ACTA CHIMICA

ACADEMIAE SCIENTIARUM HUNGARICAE

TOMUS 63 FASCICULUS 1

AKADÉMIAI KIADÓ, BUDAPEST

1970

ACTA CHIM. ACAD. SCI. HUNG.

ACTA CHIMICA

A MAGYAR TUDOMÁNYOS AKADÉMIA KÉMIAI TUDOMÁNYOK OSZTÁLYÁNAK IDEGEN NYELVŰ KÖZLEMÉNYEI

SZERKESZTI

LENGYEL BÉLA

TECHNIKAI SZERKESZTŐK

DEÁK GYULA és HARASZTHY-PAPP MELINDA

Az Acta Chimica német, angol, francia és orosz nyelven közöl értekezéseket a kémiai tudományok köréből.

Az Acta Chimica változó terjedelmű füzetekben jelenik meg, egy-egy kötet négy füzetből áll. Évente átlag négy kötet jelenik meg.

A közlésre szánt kéziratok a szerkesztőség címére (Budapest 112/91 Műegyetem) küldendők.

Ugyanerre a címre küldendő minden szerkesztőségi levelezés. A szerkesztőség kéziratokat nem ad vissza.

Az Acta Chimica előfizetési ára kötetenként belföldre 120 Ft, külföldre 165 Ft. Megrendelhető a belföld számára az „Akadémiai Kiadó"-nál (Budapest V., Alkotmány utca 21. Bankszámla 05-915-111-46), a külföld számára pedig a „Kultura" Könyv- és Hírlap Külkereskedelmi Vállalatnál (Budapest I., Fő utca 32. Bankszámla: 43-790-057-181) vagy annak külföldi képviseleteinél és bizományosainál.

Die Acta Chimica veröffentlichen Abhandlungen aus dem Bereiche der chemischen Wissenschaften in deutscher, englischer, französischer und russischer Sprache.

Die Acta Chimica erscheinen in Heften wechselnden Umfanges. Vier Hefte bilden einen Band. Jährlich erscheinen 4 Bände.

Die zur Veröffentlichung bestimmten Manuskripte sind an folgende Adresse zu senden:

Acta Chimica
Budapest 112/91 Műegyetem

An die gleiche Anschrift ist auch jede für die Redaktion bestimmte Korrespondenz zu richten.

Abonnementspreis pro Band: 165 Forint. Bestellbar bei dem Buch- und Zeitungs-Außenhandels-Unternehmen »*Kultura*« (Budapest I., Fő utca 32. Bankkonto No. 43-790-057-181) oder bei seinen Auslandsvertretungen und Kommissionären.

ACTA CHIMICA

ACADEMIAE SCIENTIARUM HUNGARICAE

TOMUS 63

AKADÉMIAI KIADÓ, BUDAPEST

1970

ACTA CHIMICA

TOMUS 63

Fasciculus 1 : 1970
Fasciculus 2 : 1970
Fasciculus 3 : 1970
Fasciculus 4 : 1970

INDEX

Acta Chimica Academiae Scientiarum Hungaricae, Tomus 63 (1), pp. 1—8 (1970)

MÖSSBAUER PARAMETERS OF IRON(II)-SALT HYDRATES

A. VÉRTES*, T. SZÉKELY** and T. TARNÓCZY***

*(*Department of Physical Chemistry and Radiology, Eötvös L. University of Sciences, **Department of Inorganic and General Chemistry, Eötvös L. University of Sciences, ***Central Research Institute for Physics)*

Received May 24, 1968

The Mössbauer parameters of iron(II) chlorides and sulfates containing various amount of water of crystallization were investigated. It has been found that increasing the water content the values of isomer shift and quadrupole splitting are increasingly determined by the linkage between the water molecule iron(II) ion. As an example, the high nepheloauxetic effect of chlorine – measured in $FeCl_2$ – is almost entirely screened by the H_2O molecules in $FeCl_2 \cdot 4H_2O$. The thermal behaviour of $FeSO_4 \cdot 4H_2O$ was investigated and on the basis of the measurements it has been estabilished that in the presence of air on 200°C this compound is oxidized to a basic iron sulfate, which is antiferromagnetic below —80°C.

The isomer shift (δ), the quadrupole splitting (ΔE) and the magnetic splitting (H) are the most important parameters of Mössbauer spectra [1, 2]. Although it is the so-called Mössbauer nucleus (in this case Fe) whose several features are characterized by each of the above parameters*, one can get valuable information about the structure of the whole molecule or even which contains as a part the Mössbauer nucleus.

*The isomer shift arises from the interaction between the nucleus and the surrounding electric charge, which can be represented by the charge density of electrons around the nucleus:

$$\delta = KZ\, e^2\, [|\psi(0)|_a^2 - |\psi(0)|_s^2] \cdot (R_e^2 - R_g^2)$$

where K is a constant, characterizing the substance Z is the atomic number,

$$|\psi(0)|_a^2 \text{ and } |\psi(0)|_s^2$$

are eletronic densities at the Mössbauer nuclei of absorber and source; R_e and R_g are the radii of the nucleus in the ground and excited states, respectively.

The quadrupole splitting is due to the interaction between the electric field gradient and the quadrupole moment of the nucleus (Stark effect). In the case of iron nuclei

$$\Delta E = \frac{1}{2} e^2\, q\, \Theta \left(1 + \frac{\eta^2}{3}\right) 1/2$$

where eq is the electric field gradient along the "Z" direction (Z is the preferred direction belonging to the highest field gradient), Θ is the quadrupole moment of iron nucleus and

$$\eta = (V_{xx} - V_{yy})\, V_{zz}$$

where V_{xx} is the electric field gradient along the x axis.

The magnetic splitting of nucleus levels is due to the internal magnetic field of ferro- and antiferromagnetic substances (Zeeman effect); in the case of iron it consists of mostly 6 lines.

This is explained by the fact that the fine structure of the energy levels of nuclei is determined by the structure of the electron shell and this latter is affected by the atoms surrounding and connected to the central atom. Therefore, as a result, the chemical and crystal structures are closely correlated with the Mössbauer parameters.

The aim of the present paper is to investigate the extent of the effect of crystal water content on several Mössbauer parameters.

As models iron(II) compounds were chosen, because in the high spin iron(II) compounds the charge distribution of $3d^6$ electrons is rather asymmetric, which results in a high quadrupole splitting even in the absence of external field. Therefore it can be expected that the structure deformational effect of crystal water molecules results in greater absolute ΔE change in the case of iron(II) than in iron(III), where the distribution of $3d^5$ electrons is of spherical symmetry. (The relative change would likely be greater in the case of iron(III) compounds, directly, however, the absolute change of quadrupole splitting can be measured, and so it is wortwhile to choose the case of greater absolute change.) On the other hand various iron(II) sulfate- and chloride-hydrates can be fairly easily prepared ($FeA \cdot xH_2O$, where $A = Cl_2$ or SO_4 and $x = 0,1,2,4,7$), and they are relatively stable compounds.

Experimental and results

The $FeSO_4 \cdot 7H_2O$ used for the measurements was of "Reanal, Ph.Hg.V." grade; the $FeSO_4 \cdot 4H_2O$ and the $FeSO_4 \cdot H_2O$ crystals were prepared by recrystallizing the $FeSO_4 \cdot 7H_2O$ at controlled temperature; $FeSO_4 \cdot 4H_2O$ was crystallized at 60 ± 1°C; $FeSO_4 \cdot$ $FeSO_4 \cdot H_2O$ at 80 ± 2°C. $FeSO_4$ was prepared by heating the compound in vacuo at 250°C for 4 hours.

$FeCl_2 \cdot 4H_2O$ was of "Reanal, pro analysi" grade; $FeCl_2 \cdot 2H_2O$ and anhydrous $FeCl_2$ were prepared by heating the above compound in vacuo at about 120°C and 400°C, respectively, for 4 hours.

The crystal water content of the preparations was determined by the Karl-Fischer method as well as by potassium permanganate titration (in the latter case x values were calculated from the determined Fe(II) content of the $Fe(II)A \cdot xH_2O$ compound). The difference in the results obtained by the two methods was less than 0.1 H_2O.

The $FeSO_4$ and $FeCl_2$ solutions (of 0.06 mole/l concentration, pH = 2) were prepared from ^{57}Fe isotope, enriched to about 80%.

The Mössbauer spectra were recorded with an automatic Mössbauer spectrometer constructed by us, connected to a multichannel pulse light analyser. The mode of working and the most important parameters of the equipment have been published in details [3]. As radiation source, ^{57}Co isotope of activity 1 mCi, diffused into stainless steel was used.

The magnetic susceptibility measurements were carried out by an equipment built in the Central Research Institute of Physics. The main features of this equipment have been described earlier [4].

The thermogravimetric curve was recorded with a "massflow" thermobalance of Stanton type.

Table I

Absorber	Temperature	δ*mm/s	ΔE*mm/s
$FeSO_4$ sol.	*la*	1.54	3.36
$FeSO_4.7\ H_2O$	*la*	1.50	3.60
	r	1.40	3.20
$FeSO_4.4\ H_2O$	*la*	1.48	3.51
	r	1.32	3.17
$FeSO_4.H_2O$	*la*	1.45	3.04
	r	1.27	2.70
$FeSO_4$	*la*	1.49	3.11
	r	1.34	2.94
$FeCl_2$ sol.	*la*	1.50	3.35
$FeCl_2.4\ H_2O$	*la*	1.42	3.08
	r	1.35	2.98
$FeCl_2.2\ H_2O$	*la*	1.29	2.59
	r	1.15	2.24
$FeCl_2$	*la*	1.23	1.10
	r	1.01	0.70

la = liquid air temperature
r = room temperature
* the error of the measurements is not greater than ± 0.05 mm/s

The results of Mössbauer measurements are listed in Table I. As the character of the spectra is very similar, only two of them are published here, namely those obtained for $FeSO_4 \cdot H_2O$, measured at room temperature and at temperature of liquid air (Fig. 1).

Some of the data listed in the table ($FeCl_2$ [7], $FeCl_2 \cdot 2H_2O$ [8], $FeCl_2 \cdot 4H_2O$ [9], $FeSO_4 \cdot 7H_2O$ [10]) have been measured by other authors, and the majority of the results is in good agreement (within the error limit) with our results. Significant difference was found in the case of values measured by ONO *et al.* for $FeCl_2$. This can likely be explained by the fact that $FeCl_2$ is very hygroscopic, and due to water absorption the spectrum may be deformed. During our experiments precaution was taken, so the data in our paper seem to be more accurate.

The water content of the individual samples indicates that they are not quite homogeneous crystal hydrates but contain in some per cent (5—10%) components of different crystal content. This superposition of low intensity, however, did not affect the Mössbauer spectra to such an extent that they

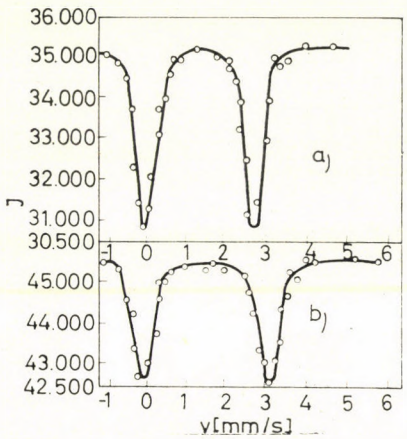

Fig. 1. The Mössbauer spectrum of $FeSO_4 \cdot 4H_2O$ *a* at room temperature, *b* at the temperature of liquid air

Table II

Water content of $FeSO_4$ (mole H_2O/mole $FeSO_4$)		δ mm/s		ΔE mm/s	
Karl—Fischer method	$KMnO_4$ titration	*la*	*r*	*la*	*r*
3.89	3.86	1.44	1.31	3.50	3.16
4.19	4.28	1.52	1.33	3.52	3.18

could not be evaluated properly. The differences in the values of Mössbauer parameters brought about by the water content change of this magnitude did not exceed the experimental error (see Table II).

If however, for any reason the quantity of "foreign" crystal hydrate increases, this results in a superposition of spectra, and not a single deformation or shift of the spectrum. For example in the spectrum of $FeCl_2$ exposed to room temperature air the lines characterizing $FeCl_2 \cdot 2H_2O$ will also appear after some hours. Having been transformed the whole sample into $FeCl_2 \cdot 2H_2O$, the latter transforms to $FeCl_2 \cdot 4H_2O$ by further water absorption. This process, whose individual steps are shown in Fig. 2, is complete within about 24 hours. In this case, however, the two superimposed spectra can be separated and evaluated. In addition, the quantity of each component can be determined on the basis of the Mössbauer intensities.

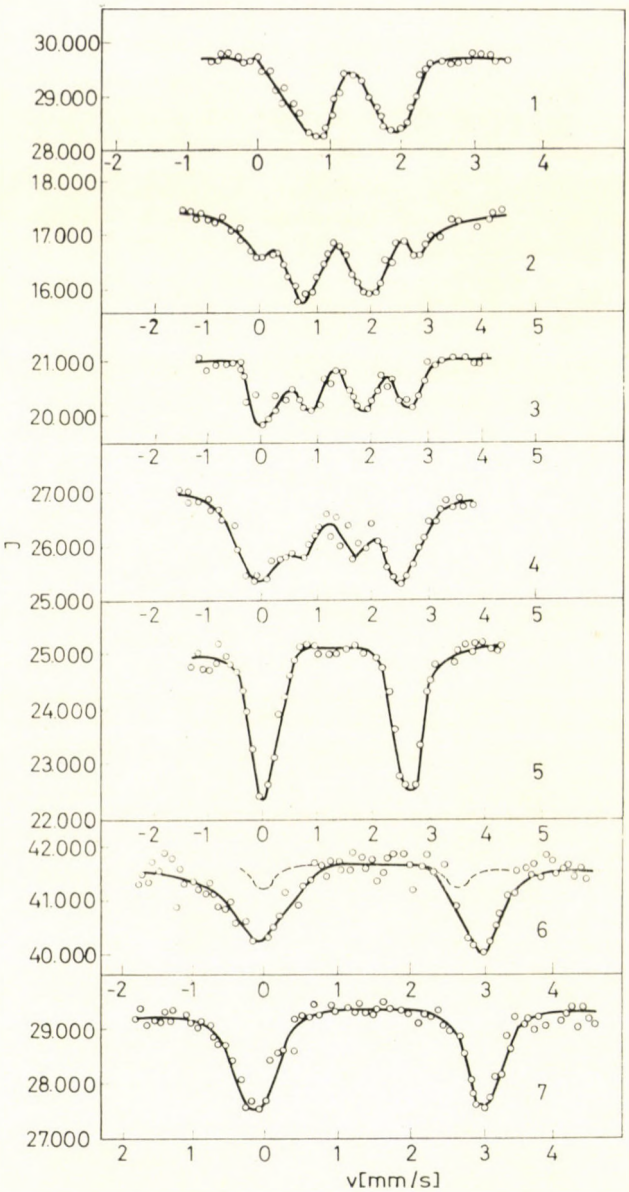

Fig. 2. Mössbauer spectra of iron(II) chloride samples containing various amount of water of crystallization, at liquid air temperature. 1. $FeCl_2$; $t_1 = 0$; 2. $FeCl_2$ ($\sim$ 85%) + $FeCl_2 \cdot 2H_2O$ ($\sim$ 15%); $t_2 = 2$ hours; 3. FeCl ($\sim$ 40%) + $FeCl_2 \cdot 2H_2O$ ($\sim$ 60%); $t_3 = 5$ hours; 4. $FeCl_2$ ($\sim$ 30%) + $FeCl_2 \cdot 2H_2O$ ($\sim$ 70%); $t_4 = 8$ hours; 5. $FeCl_2 \cdot 2H_2O$ (100%); $t_5 = 16$ hours; 6. $FeCl_2 \cdot 2H_2O$ ($\sim$ 10%) + $FeCl_2 \cdot 4H_2O$ ($\sim$ 90%); $t_6 = 22$ hours; 7. $FeCl_2 \cdot 4H_2O$ ($\sim$ 100%); $t_7 = 27$ hours (where t_i is the time of hydration of $FeCl_2$ stored in room temperature air)

Investigating the Mössbauer parameters of iron(II) chloride and sulfate samples of different crystal water content, the conclusion can be drawn that the δ and ΔE values of samples containing more crystal water are relatively near to those of dilute aqueous $FeSO_4$ and $FeCl_2$ solution samples. On the other hand it is known that in dilute aqueous iron(II) salt solutions the iron(II) ions are in the form of hexaquo-complex. According to the above it is probable that also in crystals containing more crystal water the first ligand-sphere is entirely or dominantly occupied by water molecules, consequently the Mössbauer parameters are determined by the linkage between Fe^{2+} and H_2O. In $FeSO_4 \cdot H_2O$ and $FeSO_4$ crystals, however, the connection between Fe^{2+} and SO_4^{2-} ions is more direct. This is indicated by the decrease of isomer shift and quadrupole splitting. It is even more evident in the

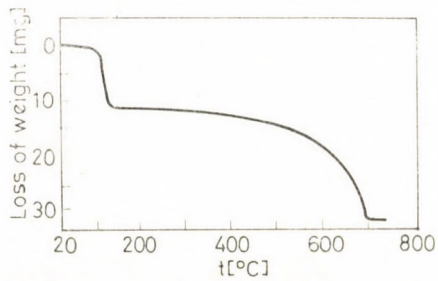

Fig. 3. The thermogravimetric diagram of $FeSO_4 \cdot 4H_2O$

case of $FeCl_2$, where the rather high nepheloauxetic effect of Cl^- is not screened by H_2O molecules and so both δ and ΔE values show significant decrease. It is worthwhile to note that changes in Mössbauer parameters can also be caused by the change in coordination number. In the present case, however, this does not seem probable, for the change of coordination number 6 would result in the increase of quadrupole splitting [6] contrary to the decrease found by us.

The thermogravimetric investigation of one of the examined samples ($FeSO_4 \cdot 4H_2O$) was also carried out. The results indicate that the water loss begins already at about 80°C and is complete below 200°C, followed by another step beginning at about 400°C (sulfate decomposition) (Fig. 3).

For investigating further the thermal behaviour of $FeSO_4 \cdot 4H_2O$ a sample was kept in air at 200°C and its Mössbauer spectrum was recorded, both on room temperature and on liquid air temperature (Fig. 4) On the basis of Fig. 4a, which is the superposition of two spectra, one can establish that the obtained product composed of a Fe^{II} compound ($\Delta E = 3.1$ mm/s, $\delta = 1.35$ mm/s) and a Fe^{III} compound ($\Delta E = 1.4$ mm/s, $\delta = 0.48$ mm/s),

this latter being present in greater quantity. The unusually high quadrupole splitting of Fe^{III} compound indicates that the charge distribution around the iron nucleus is rather asymmetric, which, regarding the $3d^5$ structure of Fe^{III} can be caused only by a great molecular asymmetry.

Also the spectrum obtained at liquid air temperature (Fig. 2b) indicates the presence of iron in two different oxidation numbers, among which the

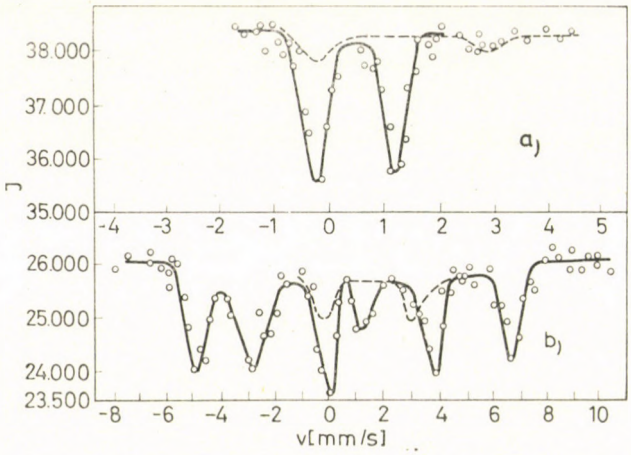

Fig. 4. The Mössbauer spectrum of basic iron(III) sulfate *a* at room temperature, *b* a liquid air temperature

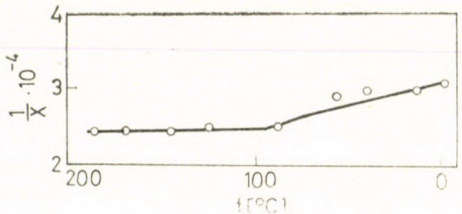

Fig. 5. The temperature dependence of the reciprocal susceptibility of basic iron(III) sulfate

Fe^{III} compound has an internal magnetic field of H = 373 KOe. On the basis of magnetic susceptibility measurements it could be established that this compound is antiferromagmetic and not ferromagnetic character at liquid air temperature, and its Néel temperature is about −80°C (Fig. 5).

On the basis of the above it seems probable that during the thermal decomposition of $FeSO_4 \cdot 4H_2O$ basic iron(III) sulfate $Fe_2O(SO_4)_2$ is formed. Consequently, one part of Fe^{II} is oxidized to Fe^{III}, and the remainder of Fe^{II} is probably in the form of $FeSO_4 \cdot 4H_2O$, as shown by the Mössbauer parameters (see Fig. 2 and Table I). Using the above assumption, on the basis

of thermogravimetric data it can be calculated that up to 200°C about 80 mole per cent of $FeSO_4 \cdot 4H_2O$ transforms into $Fe_2O(SO_4)_2$ and 20 mole per cent remains unchanged $FeSO_4 \cdot 4H_2O$.

*

The authors would like to express their thanks to L. KORECZ for discussions connected with the subject; to Miss M. KÁLDI for the Karl-Fischer titrations, and to Mrs. SUBA and Miss K. GORDON for their technical help.

REFERENCES

1. GRUVERMAN, I. J.: Mössbauer Effect Methodology, V. 2. Plenum Press, New York 1966
2. WERTHEIM, G. K.: Mössbauer Effect. Academic Press, New York, 1964
3. SOÓS, J., VÉRTES, A.: Magyar Kémikusok Lapja, **23,** 690 (1968)
4. VÉRTES, A., BURGER, K., TARNÓCZY, T., PAPP, O., EGYED, C. L.: Acta Chim. Acad. Sci. Hung. **59,** 17 (1969)
5. BURGER, K., VÉRTES, A., PAPP MOLNÁR, E.: Acta Chim. Acad. Sci. Hung. **57,** 257 (1967)
6. EDWARDS, P. R., JOHNSON, C. E., WILLIAMS, R. J. P.: J. Chem. Phys. **47,** 2074 (1967)
7. ONO, K., ITO, A., FUJITA, T.: J. Phys. Soc. Japan, **19,** 2119 (1964)
8. JOHNSON, C. E.: Proc. Phys. Soc. (London) **88,** 943 (1966)
9. DÉZSI, I., KESZTHELYI, L., MOLNÁR, B., PÓCS, L.: Investigation of Condensed Aqueous Systems by Mössbauer Effect. KFKI Közl. Budapest, 9/1967
10. DE BENEDETTI, S., LANG, G., INGALLS, R.: Phys. Rev. Lett. **6,** 60 (1961)

Attila VÉRTES; Budapest VIIII., Puskin u. 11—13.
Tamás SZÉKELY; Budapest VIII., Múzeum krt. 6—8.
Tivadar TARNÓCZY; Budapest XII., Konkoly Thege M. út.

Acta Chimica Academiae Scientiarum Hungaricae, Tomus 63 (1) pp. 9—17 (1970)

INVESTIGATIONS ON THE HYDRATIONAL AND SOLVATIONAL CONDITIONS OF IRON(II)-SALT SOLUTIONS BY MÖSSBAUER EFFECT

A. VÉRTES

(Department of Physical Chemistry and Radiology, Eötvös L. Univesity of Sciences)

Received May 30, 1968

Mössbauer spectra of frozen iron(II)-salt solutions have been investigated. In the two- and three-component solutions the change in the concentration of the components has brought about changes in the quadrupole splitting, which. according to our assumption, can be related to the transformations taking place in the hydrate indicating that in these solutions two types of iron-hydrate or solvate layers are in equilibrium.

It could be concluded that Mössbauer effect can be applied for the investigation of hydrational and solvational conditions in solutions containing Mössbauer atoms.

Introduction

It has been demonstrated earlier that Mössbauer effect can be advantageously utilized for studying the coordination and bonding in complexes containing Mössbauer atoms (*e.g.* Fe, Sn) [1—6], further for investigating the structure and magnetic behaviour of crystal hydrates [7] and in some cases also for chemical analysis and simultaneous determination of polymorphous crystal modifications [8]. The aim of this paper is to demonstrate what properties of iron(II) solutions can be examined by Mössbauer effect.

The applicability of this method for the investigation of solutions seems to be seriously reduced by the fact that recoilless resonance absorption can merely be produced by crystals, *i.e.* the Mössbauer spectrum of solutions can be recorded only after freezing the solutions. When assuming, however, that the composition of the immediate environment (the first ligand sphere) of the central ion (in this case the Fe^{2+}) does not change during rapid freezing within 10—12 seconds — and this assumption is probably valied —, on the basis of the Mössbauer spectrum of freezed solution conclusions can be drawn on the environment of the Mössbauer atoms in the original solution, *i. e.* on the composition of their hydrate and solvate layer as well.

Experimental

The equipment for recording Mössbauer spectra, which operates in pulse modulation mode and is connected to a multichannel analyser, has been described in one of our earlier papers [9]. As radiation source, a ^{57}Co isotope, diffused into stainless steel was used. The velocity *vs.* channel number

calibration was performed using $FeSO_4 \cdot 7H_2O$ absorber, for which the isomer shift on room temperature is $\delta = 1.40$ mm/s and the quadrupole splitting is $\Delta E = 3.2$ mm/s. For the spectra so many pulses were collected in each channel (10 000—60 000) that the required Mössbauer parameters could be evaluated with a 0.05 mm/s precision. Therefore the pulse number is different in each spectrum, depending on the ^{57}Fe content of the solution.

The rapid freezing of solution samples was achieved by liquid air and also the measurements were carried out at liquid air temperature in a cryostat made of plastic foam "Hungarocell".

The chemicals used were of analytical purity. Anhydrous $FeCl_2$ was prepared by heating $FeCl_2 \cdot 4H_2O$ in a vacuum furnace at about 400°C for a few hours.

For the $FeSO_4$-caprolactame-H_2O system $FeSO_4$ was prepared by dissolving metallic iron enriched in ^{57}Fe to 80% in sulfuric acid, and thus even in the case of rather low iron concentrations ($\sim$0.2 w/w%) properly measurable effects were obtained. The iron(II) perchlorate—perchloric acid solutions were prepared by dissolving ^{57}Fe (metal) in perchloric acid. In the other cases ordinary iron was used, and consequently relatively higher iron concentration was needed to obtain measurable effects. In the majority of cases solutions of concentration about 1 $\frac{\text{mole iron (II) salt}}{\text{1000 g solvent}}$ were used. In cases where this concentration could not be reached due to the low solubility, saturated solutions (with respect to $FeCl_2$) were used.

The oxidation of iron(II) was prevented by removing oxygen from the solvents by bubbling hydrogen through them before dissolving $FeCl_2$ and also by carrying out the dissolution in a hydrogen atmosphere. In more concentrated acetic acid solutions the partial oxidation of iron(II) could not be avoided even by using the above method, because some oxygen remains even after bubbling hydrogen for 1—2 hours.

Results

Aqueous solutions of $FeCl_2$, $FeSO_4$, $Fe(ClO_4)_2$; and three-component systems $FeCl_2$—$LiCl$—H_2O, $FeCl_2$—KCl—H_2O, $FeCl_2$—KF—H_2O, $FeCl_2$—NaF—H_2O and $FeSO_4$-caprolactame($C_6H_{11}NO$)—H_2O were investigated, in the latters LiCl, KCl, KF, NaF and caprolactame were employed for decreasing the activity of water. In addition, the $FeCl_2$—CH_3COOH—H_2O and $FeSO_4$—CH_3COOH—H_2O systems were used. The most important parameters of the Mössbauer spectra of the above solutions (isomer shift δ and quadrupole splitting ΔE) are listed in Table I.

The change in the value of isomer shift has scarcely exceeded the error limit; this fact is quite understandable because the isomer shift depends on

Table I

No	Components of the system	Composition in weight %	Mössbauer parameters in mm/s units		a_0*
			ΔE	δ	
1	$FeCl_2$	10.58	3.28	1.42	
	H_2O	89.42			
2	$FeCl_2$	24.64	3.25	1.50	
	H_2O	75.36			
3	$FeCl_2$	7.91			
	LiCl	24.50	3.26	1.50	0.57
	H_2O	67.59			
4	$FeCl_2$	6.91			
	LiCl	34.20	3.20	1.52	0.30
	H_2O	58.89			
5	$FeCl_2$	8.19			
	LiCl	37.80	3.30	1.40	0.24
	H_2O	54.01			
6	$FeCl_2$	6.31			
	LiCl	39.70	2.45	1.48	0.19
	H_2O	53.99			
7	$FeCl_2$	8.15			
	KCl	23.32	3.18	1.38	0.85
	H_2O	68.53			
8	$FeCl_2$	9.85			
	KF	6.31	3.18	1.52	0.96
	H_2O	83.84			
9	$FeCl_2$	9.80			
	NaF	6.73	3.24	1.50	0.95
	H_2O	83.47			
10	$FeCl_2$	12.95			
	$HClO_4$	5.98	3.20	1.44	0.99
	H_2O	81.07			
11	$FeCl_2$	8.54			
	$HClO_4$	14.90	3.28	1.48	0.92
	H_2O	76.56			
12	$FeCl_2$	9.29			
	$HClO_4$	26.80	3.33	1.46	0.76
	H_2O	63.91			

Table I continued

No	Components of the system	Composition in weight %	Mössbauer parameters mm/s units		a *
			ΔE	δ	
13	$FeCl_2$	3.46			
	$HClO_4$	43.60	3.18	1.48	0.43
	H_2O	52.94			
14	$Fe(ClO_4)_2$	0.55			
	$HClO_4$	7.69	3.33	1.46	0.95
15	$Fe(ClO_4)_2$	0.81			
	$HClO_4$	69.23	3.28	1.50	
	H_2O	29.96			
16	$FeSO_3$	0.51			
	ε-caprolactame	0.00	3.28	1.54	0.99
		99.49			
17	$FeSO_4$	0.51			
	ε-capro-lactame	41.20	3.18	1.54	0.86
	H_2O	58.19			
18	$FeSO_4$	0.51			
	ε-caprolactame	61.40	3.16	1.48	0.75
	H_2O	38.09			
19	$FeSO_4$	0.48			
	ε-caprolactame	76.70	3.20	1.54	0.66
	H_2O	22.82			
20**	$FeSO_4$	0.48			
	ε-caprolactame	76.70	1.94	1.56	
	H_2O	22.82			
21	$FeCl_2$	11.75			
	CH_3COOH	3.26	3.28	1.50	
	H_2O	84.99			
22	$FeCl_2$	9.12			
	CH_3COOH	7.22	3.22	1.53	
	H_2O	83.66			
23	$FeCl_2$	11.23			
	CH_3COOH	11.25	3.28	1.42	
	H_2O	77.52			
24	$FeCl_2$	12.91			
	CH_3COOH	29.43	3.26	1.40	
	H_2O	57.66			

Table I continued

No	Components of the system	Composition in weight %	Mössbauer parameters in mm/s units		a_0*
			ΔE	δ	
25	$FeCl_2$	9.41			
	CH_3COOH	45.20	3.30	1.46	
	H_2O	45.39	2.47		
26	$FeCl_2$	11.94	3.24		
	CH_3COOH	60.70	2.56	1.52	
	H_2O	27.36			
27	$FeCl_2$	3.66	3.20		
	CH_3COOH	81.12	2.50	1.48	
	H_2O	15.22			
28	$FeCl_2$	3.66			
	CH_3COOH	96.34	2.43	1.44	
	H_2O	0.00			
29	$FeSO_4$	11.60			
	CH_3COOH	15.55	3.32	1.42	
	H_2O	72.85			

* Water activity values were calculated using the osmotic coefficient data from literature [10]. For solutions containing caprolactame there are direct a_0 data published [11]. The a_0 values refer to solutions that do not contain iron salt.

** The solution was pre-heated at 70°C for 5 hours; the oxidation of Fe^{2+} was prevented by adding some ascorbic acid.

the electron density at the Mössbauer nucleus; on the other hand, the changes taking place in the hydrate and solvate layer can evidently affect the electron density at the central atom (which can be given by the Schrődinger wave function, $|\psi(o)|^2$) only to a negligible extent. Therefore on the basis of isomer shift data one cannot expect to obtain any information about the hydrate and solvate layer.

The value of quadrupole splitting, however, is determined by the symmetry of the charge distribution around the Mössbauer nucleus, and this can be influenced to a greater extent by the composition and symmetry of the hydrate and solvate layer. On the basis of the above fact one may assume that changes taking place in hydrate and solvate layers are reflected in the value of quadrupole splitting. In accordance with this assumption the changes found in the experimental results concerning ΔE exceed the experimental error sometimes by one order of magnitude. (See, *e.g.* the difference between measurements 5 and 6).

Discussion

On the basis of the experimental results the following conclusions can be drawn:

The Mössbauer parameters of aqueous iron(II) solutions containing different anions (Cl^-, SO_4^{2-}, ClO_4^-) are the same within the error limit, and therefore it can be concluded with great probability that in the above solutions Fe^{2+} ions are present as hexaquo ions, *i.e.* the anions do not take part in the formation of the inner coordination sphere around the Fe^{2+} ion. This, of course, does not mean that the anions may neither be present in the further, second or third spheres, since an anion effect taking place in second or third spheres does not appear in the quadrupole splitting.

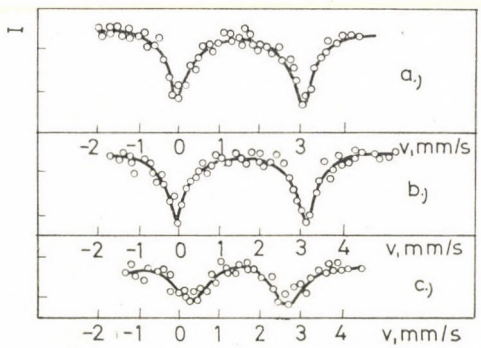

Fig. 1. The Mössbauer spectra of three-component systems $FeCl_2$—LiCl—H_2O. *a)* $FeCl_2$: 24.64 w%, LiCl: 0.00 w%, H_2O: 75.36 w%, *b)* $FeCl_2$: 6.91 w%, LiCl: 34.20 w%, H_2O: 58.89 w%, *c)* $FeCl_2$: 6.31 w%, LiCl: 39.70 w%, H_2O: 53.99 w%

The $Fe(H_2O)_6^{2+}$ complex ions remain unchanged even by increasing the iron(II) salt concentration considerably since the ΔE and δ values of saturated $FeCl_2$ solution (measurement 2) are the same as the Mössbauer parameters of $FeCl_2$ solution of 10 58 weight per cent concentration (measurement 1) and moreover as those of the 0.5 weight per cent $FeSO_4$ solution (measurement 16).

In the case, however, when the activity of water (a_0) is decreased somehow, it is possible to reach an a_0 value where the ΔE value of the solution changes, indicating certain change in the hydrate layer of the Fe^{2+} ion. If LiCl is used for decreasing a_0 (measurements 3—6) this change takes place at about $a_0 = 0.2$ (measurement 6). It seems probable that this decrease in ΔE is brought about by the fact that among the 6 coordination places of the iron two is already replaced by Cl^- ions at $a_0 < 0.2$. This assumption is supported by the tendency of ΔE change, which can be fairly correlated with the relatively high nepheloauxetic effect of chlorine [5].

It is remarkable that the exchange of H_2O molecules to Cl^- ions takes place stepwise and not continuously with the decrease of a_0 values. This fact is in correlation with the experimental results where the activity of water was decreased by KCl (measurement 7), KF (measurement 8), NaF (measurement 9), $HClO_4$ (measurement 10—15) and caprolactame (measurements 17—19). In these cases the $a_0 = 0.2$ value could not be attained (demanding that there should be dissolved iron(II) salt in quantity ensuring any Mössbauer effect); therefore in these solutions the ΔE values remained unchanged. As we have not found any data regarding the osmotic coefficient of concentrated perchloric acid solution (No. 15), its a_0 value could not be calculated.

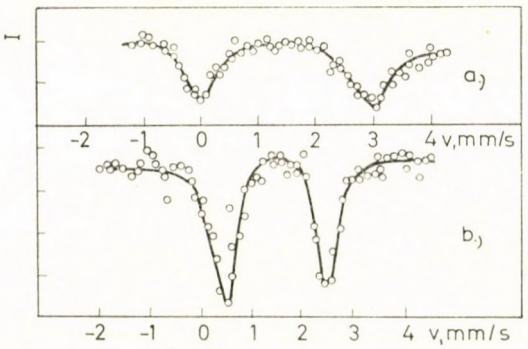

Fig. 2. Mössbauer spectra of the three-component system $FeSO_4$ 0.48 w% — ε-caprolactame 76.70 w% — H_2O 22.82 w%: *a)* without heating, *b)* after heating at 70°C for 5 hours

Our assumption concerning the correlation between ΔE change and the dissociation of hydrate layer is supported by the results of measurement 20, too. According to this experiment, in a caprolactame solution of about ~30M = = mole/1000 g solvent concentration, heated to 70°C during 5 hours (where a considerable polymerization of caprolactame has taken place resulting in gelation and through this the loosening of hydrate layer) the value of quadrupole splitting decreased by about 40 per cent (Fig. 2).

As published a_0 values or osmotic coefficients of acetic acid solutions have not been available, Table I does not include data on water activity in $FeCl_2$—CH_3COOH—H_2O systems (measurements 21—28).

On the basis of the measurements on acetic acid systems similarly the presence of $Fe(H_2O)_6^{2+}$ ions can be assumed up to about 40 weight per cent CH_3COOH content (Fig. 3a). In the solution containing 45.20 weight per cent acetic acid, however, another type of spectrum appears, too, with $\Delta E = 2.47$ mm/s quadrupole splitting (measurement 25), the intensity of which amounts to 10—15% of the entire spectrum, *i.e.* in the solution 10—15% of the total iron(II) content is not in hexaquo-complex (see Fig. 3b). In anhydrous glacial acetic acid the whole iron(II) content of the solution gives rise

to Mössbauer spectrum of such, relatively low quadrupole splitting (ΔE = = 2.43 mm/s; Fig. 3c and measurement 28). From this fact it seems very probable that in CH_3COOH solutions of higher than about 45 weight per cent concentration also another iron(II) complex is present; and while increasing the acetic acid concentration the concentration of the latter complex increases at the expense of the hexaquo-complex, and finally, in anhydrous glacial acetic acid only this latter complex — probable $FeCl_2 \cdot 4CH_3COOH$ — is existing. The probability of this structure is increased by the fact that the dielectric constant of glacial acetic acid is $\varepsilon = 6.29$ (while that of water is

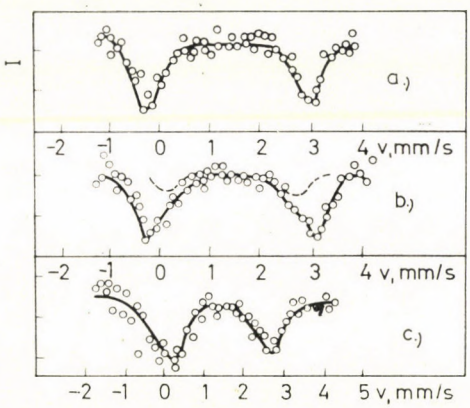

Fig. 3. Mössbauer parameters of three-component systems $FeCl_2$—CH_3COOH—H_2O: *a)* $FeCl_2$: 12.91 w%, AcOH: 29.43 w%, H_2O: 57.66 w%, *b)* $FeCl_2$: 9.41 w%, AcOH: 45.20 w%, H_2O: 45.39 w%, *c)* $FeCl_2$: 3.66 w%, AcOH: 96.34 w%, H_2O: 0.00 w%

$\varepsilon_{H_2O} = 80$) and, accordingly, the dissociation constant (K_d) of salts (e.g. LiCl, KCl) dissolved in glacial acetic acid is about 10^{-6}—10^{-7} [12].

It is worthwhile to note that in acetic acid solutions containing more than 50 weight per cent of CH_3COOH the solubility of $FeCl_2$ is surprisingly low, and as a consequence the intensity of Mössbauer spectra measured in this concentration range is very weak. Due to this fact difficulties arise in evaluating the spectra; therefore the error of measurements 26—28 (± 0.08 mm/s) slightly exceeds that of the former experiments. This fact, however, has nothing to do with the above statements because the difference between the two types of ΔE is even in this case greater by an order of magnitude than the experimental error.

In one experiment (measurement 29) — in relatively dilute acetic acid solution — $FeSO_4$ was dissolved instead of $FeCl_2$. The results obtained do not indicate any anion effect, consequently on dissolving $FeSO_4$ also in this case $Fe(H_2O)_6^{2+}$ ions are formed.

*

I would like to express my thanks to Mrs. L. SUBA for her conscientious and precise work, and to Miss K. GORDON for drawing the figures.

REFERENCES

1. KERLER, W., NEUWIRTH, W.: Z. Phys. **167,** 176 (1962)
2. HERBER, R. H., KINGSTON, W. R., WERTHWIM, G. K.: Inorg. Chem. **3,** 101 (1964)
3. GOLDANSKIJ, V. I., ROTSEV, V. J., CHRAPOV, V. V.: Dokl. Akad. Nauk. SSSR **156,** 909 (1964)
4. BURGER, K.: Modern koordinációs kémiai vizsgáló módszerek (in Hungarian) Akadémiai Kiadó, Budapest, 1967
5. BURGER, K., VÉRTES, A., PAPP MOLNÁR, E.: Acta Chim. Acad. Sci. Hung., **57,** 257 (1967)
6. VÉRTES, A., TARNÓCZY, T., PAPP MOLNÁR, E., BURGER, K., EGYED, C. L.: Acta. Chim. Acad. Sci. Hung., **59,** 19 (1969)
7. VÉRTES, A., SZÉKELY, T., TARNÓCZY, T.: Acta Chim. Acad. Sci. Hung. **63,** 1 (1970)
8. DÉZSI, I., VÉRTES, A., KISS, L.: Magy. Kém. Folyóirat **73,** 421 (1967)
9. SOÓS, J., VÉRTES, A.: Magyar Kémikusok Lapja, **23,** 690 (1968)
10. ROBINSON, R. A., STOKES, R. H.: Electrolytic Solutions. Butterworths Scientific Publ. London, 1959
11. ERDEY-GRÚZ, T., GOLOPENCZA BAJOR, O., GALLYAS, M.: Magy. Kém. Folyóirat **72,** 501 (1966)
12. JANDER, G., SPANDAU, H., ADDISSON, C. C.: Chemie in nichtwässrigen ionisierenden Lösungsmitteln. Band IV. Akademie-Verlag, Berlin, 1963

Attila VÉRTES; Budapest VIII., Puskin u. 11—13.

Acta Chimica Academiae Scientiarum Hungaricae, Tomus 63 (1), pp. 19—51 (1970)

SPECTROSCOPY OF DIFFUSE SCATTERING SYSTEMS, I

DEPENDENCE OF OPTICAL DATA ON THE QUANTITY OF THE SAMPLE

J. HUSZÁR

(Spectroscopic Laboratory, Ministry of the Interior)

Received May 27, 1968

In this apper the author deals with relations of measured optical data and the quantity of a scattering sample. Under defined conditions the scattering samples on paper basis can be considered as "quasi-homogeneous" ones. Parallelisms in the dependence of remission and transmission values on substance quantity were investigated. Relation "A" was expressed; also the "critical quantities", their formal and substantial characteristics and the special optical parameter of samples with quantities greater than the critical (Δ_r value) were determined. Validity range of the relations was discussed.

Introduction

Characteristics of optically diffuse scattering systems (further on: scattering systems) can be attributed to scattering phenomena. The fundamental processes of scattering (first of all: reflection and refraction) occur on interfaces of phases of different refractive indexes. The direction of photons becomes altered. So diffuse scattering means a multiple alteration of the direction of a beam, in every direction of space.

Great variety of samples show this phenomenon. Scattering systems are the atmosphere, hydrosphere, earths; floral and animal cell systems, leaves, blood; every emulsion and suspension; several industrial products (*e.g.* textile fabrics, papers, printed matters, paints, ceramics, most of foods and medicines, etc.). All carriers used for chromatographic, electrophoretic or spot test analysis are, with no exceptions, scattering systems. Huge majority of the visible objects in our world forms scattering systems, as diffuse scattering is one of the fundamental conditions of visibility of shapes.

Spectroscopy of scattering systems is an independent part of absorption spectroscopy [7]. Scattering — as compared to scatteringless conditions — alters the probability of the absorption processes. Formulation of the absorption spectrum, its measurement and evaluation are carried out under considerably different, more complicated conditions than in the classical absorption spectroscopy.

Measuring parameters and data of scattering samples

In the spectroscopic literature different, even contradictory symbols are used. It is reasonable to differentiate between measuring parameters, measuring data and working parameters.

Measuring parameters

Measuring parameters can be divided into three groups:

a) Internal parameters are the properties of the components and the system, influencing the optical characteristics of the scattering system.

b) Quantitative characteristics: quantity of the total sample, and quantity of the individual components (*e.g.* carrier, dye, etc.).

c) External parameters include the conditions of the illumination and observation of the optical measurement (instrumental conditions).

The measuring parameters (these three groups together) determine the content of the measuring data. In Table I the range of measuring parameters referred to in this series of papers is summarized.

Table I

Measuring parameters of the scattering sample

Internal parameters	Characteristics of components — geometric data of dispersed particles (size of particles, shape of particles) — material constants of components — absorption coefficient (*e.g.* $\varepsilon_{\lambda;1}$; $\varepsilon_{\lambda;2}$; . . .) — refractive index ($n_{\lambda;1}$; $n_{\lambda;2}$; . . .) Characteristics of the system — structural characteristics — uniformity of size and shape of the dispersed particles (by components) — uniformity of distribution of components — type of location of the components — optical characteristics — diffuse-scattering (multiple change of direction of photons) — absorption (joint result of light absorption of the individual components)
Quantitative characteristics	Substance quantity of the sample Quantity of the individual components
External parameters (instrumental conditions)	Type of illumination and observation — diffuse or directed — complex or monochromatic — polarized or non-polarized Size of illuminated area of the sample Optical arrangement (determining the instrumental constant) Sensitivity of the instrument

Data of measurement

Only the quantitative data of the scattering sample and the optical characteristics of the total sample are directly measurable. They form a related pair of values of quantitative—optical character.

In most cases the other internal parameters can be directly measured only out of the scattering system. In the scattering sample their optical effect does not appear separately, but combined with many other factors. Studies should be carried out on revealing the possibility of their determination on the base of optical measuring data (*e.g.* determination of ε_λ of the absorbing substance in the scattering sample).

a) Quantitative data: they are characteristic to the quantity of the material showing interaction with light.

The applied unit of measurement is strongly dependent on the type of the sample. Use of different units may be advantageous in the case of the scattering sample and the individual components. For example, in colored materials the quantity of the dye is usually smaller than the accuracy of determination of the quantity of the carrier. The applicability of data obtained by usual measurements of mechanical character on high quantities of samples, and the appropriateness of use of absolute or specific data must be decided after considering the actual type of sample and investigation.

b) The optical data (data of remission and transmission) give informations on the results of optical interactions.

The non-absorbed photons are removed from the sample by scattering, through one of the surfaces. Values of remission and transmission indicate the same interactions. However, the optical characteristics of the sample can be observed in different degrees and from different points of view by means of this two types of measurement.

The radiation providing optical data can always be reduced to several components [34], which take part in the absorption interactions in different degrees; and their ratio depends on many factors (*e.g.* type of sample, quantity of sample, degree of scattering—absorption, etc.).

Components of the diffuse-remitted radiation are: "external component" (sum of rays reflected "regularly" from the surface, not being passed through any particle) and the "internal component" (rays passing repeatedly through the particles of the layer).

Components of diffuse-transmitted radiation are: rays passing through the layer between the particles; those passing through the particles in unaltered direction; rays passing through the particles with multiple change of direction.

So very complex information is resulted from the optical data of a scattering sample.

c) One of the fundamental problems of spectrophotometry of scattering systems is the dependence of the optical data on the quantity of the material. Investigation of this question first results in empirical relations, discovering the direct relationship existing between the two parallel measurable groups of data. Its importance is due to the fact that studies of all the other points

(*e.g.* effect of the measuring parameters, their interactions, general relationships) are based on the optical data of an actual quantity of material (scattering system).

Review of the literature

Literature of the optical characteristics of scattering samples and their investigation is very extended and various. Several comprehensive papers are available [15, 17, 20, 21, 30, 34, 37, 42]. Results and problems indicate a beginning phase in this branch of spectroscopy.

A great number of scientists have studied the scattering systems. However, no one of the theories could take all the influencing factors into consideration because of the complexity of these factors determining the optical behaviour of the scattering samples (Table I). The validity and applicability range of a given theory is determined by the simplifications and neglections included by the physical assumptions and the selected "working" parameters.

In reviewing the theories we want to point out the relations to the quantities of the material.

*Theories on diffuse-reflection**

The relatively most general and most extended theories are based on determination of photometric characteristics of the light *reflected* by the sample.

a) Most of the theories dealing with diffuse reflections — though showing great variety of explanatory forms — are based on the theory of GUREVIC—KUBELKA—MUNK (data of elaboration: 1930—1931; fundamental publications: [11, 22, 23, 24, 27]). Premise conditions of the GKM theory:

— ideal-hypothetic sample (JUDD's term [16]): homogeneous, isotropic medium, uniformly distributed scattering and absorbing properties, plan-parallel surface

— dimension of the sample: practically infinite in the YZ plane (edge effects are negligible); thickness of the layer is high enough to result in practically non-transparent sample

— diffuse illumination by monochromatic light

— light path can be represented in a simplified manner by two components of opposite direction, perpendicular to the surface of the sample.

Relationship was deduced between one single measured datum (R_∞ remission of a sample of d_∞ layer thickness) and two "working" parameters (K and S, constants characteristic of absorption and scattering of a layer of unit thickness):

$$f(R_\infty) = \frac{K}{S} = \frac{(1 - R_\infty)^2}{2R_\infty}$$

*In the literature "diffuse-reflection" is often used in the same sense as remission.

Applying R_∞ the problem connected to the quantity of the substance is actually eliminated (change of layer thickness of the measured sample will not affect the data of remission).

The R_∞ function gives the quotient of two constants. This relation contains no assumptions regarding the members of the quotient (only their independence from the quantity of the material is supposed).

It is supposed [18] that dependence of the scattering coefficient on wavelength is negligible for small absorption values:

$$K \sim \varepsilon_\lambda \cdot \text{const.}$$

This relation is thought to be suitable for quantitative determination of low-absorbing materials. Therefore KORTÜM "dilutes" the strongly absorbing powder samples with a chemically inactive "white" substance [20, 21].

Parallel illumination of $\alpha = 0$ angle was studied by RYDE [31], his equations can ultimately be considered identical with the GKM functions.

Remission data of samples having significant transmission are dependent on the quantity of the sample and the "background" behind them (this can return the transmitted photons into the sample, increasing so the value of remission). Many functions were developed for remission of scattering samples of "definite layer thickness" [42]. In these relations the number of layers (1 and ∞) and data of the background (a black or white medium) serve to set the measuring conditions. However, no systematic study of the dependence of them on the quantity of the material was carried out yet. STENIUS [36] investigated the dependence of scattering coefficients of papers on the square weight. The obtained nonlinear curve was explained by the different scattering coefficients of the surface and central layers of the sample.

b) The theory of planparallel layers was developed in the fifties of this century [2, 3, 24, 33, 37].* Light reflection of a real scattering layer was supposed to be equivalent to reflection on a series of layers, the thickness of the individual layers being equal to the average diameter of the scattering centres. Light is partly reflected on each surface (according to the reflection coefficient), partly absorption of definite degree occurs while passing through the layer. Some authors name this explanation as "statistical" [42], others as "factorial" [32] one. Its equations are based on the optical constants of the individual particles and on R and T data of the individual layer.

The "Blattstoss-Theorie" by SCHMIDT [32] is based on the investigation of a paper "sheet-packet" of changeable number of layers. Dependence of remission values on thickness is deduced from remission of the building-up

*Starting points of the theory of planparallel layers were developed by STOKES in 1860. However, his equations cannot be used for practical purposes because of their complexity.

layers. Its fundamental idea — modelled by planparallel layers — is the following:

$$\frac{\Delta_n}{\Delta_{n+1}} = \text{const.} \qquad \text{where } \Delta_n = R_{n+1} - R_n$$

Δ_n value is the difference in remission of sheet packets of neighbouring layer numbers. According to SCHMIDT, the quotient of the succeeding Δ_n values is constant and it depends on the remission and transmission of the individual layer only. The author stated that the content of his formulas is identical with that of the GKM theory, but in a more simple form.

c) Several papers deal with the practical study and application of the two main groups of theory. Such subjects are the following:

— substitution of complicated equations by charts or nomograms [5, 6, 16]

— adjustment of experimental conditions to the theoretical starting points [21]

— determination of the limit of validity for certain types of scattering samples [15, 34].

In science and practice alike increases the application range of these methods.

d) IVANOV [15] summarized the efficiency of theories based on measurement of remission as follows:

— These theories emphasize only one of the important photometric characteristics of a scattering sample, the others (transmission, polarization properties, structure of angle distribution of the radiation, etc.) are almost perfectly neglected.

— It is not sure that reflection coefficient is a most suitable factor for spectroscopic investigation of a scattering medium, especially when considering, that this is not too sensitive to the changes of internal properties of the layer.

— Relations based on measurable parameters are very complicated. Parameters of simple formulas are not measurable. So the equations are applicable for certain details only.

Transmission of scattering samples

Studies on transmission of scattering samples could not avoid the question of dependence on the quantity of the material.

a) Differences in distribution of the substance in scattering samples result in significant errors in the measurements and strongly spreading transmission data [13]. Different instruments may give very different data of transmission. Increasing layer thickness enhances the requirements for the sensitivity of the instrument.

Therefore this type of measurement is thought to be disadvantageous [13, 32] though the higher sensitivity of evaluation based on measurement of transmission (compared to that based on measurement of remission) is admitted [12].

b) Special attention was lately drawn to the investigation of laws of extension of the radiation in greater depth of diffuse scattering liquids. Such studies were needed for investigation of the hydrosphere of the Earth. It has several advantageous possibilities. Such are:

— laws of extension of radiation are strongly simplified in greater depth, and more simplified relations are probable between the optical characteristics and spectroscopic properties of the scattering medium

— external illumination of the medium, its surface structure, etc. have no effect on the distribution of intensity.

Results of theoretical research works (summarized in [15]), are not suitable for practical application owing to the complicated mathematical treatment and the need of knowledge of the scattering indicatrix.

Experimental investigation of the "depth regime" was carried out by TIMOFEJEVA [39—41]. She established several new empirical relations on the basis of her study on transmission of milk-like media of different dilutions. According to her, the curve describing the attenuation of the directed beam in the deepness (the medium is of low-absorption) consists of three sections. The first and third ones show changes of exponential character, the second one is nearly hyperbolic.

SIDKO and TERSKOV [35] note the layer-thickness regions belonging to sections of the "depth regime" curve as d_{01}, d_{12}, d_{23}. The third section is observed usually in the case of total scattering. To this phenemenon the presence of a sample of $d_{\text{min.}} = d_{01} + d_{12}$ layer thickness is required (this is about 300 m in clear sea-water). Value of $d_{\text{min.}}$ depends on the wavelength.

c) From the beginning of the fifties of this century several research workers dealt with "direct photometry" of absorbing substances, isolated on paper (*i.e.* measuring transmission of a scattering sample), to avoid the time-consuming and error-involving operation of eluation.

The majority of investigations search for a linear relation between the quantity of the substance present on the carrier, and the measured optical data (validity of BEER's law). We do not want to deal with this question now.

References for relations between the quantity of the total sample and the corresponding transmission data are given in several papers.

— A formula was developed by FALTA, based on equations of NEUGEBAUER, which allows the assumption of validity of the BOUGUER—LAMBERT law for the transmission degree of papers of high layer thickness [9].

— Also FALTA [8] stated — based on his measurements on opaque glasses of different thicknesses — that the transmissional extinction does

not increase linearly with increasing layer thickness. For smaller thicknesses the increase is greater than for higher ones. Measurements of samples of high thickness resulted in almost linear curves.

— PRICE, HUDSON and ASHMAN [28] found a linear relationship between the number of layers and the density measured under special conditions (at 254 nm). The studied sample was adenilic acid on Whatman No. 11 filter-paper.

Uniform treatment of scattering systems

Theories and relations based on measurement of remission or transmission only, must be regarded as very restricted ones. Both the theoretical and the empirical investigations make efforts to develop relations between the measured optical data and characteristics of scattering and absorption. However, measurements are usually carried out by one type of them only. Parallel studies of the two phenomena are very rarely found in the literature.

An interesting initiation is the description of the optical properties of scattering samples by functions of path-length of the light. In the paper by MAJOR [25] parallel considerations are found concerning remission and transmission of scattering samples. Certain part-results are proved by measured data of powders and samples on paper basis.

Parallel experimental studies of remission and transmission of scattering samples are accompanied by serious difficulties. Such are:

— Certain types of samples (*e.g.* powders, textile fabrics, printed products, earths, ceramics, etc.) are available only for measuring of remission, while others are suitable only for measurements of transmission only (*e.g.* atmosphere, hydrosphere, emulsions, suspensions, etc.), possibilities of measuring their remission are restricted.

— Definite conditions of measurement for optical investigation of scattering samples indicate a difficult and neglected problem. Only few attention was drawn to it, in some studies on analytical subject, and in the field of remission measurements [13, 19, 21, 29].

— The general, multilateral investigation of the dependence of measured optical data on the quantity of the material is missing yet. It is expected that the individual types of scattering samples will provide different points of view for the researchers.

Subject of the present investigation

Purpose of our investigation published in the present paper are:

— development of defined conditions for measurements of scattering samples on paper basis by spectrophotometer for routine work, for parallel measurement of remission and transmission

— study of relations between the optical and quantitative data of the sample (corresponding measurements of remission of the examined type of sample, but no transmission measurements were found in the literature).

The published data and conclusions are of photometric character; no discussion of dependence on wavelength is given here. Both colored and colorless substances were studied as scattering ones. The effect of coloring of colorless samples or measurements at different wavelengths on the principal character of the obtained empirical relations was studied. (No discussion of the appearance of the spectrum of the absorbing substance present on the carrier, in connection to the wavelength dependence of the optical data of the scattering sample is presented here.)

2. Experimental

Instruments, procedures

It was investigated, whether conditions suitable for defined measurement of scattering samples on paper basis can be assured by means of a recording routine spectrophotometer, designed for measurement of absorption of solutions. Measurements on a Unicam SP 700 spectrophotometer prove the multilateral applicability of the instrument for determination of the optical characteristics of papers (and other scattering samples).

As regards the observation of the radiation falling on the detector, the possibilities of the instrument are the same by measurement of solutions and scattering samples too. The detector is insensitive to the origin of the observed radiation. Applicability of an instrument depends on utilization of the character of the instrument and knowledge of the dependence of measured data on it.

Instrumental conditions and their use for investigation of scattering samples

Scattered radiation leaves the surface of a sample with a definite intensity distribution, after it no changes of wavelength or indicatrix are possible. By measuring remission or transmission by different instruments the intensity of light, reaching the detectors may be significantly different — sometimes they are of different orders [32]. Different instruments — due to their dissimilar optical arrangements — use different portions of the radiation leaving the sample. Also the external parameters of measurements are dissimilar. The measured data contain different values of instrumental constants.

Instrumental constant of remission measurement by a Unicam SP 700 spectrophotometer, with optical arrangement shown in Fig. 2 is:

$$E_{(MR)} \sim 2.6$$

that of transmission measurement:

$$E_{(MT)} \sim 1.8$$

However, the detector (PM 6256) of the instrument is so sensitive, that $E \sim 4.5$ values can be reliably measured in the visible spectral region. Full intensity range of remission measurement is about one order; there are three orders for measurement of transmission. Utilization of light in transmission measurements can be increased by almost one order (with decrease of the instrumental constant) by placing a condenser lens closely after the sample (Fig. 2).

Value of the instrumental constant is influenced by the location of the sample in the cuvette space. This means change of the distance between the sample and the first lens. The spatial angle, from which photons can reach the detector, also changes. Placing of the sample means also a very sensitive source of error. To avoid it, a special sample holder and a base plate is required for a well defined placement in the cuvette space.

Acta Chim. Acad. Sci. Hung. 63, 1970

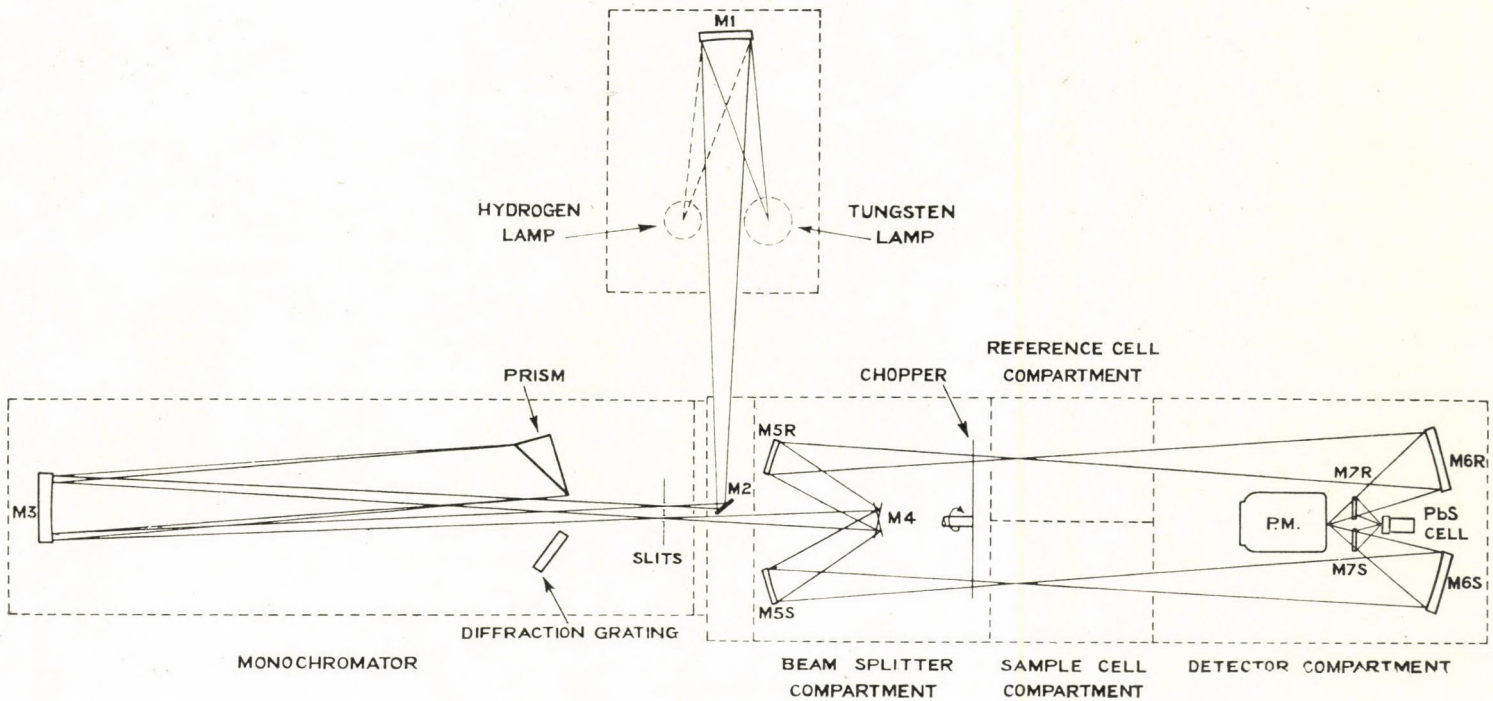

Fig. 1. Optical arrangement of Unicam SP 700 spectrophotometer

Springs compressing the surfaces of the sample holder provide identical compression of samples of different layer numbers. Reproducible placement of square paper pieces is made easier by adjusting plate. In the reference beam a series of grating was applied for weakening the light. They were prepared by cautery of brass plates. Reproducibility of their placement into the ligth path is ensured by base plates similar to those of the sample holders.

The instrument, equipped with special sample holders, a series of gratings and special base plates of the holders, can be used with the same sensitivity, accuracy and reproducibility

remission measurement transmission measurement

Fig. 2. Optical path in the cuvette space when examining scattering samples. Representation of light path is quite schematic; after point S the light is scattered in all direction in reality

S — sample; M — mirror; K — condenser

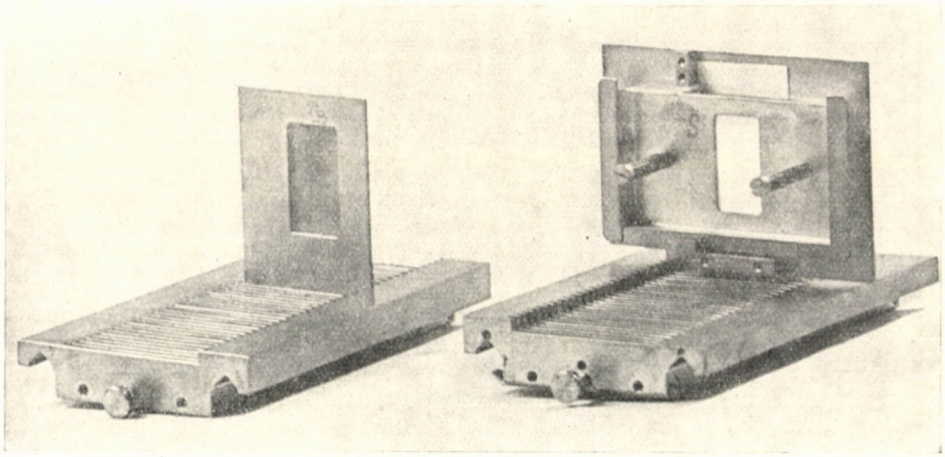

Fig. 3. The special base plate, sample holder and the grating for weakening the light

degrees as at measurement of solutions. (Even in the case of very uneven papers, the spread of the obtained results is less than 0.005 extinction unit.) Correct and reliable data are obtained by measuring the colored sample and the colorless carrier being placed after each other in the light path. (In the reference beam the grating is found.)

The 100% value being set for air cannot be used for scattering samples, if also in the reference light path a scattering sample is used. It must be set by using identical quantity of sample for every case.

The instrument is suitable for examination of scattering samples on paper basis in the 0.250—2.0 micron wavelength range. Number of layers of the sample measurable in transmission is strongly dependent on the quality of the sample and spectral sensitivity of the instrument.

Dependence on the instrument

Some of the measured optical data depend upon the used instrument. These contain an instrumental constant. According to the notation given in Table III these are:

by measuring remission: R_n; $E_n^{(R)}$

by measuring transmission: T_n; $E_n^{(T)}$

However, using the ratio of intensities (or extinction differences) the instrumental constant is eliminated. Value of these data must be identical when measured by different instruments.

Table II

Effect of instrumental constant on the data of transmission

Sort of filter-paper	SP 700 (625 nm)		SzF-10 M (625 nm) Beckman DK-2		Luxmeter (white light)	
	$E^{(T)}$	$\Delta E^{(T)}$	$E^{(T)}$	$\Delta E^{(T)}$	$E^{(T)}$	$\Delta E^{(T)}$
Whatman No 1 (W1)	2.514	0.268	0.602	0.264	0.626	0.252
Macherey-Nagel 214 (MN 214)	2.782		0.866		0.878	

$E^{(T)}$ — transmission extinction

$\Delta E^{(T)} = E_{(MN214)} - E_{(W1)}$

Table II summarizes data of two filter papers measured by three types of instruments, with strongly different optical arrangements. Values of the corresponding $E^{(T)}$ data are very different, while values of $\Delta E^{(T)}$ are almost identical.

Similar agreement was found in $\Delta_n^{(T)} = E_{n+1}^{(T)} - E_n^{(T)}$ data of the W1 filter paper with increasing number of layers (from 1 to 10), measured by different instruments. Measurements carried out on instruments equipped with Ulbricht sphere (SzF-10 M and Beckman DK-2) are used as references. The spherical angle, from they accommodate photons leaving the sample, corresponds to almost the total half sphere. Agreement in data obtained by the Unicam SP 700 and instruments equipped with U-sphere indicates no effect of layer number of samples on the instrumental constant of Unicam SP 700. Thus this instrument is suitable for examination of samples on paper basis under defined conditions.

The adapter, used for remission measurements is of "mirror" arrangement (Fig. 2). Spectra recorded by use of it show excellent agreement with those obtained by instruments equipped with U-sphere [26]. This "mirror" arrangement excludes the measurement of radiation resulted by regular reflection on the surface of the sample (in this case). Most of these photons comes from the inside of the sample. After multiple direction changes they leave the surface of the sample under the same angle as that of the examining beam, entering into it.

Examined samples

We studied, whether suitable conditions of defined optical measurements can be assured for scattering samples on paper base (filter papers, colored filter papers, post- and printing papers, etc.) or not.

Unevenness in distribution of substances

In the literature "evenness" and "unevenness" of papers are parallel used concepts to characterize the distribution of substance in the sample. Irregular distribution of unevenness statistically results in a certain degree of evenness.

— No macroscopic cavities (holes, bubbles inside the sample, watermark, strong surface structure) may appear. "Cavity effects" mean optically uncontrollable sources of error. In their presence defined spectroscopic measurements cannot be carried out.

— It is impossible to eliminate the "structural" cavities. They are parts of structure of the system (small holes appearing between fibres of the paper). Therefore, also strongly smoothed papers do not provide samples of "even" distribution of substance.

— Unevenness in distribution of substance in the sample influences the reproducibility of measurement; this effect depends on the size of the examining beam. The smaller the cross-section of the light beam, the smaller is the possibility of "equalization" of unevenness (this is one of the important problems of micro-measurements of scattering samples). The greater

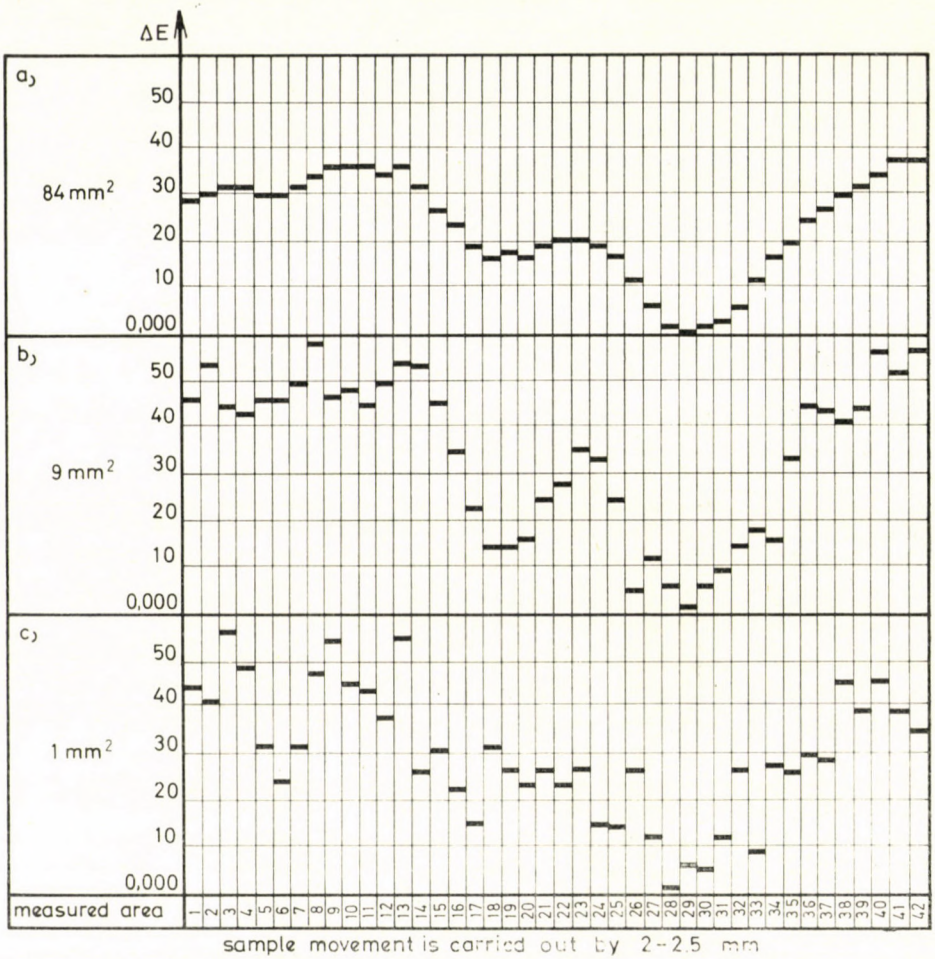

Fig. 4. Optical effect of unevenness of W1 filter paper

the cross-section of the examining light beam, the better is the agreement between optical data and the average value of sample quantity.

Data of Fig. 4 show that in examination of the W1 filter paper, an about 2 mm shift of the sample results in 0.020—0.030 extinction unit difference, if the size of the light spot is 1 mm². In the case of a 84 mm² cross-section similar movement results in such a difference of data (0.005 extinction unit), which is regarded as good reproducibility even in spectroscopy of solutions too.

At examination of filter papers the shape of cross-section (given in mm²) has no importance.

Unevennesses of the scattering sample influence measurement of transmission in greater degree, than that of remission. This is one of the reasons of neglecting measurement of transmission [13].

Optical effect of unevennesses is greatest at measurement of a single layer of the given type of sample, both in remission and transmission. Increase of layer thickness decreases the importance of unevennesses. At transmission measurements unevennesses of the sample are placed on each other, resulting in equalization in the course of increasing number of layers. At remission measurements this is supplemented by the fact, that optical effects of the second, third, etc. layers are considerably smaller, than that of the first.

Defined portioning of substance

Fig. 4 shows that the W1 filter paper (and every other paper) contains also greater zones of unevennesses. Measurements carried out on areas in several cm distances gave significantly different optical data. For our investigation we needed paper layers with identical quantities interacting with a light beam of given cross-section. Mechanical data (thickness or square weight) are not suitable for such selection.

Optical measurements may be used of select layers of identical optical effect. This is carried out by transmission measurement (at wavelength used for examinations later). Requirements:

— identical transmission data, determined as single layer

— identical effect on the transmission value, present in a sample of any number of layers and being anyone of them. These requirements are fulfilled only by identical quantities of identical type of sample.

Samples obtained from one single sheet of W1 filter paper (size of the cross-section of the examining light beam was about 95 mm^2; wavelength: 625 nm) gave ± 0.020 extinction unit deviation from the average. Among 100 samples obtained from such a sheet there are 6—8 pieces fulfilling the above requirements (extreme of differences $\Delta E < 0.005$). The thicker and more even MN214 filter paper shows better ratio.

Portioning of quantity of the sample was accomplished by producing sheet packets. The *sheet packet* is a sample consisting of paper layers being assured, that the selected parts of sample cover each other and are placed so in the light path.

Further on a "single sheet packet" means a sheet packet prepared from layers of identical optical effects and a "combined sheet pocket" is a sample consisting of layers of different quality.

Role of articulation of the sample was investigated by means of hand-made papers (made of bleached sulphite celluloze). Layers of different square weight were used to make sheet packets of 80, 120 and 160 g/m^2. Measured data of sheet packets consisting of 1, 2, 3 layers, with given weight/m^2 were practically identical. Significant difference appeared, when the individual layers were too thin (at 20—30 g/m^2 small holes appear) and above 150 g/m^2 (drying resulted in roughness on one surface).

SCHMIDT [32] — who introduced the name "sheet packet" — gives no requirements for external or internal structure of the examined papers. There are also very transparent, shining, very thin papers among the samples. He did not select the layers for sheet packets.

Colored filter paper samples

Coloration of filter papers was carried out by alcoholic solutions of di- and tri-arylmethane derivatives.* Use of alcohol avoided swelling of celluloze fibres (water results in strong swelling of them; after drying the structure is more loose, than in untreated state. wavyness may occur, etc.). Alcohol is more advantageous in drying too. About 0.5% glacial acetic acid was added to the alcoholic colourant solution to prevent formation of carbinol base from the dyestuff salt. Stability of the samples is good. Proper storage gives unchanged optical behaviour for weeks (sometimes for months).

After coloration of the selected filter paper layers of identical optical characteristics, repeated selection gave identical layers with respect to the carrier and the quantity of dyestuff too.

*M-marked paints were made by Malachite Green ANS; ICI
A-marked paints were made by Auramin O

Notation of measured data

a) Quantitative data of scattering samples on paper base can be given in:

square weight:	$[Q] = g/m^2$
layer thickness:	$[d] = mm$
number of layers:	n

Quantity of material in a scattering sample is most accurately given by Q (as noted by VAN DEN AKKER [1] too). Therefore we present concrete quantitative data in square weight.

Use of d is very extended in the literature. Layer thickness is a geometric datum, proportional to the quantity of material. (Concrete thickness data are usually given only for liquids.) We will use it for the sake of comparison to literature. It has special importance in characterizing processes taking place in different depths of scattering samples.

Layer number is suitable to describe a combined sample prepared from identical units. It can be used to give the concrete quantity of material only, if Q_1 is known. However, for investigation of dependence on substance quantity, layer number is the most simple way to describe changes of quantities.

b) Optical data of a sample are noted as follows:
transmission of a not-scattering sample (*e.g.* a solution):

$$\tau = \frac{I_\tau}{I_0}$$

transmission of a scattering sample:

$$T = \frac{I_T}{I_0}$$

remission of a scattering sample:

$$R = \frac{I_R}{I_0}$$

where I_0 is the intensity of light falling on the sample (directed beam)
I_τ is the intensity of light passed through a non-scattering sample
I_R and I_T are the intensity of light reflected or transmitted by a scattering sample, resp. τ gives the ratio of intensities of the incident and the total transmitted light, with respect to the incident one. Measured T and R contain instrumental constant too.

In every absorption spectrum wavelength-dependent radiation losses, due to interaction of electromagnetic radiation and the substance are shown. It is advantageous to apply the concept of extinction to characterize these radiation losses:

$$E^{(\tau)} = -\lg \tau$$

$$E^{(T)} = -\lg T$$

$$E^{(R)} = -\lg R$$

(τ, T and R are used as upper indexes to allow layer numbers to be the lower ones. Layer number as the upper index would suggest an exponent.)

The only loss-component of τ and $E^{(\tau)}$ derived from it is light absorption. However, for scattering samples in both optical data several reasons of radiation losses must be considered. Expressing every loss component as extinction, those of the measured data symbolically are the following:

$$E^{(T)} = f(E_{(R)};\ E_{(A)};\ E_{(0)};\ E_{(MT)})$$

$$E^{(R)} = f(E_{(T)};\ E_{(A)};\ E_{(0)};\ E_{(MR)})$$

where $E_{(T)}$ Lofs component of remission measurement originated from transmission
$E_{(R)}$ Lofs component of transmission measurement originated from remission
$E_{(A)}$ rays absorbed by the layer
$E_{(0)}$ lateral losses (in a sample of "infinite" in lateral extension)
$E_{(MT)}$ instrumental constant of transmission measurement
$E_{(MR)}$ instrumental constant of remission measurement.

Table III

Applied notation

Data of a sheet packet								
Substance quantity			Remission data			Transmission data		
weight of m^2	thickness	layer number	$\Delta_n^{(R)} = E_{n+1}^{(R)} - E_n^{(R)}$	$E_n^{(R)} = -\lg R_n$	R_n	T_n	$E_n^{(T)} = -\lg T_n$	$\Delta_n^{(T)} = E_{n+1}^{(T)} - E_n^{(T)}$
Q_1	d_1	n_1	$\Delta_1^{(R)}$	$E_1^{(R)}$	R_1	T_1	$E_1^{(T)}$	$\Delta_1^{(T)}$
Q_2	d_2	n_2	$\Delta_2^{(R)}$	$E_2^{(R)}$	R_2	T_2	$E_2^{(T)}$	$\Delta_2^{(T)}$
Q_3	d_3	n_3	$\Delta_3^{(R)}$	$E_3^{(R)}$	R_3	T_3	$E_3^{(T)}$	$\Delta_3^{(T)}$
Q_4	d_4	n_4		$E_4^{(R)}$	R_4	T_4	$E_4^{(T)}$	
.	.	.	.	.	.	.	.	.
.	.	.	.	.	.	.	.	.
.	.	.	.	.	.	.	.	.
Q_n	d_n	n_n	$\Delta_n^{(R)}$	$E_n^{(R)}$	R_n	T_n	$E_n^{(T)}$	$\Delta_n^{(T)}$
Q_{n+1}	d_{n+1}	n_{n+1}		$E_{n+1}^{(R)}$	R_{n+1}	T_{n+1}	$E_{n+1}^{(T)}$	

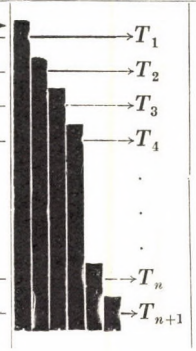

Extinction of the complete sheet packet: negative logarithm of measured optical data of a sheet packet containing n layers:

$$E_n^{(T)} = -\lg T_n$$

and

$$E_n^{(R)} = -\lg R_n$$

$E_n^{(T;R)}$ is resulted by total losses of radiation present in the measured value; every further calculations are based on it.

$\Delta_n^{(T;R)}$ *series* is obtained from differences between two neighbouring $E_n^{(T;R)}$ values:

$$\Delta_n^{(T)} = E_{n+1}^{(T)} - E_n^{(T)} \quad \text{thus} \quad \Delta_1^{(T)} = E_2^{(T)} - E_1^{(T)}$$

$$\Delta_2^{(T)} = E_3^{(T)} - E_2^{(T)}; \text{ etc.}$$

$$\Delta_n^{(R)} = E_{n+1}^{(R)} - E_n^{(R)}$$

Remission of a sheet packet increases with increasing layer number ($E_n^{(R)}$ value decreases) and radiation losses due to transmission are smaller. Thus actual $\Delta_n^{(R)}$ values are **negative.**

The $\Delta_n^{(T;R)}$ data represent not the extinction of the n^{th} layer, but a change of the extinction value of the complete sheet packet, due to a quantity increase corresponding to one layer. Notation applied for measured data of scattering samples are given in Table III.

According to IVANOV [14] between plots of remission data it is not the $-\lg R = f(\lambda)$, which gives optimal following of $-\lg \tau = f(\lambda)$ curve of the same absorbing substance. In our case the only requirement was to use equal units for the parallel measured data of the two types of measurement. (Later on will only be investigated the reason of not perfect following of $-\lg \tau = f(\lambda)$ curve of the solution by the $-\lg R = f(\lambda)$ curve.)

Model measurements

Data of tables and graphs were obtained from sheet packets of optically equivalent layers.

a) Table IV and Fig. 5 illustrate changes in extinction values of remissional and transmissional origin, due to changes of layer number. Designation of the measured samples:

WA — Whatman No. 1. filter paper (in alcohol, soaked under the same conditions as colored paints M_I and M_{II}).

M_I — colored sample made by a solution of Malachite Green ANS; ICI. (conc. of solution: $9 \cdot 10^{-6}$ mole/l)

M_{II} — paint made by a solution of Malachite Green ANS; ICI. (conc. of solution: $4 \cdot 10^{-5}$ mole/l).

Table IV

Change of $E_n^{(R;T)}$ values according to the number of layers

Sample	$E_1^{(R)}$	$E_2^{(R)}$	$E_3^{(R)}$	$E_4^{(R)}$	$E_5^{(R)}$	$E_6^{(R)}$	$E_7^{(R)}$	$E_8^{(R)}$
WA	2.815	2.750	2.728	2.718	2.713	2.708	2.705	2.702
M_I	2.827	2.777	2.764	2.761	2.758	2.760	2.760	2.757
M_{II}	2.857	2.839	2.832	2.835	2.832	2.835	2.832	2.830

Sample	$E_1^{(T)}$	$E_2^{(T)}$	$E_3^{(T)}$	$E_4^{(T)}$	$E_5^{(T)}$	$E_6^{(T)}$	$E_7^{(T)}$	$E_8^{(T)}$
WA	2.436	2.697	2.866	2.995	3.107	3.215	3.310	3.394
M_I	2.458	2.776	3.032	3.275	3.506	3.740	3.974	4.204
M_{II}	2.493	2.906	3.310	3.690	4.070	—	—	—

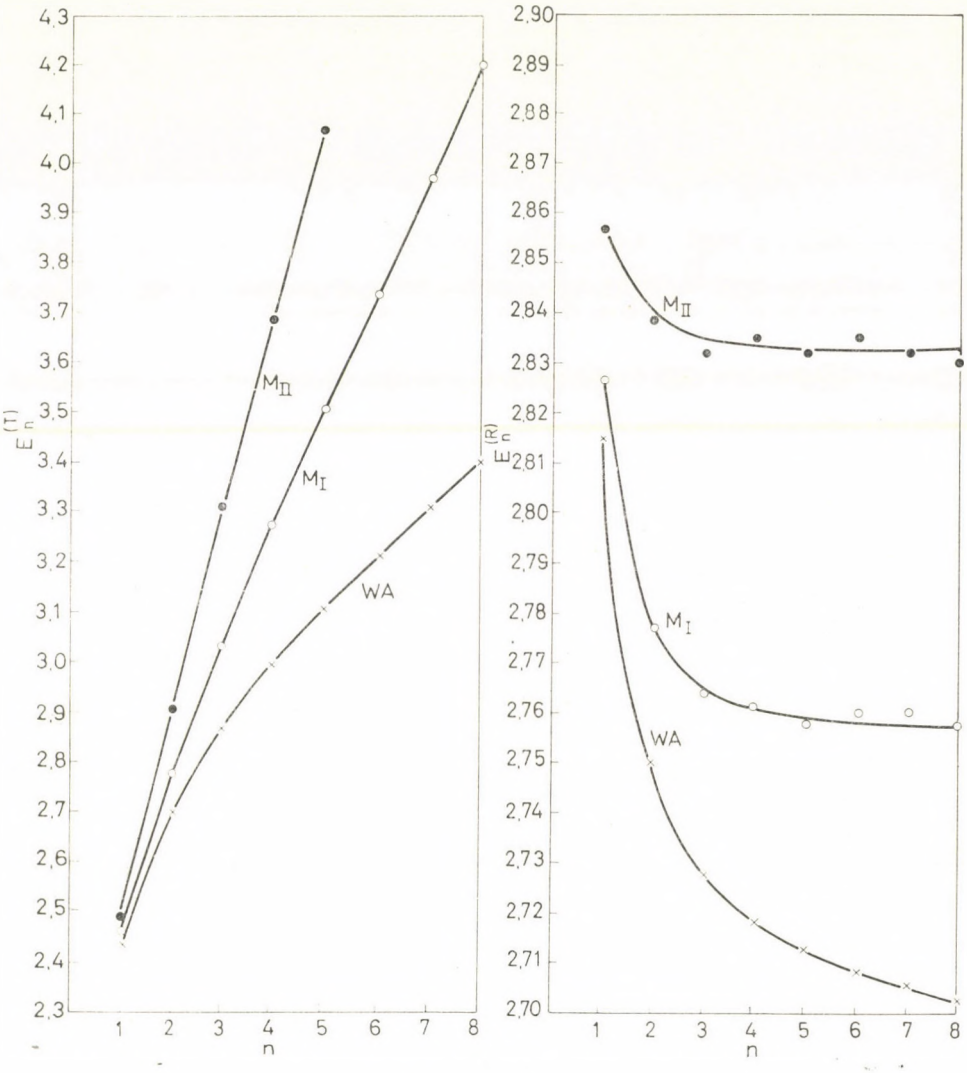

Fig. 5. Alteration of $E_n^{(R;T)}$ values in function of layer number

b) Curves of both types of measurement showed linear character with increasing layer number. More accurate studies were based on $\Delta_n^{(R;T)}$ values.

c) Effects of changes of layer number on the remission data ($R_1 \rightarrow R_\infty$) were investigated previously, also its character was determined with regard to papers [9], [32]. Thus a detailed investigation of the relation between transmission and quantity of material — which field is still less studied though showing far more distinct changes — was carried out by us.

On increasing layer number of a sheet packet, transmissional radiation losses alter at first in non-linear manner; however, above a certain substance quantity this relation becomes linear. At 625 nm, under defined conditions of measurement, transmissional density change of a W1 sheet packet was followed up to 20 layers ($E_{20}^{(T)} = 4.330$). No measured data indicated change of the linear character.

Table V

$E_1^{(T)}$ and $\Delta_n^{(T)}$ values of Whatman No. 1 filter paper in function of wavelength

λ (nm)	$E_1^{(T)}$	$\Delta_1^{(T)}$	$\Delta_2^{(T)}$	$\Delta_3^{(T)}$	$\Delta_4^{(T)}$	$\Delta_5^{(T)}$	$\Delta_6^{(T)}$	$\Delta_7^{(T)}$	$\Delta_8^{(T)}$	$\Delta_9^{(T)}$	$\Delta_{10}^{(T)}$
400	2.516	0.345	0.285	0.257	0.251	0.247	0.244	0.249	0.246	0.247	0.251
417	2.500	0.327	0.264	0.233	0.226	0.220	0.224	0.218	0.225	0.225	0.226
435	2.495	0.313	0.245	0.215	0.197	0.195	0.199	0.195	0.195	0.195	0.197
455	2.477	0.301	0.232	0.201	0.187	0.184	0.180	0.178	0.185	0.179	0.186
476	2.470	0.292	0.217	0.186	0.169	0.160	0.162	0.159	0.167	0.162	0.164
500	2.462	0.283	0.207	0.169	0.155	0.147	0.146	0.148	0.152	0.145	0.146
526	2.448	0.277	0.203	0.162	0.143	0.132	0.135	0.132	0.135	0.138	0.135
556	2.435	0.275	0.192	0.156	0.134	0.121	0.123	0.118	0.124	0.119	0.117
588	2.417	0.271	0.188	0.150	0.127	0.111	0.115	0.108	0.104	0.102	0.107
625	2.416	0.266	0.184	0.142	0.126	0.108	0.108	0.097	0.099	0.102	0.100
667	2.413	0.266	0.184	0.145	0.123	0.109	0.109	0.103	0.098	0.093	0.097
715	2.413	0.266	0.182	0.146	0.121	0.110	0.109	0.102	0.097	0.095	0.096
770	2.404	0.263	0.182	0.143	0.122	0.107	0.109	0.097	0.092	0.096	0.092
833	2.391	0.264	0.184	0.144	0.122	0.107	0.104	0.101	0.094	0.093	0.094
910	2.376	0.263	0.183	0.141	0.122	0.110	0.104	0.104	0.096	0.097	0.099
1000	2.369	0.268	0.186	0.150	0.132	0.121	0.121	0.114	0.118	0.114	0.115
1111	2.344	0.262	0.182	0.147	0.123	0.115	0.109	0.111	0.100	0.101	0.101
1250	2.327	0.286	0.219	0.192	0.176	0.170	0.165	0.163	0.166	0.161	0.166
1326	2.306	0.276	0.204	0.171	0.155	0.147	0.146	0.143	0.143	0.147	0.145

Table V shows dependence of transmissional radiation losses on the layer number at different wavelengths.

Note: $\Delta_n^{(T)}$ values are very sensitive to the substance quantity and contaminations of the individual layers, to aging processes during storage (especially in chemical laboratories), etc. In the course of examination of several sheets of W1 filter paper, for example, the series of highest transmittance gave $\Delta_1^{(T)} = 0.260$ at 625 nm; the sheet packet reached Δ_r after 9 layers, with measured values fluctuating between 0.074 and 0.078. (Similarly lower $\Delta_n^{(T)}$ values were obtained at the other wavelengths too, as compared to those of Table V.)

This relation was studied on other types of filter paper (samples No. 1—7); on post- and printing papers containing solid components other than celluloze too (samples 8—10); and on colored filter papers (designation M means paint by Malachite Green, A means paint by Auramin O); and on colored commercial papers (samples 14—18).

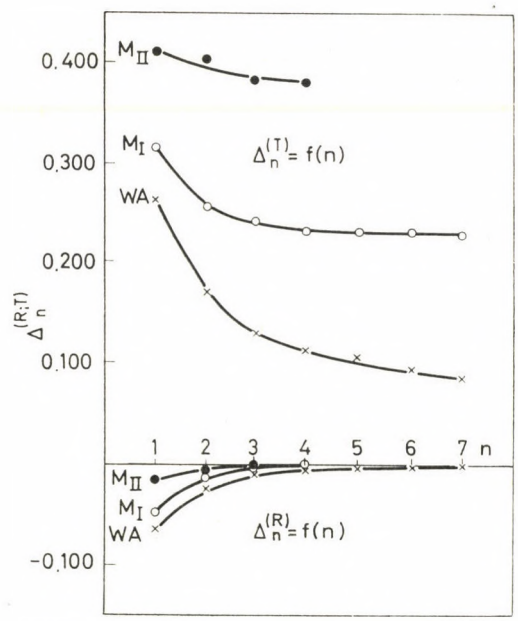

Fig. 6. Alteration of $\Delta_n^{(R;T)}$ values in function of layer number

Discussion

The "quasi-homogeneous" sample

Scattering samples are heterogeneous systems. Thus it is theoretically impossible to consider them "homogeneous" in the same sense as the solutions.

The ideal-hypothetic type of sample (homogeneous and isotropic) introduced by the GKM theory, does not exist. Best approximation of that are the powder samples prepared by KORTÜM; these were ground and sieved with great care before measurement [18]. However, perfectly uniform particle size could not be obtained even with grinding for 48 hours. Accurate portion-

ing of thickness of the powder layer is extraordinarily difficult, especially for transmission measurements.

A real type of sample was required for experimental investigation of optical properties of scattering samples. Requirements:

— in the sample optical inhomogeneities should statistically result in a distribution, which can be handled similarly to "homogeneity";

— defined portioning of substance quantity of the sample is required (free of macro hole effects; the disperging medium should be the same as that the light is coming from; etc.)

The above requirements are well fulfilled by paper sheet packets. The optically equivalent layers may be considered as defined building units. From the point of optical interactions, the sample constructed from them shows a "continuous" internal structure, changes of layer number have no effects on it. Addition of a further layer alter only the substance quantity of the sample of given structure, optically the individual layer surfaces are ineffective. In this sense the system may be regarded as "quasi-homogeneous". Also alteration of quantity of a "quasi-homogeneous" sample is considered to be defined, similarly to change of layer thickness of solutions.

A "quasi-homogeneous" sample can also be optically anisotropic. It is well known that filaments of paper are made of celluloze, and it is birefringent, further on, that these celluloze fibres are in a certain degree directed in the paper layers.

By preparing sheet packets, special conditions of measurements can be provided, which can be applied for systematic investigation of dependence of optical data on substance quantity; of results of scattering and absorption relationships; of effect of inhomogeneities, etc.

Dependence of remission and transmission on substance quantity of the sampl

Layers used for sheet packets are "optically equivalent", *i.e.* represent equal substance quantities. However, extinction of a sheet packet can never be expressed as sum of extinctions of the individual layers (no extinction of remissional or transmissional origin). This dependence on layer number results in characteristic curve shape.

The value of *remission** increases with increasing substance quantity, and at a certain layer thickness characteristic to the sample (denoted as d_∞ in the literature) a limit value is reached. Afterwards the remission datum remains unchanged with increasing layer number; it is denoted as R_∞. Extinction of remissional origin ($E_n^{(K)}$) decreases to a limit value (Fig. 5).

*Remission refers to "remission with black background". (Presence of reflecting background should be specially noted.)

Transmission decreases with increasing substance quantity. Extinction of a sheet packet has no limiting value. However, magnitude of changes due to addition of one more layer tends to a limiting value. Extinctions ($E_n^{(T)}$) obtained by transmission measurement increase non-linearly under a certain quantity of material, above that linear change of extinction is observed with change of substance quantity (Fig. 5).

Relation "A"

Tendency of change of remission data as a function of layer number has been investigated for a long time. However, dependence of transmissional radiation losses on substance quantity requires more detailed studies. Further on the above described empirical relation will shortly be called as relation "A"

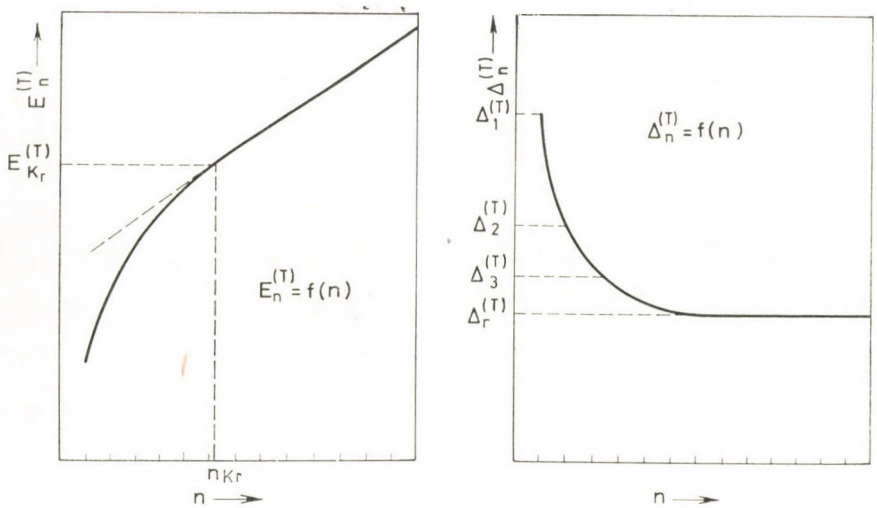

Fig. 7. Relation "A"

Relation "A" can be illustrated as follows (Fig. 7):

a) one method is to show the relation between transmissional radiation loss of the total sheet packet and the layer number (or substance quantity expressed in any other form); this is a plot of $E_n^{(T)} = f(n)$ function

b) the other method represents the extinction changes due to addition of one more layer to the sheet packet, as a function of layer number: $\Delta_n^{(T)} = f(n)$.

The two representations show different sides of the same relation, in generalized form.

Details of relation "A" will be examined on the basis of function $\Delta_n^{(T)} = f(n)$.

The $\Delta_n^{(T)}$ series describes optical consequences of changes in substance quantity after the first layer. To show characteristics of location on curve "A", two group designations were introduced.

Δ_i — $\Delta_n^{(T)}$ value, belonging to the non linear section; Δ_i values of a sheet packet are not equal to each other; $\Delta_1^{(T)} \neq \Delta_2^{(T)} \neq \ldots \neq \Delta_i$ (the last one)

Δ_r — $\Delta_n^{(T)}$ value, belonging to the linear section; Δ_r values of a sheet packet are practically equal. $\Delta_{r_1} = \Delta_{r_2} = \ldots = \Delta_r$

In every case the $\Delta_n^{(T)}$ series — with increasing substance quantity — tends to Δ_r.

In the tables wide variation of Δ_r values is shown between 0.070 and 1.300. The smaller Δ_r value is approximated by the $\Delta_n^{(T)}$ series, the more detailed and minute appearance of the non-linear section is observed. The higher is the value of Δ_r, the shorter will the non-linear section be. There are layers of so small transmittance, when fraction of layer thickness represents the critical substance quantity. Non-linear section of such samples cannot be studied on the given layers.

(Note: Points corresponding to $\Delta_n^{(T)}$ data are connected with a continuous line only for the sake of descriptiveness, as the high number of measured points would not give a clear picture.)

We point to the importance of defined conditions of measurements. In addition to those factors, which also in spectroscopy of solutions deform the spectra *(e.g.* luminescence, non-adequately monochromatic light, poor sensitivity of the instrument, etc.), several characteristics of the system itself can put out of shape the above relations (*e.g.* hole effects, strongly shining surface, uneven substance distribution of the carrier or the dye, etc.)

"Pausz" and "pvc" curves in Fig. 8 were obtained from such not "quasi-homogeneous" samples.

In the case of scattering samples on paper basis the empirical relation "A" consists of two sections. Characteristics of the curve:

— beginning value of relation "A" ($E_1^{(T)}$) (as well seen in Tables V and VI) is not in unambiguous relation with the $\Delta_n^{(T)}$ series (compare data of W1 filter paper at 435 nm and those of W3 filter paper at 625 nm);

— non-linear section of curve "A" is of hyperbolic character. It is indicated by data of Table VII. As a model, $\Delta_n^{(T)}$ series of W1 filter paper (measured at 590 nm) was evaluated according to the following equation:

$$\Delta_n^{(T)} = (\Delta_1^{(T)} - \Delta_r) \cdot \frac{1}{2^{n-1}} + \Delta_r$$

— linear section of curve "A" shows exponential dependence of transmission data on substance quantity.

Table VI

$E_1^{(T)}$ and $\Delta_n^{(T)}$ values of different paper samples

No	Sample	g/m²	λ (nm)	$E_1^{(T)}$	$\Delta_1^{(T)}$	$\Delta_2^{(T)}$	$\Delta_3^{(T)}$	$\Delta_4^{(T)}$	$\Delta_5^{(T)}$	$\Delta_6^{(T)}$	$\Delta_7^{(T)}$	$\Delta_8^{(T)}$	$\Delta_9^{(T)}$	$\Delta_{10}^{(T)}$
1	MN 214	140	625	2.698	0.314	0.226	0.202	0.189	0.182	0.177	0.177	0.175	0.174	0.178
2	937	85	625	2.343	0.261	0.166	0.136	0.116	0.105	0.103	0.098	0.093	0.091	0.093
3	W 3	176	625	2.768	0.312	0.233	0.208	0.193	0.191	0.194	0.200	0.194	0.197	0.202
4	Sch-Sch 2040/A	88	625	2.406	0.268	0.184	0.147	0.125	0.123	0.120	0.114	0.114	0.113	0.115
5	Sch-Sch 2043/B	125	625	2.515	0.295	0.211	0.178	0.169	0.166	0.158	0.158	0.153	0.156	0.156
6	Filtrec	78	625	2.442	0.281	0.196	0.157	0.147	0.141	0.139	0.133	0.131	0.132	0.132
7	MN 619	93	625	2.507	0.269	0.177	0.137	0.115	0.101	0.094	0.090	0.088	0.092	0.088
8	"Bank-post"	70	625	2.512	0.394	0.362	0.338	0.339	0.334	0.341	0.340	—	—	—
9	Semi wood-free book paper	100	625	2.845	0.682	0.676	0.652	0.665	0.663	0.660	—	—	—	—
10	"India-paper"	44	625	2.586	0.273	0.184	0.148	0.130	0.122	0.115	0.116	0.105	0.103	0.105
11	M_I	88	632	2.440	0.425	0.387	0.382	0.396	0.398	0.390	0.395	—	—	—
12	M_I	88	513	2.450	0.284	0.210	0.183	0.159	0.149	0.146	0.145	0.146	0.148	0.143
13	M_{II}	88	632	2.500	0.893	0.848	0.850	0.880	—	—	—	—	—	—
14	A_I	88	435	2.480	0.440	0.403	0.394	0.392	0.415	0.402	0.399	—	—	—
15	A_I	88	625	2.410	0.274	0.182	0.146	0.120	0.115	0.112	0.101	0.096	0.101	0.095
16	F_p	40	632	—	0.699	0.296	0.248	0.232	0.240	0.247	0.260	0.247	0.254	0.260
17	F_p	40	535	—	0.544	0.231	0.187	0.182	0.172	0.189	0.181	0.171	0.180	0.169
18	R	100	500	—	1.287	1.252	1.263	—	—	—	—	—	—	—

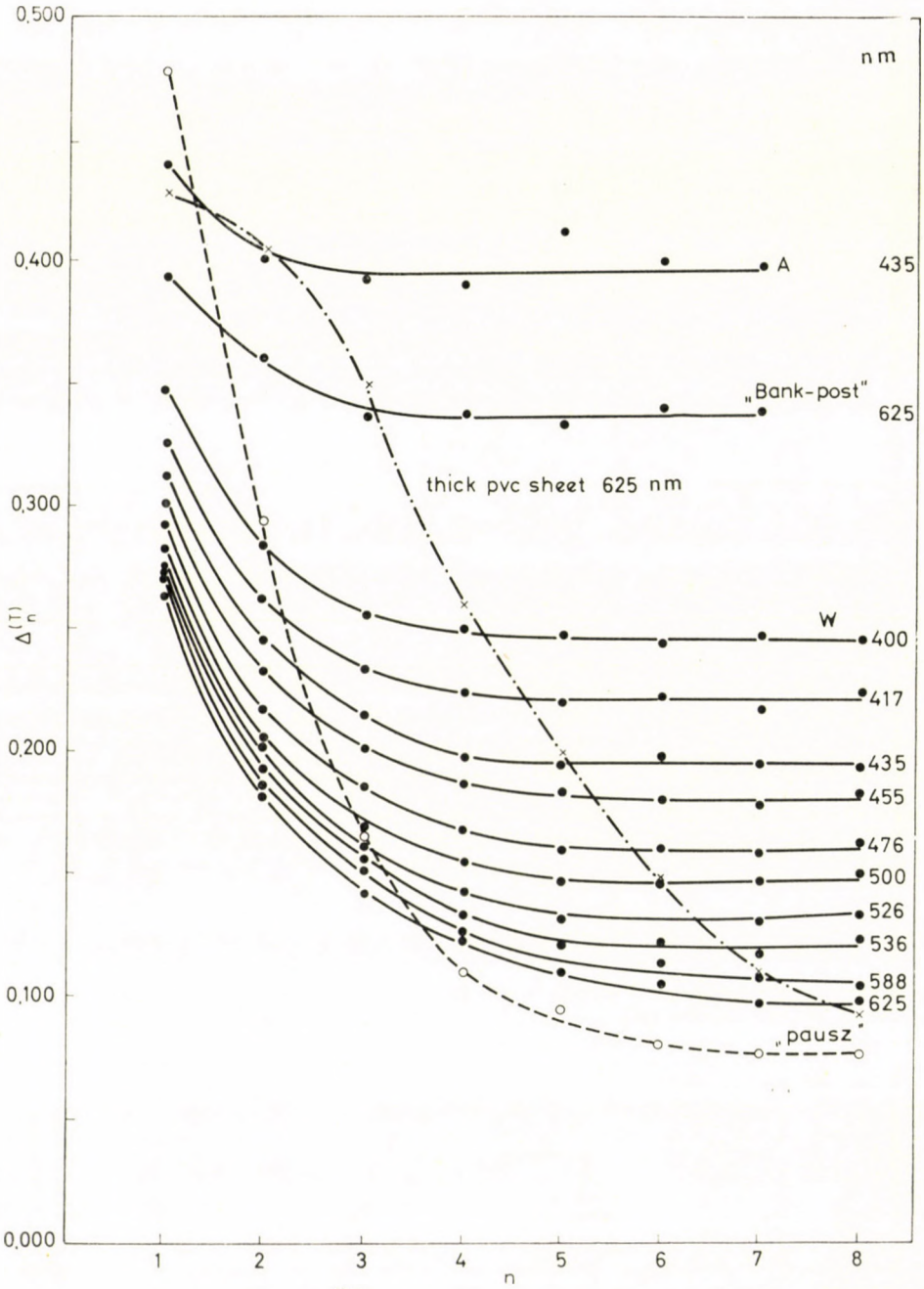

Fig. 8. Empiric 1 $\Delta_n^{(T)} = f(n)$ curves

Table VII

Measured and calculated $\Delta_n^{(T)}$ series. (W1 filter paper: at 590 nm)

$\Delta_n^{(T)}$	$\Delta_1^{(T)}$	$\Delta_2^{(T)}$	$\Delta_3^{(T)}$	$\Delta_4^{(T)}$	$\Delta_5^{(T)}$	$\Delta_6^{(T)}$	$\Delta_7^{(T)}$	$\Delta_8^{(T)}$	$\Delta_9^{(T)}$
measured	0.271	0.188	0.150	0.127	0.111	0.115	0.108	0.104	0.105
calcd.	0.271	0.188	0.147	0.126	0.116	0.110	0.107	0.106	0.105

The first exponential section — noticed by the theory of "depth" regime [39] — was not observed in scattering systems on paper basis. This section was determined with so small substance quantities that radiation transmitted by them contains significant quantity of non-scattered radiation too. Paper samples of such layer thickness cannot be measured definitely because of macro hole-effects.

According to PRICE, HUDSON and ASHMAN [28], the relation expresses one single linear section only. Graphs published by them indicated that their paper layers had Δ_r values 10—21 times greater than ours. (One layer of Whatman No. 11 filter paper alters the extinction of the sample with about 1 extinction unit, and one containing also adenilic acid has an effect of about 2.1 extinction units.) It is interesting to note that in their graphs all measured data belonging to one layer fall under the line. (Appearance of the non-linear interval).

Parallelism of changes

Tendencies of changes of remission and transmission (due to changes of layer number) are emphasized in Table VIII. These parallel changes are:

— in remission: $E_{Kr}^{(R)} - E_n^{(R)}$

in series of $E_n^{(R)}$ data it characterizes formation of remission corresponding to $E_{Kr}^{(R)}$; (as R_∞ is the highest remission value of the series, it represents the smallest extinction value; differences describing the changes are negative.)

— in transmission: $\Delta_n^{(T)} - \Delta_r$

in series of $\Delta_n^{(T)}$ data it characterizes formation of $\Delta_n^{(T)}$ value, Δ_r in the linear section.

As seen from Table VIII, configuration of these differences in the two types of measurement point to the following parallelism:

— ends at the same layer number;

— at both types of measurement that series, which starts with higher value, will have longer course, while that starting with lower value, will have shorter one;

— numerical values of the parallel differences are of corresponding magnitude. Data of remissional origin, starting with higher value correspond to higher values of data of transmissional origin.

Table VIII

Optical changes due to changes of layer number

λ (nm)	835		625		1000		525		475		417		400	
n	rem.	trans	rem.	trans.	rem.	trans.	rem.	trans.	rem.	trans.	rem.	trans.	rem.	trans.
1.	0.107	0.186	0.106	0.176	0.103	0.164	0.094	0.148	0.080	0.135	0.067	0.094	0.059	0.085
2.	0.043	0.095	0.046	0.086	0.039	0.076	0.036	0.069	0.026	0 054	0.020	0.027	0.017	0.020
3.	0.019	0.062	0.020	0.061	0.017	0.051	0.017	0.041	0.012	0.032	0.007	0.008	0.005	0.006
4.	0.010	0.034	0.013	0.029	0.008	0.020	0.009	0.018	0.004	0.014	0.002	0.002	0.002	0.006
5.	0.006	0.016	0.008	0.018	0.003	0.013	0.005	0.009	0.001	0.009	—	—	—	—
6.	0.004	0.008	0.005	0.007	—	0.004	0.004	0.003	—	0.002	—	—	—	—
7.	0.002	0.004	0.003	0.003	—	—	0.002	—	—	—	—	—	—	—

Data of this Table refer to Whatman No. 1 filter paper, and in remission $E_{Kr}^{(R)} - E_n^{(R)}$ so all remission data are negative in transmission $\Delta_n^{(T)} - \Delta_r$

"Critical" quantities

Parallel measurements on a given sheet packet showed that *at producing sheet packets the d_∞ substance quantity of remission measurement is the same value, as at which in transmission the change of radiation losses — due to change of substance quantity — will become linear.*

Thus critical substance quantities of the two types of measurement are equal; more accurately, they are identical. It is reasonable to use uniform designation: *Kr* may refer to the optically critical substance quantity. For characteristics of substance quantity:

n_{Kr} — critical layer number
Q_{Kr} — critical square weight
d_{Kr} — critical layer thickness.

For optical characteristics:

$E_{Kr}^{(T)}$ — extinction value calculated from transmission datum of critical substance quantity
$E_{Kr}^{(\kappa)}$ — extinction value calculated from remission value of critical substance quantity.

The (optically) critical substance quantity is a parameter indicating a limit in dependenc of optical data on substance quantity; above and under it alteration of the optical data — due to changes of substance quantity — take place according to different functions.

In the literature the "critical substance quantity" of remission measurement and all quantities of the sample higher than that are denoted by d_∞. This is disturbing in parallel evaluation and interpretation of the measured remission and transmission data.

In transmission measurements — for practical purposes — that quantity is considered to be critical substance quantity, for which the value of $\Delta_n^{(T)}$ will be smaller than 1.1 times the value of $\Delta_n^{(T)}$ value of the linear section. In most cases n_{Kr} appears at fraction of layer number.

Actual value of critical substance quantity may strongly differ by samples and wavelengths. In the case of W1 filter papers value of Q_{Kr}, expressed in square weight is about 350 g/m^2 at 435 nm, while 550 g/m^2 at 625 nm.

It is interesting that in transmission measurement of filter papers, very different $E_1^{(T)}$ and $\Delta_n^{(T)}$ series gave $E_{Kr}^{(T)}$ values between 3.2 and 3.4 ($E_{Kr}^{(\cdot)}$ being determined according to the mentioned conventional definition; it contains instrumental constant too). Taking into consideration the inaccuracy of measurement and estimation, *value of $E_{Kr}^{(T)}$ can be regarded approximately constant.*

Appearance of parameters of the critical substance quantity results in isolation of further formation of quantities of photons coming out on

the two surfaces, by the substance quantity of "quasi-homogeneous" scattering system between the two surfaces of the sample. Decrease of quantity of transmitted photons due to further increase of layer thickness has no significant effect on the quantity of remitted photons. The remission becomes constant, so — as a loss component — does not cause changes in the transmission value.

Actual value of the critical substance quantity expresses the required quantity of a sample of given optical properties to assure by interactions the critical extinction level of optical data of diffuse scattering systems.

Optical data of samples with quantities greater than the critical

a) One important consequence of existence of optically critical substance quantity is to make available such a range of optical properties of diffuse scattering systems, which is inaccessible for remission measurement.

$$\lim_{n \to n_{Kr}} \Delta_n^{(R)} \to 0$$

$$\lim_{n \to n_{Kr}} \Delta_n^{(T)} \to \Delta_r$$

Δ_r is the smallest $\Delta_n^{(T)}$ value, but always higher than any of $\Delta_n^{(R)}$ values.

$$\Delta_r = \Delta_{n,\min.}^{(T)} > \Delta_n^{(R)}$$

Δ_r is linearly proportional to the corresponding $(d_{n+1} - d_n)$ sample quantity, and can linearly be interpolated and extrapolated.

b) Linear section of relation "A" shows formal similarity to the Bouguer—Lambert—Beer law. (When the BLB law is valid, a change of quantity of the examined absorbing substance will be followed by linearly proportional change of extinction of the sample.) However, for scattering samples:

— quantitative changes will only be followed by a linear extinction change above a definite and "critical" substance quantity, characteristic for the actual type of sample

— it is valid only for quantity changes by means of change of layer thickness (if "concentration" of the absorbing substance is altered, the whole scattering system itself is altered). So analogy is present only to the Bouguer—Lambert law.

No analogies to BLB law were found in data of remissional origin.

c) Linear section of relation "A" indicated essential analogy to BL law too.

Magnitude of radiation losses involved in the optical data, and their ratio in proportion to each other is in close relationship with the quantity of scattering sample. It shows characteristic changes with change of substance quantity of the sample. It is supposed, that increasing quantity of substance

— gives maximal value of loss component ($E_{(R)}$) of remission at the critical substance quantity; there are no changes further on (this is experimental fact)

— lateral loss component ($E_{(0)}$) with respect to layer number is unchanged

— identical instrumental constants ($E_{(MT)}$) exist for every layer number.

For quantities greater than the critical, dominating and determining component of transmissional radiation losses is $E_{(A)}$, the loss component due to absorption.

In scattering systems the BL law exists under special conditions. Here effects of absorption are involved in an other phenomenon, scattering. Diffuse scattering increases the optical path length, thus increasing the probability of absorption interactions too.

d) The Δ_r value is a measure of optical properties determined by internal parameters of the sample, expressed by the substance quantity of one layer. When it is converted to any unit quantity — *e.g.* 100 g/m^2 — a specific optical datum is obtained, suitable to characterize optical behaviour of the given type of sample.

Special possibilities of employment of Δ_r^{100} value are the following:

— it is suitable to compare different types of samples (or data obtained at different wavelengths)

Table IX

Specific Δ_r values

λ (nm)	400	417	435	455	476	500	526	556	588	625
W 1	0.259	0.235	0.209	0.187	0.160	0.152	0.132	0.117	0.106	0.098
MN 214	0.308	0.273	0.240	0.213	0.192	0.170	0.153	0.139	0.128	0.118
2043/B	0.395	0.355	0.323	0.290	0.260	0.238	0.198	0.177	0.151	0.143
"India paper"	1.100	0.965	0.750	0.650	0.565	0.500	0.447	0.380	0.333	0.297

— W1 and MN 214 in Table IX have very similar optical properties, but differences of their Δ_r^{100} values are greater than the experimental error. 2043/B is a filter paper being more compact than the two previous ones. "india paper" is printing paper containing fillers. (At 625 nm its $\Delta_n^{(T)}$ series is almost identical with that of W1; see Tables V and VI.)

— "Spectrum Δ_r^{100}" provides the most defined possibility of characterization of absorption properties of a paper layer. The only optical datum of a scattering sample is Δ_r, which can be linearly extrapolated or interpolated with respect to substance quantity. The $E_1^{(R;T)}$, Δ_i and $\Delta_n^{(R)}$ values cannot be specificated in the above manner. "Δ_r^{100} spectrum" of W1 filter paper is shown in Fig. 9.

— The Δ_r^{100} value expresses light absorption properties of a paper layer in a simple sheet packet in the possibly most differentiated way. True enough, the $\Delta_n^{(R;T)}$ values decrease until the critical substance quantity is reached. However, with increase of d the absorption loss component ($E_{(A)}$) shows continuous increase up to $d_{\infty r}$ in the $\Delta_n^{(R;T)}$ values.

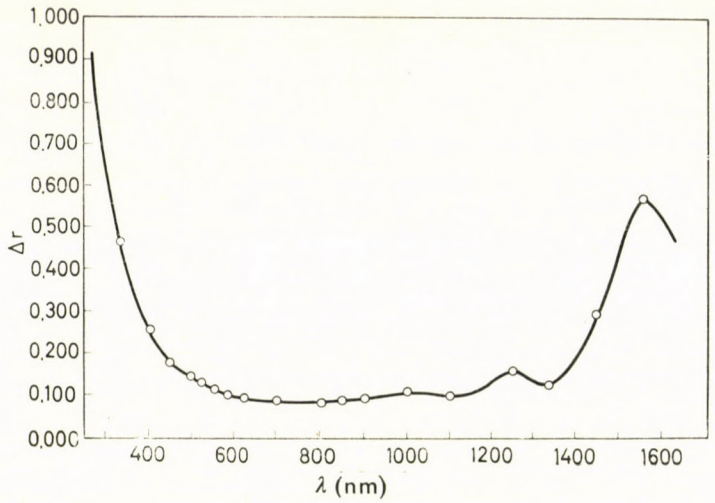

Fig. 9. "Δ_r^{100} spectrum" of W1 filter paper

Optical effect of one layer in a sheet packet

Internal parameters of an actual scattering system determine the optical properties of a sample prepared from it. However, their appearance is not unilateral (as in the case of non-scattering samples — solutions — studied under defined conditions). Optical properties of scattering samples become available through dependence of optical data on substance quantity.

In an inarticulated "quasi-homogeneous" sample participation of a layer in the series of optical interactions depends on its location and thickness of sample. Optical role of the surface layers is obviously different from that of the internal layers (though having identical optical properties).

Concept of "quasi-homogeneity" combines two sides of optical role of the individual layers:

— in one respect: the layer increases substance quantity of the sheet packet; position of the layer resulting the increase is ineffective to the extinction value of the whole sheet packet

— in the other respect: magnitude of participation of a layer in development of extinction value of the sheet packet depends on its location.

This fact has special importance at the formation and evaluation of absorption spectrum of a scattering sample.

Limits of range of the examined phenomena

Internal parameters of scattering samples and external parameters of measurements can be extraordinarily various and diverse. Thus measured data regarding empirically stated relations are conclusive for the actual type of investigation only.

Scattering samples on paper basis show relatively small absorption and high scattering. Value of regular reflection is about 4% [36]. Quantity of rays transmitted in unaltered direction is negligible (lower limit of layer thickness was selected so). Measurements were carried out under conditions provided by the optical arrangement of Unicam SP 700 spectrophotometer. Directed, non-polarized and monochromatic light was used for illumination.

It is supposed that the obtained relations are valid for other — similar — scattering sample too; yet, verification needs actual measured data. "Quasi-homogeneous" samples on paper basis were found to be the most suitable for investigation of the discussed phenomena.

*

The author's thanks are due to Dr. L. LÁNG and G. MAJOR for their many valuable advices and help in design of optimal instrumental conditions.

REFERENCES

1. VAN DEN AKKER, J. A.: TAPPI. **32,** 498—501 (1949)
2. ANTONOV-ROMANOVSKI, V. V.: Zh. E. T. F. **26,** 459—472 (1954)
3. BODÓ, Z.: Acta Phys. Acad. Sci. Hung. **1,** 135—150 (1951)
4. BRAUMBECK, J.: Angew. Chem. **72,** 31—33 (1960)
5. CAMPBELL, W. B., BENNY, J.: Pulp and Paper Magazine of Canada **6,** 74—78 (1946)
6. DARBEY, A.: Amer. Dyestuff Rep. **46,** 465—471 (1957)
7. DOBOZY, O., LÁNG, L.: MTA Kémiai Tud. Oszt. Közl. **18,** No. 2, 221—242 (1962)
8. FALTA, W.: Jenaer Jahrbuch. **1955,** II. 212—246
9. FALTA, W.: Jenaer Jahrbuch. **1956,** 94—124
10. GRASSMANN, W., HANNIG K.: Klinische Wochenschrift **32,** 838—846 (1954)
11. GUREVIC, M.: Physik. Zeitschrift **31,** 753—763 (1930)
12. HEBER, U.: Zeiss-Mitteilungen. **2,** Heft 1. 1—13 (1960)
13. INGLE, R. B., MINSHALL, E.: J. Chrom. **8,** 369—385; 386—392 (1962)
14. IVANOV, A. P.: Opt. i. Spectr. **2,** 524—529 (1957)
15. IVANOV, A. P.: Spectr. Svr. Sred. Sbornik. Minsk 42—53 (1963)
16. JUDD, B. D.: J. Res. Nat. Bureau of Stand. **19,** 288—317 (1937)
17. JUDD, D. B., WYSZECKI, G.: Color in Business, Science and Industry, Part III. Physics and Psychophysics of Colorant Layers. Wiley, New York 1963. p. 297—340
18. KORTÜM, G., HAUG, P.: Z. Naturforsch. 8.a. 372—379 (1953)
19. KORTÜM, G., VOGEL, J.: Z. physik. Chem. Frankfurter Ausg. **18,** 230—241 (1958)
20. KORTÜM, G.: Rev Univ. des Mines. 9-série. T. XV. No. 5. 495—506
21. KORTÜM, G., BRAUN, W.: Angew. Chem. **75,** 653—661 (1963)
22. KUBELKA, P., MUNK, F.: Z. techn. Phys. **12,** 593—601 (1931)
23. KUBELKA, P.: J.O.S.A. **38,** 448—457 (1948)
24. KUBELKA, P.: J.O.S.A. **44,** 330—335 (1954)
25. MAJOR, GY.: Cand. Chem. Thesis, Leningrad, 1968.
26. MAJOR, GY., PAP, F., SZOVIK, J.: Mérés és Automatika (in Hungarian). (In the press)
27. MUNK, F.: Dtsch. Farben Ztschr. **11,** No. 3. 84—90 (1957)
28. PRICE, T. D., HUDSON, P. B., ASHMAN, D. F.: Nature **175,** 45—46 (1955)
29. RÁCZ, I., LÁNG, L.: Magyar Grafika **8,** 366—371 (1964)

30. ROZENBERG, G. V.: Usp. Fiz. Nauk. **69,** 57—104 (1959)
31. RYDE, J. W.: Proc. Roy. Soc. London. **A. 131,** 451—464; 464—475 (1931)
32. SCHMIDT, G.: Das Papier, **13,** 141—150 (1959), **14,** 445—452 (1960)
33. SCHULTZ, G.: Ann. der Phys. **6,** 345—354 (1960)
34. SAVOSTIANOVA, M. B.: Spektr. Svr. Sred. Sbornik. Minsk. 179—200 (1963)
35. SIDKO, F. J., TERSKOV, I. A.: Izv. Vuzov Fizik No. 2. 164—170 (1961)
36. STENIUS, A.: Svensk. Papperstidning. **54,** 663—670 701—709 (1951); **56,** 607—614 (1953)
37. STEPANOV, B. I.: Izv. A. N. USSR. Ser. Fiz. **21,** 1485—1493 (1957)
38. STEPANOV, B. I., TSEKALINSKAYA, J. I., GIRIN, O. P.: Trudu In. Fiz. i Mat. A. N. B.S.S.R. No. 1. 152—175 (1956)
39. TIMOFEJEVA, V. A.: D.A.N. USSR. **76,** 677—680 (1951), **113,** 556—559 (1957)
40. TIMOFEJEVA, V. A., GOROBEC, F. I.: Izv. A. N. USSR. Fiz. atm. i. ok. **3,** 291—295 (1967)
41. TIMOFEJEVA, V. A.: Izv. A.N. USSR. Ser. Geofiz. 265—272 (1957)
42. WENDLANDT, W., HECHT, H. G.: Reflectance Spectroscopy. Interscience Publishers. 1966. New York, London, Sydney

Jenő HUSZÁR; Budapest VI., Népköztársaság útja 17.

Acta Chimica Academiae Scientiarum Hungaricae, Tomus 63 (1), pp. 53—58 (1970)

INVESTIGATION OF THE ELECTRONIC STRUCTURE OF NUCLEOTIDE BASE ANTIMETABOLITE-TYPE POSSIBLE ANTICARCINOGENS, II

MONOSUBSTITUTED PURINES, ADENINES AND GUANINES

J. LADIK and G. BICZÓ

(Central Research Institute for Chemistry of the Hungarian Academy of Sciences, Budapest)

Received November 26, 1968

The π electron charge densities of different monosubstituted purines, adenines and guanines have been calculated with the aid of the semiempirical SCF LCAO MO method. The substituents were the same as in the previous paper.

On the basis of the obtained charge distributions some probable correlations seem to exist between the charge densities and the anticarcinogenic activity of the tested compounds. To establish better these correlations the calculation of further quantum chemical indices is necessary.

Introduction

In our previous paper [1], the charge distributions obtained from our semiempirical SCF LCAO MO calculations for a series of monosubstituted pyrimidines, uracils, thymines and cytosines have been given. In the present paper we give the SCF charge distributions obtained with the aid of the same method and using everywhere the same parameters (I_i, E_i, Z_i, $\beta_{i,j}$

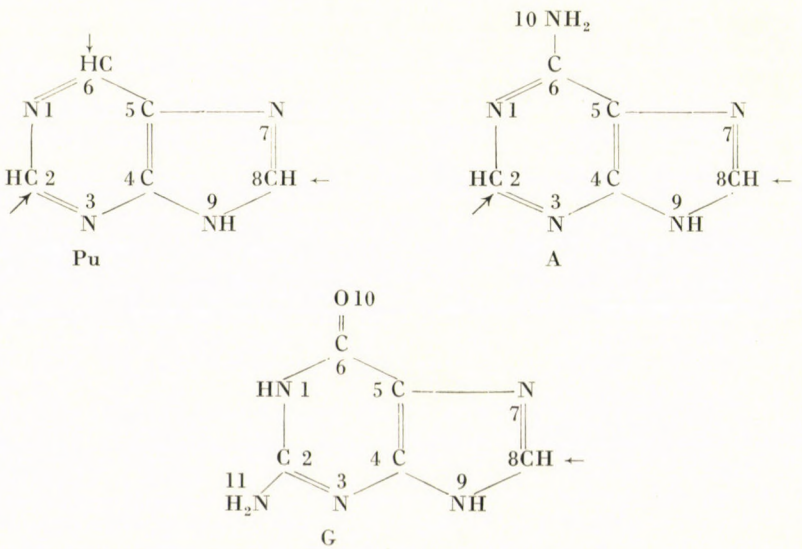

Fig. 1. The numbering of atoms in purine (Pu), adenine (A) and guanine (G). The arrows indicate those positions of substitution for which the calculations have been performed

Acta Chim. Acad. Sci. Hung. 63, 1970

Table I

SCF charge densities of monosubstituted purines

Substituent/Position	1	2	3	4	5	6	7	8	9	10	11	12
Pu	1.122	0.908	1.136	0.949	1.012	0.924	1.140	0.933	1.876	—	—	—
2—F	1.144	0.880	1.162	0.946	1.023	0.921	1.139	0.939	1.877	1.968	—	—
2—Cl	1.133	0.898	1.149	0.948	1.018	0.923	1.139	0.937	1.877	1.979	—	—
2—Br	1.125	0.905	1.140	0.949	1.014	0.924	1.140	0.934	1.876	1.993	—	—
2—J	1.122	0.908	1.137	0.949	1.012	0.924	1.140	0.933	1.876	1.999	—	—
6—F	1.149	0.905	1.148	0.948	1.034	0.894	1.141	0.939	1.876	1.967	—	—
6—Cl	1.135	0.907	1.143	0.948	1.023	0.913	1.140	0.937	1.876	1.978	—	—
6—Br	1.126	0.908	1.138	0.949	1.015	0.921	1.140	0.934	1.876	1.993	—	—
6—J	1.122	0.908	1.136	0.949	1.013	0.924	1.140	0.933	1.876	1.999	—	—
8—F	1.122	0.914	1.136	0.958	1.007	0.930	1.180	0.904	1.881	1.967	—	—
8—Cl	1.122	0.912	1.136	0.954	1.009	0.928	1.160	0.928	1.879	1.977	—	—
8—Br	1.122	0.909	1.136	0.950	1.011	0.925	1.146	0.930	1.877	1.993	—	—
8—J	1.122	0.908	1.136	0.949	1.012	0.924	1.141	0.933	1.876	1.999	—	—
2—OH	1.144	0.866	1.162	0.946	1.023	0.922	1.139	0.940	1.877	1.963	—	—
2—O—C—H_3	1,143	0.891	1.160	0.945	1.022	0.921	1.139	0.938	1.876	1.950	0.921	1.093
2—SH	1.132	0.898	1.148	0.948	1.017	0.923	1.140	0.936	1.876	1.982	—	—

2—NH_2	1.144	0.892	1.162	0.946	1.024	0.921	1.139	0.941	1.877	1.954	—	—
2—C—H_3	1.120	0.916	1.134	0.949	1.010	0.923	1.140	0.931	1.876	0.924	1.077	—
2—C(=O)—O—H	1.088	0.953	1.095	0.950	0.986	0.923	1.143	0.913	1.874	0.565	1.756	1.754
6—OH	1.148	0.905	1.149	0.947	1.033	0.899	1.141	0.939	1.876	1.962	—	—
6—O—C—H_3	1.147	0.905	1.147	0.946	1.032	0.905	1.138	0.942	1.874	1.950	0.921	1.093
6—SH	1.134	0.907	1.142	0.948	1.022	0.913	1.140	0.936	1.876	1.982	—	—
6—NH_2	1.149	0.905	1.149	0.948	1.033	0.906	1.141	0.940	1.876	1.953	—	—
6—C—H_3	1.120	0.907	1.134	0.949	1.010	0.932	1.141	0.930	1.876	0.925	1.077	—
6—C(=O)—O—H	1.082	0.907	1.110	0.949	0.974	0.973	1.137	0.913	1.876	0.568	1.756	1.756
8—OH	1.122	0.914	1.136	0.958	1.007	0.930	1.180	0.914	1.881	1.962	—	—
8—O—C—H_3	1.122	0.913	1.136	0.957	1.008	0.929	1.175	0.916	1.881	1.949	0.926	1.008
8—SH	1.122	0.911	1.136	0.953	1.010	0.927	1.155	0.925	1.879	1.981	—	—
8—NH_2	1.122	0.915	1.136	0.958	1.007	0.931	1.181	0.917	1.882	1.952	—	—
8—C—H_3	1.122	0.906	1.136	0.947	1.013	0.923	1.134	0.941	1.877	0.930	1.073	—
8—C(=O)—O—H	1.121	0.888	1.136	0.925	1.021	0.906	1.062	0.976	1.875	0.576	1.754	1.761

Table II

SCF charge densities of monosubstituted adenines

Substituent/Position	1	2	3	4	5	6	7	8	9	10	11	12	13
A	1.149	0.905	1.149	0.948	1.033	0.906	1.141	0.949	1.876	1.953	—	—	—
2—F	1.171	0.878	1.175	0.945	1.044	0.904	1.140	0.946	1.877	1.953	1.968	—	—
2—Cl	1.160	0.896	1.162	0.946	1.039	0.905	1.140	0.944	1.876	1.953	1.979	—	—
2—Br	1.152	0.903	1.153	0.947	1.035	0.906	1.141	0.941	1.876	1.953	1.993	—	—
2—J	1.149	0.905	1.150	0.948	1.033	0.906	1.141	0.940	1.876	1.953	1.999	—	—
8—F	1.149	0.912	1.149	0.958	1.028	0.917	1.181	0.911	1.881	1.953	1.967	—	—
8—Cl	1.149	0.909	1.149	0.953	1.030	0.910	1.162	0.930	1.879	1.953	1.978	—	—
8—Br	1.149	0.907	1.149	0.949	1.032	0.907	1.147	0.932	1.877	1.953	1.993	—	—
8—J	1.149	0.906	1.149	0.948	1.033	0.907	1.142	0.940	1.876	1.953	1.999	—	—
2—OH	1.171	0.883	1.174	0.945	1.044	0.904	1.140	0.947	1.877	1.953	1.963	—	—
2—O—C—H_3	1.170	0.889	1.173	0.944	1.042	0.904	1.140	0.945	1.876	1.952	1.950	0.921	1.093
2—SH	1.159	0.896	1.161	0.947	1.038	0.905	1.141	0.943	1.876	1.953	1.982	—	—
2—NH_2	1.171	0.890	1.175	0.945	1.044	0.904	1.140	0.947	1.877	1.953	1.954	—	—
2—C—H_3	1.147	0.914	1.147	0.948	1.031	0.906	1.141	0.938	1.876	1.952	1.923	1.079	—
2—C(=O)—O—H	1.116	0.950	1.108	0.949	1.037	0.905	1.144	0.920	1.874	1.952	0.565	1.755	1.755
8—OH	1.149	0.912	1.149	0.957	1.028	0.912	1.180	0.916	1.881	1.953	1.962	—	—
8—O—C—H_3	1.148	0.910	1.149	0.957	1.029	0.911	1.176	0.922	1.881	1.950	0.925	1.089	—
8—SH	1.149	0.909	1.149	0.952	1.031	0.909	1.159	0.930	1.878	1.953	1.982	—	—
8—NH_2	1.149	0.912	1.149	0.957	1.028	0.913	1.182	0.924	1.881	1.953	1.952	—	—
8—C—H_3													
8—C(=O)—O—H	1.148	0.885	1.149	0.923	1.041	0.889	1.063	0.983	1.874	1.950	0.578	1.755	1.761

Table III

SCF charge densities of monosubstituted guanines

Substituent/Position	1	2	3	4	5	6	7	8	9	10	11	12	13	14
G	1.887	0.869	1.188	0.953	1.051	0.761	1.119	0.962	1.861	1.405	1.944	—	—	—
8—F	1.886	0.879	1.185	0.969	1.044	0.763	1.155	0.931	1.867	1.408	1.946	1.968	—	—
8—Cl	1.885	0.875	1.185	0.962	1.046	0.763	1.137	0.991	1.864	1.408	1.945	1.978	—	—
8—Br	1.886	0.872	1.186	0.956	1.048	0.763	1.124	0.960	1.862	1.407	1.945	1.993	—	—
8—J	1.885	0.871	1.186	0.954	1.049	0.763	1.119	0.963	1.867	1.407	1.945	1.999	—	—
8—OH	1.886	0.879	1.185	0.969	1.044	0.763	1.155	0.936	1.867	1.408	1.946	1.963	—	—
8—O—$C—H_3$	1.887	0.865	1.194	0.961	1.046	0.756	1.146	0.939	1.866	1.415	1.946	1.971	0.919	1.089
8—SH	1.885	0.875	1.186	0.961	1.046	0.763	1.135	0.951	1.864	1.408	1.945	1.982	—	—
$8—NH_2$	1.886	0.880	1.185	0.970	1.044	0.763	1.155	0.944	1.867	1.409	1.946	1.953	—	—
$8—CH_3$	1.885	0.867	1.187	0.949	1.049	0.763	1.112	0.971	1.862	1.406	1.944	0.928	1.077	—
$8—C\begin{matrix}O\\O—H\end{matrix}$	1.884	0.843	1.190	0.909	1.054	0.763	1.045	1.009	1.859	1.398	1.941	0.582	1.765	1.766

values) as in the previous paper (see Tables I and II of [1]), for monosubstituted purines, adenines and guanines. The substituents were also the same, as previously (—F, —Cl, —Br, —J. —OH, —O—CH_3, —SH, —NH_2, —CH_3, and —COOH).

The numbering of the parent compounds, together with those positions of substitutions which do not interfere with their ability to build in to DNA and for which therefore the calculations have been performed, are shown in Fig. 1. The geometry used for the parent compounds was taken again from SPENCER [2]. The numbering of the substituents is the same as in [1].

Results and discussion

In Tables I, II and III we give the resulting SCF charge densities obtained for the calculated compounds.

From the data given in the Tables we can see, as in the case of monosubstituted pyrimidine-type compounds [1], that in most cases the charge densities of the parent compounds are changed in a larger amount only at the position of substitution and at the two neighbouring atoms. In some cases, however, the substitution causes a rather large change in the charge distribution of the whole molecule (for instance in the cases of 2—COOH—A and 8—COOH—G). It is further worthwhile to mention that the charge density of nitrogen atom 9 (where these compounds bind to the sugar in the nucleic acids) changes in all cases only very little also by substitution at carbon atom 8.

Comparing the charge densities of the tested and active compounds [4] with those of the untested ones it seems again possible to find some probable correlations between the SCF π electron charges and the anticarcinogenic activity. To establish, however, better these correlations, it is necessary again, as in the case of the monosubstituted pyrimidine-type compounds, to determine further, more characteristic quantum chemical indices. These calculations are in progress.

*

We should like to express our gratitude to Dr. A. UDVARDY for collecting many data in the literature about the experimentally tested anticarcinogenic activity of a part of the investigated compounds. We are further indebted to Miss A. JESZENÁK for tabulating the calculated charge densities.

REFERENCES

1. LADIK, J., BICZÓ, G.: Acta Chim. Acad. Sci. Hung. **62,** 401 (1969)
2. SPENCER, M.: Acta Cryst. **12,** 59 (1959)
3. HINZE, T., JAFFÉ, J.: J. Am. Chem. Soc. **84,** 540 (1962)
4. Cancer Chemotherapy Screening Data. V—VIII. in Cancer Research **20** (1960); *ibid.* IX—XII. in Cancer Research **21** (1961)

János LADIK
Géza BICZÓ
Budapest II., Pusztaszeri út 57—69.

Acta Chimica Academiae Scientiarum Hungaricae, Tomus 63 (1) pp. 59—66 (1970)

POTENTIAL AND ELECTRON ENERGY CURVES OF ISOELECTRONIC MOLECULES

S. Szőke, Zs. Vajna and G. Jalsovszky

(Central Research Institute for Chemistry of the Hungarian Academy of Sciences, Budapest)

Received November 26, 1968

Potential energy curves of isoelectronic molecules have been calculated by a combined method using adjusted parameters. For these molecules electronic energy curves and electronic force constants are given.

The potential energy curves of isoelectronic diatomic molecules, having the same orbital configuration, show similarity in their position as well as in their shape. The same statement has been found valid for the electronic energy curves, obtained by subtracting Coulomb attraction terms from the potential energy data and by taking into consideration formulas coming from Bingel united atom theory.

The electronic structure of the SiO molecule can be written according to Mulliken [1]:

$$SiO\ [KLK\ (\sigma x)^2\ (\sigma y)^2\ (\pi)^4\ (\sigma z)^2].$$

The same structure can be drawn for the PN and CS molecules despite the the fact that in the classical description PN has a triple bond, while CS and SiO have double ones. Similar is the situation, of course, in the case of the P_2 and SiS molecules.

Several parameters of the above molecules are in close similarity, among others their reduced masses, bond lengths, the geometrical means of the electronegativities, those of ionization potentials, and effective nuclear charges. There is no decisive difference in dissociation energies, either. The influence on the shape of the curves exerted by the differences in dissociation energies acts, anyway, mainly in the region of higher quantum numbers. Some of the aforesaid parameters are listed in Table I.

On the basis of the similarity of the most important spectroscopic constants — some of them being familiar as potential energy derivatives of different order — analogies may be expected in potential energy curves. For a reasonable justification of the assumptions about the analogous behaviour of electronic energy curves, beyond the Bingel rules in the $R \ll R_e$ region where routine calculations can hardly be carried out, a more accurate potential energy expression is required for medium and high quantum numbers as well.

Table I

Parameters of isoelectronic molecules
(Interatomic distances in Å, anharmonicity constants, rovibrational coupling constants and rotational constants in cm^{-1})

	R_e	$\omega_e x_e$	α_e	B_e
SiO	1.510	6.05	0.0049	0.7623
CS	1.534	6.50	0.0062	0.8205
PN	1.491	6.98	0.0055	0.7862
P_2	1.894	2.80	0.0014	0.3032
SiS	1.928	2.56	0.0015	0.3036

In the following a more suitable method is proposed for deriving potential energy expressions of improved accuracy in the field of some isoelectronic molecules.

The experimental potential energy curves

The Rydberg–Klein–Rees (RKR) experimental curves were calculated on the basis of data taken from the monograph of PEARSE and GAYDON [2]. The spectrum of PN was measured by CURRY and HERZBERG [3], that of CS

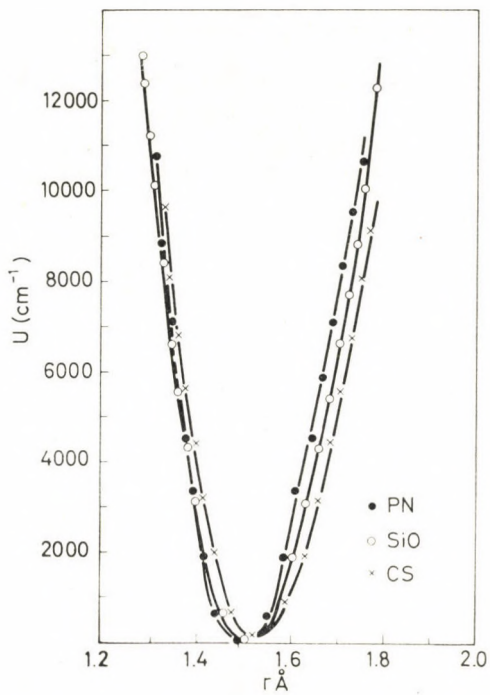

Fig. 1. Experimental curves of PN, SiO and CS

by JEVONS and by CRAWFORD [4, 5] while the spectrum of SiO was measured by JEVONS and SHARMA [6], and that of SiS by BARROW and JEVONS [7].

The potential energy curves of PN and P_2 were recently calculated by RAI and SINGH [8]. R_{max} and R_{min} values were calculated for the $^1\Sigma$ states and it has been found that the shapes of the curves of the isoelectronic molecules are very similar. The $R_{max}-R_{min}$ values are in close agreement at low and medium quantum numbers.

The experimental curves of these molecules show that the agreement between SiO and CS is better than between PN and SiO or PN and CS, respectively, justifying the assumption that there is a moderate difference between PN and the others (Fig. 1).

Empirical potential energy functions using adjusted parameters

The completeness of the calculation of RKR potentials is limited by the lack of sufficient spectroscopic data defining the whole potential. In order to obtain a complete electronic energy curve, the first step is to select a suitable empirical function for the high and medium quantum numbers. With the advent of digital computers this problem has become very simple. Programs can be written able to calculate five or six (or even more, if it is worthwhile) empirical functions at once, and to select the most convenient one with regard of the RKR values. In areas where no more experimental data exist calculations can be carried out by the optimal empirical function.

When no empirical function can be found that fits the experimental data, the term determining the shape of the curve can be adjusted by replacing coherent U and R values (R_{max} or R_{min}) into the empirical equation selected before.

A program has been written with the above claim and it has been found that it is the Rydberg empirical function that fits well the experimental data. By adjusting the $(k/D)^{1/2}$ expression the Rydberg "b" constant leeds to more accurate curve. The Rydberg function has the form

$$D_e - U(R) = D_e(1 + b\varrho)\, e^{-b\varrho} \tag{1}$$

where $b = (k_e/D_e)^{1/2}$ and $\varrho = R - R_e$.

Let the equation be transformed into

$$\frac{D_e - U(R)}{D_e} = (x + 1)\, e^{-x}.$$

By Newton's successive approximation,

$$x_n = x_{n-1} - f(x_{n-1})/f'(x_{n-1})$$

Acta Chim. Acad. Sci. Hung. 63, 1970

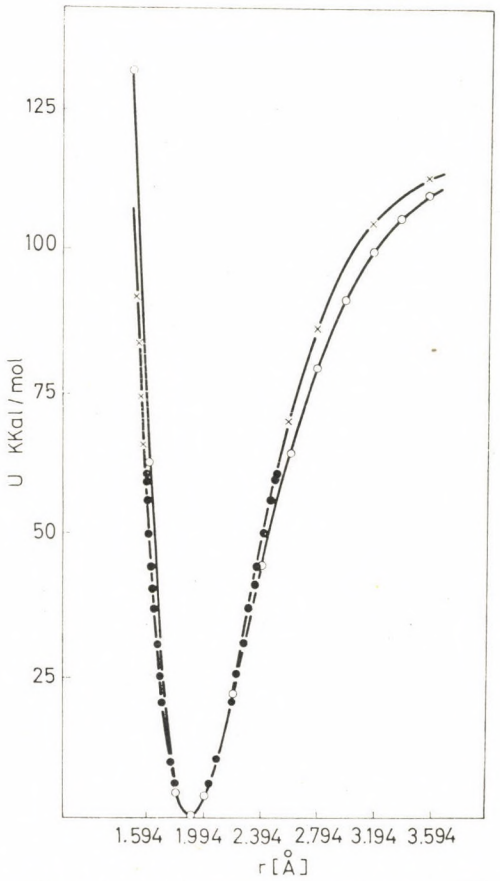

Fig. 2. Potential curves of P_2. ● denotes RKR-, ○ empirical Rydberg- and x the adjusted Rydberg data

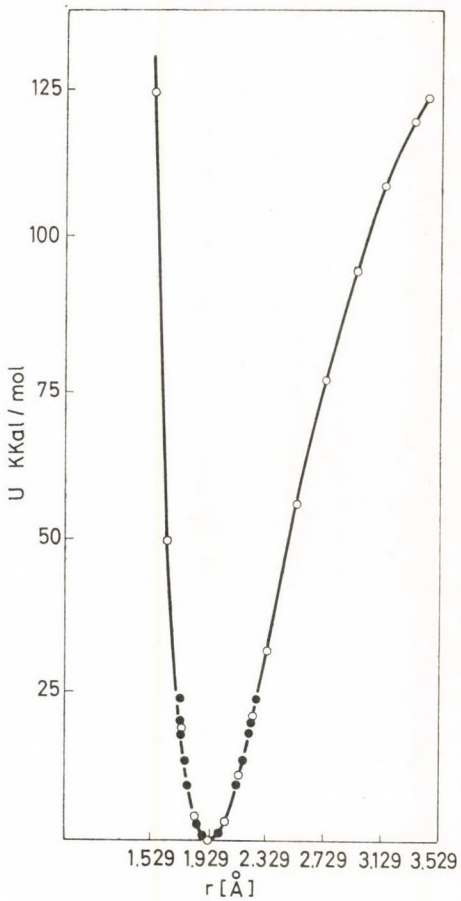

Fig. 3. Potential curves of SiS. ● denotes RKR-, and ○ the adjusted Rydberg data

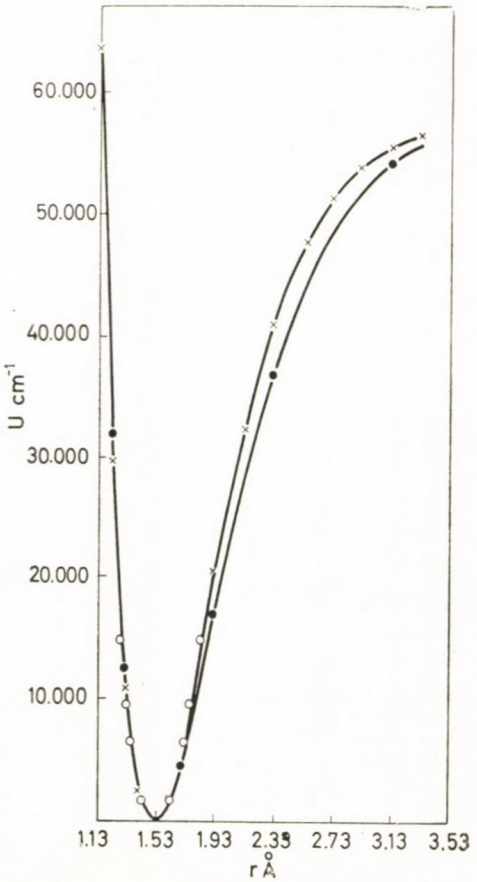

Fig. 4. Potential curves of SiO. ○ denotes RKR-, ● empirical Rydberg- and x the adjusted Rydberg data

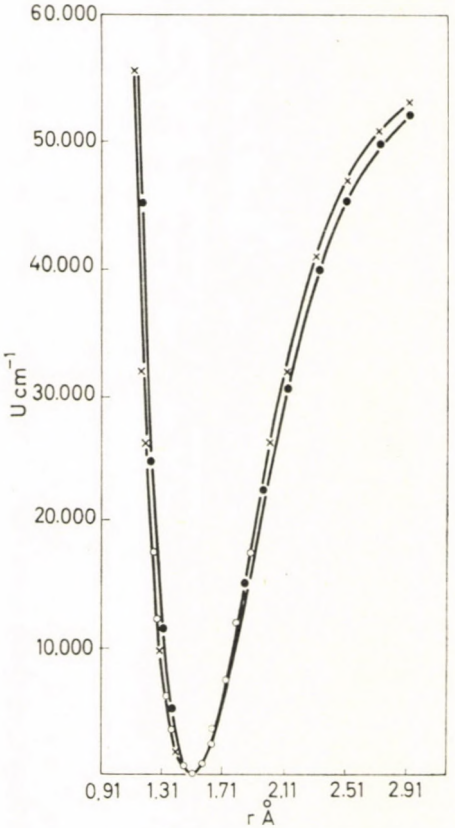

Fig. 5. Potential curves of CS. ○ denotes RKR-, ● empirical Rydberg- and x the adjusted Rydberg data

Acta Chim. Acad. Sci. Hung. 63, 1970

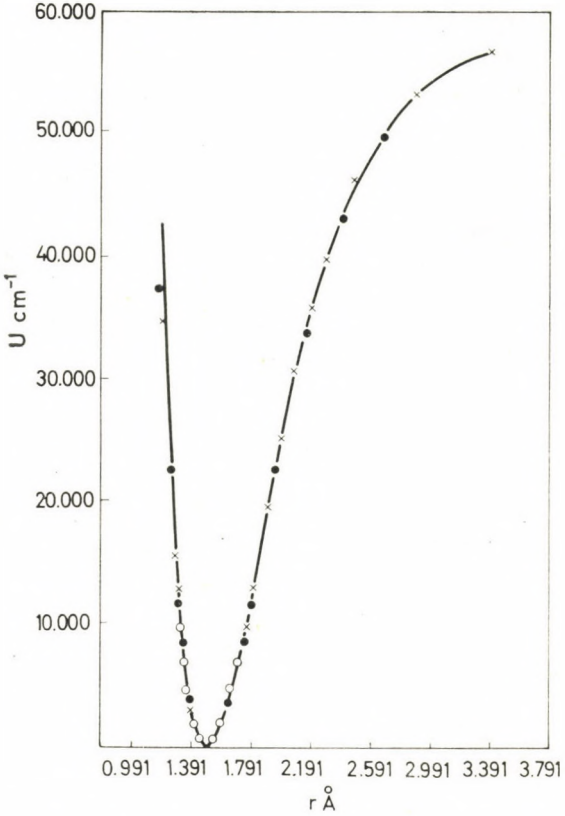

Fig. 6. Potential curves of PN. ○ denotes RKR-, ● empirical Rydberg-, and x thea djusted Rydberg data

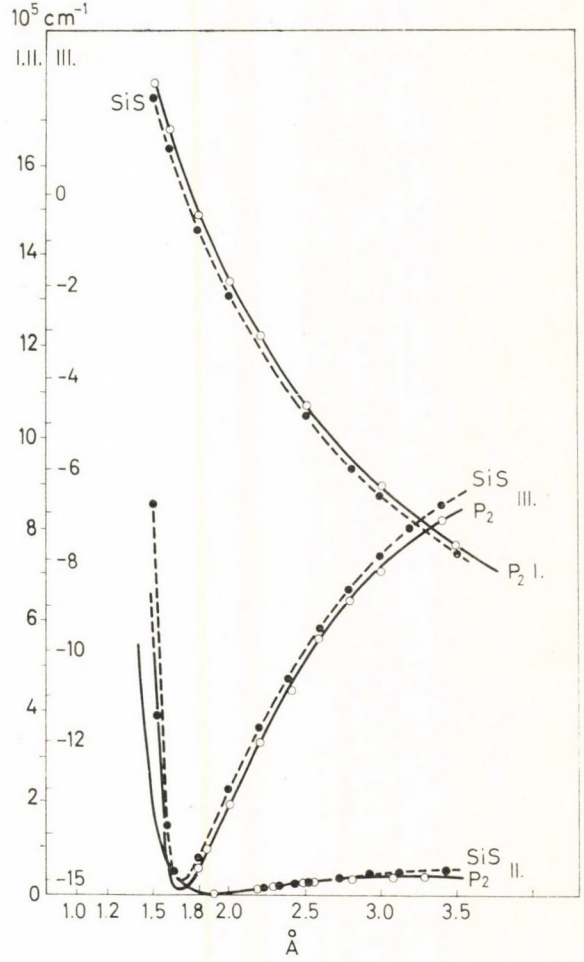

Fig. 7. Energy curves of P_2 and SiS. I: Coulomb energy, II: total potential energy, III: electronic energy

an iterative solution can be given for x at definite (U, R) values from which k as a variable parameter obtains a value different from k_e used in Eq (1). This parameter leeds to better empirical approach than the original one, where k is taken from the literature.

Figures 2, 3, 4, 5, and 6 give the experimental, the Rydberg empirical and the adjusted Rydberg curves of SiO, CS, PN, P_2 and SiS molecules.

The electron energy function of isoelectronic molecules

According to one of the potential assumptions the potential energy can be written as a sum of two terms, namely the Coulomb attraction and the electronic energy:

$$U(R) = Z_A Z_B / R_{AB} + U_{el} .$$

In the region where $R \ll R_e$ the electronic energy can be given as a power series expression [9]:

$$U_{el} = E(0) + E_2 R^2 + E_3 R^3 ,$$

where $E(0)$ is the united atom energy, E_2 and E_3 are electron energy coefficients whose more accurate definition can be derived from the BINGEL rules [10]

$$E_2 = \frac{Z_A Z_B}{Z_A + Z_B} \left\{ [\varrho_{0,0}(0)/6] - \int_0^\infty R \varrho_{2,0}(R)\, dR \right\}$$

and

$$E_3 = \frac{Z_A Z_B (Z_B^2 + Z_A^2)}{(Z_A + Z_B)^2} \cdot \frac{1}{12} \left(\frac{d\varrho_{0,0}}{dR} \right)_0$$

where ϱ denotes electronic densities and transition densities, respectively.

When the united atom is common and MO configurations are the same, the electronic curves should be also very similar in the indicated field, and, as a consequence, also over the whole range of interatomic separations.

Figure 7 shows the Coulomb, the potential and the electronic energy functions of P_2 and SiS molecules in the area where calculations can be performed. It has been easily demonstrated that the electronic energy curves are similar to each other in shape as well as in the energy values.

Electronic force constants of isoelectronic molecules

According to the Hellmann—Feynman theory the electronic force constants can be obtained by the differentiation of the Hamiltonian of diatomic molecules:

$$H = -\frac{1}{2} \sum_i \Delta_i - \sum_{i,j} \frac{Z_j}{r_{ij}} + \sum_{i<j} \frac{1}{r_{ij}} + \frac{Z_A Z_B}{R_{AB}} .$$

The second derivative has the form

$$f_{AB} = \frac{2Z_A Z_B}{R_{AB}^3} - Z_B \left\{ \int \varrho(r, R) \frac{3\cos^2 \Theta_b - 1}{r_b^3} d\tau - \right.$$
$$\left. - \frac{4}{3} \pi \varrho(B, R) \right\} + Z_B \int \frac{d\varrho}{dR} (r, R) \frac{\cos \Theta_b}{r_b^2} d\tau . \qquad (2)$$

The Coulomb attribution is easily separated and the remainder in expression (2) is the electronic force constant. When accepting MURREL's proposition for calculating the Coulomb term [11], we are able to justify the assumption that the electronic force constants of isoelectronic molecules are very similar to each other. Table II shows some electronic force constants of isoelectronic molecules of the same orbital configuration.

Table II

Force constants, interatomic distances and electronic force constants of isoelectronic molecules

	k_e	R_e	b
CP	7.83	1.562	16.4
SiN	7.29	1.572	16.5
CO	19.02	1.128	58.3
N_2	22.96	1.094	65.2
CS	8.49	1.534	22.2
PN	10.16	1.491	24.5
SiO	9.25	1.510	23.0
P_2	5.56	1.894	11.5
SiS	4.94	1.928	10.6

REFERENCES

1. MULLIKEN, R. S.: Rev. Mod. Phys. **4,** 1 (1932)
2. PEARSE, R. W. B., GAYDON, A. G.: The Identification of Molecular Spectra. Chapman and Hall Ltd., London, 1963
3. CURRY, J., HERZBERG, G.: Z. Physik **86,** 348 (1933)
4. JEVONS, W.: Proc. Roy. Soc. **117,** 351 (1928)
5. CRAWFORD, F. H., SHURCLIFF, W. A.: Proc. Roy. Soc. **145,** 860 (1934)
6. JEVONS, W.: Proc. Roy. Soc. **106,** 174 (1924); SHARMA, D.: Proc. Nat. Acad. Sci. India **A14,** 37 (1944)
7. BARROW, R. F., JEVONS, W.: Proc. Roy. Soc. **169,** 45 (1938)
8. RAI, D. K., SINGH, R. B.: Indian J. Pure Appl. Phys. **4,** 102 (1966)
9. PREUSS, H.: Theoret. chim. Acta (Berl.) **2,** 102 (1964)
10. BINGEL, W.: J. Chem. Phys. **30,** 1250 (1959), *ibid.* **30,** 1254 (1959)
11. MURRELL, J. N.: J. Mol. Spectra. **4,** 446 (1960)

Sándor SZŐKE
Zsuzsanna VAJNA
György JALSOVSZKY
Budapest II., Pusztaszeri út 57/69

Acta Chimica Academiae Scientiarum Hungaricae, Tomus 63 (1) pp. 67—85 (1970)

MULTILAYER ADSORPTION FROM LIQUID MIXTURES, I

J. TÓTH

(Industrial Research Laboratory of Oil and Gas Mining, Nagykanizsa)

Received December 6, 1968

The generalization of the monolayer model of adsorption from liquid mixtures leads to contradictions. Properties related to the structure of the liquid (association, H-bonding, etc.) point to multilayer adsorption in the case of several $\Gamma - x$ isotherms for which precise calculations of the specific surface area of the adsorbent indicate monolayer adsorption. Furthermore, multi-valued and "oscillating" free-energy functions are obtained for certain linear isotherms which is impossible to interpret. These contradictions can be resolved by assuming that the monomolecular individual adsorbed amounts Γ_1 and Γ_2 are mixed with one or more molecular layers of the bulk phase under the influence of surface forces due to structural factors. Thus a multilayer surface phase is formed in which the experimentally observed excess substance is the same as with monolayer adsorption. The resulting multilayer adsorption can be described by exact mass balance equations.

1. Monolayer adsorption of liquids

Since all considerations described in the present paper are based on the general mass balance equation of OSTWALD and DE IZAGUIRRE [1] for the adsorption of binary liquid mixtures on the surface of solids, this expression will first be derived. The basic relationships are

$$x_0 = \frac{\Gamma_{1,0}}{\Gamma_{1,0} + \Gamma_{2,0}} = \frac{\Gamma_{1,0}}{\Gamma_0} \tag{1}$$

$$x = \frac{\Gamma_{1,0} - \Gamma_1}{\Gamma_{1,0} - \Gamma_1 + \Gamma_{2,0} - \Gamma_2} \tag{2}$$

where x_0 and x are the initial and equilibrium mole fractions, respectively, $\Gamma_{1,0}$ and $\Gamma_{2,0}$ are the number of moles of the two components in the initial mixture prior to adsorption, Γ_0 is their sum, *i.e.* the total number of moles initially present, and Γ_1 and Γ_2 are the experimentally observable amounts of the two components which disappear from the bulk phase as a result of adsorption. The possibility of experimental observation is due to the fact that from Eqs (1) and (2) one obtains

$$\Gamma_0(x_0 - x) = \Gamma_1(1 - x) - \Gamma_2 x \tag{3}$$

where $\Gamma \equiv \Gamma_0(x_0 - x)$ is a directly measurable quantity referred to in the literature as the "apparent" amount of adsorbed substance, the term not being a most fortunate one. SCHAY and NAGY [2] have pointed out that the term "apparent" is not justified since Γ is identical with the excess substance in the boundary phase as defined by GIBBS and, therefore, it is an exact thermodynamic notion.

The derivation of Eq. (3) involves no assumptions about the magnitude of Γ_1 and Γ_2 thus it does not provide information concerning the thickness of the adsorption phase, *i.e.* the number of adsorbed layers. As for the latter, one can only make assumptions. In this respect two opposite concepts are currently in use: (i) the monolayer (monomolecular) model, and (ii) the pore-filling model to be regarded essentially as multilayer adsorption [3—7], the latter being used especially with porous adsorbents. The best currently available monolayer theory supported by convincing evidence has been developed by SCHAY and NAGY [2, 8—13]. The fruitfulness of their theory is due to having rejected the analogy with gas adsorption and showing that the surface is always fully covered in liquid adsorption. Thus any exchange of mass in the boundary phase is only possible by mutual displacement of the components. Since the results of the above authors are of fundamental importance, the main points of the theory will be outlined here with special reference to the evidence pointing to monolayer adsorption. It will also be shown that this evidence is necessary but not sufficient to prove monolayer adsorption, resulting in certain contradictions which, in our opinion, can only be resolved by assuming the existence of a special type of multilayer adsorption to be described more precisely in the subsequent sections of this paper.

SCHAY and NAGY regard quantities Γ_1 and Γ_2 as referring to monomolecular adsorption, and introduce equation

$$\Gamma_1\Phi_1 + \Gamma_2\Phi_2 = 1 \tag{4}$$

where Γ_1 and Γ_2 are the individual adsorbed amounts (μmole/m^2) in monolayer adsorption, Φ_1 and Φ_2 are the molar requirements of surface area by the components m^2/μmole. The composition of the boundary phase (x') can be calculated easily from Eqs (3) and (4). The results are

$$\Gamma_1 = \frac{x + \Gamma\Phi_2}{(\Phi_1 - \Phi_2)\,x + \Phi_2} \tag{5}$$

$$\Gamma_2 = \frac{(1 - x) - \Gamma\Phi_1}{(\Phi_1 - \Phi_2)\,x + \Phi_2} \tag{6}$$

$$x' = \frac{\Gamma_1}{\Gamma_1 + \Gamma_2} = \frac{x + \Gamma\Phi_2}{1 + \Gamma(\Phi_2 - \Phi_1)} \tag{7}$$

Φ_1 and Φ_2 in Eqs (5)—(7) are usually calculated from vapor adsorption data while Γ is a directly measurable quantity in liquid-solid boundary adsorption as a result of the following expression

$$\Gamma \equiv \Gamma_0(x_0 - x) .$$

Γ cannot be directly measured in the case of free-surface adsorption, the only possibility being the calculation of Γ by integrating the Gibbs equation if the surface tension *vs.* composition relationship is known. Otherwise, there is a far-reaching analogy between free-surface and liquid-solid adsorptions, therefore, the followers of the monolayer adsorption theory regard Eqs (3)—(7) valid for the free surface, too.

The measured or calculated $\Gamma - x$ isotherms have been subdivided by SCHAY and NAGY into five groups (types) shown in Fig. 1.

Next to the $\Gamma - x$ isotherm types in Fig. 1 we have shown the $x' - x$, $\Gamma_1 - x$, and $\Gamma_2 - x$ isotherms, too, that have been calculated from Eqs (5)—(7) and thus involve the assumption of monolayer adsorption. Types II, III, and IV show a well-separated linear section as opposed to the other types. If Eq. (3) is re-written as

$$\Gamma = -(\Gamma_1 + \Gamma_2)\, x + \Gamma_1 \tag{8}$$

it can easily be seen that on the linear sections Γ_1 and Γ_2 and, consequently, also x' are constant, *i.e.* the composition of the surface phase does not change.

The second important consequence of linearity is that by extrapolation to $x = 0$ and $x = 1$ (*cf.* Fig. 1) one can determine Γ_1 and Γ_2 which are constant in the linear interval. This means that the specific surface area of an adsorbent (F) can be determined by using the following equation

$$\Gamma_1\Phi_1 + \Gamma_2\Phi_2 = F \tag{9}$$

where Γ_1 and Γ_2 are now the individual adsorbed amounts per unit weight of the adsorbent (μmole/g) obtained by extrapolation. If F is known or one deals with a free-surface isotherm, *i.e.* Γ_1 and Γ_2 are obtained in μmole/m^2 units, the result of the extrapolation should be in agreement with Eq. (4). The calculation of F by linear extrapolation has been given the name "graphical method of surface area determination" and as such it has been widely used. (In the subsequent parts of this paper the linear sections of the $\Gamma - x$ isotherms from which one can calculate the correct value for the surface area will be termed as F-linear sections, while the notion itself, as F-linearity).

The practical application of the method of graphical surface determination has led, under proper conditions, to good agreement with F values obtained by other procedures. The F-linear sections for a given pair of liquids on different adsorbents follow the variations of the specific surface area.

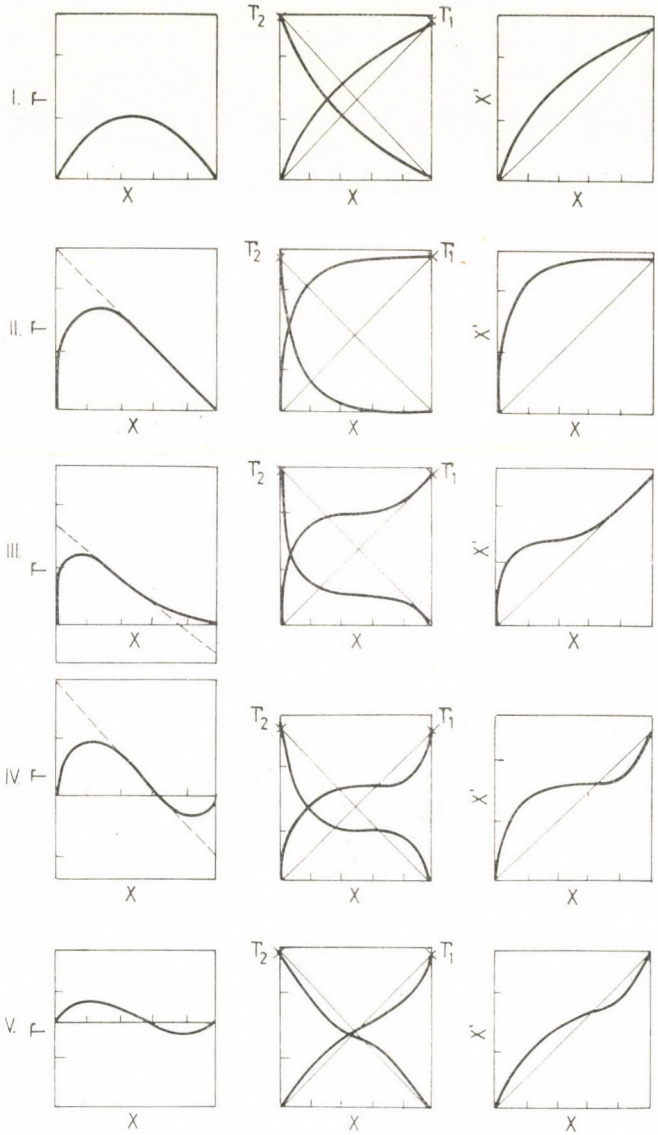

Fig. 1. Basic types of adsorption isotherms of liquid mixtures according to SCHAY and NAGY

These are the undisputable facts regarded by the supporters of the monolayer theory as evidence for monomolecular adsorption also outside the *F*-linear isotherm sections with the exception of only a few chemisorption phenomena. However, it can be seen from Eqs (1)—(2) that the evidence based on the fact of *F*-linearity only proves that the experimentally observed amounts of mass exchanged between the bulk and surface phases are in

agreement with the monomolecular concept. The equations derived from Eq. (3) cannot give information about the "fate" on the surface of the amounts Γ_1 and Γ_2 that have disappeared from the bulk phase, *i.e.* whether the two substances remain discretely separated in a single layer, or they mix with one or more molecular layers of the bulk phase in an experimentally inaccessible manner. The rejection of the possibility concerning the mixing of Γ_1 and Γ_2, *i.e.* the complete adherence to the monolayer model, may lead to serious contradictions. The two most important contradictions will be analyzed in detail.

The generalization of monolayer adsorption contradicts the individual structural properties of liquid systems such as association, hydrogen bond formation, polar and unpolar structures, etc. These phenomena support, and in many cases also prove multilayer adsorption. For example, it is known that on the basis of the van der Waals theory, assuming a surface with a monomolecular thickness the Eötvös constant can be written as

$$k_E = \frac{k N^{2/3}}{1 - b/V} \approx 2 \qquad \text{erg/mole} \cdot \text{degree} \tag{10}$$

where k is the Boltzmann constant, N is the Avogadro number, b is the van der Waals "constant", and V is the molar volume. If b is regarded as a variable together with the volume and equal to one half of the molar volume, one obtains the value of 2 erg/mole·degree in good agreement with the experiment. However, Eötvös constants are often obtained which are strongly different from the value calculated from the assumption of a monolayer boundary surface. Thus, for water, ethanol, methanol, formic acid, acetic acid, etc. the experimental k_E values are in the interval of 0.6—1.35. According to our present knowledge, this indicates the association of molecules on the surface and the formation of multimolecular structures due to H-bonds or other factors.

As a consequence of this, the strict F-linearity of the ethanol–water free surface *(cf.* Fig. 3) and of the liquid isotherms for the ethanol–water–charcoal system [13], [14] at 25°C must involve a contradiction. "Strict" linearity means that on the linear section of the free-surface isotherm the $\Gamma_1\Phi_1 + \Gamma_2\Phi_2$ sum equals unity, and the specific surface area calculated from the isotherm on charcoal is, within 1—5%, equal to that determined by the BET method. Numerous other examples are available in the literature for which the possibility of correct specific surface area calculations indicates monolayer adsorption while other physical parameters and the anomalies of the Eötvös constant are indicative of multilayer adsorption.

The other contradiction concerns the thermodynamic approach to the adsorption of liquid mixtures. The general thermodynamic Gibbs-equation

of adsorption can be written for the adsorption from a binary liquid mixture (2) as

$$\Gamma_{1,G} = -\frac{1}{RT}\,\frac{d\gamma}{d\ln(f_1 x)} \tag{11}$$

where $\Gamma_{1,G}$ is the excess of component 1 in the surface phase (μmole/m^2), f_1 is the rational activity coefficient, *i.e.* $f_1 x$ is the activity of component 1 in the bulk of the liquid phase, and γ is the surface tension of the mixture measured

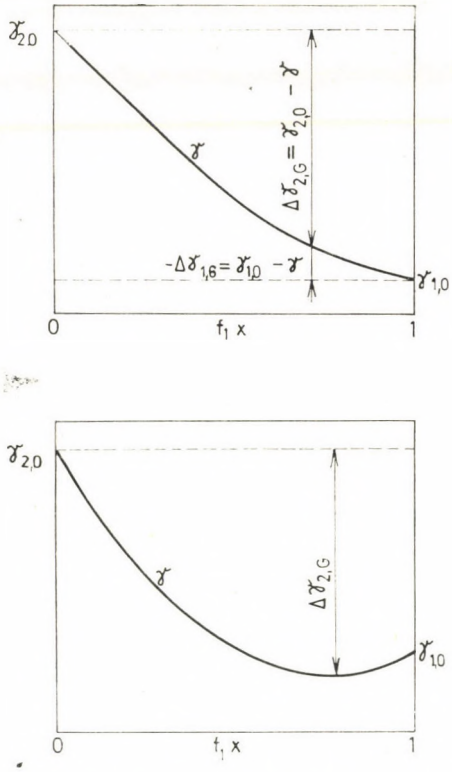

Fig. 2. Variation of the surface free-energy as a function of the activity of component *1*

at concentration x (at activity $f_1 x$). For adsorption on a solid surface γ is the excess free-energy of the phase-boundary layer with respect to the bulk phase of identical composition.

SCHAY and NAGY [2] have shown that $\Gamma_{1,G}$ in the Gibbs-equation and Γ determined from the OSTWALD—DE IZAGUIRRE equation

$$\Gamma = \Gamma_0(x_0 - x) \tag{12}$$

are related by the expression

$$\Gamma_{1,G} = \frac{\Gamma}{1 - x}. \tag{13}$$

Using Eq. (13), the Gibbs-equation integrated between limits $0 - f_1 x$ can be written as

$$\int_0^{f_1 x} d\gamma = \Delta\gamma_{2,G} = \mathrm{RT} \int_0^{f_1 x} \frac{\Gamma}{1 - x} d\ln(f_1 x). \tag{14}$$

If the experimental $\Gamma - x$ isotherms plotted as $\Gamma/(1 - x)$ *vs.* $\ln f_1 x$ permit graphical or other approximate integration, the free-energy change $\Delta\gamma_{2,G}$ can be calculated. The latter is obtained as the $\gamma_{2,0} - \gamma$ difference, where

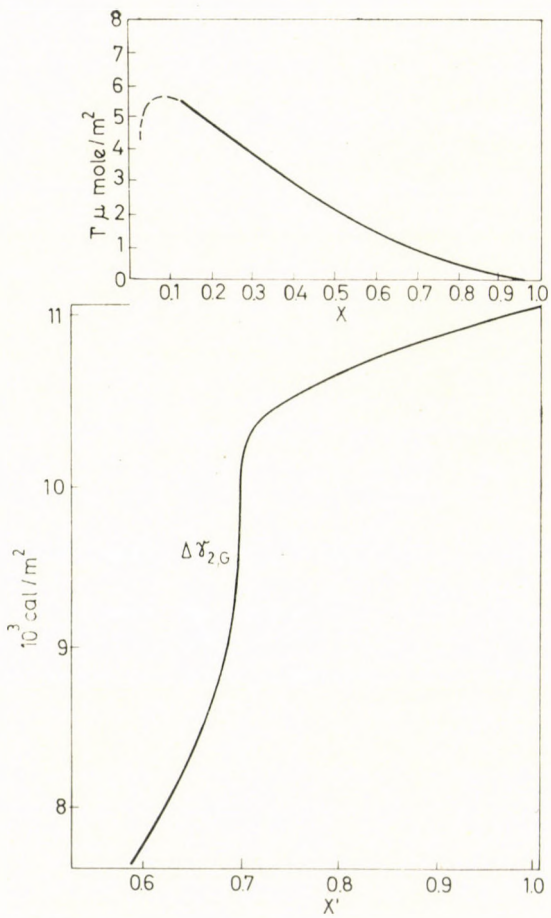

Fig. 3. Free-surface isotherm for ethanol–water and the free-energy function calculated on the basis of monolayer adsorption

$\gamma_{2,0}$ is the surface free energy (surface tension) at activity $f_1x = 0$, *i.e.* that for pure component *2*.

Thus the free-energy change illustrated in Fig. 2 can be calculated on the basis of Eq. (14).

If Eq. (14) is integrated between limits 1 and f_1x, one obtains the $-\Delta\gamma_{1,G} = \gamma_{1,0} - \gamma$ free-energy change.

The ethanol–water free-surface $\Gamma - x$ isotherm calculated by integrating the Gibbs equation, and the free-energy function obtained by means of Eq. (14) are shown in Fig. 3.

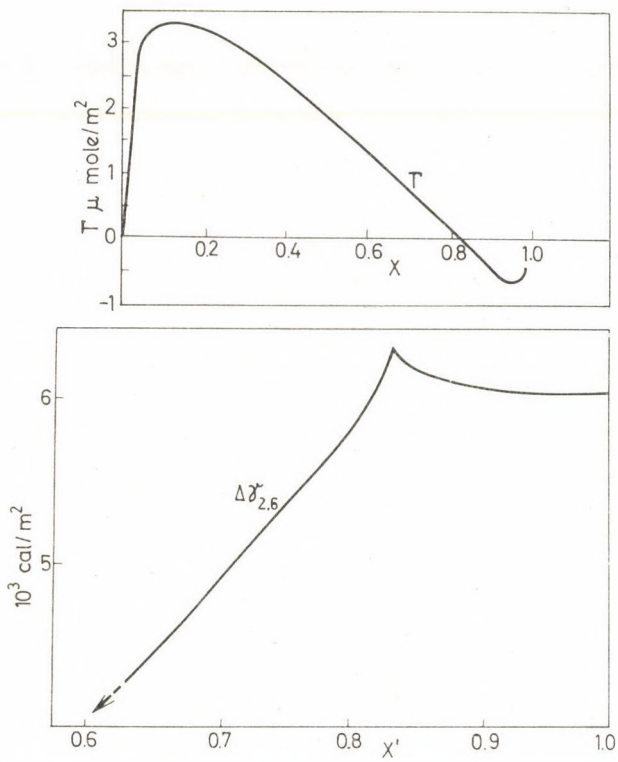

Fig. 4. Benzene–ethanol–charcoal (720 m^2/g) isotherm and the free-energy function calculated on the basis of monolayer adsorption

The assumption of monolayer adsorption involves that on the linear section of the $\Gamma - x$ isotherm x' is constant, consequently, the $\Delta\gamma_{2,0}$ *vs.* x' function is multi-valued which is thermodynamically incorrect because it means that more than one $\Delta\gamma_{2,0}$ can be calculated from a single surface phase composition.

It is even more difficult to interpret the free-energy function for a $\Gamma - x$ isotherm which changes sign and is linear in the vicinity of (prior to and

after) the location where this occurs. The γ *vs.* $f_1 x$ function has a minimum at $\Gamma = 0$ for such isotherms *(cf.* Fig. 2), *i.e.* the $\Delta\gamma_{2,G}$ *vs.* x' has a maximum. Consequently, $\Delta\gamma_{2,G}$ increases prior to, and decreases after, the change in the sign. If this occurs in a linear isotherm section, the free-energy change at a given x' will be not only multi-valued but "oscillating". For example, this is manifested on the free-energy function of the type IV isotherm for the benzene–ethanol–charcoal system (720 m^2/g) in such a manner (2) that the maximum almost collapses into a vertical line (*cf.* Fig. 4). On the basis of this phenomenon, inexplicable both physically and thermodynamically, we have reached the conclusion that the monolayer adsorption model does not apply in the above mentioned cases. The $\Delta\gamma_{2,G}$ values of the $\Delta\gamma_{2,G}$ *vs.* x' free-energy function have been calculated from Eq. (14) which is correct in all respects, therefore, the inexplicability of the free-energy functions can only be due to the x' values calculated on the basis of monomolecular adsorption.

Summarizing briefly the above considerations, we have shown that F-linearity, a convincing evidence for the validity of the monolayer model, may contradict to the physical and thermodynamic properties of liquid mixtures. In our opinion, this contradiction is due to the fact that in the monolayer model Γ_1 and Γ_2 originating in the bulk phase are regarded as discreetly separated quantities, disregarding the possibility that they may interact with the bulk phase, although in a way that has escaped experimental detection as yet. If the extent of these interactions are reckoned with on the basis of the laws of liquid adsorption, all contradictions can be resolved and perhaps a more general pictur of the adsorption of liquid mixtures will emerge.

2. Multilayer adsorption as a result of mass transport

Any interaction between Γ_1, Γ_2 and the bulk phase is only possible by means of mutual displacement, *i.e.* the principle of full coverage must remain valid. Therefore, we shall assume that as a result of the above mentioned specific surface forces which are due to structural factors, an amount $\Gamma_{1,d}$ of component *1* is transferred into layer *2* with concentration x. In accordance with the principle of displacement, an amount $\Gamma_{2,d}$ of component *2* is simultaneously transferred from layer *2* into layer *1*. As a result of displacement

$$\Gamma_{1,d}\,\Phi_1 = \Gamma_{2,d}\,\Phi_2\,.$$

After mass transport has taken place, we have

$$\Gamma_{1,1} = \Gamma_1 - \Gamma_{1,d} \tag{15}$$

and

$$\Gamma_{2,1} = \Gamma_2 + \Gamma_{2,d} \tag{16}$$

where $\Gamma_{1,1}$ and $\Gamma_{2,1}$ are the amounts of the two components in layer *1* after the exchange of mass has gone to completion. (In the subsequent parts of this paper, the first and second numerals of a double subscript will refer to the component and the layer, respectively. A single subscript refers to a component participating in monolayer adsorption.) Prior to mass transport, one can write for amounts $W_{1,2}$ and $W_{2,2}$ present in layer *2* which, according to the monolayer model, are not adsorbed

$$x = \frac{W_{1,2}}{W_{1,2} + W_{2,2}} \tag{17}$$

and

$$W_{1,2}\,\Phi_1 + W_{2,2}\,\Phi_2 = 1\,. \tag{18}$$

From Eqs (17) and (18) one obtains

$$W_{1,2} = \frac{x}{(\Phi_1 - \Phi_2)\,x + \Phi_2}\,. \tag{19}$$

Similarly,

$$W_{2,2} = \frac{1 - x}{(\Phi_1 - \Phi_2)\,x + \Phi_2}\,. \tag{20}$$

After mass transport has taken place, the amounts in layer *2* may again be denoted by Γ reserved for the adsorbed amounts because, here too, the concentration is different from the equilibrium value x:

$$\begin{aligned} \Gamma_{1,2} &= W_{1,2} + \Gamma_{1,d} \\ \Gamma_{2,2} &= W_{2,2} - \Gamma_{2,d}\,. \end{aligned} \tag{21}$$

Thus the total adsorbed amounts of the components are

$$\Gamma_{1,t} = \Gamma_1 + W_{1,2} \tag{22}$$

$$\Gamma_{2,t} = \Gamma_2 + W_{2,2}\,. \tag{23}$$

Since the OSTWALD—DE IZAGUIRRE equation should be valid in this case, too, we have

$$\Gamma = \Gamma_{1,t}\,(1 - x) - \Gamma_{2,t}\,x\,. \tag{24}$$

Inserting Eqs (22) and (23) into Eq. (24), and taking into account Eqs (19) and (20), one obtains

$$\Gamma \equiv (\Gamma_1 + W_{1,2})\,(1 - x) - (\Gamma_2 + W_{2,2})\,x \equiv \Gamma_1\,(1 - x) - \Gamma_2\,x\,. \tag{25}$$

If, instead of two, mass transport involves n layers, it is easy to see that

$$\Gamma_{1,t} = \Gamma_1 + W_{1,2} + \ldots + W_{1,n} = \Gamma_1 + \frac{(n-1)\,x}{(\Phi_1 - \Phi_2)\,x + \Phi_2}$$

and (26)

$$\Gamma_{2,t} = \Gamma_2 + W_{2,2} + \ldots + W_{2,n} = \Gamma_2 + \frac{(n-1)\,(1-x)}{(\Phi_1 - \Phi_2)\,x + \Phi_2} \,.$$

Thus identity (25) may be written in a general form as

$$\Gamma \equiv \Gamma_{1,t}\,(1-x) - \Gamma_{2,t} \equiv \Gamma_1\,(1+x) - \Gamma_2\,x\,. \tag{27}$$

This means that mass transport may lead to a multilayer adsorption phase in which the excess amount Γ is identical with that in a monolayer phase.

The total concentration (x_t) in the layers depends on the "depth" (n) of mass exchange, *i.e.*

$$x_t = \frac{\Gamma_{1,t}}{\Gamma_{1,t} + \Gamma_{2,t}} = \frac{[(\Phi_1 - \Phi_2)\,x + \Phi_2]\,\Gamma_1 + (n-1)\,x}{[(\Phi_1 - \Phi_2)\,x + \Phi_2]\,[\Gamma_1 + \Gamma_2] + (n-1)} \,. \tag{28}$$

If in Eq. (28) Γ_1 and Γ_2 are inserted according to Eqs (6) and (5), one obtains

$$x_t = \frac{nx + \Gamma\Phi_2}{n + \Gamma(\Phi_2 - \Phi_1)} \tag{29}$$

which for $n = 1$ becomes identical with equation (7) derived by SCHAY and NAGY.

Eq. (27) shows that the $\Gamma - x$ isotherm for multilayer adsorption due to mass transport is identical with that for monolayer adsorption, the two isotherms being indistinguishable. For brevity's sake, this multilayer adsorption equivalent to monolayer adsorption will subsequently be referred to as *(e*quivalent *m*ultilayer) *e.m.* adsorption.

It is clear from the above considerations that *e.m.* adsorption is impossible if mass transport with one or both components is by some reason forbidden (the layers are closed). This is the case if chemisorption occurs in the first layer but physical adsorption takes place in all subsequent layers. Similarly closed layers are present on adsorbents whose pores are accessible only for one of the components (molecular sieves), or if the physical adsorption of one of the components results in *complete* displacement of the other from the surface (type II isotherm). Therefore, *if* multilayer adsorption occurs in such cases, this may only lead to a $\Gamma - x$ isotherm which is *different* from that for monolayer adsorption (Eq. (27) does not hold).

In connection with the interpretation of these mass transport equations it should be emphasized that no conclusions should be drawn about the time course of *e.m.* adsorption on the basis of the mass transport mechanism outlined above. Thus we may not state that monolayer adsorption occurs first and mass transport towards deeper-lying layers takes place subsequently. Obviously, the forces resulting in multilayer adsorption are operative during the whole time interval required to reach adsorption equilibrium. Therefore, it is completely unlikely that an extended period exists during which only monolayer adsorption occurs. The above separation in time of the two kinds of adsorption was required only by the nature of the mathematical treatment used. For example, the states prior to and after mass exchange mentioned in connection with Eqs (16) and (17) probably do not exist for the surface forces. As far as these forces are concerned, there exists only a post-exchange state because it is the very existence and effect of surface forces causing multilayer adsorption that prevent the pre-exchange state (monolayer adsorption) from being a reality. Thus the kinetics of *e.m.* adsorption can be assumed as the transfer of amounts Γ_1 and Γ_2 from the bulk to the surface phase where they become mixed between n layers prior to adsorption on the surface as a result of the variation of γ with "depth". After the exchange of mass has taken place, the surface phase is set up according to concentrations $x_1' \ldots x_n'$ characteristic for multilayer adsorption without the previous existence of monolayer adsorption. However, it is possible, too, that a layer of composition x' comes into existence but is instantaneously mixed with the bulk phase. Whichever of the assumptions is valid, the fact remains that the mechanism of mass exchange has not been used to describe the time course of *e.m.* adsorption but only to illustrate the nature of surface forces causing multilayer adsorption, *i.e.* that in the case of open layers these short-range forces (with a range of one or perhaps a few molecular diameters) exert their influence via *mass exchange*.

3. Mass balance equations for multilayer liquid adsorption

The assumed mechanism of mass exchange leading to *e.m.* adsorption can be regarded as complete only if its consistence with the general mass balance equations for *any* multilayer liquid adsorption is demonstrated. The starting point of the procedure is again the OSTWALD—DE IZAGUIRRE equation (24) but now it is not necessary to assume that $\Gamma_{1,t}$ and $\Gamma_{2,t}$ have been reached by "mixing".

If the treatment is temporarily restricted to double-layer adsorption, one may write

$$\Gamma = (\Gamma_{1,1} + \Gamma_{1,2})(1 - x) - (\Gamma_{2,1} + \Gamma_{2,2})\, x \qquad (30)$$

where

$$\Gamma_{1,t} = \Gamma_{1,1} + \Gamma_{1,2}$$

and

$$\Gamma_{2,t} = \Gamma_{2,1} + \Gamma_{2,2}\,.$$

Eq. (30) can be re-written as

$$\Gamma = \Gamma_{1,1}(1 - x) - \Gamma_{2,1}\,x + \Gamma_{1,2}(1 - x) - \Gamma_{2,2}\,x \tag{31}$$

Eq. (31) indicates that the excess mass Γ is a sum of the corresponding excesses in layers *1* and *2*, *i.e.*

$$\Gamma = \Gamma^1 + \Gamma^2 \tag{32}$$

where

$$\Gamma^1 = \Gamma_{1,1}(1 - x) - \Gamma_{2,1}\,x \tag{33}$$

and

$$\Gamma^2 = \Gamma_{1,2}(1 - x) - \Gamma_{2,2}\,x\,. \tag{34}$$

As a result of full coverage and the validity of the displacement principle, one can write for the individual adsorbed amounts that

$$\Gamma_{1,1}\Phi_1 + \Gamma_{2,1}\Phi_2 = 1 \tag{35}$$

$$\Gamma_{1,2}\Phi_1 + \Gamma_{2,2}\Phi_2 = 1\,. \tag{36}$$

The concentrations in the two layers are given by

$$x_1' = \frac{\Gamma_{1,1}}{\Gamma_{1,1} + \Gamma_{2,1}}\,, \qquad x_2' = \frac{\Gamma_{1,2}}{\Gamma_{1,2} + \Gamma_{2,2}}\,. \tag{37}$$

The individual adsorbed amounts in the two layers are obtained from Eqs (35)—(37)

$$\Gamma_{1,1} = \frac{x_1'}{(\Phi_1 - \Phi_2)\,x_1' + \Phi_2} \tag{38}$$

$$\Gamma_{2,1} = \frac{1 - x_1'}{(\Phi_1 - \Phi_2)\,x_1' + \Phi_2} \tag{39}$$

and

$$\Gamma_{1,2} = \frac{x_2'}{(\Phi_1 - \Phi_2)\,x_2' + \Phi_2} \tag{40}$$

$$\Gamma_{2,2} = \frac{1 - x_2'}{(\Phi_1 - \Phi_2)\,x_2' + \Phi_2}\,. \tag{41}$$

From Eqs (38)—(41) and (33)—(34) one obtains

$$\Gamma^1 = \frac{x_1' - x}{(\Phi_1 - \Phi_2)\, x_1' + \Phi_2} \tag{42}$$

and

$$\Gamma^2 = \frac{x_2' - x}{(\Phi_1 - \Phi_2)\, x_2' + \Phi_2} . \tag{43}$$

On the basis of Eqs (42) and (43), Eq. (32) can be re-written as

$$\Gamma - \frac{x_1' - x}{(\Phi_1 - \Phi_2)\, x_1' + \Phi_2} = \frac{x_2' - x}{(\Phi_1 - \Phi_2)\, x_2' + \Phi_2} . \tag{44}$$

If at a given x, the left-hand and right-hand sides of Eq. (44) are plotted against x_1' and x_2', respectively, one obtains the graphs shown in Fig. 5. The upper graph refers to positive and the lower one to negative Γ.

The nature of the plot involves that Eq. (44) is satisfied by every x_1', x_2' pair corresponding to points where the solid curves in Fig. 5 intersect with horizontal straight lines. (*Cf.*, for example $x_1' = 0.600$ and $x_2' = 0.126$, etc., in Fig. 5.)

Consequently, only one x_2' may belong to a given x_1'. In spite of this, an infinite number of x_1', x_2' concentration pairs can be selected mathematically which yield identical Γ-s at a given x. For the overall concentration of the two layers one may write

$$x_t = \frac{\Gamma_{1,t}}{\Gamma_{1,t} + \Gamma_{2,t}} . \tag{45}$$

from which, taking Eq. (24) into account, one obtains

$$\Gamma_{1,t} = \frac{x_t}{x_t - x}\, \Gamma \tag{46}$$

and

$$\Gamma_{2,t} = \frac{1 - x_t}{x_t - x}\, \Gamma . \tag{47}$$

At given x and Γ, x_t must be independent of all the possible concentration pairs x_1', x_2' for the two layers because in the opposite case, according to Eqs (46)—(47), $\Gamma_{1,t}$ and $\Gamma_{2,t}$ would not be constant which is impossible. This constancy of x_t is true for all x_1', x_2' pairs including $x_1' = x_2' = x_t$. For this case, Eq. (44) can be written as

$$\Gamma = \frac{2(x_t - x)}{(\Phi_1 - \Phi_2)\, x_t + \Phi_2} . \tag{48}$$

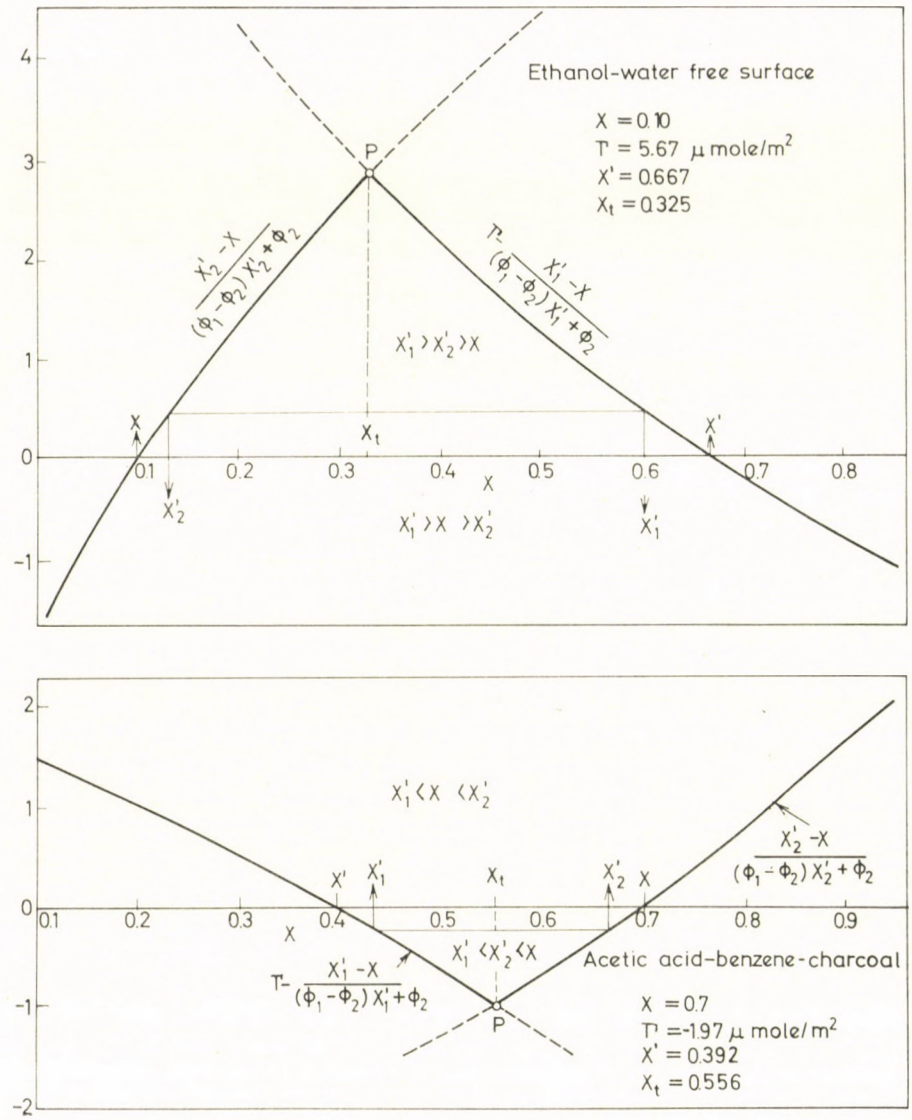

Fig. 5. Graphical determination of the concentration distribution in the adsorbed phase for double-layer adsorption

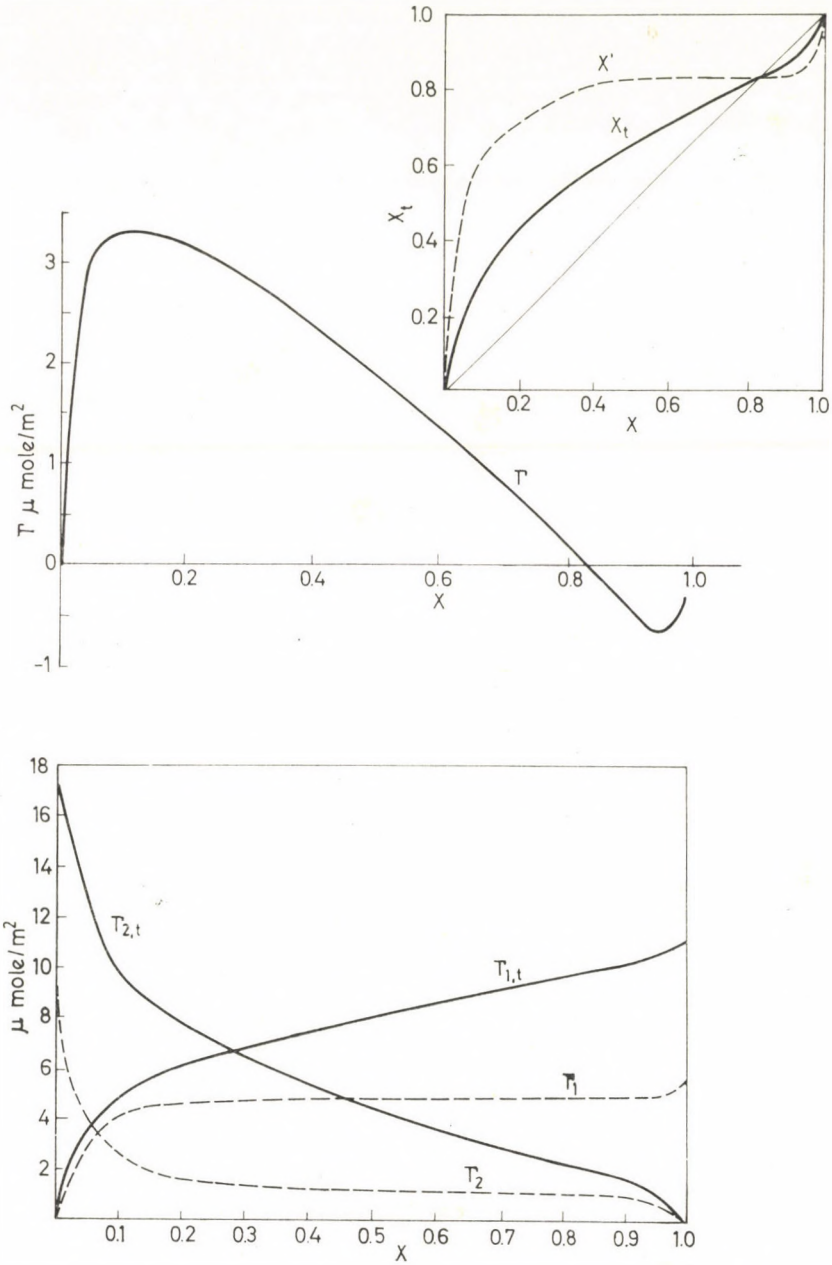

Fig. 6. Individual isotherms $x' - x$ and $x_t - x$ relationships for the benzene–ethanol–charcoal system (720 m^2/g) at 25°C calculated for monolayer and double-layer adsorptions

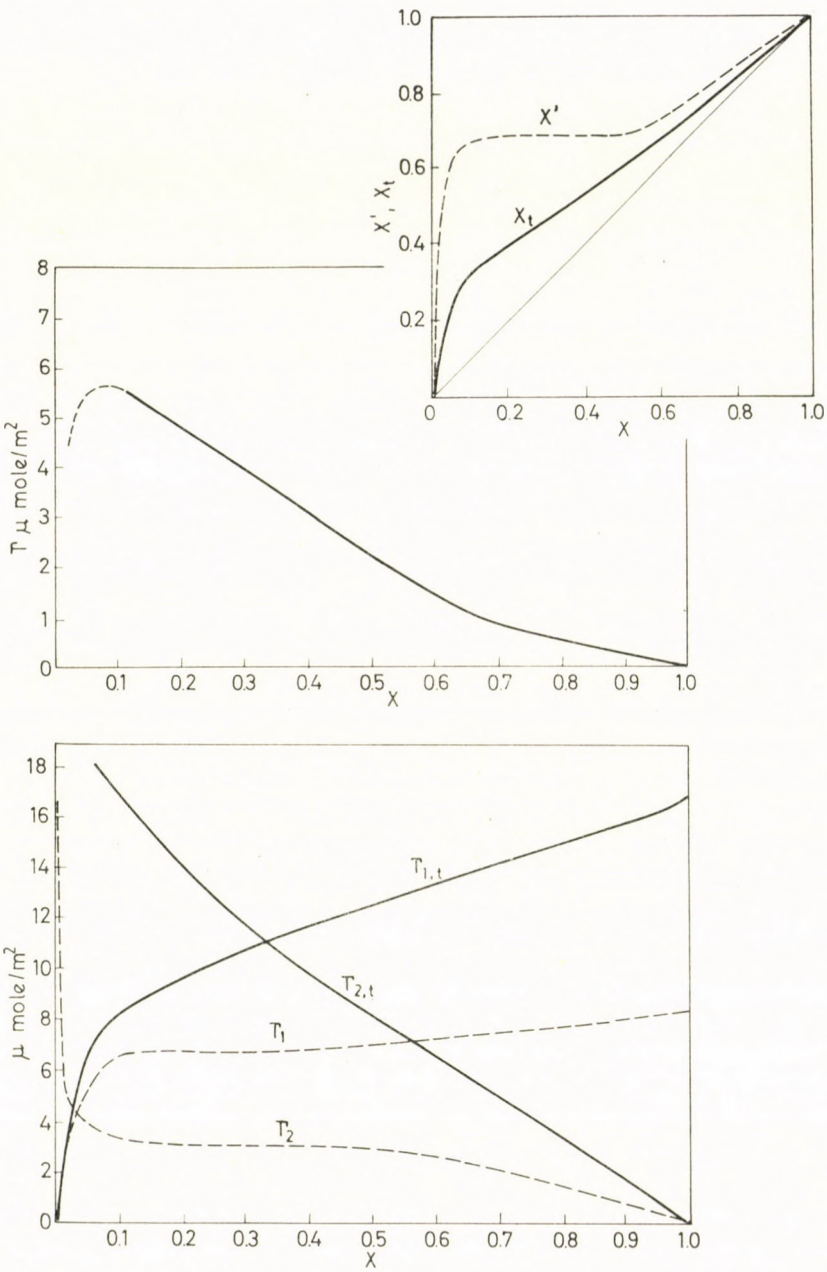

Fig. 7. Ethanol–water free-surface at 25°C. Individual isotherms, $x' - x$ and $x_t - x$ relationships calculated for monolayer and double-layer adsorptions

The value of the x_t coordinate of the intersection point P shown in Fig. 5 can be calculated from Eq. (48):

$$x_t = \frac{2x + \Gamma\Phi_2}{2 + \Gamma(\Phi_2 - \Phi_1)} \,. \tag{49}$$

This expression is identical with Eq. (29) for the special case when $n = 2$ thus we have proved the full consistency between the mechanism of mass transport and the mass balance equations.

It follows from the determination of the x_1', x_2' pairs illustrated in Fig. 5 that the concentration pairs can be subdivided into two groups. The first group consists of those pairs indicating adsorption of the same sign for both layers (positive-positive or negative-negative), *i.e.* $x_1' > x_2' > x$ or $x_1' < x_2' < x$. The values for the corresponding pairs are obtained between point P and the abscissa. The two functions in Eq. (44) reach the horizontal (concentration) axis at points x' and x, *i.e.* this corresponds to the concentration distribution for monolayer adsorption. For the x_1', x_2' pairs obtained at the opposite side of intersection point P we have $x_1' > x > x_2'$ or $x_1' < x < x_2'$, indicating adsorption with opposite signs in the two layers. The concentration values associated with the first group can be interpreted by assuming that the physical nature of the surface forces is the same in both the first and second layers, being but slightly weaker in the second. Consequently, a capillary-active (or inactive) substance with respect to the first layer shows the same behaviour in the second layer and thus there is a gradual transition between the concentrations in the surface and in the bulk phase. (For example, in Fig. 5, $x_1' = 0.600$, $x_2' = 0.126$, $x_3' = x = 0.100$, or for negative adsorption $x_1' = 0.425$, $x_2' = 0.600$, $x_3' = x = 0.700$.) The concentration pairs characteristic for the second group involve that the effects of surface forces are essentially opposite in the first and in the second layers.

The above concentration distribution for concrete systems as well as their interpretation will be treated in detail in Part II of this series.

It should be mentioned briefly that the assumption of the *e.m.* adsorption resolves the physical and thermodynamic contradictions associated with the F-linearity of the $\Gamma - x$ isotherms since the composition of the surface phase is not constant in these regions. This is proved by Figs 6 and 7 showing the values for $\Gamma_{1,t}$, $\Gamma_{2,t}$ and x_t calculated from the above mentioned isotherms for $n = 2$ using Eqs (46), (47), and (49), as compared to the Γ_1, Γ_2 and x' functions calculated on the basis of monolayer adsorption.

The calculation of free-energy functions allowed by *e.m.* adsorption will be shown in Part II, together with the most important concept of the physical justification of *e.m.* adsorption, *viz.* why is multilayer adsorption precisely equivalent to monomolecular adsorption.

REFERENCES

1. OSTWALD, W., DE IZAGUIRRE, R.: Kolloid-Z. **30,** 279 (1922)
2. NAGY, L. GY., SCHAY, G.: Magy. Kém. Foly. **70,** 33 (1964)
3. JONES, D. C., OUTRIDE, L.: J. Chem. Soc. **1930,** 1574
4. DOSS, K. S. G.: J. Chem. Soc. **1931,** 2027
5. HANSEN, R. D., HANSEN, R. S.: J. Coll. Sci. **1954,** 1
6. HANSEN, R. S., HANSEN, R. D.: J. Phys. Chem. **59,** 496 (1955)
7. JONES, D. C., MILL, G. S.: J. Chem. Soc. **1957,** 213
8. NAGY, L. GY., SCHAY, G.: Magy. Kém. Foly. **66,** 31 (1960)
9. SCHAY, G., NAGY, L. GY., SZEKRÉNYESY, T.: Magy. Kém. Foly. **66,** 271 (1960)
10. SCHAY, G., NAGY, L. GY.: J. Chim. Phys. **1961,** 149
11. NAGY, L. GY., SCHAY, G.: Acta Chim. Hung. **39,** 365 (1963)
12. SCHAY, G., NAGY, L. GY.: Magy. Kém. Lapja **19,** 173 (1964)
13. NAGY, L. GY.: MTA Kémiai Közl. **27,** 323 (1967)
14. ERDEY-GRÚZ, T., SCHAY, G.: Theoretical Phsyical Chemistry. 4th Edition, Vol. II. p. 331. Tankönyvkiadó, Budapest 1964

József TÓTH; Nagykanizsa, Vár u. 8. Hungary

Acta Chimica Academiae Scientiarum Hungaricae, Tomus 63 (1) pp. 87—95 (1970)

HYDANTOINS, THIOHYDANTOINS, GLYCOCYAMIDINES, XXVIII*

REACTION OF THE 3-METHYL-2,5-BIS(METHYLTHIO)-4,4-DIPHENYL-4*H*-IMIDAZOL-3-IUM CATION WITH BENZYLAMINE

K. LEMPERT*, P. SOHÁR** and K. ZAUER*

*(*Department of Organic Chemistry, Technical University, Budapest and **Pharmaceutical Research Institute, Budapest)*

Received November 19, 1968

3-Methyl-2,5-bis(methylthio)-4,4-diphenyl-4*H*-imidazol-3-ium (**1**) methosulfate, when treated with pyridine and benzylammonium chloride, furnishes 2-benzylimino-1-methyl-5,5-diphenyl-4-imidazolidinethione (**5**) as the main product, formed through **3** by successive benzylaminolysis and *S*-demethylation, and, as a by-product, the hydrochloride of 2,4-di(benzylimino)-1-methyl-5,5-diphenylimidazolidine (**8**). *S*-Demethylation during the formation of **5** is effected by pyridine. The IR and NMR spectra of some of the compounds (**2**—**5**) revealed finer structural details, such as the electronic distribution and, in the case of potentially tautomeric compounds, the tautomeric structures.

In Part XXIII [1] of the present series, the reaction of 3-methyl-2,5-bis(methylthio)-4,4-diphenyl-4*H*-imidazol-3-ium cation (**1**; in the paper cited: **II**) with bezylammonium chloride in pyridine was described. To the main product (m.p. 313—4°C) of the reaction the structure of 2-benzylimino-1-methyl-4-methylthio-5,5-diphenyl-3-imidazoline (**3**; in the paper cited: **V**) was assigned, mainly on the basis of analytical results and on the fact that the compound was found different from 4-benzylimino-1-methyl-2-methylthio-5,5-diphenyl-2-imidazoline (**2**; in the paper cited: **XII**) (m.p. 111—2°C) which has been prepared by structure proving synthesis.

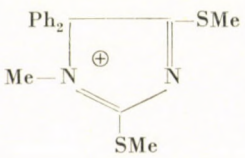

1

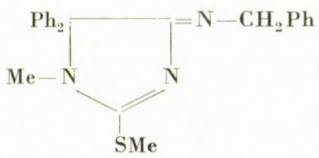

2

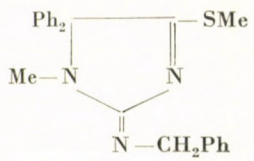

3

Recently NMR spectra of the compound melting at 313—4°C and of **2** have been obtained. While in the latter case the spectrum was consistent with the structure derived by chemical means, structure **3** was definitely excluded for the compound melting at 313—4°C by its NMR spectrum. In

*Part XXVII: J. NYITRAI, R. MARKOVITS-KORNIS, K. LEMPERT: Acta Chim. Acad. Sci. Hung. **60**, 141 (1969).

the spectrum (in $CDCl_3$) of compound **2** two singlets at $\delta = 2.65$ and 2.80 ppm, corresponding to the *N*- and *S*-methyl groups, respectively, were found, while the spectrum (in DMSO-d_6) of the compound melting at 313—4°C had only one methyl signal (at 2.75 ppm). This obviously means that, in the course of the reaction of **1** with benzylammonium chloride in pyridine, besides benzylaminolysis partial demethylation (at the nitrogen or sulfur) had occurred; this was originally overlooked, since it does not affect significantly the percentage elemental composition of the product.*

Consequently, the compound melting at 313—4°C should be identical with an isomer of the known [1] 4-benzylamino-1-methyl-5,5-diphenyl-3--imidazoline-2-thione (**4**; in the paper cited: **IX**; m.p. 258—9°C).

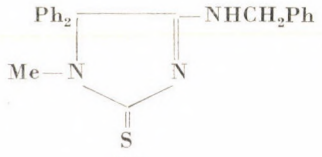

4**

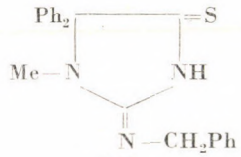

5**

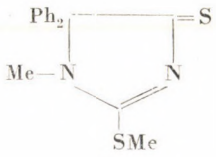

6

Since *S*-demethylations of compounds similar to **1** by amines have been repeatedly observed by us (*cf.*, *e.g.* [2]), structure **5** (*i.e.* 2-benzylimino--1-methyl-5,5-diphenyl-4-imidazolidenethione) was next taken into consideration, this structure being in good agreement with the IR spectrum which clearly contained a *v*NH band, and with the resistance of the compound towards acid hydrolysis [1]. Earlier, when structure **3** was still accepted, this resistance was explained on the basis of the observation that methylthio groups at position 4 are generally much more resistant towards acid hydrolysis than those at position 2 (*e.g.* that in compound **2**) [1].

Structure **5** could finally be proved unequivocally by synthesis of the compound melting at 313—4°C, starting with 1-methyl-2-methylthio-5,5--diphenyl-2-imidazoline-4-thione (**6**).

The question next arises as to exactly how **5** is formed in the reaction of **1** and benzylammonium chloride in the presence of pyridine, and which of the two amines present in the reaction mixture is the actual demethylating agent. Two routes, differing only in the sequenc of benzylaminolysis and *S*-demethylation, could namely lead from **1** to **5**, as shown in Scheme 1.

*Found: C 74.63, 74.60; H 5.97, 6.06; N 11.39, 11.23; S 8.06, 8.59 [1]. Calcd. for **3**, $C_{24}H_{23}N_3S$ (385.5): C 74.78; H 6.01; N 10.90; S 8.30; for $C_{23}H_{21}N_3S$ (371.4): C 74.37; H 5.70; N 11.31; S 8.62%.

**Potentially tautomeric compound. The tautomeric structure was elucidated by spectroscopic studies which will be described below.

Scheme 1

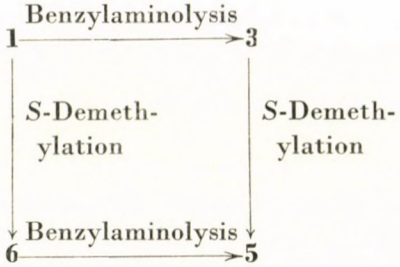

It will be shown below that **3** may indeed be prepared by benzylaminolysis of **1** under proper conditions, and *S*-demethylation of **3** may be effected as well. On the other hand, in connection with the structure proving synthesis of **5** it was seen that benzylaminolysis of **6** may also be achieved. In spite of our previous finding [2] that **1**, too, may be *S*-demethylated by pyridine, reaction sequence **1** → **6** → **5** may nevertheless be considered as to be out of question, since *S*-demethylation of **1** yields the isomeric **7** instead of **6** [2].

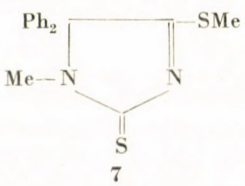

7

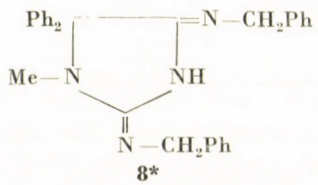

8*

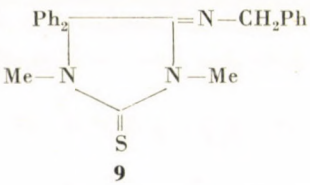

9

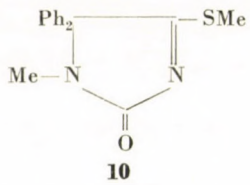

10

The question of the actual demethylation agent in the reaction **3** → **5** shall be taken up again below, after having discussed reaction **1** → **3**.

By reacting **1** and benzylamine in chloroform in the presence of the hydrochloride of the latter, a compound (m.p. 135—6°C) different from **5** was obtained which, on the basis of analytical results and its NMR spectrum, was actually identical with the desired compound, **3**. For the purpose of identification the two singlets ($\delta = 2.50$ and 2.65 ppm) in the NMR spectrum ($CDCl_3$), corresponding to the *S*- and *N*-methyl groups of the product were

*Potentially tautomeric compound, its tautomeric structure being an open question since the spectroscopic properties of its hydrochloride have only been studied.

especially of importance. Final proof for this structure assignment was obtained by synthesis. Methylation of **5** by methyl iodide furnished the compound of m.p. 135—6°C as well, and the two products obtained by different routes were found to be identical also by comparing their IR spectra.

An authentic sample of **3** being at our disposal, we could proceed to the solution of the problem as to which of the two amines present is the actual demethylating agent in the course of the synthesis of **5** achieved by reacting **1** with benzylammonium chloride in pyridine, the intermediate of this reaction being **3**, as demonstrated above. Since, when heated with pyridine in the presence of pyridinium chloride, **3** becomes demethylated to **5** while, when heated with benzylamine in the presence of benzylammonium chloride, it yields another product, it follows that in the second step of conversion **1** → **5** pyridine must be the actual demethylating agent.

For the product obtained from **3** with benzylamine, structure **8** could be deduced from its analytical data, although only the hydrochloride but not the free base could be obtained in crystalline form. The same compound results as a by-product when **1** is reacted with benzylammonium chloride in pyridine. This may be considered as further evidence for the role of **3** as an intermediate in the reaction **1** → **5**.

Spectroscopic studies

IR and NMR spectra of compounds **6** and **7** were discussed elsewhere [3, 4]. Now the results of a study of the IR and NMR spectra of the isomeric pairs **2** and **3**, and **4** and **5**, respectively, allowed not only to corroborate the gross structures of these compounds as deduced from preparative work (see above), but also to gain some information regarding the fine structures (tautomeric state, electron distribution).

Comparing the IR and NMR spectra of compounds **2** and **3**, the following conclusions could be drawn (*cf.* Tables 1 and 2):

(1) The $\nu C = N$ band appearing at higher wave numbers (1675 cm^{-1}) and being more intense in the case of **3**, may be assigned in the IR spectra of both compounds to the exocyclic C=N bond. The second $\nu C=N$ band, belonging to the endocyclic C=N bond is found at higher wave numbers in the spectrum of **3**, and it has lower intensity. Consequently, the exocyclic C=N bond must participate in the conjugation to the same degree in both isomers and, furthermore, the bond order of the endocyclic C=N bond in **2** must be less than in **3**. Thus the electronic displacement in the conjugated system towards the nitrogen atom bearing the benzyl group causes greater distortion of the electron cloud in **2** than in **3**, because the + M effects of the nitrogen and sulfur atoms in **2** mutually enhance each other, whereas in **3** they counter-act each other.

Table I

NMR Spectra

Compound	Solvent	δ [ppm]*, TMS=O				NH
		S—CH_3	N—CH_3	N—CH_2—Ph	ArH	
2	$CDCl_3$	2.80	2.65	4.9	7.1 ($PhCH_2$); 7.3 (Ph)	—
3		2.50	2.65	5.0	7.3 ($PhCH_2$ + + Ph)	—
4	DMSO—d_6	—	2.85	4.5 (d), J = 8 Hz	405—450 Hz (m)	8.85 (tr), J = 8 Hz
5		—	2.75	4.7 (s)	7.25 (s)	8.7
8·HCl	DMSO—d_6	—	2.70	4.60 and 4.70	7.20 (4-$PhCH_2$); 7.40 (2-$PhCH_2$ + + Ph)	3.45**
9	$CDCl_3$	—	2.95 and 3.50	4.25 (s)	7.30 and 400—430 Hz (m);	—

* d = doublet, m = multiplet, s = singlet, tr = triplet

** Merged with the H_2O signal due to the water content of the solvent

Table II

*IR Spectra (KBr pellets)**

Compound	νC=N [cm⁻¹]		νNH [cm⁻¹]	νC=S [cm⁻¹]
	Exo	Endo		
2	1675 s	1490 vs	—	—
3	1675 vvs	1530 vs	—	—
4	—	1610	3350—3150	1290
5	1640	—	3350—2600	1330
8·HCl	1680**	1620	3300—2600***	—
9	1690	—	—	1320

* s = strong, vs = very strong, vvs = very-very strong

** This band is, perhaps, a $\nu C=\overset{\oplus}{N}$ band

*** $\nu(>\overset{\oplus}{N}H_2)$ or $\nu(>\overset{\oplus}{N}H)$ band

(2a) The signal of the aromatic protons in the NMR spectrum of **3** appears as a singlet at $\delta = 7.3$ ppm while, in the spectrum of **2**, the same signal is split. In the latter case, namely, the aromatic ring of the benzyl group falls into the shielding zone of the two phenyl groups; therefore, its signal undergoes an upfield shift. In compound **3**, these groups are situated too far from each other, therefore, the above effect does not operate.

(2b) In contrast, it is compound **3** in whose NMR spectrum the signal of the *S*-methyl group is found shifted upfield (at 2.5 ppm as compared with 2.8 ppm in the case of **2**), the reason being the same as above.

(2c) Finally, the signal of the methylene protons is found in the spectrum of **3** to be somewhat shifted upfield as compared with the spectrum of **2.** This seems to be a consequence of the fact that the exocyclic nitrogen atom is more negatively polarized in the former compound; this is also indicated by the higher intensity of the νC=N band corresponding to the exocyclic C=N bond in the IR spectrum of **3** as compared with **2** *(cf.* (1)).

A study of the IR and NMR spectra of **4** and **5** has led to the following conclusions:

(1a) During a study of the IR spectra of 5,5-diphenyl-hydantoins and -thiohydantoins [5] it has previously been found that the presence of an NH group at position 3 leads, under participation of the electronegative atom attached to the ring at position 2, to the formation of cyclic dimeric associates which are characterized in the IR spectra by broad diffuse νNH bands considerably extending towards lower wave numbers [6]. The νNH band extending from 3350 to as low as 2600 cm^{-1} in the IR spectrum of **5** has exactly these properties, while the spectrum of **4** has a less diffuse νNH band at somewhat higher wave numbers, in the region of 3350—3150 cm^{-1}, characteristic for simple intermolecular association. The NH group, threrefore, may be presumed to occupy an exocyclic position in compound **4** and an endocyclic position in compound **5.** Thus, **4** and **5** should exist, in crystalline state, in form of the 3-imidazoline-2-thione and imidazolidine-4-thione tautomer, respectively.

(1b) The νC=N and νC=S bands in the spectrum of **4** are found at lower wave numbers than in that of **5** (at 1610 and 1290 cm^{-1} as compared with 1640 and 1330 cm^{-1}, respectively); this fact well corroborates the above conclusion.

(1c) The suggested tautomeric structure of compound **4** is further corroborated by the IR spectrum of the known [1] compound **9** (in the cited paper: **XI**), whose imidazolidine-2-thione structure is certain; in the IR spectrum of the latter compound the νC=N and νC=S bands are found at 1680 and 1320 cm^{-1}.

(2a) According to the NMR spectra obtained in DMSO-d_6, the tautomeric structures do not change even on dissolution. This may be concluded from the fact that, in the spectrum of **5**, both the CH_2 and ArH signals appear as singlets (at $\delta = 4.7$ and 7.25 ppm, respectively) while in the spectrum of **4** the methylene peak is split into a doublet ($\delta = 4.5$ ppm; $J = 8$ Hz); in the latter case the ArH signal appears as a multiplet. The doublet splitting of the CH_2 signal is caused by spin-spin coupling with the NH proton and, as a consequence, the signal of the latter, too, appears as a triplet ($\delta = 8.7$ ppm; $J = 8$ Hz). The downfield shift of the CH_2 signal in the case of compound **5** as com-

pared with its position in the case of compound **4** is, of course, caused by the neighbouring C=N group. The multiplet structure of the ArH signal in the spectrum of compound **4** is caused by the shielding effect of the phenyl groups at position 5 exerted on the 4-benzyl group (*cf.* the NMR spectrum of compound **2**, discussed above).

(2b) In compound **5** the deshielding effect of the aromatic ring of the benzyl group exerted on the 1-methyl group may be observed, as a consequence of which the signal of the latter is shifted upfield in comparison with the signal of the same group in compound **4** (δ = 2.75 and 2.85 ppm, respectively).

Experimental

The IR spectra were obtained in KBr pellets with a Spectrometer of Type UR-10 (Carl Zeiss, Jena, GDR); the NMR spectra were recorded at 60 MHz with a JNM-C-60 Spectrometer (Japan Electron Optics Laboratories, Tokyo) using TMS as internal standard. All m.p.'s are uncorrected.

Reaction of 3-methyl-2,5-bis(methylthio)-4,4-diphenyl-4*H*-imidazol-3-ium(1) methosulfate with benzylammonium chloride in pyridine

The reaction was performed as described earlier [1] but, in order to facilitate the isolation of the by-products (which previously were discarded), sixfold quantities of the reactants were used, *i.e.* the experiment was made with 5.25 g (12 mmoles) of 1-methosulfate. The crude **5** obtained (which previously had been believed to be **3**, see page 87) was, according to its IR spectrum, contaminated with **10**, the partial hydrolysis product [1] of **1**. In order to remove this contaminant, the crude product was extracted with a small quantity of hot *n*-propanol in which **5** is much less soluble than **10**. According to its m.p. (313—4°C, from a mixture of pyridine and ethanol), mixed m.p., and IR spectrum, the purified product proved to be identical with authentic **5** (see below).

By diluting the aqueous pyridine mother liquor of **5** with further 100 ml of water, 0.65 g of crude **8** · HCl was precipitated. This product was purified by reprecipitating it from its solution in 10 ml *n*-propanol with 10 ml of ether to obtain 0.45 g (8.4%) of pure **8** · HCl, m.p. 301°C (dec.), which by mixed m.p. and IR spectrum proved to be identical with an authentic sample (see below).

1-Methyl-2-methylthio-5,5-diphenyl-2-imidazoline-4-thione (6)

6 may be obtained as a minor by-product in the methylation of 1-methyl-5,5-diphenyldithiohydantion [7] if the prescription given below is strictly followed.

A solution of 1-methyl-5,5-diphenyldithiohydantoin (10 g; 35 mmoles) in acetone (150 ml) is mixed with an aqueous (10 ml) solution of K_2CO_3 (5.0 g; 36 mmoles). To the heterogeneous mixture obtained, a solution of methyl iodide (2.3 ml; 37 mmoles) in acetone (3 ml) is added in portions under continuous shaking within about 5 min. A bright yellow homogeneous solution is obtained, which soon begins to deposit yellow plates. (The crystals proved to be identical with the known [7] **7**.) 15 min. after the methylation has been started, the mixture is diluted with water (100 ml), shaken for 2 min. and subsequently the crystals are filtered off and washed first with aqueous acetone (50 ml; 1 : 1 v/v) and then with water (60 ml). The washings should be thoroughly removed by pressing the crystals on the Büchner funnel. The wet product is then boiled for a few min. with methanol (50 ml) and the insoluble material immediately filtered off and washed with 10 ml of hot methanol. This material proved to be a mixture (9.0 g; 82.4%) of the isomers — **7** and 1,3-dimethyl-5,5-diphenyldithiohydantoin [7] — of the desired **6**.

The methanolic filtrate is combined with the original aqueous acetonic filtrate and the aqueous washings, diluted with 50 ml of water, and extracted with three 10-ml and three 5-ml portions of chloroform. The gummy residue, obtained on drying the chloroform solution and evaporating the solvent, is dissolved in warm ethanol (10 ml). After some standing bright yellow crystals will start to precipitate; the mother liquor is sucked off while still warm (50°C), and the crystals are washed with 4 ml of warm ethanol. The crude product (0.40 g) is finally recrystallized from ethanol (18 ml) to yield 0.29 g (2.7%) of **6**, m.p. 204°C.

$C_{17}H_{16}N_2S_2$ (312.40). Calcd. C 65.37; H 5.16; N 8.97; S 20.49. Found C 65.20; H 5.17; N 8.81; S 20.21%.

The structure of the product follows, besides its analysis, from its IR spectrum and its non-identity with the two other isomers (see above) also formed on methylation of 1-methyl-5,5-diphenyldithiohydantoin.

2-Benzylimino-1-methyl-5,5-diphenyl-4-imidazolidinethione (5)

(a) *Authentic sample:* A mixture of **6** (44.2 mg; 0.142 mmoles), benzylamine (0.03 ml; 0.275 mmoles), benzylammonium chloride (1 mg; 7 μmoles) and dry ethanol (5 ml) was refluxed for 5 hrs. The product was precipitated in crystalline form by the addition of 2 ml of water, filtered off, and washed with water and then with methanol to yield 40 mg (76%) of a product, m.p. 314°C, which by mixed m.p. and IR spectrum proved to be identical with a product previously prepared [1] from **1** with benzylammonium chloride and pyridine and erroneously believed to possess structure **3** (in the cited paper: **V**). For the analysis results, see footnote* on p. 88.

(b) A mixture of **3** (1.0 g; 2.6 mmoles), pyridinium chloride (1.0 g; 8.7 mmoles) and pyridine (6 ml) was refluxed for 3 hrs. and then concentrated to about 3 ml. Water (10 ml) was then added to precipitate 0.80 g (83%) of **5** as a yellow product, m.p. 312°C. The IR spectrum proved that this substance was identical with the sample prepared according to (a).

2-Benzylimino-1-methyl-4-methylthio-5,5-diphenyl-3-imidazoline (3)

(a) A mixture of **1**-methosulfate (12.5 g; 28.6 mmoles), benzylammonium chloride (0.3 g; 2 mmoles), benzylamine (3.2 g; 30 mmoles) and dry chloroform (20 ml) was slowly heated to its b.p. and then refluxed for 6 hrs. The residue, obtained on evaporation of the solvent and volatile materials, was washed by thoroughly shaking it twice with 15-ml portions of water and then with 20 ml of 6% aqueous KOH. Finally, it was dissolved in 10 ml of hot methanol. After the addition of 1 ml of water, the product slowly crystallized to yield 6.2 g (56%) of **3**, m.p. 135°C (from aqueous methanol).

$C_{24}H_{23}N_3S$ (385.51); Calcd. C 74.78; H 6.01; N 10.90; S 8.30. Found C 74.94; H 5.54; N 10.79; S 8.24%.

(b) *Authentic sample:* A solution of **5** (0.40 g; 1.1 mmole) in *n*-propanol (90 ml) was mixed with methyl iodide (0.5 ml; 8.3 mmoles) and an aqueous (5 ml) solution of K_2CO_3 (0.30 g; 2.2 mmoles), and allowed to stand for 3 days. The mixture was then filtered, the filtrate evaporated to dryness, and the residue extracted, after the addition of 5 ml of water, with three 3-ml portions of chloroform. After evaporation of the solvent, the residue was dissolved in methanol (1 ml). On the addition of 2 ml of water the product (0.20 g; 48% of **3**) precipitated in crystalline form, m.p. 132—3°C. By mixed m.p. and IR spectrum it proved to be identical with the substance prepared according to (a).

2,4-Di(benzylimino)-1-methyl-5,5-diphenylimidazolidine* hydrochloride (8 · HCl)

(a) *Authentic sample:* A mixture of **3** (1.0 g; 2.6 mmoles), benzylamine (1.5 ml; 14 mmoles) and benzylammonium chloride (0.50 g; 3.5 mmoles) was heated for 25 hrs. at 120°C in a sealed tube. After being allowed to cool, the mixture was diluted with ether (10 ml) and the crystalline product filtered off, washed with ether and then with water to yield 1.2 g (97%) of **8** · HCl, m.p. 301°C (dec., from a mixture of methanol and ether).

*The tautomeric structure was not investigated.

$C_{30}H_{28}N_4 \cdot HCl$ (481.04). Calcd. C 74.90; H 6.08; Cl 7.37; N 11.65. Found C 74.86; H 6.34; Cl 7.64; N 11.38%.

The non-crystalline base may be liberated from the hydrochloride by silver oxide.

(b) A mixture of **1**-methosulfate (2.0 g; 4.6 mmoles), benzylamine (6 ml; 55 mmoles) and benzylammonium chloride (0.80 g; 5.6 mmoles) was refluxed for 10 hrs. During this period colourless plates were gradually deposited from the originally homogeneous solution. After being allowed to cool, the thick crystalline paste obtained was diluted with ether (15 ml) and then treated as described under (a) to obtain 2.2 g (100%) of **8** · HCl, m.p. 299°C (dec.) which, by mixed m.p. and IR spectrum, proved to be identical with the product prepared according to (a).

*

Acknowledgement: The authors wish to express their gratitude to Miss K. Ófalvi, Mrs. S. Viszt-Simon and Mrs. I. Zauer-Csüllög for the microanalyses.

REFERENCES

1. Lempert, K., Zauer, K.: Acta Chim. Acad. Sci. Hung. **47,** 391 (1966)
2. Lempert, K., Zauer, K.: Acta Chim. Acad. Sci. Hung. **50,** 303 (1966)
3. Sohár, P., Nyitrai, J., Zauer, K., Lempert, K.: Acta Chim. Acad. Sci. Hung. **58,** 165 (1968)
4. Sohár, P., Nyitrai, J., Zauer, K., Lempert, K.: Acta Chim. Acad. Sci. Hung.,accepted for publication
5. Sohár, P.: Acta Chim. Acad. Sci. Hung. **57,** 425 (1968)

6a. Sohár, P.: Acta Chim. Acad. Sci. Hung. **54,** 91 (1967)
6b. Sohár, P.: Magyar Kém. Foly. **71,** 415 (1965)
6c. Sohár, P., Varsányi, Gy.: Spectrochim. Acta **23A,** 1947 (1967)

7. Carrington, H. C., Waring, W. S.: J. Chem. Soc. [London] **1950,** 354

Károly Lempert; Budapest XI., Gellért tér 4.
Pál Sohár; Budapest IV., Szabadságharcosok útja 47—49.
Károly Zauer; Budapest XI., Gellért tér 4.

Acta Chimica Academiae Scientiarum Hungaricae, Tomus 63, (1) pp. 97—105 (1970)

1,5-DIKETONES, V*

CATALYTIC REDUCTION OF SOME 2-(1-ACETYLPROPYL)-BENZOPHENONES

M. LEMPERT-SRÉTER

(Institute of Organic Chemistry, L. Eötvös University, Budapest)

Received January 10, 1969

On catalytic reduction of 2-(1-acetylpropyl)-5,4′-diacetoxy-4,3′-dimethoxy-benzophenone(**1**) a loose 1 : 1 molecular compound of 2-(1-acetylpropyl)-5,4′-diacetoxy-4,3′-dimethoxy-diphenylmethane (**2**) and 2-(1-ethyl-2-hydroxypropyl)-5,4′-diacetoxy-4,3′-dimethoxy-diphenylmethane (**3**) is obtained. Under the same conditions, other 2-(1-acetylpropyl)-benzophenones (**6** and **15**) yield only reduction products analogous to **2**.

2 is not an intermediate of the transformation **1** → **3**, since it is the aliphatic ketone group of **1** which is first reduced, under formation of **14**, whose aromatic ketone group is subsequently reduced to yield **3**.

On catalytic reduction at room temperature in the presence of a palladium/charcoal catalyst in acetic acid or ethanol solution, 2-(1-acetylpropyl)-5,4′-diacetoxy-4,3′-dimethoxy-benzophenone (**1**) [1] takes up, according to the results of microhydrogenations, about 2.5 moles of hydrogen whereafter the addition of hydrogen abruptly stops. The product (**A**) could be reconverted into **1** by chromic acid oxidation, but, as shown by its IR and NMR spectra as well as by its thin layer chromatogram, in spite of the sharp melting point, it proved to be a mixture of two substances.

Direct resolution of **A** into its components by either fractional crystallization or by column chromatography could not be achieved, therefore, an indirect procedure had to be chosen. On deacetylating **A** by ethanolic sodium hydroxide, a crystalline (**5**) and an oily fraction (**4**) was obtained. Acetylation of the oily fraction yielded the diacetyl derivative of **4** which, as shown by its IR and NMR spectra as well as its TLC, was identical with one of the components (**2**) of **A**. The crystalline fraction (**5**), on the other hand, according to its elemental composition and its IR and NMR spectra proved to be a trihydroxy compound (see page 98).

Two of the three hydroxyl groups had to be, in view of the formation of **2** from **1**, phenolic hydroxyl groups, while the third one proved to be alcoholic. The second component (**3**) of **A**, therefore, must have been the derivative of **5** acetylated on its phenolic hydroxyl groups. In fact, by selective acetylation of the phenolic hydroxyl groups of **5**, **3** could be successfully prepared and

*Part IV. LEMPERT-SRÉTER M., BÁRDY, M.: Acta Chim. Acad. Sci. Hung. **57**, 181 (1968)

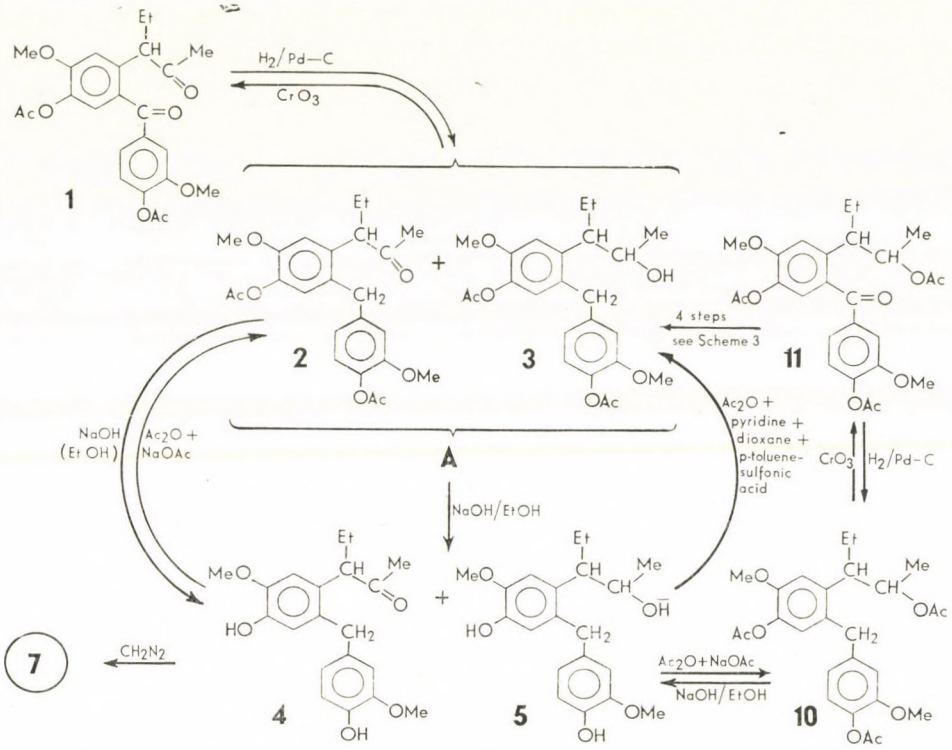

the product, according to its IR and NMR spectra as well as its TLC, proved to be identical with the second component of **A.**

The possibility of selective acylation of phenolic hydroxyl groups in the presence of alcoholic hydroxyl groups seemed quite promising in view of the kinetic investigations of MESNARD and BERTUCAT [2] according to which phenolic hydroxyl groups are acetylated thirty to sixty times faster than alcoholic ones when the acetylation is performed with acetic anhydride in a dioxane—pyridine mixture in the presence of *p*-toluenesulfonic acid. Therefore, **5** was reacted with acetic anhydride under the conditions stated above and the progress of the reaction was followed as a function of time. No phenolic hydroxyl could be detected with ferric chloride after a few minutes, nevertheless, according to the IR spectrum of the isolated product, esterification at the aliphatic hydroxyl group had not yet started.

The structure of **2** was corroborated by its transformation by deacetylation and subsequent methylation into **7**, which was prepared also by catalytic reduction (in acetic acid or ethanol solution at room temperature, in the presence of a palladium/charcoal catalyst) of 2-(1-acetylpropyl)-4,5,3′,4′-tetramethoxybenzophenone (**6**) [3].

The product obtained by catalytic reduction of **6** was previously [5] thought to possess the isochromane skeleton and to be, consequently, a stereo-

isomer of the isochromane (**9**) prepared with lithium aluminium hydride and subsequent catalytic reduction of the isobenzopyrylium salts (**8**) obtained by a treatment of **6** with mineral acids [4]. However, according to its IR spectrum, **6** contains an aliphatic ketonic carbonyl group and reacts with dinitrophenylhydrazine and gives a positive iodoform test.

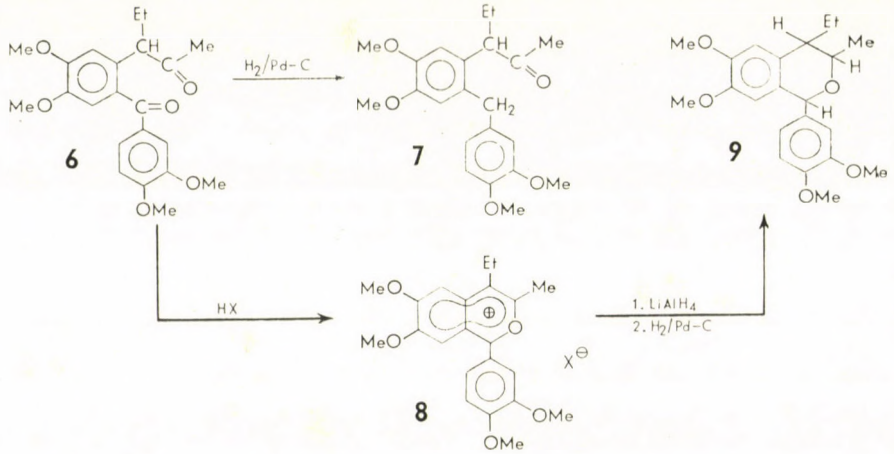

In the presence of sodium acetate, all hydroxyl groups of **5** undergo acetylation by acetic anhydride and **10** is obtained. Alkaline hydrolysis reconverts **10** into **5**; on chromic acid treatment the methylene group activated by the two neighbouring phenyl groups is oxidized to a carbonyl group and **11** is obtained. Catalytic reduction of **11** leads to **10.**

In spite of the facts that the IR and NMR spectra of **A** are the superpositions of those of its components, and that in the TLC of **A** its components migrate separately, **A** is a loose molecular associate of its components, as

Table I

Melting points of **A** *and its components*

2		124—125°C
2 + **A**	(2 : 1)	118—122°C
	(1 : 1)	115—124°C
	(1 : 2)	108—122°C
A		137—138°C
A + **3**	(2 : 1)	123—135°C
	(1 : 1)	129—134°C
	(1 : 2)	131—136°C
3		138—140°C
2 + **3**	(1 : 1)	118—127°C

may be deduced from its melting characteristics. **A** shows namely a melting point depression with either one of its components and, on the other hand, the melting point of a thoroughly ground 1 : 1 mixture of **2** and **3** differs from that of **A** (*cf.* Table I).

When, however, an equimolecular mixture of **2** and **3** was recrystallized from ethanol, a product with a sharp melting point, equal to that of **A**, was obtained.

An important observation concerning the formation of **A** is that, even under more drastic conditions than used during its preparation, **A** cannot be induced to add more hydrogen, and that, in accordance with this, **2** cannot be reduced catalytically to **3.** This observation suggests that, in the course of transformation **1** → **3**, first the aliphatic carbonyl group of **1** is reduced to a carbinol group and it is only subsequently that the aromatic carbonyl group of compound **14** thus obtained is reduced to a methylene group. The correctness of this assumption has been proved by studying the behaviour of **14** during catalytic reduction (*cf.* below).

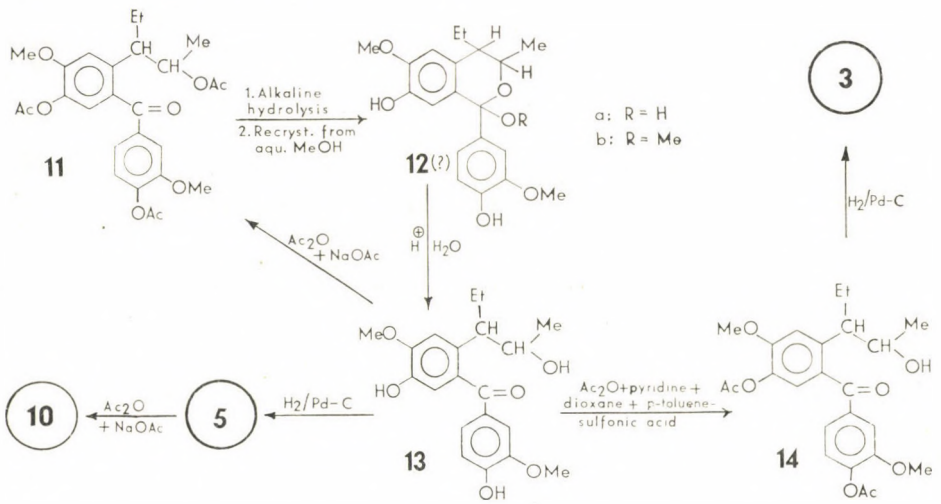

In order to prepare **14**, **11** was deacetylated by alkaline hydrolysis and the product recrystallized from aqueous methanol containing some hydrochloric acid.* Its elemental composition and IR spectrum proves structure

*When the aqueous methanol used for recrystallization did not contain acid, colourless crystals were obtained which turned pink on standing and had no sharp melting point even after repeated recrystallization. Since no carbonyl band was found in its IR spectrum, the product could not be identical with the expected **13**; it could, however, be transformed into **13** by recrystallization from aqueous methanolic hydrochloric acid. The precursor of **13**, therefore, was assumed to be identical with the cyclohemiacetal **12b** or its methylacetal **12a**, or their mixture. The wide melting point range and the diverging analytical data prevented a conclusive elucidation of the structure.

13 for the product. This structure was confirmed by the observation that upon acetylation, **13** is reconverted into **11.** By the method mentioned above, **13** was selectively acetylated at its phenolic hydroxyl groups to yield **14.**

Both **14** and the phenolic **13** could be reduced catalytically to yield **3** and **5,** respectively; the latter was identified as the totally *O*-acetylated derivative (**10**).

Surprisingly, the tetramethoxy analogue (**6**) [3] of **1,** on catalytic reduction, yielded exclusively **7,** the analogue of **2** (in about 60% yield) and, according to their IR spectra, the uncrystallizable oily byproducts did not contain a hydroxyl group either, *i.e.* a compound analogous to **3.** Similarly, on catalytic reduction of 2-(1-acetylpropyl)-4,5,4′-trimethoxybenzophenone (**15**) [6] only the monoketone analogues of **2** and **7** could be obtained. That in the case of **1** — as contrasted to those of **6** and **15** — the aliphatic carbonyl group can effectively compete with the aromatic one during catalytic hydrogenation, may perhaps be a consequence of the enhanced reactivity of the former and not of the decreased reactivity of the latter. Experiments to test the correctness of this hypothesis are in progress.

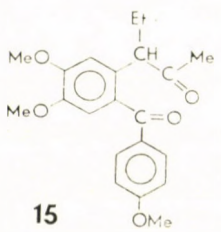

15

Experimental*

Catalytic reduction of 2-(1-acetylpropyl)-5,4'-diacetoxy-4,3'-dimethoxybenzophenone (1) [1

A suspension of **1** (6.0 g; 13.6 mmoles) in ethanol (400 ml) was hydrogenated at room temperature and 1 atm. in the presence of a 10% palladium/charcoal catalyst. Hydrogen absorption stopped after about 5—6 hrs., during which period a clear solution was formed. The catalyst was removed, the solution evaporated to dryness and the residue crystallized from ethanol to yield 4.9 g (84%) of colourless crystals of **A,** m.p.: 137—138°C.

$C_{24}H_{28}O_7 + C_{24}H_{30}O_7$ (858.9). Calcd. C 67.12; H 6.80. Found C 67.35; H 6.85%.

IR (KBr pellet): νOH: 3560, νCO: 1770 (phenyl ester) and 1715 cm^{-1} (weak, aliphatic ketone).

The NMR spectrum** of **A** contains all signals present in those of **2** and **3.**

Intensity ratios	*Found*	*Calculated for* 1 : 1 *composition*
CH_3OAr or CH_3COO : CH_3CO	28 : 7	4 : 1
CH_3OAr or CH_3COO : OH	28 : 2,5	12 : 1
$ArCH_2Ar$: CH_3CO	10 : 7	4 : 3

The same product was obtained when the reduction was performed in acetic acid solution.

*M.p.-s are uncorrected
**For the NMR spectra, *cf.* Table II

Chromic acid oxidation

A mixture of CrO_3 (0.3 g; 3 mmoles), water (0.5 ml) and acetic acid (2 ml) was added dropwise to a solution of **A** (0.5 g; 1.2 mmole) in acetic acid (10 ml) placed in an ice bath. The oxidation mixture was allowed to stand for a few hours at room temperature and then poured into water and extracted with benzene. The benzene solution was washed until neutral, dried and evaporated to dryness. The residue was recrystallized from ethanol to yield 0.18 g (30%) of **1** [1] identified by its IR spectrum, its m.p. (178—80°C) and the mixed m.p. determination with an authentic sample.

Deacetylation of A

A mixture of **A** (4.2 g; 10 mmoles) ethanol and 20% aqueous NaOH (14 ml each) was heated for 1 hr. on a steam bath and concentrated to about half of its original volume. Water (15 ml) was added and the solution acidified by the addition of aqueous HCl. The oily precipitate was dissolved in ether, the solution dried over $MgSO_4$ and evaporated to dryness. The oily residue was dissolved in the minimum amount of ether; a small amount of petroleum ether was added and the solution was allowed to stand overnight in a refrigerator. The crystalline precipitate was collected and recrystallized from aqueous methanol to yield 1.8 g (52%) of **5,** m.p. 136—137°C (turning red).

$C_{20}H_{26}O_5$ (346.4). Calcd. C 69.34; H 7.56%. Found C 69.15; H 7.26%.

IR: νO—H 3450 (broad); νC=O ø

The oily residue (1.15 g; 34%) of the mother liquor of crude **5** consisted of almost pure **4** contaminated with traces of **5.**

2-(1-Acetylpropyl)-5,4'-diacetoxy-4,3'-dimethoxy-diphenylmethane (2)

Crude **4** (0.3 g; 0.87 mmole) prepared as described above was acetylated with acetic anhydride and sodium acetate. The crude **2** which, according to its IR spectrum, contained some **10** (originating from **5** which contaminated the starting material) was purifed by repeated recrystallization from methanol to yield 0.18 g (48.5%) of **2,** m.p. 124—125°C.

$C_{24}H_{28}O_7$ (427.5). Calcd. C 67.27; H 6.59; O 26.14. Found C 67.27; H 6.65; O 26.25%.

IR: νC=O 1770 (phenyl ester) and 1710 (aliphatic ketone).

NMR spectrum: *cf.* Table II

2,4-*Dinitrophenylhydrazone*, m.p. 109—111°C (from ethyl acetate)

$C_{30}H_{32}O_{10}N_4$ (608.6). Calcd. C 59.20; H 5.30; N 9.20. Found C 59.14; H 5.65; N 8.98%.

Partial and total acetylation of 2-(1-ethyl-2-hydroxypropyl)-5,4'-dihydroxy-4,3'-dimethoxy-diphenylmethane (5)

a) 16 ml of an acetylation mixture (prepared from 7.5 ml acetic anhydride, 16 ml of dry dioxane and 0.5 g of *p*-toluenesulfonic acid) were added to a solution of **5** (0.8 g; 2.3 mmoles) in dry pyridine (8 ml). The initially positive colour spot test with ferric chloride turned negative after allowing the mixture to stand for 3 minutes at room temperature. At this moment the mixture was poured into water and the crystalline precipitate was recrystallized from methanol to yield 0.56 g (57%) of **3,** m.p. 138—140°C.

$C_{24}H_{30}O_7$ (430.5). Calcd. C 66.95; H 7.03; O 26.01. Found C 66.78; H 7.05; O 26.09%.

IR : νO—H 3565, νC=O 1760 (phenyl ester).

NMR spectrum: *cf.* Table II.

b) **5** (0.6 g; 1.7 mmoles) was acetylated with acetic anhydride and sodium acetate and the product recrystallized from aqueous methanol to yield 0.72 g (90%) of **10,** m.p. 128—130°C.

$C_{26}H_{32}O_8$ (472.5). Calcd. C 66.09; H 6.83; O 27.10. Found C 66.24; H 6.73; O 26.95%.

IR: νC=O 1735 (aliphatic ester), 1770 (phenyl ester)

NMR spectrum: *cf.* Table II.

The same product was obtained by heating **5** with the acetylation mixture described under *a)* for 10 minutes on a steam bath.

2-(1-Acetylpropyl)-4,5,3',4'-tetramethoxy-diphenylmethane (7)

a) **2** (0.15 g; 0.35 mmole) was deacetylated by refluxing with ethanolic sodium hydroxide. Water was added and the product extracted with ether. The solution was dried and treated with an ethereal diazomethane solution. The methylated product was recrystallized from aqueous methanol to yield 0.1 g (74%) of **7**, which was identified by m.p., IR and mixed m.p. with an authentic sample of **7** prepared according to *b)*.

b) By reduction of 2-(1-acetylpropyl)-4,5,3',4'-tetramethoxybenzophenone **(6)** [3]

6 (1.0 g; 2.6 mmoles), dissolved in ethanol (90 ml) was reduced at room temperature and 1 atm. in the presence of a 10% palladium/charcoal catalyst. During a period of about 1 hr. 121 normal ml (5.3 mmoles) of hydrogen was consumed. The catalyst was removed, the filtrate evaporated to dryness and the residue recrystallized from methanol to yield 0.57 g (59%) of **7**, m.p. 94—95°C.

C_{22} $H_{28}O_5$ (372.4). Calcd. C 71.00; H 7.52. Found C 71.28; H 7.58%.

IR: νC=O 1705.

The product gave a positive iodoform test.

2,4-*Dinitrophenyl hydrazone*, m.p. 161—162°C (from an ethanol–ethyl acetate mixture). $C_{28}H_{32}N_4O_8$ (552.6). Calcd. N 10.01. Found N 9.88%.

Reactions of 2-(1-ethyl-2-acetoxypropyl)-5,4'-diacetoxy-4,3'-dimethoxydiphenylmethane (10)

a) Deacetylation of **10** by ethanolic NaOH gives **5**, mp. and mixed m.p. 135—137°C.

b) Oxidation of **10** (0.3 g; 0.64 mmole) with CrO_3 in acetic acid gave 0.15 g (48.5%) of **11**, m.p. 138—139°C (from methanol).

$C_{26}H_{30}O_9$ (486.5). Calcd. C 64.19; H 6.22; O 29.6. Found C 64.16; H 6.16; O 29.34%.

IR: νC=O 1780 (phenyl ester), 1730 (aliphatic ester), 1670 (aromatic ketone).

NMR spectrum: *cf.* Table II.

Upon catalytic reduction in ethanol solution in the presence of a palladium/charcoal catalyst, **11** was reconverted into **10.**

2-(1-Ethyl-2-hydroxypropyl)-5,4'-dihydroxy-4,3'-dimethoxybenzophenone (13)

A mixture of **11** (0.48 g; 1 mmole) with ethanol and 20% aqueous NaOH (2.5 ml each) was refluxed for 1 hr. The solution turned bright red after a few minutes. It was poured into water, treated with charcoal and acidified with aqueous HCl. The oily red precipitate (0.35 g) was extracted with ether and recrystallized from dilute aqueous methanol, containing some HCl, to yield 0.14 g (40%) of **14**; cream coloured crystals, m. p. 139—141°C.

$C_{20}H_{24}O_6$ (360.4). Calcd. C 66.65; H 6.71. Found C 66.25, 66.55; H 6.60, 6.90%.

IR: νO—H 3600—2600; νC=O 1630 (aromatic ketone).

Acetylation of the product with acetic anhydride and sodium acetate reconverted it into **11,** which was identified by m.p., mixed m.p. and IR spectrum.

When the original red oil obtained by extraction with ether was recrystallized from aqueous methanol containing no HCl, 0.2 g of colourless crystals (presumably a mixture of **12a** and **b**), melting range 120—145°C, were obtained, which turned pink on standing. This product, when recrystallized from aqueous methanol containing HCl, was converted into **14** described above.

Reactions of 2-(1-ethyl-2-hydroxypropyl)-5,4'-dihydroxy-4,3'-dimethoxybenzophenone (13)

a) Partial acetylation

A solution of **13** (0.2 g; 0.55 mmole) in pyridine (4 ml) was treated for 3 min at room temperature with an acetylation mixture (4 ml) described on p. 102. When the mixture was poured into water, 0.15 g (62%) crude **14** was obtained in the form of a colourless precipitate, m.p. 191—193°C (first from dil. acetic acid and then from ethyl acetate).

$C_{24}H_{28}O_8$ (444.5). Calcd. C 64.85; H 6.35. Found C 64.52; H 6.47%.

IR : νO—H 3485 (aliphatic), νC=O 1760 (phenyl ester).

b) Catalytic reduction

13 (0.04 g; 0.11 mmole) dissolved in ethanol (10 ml) was hydrogenated in the presence of a palladium/charcoal catalyst at room temperature. The product (**5**) obtained on evaporation of the filtrate to dryness was acetylated with acetic anhydride and sodium acetate, and identified in the form of **10** by m.p., mixed m.p. and IR spectrum.

Table II

NMR spectra (in $CDCl_3$*)*
δ values (in ppm), internal reference: TMS

Group \ Compound	2*	3**	10**	11**
CH_3-CH_2 (triplet, J = 12 Hz)	0.75 ppm	0.6 ppm	0.6 ppm	0.7 ppm
$CH_3CH<^{OAc}$ (doublet, J = 12 Hz)	—	—	0.9 ppm	1.05 ppm
$CH_3-CH<^{OH}$ (doublet, J = 12 Hz)	—	0.95 ppm	—	—
$CH_3-C<^{O}$	1.8 ppm	—	—	—
$CH_3-C<^{O}_{O}$ aliph.	—	—	2.05 ppm	1.95 ppm
$CH_3-C<^{O}_{O}$ arom.	2.3 ppm	2.3 ppm	2.25 ppm	2.20 + 2.25 ppm
CH_3OAr	3.75 ppm	3.7 + 3.8 ppm	3.65 + 3.70 ppm	3.75 + 3.80 ppm
$Ar-CH_2Ar$	4.0 ppm	3.95 ppm	3.9 ppm	—
Ar—H	400—420 Hz	390—420 Hz	390—420 Hz	410—450 Hz
Intensity ratio	3 : 3 : 6 : 6 : 2 : 5	3 : 3 : 6 : (3 + 3) : 2 : 5	3 : 3 : 3 : 6 : (3 + 3) : 2 : 5	3 : 3 : 3 : (3 + 3) : : (3 + 3) : 5

* The signals of the methine group and of the methylene protons of the ethyl group could not be identified
** The signals of the two methine protons and of the methylene protons of the ethyl group could not be identified

Catalytic reduction of 2-(1-ethyl-2-hydroxypropyl)-5,4'-diacetoxy-4,3'-dimethoxybenzophenone (14)

A suspension of **14** (0.04 g; 0.09 mmole) in ethanol (10 ml) was hydrogenated at room temperature in the presence of a palladium/charcoal catalyst. The product (**3**) dissolved as soon as it formed and, after removing the catalyst, was isolated by evaporation to dryness and recrystallization from aqueous methanol. It was identified by m.p. (138—140°C), mixed m.p. and IR spectra.

Reduction of 2-(1-acetylpropyl)-4,5,4'-trimethoxy-benzophenone (15) [6]

A suspension of **15** (1.37 g; 3.8 mmoles) in ethanol (30 ml) was hydrogenated in the presence of a 10% palladium /charcoal catalyst. After 170 normal ml (7.6 mmoles) of hydrogen had been consumed, the catalyst was removed and the filtrate evaporated to dryness to yield 2-(1-acetylpropyl)-4,5,4'-trimethoxy-diphenylmethane, which resisted all attempts of crystallization.

IR: νC=O 1710 (aliphatic ketone)

Iodoform test positive.

2,4-*Dinitrophenylhydrazone*, m.p. 181—183°C (from an ethanol–ethyl acetate mixture)

$C_{27}H_{30}N_4O_7$ (522.5). Calcd. N 10.72. Found N 10.55%.

*

The author is indebted to Mrs. A. FARAGÓ for her valuable assistance in performing the experiments, to the microanalytical division of the Institute (Head: Mrs. H. MEDZIHRADSZKY-SCHWEIGER) for the microanalyses, to Dr. F. RUFF for recording the IR spectra and to Dr. P. SOHÁR for recording and interpretation of the NMR spectra.

REFERENCES

1. MÜLLER, A., HORVÁTH, A.: Chem. Ber. **76,** 855 (1943)
2. MESNARD, P., BERTUCAT, M.: Boll. Chim. Farm. **101,** 519 (1962); Chem. Abstr. **59,** 1513 (1963)
3. DOERING, W. von E., BERSON, J. A.: J. Am. Chem. Soc. **72,** 1118 (1950)
4. MÜLLER, A., SZABÓ, L.: Chem. Ber. **77,** 6 (1944)
5. MÜLLER, A., LEMPERT-SRÉTER, M., KARCZAG-WILHELMS, A.: J. Org. Chem. **19,** 1533 (1954)
6. LEMPERT-SRÉTER, M., MÜLLER, A.: Acta Chim. Acad. Sci. Hung. **41,** 451 (1964)
7. LEMPERT-SRÉTER, M., BÁRDY, M.: Acta Chim. Acad. Sci. Hung. **57,** 181 (1968)

Magda LEMPERT-SRÉTER; Budapest VIII., Múzeum krt. 4/b.

Acta Chimica Academiae Scientiarum Hungaricae, Tomus 63 (1), pp. 107—110 (1970)

ÜBER DIE OXYDATION VON SYMMETRISCHEN PYRIDYL-3-THIOÄTHERN ZU SULFOXIDEN UND SULFONEN

(VORLÄUFIGE MITTEILUNG)

W. GÖBEL und H. J. KÖNIG

(Sektion Chemie, Bereich Technische Chemie, der Technischen Universität Dresden, DDR)

Eingegangen am 3. Januar 1969

Durch Oxydation von Pyridyl-3-thioäthern mittels Wasserstoffperoxid oder Benzopersäure unter milden Reaktionsbedingungen sind die Pyridyl-3-sulfoxide, die bisher in der Literatur noch nicht beschrieben wurden, zugänglich. Werden die Thioäther schärferen Reaktionsbedingungen ausgesetzt, so können mittels Wasserstoffperoxid in Eisessig oder technischer Natriumhypochloritlösung im alkalischen Medium die entsprechenden Sulfone erhalten werden.

Pyridyl-2- bzw. -4-sulfoxide und -sulfone wurden in der Literatur bereits beschrieben; Pyridyl-3-sulfoxide und Dipyridyl-3,3'-disulfone sind aber noch nicht bekannt. Die dargestellten Verbindungen werden zur Zeit auf ihre biologische Wirksamkeit untersucht. Über die als Ausgangsprodukte für die zuletzt genannten Verbindungen geeignet erscheinenden Thioäther 1,5-Bis-(pyridyl-3-thio)-pentan (**I**), 2,2'-Bis-(pyridyl-3''-thio)-diäthylsulfid (**II**) und 2,2'-Bis-(pyridyl-3''-thio)-diäthylamin (**III**) wurde von uns kürzlich berichtet [1].

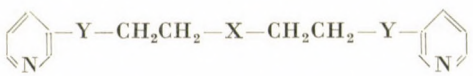

Thioäther (Y=S): **I:** X=CH_2; **II:** X=S; **III:** X=NH
Sulfoxide (Y=SO): **Ia:** X=CH_2; **IIa:** X=SO; **IIIa:** X=NH
Sulfone (Y=SO_2): **Ib:** X=CH_2; **IIb:** X=CH_2; **IIIb:** X=NH

Das Verfahren zur Darstellung von Sulfoxiden, das von SHRINER, STRUCK und JORISON [2] beschrieben wurde, erweist sich auch als geeignet zur Darstellung von Pyridyl-3-sulfoxiden. Danach wird der in Azeton gelöste Thioäther mit der stöchiometrischen Menge 30%igen Wasserstoffperoxids bei Zimmertemperatur umgesetzt.

Die Verbindung **I** wurde auch mittels Benzopersäure nach SHAW, BERNSTEIN, LOSEE und LOTT [3] zum Sulfoxid oxydiert. Die Ausbeuten sind bei beiden Verfahren in etwa gleich, die Reaktionsprodukte identisch.

Die Löslichkeit der Sulfoxide in Wasser nimmt in der Reihenfolge **Ia, IIIa** und **IIa** entsprechend der ansteigenden Polarität dieser Verbindungen zu. In gleicher Reihenfolge nimmt die Löslichkeit in wenig oder nichtpolaren organischen Lösungsmitteln ab. Die Sulfoxide sind in Wasser besser löslich als die entsprechenden Thioäther.

Die Pikrate der dargestellten Sulfoxide sind gut kristallisierende Verbindungen, die Hydrochloride von **Ia** und **IIIa** sind stark hygroskopisch.

Im Gegensatz zu den Pyridyl-3-sulfoxiden wurden Pyridyl-3-sulfone in der Literatur schon häufig beschrieben. Allerdings wurden sie meist durch Umsetzung von Sulfinsäuren mit Acyl- oder Alkylhalogeniden bzw. mit Olefinen erhalten [4, 5, 6, 7]. Durch Oxydation von Pyridyl-3-thioäthern gelangten BAMBAS [8], BURTON und DAVY [7] und TAKAHASHI und UEDA [9] zu den entsprechenden Sulfonen.

Von diesen Autoren wurden Wasserstoffperoxid, Kaliumpermanganat, Kaliumdichromat und Salpetersäure als Oxydationsmittel verwendet. Persäuren oder Natriumhypochlorit wurden in der Pyridinreihe zur Herstellung von Sulfonen noch nicht eingesetzt. Das billige Oxydationsmittel Natriumhypochlorit wurde bisher nur zur Oxydation von in Erdöl enthaltenen Sulfiden eingesetzt [10, 11, 12], wobei Sulfone entstehen. Eine Arbeitsvorschrift, die für die Oxydation von Pyridyl-3-tioäthern zu den entsprechenden Sulfonen verwendet werden könnte, wird aber von diesen Autoren nicht gegeben. Ein von uns ausgearbeitetes Verfahren liefert gute Ausbeuten; die mittels Perhydrol erreichbaren Ausbeuten liegen aber deutlich höher. Andere Oxydationsmittel wurden nicht eingesetzt, da bei deren Einsatz in stärkerem Maße Nebenreaktionen zu befürchten sind, die am Ende zu viskosen Verharzungsprodukten führen (vgl. z. B. auch KNOLL [13]).

Die Oxydation mittels Natriumhypochlorit wird im alkalischen Medium durchgeführt. Deshalb können hier leicht Salze, wie z. B. Hydrochloride, die oft leichter zugänglich sind als die freien Basen, eingesetzt werden.

Der Oxydation mittels Perhydrol wurden die Verbindungen **I, II** und **III** unterworfen; Natriumhypochlorit wurde nur zur Oxydation von **I** verwendet, nachdem das Verfahren an einem einfachen aliphatischen Thioäther entwickelt und erprobt worden war.

Während die Oxydation bei der Verbindung **I** glatt verläuft, werden aus den Verbindungen **II** und **III** Produkte erhalten, deren elementaranalytische Werte nicht den berechneten entsprechen. Die IR-Spektren weisen aber für alle Verbindungen Sulfonylgruppen aus.

Die oben formulierte Verbindung **IIb** ist ein 1,4,7-Trisulfon. Da aber bereits 1,4-Disulfone leicht in Sulfinsäure und β-Oxysulfon zerfallen [14], erscheint dieser Befund verständlich.

Das 3,5-Dinitrobenzoat des Oxydationsproduktes von **III** gibt bei der Elementaranalyse etwas zu niedrige Stickstoff- und zu hohe Kohlenstoff-

und Wasserstoffwerte:

	%N	%C	%H
Berechnet	12,75	45,85	3,46
Gefunden	11,72; 12,00	46,71; 46,96	5,21; 5,35

Bisher war es nicht möglich, die Struktur dieser Produkte — das zuletzt genannte ist auf Grund seiner physikalischen und chemischen Eigenschaften wahrscheinlich verunreinigtes **IIIb** — exakt zu ermitteln.

Die Sulfone sind wie erwartet in Wasser besser löslich als die Sulfoxide.

Beschreibung der Versuche

Sulfoxide

1. Oxydation mittels 30%igen Wasserstoffperoxids:

5 g **I** (0,017 Mol) werden in 30 ml Azeton gelöst, mit 4 g (0,035 Mol) 30%igem Wasserstoffperoxid versetzt und 48 Stunden bei Zimmertemperatur stehen gelassen. Nach Abdestillation des Lösungsmittels im Vakuum auf dem Wasserbad wird in Alkohol aufgenommen, mit Aktivkohle entfärbt und das Lösungsmittel wie oben wieder abdestilliert.

Ausbeuten: 4,4 g **Ia** entsprechend 79% d. Th.
n_D^{20}: 1,6062, gelbliche Flüssigkeit
3,4 g **IIa** entsprechend 59% d. Th.
umkrist. aus Azeton
F. 134—136 °C, farblose Kristalle
3,0 g **IIIa** entsprechend 54% d. Th.
hellbraune Flüssigkeit

Die Pikrate zeigen folgende F.:

Ia: 147—148 °C
IIa: 248—250 °C (Z.)
IIIa: 185—188 °C (Z.)

Die beschriebenen Sulfoxide sind löslich in Wasser, verd. Salzsäure, Alkohol und Azeton, schwer oder unlöslich in Äther, Benzol und verd. Natronlauge.

2. Oxydation mittels Benzopersäure:

5 g **I** (0,017 Mol) werden in 30 ml Chloroform gelöst und unter Rühren innerhalb 30 Min. bei 10 °C mit 22 ml 1,53 molarer Lösung von Benzopersäure (0,03 Mol) in Chloroform versetzt. Der Ansatz wird noch 3 Std. bei 10 °C gerührt. Das Reaktionsgemisch wird zweimal mit kalter gesättigter Sodalösung, einmal mit 5%iger Natronlauge und zweimal mit Wasser gewaschen. Nach Abdestillation des Lösungsmittels erhält man eine Ausbeute von 4 g entsprechend 72% d. Th.; n_D^{20}: 1,6049.

Tabelle I

Analytische Daten dargestellter Pyridin-3-sulfoxide

Verbindung	Bruttoformel	Molekulargewicht	S ber. (%)	S gef. (%)	N ber. (%)	N gef. (%)	Absorption im IR-Spektrum
Ia	$C_{15}H_{18}N_2O_2S_2$	322	19,89	20,04	8,69	8,54	1050 cm^{-1}
IIa	$C_{14}H_{16}N_2O_3S_3$	356	26,98	26,86	7,86	7,81	1040 cm^{-1}
IIIa-pikrat	$C_{20}H_{20}N_6O_9S_2$	552	11,62	11,43	15,20	15,13	1042 cm^{-1}

Sulfone

1. Oxydation mittels 30%igen Wasserstoffperoxids:

5 g (0,017 Mol) **I** werden in 20 ml Eisessig gelöst und mit 12 ml (0,106 Mol) Perhydrol versetzt. Nun wird 2 Std. unter Rückfluß erhitzt. Bei Eingießen des Reaktionsgemisches in 300 ml eiskalte Sodalösung kristallisiert das Sulfon aus. Nach Absaugen läßt sich aus dem Filtrat durch Extraktion mit Chloroform eine zweite Fraktion gewinnen. Das Rohsulfon wird aus Azeton umkristallisiert.

Ausbeute: 5,8 g entsprechend 95% d. Th.;
F. 144—144,5 °C

Die Substanz ist löslich in heißem Wasser, leicht löslich in verd. HCl und Chloroform, in heißem Alkohol und Azeton, wenig löslich in Äther und Benzol und unlöslich in verd. NaOH.

Pikrat: F. 171—172 °C
Dihydrochlorid: F. 200—202 °C

S ber. 18,09 N ber. 7,91
S gef. 17,88 N gef. 7,94

Absorptionen im IR-Spektrum:
1153 cm^{-1}; 1300 cm^{-1}

2. Oxydation mittels Natriumhypochlorit:

Zu 5 g (0,017 Mol) **I** werden unter Rühren bei 30 °C innerhalb 30 Minuten 42 ml (0,068 Mol) 1,6 *n*-Natriumhypochloritlösung getropft und die Reaktionsmischung noch 2 Std. bei dieser Temperatur gerührt. Nach Abkühlung extrahiert man das gebildete Sulfon mit Chloroform, destilliert dann das Extraktionsmittel ab und kristallisiert den Rückstand aus Azeton um.

Ausbeute: 3,8 g entsprechend 62,3% d. Th.
F. 141—143 °C

Mischschmelzpunkt mit dem unter 1. erhaltenen Sulfon:
Keine Depression

REFERENCES

1. Heltzig, M., Göbel, W., König, H. J.: J. prakt. Chem. **311,** 174 (1969)
2. Shriner, R. L., Struck, H. C., Jorison, W. J.: J. Amer. Chem. Soc. **52,** 2060 (1930)
3. Shaw, E., Bernstein, J., Losee, K., Lott, W. A.: J. Amer. Chem. Soc. **72,** 4362 (1950)
4. Goldberg, W. M., Teitel, S.: US Pat. 2 761 865 und 2 761 866 entspr. Österr. Pat. 193 876 und 193 877; Ref. C. **1959**, 1218; Österr. Pat. 193 878; Ref. C. **1959**, 1219
5. Lewis, T. R., Archer, S.: J. Amer. Chem. Soc. **73,** 2109 (1951)
6. Foldi, E.: Acta Chim. Acad. Sci., Hung. **19,** 205 (1959), Ref. C. A. **54,** 2325 c (1960)
7. Burton, A., Davy, W. A.: J. Chem. Soc. (London) **1947**, 52
8. Bambas, L. L.: J. Amer. Chem. Soc. **67,** 668 (1945)
9. Takahashi, I., Ueda, K.: J. Pharm. Soc. Japan, **73,** 442 (1953); Ref. C. A. **48,** 5187 h (1954)
   Ueda, K.: Pharm. Bull. (Tokio) **4,** 396 (1956)
10. Birch, S. F., Norris, W. S.: J. Chem. Soc. (London) **127,** 1934 (1925)
11. Wood, A. E., Greene, A. R., Provine, R. W.: J. Ind. Eng. Chem. **18,** 823 (1926)
12. Wood, A. E., Travis, E. G.: J. Amer. Chem. Soc. **50,** 1226 (1928)
13. Knoll, R.: J. prakt. Chem. **113,** 40 (1926)
14. Houben-Weyl: Methoden der organischen Chemie 4. Aufl., Band 9, S. 257. G. Thieme-Verlag, Stuttgart, 1955

Wolfgang Göbel; 8020 Dresden, Teplitzer Str. 58
Hans-Joachim König; 69 Jena, Arvid-Harnack Str. 22

Acta Chimica Academiae Scientiarum Hungaricae, Tomus 63 (1), pp. 111—114 (1970)

BOOK REVIEWS — BUCHBESPRECHUNGEN — РЕЦЕНЗИИ КНИГ

G. M. BADGER: *Aromatic Character and Aromaticity.*

University Press, Cambridge 1969. 133 pages.

This book by Professor BADGER (Adelaid) has been published as a volume of the Cambridge Chemistry Textbook Series. The purpose of the Series is rather to highlight the principal theoretical backgrounds than to supply the reader with detailed information.

The concepts of "aromatic character" and "aromaticity" have recently become rather vague, as a number of short-lived, unstable chemical entities have been synthesized, to which, in a certain sense, an aromatic character may be assigned, *e.g.* the dianione derived from cyclooctatetraene. Therefore, the classic usage according to which the expression "aromatic" was next to synonymous to "benzenoid", can only be maintained with difficulty. At the same time, in preparative practice, a certain reactivity is still expected as a criterion of aromatic character. This problem also involves difficulties in didactics.

Attempts have been made in the present book to clarify these contradictions, or apparent contradictions, and in the opinion of the reviewer, this endeavour has been successful.

In Chapter 1 (38 pages) a brief historical survey is given, followed by a review of the physical-chemical methods suitable for the determination of the structure of benzene, the applicability of wave mechanics, benzenoid polycyclic compounds, and finally aromatic heterocycles. At the end of the Chapter an attempt is made to define the concept of aromaticity.

In the subsequent Chapters the consequences of this definition are taken one after the other.

In Chapter 2 (32 pages) the problems of bond length, resonance energy and electronic absorption spectra are discussed. The same Chapter deals with induced ring currents, a topic which has recently given rise to much dispute in connection with aromatic character, and which is experienced most distinctly in the NMR spectroscopic analysis of aromatic compounds.

Chapter 3 (39 pages) is concerned with non-benzenoid hydrocarbons. On basis of the well-known Hückel rule, the 2π-, 4π-, 6π-, 8π-, 10π-, 12π-, 14π-, 16π-, 18π-, 20π-, 24π-, and 30π- electron systems are dealt with one by one. The Chapter is concluded with an evaluation of the Hückel rule.

The last Chapter, Chapter 4 (15 pages) is devoted to some more complex systems, such as fulvenes, fulvalenes, metallocenes, etc., giving a short survey again.

The get-up of the book and the typographical implementation of the formulas are good.

The lucid presentation and discussion of the subject-matter makes the book highly recommendable both to beginners and advanced workers in organic chemistry.

CS. SZÁNTAY

K. KÜHNE: *Zur Kenntnis silikatischer Werkstoffe und der Technologie ihrer Herstellung im 2. Jahrhundert vor unserer Zeitrechnung.*

Akademischer Verlag, 1969. 46 Seiten, 6 Abb., 20 Qu.

Im Rahmen der Abhandlungen der Deutschen Akademie der Wissenschaften zu Berlin, Jahrgang 1969, erschien eine Monographie, die seitens der Archeologen und der Glasexperten besondere Beachtung verdient. Sie zeigt den Archeologen, wie uns die zeitgemäße Glaskunde Aufschlüsse über technische Kenntnisse in einer vergangenen Zeit geben kann, während die

Forscher der Glasindustrie ein Beispiel dafür kennen lernen, wie der Glasfachmann eine archeologische Frage lösen kann. In dieser Hinsicht ist die KÜHNEsche Arbeit beispielhaft.

Die Monographie befaßt sich mit der Frage der Erzeugung silikatischer Werkstoffe im 2. Jahrhundert v. u. Z. Die untersuchten Fundstücke stammen aus Tell-el-Amarna; sie sind von der Deutschen Orientgesellschaft in den zwanziger Jahren ausgegraben worden und werden — geteilt zwischen Ägypten und Deutschland — in den Museen von Kairo und Berlin aufbewahrt.

In der behandelten Zeit wurden ägyptische Fayencen und Gläser erzeugt. Beide stammen aus der Zeit um 1358—1347 v. u. Z. Die ägyptischen Fayencen werden vom Verfasser Kieselkeramiken genannt, was damit begründet wird, daß sie 90,95% Kieselsäure enthalten.

Im ersten Abschnitt wird kurz die Geschichte Ägyptens geschildert, insbesondere die der Amarna-Epoche, aus welcher die behandelten Funde stammen. Diesen Abschnitt hat St. WENIG, ein erfahrener Ägyptologe geschrieben.

Der zweite Abschnitt behandelt die Ausgrabungen der Deutschen Orientgesellschaft in Tell-el-Amarna. Mit den Kieselkeramiken befaßt sich der dritte Abschnitt. Aus disem Stoff wurden Amulette, Platten mit reliefartigen Darstellungen, Schmuckstücke, Ringe, Gefäße hergestellt. Die Grundsubstanz war fein gemahlener Quarz, der mit einer Glasur überzogen wurde. Auf Grund mikroskopischer Untersuchungen von Dünnschliffen und qualitativer Spektralanalyse konnte auch die Zusammensetzung der Glasur festgestellt werden. Die Formgebung und Verarbeitung der Kieselkeramiken its der des Glases gegenüber sehr einfach, weshalb die schon in vordynastischen Zeiten hergestellten Kieselkeramiken erst sehr viel später — in der Zeit der 18. Dynastie, um 1450 v. u. Z. — durch das Glas verdrängt worden sind.

Der vierte Abschnitt faßt die an den Gläsern aus Tell-el-Amarna durchgeführten Untersuchungen zusammen. Die chemische Analyse wurde auf spektroskopischem Weg ausgeführt. Als ein interessantes Ergebnis hat sich herausgestellt, daß diese Gläser Kobaltoxyd bis 0,13% enthalten, obwohl in ägyptischen Gläsern Kobaltoxyd sonst nicht gefunden wurde. Der Verfasser vermutet daher, daß die zur Dekoration verwendeten Stäbe nicht in Tell-el-Amarna geschmolzen wurden, sondern aus Vorderasien eingeführt worden sind. Die blauen Farben wurden mit Kupferoxydul und Kobaltoxyd, die braunen mint Eisenoxyd, die gelben mit Antimonoxyd, die grünen mit einer Mischung aus gelben und blauen Gläsern, die zwei roten mit Kupferoxydul und Zinnoxyd gefärbt. Die Erzeugung der Gläser wurde auf zwei Wegen ausgeführt und zwar mit der Sandkerngefäßherstellung und mit dem Wickelverfahren. Beide Verfahren konnten getreu reproduziert werden.

Die Monorgaphie vermittelt uns neue Kenntnisse über den Stand des Wissens und der Technik der alten ägyptischen Kultur. Sie ist bemerkenswert u. a. weil sie beweist, daß eine enge Zusammenarbeit zwischen Archeologen und Glasfachleuten äußerst fruchtbar sein kann.

O. KNAPP

H. KANGRO: *Joachim Jungius' Experimente und Gedanken zur Begründung der Chemie als Wissenschaft.*

Franz Steiner Verlag, Wiesbaden 1968, 476 S.

Werke der Chemiegeschichte werden in unserem Jahrhundert nur sehr selten mit so ausführlichem wissenschaftlichem Apparat versehen, wie das von Hans KANGRO. Die beiden Hauptteile: I. JUNGIUS' Forschungen zur Chemie und II. JUNGIUS' Gedanken, den zeitgenössischen Anschauungen gegenübergestellt, machen einen Umfang von 251 Seiten aus. Das übrige ist der Apparat. Originaltexte in lateinisch und ihre Übersetzungen, Lebensläufe der zitierten Autoren, Zeittafel, Literatur, in 35 Bildtafeln die Photokopien sämtlicher Werke von JUNGIUS und Register.

Die meisten Nationen haben ihre »vergessenen« Wissenschaftler, deren Verdienste ungewürdigt geblieben sind. Von späten Nachfahren entdeckt, wird ihnen dann Anerkennung gezollt, man versucht dann aber auch vielfach zu große Verdienste zu entdecken und ihnen eine Rolle zuzuschreiben, die weit übertrieben ist. Sicherlich finden sich in vergessenen Schriften oft unbeachtet gebliebene wertvolle Gedanken; wahr ist aber auch, daß Gedanken, die zu ihrer Zeit ohne Wirkung waren, für die Entwicklung der Wissenschaft auch nie von besonderer Bedeutung gewesen sind.

Mir selbst schien es schon lange, daß JUNGIUS diese vergessene Gestalt in der deutschen Chemie sei. Viele Andeutungen ließen das durchblicken; man las z.B., BOYLE hätte viele seiner Ideen, so den Elementbegriff oder die Definition der chemischen Analyse von JUNGIUS geschöpft. Deshalb hat es mich besonders gefreut, nun sehen zu können, was JUNGIUS eigentlich geschaffen hat.

Ich bin dabei zu der Überzeugung gelangt, daß sich BOYLE JUNGIUS' Ideen nicht einmal in ihren Keimen entliehen hat. Dies wäre auch schwer möglich gewesen, zumal die Werke von JUNGIUS — der zwar vor BOYLE gelebt hat — alle erst nach seinem Tode erschienen sind, seine Doxoscopie z. B. ein Jahr nach BOYLES Sceptical Chymist. Auch läßt sich BOYLES klarer Stil nicht mit JUNGIUS' schwerfälliger und komplizierter Ausdrucksweise vergleichen. Auch KANGRO gelangt in seiner Schlußbetrachtung zu der Folgerung, daß zwischen dem Elementenbegriff von JUNGIUS und dem von BOYLE — im Gegensatz zu zahlreichen Behauptungen — große Unterschiede zu erkennen sind. Daran ändert meines Erachtens auch die Möglichkeit nichts, daß BOYLE über HARTLIEB einige Disputationes von JUNGIUS vielleicht doch kennen lernen konnte. Mir selbst scheint auch die Atomlehre von JUNGIUS nicht von besonderer Bedeutung gewesen zu sein, wenn ich sie z. B. mit der Lehre SENNERTS vergleiche. Mit den übrigen — besonders der von GASSENDI und BOYLE — verglichen war SENNERTS Atomlehre vielleicht die »chemischeste« jenes Jahrhunderts.

Damit soll natürlich nicht behauptet werden, JUNGIUS sei nicht ein wertvoller Denker seiner Zeit gewesen. Ob er auch experimentell tätig war, ist ziemlich unklar geblieben; man hat eher den Eindruck, er hätte sich lediglich auf die Auslegung von Versuchsergebnissen beschränkt, was er aber oft besser tat als der Experimentator selbst.

KANGRO zitiert wenig und gibt JUNGIUS' Darstellungen meist mit seinen eigenen Worten wieder. Ob aber Sätze, wie z. B. »Elemente sind nicht in einander überführbar und aus ihnen als ersten Bestandteilen ist ein Naturkörper aufgebaut« usw., nicht mehr aussagen, als JUNGIUS selbst ausgedrückt hatte, sei dahingestellt. Interessant ist, daß JUNGIUS das Wort »analyses« schon im heutigen Sinne der chemischen Analyse gebraucht haben soll. Aber auch darin ist ihm BOYLE — zumindest in Druck — zuvorgekommen.

Das besprochene Buch läßt ein imponierendes Wissen und sehr eingehende chemische, philosophische und literarische Kenntnisse seines Verfassers erkennen. Er kennt sich in der Literatur des 17. Jahrhunderts aus, wie man sich im eigenen Bücherschrank auskennt. Bei der Fülle der detaillierten Besprechung von JUNGIUS' Darlegungen, bei den Bemerkungen, Literaturhinweisen usw. entbehrt man jedoch eine eigentliche Zusammenfassung des Wesentlichen. Die Schlußbetrachtung verfehlt dieses Ziel, sie gibt uns kein genügend komprimiertes und kritisches Bild von JUNGIUS' Schaffen. Auch die Persönlichkeit von JUNGIUS habe ich vermißt. Der Autor hat sie bewußt weggelassen. Für mich ist es aber immer unvollständig, wenn man nur von Schriften ausgeht und Persönlichkeit und Umstände ihres Verfassers ganz außer Acht läßt.

Mit mühsamer Arbeit hat KANGRO der Chemiegeschichte ein Quellenwerk von bleibendem Wert geschenkt. Sein Stil ist aber kein leichter. Ihn zu lesen macht starkes Konzentrieren notwendig.

F. SZABADVÁRY

Quantitative Paper and Thin-Layer Chromatography. Edited by E. J. Shellard.

Academic Press, London and New York, 1968, 140 pages

The book consists of eleven lectures held by invited speakers at a Symposium on the title topics in the Chelsea College of Science and Technology, London, January 3—4, 1968. A detailed analysis of possible sources of error in the application of procedures described in the literature is given. On the basis of control examinations, as well as literary data, the authors provide numerical values for the expected precision of the principles involved and the apparatuses used in the measurements, thus for the accuracy of the results. In this way, the reader is supplied with instructions for the solution of his own microanalytical problems, in the selection of both the suitable method and the apparatus.

The titles of the eleven Chapters are: 1. Factors Involved in Producing Uniform Spots. 2. Quantitation of Paper Chromatograms. 3. Quantitative Thin-Layer Chromatography using Elution Techniques. 4. Quantitative Thin-Layer Chromatography using Densitometry. 5.

Quantitative Thin-Layer Chromatography using Fluorimetry. 6. Advantages and Problems of Direct Spectrophotometry on Thin-Layer Chromatograms. 7. The Application of Spectroscopy to Thin-Layer Chromatography. 8. The Visual Assessment of Thin-Layer Chromatograms. 9. Quantitative Scanning of Radioactive Thin-Layer Chromatograms. 10. Bidimensional Radiochromatogram Scanning. 11. The Evaluation of Radiochromatograms using a Spark Chamber.

Each chapter is provided with references to periodicals and books. The titles of the chapters show that the reader will find valuable information in the book, covering the whole field of the selected subject.

The book is an indispensable collection of experiences and a source of consultative information to chemists and engineers interested in quantitative paper and thin-layer chromatography.

P. BITE

INDEX

PHYSICAL CHEMISTRY — PHYSIKALISCHE CHEMIE — ФИЗИЧЕСКАЯ ХИМИЯ

ORGANIC CHEMISTRY — ORGANISCHE CHEMIE — ОРГАНИЧЕСКАЯ ХИМИЯ

Printed in Hungary

A kiadásért felel az Akadémiai Kiadó igazgatója — Műszaki szerkesztő: Farkas Sándor

A kézirat nyomdába érkezett: 1969. IX. 24. — Terjdedelem: 10 (A/5) ív, 36 ábra

69.68353 Akadémiai Nyomda, Budapest — Felelős vezető: Bernát György

The AALC collection, including approx. 5500 punched cards gives the individual the advantages of modern data processing, without the need for expensive machines.

The advantages of cards!

The AALC collection of cards offers many advantages to its user. First, because only a card-file can be kept complete and up-to-date at any time. Book-form bibliographies are difficult to handle and are not apt for cross-indexing. Secondly with a card-file you do not have to make personal notes. If you wish to retain items of information from a book-bound bibliography, you cannot avoid noting them down (if you don't want to tear out the relevant pages!); with the AALC-file, however, you can indulge in the luxury of picking out the cards you are looking for.

The advantages of p u n c h e d cards!

By having the AALC collection on *punched* cards, you never have to replace cards in any particular order. Through the selection operation the cards you are looking for fall unerringly from the whole pack, irrespective of the place they occupy in the card-file. Using simple methods, you can collect all the cards that are particularly important for the topical field you are engaged in at a given time. A punched card file allows any questions to be combined according to the nature of your problem: it allows cross-indexing as well.

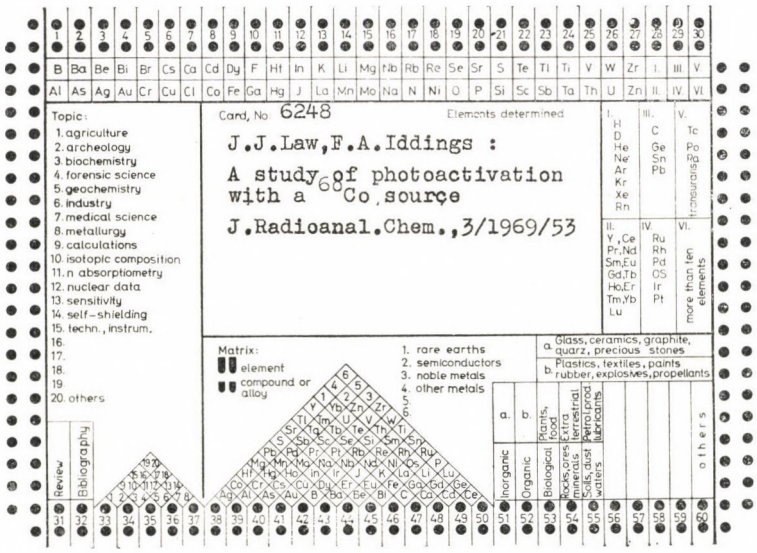

AALC—File
ACTIVATION
ANALYSIS
LITERATURE
CARDS
1935—1968

Unslotted:
US$ 0.05/card

Slotted:
US$ 0.06/card

IN PREPARATION

Ask for leaflets at the following address

AKADÉMIAI KIADÓ

Publicity Department, Budapest 502. P.O.B. 24

ACTIVATION ANALYSIS DOCUMENTATION CENTER

AKADÉMIAI KIADÓ

PUBLISHING HOUSE OF THE HUNGARIAN ACADEMY OF SCIENCES

ACTA CHIMICA

ТОМ 63 — ВЫП. 1

РЕЗЮМЕ

Параметры Мёссбауэра для гидратов солей железа (II)

А. ВЕРТЕШ, Т. СЕКЕЙ и Т. ТАРНОЦИ

Изучались параметры Мёссбауэра для хлоридов и сульфатов железа(II) с различным содержанием кристаллической воды. Было установлено, что с увеличением содержания воды связь железо-вода все более и более определяет изомерный сдвиг и величины квадрупольного расщепления; так например, нефелоауксетическое влияние хлора, установленное в $FeCl_2$, почти полностью экранируется в $FeCl_2 \cdot 4H_2O$ молекулами H_2O. Изучалось термическое поведение $FeSO_4 \cdot 4H_2O$, на основе чего было установлено, что в присутствии воздуха данное вещество окисляется при 200° С до основного сульфата железа с антиферромагнитным поведением при —80° С.

Изучение гидратационных и сольватационных условий растворов солей железа (II) с помощью эффекта Мёссбауэра

А. ВЕРТЕШ

Приводятся спектры Мёссбауэра замороженных растворов солей железа(II). В двух- и трехкомпонентных растворах изменение концентрации отдельных компонентов приводит к изменению квадрупольного расщепления, что, по нашему мнению, может быть связано с превращениями, протекающими в гидратной или сольватной оболочках. В отдельных случаях появляются два различных (суперпонированных) спектра. Это указывает на то, что в данном растворе находятся две различные гидратные и сольватные оболочки, в равновесии друг с другом.

На основе вышесказанного может быть установлено, что эффект Мёссбауэра является методом, пригодным для изучения гидратационных и сольватационных условий растворов, содержащих атомы Мёссбауэра.

Спектроскопия диффузионных рассеиваюших систем, I

Зависимость оптических данных от количества вещества в образце

Е. ХУСАР

В работе обсуждаются зависимости между количеством вещества в рассеивающем образце и оптическими (измеренными) данными.

Рассеивающие образцы на бумажной основе — в разработанных, определенных условиях измерений — можно рассматривать как «квази-гомогенные».

Изучались параллельности, наблюдаемые в зависимости величин ремиссии и трансмиссии от количества вещества. Были установлены: зависимость «А»; «критические количества», а также характеристики их формы и содержания; а также характерный оптический параметр для образцов, содержащих больше, чем критическое количество, — величина Δr.

Изучались пределы справедливости зависимостей.

Расчет электронной структуры потенциальных антикарциногенов — нуклеотидных оснований антиметаболитного типа, II

Монозамещенные пурины, аденины и гуанины

Я. ЛАДИК и Г. БИЦО

π-Электронная структура различных монозамещенных муринов, аденинов и гуанинов рассчитывалась с помощью полуэмпирического метода ССП ЛКАО МО. Заместители были теми же, что и в предыдущем сообщении.

Кажется вероятным наличие таких же корреляций между плотностями заряда изученных веществ и их антикарциногенными свойствами и для данных веществ, как в случае соединений, описанных в предыдущем сообщении. Для уточнения и обобщения корреляций необходимо определение дальнейших квантово-химических индексов.

Потенциальные кривые и кривые электронной энергии изоэлектронных молекул

Ш. СЁКЕ, Ж. ВАЙНА и Дь. ЯЛШОВСКИЙ

Рассчитывались потенциальные кривые изоэлектронных двухатомных молекул с помощью комбинированного метода с использованием пригонки параметров. Приводятся рассчитанные таким образом кривые электронной энергии и электронные силовые постоянные изоэлектронных молекул.

Многослойная адсорбция смеси жидкостей, I

Й. ТОТ

Обобщение однослойной модели адсорбции смеси жидкостей приводит к противоречиям. Так, в случае многих линейных изотерм Г-х, для которых возможность точного измерения удельной поверхности адсорбента указывает на однослойную адсорбцию, свойства, определяемые строением жидкости (ассоциирующая способность, водородные мостики и т. д.) должны обусловливать многослойную адсорбцию. Помимо этого, в случае линейных изотерм может быть рассчитана многослойная и «осциллирующая» зависимость свободной энергии, интерпретация которой невозможна. Эти противоречия могут быть разрешены, если полагать, что отдельные мономолекулярные адсорбированные количества Γ_1, Γ_2 под влиянием поверхностных сил, обусловленных структурными возможностями, смешиваются с одним (или возможно с несколькими) молекулярным слоем внутренней фазы. Образуется такая многослойная поверхностная фаза, в которой избыток вещества, определяемый экспериментально, таков же, как и в случае однослойной адсорбции. Такая многослойная адсорбция может быть описана совершенно точными уравнениями материального баланса.

Хидантоины, тиохидантоины и гликоциамидины, XXVIII

Реакция катиона 3-метил-2,5-бис(метилтио)-4,4-дифенил-4Н-нимидазоль-3-иума с бензиламином

К. ЛЕМПЕРТ, П. ШОХАР и К. ЗАУЭР

Под влиянием хлористого бензиламмония в пиридине катион 3-метил-2,5-бис(метилтио)-4,4-дифенил-4*Н*-имидазоль-3-иума (**1**) превращается в два различных продукта. Главным продуктом является 2-бензилимино-1-метил-5,5-дифенил-4-имидазолидинтион (**5**) образовавшийся путем бензиламинолиз и с дальнейшим *s*-деметилирования через образование **3**-она, а в качестве побочного продукта образуется гидрохлористый 2,4-ди (бензилимино)-1-метил-5,5-дифенилимидазолидин (**8**). В процессе образования **5** *s*-деметилирование вызвано пиридином. Для некоторых из полученных соединений (**2**—**5**) снимались ИК и ЯМР спектры, на основе которых делались заключения относительно их тонкой структуры (электронное распределение, строение таутомеров).

1,5-Дикетоны, V

Каталитические реакции некоторых 2-(1-ацетилпропил)-бензофенонов

М. ЛЕМПЕРТ-ШРЕЙТЕР

Каталитическое восстановление 2-(1-ацетилпропил)-5,4'-диацетокси-4,3'-диметокси-бензофенона (**1**) приводит к образованию слабого молекулярного соединения между 2-(1-ацетилпропил)-5,4'-диацетокси-4,3'-диметокси-дифенилметаном (**2**) и 2-(1-этил-2-гидроксипропил)-5,4'-диацетокси-4,3'-диметокси-дифенинилметаном (**5**), с соотношением компонентов 1 : 1. Другие 2-(1-ацетилпропил)-бензофеноны (**6** и **15**) в подобных условиях дают продукты восстановления, аналогичные исключительно соединению **2**.

В реакции превращения **1** в **3**, соединение **2** не является промежуточным продуктом, т. к. в процессе превращения вначале восстанавливается алифатическая кетокарбонильная группа соединения **1**, и лишь за этим следует восстановление ароматического кетонкарбонила соединения **14** до метиленовой группы.

The Acta Chimica publish papers on chemistry in English, German, French and Russian.

The Acta Chimica appear in volumes consisting of four parts of varying size, 4 volumes being published a year.

Manuscripts should be addressed to

Acta Chimica
Budapest 112/91 Műegyetem

Correspondence with the editors should be sent to the same address.

The rate of subscription is 165 forints a volume. Orders may be placed with "*Kultura*" Foreign Trade Company for Books and Newspapers (Budapest I., Fő utca 32. Account No. 43-790-057-181) or with representatives abroad.

Les Acta Chimica paraissent en français, allemand, anglais et russe et publient des mémoires du domaine des sciences chimiques.

Les Acta Chimica sont publiés sous forme de fascicules. Quatre fascicules seront réunis en un volume (4 volumes par an).

On est prié d'envoyer les manuscrits destinés à la rédaction à l'adresse suivante:

Acta Chimica
Budapest 112/91 Műegyetem

Toute correspondance doit être envoyée à cette même adresse.

Le prix de l'abonnement est de 165 forints par volume.

On peut s'abonner à l'Entreprise pour le Commerce Extérieur de Livres et Journaux «*Kultura*» (Budapest I., Fő utca 32. Compte-courant No. 43-790-057-181) ou à l'étranger chez tous les représentants ou dépositaires.

«*Acta Chimica*» издают трактаты из области химической науки на русском, французском, английском и немецком языках.

«*Acta Chimica*» выходят отдельными выпусками разного объема. 4 выпуска составляют один том. 4 тома публикуются в год.

Предназначенные для публикации рукописи следует направлять по адресу:

Acta Chimica
Budapest 112/91 Műegyetem

По этому же адресу направлять всякую корреспонденцию для редакции.

Подписная цена «*Acta Chimica*» — 165 форинтов за том. Заказы принимает предприятие по внешней торговле книг и газет «*Kultura*» (Budapest I., Fő utca 32. Текущий счет № 43-790-057-181) или его заграничные представительства и уполномоченные.

Reviews of the Hungarian Academy of Sciences are obtainable at the following addresses:

ALBANIA

Ndermarja Shtetnore e Botimeve
Tirana

AUSTRALIA

A. Keesing
Box 4886, GPO
Sydney

AUSTRIA

Globus Buchvertrieb
Salzgries 16
Wien I

BELGIUM

Office International de Librairie
30, Avenue Marnix
Bruxelles 5
Du Monde Entier
5, Place St. Jean
Bruxelles

BULGARIA

Raznoiznos
1, Tzar Assen
Sofia

CANADA

Pannonia Books
2, Spadina Road
Toronto 4, Ont.

CHINA

Waiwen Shudian
Peking
P. O. B. 88

CZECHOSLOVAKIA

Artia
Ve Smečkách 30
Praha 2
Poštová Novinová Služba
Dovoz tisku
Vinohradská 46
Praha 2
Mad'arská Kultura
Václavské nám. 2
Praha I
Poštová Novinová Služba
Dovoz tlače
Leningradská 14
Bratislava

DENMARK

Ejnar Munksgaard
Nörregade 6
Copenhagen

FINLAND

Akateeminen Kirjakauppa
Keskuskatu 2
Helsinki

FRANCE

Office International de Documentation et Librairie
48, rue Gay Lussac
Paris 5

GERMAN DEMOCRATIC REPUBLIC

Deutscher Buch-Export und Import
Leninstraße 16
Leipzig 701
Zeitungsvertriebsamt
Fruchtstrasse 3—4
1004 Berlin

GERMAN FEDERAL REPUBLIC

Kunst und Wissen
Erich Bieber
Postfach 46
7 Stuttgart S.

GREAT BRITAIN

Collet's Holdings Ltd.
Dennington Estate
London Rd.
Wellingborough. Northants.
Robert Maxwell and Co. Ltd.
Waynflete Bldg. The Plain
Oxford

HOLLAND

Swetz and Zeitlinger
Keizersgracht 471—487
Amsterdam C.
Martinus Nijhof
Lange Voorhout 9
The Hague

INDIA

Current Technical Literature
Co. Private Ltd.
India House OPP
GPO Post Box 1374
Bombay I

ITALY

Santo Vanasia
Via M. Macchi 71
Milano
Libreria Commissionaria Sansoni
Via La Marmora 45
Firenze

JAPAN

Nauka Ltd.
92, Ikebukur O-Higashi 1-chome
Toshima-ku
Tokyo
Maruzen and Co. Ltd.
P. O. Box 605
Tokyo-Central
Far Eastern Booksellers
Kanda P. O. Box 72
Tokyo

KOREA

Chulpanmul
Phenjan

NORWAY

Johan Grundt Tanum
Karl Johansgatan 43
Oslo

POLAND

Ruch
ul. Wronia 23
Warszawa

ROUMANIA

Cartimex
Str. Aristide Briand 14—18
Bucureşti

SOVIET UNION

Mezhdunarodnaya Kniga
Moscow G—200

SWEDEN

Almquist and Wiksell
Gamla Brogatan 26
Stockholm

USA

Stechert Hafner Inc.
31, East 10th Street
New York, N. Y. 10003
Walter J. Johnson
111, Fifth Avenue
New York, N. Y. 10003

VIETNAM

Xunhasaba
19, Tran Quoc Toan
Hanoi

YUGOSLAVIA

Forum
Vojvode Mišića broj 1
Novi Sad
Jugoslovenska Knjiga
Terazije 27
Beograd

ACTA CHIMICA

ACADEMIAE SCIENTIARUM HUNGARICAE

TOMUS 63 FASCICULUS 2

AKADÉMIAI KIADÓ, BUDAPEST

1970

ACTA CHIM. ACAD. SCI. HUNG.

ACTA CHIMICA

A MAGYAR TUDOMÁNYOS AKADÉMIA KÉMIAI TUDOMÁNYOK OSZTÁLYÁNAK IDEGEN NYELVŰ KÖZLEMÉNYEI

Az Acta Chimica német, angol, francia és orosz nyelven közöl értekezéseket a kémiai tudományok köréből.

Az Acta Chimica változó terjedelmű füzetekben jelenik meg, egy-egy kötet négy füzetből áll. Évente átlag négy kötet jelenik meg.

A közlésre szánt kéziratok a szerkesztőség címére (Budapest 112/91 Műegyetem) küldendők.

Ugyanerre a címre küldendő minden szerkesztőségi levelezés. A szerkesztőség kéziratokat nem ad vissza.

Megrendelhető a belföld számára az „Akadémiai Kiadó"-nál (Budapest V., Alkotmány utca 21. Bankszámla 05-915-111-46), a külföld számára pedig a „Kultura" Könyv- és Hírlap Külkereskedelmi Vállalatnál (Budapest I., Fő utca 32. Bankszámla: 43-790-057-181) vagy annak külföldi képviseleteinél és bizományosainál.

Die Acta Chimica veröffentlichen Abhandlungen aus dem Bereiche der chemischen Wissenschaften in deutscher, englischer, französischer und russischer Sprache.

Die Acta Chimica erscheinen in Heften wechselnden Umfanges. Vier Hefte bilden einen Band. Jährlich erscheinen 4 Bände.

Die zur Veröffentlichung bestimmten Manuskripte sind an folgende Adresse zu senden:

Acta Chimica
Budapest 112/91 Műegyetem

An die gleiche Anschrift ist auch jede für die Redaktion bestimmte Korrespondenz zu richten.

Bestellbar bei dem Buch- und Zeitungs-Außenhandels-Unternehmen »*Kultura*« (Budapest I., Fő utca 32. Bankkonto No. 43-790-057-181) oder bei seinen Auslandsvertretungen und Kommissionären.

Acta Chimica Academiae Scientiarum Hungaricae, Tomus 63 (2), pp. 115—121 (1970)

THE STUDY OF SOLVATATION OF IRON(II)CHLORIDE WITH THE AID OF THE MÖSSBAUER EFFECT

K. BURGER*, A. VÉRTES**, and I. N. CZAKÓ**

*(*Institute for Inorganic and Analytical Chemistry, Eötvös Loránd University, Budapest, **Institute of Physical Chemistry and Radiology, Eötvös Loránd University, Budapest)*

Received July 22, 1968

The Mössbauer parameters of the frozen solutions of $FeCl_2$, $FeSO_4$ and $FeCl_2 \cdot 4H_2O$, dissolved in various solvents, were measured. On the basis of measurements carried out at liquid air temperature, it could be established that Mössbauer parameters can give valuable information on the structure and composition of the solvate sheaths.

Mössbauer investigations in frozen solutions [1, 2, 3] raised the possibility that the Mössbauer spectrum of various frozen solutions may also furnish information on the species in the original solution, besides that of the frozen one [4]. Mössbauer spectra are hoped to yield informations concerning ion solvation phenomena, if a rapid freezing of a solution is resulted in the "freezing-in" of the corresponding equilibria. It is to be expected, therefore, that the Mössbauer investigation of complex equilibria or solvatation will yield valuable informations.

The application of the method is justified by the assumption that in solutions solidified by rapid freezing, the composition of the immediate environment of the dissolved ions and molecules (the inner ligand sphere) will remain unchanged. The validity of this latter assumption is not influenced by the circumstance that ligand exchange may proceed in the solid phase with an altered rate (excluding naturally the possibility that ligand exchange has a phase effect, that is to say, that the ratio of the exchange rates of single components in the solvate sheath is different in the liquid and the solid phase).

Our aim was the study of iron(II) solvates by the Mössbauer investigation of frozen iron(II) salt solutions, prepared with various non-aqueous solvents. A high spin iron(II) salt was chosen as model system, because especially one of the Mössbauer parameters of this salt *viz.* the quadrupole splitting is a sensible indicator even for small changes in the electron system of iron.

On the dissolution of iron salts in various solvents, the electron configuration of iron, and consequently its Mössbauer spectrum, is determined by several effects. Out of these, two are fundamental*: (1) the coordination of the

* Since in general the Mössbauer effect reflects only changes in the inner coordination sphere of iron, the formation of complexes of outer sphere type, and changes in the structure of the solution which do not affect the inner coordination sphere, appear only weakly, or not at all, in the Mössbauer spectrum.

solvent molecules to iron, and (2) the degree of ion-association between iron(II) ion and the particular anion.

The investigations are rendered more difficult by the fact that anhydrous iron salts are poorly soluble in most of the organic solvents, so that the Mössbauer spectra of the frozen solutions of various iron salts can be compared only in rare cases. Moreover, little is known on the dissociation conditions of iron salts in organic solvents.

Among anhydrous iron(II) salts, only iron(II)chloride was soluble in all the solvents investigated by us (methanol, pyridine, glycol, formamide and dimethylformamide). With anhydrous iron(II) sulfate containing iron enriched in iron-57, the Mössbauer investigation of the solutions of this salt in methanol and in glycol became also possible. To obtain as much information as possible from the Mössbauer spectra, Mössbauer measurements were supplemented by conductivity measurements.

Experimental

Mössbauer spectra were recorded on the apparatus described earlier [5]. The samples were kept during the measurements at liquid air temperature. Cobalt–57 diffused into stainless steel was used as Mössbauer source.

Chemicals and solvents used were of analytical purity. Anhydrous iron(II) chloride was prepared from $FeCl_2 \cdot 4H_2O$, by heating in vacuum oven at 400 °C.

Anhydrous iron(II) sulfate was prepared from metallic iron enriched in iron–57 to 80 per cent, by dissolving it in the calculated amount of sulfuric acid under H_2 atmosphere. Then the solution was evaporated. The crystal water of iron(II) sulfate was removed in a vacuum oven at 250 °C.

Dissolved oxygen was expelled from the solvents by bubbling hydrogen gas through them. Oxygen could not be always completely removed from the solvents by hydrogen, and therefore, iron(II) was oxidized partly (to 10—15 per cent) to iron(III). The Mössbauer spectra of such solutions showed low intensity iron(III) lines, too, *(e.g.* in the system formamide-$FeCl_2 \cdot 4H_2O$), and this circumstance lowered the accuracy of the Mössbauer parameters to ± 0.1 mm/s, which otherwise could be evaluated within ± 0.05 mm/s.

The concentration of the solutions with respect to $FeCl_2$ and $FeCl_2 \cdot 4H_2O$ was 1 mole/1000 g of solvent, while in the case of lower solubilities saturated solutions were used. The concentration of iron(II) sulfate solutions was 0.04 mole/1000 g of solvent.

Conductivity was measured with an a.c. Wheatstone bridge circuit.

The $\varkappa_{el}$ values of anhydrous iron(II) chloride solutions prepared with various solvents and having a concentration of 0.1 mole/1000 ml solution were determined at 25 °C, where $\varkappa_{el} = \varkappa_{solution} - \varkappa_{solvent}$; $\varkappa_{solution}$ and $\varkappa_{solvent}$ being the specific conductivity of the solution and the solvent, respectively.

Results and discussion

It is well known that an aqueous solution of iron(II) chloride contains iron(II)-hexaquo ions and chloride ions, which are not directly linked [6]. However, in solvents of lower solvatation power than water, the chloride can be accommodated in the inner coordination sphere of iron(II).

The specific conductivity of iron(II) chloride solutions in various solvents shows (Table I) that the degree of dissociation of iron(II) chloride in methanol and in formamide is substantially greater than in pyridine, glycol or in dimethylformamide.

Table I

The specific conductivity of anhydrous iron(II)chloride in various solvents
(25 °C, concentration: 0.1 mole/l solution)

Solvent	$\varkappa_{solution}$ Ω^{-1} cm^{-1}	$\varkappa_{solvent}$ Ω^{-1} cm^{-1}	$\varkappa_{el}$ Ω^{-1} cm^{-1}
Methanol	$2.882 \cdot 10^{-3}$	$4.341 \cdot 10^{-6}$	$2.877 \cdot 10^{-2}$
Pyridine	$1.072 \cdot 10^{-4}$	$2.535 \cdot 10^{-7}$	$1.069 \cdot 10^{-4}$
Ethyleneglycol.....	$7.140 \cdot 10^{-4}$	$2.356 \cdot 10^{-7}$	$7.137 \cdot 10^{-4}$
Formamide.....	$3.181 \cdot 10^{-3}$	$7.570 \cdot 10^{-4}$	$2.424 \cdot 10^{-3}$
Dimethylformamide	$1.452 \cdot 10^{-4}$	$9.233 \cdot 10^{-7}$	$1.442 \cdot 10^{-4}$

Thus, according to conductivity measurements, the Mössbauer parameters of iron(II) chloride solutions in methanol and formamide ought to give a pattern characteristic of the solvate parent complex, while solutions in pyridine, glycol and dimethylformamide show a pattern characteristic of mixed complexes, containing also chloride ions besides solvent molecules in the inner coordination sphere of iron(II).

Even when using a preparation enriched in iron-57, the Mössbauer investigation of anhydrous iron(II) sulfate could be performed only in methanol and glycol due to the low solubility of this salt in other solvents.

Mössbauer parameters of the systems investigated are shown in Table II. Conclusions to be drawn from experimental data can be summarized as follows:

Table II

The Mössbauer parameters of frozen iron(II)chloride and iron(II)sulfate solutions

Dissolved substance	Solvent	ΔE, mm/s	δ, mm/s
$FeCl_2$	Methanol	3.50	1.41
$FeSO_4$	Methanol	3.48	1.39
$FeCl_2$	Ethyleneglycol	3.20	1.20
$FeSO_4$	Ethyleneglycol	3.06	1.48
$FeCl_2 \cdot 4H_2O$	Methanol	3.24	1.48
$FeCl_2$	Methanol + water	3.33	1.40
$FeCl_2$	Water	3.20	1.51
$FeCl_2$	Pyridine	3.52	1.36
$FeCl_2$	Formamide	1.89	1.43
$FeCl_2$	Dimethylformamide	1.38	0.54
$FeCl_2 \cdot 4H_2O$	Formamide	2.71	1.41
$FeCl_2 \cdot 4H_2O$	Dimethylformamide	2.67	1.25
		1.31	0.41

1. In methanol-ice, iron(II) sulfate gave a Mössbauer spectrum, completely identical with that of iron(II) chloride, while in glycol-ice the Mössbauer parameters of the two salts were different. Thus, in their methanolic solutions both iron(II) salts formed iron(II) solvate complexes of identical composition, while in glycolic solution the composition of the coordination sphere of iron(II) depends also on the anion.

On comparing the Mössbauer parameters of the methanol solvate with those of the aquocomplex, it can be seen that with the first the electric field gradient at the iron nucleus is higher than with the latter. This is consistent with the fact that methanol molecules have a lower symmetry than water molecules.

2. When iron(II) chloride containing crystal water ($FeCl_2 \cdot 4H_2O$) was dissolved in methanol, Mössbauer parameters obtained differed significantly from those measured for anhydrous iron(II) chloride solution.

This fact shows that in the course of the dissolution of the salt in methanol the solvent molecules do not displace the water molecules from the coordination sphere of the iron(II).

When a calculated amount of water (4 molecules of water for each Fe atom) was added to the solution of anhydrous iron(II) chloride in methanol, the frozen solution gave after 24 hours a spectrum almost identical with that of the solution of $FeCl_2 \cdot 4H_2O$ in absolute methanol.

Thus, the affinity of water molecules for iron(II) is stronger than that of the methanol molecules, so that even under the given extreme concentration conditions the solvatation equilibrium is shifted in the direction of the formation of the aquocomplex.

3. On comparing the isomer shift value of the frozen solutions of anhydrous iron(II) chloride in pyridine, glycol and dimethylformamide with those measured in its frozen solutions in water, methanol and formamide, it can be seen that in the former solutions, where, according to conductivity data, also the chloride ions are presumably bound in the inner coordination sphere of iron, the isomer shift values are smaller than in the case of the latter solutions, in which chloride ions are not linked to iron(II) (Fig. 1).

This phenomenon can be interpreted with the nephelauxetic effect of chloride [7]. It is due to this effect that chloride in the inner coordination sphere of iron diminishes the d electron density on iron. By decreasing the shielding effect of d electrons, it increases the electron density at the nucleus. This is reflected in the diminution of the isomer shift values.

In case of iron(II) compounds, the nephelauxetic effect diminishes generally also the ΔE value [7]. However, the symmetry-reducing action of the chloride ion in the solvate sheath may act in the opposite direction, so that an increase in ΔE may occur. Depending on the circumstance which of these two counteracting effects predominates, the value of quadrupole split-

ting may be smaller or larger than that of the analogous solvate which does not contain chloride. In the solution of iron(II) chloride in glycol $\Delta E = 3.20$, while in the solution of iron(II) sulfate in glycol $\Delta E = 3.06$, *i.e.* quadrupole splitting is not reduced by the nephelauxetic effect. However, isomer shift values ($FeCl_2$ $\delta = 1.20$ and $FeSO_4$ $\delta = 1.48$) unequivocally reflect that effect.

4. In the glycol—$FeCl_2 \cdot 4H_2O$ system, the water molecules cannot be displaced from the solvent sheath by the glycol molecules, similarly to the case of the methanolic solution, where water molecules are not replaced by methanol molecules (here ΔE and δ values are near those obtained for aqueous

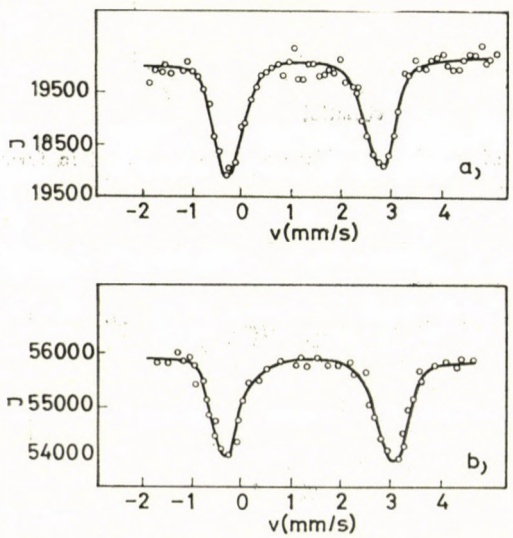

Fig. 1. Mössbauer spectra of the frozen solutions of $Fe(II)Cl_2$ (a) in glycol and (b) in methanol at liquid air temperature

solutions). Indeed, as in the preceding case, this is in accord with the fact that the coordination power of water molecules is considerably greater than that of glycol molecules (or methanol molecules).

The Mössbauer parameters of the precipitate formed in the glycol-$FeCl_2$ system are practically the same as those obtained for the solution.

The relatively small ΔE values obtained for the solutions of iron(II) chloride in formamide and dimethylformamide, respectively, are indicative of the fact that the solvent sheath containing formamide molecules or dimethylformamide molecules increases the symmetry of the electron cloud of the central iron atom (Fig. 2).

The large difference between the δ values for the solvents formamide and dimethylformamide can be interpreted on the basis of conductivity measurements by the finding that in the formamide solvate no chloride ions

are accommodated in the solvate sheath of iron(II), while in the case of dimethylformamide also chloride ions are coordinated in the inner coordination sphere, and owing to their strong nephelauxetic effect, increase the s electron density at the central iron atom.

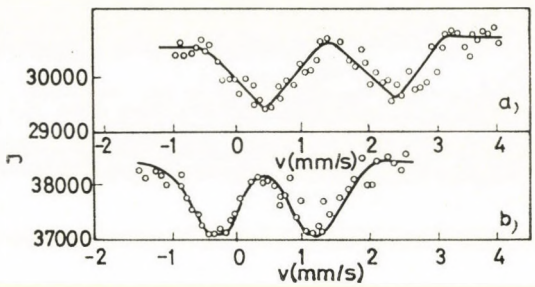

Fig. 2. Mössbauer spectra of the frozen solutions of $Fe(II)Cl_2$ (a) in formamide and (b) in dimethylformamide at liquid air temperature

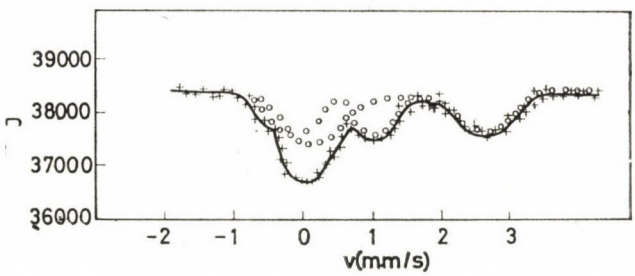

Fig. 3. Mössbauer spectrum of the frozen solution of $Fe(II)Cl_2 \cdot 4H_2O$ in dimethylformamide (+ spectrum measured; o components of the superposed spectrum)

Mössbauer parameters measured in the systems formamide-$FeCl_2 \cdot 4H_2O$ and dimethylformamide-$FeCl_2 \cdot 4H_2O$ show that water is displaced in several steps from the solvent sheath by these solvents, so that intermediate mixed complexes are formed. For example, in the system dimethylformamide-$FeCl_2 \cdot 4H_2O$, lines corresponding to a solvate sheath containing also water ($\Delta E = 2.67$ mm/s, $\delta = 1.25$ mm/s) and those corresponding to a solvate sheath already free of water ($\Delta E = 1.31$ mm/s, $\delta = 0.41$ mm/s) appear together in the Mössbauer spectrum (Fig. 3).

*

The authors wish to thank Dr. E. KUGLER for her useful advice concerning conductivity measurements, to Mrs. L. SUBA for her conscientious, precise work, and to B. MOLNÁR (Central Research Institute for Physics) for his help in the preparation of anhydrous $FeCl_2$.

REFERENCES

1. Dézsi, I., Keszthelyi, L., Pócs, I., Korecz, L.: Phys. Letters **14,** 14 (1965)
2. Nozik, A. J., Kaplan, M.: J. Chem. Phys. **47,** 2960 (1967)
3. Vértes, A.: Magy. Kém. Folyóirat **75,** 175 (1969)
4. Vértes, A., Burger, K., Suba L.: Acta Chim. Acad. Sci. Hung. **63,** 123 (1970)
5. Soós, J., Vértes, A.: Magyar Kémikusok Lapja **23,** 690 (1968)
6. Po, H. N., Sutin, N.: Inorg. Chem. **7,** 621 (1968)
7. Burger, K., Vértes, A., Papp-Molnár, E.: Acta Chim. Acad. Sci. Hung. **57,** 257 (1968)

Kálmán Burger
Attila Vértes
Ilona N. Czakó

Budapest VIII., Múzeum krt 4/b

Acta Chimica Academiae Scientiarum Hungaricae, Tomus 63 (2), pp. 123—127 (1970)

INVESTIGATION OF THE SOLVATATION OF ANHYDROUS IRON(II)CHLORIDE IN METHANOL–FORMAMIDE MIXTURES WITH THE AID OF THE MÖSSBAUER EFFECT

A. VÉRTES*, K. BURGER** and M. SUBA*

*(*Institute of Physical Chemistry and Radiology, L. Eötvös University, Budapest,*
***Institute of Inorganic and Analytical Chemistry, L. Eötvös University, Budapest)*

Received November 23, 1968

The Mössbauer spectra of $FeCl_2$, dissolved in methanol–formamide mixtures of various composition were recorded. It can be established on the basis of these measurements that in these mixtures two kinds of iron(II) solvates, in equilibrium with each other, are formed.

Although Mössbauer effect can be observed only in the solid phase DÉZSI's [1] investigations disclosed the possibility for studying liquid systems as well [2, 3, 4, 5]. It is to be assumed that in equilibrium systems, in which the equilibria in the solution can be frozen in by a rapid freezing of the solution, the study of the solid solution containing a Mössbauer atom permits to draw conclusions on the system which existed in the solution. In view of the fact that the shift of complex formation equilibria, and thus, the extent of solvatation is accompanied by the displacement of ions or molecules, the rate of equilibrium reactions should be lowered considerably by freezing. Presuming that solvents cooled rapidly to liquid air temperature will form solid solutions, the structure of which is similar to that of the original solution, and is transformed only with time to a structure characteristic of ice [5], the Mössbauer method appears to be suitable for the studying of solvatation phenomena. In the following, we report on the application of this technique.

For the purposes of these investigations, solvent mixtures had to be selected, the components of which considerably change the Mössbauer spectrum of the dissolved substance [4]. This permits to follow from the spectrum of the solvent mixture on the solvates formed in it. As model system, the solutions of iron (II) chloride in methanol–formamide mixtures of various composition were chosen. We present the Mössbauer spectra of the frozen solutions, and discuss the conclusions, which can be drawn from these spectra on the structure of the solution.

Experimental

The measuring equipment constructed by us for the recording of the Mössbauer spectra has been described earlier [6]. 5 mCi of Co^{57} isotope, diffunded into stainless steel, of the marking "CTD 3", manufactured by the Radiochemical Centre Amersham, was used as radiation source.

Measurements were carried out at liquid air temperature.

Chemicals used for the preparation of the solutions were of analytical grade.

To prevent the oxidation of iron(II), before dissolution, hydrogen gas was bubbled through the solvents for 40 minutes.

The concentration of the solutions was 0.7 mole per 1000 g of solvent.

In each case, the solutions were prepared by dissolving the anhydrous iron(II) chloride in the solvent mixture prepared previously.

Results and discussion

The Mössbauer spectra of the solid solutions, obtained by the rapid freezing of the solutions of iron(II) chloride in methanol, in formamide, and in their mixtures of various proportion on the temperature of liquid air, is shown in Fig. 1. The most important parameters of these spectra are summarized in Table I.

It can be seen in Fig. 1 that the difference between the values of the Mössbauer quadrupole splitting, ΔE, in methanol and in formamide is sufficiently large to permit the differentiation of the single solvates in the solvent mixtures. On the other hand, the isomere shift values (δ) are nearly identical. A comparison of these quadrupole splitting values with that of the frozen aqueous iron(II) chloride solution shows that the electric field gradient at the iron nucleus is smaller in the formamide solvate, while larger in the methanol solvate than in the aquosolvate.

The spectra of the frozen solutions prepared with solvent mixtures clearly show that each of them is a superposition of two spectra exhibiting quadrupole splitting. This indicates unequivocally that two different species containing iron are present in the frozen solutions. That part of the spectrum which exhibits a smaller quadrupole splitting, has a ΔE value near to that measured in the formamide solution (see Table I). Therefore, this is probably a line pair arising from a solvent sheath consisting totally or predominantly of formamide molecules. The greater ΔE value can be associated with the solvate sheath built up from methanol molecules, since it lies near the ΔE value of the pure methanolic solution (Table I).

It should be mentioned that larger and smaller ΔE values cannot be considered as completely identical with the quadrupole splitting value $\Delta E = 3.54 \pm 0.05$ mm/s of the solution in pure methanol and $\Delta E = 1.89 \pm 0.05$ mm/s of the solution in pure formamide. (The isomer shift values δ are, within the limits of experimental error, identical for the mixtures and the pure solvents.) The difference in the values of quadrupole splitting measured in the

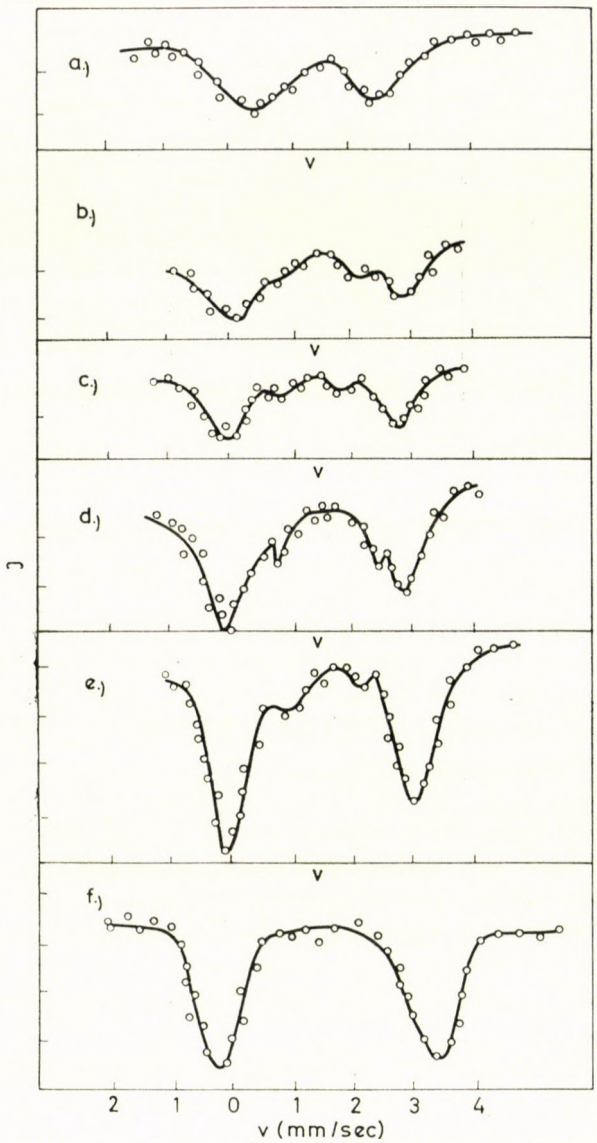

Fig. 1. The Mössbauer spectra of the frozen solutions of $FeCl_2$ in methanol–formamide mixtures of various composition

a) 0.0 w/w% of methanol + 100.0 w/w% of formamide;
b) 20.04 ,, ,, ,, + 79.96 ,, ,, ,,
c) 37.60 ,, ,, ,, + 62.40 ,, ,, ,,
d) 59.00 ,, ,, ,, + 41.00 ,, ,, ,,
e) 79.50 ,, ,, ,, + 20.50 ,, ,, ,,
f) 100.0 ,, ,, ,, + 0.0 ,, ,, ,,

Table I

Composition of the mixture methanol + formamide, w/w per cent		Mössbauer parameters	
		ΔE* mm/s	δ* mm/s
0.00	100.00	1.89	1.43
20.04	79.96	2.80 1.45	1.50
37.60	62.40	2.86 1.36	1.45
59.00	41.00	2.92 1.60	1.40
79.50	20.50	3.10 1.55	1.47
100.00	0.00	3.54	1.34

* Accuracy of the measurements ± 0.05 mm/s

pure solvents and the mixtures may arise from the fact that the solvent sheaths of two kinds do not consist exclusively of methanol and formamide molecules, respectively, but also "mixed solvates" are formed. On the other hand, this degree of change in the quadrupole splitting value may be due to a difference in crystal structure of the frozen solvent mixture and the frozen pure methanol or formamide. These differences in the crystal structure may cause a slight difference in the symmetry of the charge distribution in the environment of the iron nucleus.

It follows from the aforesaid that it cannot be unambiguously decided on the basis of the Mössbauer spectra whether mixed or pure solvate sheaths are formed in methanol – formamide mixtures. However, it can be established beyond doubt that two kinds of solvate sheaths are present.

It is noteworthy that the intensity of the lines belonging to the smaller ΔE values of the spectra is for each composition of the mixture (even for formamide w/w% > 50) lower than that of the lines belonging to the region of the larger ΔE values. Assuming that the probablity of recoil-free absorption (f) is identical for the two solvate sheaths in the solvent mixture, this means that the relative quantity of the solvate belonging to the larger ΔE value (methanol solvate) is in each case greater than the relative quantity of the solvate resulting a smaller ΔE value. This is remarkable in view of the fact that the dipole moment of formamide ($\mu = 3.37$) is considerably larger than that of methanol ($\mu = 1.66$) so that formamide would be expected to have a more intense solvating effect. On the other hand, the oxygen atom of methanol actually can be sonsidered as a stronger Lewis base, than the donor atom of formamide, which is consistent with the phenomenon observed.

However, it can be seen from the spectra that the relative intensity of the line pair belonging to the smaller ΔE value diminishes with a decreasing formamide content of the mixtures. This indicates an equilibrium between the two kinds of solvate complexes.

The slight antisymmetry of the spectra presumably arises from the fact that notwithstanding the pretreatment with hydrogen, a small part of the iron(II) chloride oxidizes, and, owing to the superposition of the lines arising from iron(III), the intensity of the lines belonging to smaller velocities slightly increases. However, this circumstance does not interfere in the evaluation of the lines of higher intensity, due to iron(II).

We tried to study the above system by infrared spectrometry at room temperature. However, the formation of the solvate complexes distorts the infrared spectrum of the solvent molecules only to such a small extent that this change could not be observed in the presence of the large excess in free solvent molecules. Owing to the relatively poor solubility of iron(II) chloride, the solutions were 0.7 molar with respect to iron, so that coordinated solvent molecules amounted to not more than 10–15 per cent of the total of solvent molecules. Therefore, the small shift of bands, characteristic of solvates, was completely masked by the bands of the free solvent molecules. The stretching frequencies of the iron–solvate–donor atom coordinate bond appear at such low frequencies, which makes their observation and assignement impossible.

Further results are to be expected from the NMR study of the systems.

REFERENCES

1. DÉZSI, I., KESZTHELYI, L., PÓCS, L., KORECZ, L.: Phys. Letters **14**, 14 (1965)
2. DÉZSI, I., VÉRTES, A., KOMOR, M.: Inorg. Nucl. Chem. (in print)
3. VÉRTES, A.: Magy. Kém. Folyóirat (in the press)
4. BURGER, K., VÉRTES, A., N. CZAKÓ, I.: Acta Chim. Acad. Sci. Hung. **63**, 115 (1970)
5. NOZIK, A. J., KAPLAN, M.: J. Chem. Phys. **47**, 2960 (1967)
6. SOÓS, I., VÉRTES, A.: Magy. Kémikusok Lapja (in print)

Attila VÉRTES
Kálmán BURGER
Magdolna SUBA
Budapest VIII., Puskin-u. 7.

Acta Chimica Academiae Scientiarum Hungaricae, Tomus 63 (2), pp. 129—141 (1970)

HALBEMPIRISCHE METHODE ZUR ANNÄHERNDEN BERECHNUNG DES DAMPF–FLÜSSIGKEIT-GLEICHGEWICHTES VON BINÄREN ALKOHOL–KOHLENWASSERSTOFF-GEMISCHEN*

F. RATKOVICS und L. MÉSZÁROS

(Elektrochemische Forschungsgruppe der Ungarischen Akademie der Wissenschaften bei dem Lehrstuhl für Physikalische Chemie der Chemisch-technischen Universität, Veszprém)

Eingegangen am 5. Oktober 1968

Es wird ein halbempirisches Verfahren zur Berechnung der Dampf–Flüssigkeit-Gleichgewichtsdaten von Gemischen aus Alkohol und Kohlenwasserstoff beschrieben, wobei das Gemisch der Alkoholkomponente des zu berechnenden Gemisches mit einem anderen Kohlenwasserstoff als Bezugssystem verwendet wird. Sind die Eigenschaften des Bezugsgemisches bekannt, so können die Dampf–Flüssigkeit-Gleichgewichte für sämtliche binäre Gemische des Alkohols mit beliebigen Kohlenwasserstoffen berechnet werden, wenn der Hildebrandsche Lösungsparameter des Kohlenwasserstoffes bekannt ist. Der Fehler der berechneten Gleichgewichtsdaten blieb in den geprüften Fällen unterhalb $\pm$ 3 Mol% bzw. $\pm$ 7 Torr. Das Verfahren wird zur Bestimmung der zur Berechnung von Vielkomponentengemischen aus Alkoholen und Kohlenwasserstoffen nötigen Ausgangsdaten (Wilson-Konstanten von binären Gemischen) empfohlen.

Zur Berechnung des Dampf–Flüssigkeit-Gleichgewichtes von Mehrkomponentengemischen, welche auch polare Komponenten enthalten, sind nur Methoden bekannt, bei denen als Ausgangsdaten die Kenntnis der Gleichgewichtsdaten sämtlicher möglichen binären Gemische aus den Komponenten des Mehrkomponentengemisches erforderlich ist [1]. In unseren früheren Arbeiten [2, 3, 4] wurde darüber berichtet, daß das Dampf–Flüssigkeit-Gleichgewicht des Äthanol–Kohlenwasserstoff-Gemisches auch auf der Basis eines Modells berechnet werden kann, welches auf der Annahme beruht, daß das Äthanol selbst ein ideales binäres Gemisch aus monomeren und dimeren Alkoholmolekülen ist, während sein Gemisch mit Kohlenwasserstoffen ein reguläres ternäres Gemisch ist. Diese Berechnungsart hat den Nachteil, daß einerseits die Kenntnis des Assoziationsgleichgewichtes des Alkohols erforderlich ist, und daß andererseits — wegen der Trennung der monomeren und dimeren Alkoholmoleküle — die in der Berechnung angewendeten Molenbrüche zahlenmäßig von den Molenbrüchen im üblichen Sinne abweichen. In der vorliegenden Mitteilung wird über ein Berechnungsverfahren berichtet, welches im wesentlichen auf dem erwähnten Modell des regulären ternären Gemisches beruht, die bei seiner Anwendung auftretenden Schwierigkeiten jedoch beseitigt.

Prinzip der Methode

Beim regulären ternären Gemisch-Modell zur Berechnung der Alkohol–Kohlenwasserstoff-Gemische wurde die Gültigkeit folgender Zusammenhänge angenommen:

Gesamtdruck des Gemisches

$$P = p_A + p_{AA} + p_B. \tag{1}$$

Die Assoziationsgleichgewichtskonstante des Alkohols ist nur von der Temperatur abhängig und beträgt

$$K = \frac{X_{AA}}{X_A^2} \cdot \frac{\gamma_{AA}}{\gamma_A^2} = \text{konst.}, \tag{2}$$

wo

$$\ln \gamma_A = \ln \gamma_{AA} = q X_B^2 \tag{3}$$

und

$$\ln \gamma_B = q(1 - X_B)^2 \tag{4}$$

$$q = \frac{\Delta E}{RT} \tag{5}$$

$$p_i = P_i^0 X_i \gamma_i . \tag{6}$$

Im weiteren werden folgende vereinfachende Annahmen benützt:

1) Bei niedrigen Drucken ist der Partialdruck der Fugazität gleichzusetzen.

2) Der Partialdruck des dimeren Alkohols kann stets vernachlässigt werden [4].

In diesem Fall können für den Partialdruck des Alkohols bzw. des Kohlenwasserstoffs je zwei Gleichungen geschrieben werden, die eine aufgrund des regulären ternären Gemischmodells, die andere auf die übliche Art:

$$p_A = P_A^0 X_A \gamma_A \quad \text{oder} \quad p_1 = P_1^0 X_1 \gamma_1 \tag{7}$$

$$p_B = P_B^0 X_B \gamma_A \quad \text{oder} \quad p_2 = P_2^0 X_2 \gamma_2 \tag{8}$$

Da $p_B = p_2$ und $p_A \approx p_1$, ist

$$P_A^0 X_A \gamma_A = P_1^0 X_1 \gamma_1 \tag{9}$$

$$P_B^0 X_B \gamma_B = P_2^0 X_2 \gamma_2 . \tag{10}$$

Aus Gl (9) und (10), unter Verwendung der Gl. (2), (3) und (4) sowie aus der vereinfachenden Annahme

$$\frac{1-X_2-X_A}{1+X_2} \approx \frac{1-X_2}{1+X_2}$$

d. h., daß in der Flüssigkeitsphase nur geringe Mengen von monomeren Alkoholmolekülen vorhanden sind [4], ergeben sich folgende Zusammenhänge für die Aktivitätskoeffizienten:

$$\ln \gamma_1 = \frac{1}{2} \ln \frac{1}{(1+X_2)X_1} + 2q \left(\frac{X_2}{1+X_2} \right)^2 \tag{11}$$

$$\ln \gamma_2 = \ln \frac{2}{1+X_2} + q \left(\frac{X_1}{1+X_2} \right)^2 . \tag{12}$$

Das erste Glied der rechten Seite in Gl. (11) wird bei $X_1 = 0$ unendlich; die Gleichung ist also in der vorliegenden Form im Gebiete der geringen Werte von X_1 (wegen der Vernachlässigung $1-X_2-X_A \approx 1-X_2$) unbrauchbar. Nähert sich nämlich der Wert von X_2 dem Wert 1, so assoziiert der Alkohol wegen der hohen Verdünnung nur in geringem Maße, folglich ist die Vernachlässigung des monomeren Alkohols unbegründet. Es ist bemerkenswert, daß die Konstante q, welche die Wechselwirkung der Moleküle charakterisiert, im ersten Glied der rechten Seite der Gleichungen nicht enthalten ist, während das zweite Glied der rechten Seite vor allem von diesem — die Austauschenergie ΔE enthaltenden — Wert q abhängig ist. Nach dieser Erkenntnis wurde unsere Methode auf folgende Betrachtungen aufgebaut:

1) Die Ungenauigkeit der Gl. (11) und (12) wird vor allem durch die Ungenauigkeit des die Assoziation beinhaltenden Glieds verursacht. Die Gleichung kann also dann genauer geschrieben werden, wenn diese Glieder durch die vorläufig unbekannten Funktionen $f(X_2)$ bzw. $g(X_1)$ ersetzt werden:

$$\ln \gamma_1 = f(X_1) + 2q \left(\frac{X_2}{1+X_2} \right)^2 \tag{13}$$

$$\ln \gamma_2 = g(X_1) + q \left(\frac{X_1}{1+X_2} \right)^2 \tag{14}$$

2) Die Konstante $q = \Delta E/RT$, welche die Wechselwirkungsenergie beinhaltet, ist offensichtlich von der Energie der Weschselwirkungen zwischen den Alkohol- und Kohlenwasserstoffmolekülen abhängig. Da jedoch zwischen den größtenteils in Form von Assoziaten vorliegenden Alkoholmolekülen und

den Kohlenwasserstoffmolekülen vor allem eine Wechselwirkung aufgrund von Dispersionskräften vorstellbar ist, kann erwartet werden, daß der Wert q in eindeutigen Zusammenhang mit dem die Eigenschaften der Kohlenwasserstoff-Kohlenwasserstoff-Gemische charakterisierenden Hildebrandschen Lösungsparameter gebracht werden kann. Diese Annahme, wie im weiteren noch gezeigt werden soll, erwies sich als richtig.

3) Eine Möglichkeit zur Bestimmung der vorerst unbekannten Funktionen $f(X_1)$ und $g(X_1)$ ergibt sich aus dem Umstand, daß der Assoziationsgrad eines gegebenen Alkohols bei gegebener Konzetration und gegebener Temperatur in Gemischen mit verschiedenen Kohlenwasserstoffen in guter Annäherung identisch ist. Die gesuchten Funktionen können also — in Kenntnis der Eigenschaften eines einzigen binären Gemisches — für die Gemische des betreffenden Alkohols mit allen sonstigen Kohlenwasserstoffen bestimmt werden.

Zusammenhang zwischen der Austauschenergie und dem Hildebrandschen Lösungsparameter

Um den Zusammenhang zwischen der Austauschenergie ΔE und dem Lösungsparameter δ zu bestimmen, wurden die Angaben $X - Y$ und $P - X$ der in Tabelle I zusammengefaßten binären Gemische bearbeitet.

Tabelle I

Untersuchte binäre Gemische

Komponenten		Temperatur °C	Literatur
A	*B*		
Äthanol.....	Benzol	40	[5]
Äthanol.....	Toluol	60	[6]
Äthanol.....	*n*-Pentan	20	[7]
Äthanol.....	*n*-Hexan	30	[8]
Äthanol.....	*n*-Heptan	30 u. 70	[9, 10]
Äthanol.....	Cyclohexan	30	[11]
Äthanol.....	Methylcyclohexan	30 u. 55	[8]

Gl. (11) und (12) wurde im Molenbruchbereich $X_1 = 0.1 - 0{,}9$ zur Beschreibung der Versuchsergebnisse angewendet und die den Vesuchsergebnissen am besten entsprechenden Werte von q und ΔE wurden festgestellt. Wegen der bereits erwähnten Unbrauchbarkeit der Gleichung in den Molenbruchgebieten $X_1 < 0{,}1$ bzw. $X_1 > 0{,}9$ wurden diese Gebiete außer acht gelassen.

Als Beispiel ist in Abb. 1 das Ergebnis für das Gemisch Äthanol – *n*-Heptan bei 70 °C dargestellt. Die gemessenen bzw. berechneten Werte sind in Tabelle II zusammengestellt.

Tabelle II

Berechnete Werte			*Gemessene Werte* [10]		
X_1	Y_1	P, torr	X_1	Y_1	P, torr
0,1	0,4854	571	0,0567	0,4685	500,3
0,2	0,5660	630	0,1180	0,5531	614,3
0,3	0,6149	664	0,1573	0,5790	648,0
0,4	0,6365	687	0,2575	0,6000	689,6
0,5	0,6527	699	0,3633	0,6114	705,9
0,6	0,6638	702	0,4290	0,6213	712,1
0,7	0,6736	704	0,5069	0,6241	715,7
0,8	0,6891	693	0,5968	0,6280	717,7
0,9	0,7395	679	0,6648	0,6383	717,7
			0,7174	0,6483	717,7
			0,8200	0,6516	704,9
			0,8600	0,6713	693,4
			0,8940	0,7293	676,5
			0,9250	0,8013	651,8
			0,9564	0,8639	610,0
			0,9827	0,9211	569,4

Der graphische Vergleich der Ergebnisse (Abb. 1) weist auf den charakteristischen Fehler der Methode hin. Die Abweichung der berechneten von den gemessen Angaben war in sämtlichen untersuchten Fällen von gleichem Charakter und ähnlicher Größe.

Aus der Bearbeitung der in Tabelle I angeführten binären Gemische standen uns nun die den Versuchsergebnissen am nächsten liegenden Werte q zur Verfügung. Diese sind in Tabelle II angeführt, und zwar zwecks besserer Vergleichbarkeit der Werte in die von der Temperatur unabhängige Form $q \cdot RT = \Delta E$ cal/mol gebracht.

Nun suchten wir einen Zusammenhang zwischen den Angaben in Tabelle III und dem Lösungsparameter der Kohlenwasserstoffe. Definitionsgemäß ist der Lösungsparameter [12]

$$\delta_i = \left(\frac{\Delta e}{V_i}\right)^{1/2}. \tag{15}$$

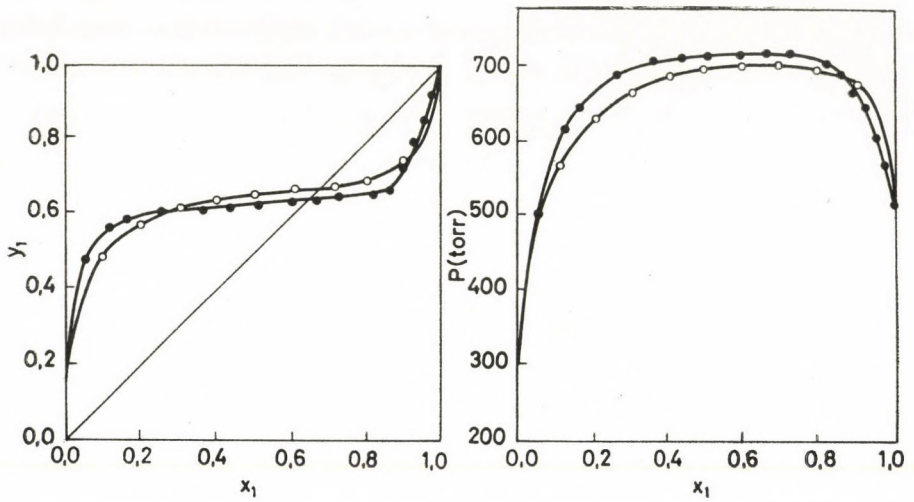

Abb. 1. Gemisch Äthanol–*n*-Heptan bei 70 °C. o berechnete Werte; * gemessene Werte

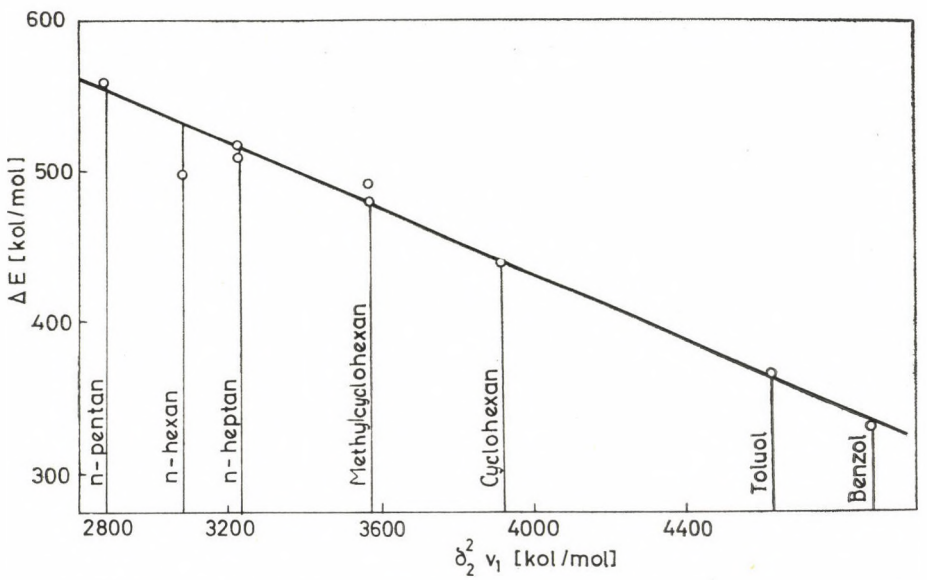

Abb. 2. ΔE-Werte in Gemischen von Äthanol mit verschiedenen Kohlenwasserstoffen *n*-Pentan, *n*-Hexan, *n*-Heptan, Methylcyclohexan, Cyclohexan, Toluol, Benzol

Da $\Delta e/V_i$ die Dispersionsenergiedichte bedeutet, dividierten wir die Austauschenergie durch das Molvolumen des Alkohols und suchten den Zusammenhang, indem der Wert $q \cdot RT = \Delta E$ als Funktion von $\Delta e/V_2 \cdot V_1 = \delta_2^2 \cdot V_1$ dargestellt wurde.

Tabelle III

Den Versuchsergebnissen am nächsten liegende Austauschenergien

Gemische		ΔE, [cal/mol]
Äthanol.....	*n*-Pentan	561
Äthanol.....	*n*-Hexan	498
Äthanol.....	*n*-Heptan	517, 510
Äthanol.....	Methylcyclohexan	479, 490
Äthanol.....	Cyclohexan	440
Äthanol.....	Toluol	366
Äthanol.....	Benzol	326

Die Ergebnisse sind in Abb. 2 dargestellt. Wie ersichtlich, können die Meßpunkte ausreichend durch eine Gerade angenähert werden, deren Gleichung folgende ist:

$$E_{12} = 875 - 0{,}111\,\delta_2^2 \cdot V_1. \tag{16}$$

Anwendung der Berechnungsmethode

Mittels der Gleichung (16), welche den Zusammenhang zwischen der Austauschenergie und dem Lösungsparameter beschreibt, sowie mit Gl. (13) und (14) wurde — in Kenntnis der Dampf–Flüssigkeit-Gleichgewichtsangaben eines als Referenzsystem gewählten Alkohol–Kohlenwasserstoff-Gemisches — die Berechnung der Dampf–Flüssigkeit-Gleichgewichte von Gemischen desselben Alkohols mit anderen Kohlenwasserstoffen ermöglicht.

Es seien die Angaben des Gemisches 1—2 bekannt und es sollen die Aktivitätskoeffizienten des Gemisches 1—3 berechnet werden.

Da im Gemisch 1—2

$$\ln \gamma_{1(2)} = f(X_1) + 2\,\frac{\Delta E_{12}}{RT}\left(\frac{1 - X_1}{2 - X_1}\right)^2$$

und

$$\ln \gamma_{2(1)} = g(X_1) + \frac{\Delta E_{12}}{RT}\left(\frac{X_1}{2 - X_1}\right)^2,$$

während im Gemisch 1—3 die unbekannten Aktivitätskoeffizienten

$$\ln \gamma_{1(3)} = f(X_1) + 2\,\frac{\Delta E_{13}}{RT}\left(\frac{1 - X_1}{2 - X_1}\right)^2$$

und

$$\ln \gamma_{3(1)} = g(X_1) + \frac{\Delta E_{13}}{RT}\left(\frac{X_1}{2 - X_1}\right)^2$$

sind, ergibt sich

$$\ln \gamma_{1(3)} = \ln \gamma_{1(2)} + 2 \frac{\Delta E_{13} - \Delta E_{12}}{RT} \left(\frac{1 - X_1}{2 - X_1} \right)^2$$

und

$$\ln \gamma_{3(1)} = \ln \gamma_{2(1)} + \frac{\Delta E_{13} - \Delta E_{12}}{RT} \left(\frac{X_1}{2 - X_1} \right)^2 .$$

Es ist selbstverständlich, daß es sich um $\gamma_{1(2)}$ und $\gamma_{2(1)}$-Werte bei dem X_1-Wert handelt, auf welche sich die Berechnung bezieht.

Die Werte von ΔE_{12} und ΔE_{13} werden in Kenntnis der Lösungsparameter der Kohlenwasserstoffe mittels Gl. (16) berechnet.

Im weiteren werden die Ergebnisse einiger Berechnungen angeführt. Die untersuchten Gemische sind:

1) Äthanol – *n*-Hexan (Referenzsystem Äthanol–Benzol);
2) Äthanol – Methylcyclohexan (Referenzsystem Äthanol–Benzol);
3) Isopropanol – Cyclohexan (Referenzsystem *i*-Propanol–Benzol) [13].

Aus den bei 40 °C gemessenen Angaben des Systems Äthanol–Benzol [5] wurden die Aktivitätskoeffizienten beider Komponenten bestimmt. Die Angaben für die Meßpunkte bzw. für »runde« Molenbrüche von 0,1; 0,2; 0,3 usw. sind in Tabelle IV enthalten.

Aus den Angaben der Tabelle IV können die für das Äthanol charakteristischen Funktionen $g(X)$ und $f(X)$ bestimmt werden. Der Wert von ΔE wird dazu aus dem Zusammenhang $\Delta E = 875 - 0{,}111 \cdot \delta_2^2 \cdot V_1$ berechnet:

$$\delta_2 = 9{,}158\,(\text{cal cm}^{-3})^{1/2}\,[12]$$

$$V_1 = \frac{46{,}07}{0{,}798} = 58{,}3\ (\text{cm}^3\ \text{mol}^{-1})\,[14],$$

Tabelle IV

Aktivitätskoeffizienten des Systems Äthanol–Benzol bei 40 °C

Meßdaten				Graphisch bestimmte Daten			
X_1	$\lg \gamma_{1\,(2)}$	$\lg \gamma_{2\,(1)}$	P, torr	X_1	$\lg \gamma_{1\,(2)}$	$\lg \gamma_{2\,(1)}$	P, torr
0,020	1,051	—0,003	208,4	0,0	—	0,000	184
0,095	0,722	0,016	239,8	0,1	0,695	0,018	241
0,204	0,479	0,056	249,1	0,2	0,490	0,052	248
0,378	0,255	0,148	252,3	0,3	0,355	0,097	252
0,490	0,162	0,215	248,8	0,4	0,230	0,150	252
0,592	0,097	0,289	245,7	0,5	0,155	0,220	248
0,702	0,044	0,385	237,3	0,6	0,090	0,285	244
0,802	0,016	0,474	219,4	0,7	0,042	0,375	236
0,880	0,002	0,548	196,3	0,8	0,013	0,465	219
0,943	0,000	0,611	169,5	0,9	0,000	0,555	190
0,987	0,000	0,731	145,6	1,0	0,000	—	134

Tabelle V

Korrektionsfunktionen aufgrund der Angaben des Systems Äthanol–Benzol bei 40 °C

X_1	$f(X_1)$	$g(X_1)$
0,0	—	0,000
0,1	0,448	0,017
0,2	0,273	0,045
0,3	0,168	0,080
0,4	0,074	0,116
0,5	0,033	0,159
0,6	0,000	0,184
0,7	—0,016	0,215
0,8	—0,017	0,220
0,9	—0,009	0,186
1,0	0,000	—

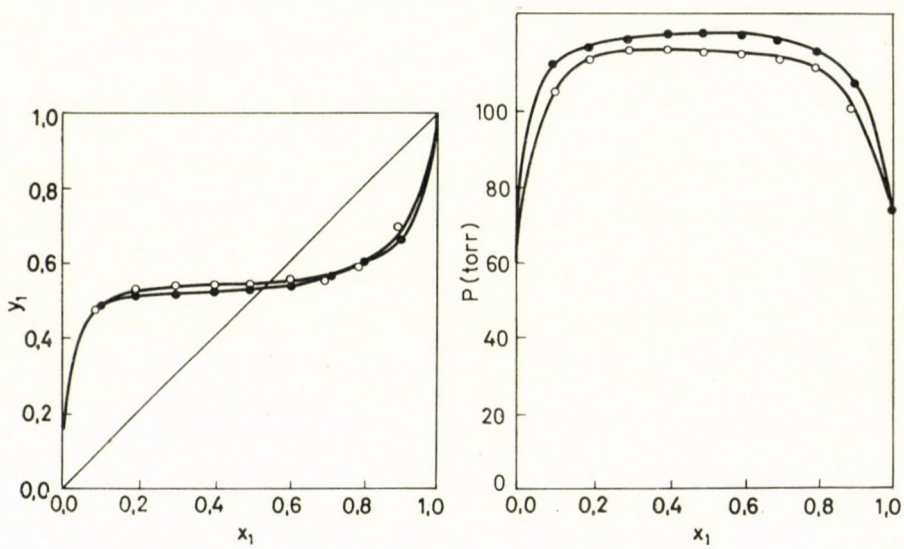

Abb. 3. Gemisch Äthanol–Methylcyclohexan bei 30 °C. o berechnete Werte; * gemessene Werte

folglich ist $\Delta E_{12} = 332$ cal/mol. Die Korrektionsfunktionen für die Assoziation sind in Tabelle V für »runde« Werte des Molenbruchs angegeben.

Auf ähnliche Art wurde auch im Fall des Systems Isopropanol–Benzol verfahren.

Der Vergleich der mit den Daten des Referenzsystems Äthanol–Benzol berechneten und der gemessenen Ergebnisse ist in Abb. 3, 4 und 5, bzw. für »runde« Molenbrüche in Tabelle VI enthalten.

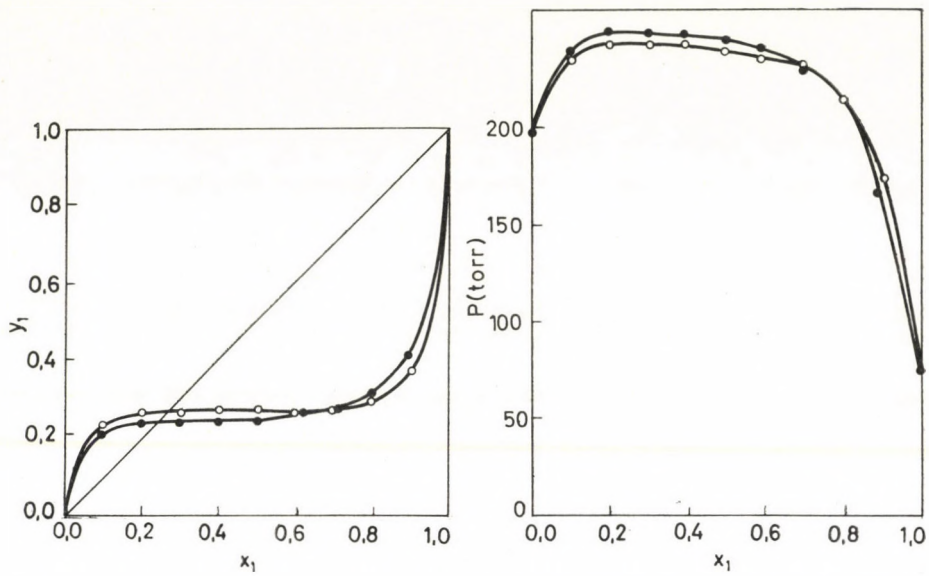

Abb. 4. Gemisch Äthanol–*n*-Hexan bei 30 °C. o berechnete Werte; * gemessene Werte

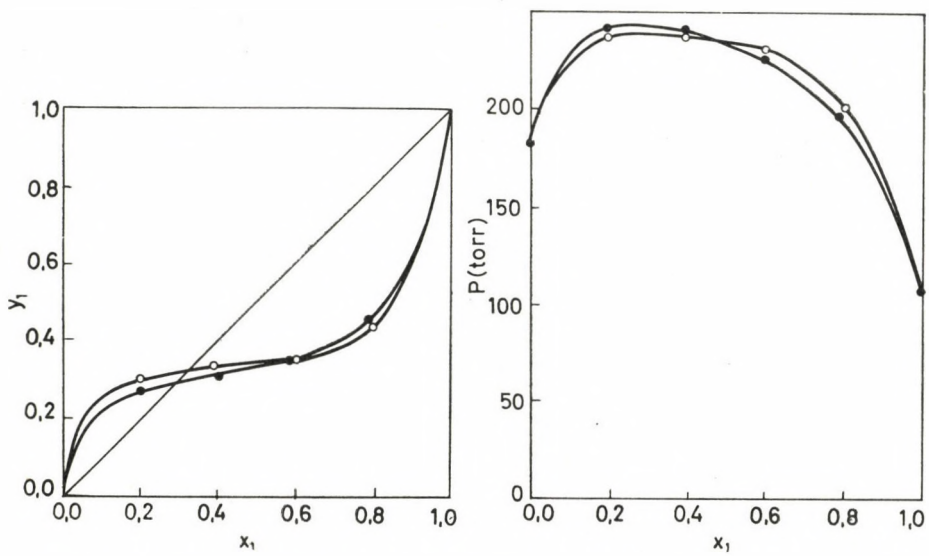

Abb. 5. Gemisch Isopropanol–Cyclohexan bei 40 °C. o berechnete Werte; * gemessene Werte

Tabelle VI

Vergleich der berechneten und gemessenen Angaben für Dampf–Flüssigkeit-Gleichgewichte

Äthanol–Methylcyclohexan bei 30 °C

X_1	Y_1 (exp.)	Y_1 (ber.)	P (exp.)	P (ber.)
0,0	0,000	0,000	59,8	59,8
0,1	0,486	0,482	112,2	105,3
0,2	0,516	0,527	117,3	114,6
0,3	0,524	0,545	118,8	117,5
0,4	0,528	0,542	119,8	116,2
0,5	0,535	0,544	1120,3	116,3
0,6	0,544	0,552	120,1	115,2
0,7	0,563	0,562	118,9	114,7
0,8	0,598	0,596	115,7	112,4
0,9	0,668	0,690	108,2	102,6
1,0	1,000	1,000	77,5	77,5

Äthanol–*n*-Hexan bei 30 °C

X_1	Y_1 (exp.)	Y_1 (ber.)	P (exp.)	P (ber.)
0,0	0,000	0,000	196	196,0
0,1	0,210	0,225	238	235,7
0,2	0,240	0,265	247	242,0
0,3	0,240	0,268	247	242,3
0,4	0,245	0,270	246	242,0
0,5	0,250	0,270	244	237,2
0,6	0,270	0,271	240	237,0
0,7	0,275	0,272	229	232,0
0,8	0,320	0,295	217	215,0
0,9	0,415	0,377	167	174,0
1,0	1,000	1,000	76	76,0

i-Propanol–Cyclohexan bei 40 °C (Referenzsystem: *i*-Propanol–Benzol)

X_1	Y_1 (exp.)	Y_1 (ber.)	P (exp.)	P (ber.)
0,0	0,000	0,000	184	184,0
0,2	0,267	0,294	241	237,7
0,4	0,315	0,339	240	238,9
0,6	0,352	0,349	228	232,2
0,8	0,452	0,440	199	202,5
1,0	1,000	1,000	106	106,0

Hinsichtlicht der Anwendbarkeit der Methode ist die Wahl des Referenzsystems keineswegs gleichgültig, da die berechneten Ergebnisse umso genauer sind, je ähnlicher die Kohlenwasserstoffkomponenten des berechneten Systems und des Referenzsystems sind. Mit den angeführten Beispielen sollte ein Begriff darüber vermittelt werden, daß auch Kohlenwasserstoffe mit wesentlich voneinander abweichenden Strukturen, wie z. B. *n*-Hexan und Benzol dazu geeignet sind, als Referenzsystemkomponente zur Berechnung des Gemisches der anderen Komponente zu dienen. Die quantitative Analyse dieser Frage benötigt noch recht viele Untersuchungen; mit dem zur Zeit zur Verfügung stehenden Angabenmaterial können wir dies noch unternehmen. Der Fehler der Berechnungsmethode beträgt in den angeführten Beispielen nicht mehr als 3 Molprozent bzw. 7 torr, die Ergebnisse können also als gute Annäherungen betrachtet werden.

Die Anwendung der vorgeführten Berechnungsmethode ist besonders dann angezeigt, wenn es zur Berechnung der Rektifikation von Vielkomponentengemischen aus Kohlenwasserstoffen und Alkoholen erforderlich ist, die Angaben sämtlicher möglichen binären Gemische zu bestimmen. Auf experimentellem Weg ist diese Arbeit äußerst zeitraubend und benötigt schwer anschaffbare Alkohol- und Kohlenwasserstoffkomponenten sowie entsprechende Apparaturen, während die Berechnung — obwohl weniger genau — durch Bearbeitung einiger Literaturangaben die nötigen Ergebnisse liefert.

Symbole

X	Molenbruch in der Flüssigkeitsphase
Y	Molenbruch in der Dampfphase
P	Druck
p	Partialdruck
P°	Gleichgewichtsdampfdruck
K	Gleichgewichtskonstante
γ	Aktivitätskoeffizient
$\gamma_{1(2)}$	Aktivitätskoeffizient der Komponente 1 in ihrem Gemisch mit Komponente 2
ΔE_{ij}	Austauschenergie im Gemisch ij
Δ_e	Dispersionsenergie
R	universale Gaskonstante
T	absolute Temperatur
q	temperaturabhängige Konstante
V_i	Molvolumen
δ_i	Hildebrandscher Parameter

Indexe

A	monomerer Alkohol
AA	dimerer Alkohol
B	Kohlenwasserstoff
1	Alkohol, ohne Berücksichtigung der Assoziation, im Gemisch im üblichen Sinne des Wortes
2	Kohlenwasserstoff im Gemisch im üblichen Sinne des Wortes.

LITERATUR

1. PRAUSNITZ, J. M., ECKERT, C. A., ORYE, R. V., O'CONNEL, J. P.: Computer Calculations for Multicomponent Vapor-Liquid Equilibria, London 1967
2. LISZI, J., RATKOVICS, F., SALAMON, T.: Acta Chim. Acad. Sci. Hung. **55,** 165 (1968)
3. LISZI, J., RATKOVICS, F., SALAMON, T.: Acta Chim. Acad. Sci. Hung. **55,** 179 (1968)
4. RATKOVICS, F.: Acta Chim. Acad. Sci. Hung. **49,** 85 (1966)
5. UDOWENKO, W. W., FATKULINA, L. G.: Sh. Fis. Chim. **26,** 719 (1952)
6. WRIGHT, W. A.: J. Phys. Chem. **37,** 233 (1933)
7. ISII, N.: J. Soc. Chem. Ind. Japan **38,** 705 (1935)
8. ISII, N.: J. Soc. Chem. Ind. Japan **38,** 659 (1935)
9. FERGUSON, J. B., FREED, M., MORRIS, A. C.: J. Phys. Chem. **37,** 87 (1933)
10. SMITH, C. P., ENGEL, E. W.: J. Amer. Chem. Soc. **51,** 2660 (1929)
11. NAGAI, J., ISII, N.: J. Soc. Chem. Ind. Japan, **38,** 86 (1935)
12. RIED, R. C., SHERWOOD, T. K.: The Properties of Gases and Liquids. London, 1958
13. STORONKY, A. W., MORATSCHEWSKY, A. G.: Sh. Fiz. Chim. **30,** 1297 (1956)
14. PERRY, J. H.: Chemical Engineers' Handbook. London 1950

Ferenc RATKOVICS
Lajos MÉSZÁROS
Veszprém, Schönherz Z. u. 12. Ungarn

Acta Chimica Academiae Scientiarum Hungaricae, Tomus 63 (2), pp. 143—155 (1970)

AN ELECTRON DIFFRACTION STUDY ON THE MOLECULAR STRUCTURE OF $(CH_3)_2NSON(CH_3)_2$

I. HARGITTAI and L. V. VILKOV

(Research Laboratory for Chemical Structures of the Hungarian Academy of Sciences, Budapest and Electron Diffraction Laboratory, Department of Physical Chemistry, Moscow State University, Moscow)

Received November 1, 1968

The molecular structure of $(CH_3)_2NSON(CH_3)_2$ was studied by the sector-microphotometer electron diffraction method. Using a least-squares refinement the following bond lengths and angles were obtained: r(C—H) 1.103 ± 0.008 Å, r(C—N) 1.460 ± 0.008 Å, r(S—O) 1.480 ± 0.009 Å, r(S—N) 1.693 ± 0.004 Å, ∢ HCN 110.7 ± 1.6°, ∢ SNC 116.1 ± 0.5°, ∢ CNC 113.9 ± 1.5°, ∢ NSN 96.9 ± 1.2° and ∢ OSN 105.5 ± 0.8°. Three internal rotational forms were found as most probable. Some problems of the sulfur and nitrogen stereochemistry were discussed. In particular, the comparison of the nitrogen bond configuration in some silicon-, phosphorus-, sulfur- and chlorine-derivatives made possible to predict the nitrogen configuration in some other sulfur- and chlorine-derivatives.

Introduction

It has been shown in our previous paper [1] that trivalent nitrogen atom bond configuration changes from peaked pyramidal to planar depending on the nature of atoms or atomic groups bound to the nitrogen atom. The sector-microphotometer method of electron diffraction was used for studying the structure of a series of compounds containing trivalent nitrogen atom in order to examine the influence of atoms or atomic groups connected with the nitrogen atom on its bond configuration [2].

The molecular structure study of dimethyl-sulfamoyl chloride, $(CH_3)_2NSO_2Cl$ (hereafter referred to as DMSC), by electron diffraction [1, 3], showed a pyramidal nitrogen bond configuration with an average bond angle around the nitrogen (α_N) of 112°. Comparing the results of this investigation with those of an X-ray one of tetramethyl-sulfamide, $(CH_3)_2NSO_2N(CH_3)_2$ (TMSA) in crystal [4], two significant differences were noticed. These were that the S–N bond was about 0.07 Å shorter and α_N about 5° less in DMSC vapours than in TMSA crystal.

In the present paper the electron diffraction sector-microphotometer study on the molecular structure of tetramethyl-sulfurous diamide, $(CH_3)_2NSON(CH_3)_2$ (TMSDA), is reported. Two other members of the same compound series, namely N,N'-thio-bis(dimethylamine), $(CH_3)_2NSN(CH_3)_2$ (TBDA) and TMSA are under investigation also in vapour phase by the Budapest Group. The structure of TMSDA itself also poses several interesting questions.

There is not too much known on the stereochemistry of tetravalent sulfur. Considering similar molecules, only $(CH_3)_2SO$ (by electron diffraction in an earlier work [5] and more recently by microwave spectroscopy [6]) and $SOCl_2$ (using the sector-microphotometer technique by one of us [7]) have been investigated in vapour phase. Also some X-ray work will be mentioned below. The sulfur bond configuration having a pyramidal arrangement does not change significantly in these cases. Reviewing the literature from point of view of the nature of the S—O bond one can be convinced that the problem needs further distance data. The most interesting problem in the structure of TMSDA seems to be the influence of the sulfoxide group on the nitrogen bond configuration which can be characterized first of all by the length of the S—N bond and the nitrogen bond angles. The structure investigation of TMSDA is made more interesting by the fact that VILKOV *et al.* have recently reported the results of an electron diffraction study of an analogous compound, the tetramethyl-urea $(CH_3)_2NCON(CH_3)_2$ (TMU) [8]. In this case the nitrogen bond configuration was found to be close to planar, $\alpha_N \sim 117.5°$. The whole molecular skeleton excluding the hydrogen atoms showed co-planar arrangement in spite of the significant steric hindrance.

Experimental procedure

Sample of TMSDA was provided through the courtesy of E. PÁLDI of the Research Group of Inorganic Chemistry of the Hungarian Academy of Sciences. PÁLDI obtained the compound slightly modifying [9] the method described in the literature [10]. The sample was further purified by vacuum sublimation and its purity was checked by J. TAMÁS using a mass-spectrometer in the Budapest Laboratory. No impurities were detected and the compound was stable in the mass-spectrometer at about 100 °C [11].

Electron diffraction photographs were taken at a nozzle temperature of about 100 °C with an EG—100A diffraction unit of the Physical-Chemistry Department, Moscow State University, during a visit of one of us (I.H.). A new evaporator system was used. Data were obtained from 19 and 41 cm camera distances using 60kV electrons. (Some plates were recorded from 41 cm using 40kV electrons too. However, this pattern did not contain significantly more information, therefore it was not used in the final data reduction).

Traces of the optical density of the diffraction pattern were obtained using a Zeiss GIII fastphotometer of the Budapest Laboratory. NH_4Cl served as crystal standard and a Zeiss Abbe-comparator and a KM—5 cathetometer were used for measuring NH_4Cl diffraction rings and nozzle to plate distances, respectively. The scale error caused by the uncertainties in measuring the wave length and the nozzle to plate distances was about 0.1 per cent.

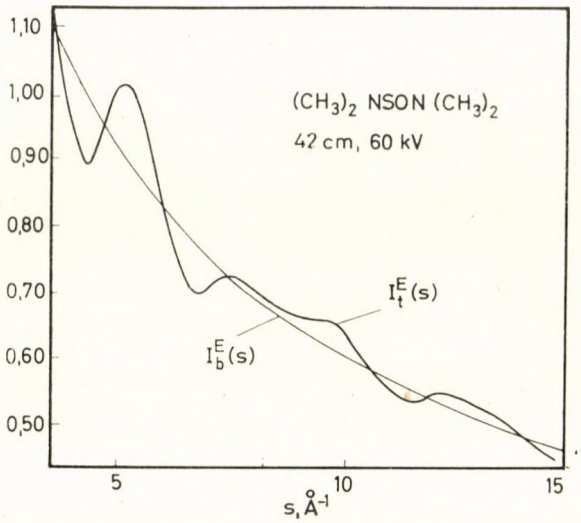

Fig. 1. The total experimental intensities and the experimental background for the 41 cm nozzle-to-plate distance

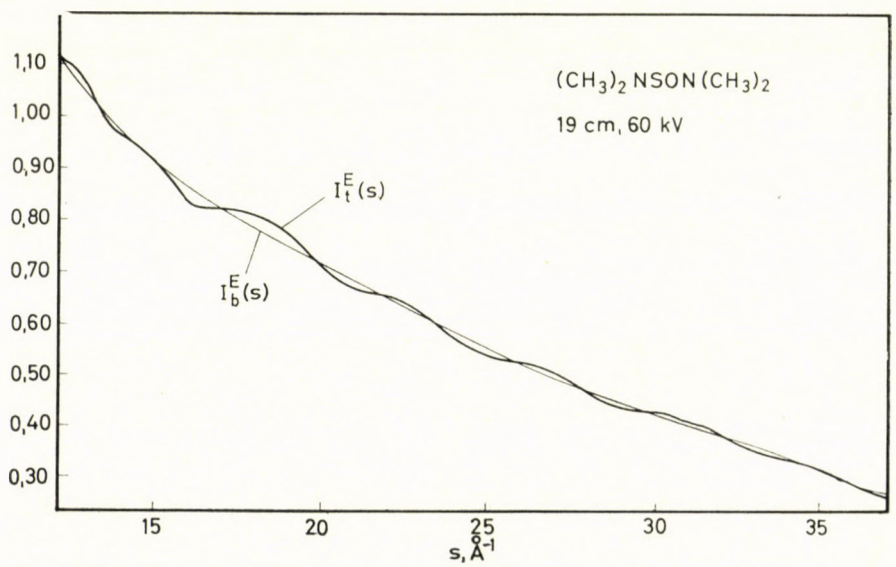

Fig. 2. The total experimental intensities and the experimental background for the 19 cm nozzle-to-plate distance

Data reduction

Figs. 1 and 2 show the total experimental intensities corresponding to two camera distances. The experimental background which was drawn in arbitrarily by a usual manner is shown too.

Then, the experimental molecular intensities modified by the experimental background, $sM^E(s) = [I_t^E(s) - I_b^E(s)]/I_b^E(s)$, were obtained for both

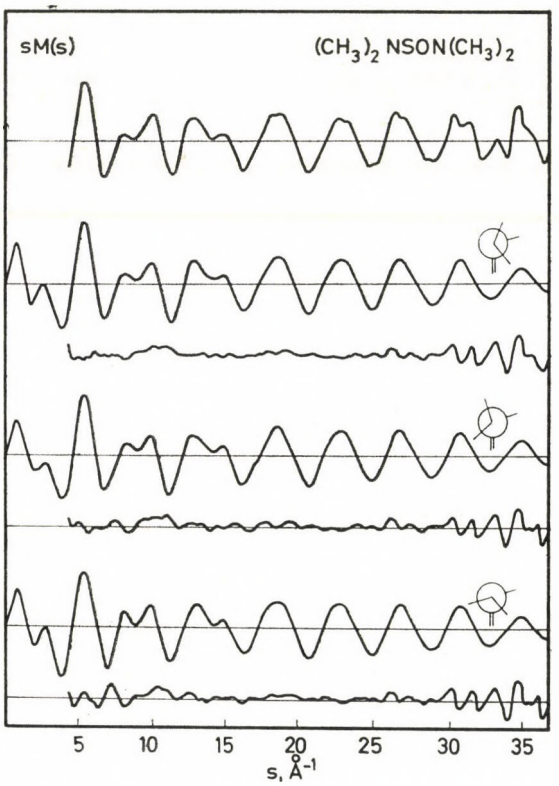

Fig. 3. Experimental and theoretical molecular intensities. The theoretical curves were computed using the final parameter values of Table II in the cases of the rotational forms shown in Fig. 7

camera geometries. After scaling and averaging these two curves, the entire experimental molecular intensity curve was produced. In the final section of the structural analysis a modification of the background was carried out for eliminating the trend in the difference curves between experimental and molecular intensities. This final experimental molecular intensity curve is shown in Fig. 3 and its numerical values are listed in Table I.

Experimental radial distribution functions were calculated using a theoretical intensity function from $s = 0$ to $s = 4$ Å^{-1} and experimental

Table I

s	$sM(s)$	s	$sM(s)$	s	$sM(s)$
4.25	−0.164	15.25	0.007	26.25	0.182
4.50	−0.079	15.50	−0.045	26.50	0.200
4.75	0.109	15.75	−0.138	26.75	0.152
5.00	0.312	16.00	−0.188	27.00	0.150
5.25	0.419	16.25	−0.217	27.25	0.130
5.50	0.400	16.50	−0.173	27.50	0.067
5.75	0.254	16.75	−0.123	27.75	−0.014
6.00	0.093	17.00	−0.072	28.00	−0.066
6.25	−0.123	17.25	−0.007	28.25	−0.134
6.50	−0.240	17.50	0.039	28.50	−0.133
6.75	−0.254	17.75	0.102	28.75	−0.136
7.00	−0.200	18.00	0.157	29.00	−0.144
7.25	−0.090	18.25	0.189	29.25	−0.121
7.50	−0.010	18.50	0.188	29.50	−0.075
7.75	0.043	18.75	0.201	29.75	0.000
8.00	0.049	19.00	0.190	30.00	0.097
8.25	0.036	19.25	0.158	30.25	0.187
8.50	0.022	19.50	0.096	30.50	0.152
8.75	0.032	19.75	0.001	30.75	0.097
9.00	0.053	20.00	−0.088	31.00	0.102
9.25	0.099	20.25	−0.170	31.25	0.112
9.50	0.155	20.50	−0.211	31.50	0.127
9.75	0.194	20.75	−0.216	31.75	0.073
10.00	0.198	21.00	−0.183	32.00	−0.111
10.25	0.114	21.25	−0.137	32.25	−0.134
10.50	−0.020	21.50	−0.078	32.50	−0.128
10.75	−0.126	21.75	−0.014	32.75	−0.094
11.00	−0.196	22.00	0.056	33.00	−0.040
11.25	−0.234	22.25	0.110	33.25	0.002
11.50	−0.198	22.50	0.142	33.50	−0.016
11.75	−0.100	22.75	0.152	33.75	−0.074
12.00	0.017	23.00	0.139	34.00	−0.140
12.25	0.104	23.25	0.140	34.25	−0.030
12.50	0.149	23.50	0.101	34.50	0.154
12.75	0.165	23.75	0.055	34.75	0.215
13.00	0.151	24.00	−0.014	35.00	0.221
13.25	0.127	24.25	−0.113	35.25	0.082
13.50	0.102	24.50	−0.168	35.50	0.055
13.75	0.030	24.75	−0.184	35.75	0.035
14.00	0.012	25.00	−0.163	36.00	−0.004
14.25	0.038	25.25	−0.150	36.25	0.009
14.50	0.052	25.50	−0.099	36.50	−0.174
14.75	0.050	25.75	−0.003	36.75	−0.174
15.00	0.047	26.00	0.135	37.00	−0.051

intensity data from $s = 4.25$ to $s = 37$ Å^{-1}. In all comparisons shown in Fig. 4 the theoretical contribution to the experimental radial distribution is consistent with the corresponding theoretical function. Radial distribution functions were computed several times using different values of a in the damping factor $\exp(-as^2)$. In the cases of the curves shown in Fig. 4 this value was 0.002 Å^2, except one additonal experimental radial distribution computed with $a = 0$, shown on the top of the figure.

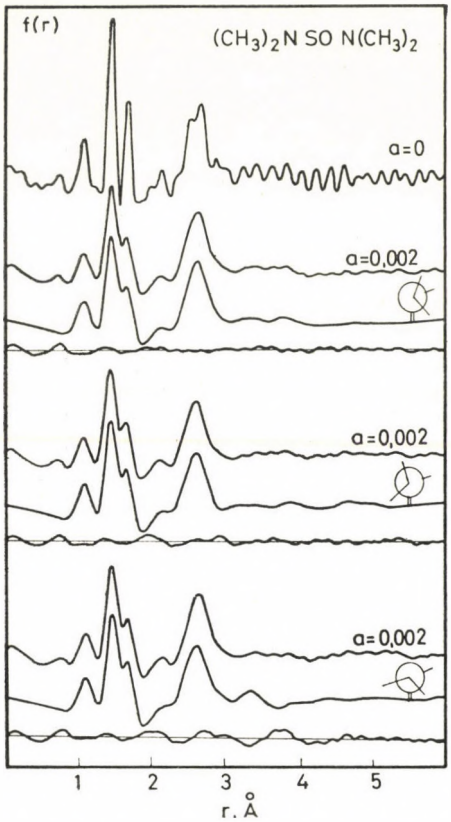

Fig. 4. Experimental and theoretical radial distributions. The theoretical curves of this figure correspond to those of Fig. 3

Structure analysis

There were three different sources for collecting a trial structure (*i.e.* the initial values of Table II) for carrying out a least-squares refinement. Some of the parameters were assumed, some derived directly from the experimental radial distribution and some estimated by trial and error method, considering both the molecular intensities and the radial distributions.

The first structural maximum on the experimental radial distribution at 1.10 Å corresponded to the C—H bond. The next compound maximum had two peaks and corresponded to three bonds *i.e.* C—N, S—O and S—N. Assuming for r(C—N) 1.47 Å and also that the S—O bond is shorter than the S—N bond, the values of 1.47 and 1.69 Å were obtained for r(S—O) and r(S—N), respectively, by subtracting the corresponding peaks from the entire maximum. Assuming l(C—N) 0.05 Å the mean amplitude values of 0.07, 0.04 and 0.05 Å were estimated for l(C—H), l (S—O) and l (S—N), respectively. The biggest maximum for non-bonded distances appeared at about

2.64 Å including the distances r(S . . . C), r(O . . . N) and others. Since r(S . . . C) had the greatest weight in forming this maximum, an approximate value of 114° was estimated for the bond angle SNC.

Theoretical molecular intensities and radial distributions were calculated for numerous molecular models using the trial and error method for finding the other bond angles, except the bond angle HCN which at once was assumed to be 110°. Also, it was assumed in these preliminary calculations that the C_2NSNC_2 skeleton had two planes of symmetry according to a Newman projection of this skeleton shown in Fig. 5. Here one of the S—N bonds is perpendicular to the plane of the picture. Varying the bond angles CNC, NSN and OSN in the intervals of about 109—120°, 80—130° and 100—108°,

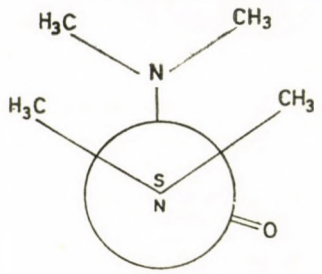

Fig. 5

respectively, the values listed in Table II as initial values were estimated for the angles NSN and OSN. No significant change could be observed in the curves obtained by varying the angle CNC; therefore it was assumed to be equal to the angle SNC.

In all these calculations constant values were used as scattering functions in the theoretical molecular intensity expression. Visiting the Oslo Electron Diffraction Group it was possible to continue the structure analysis using the following scattering functions

$$g_{ij/B}(s) = \frac{n_{ij}|f_i(s)|\,|f_j(s)|}{I_b^T(s)} \cos[\eta_i(s) - \eta_j(s)],$$

where $|f(s)|$ and $\eta(s)$ are the absolute value and phase of the atomic complex scattering amplitude and $I_b^T(s)$ denotes the theoretical background function. A description of the theory can be found in the literature [12]. It should be mentioned that instead of the theoretical background the experimental one could not be used as a modification function for the theoretical molecular intensities, because it was unknown after averaging the experimental molecular intensities corresponding to two camera geometries.

The partial waves electron scattering factors for hydrogen, carbon, nitrogen, oxygen and sulfur atoms at 60 kV accelerating voltage as well as

the scattering functions were calculated using STRAND's programs ([13] and [14], respectively). Fig. 6 shows some of the $g_{ij/B}(s)$ functions. In this figure the scattering functions for the atomic pairs OH and CH were omitted trying not to make the picture overcrowded. These scattering functions are quite similar to that for the atomic pair NH shown in the Figure.

In the structure analysis the next step was to give up one of the planes of symmetry and rotate the $(CH_3)_2N$ groups. The plane of symmetry kept was the one which went through the lines of the S—O bond and the bisectrix of

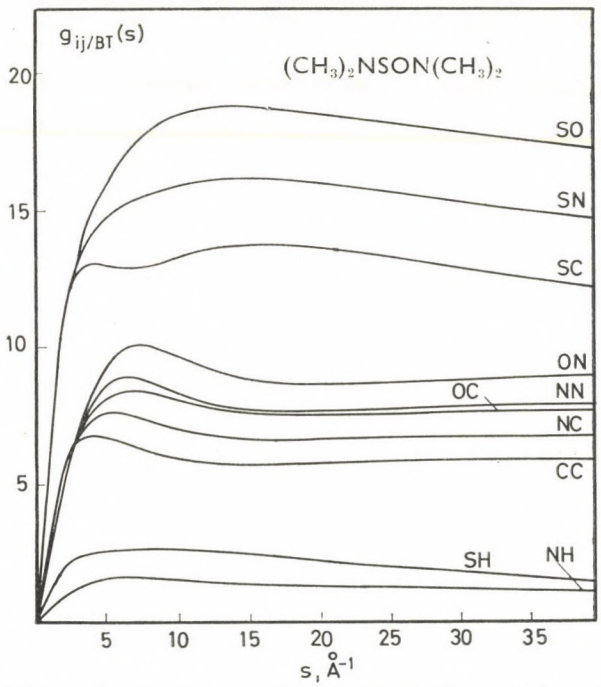

Fig. 6. Scattering functions used in the final refinement (see text)

the NSN bond angle. The rotation was carried out from $\varphi = 0°$ to $\varphi = 360°$ using an interval of $\Delta\varphi = 30°$ for the input in the least-squares calculations in which all the "initial values" of Table II were kept constant and only the angle φ was varied. Here the rotational angle φ is consistent with that of Fig. 7. All these least-squares calculations and also those mentioned hereafter were based on the intensity functions using SEIP's program [15]. The following weighting scheme was used [16]:

$$W = \exp\left[-W_1(s_1 - s)^2\right] \quad \text{for } s < s_1$$

$$W = 1.00 \quad \text{for } s_1 \leq s \leq s_2$$

$$W = \exp\left[-W_2(s_2 - s)^2\right] \quad \text{for } s > s_2$$

where W_1, W_2, s_1 and s_2 were suitable constants. Comparing the $\Sigma W \Delta^2$ values, where the sum is over all observations and Δ is the difference between the experimental and the scaled theoretical intensities, three minima were observed corresponding to three rotational forms having the values of 99, 251 and 352° for the angle φ.

Because of the smallest value of $\Sigma W \Delta^2$, the rotational form corresponding to $\varphi = 99°$ was chosen and kept for further least-squares refinement of the bond lengths, angles, the mean amplitudes of vibration for bond distances and some of those for non-bonded distances as well. The other mean amplitudes for non-bonded distances were assumed to be from about 0.10 to about

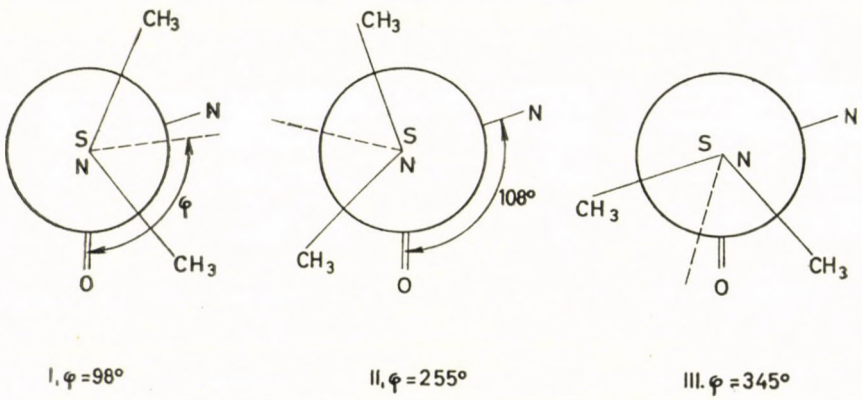

Fig. 7. The internal rotational forms found as most probable

0.15 Å. Even having these restrictions it was not possible to vary all independent parameters mentioned above at the same time. Therefore, several groups of the parameters were formed to be refined together and there was a good deal of overlapping between the parameters belonging to one or another group. The mean amplitude of vibration for the S—O bond could not be refined since giving an improbably small value, therefore it was decided to keep it constant at a value of 0.035 Å. The results of this least-squares refinement are listed in Table II. The standard deviations are also shown. Although these standard deviations were collected for every parameter as the biggest ones from different refinements they still seem to be too small. It is very difficult, if not impossible, to give any physical meaning to these standard deviations, if considering the numerous restrictions used throughout this structure analysis.

Finally, using the results of the least-squares refinement for the bond distances, angles and mean amplitudes, the rotational angle φ was refined again for the three rotational forms found as most probable and mentioned above. The final values for φ in these three cases were 97, 255 and 345° (see Fig. 7).

Table II

The result of the least-squares refinement

Parame ers	Initial values	Final values with their standard deviations
r (C—H), Å	1.10	1.103 ± 0.008
l (C—H), Å	0.07	0.063 ± 0.008
r (C—N), Å	1.47	1.460 ± 0.008
l (C—N), Å	0.05	0.046 ± 0.009
r (S—O), Å	1.47	1.480 ± 0.009
l (S—O), Å	0.04	0.035 (assumed)
r (S—N), Å	1.69	1.693 ± 0.004
l (S—N), Å	0.05	0.049 ± 0.004
angle HCN	110°	$110.7 \pm 1.6°$
SNC	114°	$116.1 \pm 0.5°$
CNC	114°	$113.9 \pm 1.5°$
NSN	96°	$96.9 \pm 1.2°$
OSN	103°	$105.5 \pm 0.8°$

It must be emphasized that the main purpose of the present study was to determine the geometry of the sulfur and the nitrogen bonds and not the rotational forms. No attempt has been made to investigate the rotation of the methyl groups. A more precise study of the internal rotation needs more information about the scattered intensity in the small angle region. Nevertheless, it can be stated that on the basis of the available experimental data the most probable internal rotational forms in the vapour phase in the conditions of the experiment are those shown as Newman projections in Fig. 7. After the modification of the background the values of 1.680, 1.890 and 2.190 were obtained for $\Sigma W \Delta^2$ for the rotational forms I, II and III, respectively. This means that the most probable is the form I and the less is III. Naturally, the existence of other rotational forms cannot be excluded either. It should also be mentioned that no models not having symmetrically rotated $(CH_3)_2N$ groups have been tried although there is no reason to exclude their existence.

Discussion

There is generally a good agreement between the values obtained for bond lengths and bond angles for TMSDA and those found for related molecules in the literature. In particular, the bond angles of the sulfur atom in TMSDA vapours agree well with those found in $(CH_3)_2SO$ [5, 6] and $SOCl_2$ [7] vapours and also in $(CH_3)_2SO$ and $C_6H_4(SO)_2C_6H_4$ [18] crystals. Some S—O

bond distances have been collected and compared in a previous work [19]. The value of 1.480 Å for r(S—O) in TMSDA agrees well with the generally observed phenomenon concerning the difference between the bond lengths of hexavalent and tetravalent sulfur atoms in analogous molecules and also agrees well with the conclusion made about the tendency of lengthening of the S—O bond, when X changes from chlorine to CH_3 or $(CH_3)_2N$ in SOX_2 molecules [19].

The value determined for r(S—N) in TMSDA is the same (but less uncertain) as that in DMSC. If considering the generally observed phenomenon mentioned above according to which the bonds of tetravalent sulphur are longer by some hundredths of an Å than the analogue bonds of tetravalent sulphur [26], the S—N bond in TMSDA can be considered stronger *i.e.* having more double bond character than the S—N bond in DMSC. This fact indicates a stronger delocalization of the nitrogen lone pair electrons. This is in accordance with the observed difference of about 3° in the average nitrogen angles in the two molecules. The nitrogen configuration is less pyramidal in TMSDA than in DMSC. On the other hand, a shorter S—N bond (1.623 Å) and less pyramidal nitrogen configuration ($\alpha_N \sim 117°$) was obtained in TMSA crystal by X-ray diffraction [4]. However, one must be very cautious, if comparing structural data on nitrogen configuration obtained in vapours and in crystal. It is a well-known fact that the inversion energy of the nitrogen atom of amino-derivatives in the vapour phase is of the same order of magnitude as the crystal lattice energy and in particular, the hydrogen bond energy in crystal is even more. Therefore it is desirable to compare the molecular structures of TMSDA and TMSA belonging to the vapour phase in both cases. An electron diffraction investigation of TMSA is in progress at the Budapest Group.

It is interesting to compare the nitrogen bond configurations in molecules where Si, P, S or Cl atom is connected with the nitrogen. In $(SiH_3)_3N$ this configuration was found to be planar, as studied by the visual method of electron diffraction [20]. A sector-microphotometer electron diffraction study showed 120 and 116° average nitrogen bond angles in $(CH_3)_2NPCl_2$ and $(CH_3)_2NPOCl_2$, respectively [21]. In $(CH_3)_2NCl$ and CH_3NCl_2 α_N is 107 and 108°, respectively, according to a visual electron diffraction study [22]. Finally, sector electron diffraction results showed $\alpha_N \sim 104°$ in NF_2Cl [23]. Data for some sulfur-nitrogen compounds have been mentioned above. The comparison shows that going from silicon to chlorine the nitrogen configuration changes from planar to peaked pyramidal. In connection with this, it is remarkable to remember CRUICKSHANK's observation on the definite tendency for the X—O—X angles to get smaller as X changes from silicon to chlorine [24]. Considering the data on nitrogen configuration one can expect a pyramidal configuration for the nitrogen bonds in chlorine-derivatives *i.e.* in $\rangle N—Cl=$,

$\rangle N-Cl\langle$ and $\rangle N-Cl=$. On the other hand, a close to planar nitrogen configuration can be predicted for $\rangle N-S-N\langle$. An electron diffraction investigation of TBDA is also in progress at the Budapest Group. It is interesting to mention here that the SNHS grouping was found to be co-planar in $S_4N_4H_4$ crystal by a neutron diffraction study [25].

As for the internal rotation forms found most probable for TMSDA we can refer only to the steric effects caused by the four methyl groups. The co-planar arrangement found for the C_2NCONC_2 skeleton in TMU in spite of the significant steric hindrance, indicates a great potential barrier for the rotation around the $\rangle C-N\langle$ bond. This bond is significantly shorter than the $-C-N\langle$ bond. If comparing the values of $r(\rangle C-N\langle) = 1.338$ Å in TMU and $r(S-N) = 1.693$ Å in TMSDA with the corresponding calculated single bond values of 1.47 and 1.74 Å, for the C—N and S—N bonds, respectively, the double bond character of $\rangle C-N\langle$ bond seems to be stronger in TMU than that of the S—N bond in TMSDA. Therefore it seems to be reasonable to believe that the rotational barrier in TMSDA is smaller than that in TMU, if other factors are not taken into account.

*

The authors are indebted to Professor S. LENGYEL for his interest and encouragement, and to Mr. A. GOLUBINSKIJ and Mrs. J. SZILÁGYI for their help in the experimental and calculation work. One of us (I.H.) is grateful to Professor O. BASTIANSEN for providing the opportunity of working in his Group and also to Cand. real. R. STÖLEVIK and Dr. T. G. STRAND for their help in using SEIP's and STRAND's programs.

REFERENCES

1. VILKOV, L. V., HARGITTAI, I.: Acta Chim. Acad. Sci. Hung., **52,** 423 (1967)
2. VILKOV, L. V.: Acta Cryst., **21,** part 7, 8.101 (1966)
3. HARGITTAI, I. J.: Acta Cryst., **21,** part 7, 8.44 (1966)
   Вилков, Л. В., Харгиттаи, И. Я.: Докл. АН СССР, **168,** 1065 (1966)
4. JORDAN, I., SMITH, H. W., LOHR, L. L. JR., LIPSCOMB, W. N.: J. Am. Chem. Soc., **85,** 846 (1963)
5. BASTIANSEN, O., VIERVOLL, H.: Acta chem. Scand., **2,** 702 (1948)
6. DREIZLER, H., DENDL, G.: Z. Naturforschg., **19a,** 542 (1964)
7. HARGITTAI, I.: Acta Chim. Acad. Sci. Hung., **59,** 351 (1969)
8. Вилков, Л. В., Акишин, П. А., Литовцева, И. Н.: Ж. структ. химии, **7,** 3 (1966)
9. PÁLDI, E.: private communication (to be published)
10. Methoden der organischen Chemie (HOUBEN—WEYL), **XI,** Teil 2, p. 737, Stuttgart, 1958
11. TAMÁS, J.: private communication
12. SEIP, H. M.: Selected topics in Structure Chemistry. Universetetsforlaget, Oslo, 1967
13. STRAND, T. G.: Program for calculation of partial waves electron scattering factors of the atoms. Oslo, 1968
14. STRAND, T. G.: Program for calculation of modification- and scattering-functions. Oslo, 1968
15. SEIP, H. M.: Program for least-squares refinement. Oslo, 1968
16. SEIP, H. M.: Acta Chem. Scand., **19,** 1955 (1965)
17. THOMAS, R., SHOEMAKER, C. B., ERIKS, K.: Acta Cryst., **21,** 12 (1966)

18. Hosoya, S.: Acta Cryst., **21,** 21 (1966)
19. Hargittai, I.: Acta Chim. Acad. Sci. Hung., **59,** 351 (1969)
20. Hedberg, K.: J. Am. Chem. Soc., **77,** 6491 (1955)
21. Вилков, Л. В., Хайкин, Л. С.: Докл. АН СССР, **168,** 810 (1966)
22. Stevenson, D. P., Schomaker, V.: J. Am. Chem. Soc., **62,** 1913 (1940)
23. Вилков, Л. В., Назаренко, И. И.: Ж. структ. химии, **8,** 346 (1967)
24. Cruicshank, D. W. J.: J. Chem. Soc., 5486 (1961)
25. Sabine, T. M., Cox, G. W.: Acta Cryst., **23,** 547 (1967)
26. Truter, M. R.: J. Chem. Soc., 3400 (1962)

István Hargittai; Budapest VIII., Puskin u. 11—13.
Lev V. Vilkov; Moscow V-234 MGU Department of Physical Chemistry U.S.S.R.

Acta Chimica Academiae Sientiarum Hungaricae, Tomus 63 (2), pp. 157—166 (1970)

ELECTRON PARAMAGNETIC RESONANCE STUDIES OF TETRAHEDRALLY COORDINATED Cu^{2+} IONS IN CU(1-BENZENE-AZO-N-PHENYL-2-NAPHTHYLAMINE)$_2$*

A. ROCKENBAUER

(Central Research Institute for Chemistry of the Hungarian Academy of Sciences, Budapest)

Received November 4, 1968

The electron paramagnetic resonance spectrum of Cu(1-benzene-azo-N-phenyl-2-naphthylamine)$_2$ was measured in diamagnetically diluted polycrystalline samples. Analysis of the spectrum led to the following parameters:

$$g_{\parallel} = 2.168 \pm 0.005,\ g_{\perp} = 2.040 \pm 0.005;$$

$$|A_{\parallel}| = (123 \pm 5)\ 10^{-4}\ \text{cm}^{-1},\ |A_{\perp}| < 20\ 10^{-4}\ \text{cm}^{-1}.$$

These values suggest a square-planar arrangement of the four nitrogen atoms in contrast to earlier chemical evidence indicating a tetrahedral symmetry for the given complex. This contradiction was resolved by demonstrating that if the tetrahedron is submitted to a large tetragonal compression, the spectral parameters can be undistinguishable from those of the square-planar structure. The large distortion which corresponds to the measured parameters can be explained by ligand flexibility.

MESSMER and SZIMÁN [1] prepared Cu(1-benzene-azo-N-phenyl-2-naphthylamine)$_2$ (CuBFNA) chelate (Fig. 1). They supposed that the planes of two BFNA groups attached to Cu^{2+} ion are perpendicular to each other, since their planar arrangement would result in a strong steric compression. Thus the four nitrogens bonded to the Cu^{2+} ion form a tetrahedron (Fig. 2). So far only a few studies [2—12] have dealt with the electron resonance spectra of tetrahedrally coordinated Cu^{2+} ion, therefore it is of interest to study the spectra of CuBFNA which may supply new information about this special coordination.

The measurements were made on polycrystalline samples of an undiluted and diamagnetically diluted complex. The dilution was made with NiBFNA in a ratio 100 : 1. X-band spectra were recorded at 77° and 300°K using a JES P—10 spectrometer.

The spectrum of an undiluted complex exhibits a single line with an anisotropic g factor, whereas in case of a diluted sample a partially resolved hyperfine structure can be observed (Figs 3 and 4). Attempts at obtaining a spectrum with higher resolution were unsuccessful.

* Presented in the XVth Colloque A. M. P. E. R. E. (16—20 September 1968, Grenoble) in the Session Electron Spin Resonance in Organic Solids.

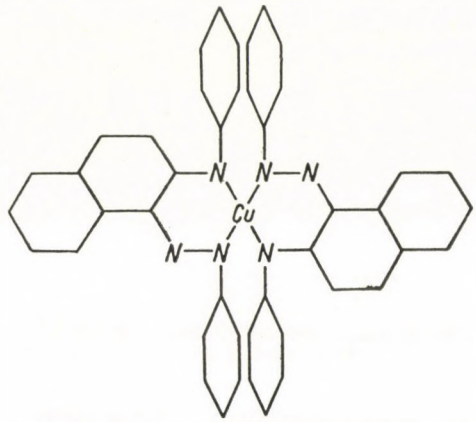

Fig. 1. The formula of Cu(1-benzene-azo-N-phenyl-2-naphthylamine)$_2$

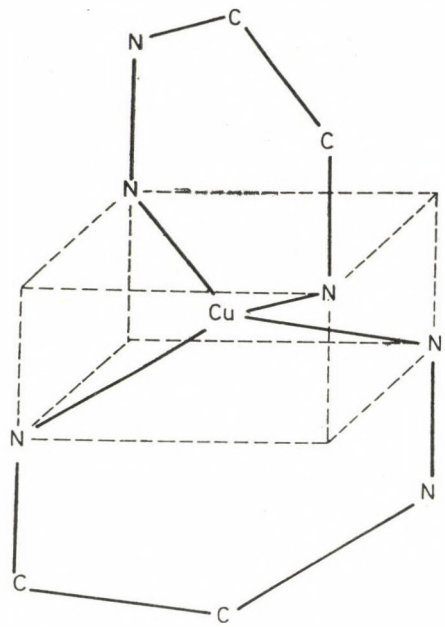

Fig. 2. The geometrical arrangement of the central group in CuBFNA

The spectra can be described by the spin Hamiltonian:

$$\mathcal{H} = g_{\prime\prime} H_z S_z + g_\perp (H_x S_x + H_y S_y) + A_{\prime\prime} I_z S_z + A_\perp (I_x S_x + I_y S_y) ,$$

with

$$g_{\prime\prime} = 2.158 \pm 0.005, \quad g_\perp = 2.041 \pm 0.005 ,$$

$$|A_{\prime\prime}| = (123 \pm 5)\, 10^{-4}\,\mathrm{cm}^{-1}, \quad |A_\perp| \leq 20\, 10^{-4}\,\mathrm{cm}^{-1} .$$

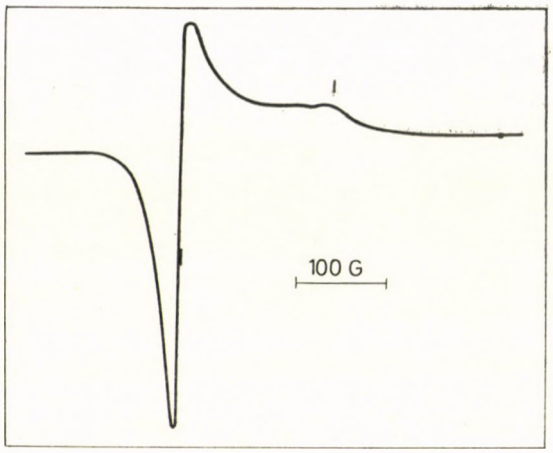

Fig. 3. The electron paramagnetic spectrum of undiluted CuBFNA polycrystal

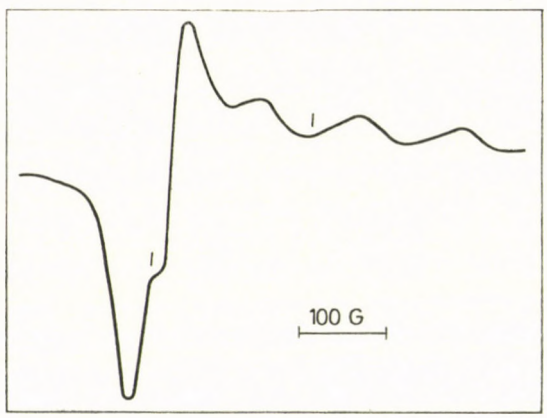

Fig. 4. The electron paramagnetic spectrum of diluted CuBFNA polycrystal. The dilution was made with NiBFNA in a ratio 100 : 1

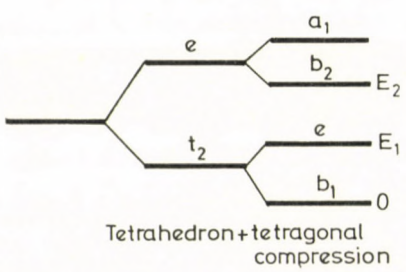

Fig. 4a. Energy levels of 3d hole electron in tetrahedral and tetragonally compressed tetrahedral crystal fields

Since only one of the hyperfine tensor components is known and its orientation is undetermined, we can arbitrarily select common principal axes for the g and hyperfine tensors. Although an axial g tensor is compatible both with trigonally and tetragonally distorted tetrahedral crystal fields we shall deal with tetragonal distortion only, since it is more likely in case of CuBFNA.

Supposing a compressed tetrahedron, the ground state of $3d^1$ hole electron is $d_{xy}(b_1)$ and the next two pertinent crystal field levels are d_{xz}, $d_{yz}(e)$ and $d_{x^2-y^2}(b_2)$ (Fig. 4a). Their energy separation from the ground state are E_1 and E_2. While E_1 is roughly proportional to the distortion of the tetrahedron, E_2 depends only slightly on it. In the following, we shall characterise the measure of distortion by E_1. An adequate description of a hole electron can be given by molecular orbital in which the *3d—4p* hybridization and antibonding character are taken into account:

$$b_1 = \alpha_0 d_{xy} + \beta_0 p_z + \gamma_0 \sigma_{xy},$$

$$e = \begin{cases} \alpha_1 d_{xz} + \beta_1 p_y + \gamma_1 \sigma_{xz} + \delta_1 \pi_{xz}, \\ \alpha_1 d_{yz} + \beta_1 p_x + \gamma_1 \sigma_{yz} + \delta_1 \pi_{yz}, \end{cases}$$

$$b_2 = \alpha_2 d_{x^2-y^2} + \delta_2 \pi_{x^2-y^2},$$

where the σ and π orbitals are built up from the *2s* and *2p* atomic orbitals of four neighbouring nitrogen atoms, the coefficients γ, δ, and β stand for the strength of covalent bonding and hybridization. It is unusual that in the "e" doublet both σ and π bondings were taken into account. It is a special consequence of our treating the square-planar arrangement as a limiting case of tetragonally distorted tetrahedron. The σ — and π — character of this bonding changes, depending on whether the geometrical arrangement is nearer to regular tetrahedron or to square-planar structure.

For determining the ground magnetic doublet, the spin-orbit coupling is taken into consideration by diagonalization in case of the first two levels and by perturbation procedure in case of the higher b_2 level. The following expressions for spin Hamiltonian parameters are calculated by the usual perturbation method:

$$g_{\prime\prime} = g_0 (\cos^2 \vartheta - \sin^2 \vartheta) - 2k_{11} \sin^2 \vartheta - 8k_{02} \cos \vartheta \frac{Z}{E_2},$$

$$g_\perp = g_0 \cos^2 \vartheta + 2\sqrt{2} k_{01} \sin \vartheta \cos \vartheta - 2\sqrt{2} k_{12} \sin \vartheta \frac{Z}{E_2},$$

where the real k parameters are the matrix elements of orbital momenta:

$$k_{01} = i(b_1 |l_x| e_{xz}) = \alpha_0 \alpha_1 - \beta_0 \beta_1 - \frac{1}{\sqrt{2}} \gamma_0 \delta_1 T(n) +$$

$$+ \gamma_1 (\alpha_0 S_d^{(1)} - \beta_0 S_p^{(1)} + \gamma_0 (\alpha_1 S_d^{(0)} - \beta_1 S_p^{(0)}),$$

$$k_{11} = - i(e_{yz} |l_z| e_{xz}) = \alpha_1^2 - \beta_1^2 + 2\gamma_1 (\alpha_1 S_d^{(1)} - \beta_1 S_p^{(1)}),$$

$$k_{02} = - \frac{i}{2} (b_1 |l_x| b_2) = \alpha_0 \alpha_2 + \alpha_2 \gamma_0 S_d^{(0)} - \frac{1}{2} \gamma_0 \delta_2 \cos \varepsilon \, T(n),$$

$$k_{12} = - i(b_2 |l_x| e_{yx}) = \alpha_1 \alpha_2 + \alpha_2 \gamma_1 S_d^{(1)} - \frac{1}{\sqrt{2}} \gamma_1 \delta_2 \sin \varepsilon \, T(n) +$$

$$+ \frac{1}{\sqrt{2}} \delta_1 \delta_2 \cos \varepsilon .$$

The distortion is characterized by

$$\operatorname{tg} \vartheta = \frac{1}{2} (W + \sqrt{W^2 + 2}),$$

and

$$W = E_1/Y + X/2Y,$$

the symbols X, Y and Z can be considered as reduced spin-orbit coupling constants:

$$X = \alpha_1^2 \lambda_d - \beta_1^2 \lambda_p,$$

$$Y = \alpha_0 \alpha_1 \lambda_d - \beta_0 \beta_1 \lambda_p,$$

$$Z = \alpha_2 \left(\alpha_0 \cos \vartheta - \frac{\alpha_1}{\sqrt{2}} \sin \vartheta \right) \lambda_d .$$

Overlap integrals (S) are only accounted for in case of σ bonding, their indices correspond to the indices of molecular orbitals. The symbol ε stands for the geometrical distortion of tetrahedron, in case of a regular tetrahedron $\operatorname{tg}\varepsilon = 1/\sqrt{2}$, in case of a square-planar structure $\operatorname{tg}\varepsilon = 0$. T(n) is an integral consisting of radial wave-functions of neighbouring ligands, and variable n characterizes the hybridization between s and p functions of ligands (GERSMANN and SWALEN [13]).

In the expressions of hyperfine coupling constants, the integrals concerning ligand orbitals are being neglected. Table I presents the calculated formulas in which the symbols P_d and P_p are the expectation values of $2\gamma\beta\beta_N r^{-3}$ in the states $3d$ and $4p$, resp.

Table I

$$A_{\parallel} = \frac{1}{1+\mathrm{tg}^2\vartheta}\left\{-\varkappa\left[\alpha_0^2 P_d + \beta_0^2 P_p - (\alpha_1^2 P_d + \beta_1^2 P_p)\,\mathrm{tg}^2\vartheta\right] - \right.$$

$$- \frac{4}{7}\alpha_0^2 P_d + \frac{4}{5}\beta_0^2 P_p + \left[\frac{6\sqrt{2}}{2}\alpha_0\alpha_1 P_d + \frac{6\sqrt{2}}{5}\beta_0\beta_1 P_p\right]\mathrm{tg}\,\vartheta - \left[\frac{16}{7}\alpha_1^2 P_d - \right.$$

$$\left. - \frac{12}{5}\beta_1^2 P_p\right]\mathrm{tg}^2\vartheta - \alpha_2^2\left[8\alpha_0 - \frac{6\sqrt{2}}{7}\alpha_1\,\mathrm{tg}\,\vartheta\right]\left[\alpha_0 - \frac{1}{\sqrt{2}}\alpha_1\,\mathrm{tg}\,\vartheta\right]\frac{\lambda_d}{E_2}P_d\Big\},$$

$$A_{\perp} = \frac{1}{1+\mathrm{tg}^2\vartheta}\left\{-\varkappa(\alpha_0^2 P_d + \beta_0^2 P_p) + \frac{2}{7}\alpha_0^2 P_d - \frac{2}{5}\beta_0^2 P_p + \right.$$

$$+ \left[\frac{11\sqrt{2}}{7}\alpha_0\alpha_1 P_d - \frac{13\sqrt{2}}{5}\beta_0\beta_1 P_p\right]\mathrm{tg}\,\vartheta - \frac{6}{5}\beta_1^2 P_p\,\mathrm{tg}^2\vartheta - $$

$$\left. - \frac{11\sqrt{2}}{7}\alpha_1\alpha_2^2\left[\alpha_0 - \frac{1}{\sqrt{2}}\alpha_1\,\mathrm{tg}\,\vartheta\right]\mathrm{tg}\,\vartheta\,\frac{\lambda_d}{E_2}P_d\right\}.$$

The above expressions of spin Hamiltonian parameters agree with those of the square-planar structure [13], when

$$\mathrm{tg}\vartheta \approx -1/\sqrt{2}W \ll 1,$$

while $\mathrm{tg}\vartheta = \sqrt{2}$, that is $\vartheta = 54.4°$ limit case corresponds to the regular tetrahedron. The distortion dependence of spin Hamiltonian parameters can be demonstrated by neglecting the effects of covalent bonding and hybridization. In Fig. 5 the contributions to g factors from t_2 states (b_1 and e) and from b_2 state, resp., are given in the function of ϑ.

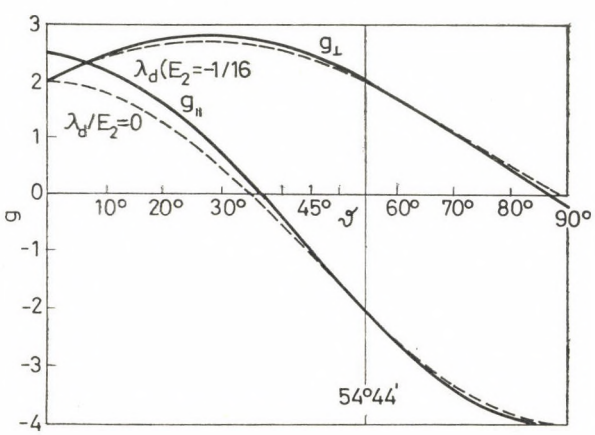

Fig. 5. Distortion dependence of g factors. The contribution of the b_2 level is demonstrated separately. Covalent bonding and hybridization are neglected. In case of $\vartheta > 54.4°$, it corresponds to an elongated tetrahedron, when $\vartheta < 54.4°$, it is a compressed tetrahedron and when $\vartheta \approx 2°$, it can be considered a square-planar structure

It can be seen that $g_{\prime\prime}$ varies very strongly, and at a special value of distortion even its sign changes. The sign of $g_{\prime\prime}$ was chosen equal to that of the product of the three principal g values, as it was proposed by PRYCE [9], thus the sign of $g_{\prime\prime}$ corresponds to the rotational direction of the magnetic momentum in an external magnetic field. The absolute values of the g factors unambiguously reveal whether the tetrahedron is only slightly or highly distorted.

In case of slight distortion (either compression or elongation) at least one of the g factors is smaller than 2, while in case of strong distortion (tetragonal distortion) both g factors are larger than 2.

By using this fact, the previously investigated tetrahedral complexes of Cu(II) can be classified. Other ions of $3d^1$ hole electronic configuration, *e.g.* Ni(I), can also be involved in this description. The principal values of g and hyperfine tensors for several substances of this kind are listed in Table II.

Table II

	$g_{\prime\prime}$	$g_\perp$	$\lvert A_{\prime\prime} \rvert$ (10^{-4} cm^{-1})	$\lvert A_\perp \rvert$ (10^{-4} cm^{-1})	References
CuBFNA	2.158	2.041	123	$\leq$20	this paper
CuISA	2.159	2.053*	125	21.5**	[6]
CuTC	2.384	2.094*	25	48.5**	[3]
CuDPM	2.283	2.075*	—	—	[5]
Cu/ZnO	−0.74	1.531*	195	231**	[4]
Cu/BeO	1.712	2.378	52.4	108	[10]
Ni(I)/ZnS	1.40	1.40	—	—	[8]

* $g_\perp = 1/2\,(g_x + g_y)$, ** $A_\perp = 1/2\,(A_x + A_y)$

In this table the following abbreviations are used:
CuISA for bis-(N-isopropylsalicylaldiminato)copper(II),
CuTC for tetrachlorocuprate(II) ion, and CuDPM for Cu((α,α'bromo)dipyrromethan)$_2$.

On comparing the data of Table II with the g-curves in Fig. 5, it can be seen that CuDPM, CuISA, CuTC and CuBFNA have highly compressed tetrahedral geometry. Two examples of trigonal distortion are also included in Table II: Cu(II) in ZnO and BeO lattices. It is remarkable that although our formulas should only be valid in case of tetragonal distortion, the experimental g values fit our formulas at least as well as those of DE WIT and REINBERG [10] who used trigonally distorted tetrahedral crystal field. Fig. 5 reveals that the Cu(II) ion in BeO has a medium-distorted while in ZnO, a slightly distorted tetrahedral crystal field. In case of slight distortion the ratio of orbital and spin contributions to the g values is 2 : 1, therefore, the covalency and hy-

bridization can significantly decrease the g values. This explains that in the case of Cu(II)/ZnO and Ni(I)/ZnS $g_\perp$ is significantly smaller than 2.

In Fig. 6 the hyperfine constants are shown as a function of ϑ for the cases when $\lambda_d/E_2 = 0$, and $|\lambda_d/E_2| = 1/16$. It is remarkable that while $A_\perp$ covers a wide range, $A_{,,}$ varies only to a small extent. The hybridization, however, can profoundly decrease the value of $A_{,,}$ and, therefore, this parameter is suitable for estimating the hybridization. Considering the above examples, the estimated hybridization is strong in case of CuDPM, medium in case of CuTC, and negligible in case of CuISA. The strong hybridization in

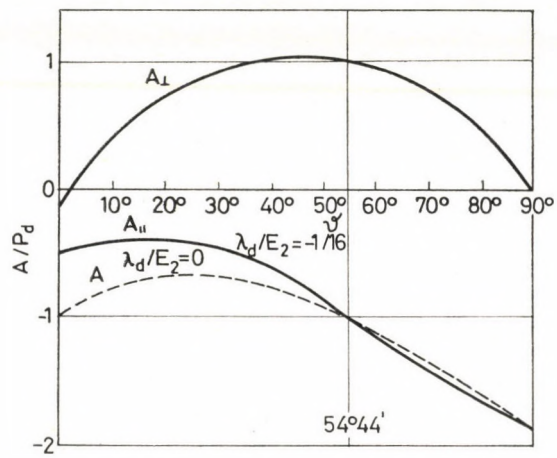

Fig. 6. Distortion dependence of hyperfine constants. The effect of the b_2 level is also illustrated. Covalent bonding and hybridization are neglected. In case when $\vartheta = 54.4°$, it corresponds to a regular tetrahedron, when $\vartheta < 54.4°$, it is a compressed tetrahedron, when $\vartheta \approx 2°$, it can be regarded a square-planar structure

case of CuDPM is surprising, since a large tetragonal compression would, by decreasing the departure from inversional symmetry, reduce the degree of hybridization.

A rough analysis of the spectral parameters for CuBFNA reveals that in this case hybridization does not play a significant role. This analysis has been completed by reducing more or less arbitrarily the number of unknown parameters. These simplifications are listed in Table III. The Table IV shows additional constants for which the values are taken from the literature [2, 3, 13]. If the 18 000 cm^{-1} band in the optical absorption spectra of CuBFNA [1] is taken tentatively equal to E_2, the remaining parameters can be calculated. Although the sign of $A_{,}$ is unknown, it has been taken as negative, because in the opposite case hybridization would be too strong ($\beta^2 = 0.52$). Table V shows the calculated molecular orbital parameters, $\varkappa$ and E_1.

Table III

$\alpha_0 = \alpha_1 = \alpha$	$\alpha_2^2 = 0.9$
$\beta_0 = \beta_1 = \beta$	
$\gamma_0 = \gamma_1 = \gamma$	
$\delta_1 = 0$	$\delta_2^2 = 0.1$

Table IV

$\lambda_d = -829\ \text{cm}^{-1}$	$\lambda_p = -925\ \text{cm}^{-1}$
$P_d = 360\ 10^{-4}\ \text{cm}^{-1}$	$P_p/P_d = 1.1$
$S_d = S_p = 0.1$	$T(n) = 0.333$

Table V

$\alpha^2 = 0.64$	$\beta^2 = 0.00$	$\gamma^2 = 0.47$
$\varkappa = 0.386$	$E_1 = 14\,000\ \text{cm}^{-1}$	

Although the calculated value for $\varkappa$ and the zero hybridization is typical for square-planar arrangement [13], a highly distorted tetrahedral structure is not to be ruled out. The reason is that if the tetragonal compression is strong, the crystal field term responsible for the lack of inversional symmetry becomes too small to cause significant hybridization, and, since $\varkappa$ is essentially a feature of the free Cu^{2+} ion [15], there must be little difference between its values in tetrahedral and square-planar structure.

Considering the chemical evidence, we are inclined to picture the four nitrogens bonded to the Cu^{2+} ion in CuBFNA forming a tetrahedron which is highly distorted towards the square-planar structure. This kind of distortion is promoted by the JAHN-TELLER effect. The square-planar arrangement is the most favourable structure for the Cu^{2+} ion, since in this case there is a highly separated *3d* singlet level which forms a low energy level for the hole electron, while the cubic crystal field leads to a degenerate ground state. The different degrees of distortion can be explained by the different ligand flexibilities. When, *e.g.* the Cu^{2+} ion is in the rigid ZnO lattice the JAHN-TELLER distortion is very small, but when the Cu^{2+} ion is surrounded by flexible organic compounds, *e.g.* in the different chelates, this distortion is large.

*

I am most indebted to Dr. A. MESSMER for the loan of samples and to Dr. L. RADICS for the valuable discussions.

REFERENCES

1. MESSMER, A., SZIMÁN, O.: Acta Szeged. **41,** 36 (1959); and MTA KKKI Közl. **2,** 87 (1959)
2. BATES, C. A., MOORE, W. S., STANDLEY, K. J., STEVENS, K. W. H.: Proc. Phys. Soc. **79,** 73 (1962)
3. SHARNOFF, M.: J. Chem. Phys. **41,** 2203 (1964)
4. DIETZ, R. E., KAMIMURA, H., STURGE, M. D., YARIV, A.: Phys. Rev. **132,** 1559 (1963)
5. BATES, C. A.: Proc. Phys. Soc. **83,** 465 (1964)
6. FRITZ, H. P., GOLLA, B. M., KELLER, H. J.: Z. Naturforschg. **21a,** 1015 (1966)
7. WÜTHRICH, K.: Helv. Chim. Acta **49,** 1400 (1966)
8. MORIGAKI, K.: J. Phys. Soc. Japan **19,** 1240 (1964)
9. ESTLE, T. L., HOLTON, W. C., DE WIT, M., WATTS, R. K., REINBERG, A. R., SCHNEIDER, J.: Proceedings of the International Conference on Luminescence, held in Budapest, 1966, p. 2121. Akadémiai Kiadó, Budapest, 1968
10. DE WIT, M., REINBERG, A. R.: Phys. Rev. **163,** 261 (1967)
11. GOULD, D. C., EHRENBERG, A.: European J. Biochem. **5,** 451 (1968)
12. FORSTER, D., WEISS, V. W.: J. Phys. Chem. **72,** 2669 (1968).
13. GERSMANN, H. R., SWALEN, J. D.: J. Chem. Phys. **36,** 3221 (1962)
14. PRYCE, M. H. L.: Phys. Rev. Letters **3,** 375 (1959)
15. ABRAGAM, A., PRYCE, M. H. L.: Proc. Roy. Soc. A**206,** 164 (1951)

Antal ROCKENBAUER; Budapest II., Pusztaszeri út 57—69.

Acta Chimica Academiae Scientiarum Hungaricae, Tomus 63 (2), pp. 167—178 (1970)

EXTREME VALUES OF FORCE CONSTANTS AND MEAN-SQUARE AMPLITUDES OF VIBRATION IN ETHYLENE TYPE MOLECULES, I

C_2H_4 and C_2D_4

G. FOGARASI and P. MEZEY

(Institute for General and Inorganic Chemistry, L. Eötvös University, Budapest)

Received November 27, 1968

Considering ethylene and ethylene–d_4 as model molecules, they have been investigated separately and a great number of force constant matrices, reproducing the experimental normal frequencies has been calculated by the parameter method of PULAY and TÖRÖK. Sets of the mean-square amplitudes compatible with the normal frequencies have also been calculated. When the normal frequencies are the only available experimental data, the force constants can assume perfectly unreasonable values, too; however, even in this case, the investigation of their extreme values can provide useful information on the force field. The investigation of the mean-square amplitudes in a wide range of force constants has given results at variance with the electron diffraction data, indicating the uncertainty of the latter.

In most cases the amount of available experimental data (vibrational frequencies and possibly additional data such as mean-square amplitudes of vibration, Coriolis constants and centrifugal stretching constants) is insufficient for an unambiguous determination of the force constants. The assumption of various simplified force fields is a widely used compromise method.

A more exact procedure is the parameter form of force constant matrix, proposed by TAYLOR [1] and worked out in detail by PULAY and TÖRÖK [2]. It makes possible to determine all the sets of force constants which will reproduce the fundamental frequencies or, in general, all the additional experimental data. TÖRÖK has shown [3] that the mean-square amplitudes compatible with the normal frequencies can also be calculated in a similar manner.

The force field of ethylene and ethylene-d_4 has been studied by several authors [4, 5]. Our purpose was not a further improvement of these calculations. This problem can be considered to be settled since the force field is practically fixed by the isotope frequencies, some uncertainties arise only from the anharmonicity correction.

In this paper the C_2H_4 and C_2D_4 molecules will be studied separately as models of the general case, when the experimental data do not fix the force constants unambiguously. This procedure seemed to be advisable, since thus we can compare our results with reliable data. Our objective was to determine the possible range of force constants and mean-square amplitudes in the case when this is limited by the only condition that they must reproduce the fundamental frequencies. Similar calculations have been carried out with the tetrahalogenoethylenes; these results will be published in a forthcoming paper.

The parameter form of the F matrix

In WILSON's notation the well-known basic equation of the normal-coordinate analysis is as follows [7]:

$$\mathrm{G\,F\,L} = \mathrm{L}\Lambda\,. \tag{1}$$

The essence of the parameter representation is that the eigenvector matrix L can be written in the following form:

$$\mathrm{L} = \mathrm{g\,U}\,, \tag{2}$$

where $\mathrm{g} = \mathrm{G}^{1/2}$, and U is an arbitrary orthogonal matrix which can be given as a function of $\binom{n}{2}$ parameters. By changing the parameters, *i.e.* the normal coordinates, a systematic calculation of L-dependent quantities (*e.g.* force constants or mean-square amplitudes) will become possible.

On the basis of the above considerations, the F matrices reproducing the normal frequencies of a molecule will be:

$$\mathrm{F} = (\mathrm{L}^{-1})^{\top}\,\Lambda\,\mathrm{L}^{-1} = \mathrm{g}^{-1}\,\mathrm{U}\,\Lambda\,\mathrm{U}^{\mathrm{T}}\,\mathrm{g}^{-1}\,, \tag{3}$$

where the elements of the diagonal matrix Λ are obtained from the experimental $\lambda_i = 4\pi^2\nu_i^2$ values. The parameters can be, *e.g.*, angles, and by changing them in the $(-\pi/2,\ \pi/2)$ interval one can systematically map all the possible values of the force constants.

According to [3], the mean-square amplitudes can be determined in the following way: Let S and Q be the n-dimensional column matrices of the internal coordinates (suitably, symmetry coordinates) and normal coordinates, resp., where $\mathrm{n} = 3\mathrm{N}-6$, N being the number of atoms; let X be the column matrix of 3N cartesian displacement coordinates, while r a column matrix of $\binom{N}{2}$ dimensions, whose elements represent the interatomic distance deviations for an arbitrary pair of atoms. Let us define, furthermore, the following transformations:

$$r = \mathrm{K}\,Q \qquad\qquad S = \mathrm{L}\,Q$$

$$r = \mathrm{B_M}\,X \qquad\qquad S = \mathrm{B}\,X$$

The mean-square amplitudes of vibration are square roots of diagonal elements of the

$$\mathrm{P} = \widetilde{\widetilde{r\,r}}^{\top} = \mathrm{K}\,\widetilde{\widetilde{Q\,Q}}^{\top}\,\mathrm{K}^{\top} = \mathrm{K}\,\Delta\,\mathrm{K}^{\top} \tag{4}$$

matrix. The upper wavy lines denote mean values. Δ is a diagonal matrix with elements $\Delta_{kk} = \dfrac{\mathrm{h}}{8\pi^2\nu_k}\coth\dfrac{\mathrm{h}\nu_k}{2\mathrm{kT}}$, K can be written in the following form:

$$\mathrm{K} = \mathrm{B_M}\,\mathrm{M}^{-1}\,\mathrm{B}^{\top}\,\mathrm{G}^{-1}\,\mathrm{L}\,, \tag{5}$$

where M is a diagonal matrix with the atomic weights as elements. On the basis of the $L = g\ U$ relationship the mean-square amplitudes can also be calculated as functions of the parameters producing matrix U.

Experimental data

Structural parameters and normal frequencies are given in Tables I and II, resp. These data agree with those used by CYVIN and CYVIN [4]. The anharmonicity corrections have also been taken from the above paper.

Table I

Structural parameters

$CH = CD = 1.086$ Å

$CC = 1.338$ Å

$\sphericalangle HCH = \sphericalangle DCD = 117.3°$

Table II

Anharmonic (experimental) and harmonic (corrected) normal frequencies of ethylenes

Assignment	C_2H_4		C_2D_4	
	v (cm^{-1})	w (cm^{-1})	v (cm^{-1})	w (cm^{-1})
A_g S_1	3026	3427	2260	2476
S_2	1623	1634	1518	1528
S_3	1342	1296	985	960
B_{1g} S_1	3102	3096	2310	2306
S_2	1236	1262	1011	1028
B_{2u} S_1	3105	3278	2345	2442
S_2	810	827	585	594
B_{3u} S_1	2989	3200	2200	2312
S_2	1443	1491	1078	1104

Calculations

The calculations have been carried out for the in-plane vibrations only. This is permissible in the case of mean-square amplitudes, too, since the out-of-plane vibrations do not contribute to their values. The internal and symmetry coordinates are defined in Fig. 1 and Table III, respectively. Bending coordinates are not weighted by equilibrium distances. The mapping of force constants has been carried out in each symmetry species separately. In order to obtain results comparable with the experimental data, in the case of mean-

square amplitudes the total L and U matrices should be considered. Thus, for the in-plane vibrations U will be of dimensions 9 and the number of parameters is $\binom{9}{2}$. However, the number of actually independent parameters is far less, namely 6, since $\alpha_{ij} = \text{const.} = 0$, if subscripts i and j refer to coordinates of two different symmetry species. Unfortunately, even this number of parameters permits only a limited mapping.

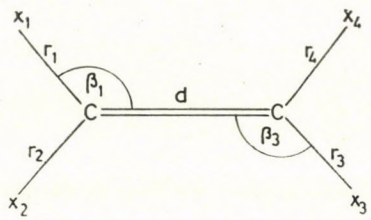

Fig. 1

Internal coordinates

Table III

In-plane symmetry coordinates

$S_1(Ag) = {}^1/_2(r_1 + r_2 + r_3 + r_4)$
$S_2(Ag) = d$
$S_3(Ag) = {}^1/_2(\beta_1 + \beta_2 + \beta_3 + \beta_4)$
$S_1(B_{1g}) = {}^1/_2(r_1 - r_2 + r_3 - r_4)$
$S_2(B_{1g}) = {}^1/_2(\beta_1 - \beta_2 + \beta_3 - \beta_4)$
$S_1(B_{2u}) = {}^1/_2(r_1 - r_2 - r_3 + r_4)$
$S_2(B_{2u}) = {}^1/_2(\beta_1 - \beta_2 - \beta_3 + \beta_4)$
$S_1(B_{3u}) = {}^1/_2(r_1 + r_2 - r_3 - r_4)$
$S_2(B_{3u}) = {}^1/_2(\beta_1 + \beta_2 - \beta_3 - \beta_4)$

Results

Force constants. In Tables IV, V and VI a map of force constants is given, where rotation angles served as parameters. Naturally, in the case of the A_g species, only a part of the full range of parameters can be given. According to our calculations carried out in the full parameter range, completely improbable extreme force constant values may also occur, *i.e.*, when the only restriction for the force constants is the reproduction of normal frequencies, the force field is practically undetermined. At the same time in all the two-dimensional species the minimum of F_{22} belonging to the bending coordinate, and the maximum of the stretching force constant F_{11} are restricted to very probable values.

Because of the problems mentioned above the extreme values of A_g force constants have been investigated under prescribed restrictions, too. Although these restrictions imposed on the off-diagonal elements involve some arbitrariness, this is far less than that associated with the simplified force fields, since, instead of fixing some elements, only wide ranges are prescribed. The results are summarized in Table VII. The force constants have not be-

Table IV

Map of the A_g-force constants of C_2H_4

Parameters (π units)			F(11)	(F12)	F(13)	F(22)	F(23)	F(33)
—.10	—.10	—.10	5.459	—2.672	—2.151	13.406	2.601	2.217
—.10	—.10	.00	5.506	—2.493	—2.074	13.797	3.061	2.264
—.10	—.10	.10	5.539	—2.439	—1.981	13.464	3.458	2.376
—.10	.00	—.10	5.899	—2.490	— .535	12.841	1.165	1.236
—.10	.00	.00	5.908	—2.415	— .448	13.421	1.657	1.262
—.10	.00	.10	5.894	—2.467	— .375	13.285	2.112	1.407
—.10	.10	—.10	5.432	—1.631	1.163	11.860	.006	1.513
—.10	.10	.00	5.393	—1.655	1.253	12.604	.485	1.540
—.10	.10	.10	5.342	—1.820	1.927	12.646	.949	1.681

Parameters			F(11)	F(12)	F(13)	F(22)	F(23)	F(33)
.00	—.10	—.10	6.349	.927	—1.943	10.359	.705	1.883
.00	—.10	.00	6.360	1.082	—1.920	10.999	1.191	1.918
.00	—.10	.10	6.378	1.203	—1.868	10.876	1.634	2.057
.00	.00	—.10	6.855	1.581	— .113	10.492	.787	1.182
.00	.00	.00	6.855	1.601	— .084	11.103	1.298	1.215
.00	.00	.10	6.853	1.578	— .062	10.950	1.765	1.366
.00	.10	—.10	6.256	2.068	1.717	10.696	1.222	1.750
.00	.10	.00	6.235	1.951	1.749	11.257	1.714	1.784
.00	.10	.10	6.223	1.785	1.740	11.050	2.154	1.926

Parameters			F(11)	F(12)	F(13)	F(22)	F(23)	F(33)
.10	—.10	—.10	6.346	4.844	—1.499	13.743	— .500	1.609
.10	—.10	.00	6.326	4.919	—1.535	14.515	— .041	1.641
.10	—.10	.10	6.313	5.056	—1.534	14.646	.410	1.783
.10	.00	—.10	6.816	5.900	.367	15.287	1.148	1.203
.10	.00	.00	6.818	5.862	.335	15.834	1.624	1.233
.10	.00	.10	6.818	5.870	.305	15.715	2.063	1.382
.10	.10	—.10	6.187	5.893	2.142	15.908	3.078	2.061
.10	.10	.00	6.202	5.734	2.115	16.200	3.529	2.094
.10	.10	.10	6.225	5.624	2.058	15.819	3.907	2.229

Table V

Map of the A_g-force constants of C_2D_4

Parameters (π units)			F(11)	F(12)	F(13)	F(22)	F(23)	F(33)
—.10	—.10	—.10	5.745	— .977	—2.299	11.266	2.331	2.474
—.10	—.10	.00	5.887	— .567	—2.058	12.157	3.319	2.611
—.10	—.10	.10	5.975	— .437	—1.785	11.874	4.179	3.012
—.10	.00	—.10	6.232	— .464	— .701	10.557	1.201	1.385
—.10	.00	.00	6.255	— .271	— .435	11.721	2.267	1.519
—.10	.00	.10	6.206	— .371	— .222	11.733	3.260	1.974
—.10	.10	—.10	5.828	.483	1.010	9.798	.483	1.553
—.10	.10	.00	5.711	.468	1.279	11.174	1.534	1.688
—.10	.10	.10	5.549	.119	1.406	11.427	2.550	2.134

Parameters			F(11)	F(12)	F(13)	F(22)	F(23)	F(33)
.00	—.10	—.10	6.611	1.255	—2.029	9.571	.830	2.037
.00	—.10	.00	6.653	1.595	—1.934	10.846	1.875	2.198
.00	—.10	.10	6.709	1.854	—1.770	10.928	2.835	2.637
.00	.00	—.10	7.124	2.192	— .175	9.809	.906	1.295
.00	.00	.00	7.124	2.250	— .073	11.011	2.005	1.456
.00	.00	.10	7.115	2.193	.000	11.010	3.013	1.932
.00	.10	—.10	6.526	2.916	1.685	10.180	1.461	1.829
.00	.10	.00	6.456	2.687	1.784	11.251	2.522	1.990
.00	.10	.10	6.410	2.320	1.760	11.108	3.465	2.439

Parameters			F(11)	F(12)	F(13)	F(22)	F(23)	F(33)
.10	—.10	—.10	6.756	3.792	—1.490	10.975	— .061	1.693
.10	—.10	.00	6.710	3.944	—1.567	12.410	.922	1.846
.10	—.10	.10	6.683	4.221	—1.539	12.887	1.903	2.298
.10	.00	—.10	7.183	5.006	.433	12.522	1.260	1.321
.10	.00	.00	7.190	4.923	.359	13.586	2.272	1.474
.10	.00	.10	7.191	4.916	.288	13.631	3.210	1.944
.10	.10	—.10	6.483	5.320	2.238	13.540	2.987	2.219
.10	.10	.00	6.512	4.984	2.170	14.164	3.938	2.374
.10	.10	.10	6.570	4.719	2.012	13.737	4.731	2.799

Table VI

Map of the B_{1g}-, B_{2u}- and B_{3u}-force constants of the C_2H_4 and C_2D_4 molecules

Parameter (π units)		F(11)		F(12)		F(22)	
		C_2H_4	C_2D_4	C_2H_4	C_2D_4	C_2H_4	C_2D_4
B_{1g}	−.50	.930	1.249	.553	.819	3.931	3.213
	−.40	1.081	1.263	− .567	− .191	3.396	2.674
	−.30	2.004	2.111	−1.249	− .783	2.449	1.874
	−.20	3.347	3.468	−1.230	− .730	1.452	1.118
	−.10	4.597	4.816	− .517	− .953	.787	.694
	.00	5.276	5.640	.615	.989	.706	.766
	.10	5.125	5.626	1.736	1.999	1.242	1.304
	.20	4.201	4.778	2.418	2.591	2.189	2.105
	.30	2.858	3.421	2.399	2.539	3.185	2.861
	.40	1.608	2.073	1.687	1.862	3.851	3.284
	.50	.930	1.249	.553	.819	3.931	3.213
B_{2u}	−.50	.370	.367	.247	.484	7.223	7.752
	−.40	.765	.662	−1.522	−1.375	6.449	6.803
	−.30	2.027	1.873	−2.621	−2.536	4.680	4.829
	−.20	3.675	3.537	−2.629	−2.554	2.592	2.584
	−.10	5.079	5.020	−1.542	−1.423	.983	.925
	.00	5.702	5.753	.223	.424	.467	.485
	.10	5.308	5.459	1.993	2.283	1.241	1.434
	.20	4.045	4.248	3.092	3.444	3.009	3.408
	.30	2.398	2.583	3.099	3.463	5.097	5.654
	.40	.994	1.101	2.013	2.332	6.706	7.313
	.50	.370	.367	.247	.484	7.223	7.752
B_{3u}	−.50	1.274	1.367	− .260	− .474	6.411	6.091
	−.40	1.804	1.972	−1.668	−1.837	6.032	5.820
	−.30	3.003	3.210	−2.537	−2.679	4.840	4.759
	−.20	4.413	4.608	−2.534	−2.677	3.291	3.313
	−.10	5.495	5.633	−1.662	−1.833	1.976	2.034
	.00	5.836	5.892	− .252	− .469	1.398	1.412
	.10	5.306	5.287	1.155	.893	1.778	1.683
	.20	4.106	4.049	2.024	1.734	2.970	2.744
	.30	2.697	2.650	2.021	1.733	4.519	4.190
	.40	1.614	1.626	1.149	.889	5.833	5.468
	.50	1.274	1.367	− .260	− .474	6.411	6.091

Table VII

Extreme values of force constants in the Ag species with the following restrictions: $|F_{12}| \leq 1$, $|F_{13}| \leq 1$, $|F_{23}| \leq 2$

	F_{11} CH str.			F_{22} C=C str.			F_{33} CCH bend.		
	min.	max.	ref [4]	min.	max.	ref [4]	min.	max.	ref [4]
C_2H_4	6.0	6.8	6.78	9.0	11.7	10.76	1.2	1.6	1.40
C_2D_4	5.8	6.9	6.78	7.7	11.6	10.76	1.3	1.8	1.40

	F_{12}			F_{13}			F_{23}		
	min.	max.	ref [4]	min	max	ref [4]	min	max	ref [4]
C_2H_4	−1.0	1.0	1.00	−1.0	1.0	−0.13	0.1	2.0	1.82
C_2D_4	−1.0	1.0	1.00	−1.0	1.0	−0.13	−0.2	2.0	1.82

Dimensions: F_{11}, F_{22}, F_{12} — mdyn/Å; F_{13}, F_{23} — mdyn; F_{33} — mdyn · Å

Table VIII

Force constants at the minimum value of F_{22}

		F_{11} CH str.	ref [4]	F_{12}	ref [4]	F_{22} CCH bend.	ref [4]
B_{1g}	C_2H_4	5.12	5.14	0.20	0.23	0.65	0.66
	C_2D_4	5.23		0.34		0.66	
B_{2u}	C_2H_4	5.68	5.69	0.03	0.04	0.46	0.46
	C_2D_4	5.68		0.03		0.46	
B_{3u}	C_2H_4	5.82	5.82	— .10	−0.13	1.39	1.39
	C_2D_4	5.84		−0.18		1.39	

Dimensions: F_{11} — mdyn/Å, F_{12} — mdyn, F_{22} — mdyn · Å

come fixed and, naturally, this cannot be expected under the applied loose restrictions, however, the results provide reliable information about the possible limits of force constants. The diagonal elements vary between acceptable values. The off-diagonal element F_{23} has a positive sign, while F_{12} and F_{23} remain undetermined.

In the case of the two-dimensional species, the force constants have been studied at the minimum of F_{22} (Table VIII). Though this has been quite an arbitrary selection from the possible solutions, it is remarkable that these force constants are in perfect agreement with CYVIN's reliable results obtained by simultaneous consideration of all the isotope frequencies. STREY's studies on nonlinear XY_2 and pyramidal XY_3 molecules [9] have led to similar results. However, it must be emphasized that the above author has examined only two-dimensional cases, since our calculations indicate evidently that this procedure cannot be extended to the three-dimensional case.

Mean-square amplitudes of vibration

As mentioned above, each in-plane vibration contributes to the mean-square amplitudes, thus their mapping can be only limited. Table IX contains the results obtained for the C_2D_4 molecule, as calculated by varying the parameters only in the A_g species, the force constants of the two-dimensional species being left unchanged. These force constants, as well as those belonging to 0,0,0 values of the parameters in the A_g species have been taken from the paper by CYVIN [4], *i.e.* the center of this mapping [10] is defined by the L_0 matrix corresponding to CYVIN's force constants, instead of the $L_0 = g$ relationship. Consequently, the amplitudes calculated at point 0,0,0 are identical with those reported by CYVIN [6]. In the present calculations $L = L_0U$. It should be noted that instead of the angle parameters another form of U matrix proposed by PULAY [10] has been applied in the present case.

Besides the results given in Table IX similar calculations have also been carried out for the C_2H_4 molecule as well as for the two-dimensional species. Table IX shows that even the reliable CYVIN's force constants calculated by considering all the isotope frequencies do not yield mean-square amplitudes compatible with the experimental values obtained by electron-diffraction techniques. The differences alone would not seem very important, but on the basis of the given mapping it is worth mentioning that the deviations from the experimental values are in the same or higher order of magnitude than the variation of the mean-square amplitudes in the whole mapped parameter range containing strongly varying force constants. Similar results have been obtained in the case of ethylene and some other molecules studied in this laboratory. Naturally, the amount of data is not sufficient to allow generalization, but this problem should be taken into account when using mean-square amplitudes obtained by electron-diffraction measurements for fixing the force field.

Table IX

Root-mean-square amplitudes of vibration[1] *at*

Parameters			F(11)	F(12	F(13)	F(22)	F(23)
−0.1	−0.1	−0.1	5.743	−0.174	0.819	11.899	2.225
−0.1	−0.1	0.0	5.845	0.103	0.814	11.358	1.505
−0.1	−0.1	0.1	5.944	0.287	0.764	10.372	0.812
−0.1	0.0	−0.1	6.095	−0.477	−0.243	12.133	2.745
−0.1	0.0	0.0	6.104	−0.440	−0.296	11.801	2.005
−0.1	0.0	0.1	6.103	−0.484	−.0364	10.979	1.262
−0.1	0.1	−0.1	6.074	−0.629	−1.303	12.324	3.352
−0.1	0.1	0.0	5.984	−0.831	−1.390	12.270	2.709
−0.1	0.1	0.1	5.887	−1.099	−1.461	11.724	2.030
0.0	−0.1	−0.1	6.389	1.222	1.113	11.038	2.435
0.0	−0.1	0.0	6.492	1.519	1.069	10.696	1.772
0.0	−0.1	0.1	6.589	1.720	0.975	9.905	1.110
0.0	0.0	−0.1	6.769	0.986	−0.031	11.077	2.527
0.0	0.0	0.0	6.783	1.004	−0.133	10.766	1.824
0.0	0.0	0.1	6.784	0.936	−0.251	9.982	1.120
0.0	0.1	−0.1	6.725	0.792	−1.188	11.132	2.719
0.0	0.1	0.0	6.644	0.530	−1.332	10.921	2.095
0.0	0.1	0.1	6.551	0.202	−1.454	10.255	1.463
0.1	−0.1	−0.1	6.781	2.864	1.404	11.510	2.868
0.1	−0.1	0.0	6.878	3.166	1.308	11.338	2.201
0.1	−0.1	0.1	6.970	3.363	1.159	10.682	1.508
0.1	0.0	−0.1	7.168	2.709	0.234	11.385	2.531
0.1	0.0	0.0	7.186	2.708	0.072	11.062	1.805
0.1	0.0	0.1	7.189	2.612	−0.105	10.253	1.077
0.1	0.1	−0.1	7.104	2.473	−0.968	11.272	2.296
0.1	0.1	0.0	7.036	2.170	−1.175	10.867	1.628
0.1	0.1	0.1	6.956	1.791	−1.358	10.013	0.978

[1] Experimental values are [8] : C = C: 0.0418 ± 0.005 Å, C—H : 0.0681 ± 0.005 Å, C . . H: 0.0925 ± 0.009 Å.

$T = 298$ °K in Å and Ag force constants for C_2D_4

F(33)	C=C	C—H	C..H	c—HH	tr—HH	gem—HH
1.676	.0416	.0647	.0822	.1392	.0963	.1063
1.476	.0407	.0646	.0825	.1406	.0964	.1056
1.414	.0406	.0645	.0831	.1415	.0968	.1044
1.675	.0429	.0643	.0825	.1417	.0978	.1014
1.427	.0414	.0643	.0831	.1434	.0987	.1009
1.321	.0408	.0644	.0840	.1446	.0997	.1000
2.164	.0443	.0648	.0829	.1436	.1006	.0969
1.909	.0424	.0649	.0837	.1454	.1021	.0967
1.773	.0412	.0650	.0847	.1467	.1035	.0962
1.773	.0431	.0644	.0816	.1384	.0945	.1056
1.554	.0421	.0644	0.818	.1397	.0946	.1051
1.465	.0419	.0644	.0823	.1407	.0950	.1041
1.633	.0441	.0641	.0819	.1413	.0962	.1004
1.398	.0427	.0641	.0825	.1429	.0971	.1000
1.303	.0420	.0641	.0833	.1440	.0980	.0993
1.994	.0451	.0646	.0825	.1435	.0994	.0959
1.784	.0433	.0647	.0833	.1453	.1008	.0956
1.698	.0423	.0647	.0843	.1465	.1021	.0952
1.902	.0442	.0644	.0808	.1378	.0931	.1051
1.647	.0430	.0645	.0810	.1391	.0934	.1049
1.519	.0427	.0645	.0815	.1400	.0937	.1040
1.626	.0448	.0642	.0812	.1409	.0951	.1000
1.389	.0434	.0642	.0818	.1425	.0959	.0997
1.293	.0427	.0642	.0825	1.435	.0967	.0991
1.845	.0454	.0648	.0819	.1435	.0986	.0956
1.664	.0437	.0648	.0828	.1452	.0999	.0953
1.616	.0429	.0647	.0838	.1462	.1010	.0949

REFERENCES

1. TAYLOR, J. W.: J. Chem. Phys. **18,** 1301 (1950)
2. PULAY, P., TÖRÖK, F.: Acta Chim. Acad. Sci. Hung. **44,** 287 (1965)
   TÖRÖK, F., PULAY, P.: Acta Chim. Acad. Sci. Hung. **56,** 285 (1968)
3. TÖRÖK, F.: Acta Chim. Acad. Sci. Hung. **59,** 303 (1969)
4. CYVIN, B. N., CYVIN, S. J.: Acta Chem. Scand. **17,** 1831 (1963); and references cited therein
5. KUCHITSU, K., MORINO, Y.: J. Mol. Spectr. **15,** 51 (1965)
6. CYVIN, B. N., CYVIN, S. J.: Acta Chem. Scand. **18,** 1690 (1964)
7. WILSON, E. B., DECIUS, J. C., CROSS, P. C.: Molecular Vibrations. McGraw-Hill, 1955
8. BARTELL, L. S., KUCHITSU, K.: J. Chem. Phys. **42,** 2683 (1965)
9. STREY, G.: J. Mol. Spectr. **24,** 87 (1967)
10. PULAY, P.: Acta Chim. Acad. Sci. Hung. **52,** 49 (1967)

Géza FOGARASI
Pál MEZEY
Budapest VIII., Múzeum krt. 6—8.

Acta Chimica Academiae Scientiarum Hungaricae, Tomus 63 (2), pp. 179—192 (1970)

MULTILAYER ADSORPTION FROM LIQUID MIXTURES, II

J. TÓTH

(Industrial Research Laboratory of Oil and Gas Mining, Nagykanizsa)

Received December 6, 1968

By means of a thermodynamic interpretation of multilayer adsorption equivalent to monolayer adsorption (e.m. adsorption) it has been shown that the contradictions resulting from an exclusive application of the monolayer adsorption model can be resolved.

On the basis of concrete properties of concrete adsorption systems, it has been established that the nature of the concentration distribution in the surface phase resulting from e.m. adsorption is of two types. The first group involves a distribution leading to continuous variation of the concentration between the surface and bulk phases. In these cases, the concentration in each layer of the surface phase exceeds that in the bulk phase but it is of decreasing tendency (positive–positive adsorption). The other possibility is that the individual layers of the surface phase are characterized by adsorption with opposite signs (positive–negative adsorption). The interpretation of experimental results taken from the literature has led to a generalized explanation for the existence of multilayer adsorption which is precisely equivalent to monomolecular adsorption.

It has been pointed out in Part I of this paper [1] that the exclusive use of the monolayer model for adsorption of liquid mixtures may lead to contradictions. Thus, complications arise in connection with the adsorption of pairs of liquid (*e.g.* ethanol–water) for which monolayer adsorption is impossible due to the ***doubtless*** presence of surface association and H-bonding. The above contradiction manifests itself when the adsorption of such components on either free or solid surfaces leads to $\Gamma - x$ isotherms characteristic for monolayer adsorption, and the extrapolation of the linear section yields a correct value for the specific surface area F(F-linear isotherms). Furthermore, calculations lead to multi-valued or "oscillating" $\Delta\gamma_{2,G}$ *vs.* x' free-energy functions with linear isotherms, a fact impossible to explain. In order to resolve the above contradictions, we have assumed that the monomolecular individual adsorbed amounts Γ_1 and Γ_2 are mixed with one or more molecular layers of the bulk phase as a result of surface forces due to structural properties, such as association and H-bonding. Thus a multilayer surface phase is formed for which the experimentally observed excess substance is the same as with monolayer adsorption. This multilayer adsorption equivalent to monolayer adsorption has been named e.m. (*e*quivalent *m*ultilayer) adsorption. This abbreviation will be used throughout this paper.

The notion of e.m. adsorption has been formulated by means of mass balance-tye equations, therefore, it is now necessary to give a thermodynamic treatment, too. The thermodymanic contradictions described in Part I can only be resolved in all details as a result of such analysis.

1. Thermodynamic interpretation of e.m. adsorption

It has been shown in Part *I* that the change in the surface free-energy

$$\Delta\gamma_{2,G} = \gamma_{2,0} - \gamma \tag{1}$$

can be calculated from the following equation:

$$\Delta\gamma_{2,G} = RT \int_0^{f_1 x} \frac{\Gamma}{1-x}\, d\ln(f_1 x) \tag{2}$$

obtained by integration of the Gibbs equation. It has also been pointed out that in multilayer adsorption the excess adsorbed amount Γ is a sum of the corresponding excesses Γ^n for all layers, *i.e.*

$$\Gamma = \Gamma^1 + \ldots + \Gamma^n\,. \tag{3}$$

Consequently, Eq. (2) may also be written as a sum:

$$\Delta\gamma_{2,G} = RT \int_0^{f_1 x} \frac{\Gamma^1}{1-x}\, d\ln(f_1 x) + \ldots + RT \int_0^{f_1 x} \frac{\Gamma^n}{1-x}\, d\ln(f_1 x)\,. \tag{4}$$

Since there is an excess substance in each layer ($\Gamma^1 \ldots . \Gamma^n$), the above integrals give the free-energy changes for the individual layers, and Eq. (4) can be regarded as if the Gibbs equation (2) were applied to each layer. Consequently

$$\Delta\gamma_{2,G} = \Delta\gamma_{2,1} + \ldots + \Delta\gamma_{2,n}\,, \tag{5}$$

where for double-layer adsorption ($n = 2$)

$$\begin{aligned} \Delta\gamma_{2,1} &= \gamma_{2,1} - \gamma_1 \\ \Delta\gamma_{2,2} &= \gamma_{2,2} - \gamma_2\,. \end{aligned} \tag{6}$$

In Eq. (6) $\gamma_{2,1}$ and $\gamma_{2,2}$ are the surface free-energies for the first and second layers, respectively, of pure component *2*, γ_1 and γ_2 are the surface free-energies of the first and second layers, respectively, of the mixture with an activity of $a_1 = f_1 x$.

It follows from Eq. (5) that the surface energies γ (surface tensions) must be additive since Eqs (1), (5) and (6) hold only if

$$\begin{aligned} \gamma &= \gamma_1 + \gamma_2 \\ \gamma_{2,0} &= \gamma_{2,1} + \gamma_{2,2} \cdot \end{aligned} \tag{7}$$

Similar equations are obtained for component *1* except that $\Delta\gamma_{1,G}$ is obtained from Eqs (2) and (4) by means of integration between $f_1 x = 1$ and $f_1 x$. Thus

$$\Delta\gamma_{1,G} = \gamma_{1,0} - \gamma = \Delta\gamma_{1,1} + \ldots + \Delta\gamma_{1,n} \tag{8}$$

and

$$\begin{aligned} \Delta\gamma_{1,1} &= \gamma_{1,1} - \gamma_1 \\ \Delta\gamma_{1,2} &= \gamma_{1,2} - \gamma_2 \\ \gamma_{1,0} \quad &= \gamma_{1,1} + \gamma_{1,2} \cdot \end{aligned}$$

On the basis of the additivity of surface energies and the generalization of the HILDEBRAND theory of monomulecular adsorption (2) it is now possible to formulate the general thermodynamic relationships for e. m. adsorption.

As a result of the equality of chemical potentials in the bulk and surface phases for a monomolecular layer, one may write for a binary system:

$$f_1 x = f_1^0 x' \quad \text{and} \quad f_2 (1 - x) = f_2^0 (1 - x'), \tag{9}$$

where f_1 and f_2 are the rational activity coefficients of the components (calculated or measured on the basis of relationships valid for regular mixtures), f_1^0 and f_2^0 are the activity coefficients in the boundary phase. According to HILDEBRAND, the latter may be written as

$$f_1^0 = f_1' \exp\left[\frac{(\gamma_{1,0} - \gamma)\,\Phi_1}{RT}\right]. \tag{10}$$

By inserting Eq. (10) into Eq. (9), one obtains

$$\Delta\gamma_{1,G} = \gamma_{1,0} - \gamma = \frac{RT}{\Phi_1} \ln \frac{f_1 x}{f_1' x'}, \tag{11}$$

or for component *2*

$$\Delta\gamma_{2,G} = \gamma_{2,0} - \gamma = \frac{RT}{\Phi_2} \ln \frac{f_2 (1 - x)}{f_2' (1 - x')}, \tag{12}$$

where $f_1' x'$ and $f_2'(1 - x')$ are the activities of the components in the surface phase with respect to a fictive reference state in which, instead of $\gamma_{1,0}$ and

$\gamma_{2,0}$, the surface tension (surface free-energy) of the pure components would be equal to γ.

These considerations permit further splitting of Eq. (10):

$$f_1^0 = f_1^* \exp\left[\frac{(\gamma_{1,0} - \gamma)\Phi_1}{RT}\right] \exp\left[-\frac{\Delta F_1 \Phi_1}{RT}\right]. \tag{13}$$

Upon inserting Eq. (13) into Eq. (9), one obtains

$$\Delta\gamma_{1,G} = \frac{RT}{\Phi_1} \ln \frac{f_1 x}{f_1^* x'} + \Delta F_1. \tag{14}$$

Similarly, for component *2*

$$\Delta\gamma_{2,G} = \frac{RT}{\Phi_2} \ln \frac{f_2 (1 - x)}{f_2^* (1 - x')} + \Delta F_2. \tag{15}$$

In the above equations f_1^* and f_2^* are the rational activity coefficients of the two components measured (or calculated) at concentration x', $f_1^* x'$, and $f_2^*(1 - x')$ are the activities of the components in the *bulk* phase if te concentration in this phase would be equal to x'. Thus the first terms in the right-hand side of Eqs (14)—(15) are exclusively those free-energy changes associated with the transfer of the components from a medium of concentration x into another with x', but without any changes of the rational activity coefficients at concentration x' due to the effect of surface forces. The free-energy changes associated with the latter effect are denoted by ΔF_1 and ΔF_2. According to the above considerations, obviously

$$\Delta F_1 = \frac{RT}{\Phi_1} \ln \frac{f_1^*}{f_1'} \tag{16}$$

and

$$\Delta F_2 = \frac{RT}{\Phi_2} \ln \frac{f_2^*}{f_2'}. \tag{17}$$

The change of the rational activity coefficients measured at concentration x'(f_1^* and f_2^*) due the effect of surface forces in case of *monolayer* adsorption is associated with a free-energy change exactly equal to ΔF_1 and ΔF_2. On the other hand, the basic concept of the thermodymanic relationships for e.m. adsorption is that *only a fraction* of free-energy changes ΔF_1 and ΔF_2 is due to changes in the activity coefficients, the remainder being caused by the formation of several adsorbed layers as a result of mass transport due to the variation of γ with the depth of the boundary phase. Consequently,

$$\Delta F_1 = \Delta F_1^C + \Delta F_1^P, \tag{18}$$

where ΔF_1^C and ΔF_1^P are the free-energy changes of component *1* due to the variation of the coefficient and the increase of the adsorbed phase, respectively. Thus the basic thermodynamic relationship for e.m. adsorption is

$$\Delta\gamma_{1,G} = \frac{RT}{\Phi_1} \ln \frac{f_1 x}{f_1^* x'} + \Delta F_1^P + \Delta F_1^C \tag{19}$$

and

$$\Delta\gamma_{2,G} = \frac{RT}{\Phi_2} \ln \frac{f_2 (1-x)}{f_2^* (1-x')} + \Delta F_2^P + \Delta F_2^C. \tag{20}$$

A more general form of Eqs (19)—(2) is obtained, if the HILDEBRAND principle for monomolecular layers as well as the splitting according to Eq. (13) are applied to each layer separately. In this way, the full free-energy change of the multilayer adsorption phase can be calculated by means of the summing procedure used with Eqs (5) and (8). If the calculation is performed for double-layer adsorption, one obtains that

$$\Delta F_1^P = \frac{RT}{\Phi_1} \ln \frac{f_1^* x'}{f_{1,1}^* x_1'} + \frac{RT}{\Phi_1} \ln \frac{f_1 x}{f_{1,2}^* x_2'} \tag{21}$$

and

$$\Delta F_2^P = \frac{RT}{\Phi_2} \ln \frac{f_2^* (1-x')}{f_{2,1}^* (1-x_1')} + \frac{RT}{\Phi_2} \ln \frac{f_2 (1-x)}{f_{2,2}^* (1-x_2')}, \tag{22}$$

where $f_{1,1}^*$ and $f_{1,2}^*$ are the rational activity coefficients measured at concentrations x_1' and x_2', respectively.

Thus the free-energy change associated with the expansion of the adsorbed phase is composed of two terms. As a result of e.m. adsorption, concentration x' is replaced by x_1' and to this is added the energy change due to the formation of a new (second) layer.

On the basis of the above thermodynamic relationships it is now possible to attempt the interpretation and description of e.m. adsorption in concrete systems.

2. Interpretation, description and generalization of e.m. adsorption from liquid mixtures in concrete systems

In addition to establishing the existence of e.m. adsorption, the most important objective in this context is to make an attempt at determining the character of the $x_1' - x_2'$ concentration distribution. It should be mentioned that while we have arrived at the hypothesis of e.m. adsorption as a result of observed facts, we can only make assumptions as far as the concentration

distribution in e.m. adsorption is concerned. However, in the subsequent section we intend to show that these assumptions are based on, and follow from, concrete physical properties of concrete adsorption systems.

First, we shall examine the data concerning the type IV *F*-linear isotherm for the benzene–ethanol–charcoal (720 m^2/g)system available from the paper by NAGY and SCHAY [2]. The "oscillating" free-energy function for this system is shown in Fig. 4 of Part I in this series. There is no better way to resolve

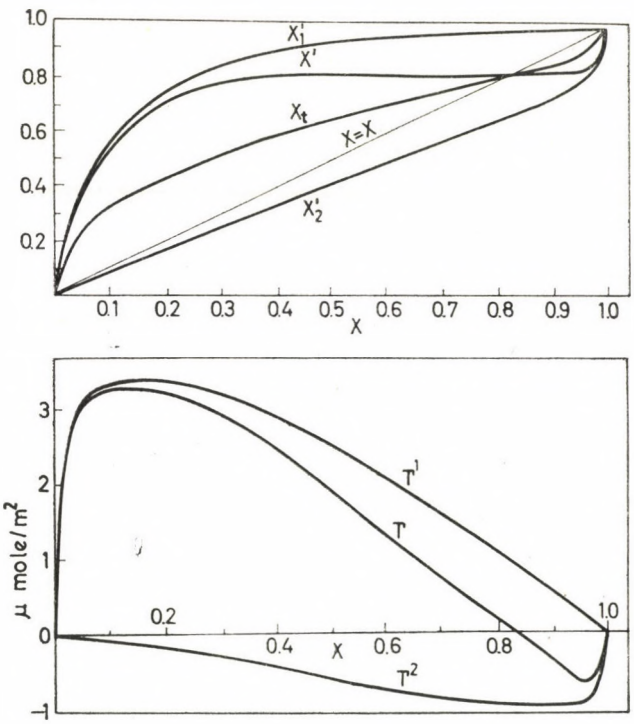

Fig. 1. Interpretation of the benzene–ethanol–charcoal (720 m^2/g) isotherm by means of double-layer adsorption

this thermodynamic contradiction than to accept the existence of e.m. adsorption which requires a surface phase of variable composition even in the linear section.

The most probable concentration distribution in e.m. adsorption is derived from the physical properties of the system. There is a significant difference in polarity between the two liquid components but the polarity of the solid surface may be regarded, though only approximately, as identical with that of one of the components. Therefore, it is assumed that on the slightly polar hydrophobic charcoal surface benzene is subjected to positive adsorption at any composition of the mixture since the latter is also unpolar and hydro-

phobic. Consequently, the more polar and hydrophilic ethanol is expelled into the second layer where it is accumulated.

On the basis of the mass transport mechanism discussed in Part I [1] this may be expressed by stating that under the influence of unpolar surface forces the liquid components of opposite properties are mixed in the surface phase in such a manner that there is positive adsorption of the apolar component on the apolar surface at any composition.

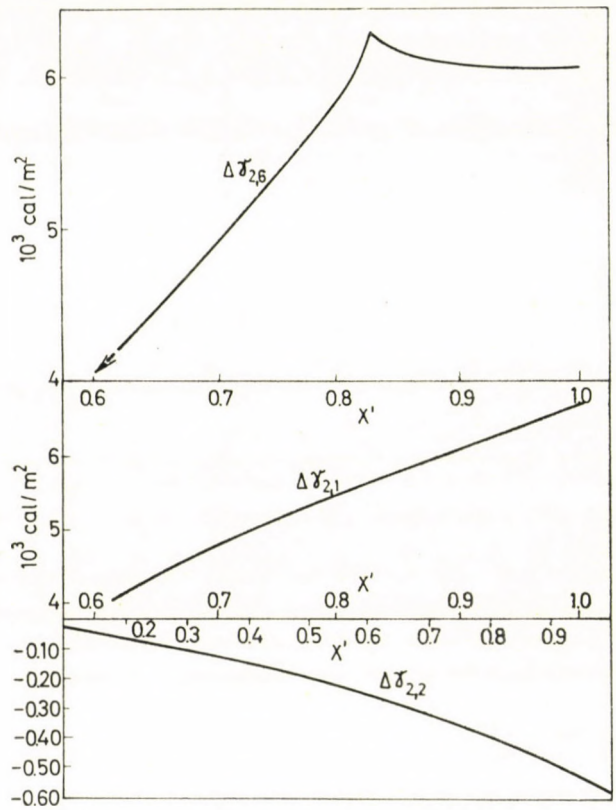

Fig. 2. Free-energy functions calculated from the benzene–ethanol–charcoal (720 m^2/g) isotherm for monolayer and double-layer adsorption

Mathematically, this concentration distribution means that the function $x_1' - x$ never intersects the $x = x$ diagonal (*cf.* Fig. 1), *i.e.* it is always true that $x_1' > x$. *One of the possible* $x_1 - x$ relationships based on this picture is shown in Fig. 1.

On the basis of this, it is possible to calculate the $x_2' - x$, $\Gamma^1 - x$ and $\Gamma^2 - x$ functions for e.m. adsorption using the equations given in Part I [1] (*cf.* Fig. 1). Furthermore, one can determine the free-energy functions of the individual layers (*cf.* Fig. 2) whose thermodynamic reality is beyond doubt.

The conclusions drawn from this concrete example may also be generalized. According to the data in Table I taken from the literature, type IV isotherms are observed *exclusively* under polarity conditions which are identical with those in the benzene–ethanol–charcoal system.

Table I

Type IV isotherms with positive–negative adsorption

Liquid components		Solid surface		Free surface	Literature
Slightly polar	Polar	Slightly polar	Polar		
Benzene (1)	Ethanol (2)	Charcoal			[2]
Benzene (1)	Acetic acid (2)	Charcoal			[4]
Benzene (1)	Propanol (2)	Charcoal			[4]
Benzene (2)	Ethanol (1)		Aluminium oxide		[4]
Carbon tetrachloride	Methanol (2)	Charcoal			[5]
Benzene (2)	Ethanol (1)		Silica gel		[6]
Benzene (1)	Methanol (2)	Charcoal			[2]
Benzene (2)	Methanol (1)			Free surface	[7]

As a rule, the positive adsorption of the component (denoted by (1) in Table I) whose polarity is approximately identical with that of the solid surface is much stronger (it is present in wider concentration and Γ intervals) than the negative adsorption of the same component. It is difficult to explain this change in the sign on the basis of the monolayer model, therefore, in our opinion, a more realistic assumption is that the adsorption of the component whose polarity is similar to that of the surface does not change its sign but this component is always negatively adsorbed in the second layer. The experimentally observed type IV isotherm is a result of the addition of these two kinds of adsorption. This physical picture may be justified and generalized also because all isotherms in Table I are F-linear, consequently, the thermodynamic unreality of monolayer adsorption demonstrated above is true in these cases.

Naturally, the polarity conditions prevailing in the cases shown in Table I are possible not only with type IV isotherms. The data shown in Table II indicate that on the basis of similar physical evidence, one may assume double-layer positive-negative adsorption with several type III and V isotherms.

The next concrete system whose properties also permit useful generalizations is the type III ethanol–water free surface isotherm [8]. This is similar to the benzene–ethanol–charcoal system due to its strict F-linearity. According to the calculations of NAGY and SCHAY [2], x' remains unchanged in the concentration interval of $x = 0.2 - 0.4$.

Table II

Various types of isotherms with positive–negative adsorption

Liquid components		Solid surface		Type and linearity of the isotherm	Literature
Apolar or slightly polar	Polar	Slightly polar	Polar		
Cyclohexane (2)	Pyridine		Aluminium oxide	III, *F*-linear	[7]
Benzene (1)	Methyl acetate (2)	Charcoal		V, not linear	[2]
Chloroform (1)	Acetone (2)	Charcoal		V, not linear	[2]
Benzene (2)	*n*-Butanol (1)		Silica gel	III, *F*-linear	[4]
Benzene (2)	*n*-Butanol (1)		Aluminium oxide	III, *F*-linear	[6]

This is surprising at first sight since the surface association of both components can be regarded as a fact due to the anomaly of the Eötvös constant. Thus monolayer adsorption cannot be explained now either thermodynamically or by other physical reasons. The constancy of the surface phase composition, while the bulk concentration is doubled, is inexplicable. On the other hand, the shape of the $\Delta\gamma_{2,G}$ *vs.* x' free-energy function shown in Fig. 4, according to which the surface free-energy is multi-valued at constant surface phase composition is impossible to interpret. The resolution of the contradictions is again possible by means of the e.m. adsorption. The $x_1' - x_2'$ concentration distribution is probably different from that for the previously discussed system. Here, both components are of identical structure (polar and hydrophilic) but no solid surface capable of modifying the interaction of the components is present. Therefore, it is completely unlikely that adsorption of opposite signs would occur with components of similar polarity and structure. Thus the most probable x_1' value for the first layer is attained under conditions when $x' > x_1' > x_l > x$. At the same time the real free-energy function (which is single valued in each point) does not permit a constant interval in the $x_1' - x$ function. *One of the possible* $x_1' - x$ relationships under these conditions is shown in Fig. 3. The rest of the data have been calculated using the equations given in Part I and are shown in Figs 3 and 4.

It can be seen from the above that the $x_1' - x$ distribution ensures a continuous transition of the concentration towards the bulk liquid since the $x_1' > x_2' > x$ relationship holds throughout the whole series of mixtures. In the light of the mass transport mechanism, this phenomenon can be described by stating that a continuous transition between the surface and the bulk phases is established as a result of mass exchange due to the structures of the two components which enable them to undergo association and H-bonding.

It should be emphasized that while the assumption of e.m. adsorption is a consequence of factual evidence, only assumptions can be made about the

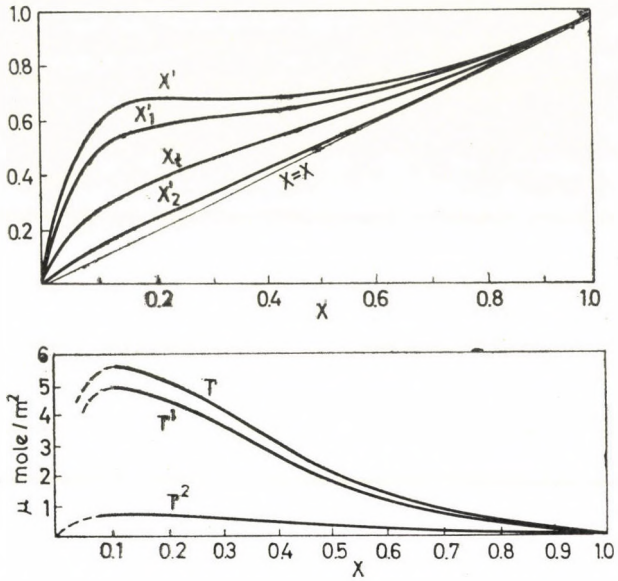

Fig. 3. Interpretation of the ethanol–water free-surface isotherm by means of double-layer adsorption

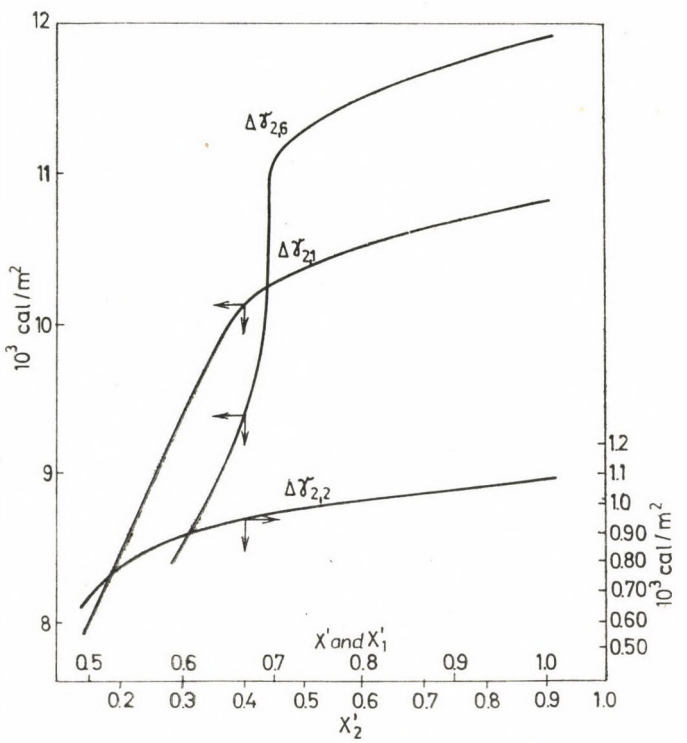

Fig. 4. Free-energy functions calculated from the ethanol–water free-surface isotherm for monolayer and double-layer adsorption

nature of the $x_1' - x_2'$ distribution. However, this assumption may be close to reality since thus, similarly to the type IV isotherms, those without a sign-change can be included into a unified picture. This unity is manifested by the lack of significant differences in polarity between liquid components involved in a large group of isotherms characterized by positive adsorption. This statement receives support from the data in Table III in which we show isotherms for

Table III

Isotherms with no change of sign and with positive–positive adsorption

Liquid components		Solid surface	Free surface	Type and linearity of the isotherm	Literature
Polar	Polar	Slightly polar			
Acetic acid	Water	Charcoal		III, *F*-linear	[4]
Pyridine	Water	Charcoal		III, *F*-linear	[4]
Ethanol	Water	Charcoal		III, *F*-linear	[2]
Acetone	Water		Free surface	III, *F*-linear	[7]
Methanol	Water		Free surface	II, *F*-linear	[7]
Ethanol	Methanol		Free surface	I, not linear	[7]
Ethanol	Water		Free surface	III, *F*-linear	[8]

liquid pairs not differing strongly in polarity. The polarity of the solid surface differs from that of the liquids but at the same time the structure of the liquids facilitates association and H-bonding, resulting in, almost certainly, multilayer adsorption. Similarly to the ethanol-water free-surface system, a continuous transition from the surface to the bulk concentration is assumed (positive-positive adsorption).

In Table IV we have shown isotherms for liquid pairs of nearly identical unpolar character which, due to their structure, are unable to H-bonding and eliminate the possibility of a surface force field ensuring continuous transition, therefore, monolayer adsorption is certain in these cases.

The thermodynamic description of e.m. adsorption and its application to the above concrete systems permit to summarize why and how multilayer adsorption occurs which is precisely equivalent to monomolecular adsorption.

The surface forces operative inside the boundary phase may and must be distinguished with respect to their effect causing concentration changes. The solid-liquid contact of the *first* layer ensures the formation of a new surface which is by several orders of magnitude larger than the free surface. Therefore, the molecules in this layer may come only from the bulk phase. Thus it is indisputable that the adsorption of the first layer results in concentration changes in the bulk phase, as considered by GIBBS. On the other hand, there is no new surface formation between the solid surface fully covered by the first layer and the bulk phase, and there is only *liquid-liquid interaction*. This

Table I

Isotherms with no change of sign and with positive monolayer adsorption

Liquid components		Solid surface		Type and linearity of the isotherm	Literature
Apolar or slightly polar	Apolar	Slightly polar	Polar		
Toluene	*n*-Heptane		Aluminium oxide	II, *F*-linear	[7]
Toluene	*n*-Heptane		Silica gel	II, *F*-linear	[7]
Benzene	Cyclohexane	Soot		I—II, nearly *F*-linear	[4]
1,2-Dichloroethane	Benzene		Silica gel	I, not linear	[2]
1,2-Dichloroethane	Benzene		Aluminium oxide	I, not linear	[2]
Benzene	Cyclohexane		Silica gel	I—II, nearly *F*-linear	[7]
Benzene	*n*-Heptane		Aluminium oxide	II, *F*-linear	[7]
Benzene	*n*-Heptane		Silica gel	II, *F*-linear	[7]

may be modified by the presence of the solid surface relative to the molecular interactions in the bulk phase. However, the range of such interactions (a few molecular diameters) is not changed by these effects which are also without influence on the general rules of liquid adsorption, according to which this interaction occurs in such a manner that the mutual displacement of the components takes place at full coverage. Mutual displacement as a result of short-range interactions can lead only to a situation where the interaction between the solid surface covered with a monomolecular layer and the bulk phase does not cause any concentration changes in the latter. On the basis of these considerations we have subdivided the surface forces into two groups. The result of the so-called "first order" forces is the formation of a *monomolecular* solid-liquid boundary surface which plays an *exclusive role* in changing the concentrations in the bulk phase and in accumulating an excess substance in the surface phase. The so-called "second order" forces act between the solid surface covered with a monomolecular layer and several molecular layers of the bulk phase, and usually are due to H-bonding, association, polar-apolar character, etc. These forces do not result in concentration changes in the bulk phase. Obviously, the mass exchange leading to e.m. adsorption is due to "second order" surface forces, the necessary free-energy or excess free-energy being supplied as ΔF_1^P and ΔF_2^P of Eqs (21) and (22). In other words, mass exchange distributes the surface free-energy change for a single adsorbed layer among several layers (*cf.* Eqs (4), (5), (8), (19), and (20)). Naturally, if there are no "second order" surface forces necessary to bring about mass transport (*e.g.* the isotherms in Table IV), actual monomolecular adsorption takes place. This can be interpreted on a concrete example. The assumed positive-negative adsorption in the benzene–ethanol–charcoal system

is equivalent to a monomolecular adsorption because the monomolecular amounts Γ_1 and Γ_2 arriving from the bulk phase are mixed with one or perhaps more layers of the latter as a result of higher "affinity" of the hydrophobic surface towards the hydrophobic liquid component.

The above consideration can be summarized in a single phrase. The excess mass in the boundary phase is due to "first order" surface forces (monomolecular adsorption) while the "second order" forces, if any, distribute this excess among several layers. It is also possible to apply this concept to adsorption on free surfaces with the obvious modification that the surface area remains unchanged during adsorption. If it is accepted that the experimentally observable mass transfer between the bulk and surface phases is always monomolecular, it should also be accepted that, of necessity, multilayer liquid adsorption always occurs in the e.m. form as a result of the described mechanism of mass transport. These statements are not valid if the transport of any component is hindered by chemisorption (molecular sieves). In such cases, *if* multilayer adsorption does occur, it cannot be of the e.m. type, *i.e.* the multilayer isotherm must be different from the monolayer one. This is supported by experimental evidence since $\Gamma - x$ isotherms different from the monolayer type are only observed in systems where it is doubtless that chemisorption or molecular sieve effects are involved.

It follows from the above considerations that, apart from certain exceptions, the $\Gamma - x$ isotherms which have a linear section can only be F-linear. Therefore, in our opinion, *F-linearity is not a property characteristic only of monomolecular adsorption but a more general trait of adsorption from liquid mixtures.* This statement reflects the fact mentioned in Part *I* that F-linearity is a necessary but not a sufficient condition for monolayer adsorption.

Finally, it is necessary to point out that although the above statements and the classification shown in Tables I — IV are consistent with the general physical picture of e.m. adsorption, it is possible that these conditions will have to be modified as the amount of available information increases. For example, it is not at all certain that the continuous transition in the concentrations between the boundary and bulk phases (positive-positive adsorption) is due to exactly two layers. It is also impossible to prove the number of layers involved in positive-negative adsorption. Modifications may become necessary also with respect to the subdivision given in Tables I—IV, because more detailed physical studies on a given system may provide evidence for "+ —" adsorption in cases where "+ +" adsorption has been assumed, or conversely.

The purpose of the above comments was to point out that the present state of our knowledge permits only theoretical conclusions about the structure of the surface phase formed as a result of adsorption from liquid mixtures and further studies are required for the precise determination of the $x_1' \ldots x_n'$ distribution and the number of layers n.

REFERENCES

1. Tóth, J.: Acta Chim. Acad. Sci. Hung. **63**, 67 (1970)
2. Nagy, L. Gy., Schay, G.: Magy. Kém. Folyóirat **70**, 33 (1964)
3. Hildebrand, J. H., Scott, N. L.: Solubility of Nonelectrolytes, p. 406—415. Reinhold, 1955
4. Nagy, L. Gy., Schay, G.: Magy. Kém. Folyóirat **66**, 31 (1960)
5. Innes, W. B., Rowleg, H. H.: J. Phys. Chem. **1947**, 1172
6. Kipling, J. J., Peakall, D. B.: J. Chem. Soc. **1954**, 4830
7. Nagy, L. Gy.: Kémiai Közlemények **27**, 323 (1967)
8. Erdey-Grúz, T., Schay, G.: Theoretical Physical Chemistry, 2nd Edition, Vol. 2., p. 331. Tankönyvkiadó, 1964

József Tóth; Nagykanizsa, Vár-u 8. Hungary

Acta Chimica Academiae Scientiarum Hungaricae, Tomus 63 (2), pp. 193—204 (1970)

POLAROGRAPHIC INVESTIGATION OF CYTOSTATIC MANNITOL DERIVATIVES, II

FURTHER STUDIES ON THE ETHYLENEIMINO DERIVATIVES OF DEGRANOL

B. JÁMBOR

(Institute for Plant Physiology, L. Eötvös University, Budapest)

Received June 26, 1968

Polarographic studies have been carried out to establish whether 1,6-ethyleneiminomannitol (II) and its isopropylidene derivative (I), investigated in detail in a previous work, give polarographic waves of identical character. An answer in the affirmative seems reasonable on the basis of the following findings:

1. The wave height is directly proportional to the square root of the mercury level and to the concentration of the depolarisator, while it is independent of the concentration of the buffer.

2. The temperature coefficient of the wave height is about 3%/°C at 15 °C; above 35 °C it is about equal the theoretical value for diffusion waves, though its evaluation is difficult.

3. At 50 °C, in neutral medium, the wave height of I diminishes rapidly, that of II more slowly.

4. The addition of gelatin does not influence the wave height, but shifts the $\pi_{1/2}$ value in the direction of more negative values.

5. Both compounds examined react at the same rate with thiosulfate to yield a product which gives a polarographic wave. About 3 hours are required under the given experimental conditions for the reaction to proceed completely as contrary to ethyleneimonium compounds, which react instantaneously.

6. At room temperature, the wave heights of both compounds diminish rapidly in slightly acid medium, and by about three times slower in slightly alkaline medium.

7. The wave heights of both compounds decrease or disappear in slightly alkaline medium as the pH of the solution polarographed is increased. The inflexion point of the curve plotted for this relationship is found at about pH 8.1 for both I and II.

Introduction

In our previous communication [1], we reported on the polarographic behaviour of two ethyleneimino derivatives of Degranol: 1,6-bis-ethyleneimino-1,6-dideoxy-3,4-monoacetate-D-mannitol(I) and 1,6-bis-ethyleneimino-1,6-dideoxy-D-mannitol diperchlorate (II).

At that time only substance I was investigated in detail, and a diffusion wave, corresponding to the uptake of 4 electrons, was found. Compound II gave a similar wave, with a half-wave potential more negative by about 100 mV. (This compound is an actual analogue of Degranol, since contrary to I, it does not contain acetone.) However, a critical investigation of the character of this wave could not be performed owing to lack of a sufficient amount of the substance. Thus, it was only assumed on the analogy with I, that both waves had the same character.

Since then, larger quantities of both compounds have been prepared, and in order to prove our assumption, a critical examination of the character of the wave was undertaken also for compound **II**. In some of these investigations, compound **I** was also included for comparison. Our present work reports the results of these investigations.

Experimental part and discussion of the results

1. *Materials and methods.* In this work, polarograms were recorded with a recording polarograph Radelkis Model OH 102. A jacketted vessel was used as the electrode vessel, and a normal calomel electrode served as the anode.

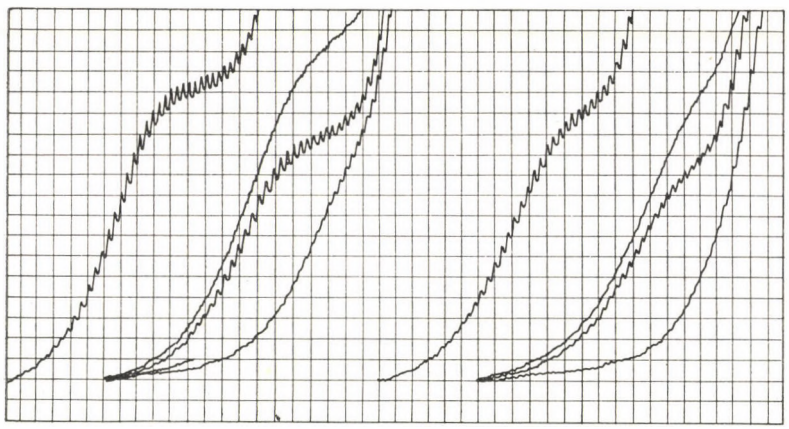

Fig. 1. Informative experiments with **I** and **II** (from left to right): 1—4: 10^{-4} *M* **I**; 1. 30 cm Hg, 30 °C; 2. 60 cm Hg, 20 °C; 3. 30 cm Hg, 20 °C; 4. 30 cm Hg, 20 °C + 0.05% of gelatin. 5—8: The polarograms of **II** under the same conditions as 1—4. All polarograms were recorded in a 0.025 *M* phosphate buffer solution of pH 6, at a galvanometer sensitivity of $16 \cdot 10^{-9}$ A, recorded from −0.8 V on. $\Delta E = 0.05$ V

With this polarograph, the reaction with thiosulfate was recorded as a function of time at constant potential. In this case, one unit on the abscissa corresponded to a period of 3 minutes. In recording the $i = f(E)$ curves, one unit on the abscissa corresponded to 0.05 V. In general, the polarograms were recorded at 20 °C. Any deviation from these parameters will be indicated when describing the various experiments.

2. *Informative comparison.* Fig. 1 shows the polarograms of compounds **I** and **II** under various experimental conditions. A comparison of the wave heights of the polarograms recorded at 20 and 30 °C shows that the temperature coefficient of the wave height is 2%/°C for both **I** and **II**, *i.e.* higher than 1.3 to 1.5%, the value characteristic of diffusion waves. This fact indicates that the waves of both compounds investigated have a small kinetic character.

Concerning the effect of the height of the Hg level, it was found that a Hg level of double height gave rise to a 1.43-fold wave height with substance **II**. A similar value (1.32-fold) was obtained for **I**, in accordance with the value reported in our previous communication [1]. Within the limit of experimental error, this value corresponds to $\sqrt{2}$, showing that the waves of both substances have predominantly diffusion character.

The presence of 0.05% gelatin has a remarkable effect on the polarograms of both substances: the waves disappear completely. Though several cases are known where the height and half-wave potential of diffusion waves are affected by the presence of colloids, complete disappearance of the waves is unusual. This phenomenon occurs usually with catalytic waves and maxima of first order.

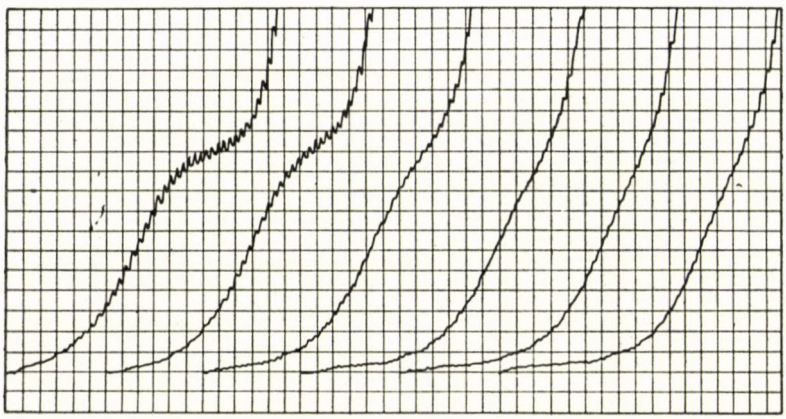

Fig. 2. Effect of gelatin on the polarogram of **I**. 10^{-4} *M* **I**, 30 cm Hg, 20 °C, in the presence of 0, 0.01, 0.02, 0.03, 0.04 and 0.05% of gelatin, respectively. For the other conditions, see Fig. 1

3. *The effect of gelatin.* To elucidate this effect, the change of the polarogram of **I** was examined in the presence of increasing amounts of gelatin added gradually. As shown in Fig. 2, as the quantity of gelatin increased, the potential of the wave of **I** shifted towards negative values, while the height of the wave remained constant. Thus, the disappearance of the wave does not arise from a suppression of the electroactive process, but is due to the merging of the wave in the final section of the polarogram. In case of maxima and catalytic waves, the height of the wave or of the maximum diminishes upon the action of colloids, that is to say, the electrode process is inhibited by the presence of the colloid. A similar behaviour is found for substance **II**, as shown in Fig. 3. The only difference as compared with **I** is that the merging of the wave in the final section of the polarogram occurs at lower gelatin concentrations. This is easy to understand, considering that the $\pi_{1/2}$ value of **II** is by about 100 mV more negative than that of **I**.

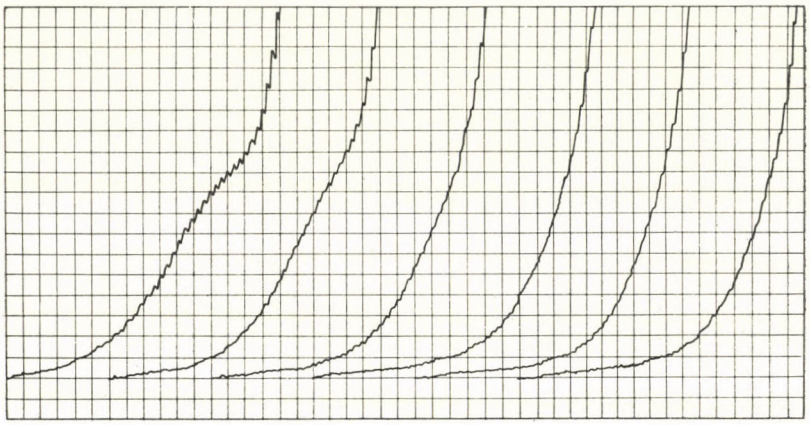

Fig. 3. Effect of gelatin on the polarogram of **II**. See Fig. 2

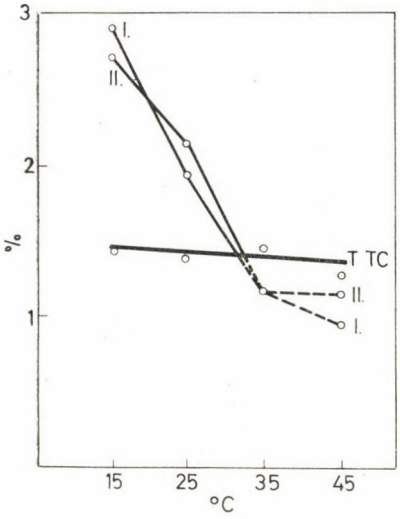

Fig. 4. The temperature coefficient of the wave of TTC, **I** and **II** at various temperatures; average values of 5 measurements each

4. *Dependence of the temperature coefficient on the temperature of the solution polarographed.* In the determination of the temperature coefficient, a wide scattering of the values was found. It became clear on further examination that the value of the temperature coefficient is highly dependent on the temperature limits used for its calculation. At the same time, this allows a comparison of compounds **I** and **II**. Fig. 4 shows the values of the temperature coefficients calculated for the substance **I** and **II** from the wave height of the polarograms recorded between +10 and +50 °C for each 10 °C. For comparison, or rather for checking, the values measured under identical conditions

for triphenyltetrazolium chloride, a compound giving a pure diffusion wave and investigated extensively by us, have also been plotted. The abscissa values mean that, for example the value of the temperature coefficient obtained on the basis of polarograms recorded at 10 and 20 °C has been plotted at 15 °C, etc.

As it is seen in the figure, the diffusion coefficient is for both compounds about 3%/°C at 15 °C, and about 1.2%/°C at 35 °C, the change between these limits being approximately linear. When the temperature is increased to higher than 35 °C, the decrease in the temperature coefficient becomes less, to fall below the value of 1.3, characteristic of diffusion waves. It can be seen from the figure that the curves of the two substances investigated have similar character. The temperature coefficient of triphenyltetrazolium chloride, plotted for comparison, has the theoretical value within the temperature range investigated.

An interpretation of the strong dependence of the temperature coefficient on temperature is rendered difficult by the fact that, to our knowledge, no similar phenomenon has been reported in the literature. If an interpretation of the phenomenon is attempted, it must begin with the presumption that the temperature coefficient is high at low temperatures, which in turn indicates that the kinetic character of the polarographic wave of the substances investigated increases. The kinetic character ceases completely near 35 °C. Therefore, it is to be assumed that a part of the compound is in a polarographically inactive state at lower temperatures, and the kinetic character of the wave is caused by its activation in the double layer surrounding the mercury drop. It seems reasonable to assume that at higher temperatures the activation energy of the formation of the polarographically active form ceases to act as a limiting factor.

If protonation is considered a precondition of polarographic activity, it can be assumed that a lower pH value and higher buffer capacity will diminish the kinetic character of the wave. The effect of the greatest possible variation of the two parameters has also been investigated (pH 5.5 and 7.5, and buffer concentrations of 10^{-2} to 5.10^{-1} M, respectively), however, contrary to expectation, they had no measurable effect on the value of the temperature coefficient. This shows that the effect of temperature has a more complicated mechanism than assumed, and is exerted indirectly.

Another unusual finding is the phenomenon that, at higher temperatures, the temperature coefficient diminishes to a value lower than that characteristic for diffusion waves. This is all the more difficult to understand, as from most of the other view-points examined the wave has a diffusion character, and the laws of diffusion, or more precisely, the role of diffusion as the rate determining factor should also prevail at higher temperatures. In this respect, a likely explanation is that both substances are unstable in the higher temperature

range used. Consequently, the height of the wave obtained at the higher temperature used for the determination of the diffusion constant may assume lower values than expected; this circumstance will be reflected in a decrease of the diffusion constant calculated on the basis of this value. Our investigations on the decomposition of the substances will be discussed in the next section. Here, we wish to mention only that every precaution was taken to diminish possible errors due to decomposition. The most important of these measures was that not the same solution was examined at increasing temperatures, but the polarographic vessel was thermostated to the required temperature, and at each temperature a fresh solution was used. Thus, the solutions on which the polarograms were recorded, were subjected only for 15 minutes to temperatures of 30, 40 and 50 °C, respectively.

Since, according to what has been said above, the value of the temperature coefficient cannot diminish below the theoretical value, obviously, the values on the curve belonging to 35 and 45 °C are lower than the actual values. This is particularly true in the case of compound **I**, which, as will be seen in the following section, is considerably less stable than **II**, so that the source of error discussed affects the values to a higher degree.

5. *Investigation of stability.* In the course of our investigations, many problems arose on account of the low stability of **I**. This makes both its preparation and its storage in solution difficult. In solution, it could not be kept even on ice for longer than 1 or 2 days, without exhibiting changes noticable by polarography. In the investigation described in the preceding section, the tendency of the substance to decompose presented difficulties. Therefore, this problem had to be examined, and moreover, it was of interest to find out, whether the wave of compound **II**, more negative by about 100 mV, is accompanied, as it is to be expected, by a higher stability.

Fig. 5 shows the percentage changes in the wave heights of compounds **I** and **II** at 50 °C, allowed to stand in solution at a pH adjusted to 6. A marked difference is to be noted in the stability of the two compounds examined, to the advantage of compound **II**. While standing for 1 hour resulted in only 20% decomposition of the latter compound, more than 80% of compound **I** decomposed under the same conditions. This decomposition does not involve only the splitting off of acetone from the molecule of **I**, because this would only cause a shift of the wave, without a decrease of its height.

The decomposition in this case probably consists in the hydrolytic splitting of the ethyleneimino ring, which was studied extensively by ANHALT and BERG [2] in the case of ethyleneiminobenzoquinones. For a comparison of the compounds investigated and intended to be investigated by us, useful information may be obtained by studying the dependence of the decomposition on the pH of the solution. ANHALT and BERG found in the case of the ethyleneiminobenzoquinones investigated by them that the rate of decomposition

was strongly enhanced in acid media, and to a lesser degree in alkaline media. However, they did not publish the whole series of data or a curve representing the whole pH range investigated by them, so that the pH value which causes minimum decomposition cannot be established.

In the case of the compounds investigated by us, the curves showing the effect of the pH did not present the characteristics of an optimum. It was found that on changing the pH value of the solution from 3 to 10, the rate of decomposition, though not linearly, decreased throughout the whole pH range. Table I shows the degree of decomposition of compounds **I** and **II** standing in solutions of weakly acid and weakly alkaline pH.

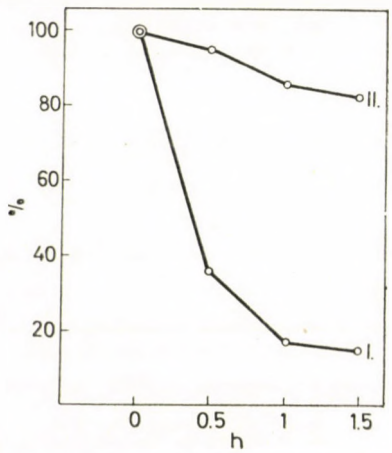

Fig. 5. The wave heights of 10^{-4} *M* solutions of **I** and **II** on standing at 50 °C in a phosphate buffer (0.025 *M*) of pH 6, expressed in percentage of the initial height. Recorded at 25 °C

Table I

Decomposition of compounds I and II in 10^{-3} M solutions at pH 5 and 9, respectively, adjusted with 0.025 M phosphate buffer, on standing for 2 days at 20 °C

	I	**II**
pH 5	42%	31%
pH 9	15%	18%

It is seen that the degree of decomposition in acid solution is higher for both compounds than in alkaline medium. It is interesting that the ratios differ from those shown in Fig. 5; however, also experimental conditions are different. On standing for 1 hour at 50 °C and pH = 6, the degree of decomposition of **I** is five times as high as the decomposition of **II**, while under the conditions listed in Table I, it is only about 1.3 times higher than that of **II**.

Under the experimental conditions described in the previous section, I exposed for 15 minutes to a temperature of 50 °C, the decomposition of the substance may be responsible for about a 30% decrease of the wave height. Thus, the wave height measured at 50 °C (to determine the value of %/°C at 45 °C) was sometimes about equal to that measured at 40 °C, which means a temperature coefficient of 0%/°C. The values corresponding to the higher temperatures in Fig. 4 could only be determined after great practice in each step of the measuring technique to reduce the thermal effect, and by repeating the measurement many times. As it has been mentioned, even so the results are rather dubious. As shown by repeated checking, at 30 °C or less the de-

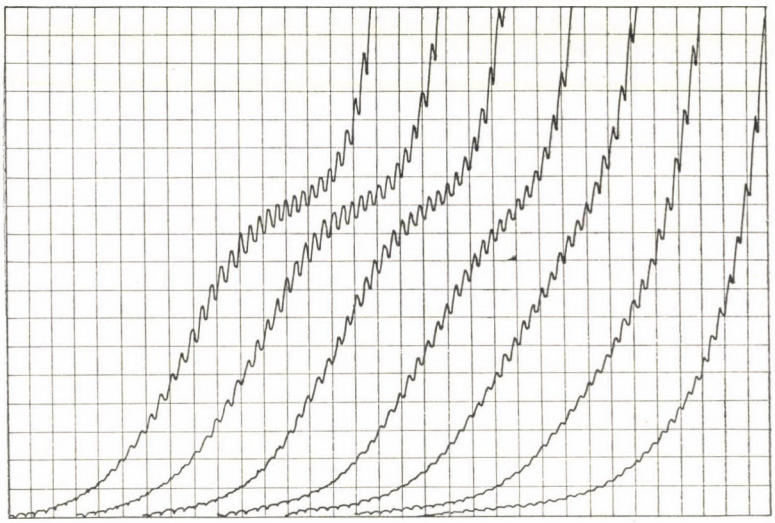

Fig. 6. Effect of the buffer concentration of the solution on the wave of **II**. $5 \cdot 10^{-5}$ *M* **II**; $S = 8 \cdot 10^{-9}$ A, pH = 6; 30 cm Hg; 25 °C; from −0.8 V on, in 0.0125, 0.025, 0.05, 0.1, 0.2, 0.4 and 0.8 *M* phosphate buffer, respectively

composition of the substance under the conditions of the determination of the thermal coefficient is negligible, so that the first section of the curves showing the dependence of the temperature coefficient on temperature can be considered reliable. For higher temperatures only the fact can be established that the curve representing the dependence on temperature has a break, and the second section is not a continuation of the first.

6. *Effect of the buffer concentration on* **II**. The polarograms shown in Fig. 6, recorded at buffer concentrations varied within very wide limits, indicate that the wave of **II** is shifted by about 100 mV towards negative values at higher buffer concentrations, and it merges into the final, ascending section of the polarogram. Before this occurs and as long as the wave can be clearly

observed (buffer concentrations between 0.0125 and 0.1 *M*), the wave height seems to be independent of the buffer concentration, in accordance with the results reported in our previous communication for compound **I** [1]. Since the wave of **I** is by 100 mV more positive, it did not merge into the final section of the polarogram at the buffer concentrations used in our previous work. The independence of the wave height of buffer capacity is a further evidence to show that the character of the wave of **II**, similarly to that of **I**, is not catalytic.

7. *Effect of the concentration of* **II**. Fig. 7 shows that the wave height of **II** is approximately proportional to the concentration of the depolarizator

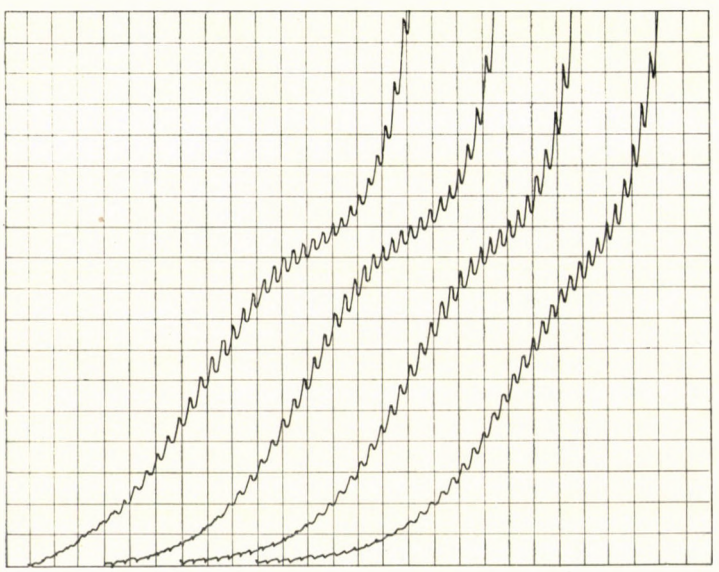

Fig. 7. Dependence of the wave height on the concentration of **II**. 25 °C; 30 cm Hg, from −0.8 V on; $\Delta E = 0.05$ V; 0.025 *M* phosphate buffer; pH = 6; concentration of **II** (from left to right): 2.5, 5, 10, and 18 · 10^{-5} *M*; *S* = 4, 8, 16 and 30 · 10^{-9} A

within the concentration range investigated. This is reflected in the figure by the almost identical height of the waves, since the sensitivity of the galvanometer recording the polarograms was selected so as to be inversely proportional to the concentration. Thus the product of sensitivity and concentration is the same for each polarogram shown in Fig. 7. Since the wave height of **II** can be determined only with considerable error, the series was repeated in 8 cases at different times. The relationship between the concentration and wave height, calculated from these average values, is shown in Fig. 8.

It can be seen that though the wave height is not strictly proportional to the concentration, the deviation is small and remains within the limits of experimental error; it hardly indicates a catalytic character of the wave.

8. *The reaction with thiosulfate.* MANTSAVINOS and CHRISTIAN [3] reported the quantitative determination of ethyleneimonium compounds, formed from true nitrogen mustards on standing, by means of titration with thiosulfate. The titration can be followed by polarography. Similar findings are reported by J. KÁDÁR-PAUNCZ [4] for ethyleneimino compounds analogous to **I** and **II**; however, in this case the reaction is not instantaneous, but, depending on the compound, it takes several hours, or even a day. She also found, that a compound is formed during the reaction which can be reduced, and thus gives a polarographic wave.

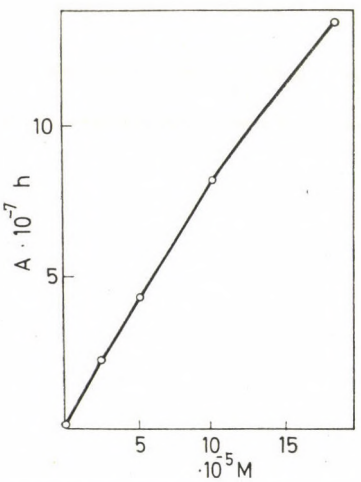

Fig. 8. Relationship between the wave height and the concentration of **II**; average of 8 repeated series. For conditions, see Fig. 7

For comparison, both **I** and **II** were reacted in the polarographic vessel with excess thiosulfate, and kinetical curves have been recorded polarographically.

Fig. 9 was plotted on the basis of the two reaction/time curves recorded under the said conditions, and gives the percentage values.

It can be seen that the reactions of **I** and **II** proceed according to an almost exactly identical time curve, and about 3 hours are required to attain the final value. This strict agreement, in accordance with the former investigations, supports the similar character of **I** and **II**. In fact, the agreement appears to be almost too good, considering that **II** is by about 0.1 V more stable towards electrolytic reduction, and there is an even more marked difference in the decomposition rate at 50 °C between the two compounds. This result indicates that the activation energy has another value in the case of the reaction with thiosulfate, than in the two other conversions mentioned.

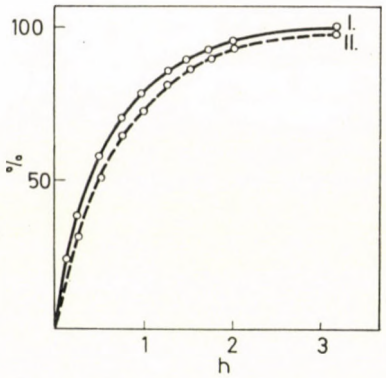

Fig. 9. The reaction of 10^{-3} *M* **I** and **II** with $3 \cdot 10^{-3}$ *M* $Na_2S_2O_3$, pH = 4; 25 °C; the results are expressed as percentages of the maximum height

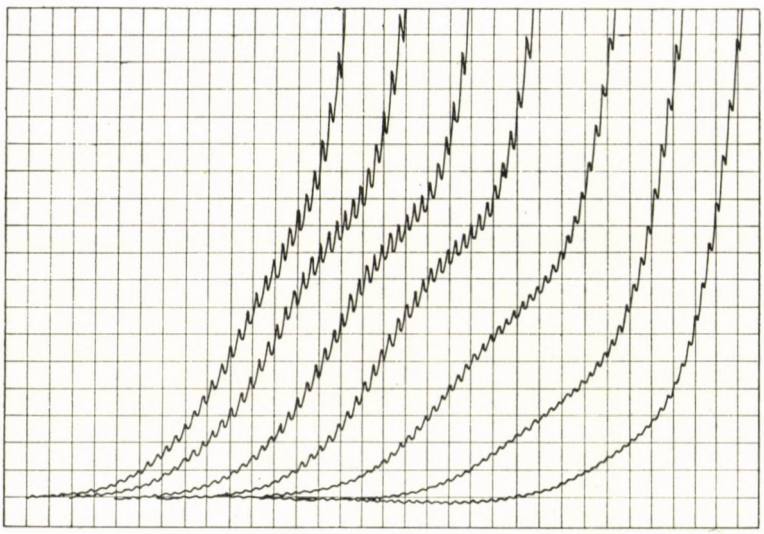

Fig. 10. The polarogram of 10^{-4} *M* **II** in 0.025 *M* phosphate buffer adjusted to pH 5, 6, 7, 7.5, 8, 8.5 and 9, respectively, recorded at 25 °C; 30 cm Hg; $S = 16 \cdot 10^{-9}$ A, from −0.8 V on; $\Delta E = 0.05$ V

The reactions of **I** and **II** and their various derivatives with thiosulfate have been examined in detail by polarography. The results will be reported in another paper.

9. *Effect of the pH on the wave of* **II**. Fig. 10 shows polarograms of **II**, recorded at various pH values. Slightly alkaline pH results in a decrease of the wave height, in the same way as it was found for **I** [1]. For comparison, the percentage changes in the wave heights of **I** and **II** are given (Fig. 11). It can be seen that the presence of the isopropylidene group in the molecule of **I**, and its absence in **II** does not affect, within the experimental error, the shape

of the curve, as contrary to its effect on the $\pi_{1/2}$ value, which is shifted by about 0.1 V [1]. If, according to what has been said above, protonation is a precondition of the formation of the wave, the inflexion points on the curves of both **I** and **II** can be considered as *pk'* values and are to be found on Fig. 11 at pH 8.1.

The investigations show unequivocally that **I** and **II** have identical polarographic behaviour. A difference is only found in stability, and in the

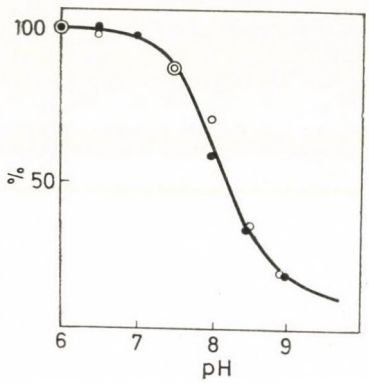

Fig. 11. The wave height of 10^{-4} *M* **I** (o—o) and **II** (•—•), recorded in 0.025 *M* phosphate buffer solution at different pH values, given as percentages of the maximum height

activation energies of various reactions. The slight deviation from linearity of the relationship wave height/concentration lies within the limit of experimental error; in fact, even if this deviation were significant, it would not substantially influence the character of the wave of **II**.

Further work is in progress to study the polarographic behaviour of Degranol with the object to establish whether it gives **II** on standing, and to clarify the effect of the experimental conditions in the course of the reaction.

*

The author's thanks are due to Drs. Irene P. Horváth and L. Institorisz for valuable discussions in the course of this work, and to Misses M. Dewath and É. Majláth for their help in the experiments.

REFERENCES

1. Jámbor, B., Horváth, I. P., Institorisz, L.: Acta Chim. Acad. Sci. Hung. **53,** 85 (1967); Magyar Kém. Foly. **73,** 332 (1967)
2. Anhalt, A., Berg, H.: J. Electroanal. Chem. **4,** 218 (1962)
3. Mantsavinos, R., Christian, J. E.: Anal. Chem. **30,** 1071 (1958)
4. Kádár-Pauncz, J.: Paper read at the Polarographic Conference, Budapest, March 22, 1965; Proc. 3rd Int. Congr. Pol., Southampton, 1964. p. 913.

Béla Jámbor; Budapest VIII., Múzeum krt 4/a

Acta Chimica Academiae Scientiarum Hungaricae, Tomus 63 (2), pp. 205—213 (1970)

POLAROGRAPHIC INVESTIGATION OF CYTOSTATIC MANNITOL DERIVATIVES, III

DEGRANOL

B. JÁMBOR

(Institute for Plant Physiology, L. Eötvös University, Budapest)

Received June 26, 1968

Every parameter investigated has shown complete identity, within the limit of experimental error, between the polarographic behaviour of the compound formed in alkaline medium from Degranol and the corresponding ethyleneimino compound, synthetized as crystalline substance.

The comparison and ascertainment of the identity were made by examining the effects of temperature, mercury level, gelatin, buffer and depolarisator concentration, and the reaction with thiosulfate on the polarographic wave. It has been found that the wave has predominantly diffusion character, mixed with a slight kinetic character and catalytic effect, however, this latter can only be observed in the section after the wave.

It is still an open question, whether also under physiological conditions a bis-ethyleneimino compound is formed from Degranol.

In two earlier communications [1], [2], the polarographic behaviour of two ethyleneimino derivatives (**I** and **II**) of Degranol, 1.6-bis-(2-chloroethyl-amino)-1.6-deoxy-D-mannitol dihydrochloride (**III**), an agent with antitumour action, has been reported. It has been found that the ethyleneimino rings, as a result of irreversible electron uptake, give polarographic waves of diffusion character, corresponding to the uptake of 2 electrons each. The influence of various experimental conditions on the wave has been studied with the object to make comparisons and to identify the compound formed from Degranol in slightly alkaline medium. It was to be presumed that Degranol is converted in the organism to a cyclic product and exerts its cytostatic action in this form.

The present work describes the polarographic behaviour of the compound formed from Degranol on standing. The object of the experiments was to clarify the problem of the assumed identity of this product and **II**.

Experimental part and discussion of the results

1. *Materials and method*

The compound (**III**) studied was the crystalline product of the Chemical Works Chinoin. The other materials and the method used were identical with those described in our previous publication [2].

As it will be seen, the characteristics of the wave formed during the conversion of **III** in slightly alkaline medium, are approximately the same as those of the wave of compound **II** (the cyclic derivative), discussed in our previous publication. In the course of our work, the evaluation of the wave of **III** posed many difficulties, owing to the following two reasons:

(*a*) The $\pi_{1/2}$ value of the wave is about -1.2 V, and it has a rather flat shape, and consequently no horizontal limiting current, which would make possible the exact determination of the wave height. Indeed, it partly melts with the final ascending part of the polarogram.

(*b*) The upper part of the wave is still more masked by the polarographic catalytic effect of one or more by-products formed during the reaction. This brings about a shift by about 0.1 V of the final section of the polarogram toward positive values, as compared with the buffer solution. This effect was observed, but not studied in detail.

Owing to these difficulties, the wave heights given in this paper cannot be regarded as accurate as usual in polarography, therefore the results must be interpreted with caution.

2. *Development of the polarographic wave*

Fig. 1 shows the polarograms of samples taken from a solution of **III**, the pH of which has been adjusted to 8. At the beginning of the reaction, samples were taken in every second hour. The development of the polarographic wave can be clearly seen in the figure. Its height at the termination of the reaction is near to that of the corresponding ethyleneimino compound [2].

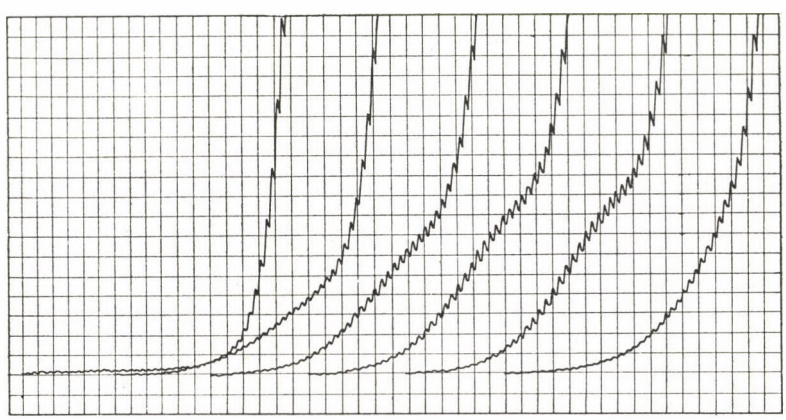

Fig. 1. Development of the wave of Degranol: $2 \cdot 10^{-4}$ *M* Degranol allowed to stand at 25 °C in 0.01 *M* phosphate buffer of pH 8, and polarographed after 0, 2, 4, 6 and 8 hours at a concentration of 10^{-4} *M* at pH 6 in 0.025 *M* phosphate buffer; $S = 16 \cdot 10^{-9}$ A; Hg level 30 cm; 25 °C; from -0.8 V on; $\Delta E = 50$ mV

In our further work, we studied the behaviour of this wave under various experimental conditions, to compare and possibly identify it with the behaviour of the waves of the corresponding ethyleneimino derivative (II). The mechanism of the reaction producing the wave, and the effect of experimental conditions on this mechanism will be discussed in further communications.

The starting material of our present investigations was in each case Degranol pretreated in the manner described, and converted by this pretreatment into the compound giving the wave.

3. *Informative experiments*

Fig. 2 shows the polarogram of the wave recorded under various experimental conditions. In these experiments the height of the mercury level, and the temperature of the solution polarographed have been varied, and the effect of the presence of gelatin has been investigated.

As it can be seen, the height of the wave increases with increasing temperature. Calculated from the polarograms recorded at 20 and 30 °C, the temperature coefficient is 2.25, similarly to that of the corresponding ethyleneimino compound [2].

Similarly, an identical behaviour was found with respect to the effect of the height of the mercury level. On the basis of the corresponding two

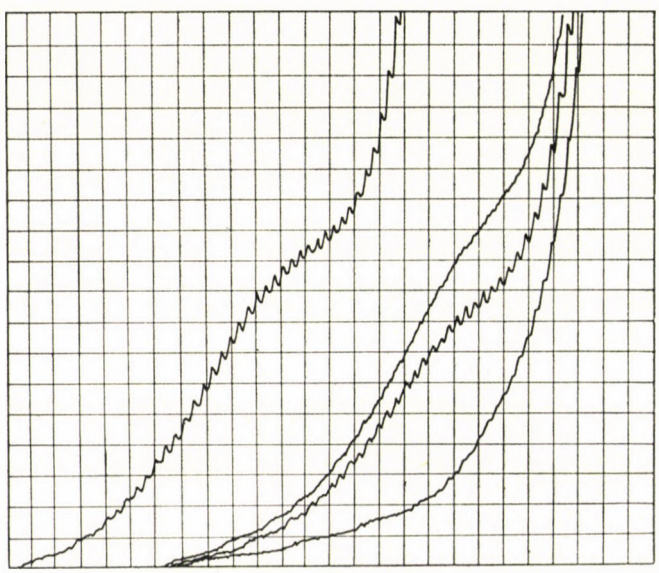

Fig. 2. Informative polarograms: Degranol allowed to stand at pH 8.5 and polarographed at a concentration of 10^{-4} *M* (from left to right): 1. 30 °C; 30 cm Hg level; 2. 20 °C; 60 cm Hg level; 3. 20 °C; 30 cm Hg level; 4. the same in the presence of 0.05% of gelatin. For the other data, see Fig. 1

curves of the figure, an about 1.4-fold wave height corresponds to a twofold mercury level height. This value is practically identical with $\sqrt{2}$, characteristic of diffusion waves.

The presence of gelatin shifts the wave in the same way in the negative direction, as it was the case with the corresponding cyclic compound (II).

4. *Effect of gelatin*

Fig. 3 shows the wave recorded at increasing gelatin concentrations. Even in the presence of 0.01% gelatin, the wave is shifted so far to the right

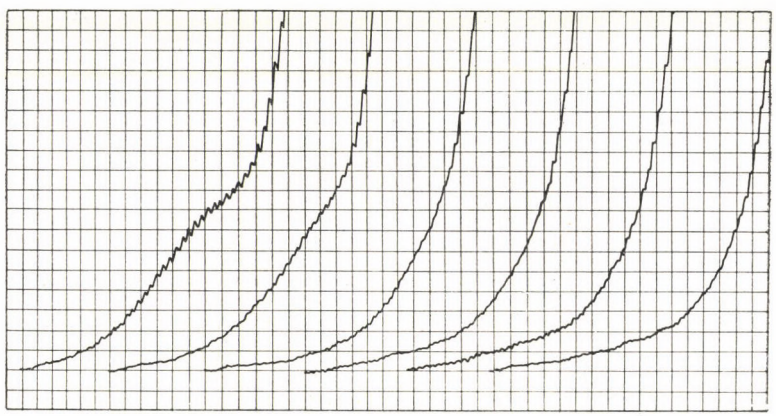

Fig. 3. The effect of gelatin. Polarograms of 10^{-4} *M* Degranol allowed to stand at pH 8.5; recorded on solutions containing (from left to right) 0, 0.01, 0.02, 0.03, 0.04 and 0.05% of gelatin

that it is almost completely merged with the end of the polarogram. When the quantity of gelatin is further increased, the wave disappears completely, and only the slope of the curve changes almost imperceptibly. The corresponding ethyleneimino compound (II) showed a completely similar behaviour [2].

5. *Effect of temperature on the temperature coefficient*

In our previous communication it has been reported that the temperature coefficient of the ethyleneimino compounds investigated decreases with increasing temperature, and at low temperatures it is indicative of the partly kinetic character of the wave. It can be seen from Fig. 4 that the wave given by the solution of III after reaction in alkaline medium shows an identical behaviour. For comparison, the values obtained for the synthetic cyclic compound (II) are also plotted in Fig. 4.

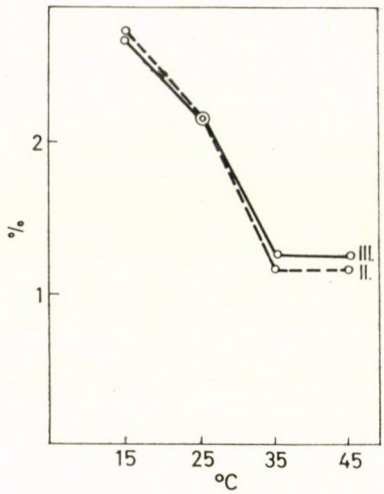

Fig. 4. Temperature coefficient of the wave. The temperature coefficient calculated from the wave-height ratios of 10^{-4} *M* Degranol after standing in alkaline medium, as a function of the temperature of the recording of the polarogram. The points plotted were calculated on the basis of waves obtained at temperatures by 5 °C lower and higher, respectively, than the temperature for which the point was plotted. o—o starting from Degranol; o---o **II** (synthetic)

6. *Decomposition of the compound producing the wave*

Fig. 5 shows the change as a function of time of the wave heights on standing at 50 °C in a solution of pH 6, for the compound formed from Degranol and for **II**. The coincidence of the two curves is obvious.

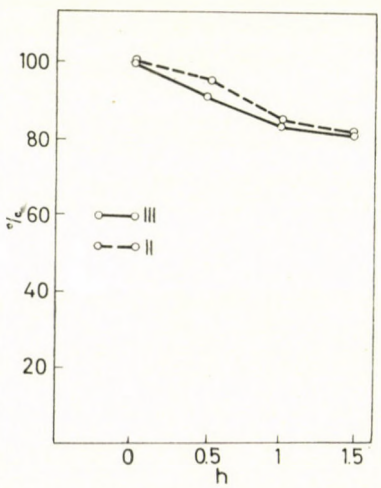

Fig. 5. Diminution of the wave height. The wave of 10^{-4} *M* Degranol after standing at pH 8.5; polarographed in a solution adjusted to pH 6, after periods of 30 min. standing at 50 °C. (Marking is the same as in Fig. 4.)

Complete similarity was also found when the above solution was allowed to stand in slightly acid or alkaline medium in 0.025 *M* phosphate buffer, at a concentration of 10^{-3} *M* and at 20 °C; a decomposition of 33% took place at pH 5, and of 15% at pH 9 after two days of standing. This is practically in accordance with the values found for **II** [2].

Concerning the nature of the reaction causing the diminution of the wave height, we refer to the work of ANHALT and BERG [3]. These authors studied the change of a bis-ethyleneimino-benzoquinone derivative in solution, and established that the ethyleneimino ring suffered hydrolytic cleavage:

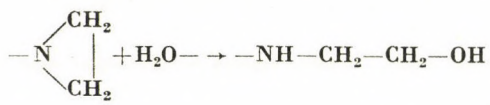

This reaction is favoured in acid medium. We have every reason to assume that an analogous reaction takes place in our case.

This reaction, as it was seen, also proceeds in a slightly alkaline medium, thus, evidently also in the case, when Degranol is allowed to stand to give a wave. However, in this case the formation of the ethyleneimino derivative does not proceed to 100%. This explains that starting with Degranol, generally a lower wave is obatined than with **II** of the same concentration.

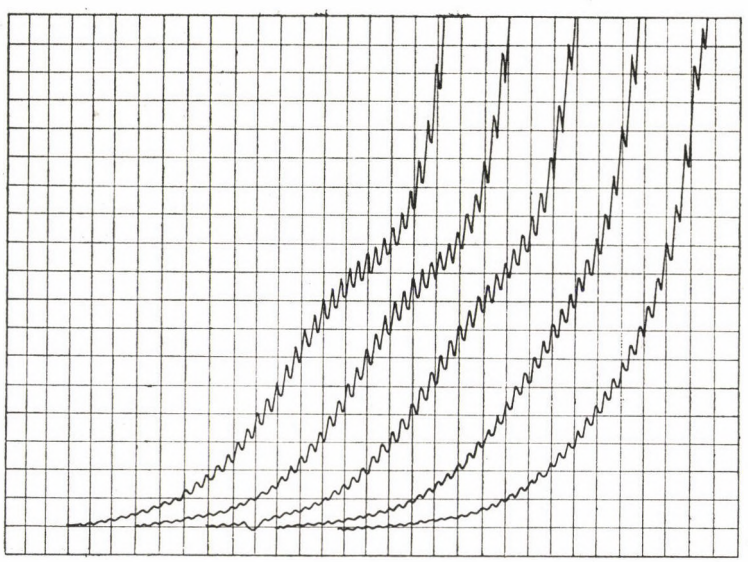

Fig. 6. Effect of the buffer concentration. $5 \cdot 10^{-4}$ *M* Degranol in 0.025 *M* phosphate buffer (pH 9), after standing at 25 °C, polarographed at a concentration of 10^{-4} *M* in solutions containing (from left to right) 0.0125, 0.025, 0.05, 0.1 and 0.2 *M* phosphate buffer, respectively. For the other data see Fig. 1

7. *Effect of the buffer concentration*

Fig. 6 shows the polarograms of the waves recorded in solutions of various buffer concentrations. It can be seen that, similarly to the case of **II**, the height of the wave is practically independent of the buffer capacity at low concentrations; at higher concentrations the wave is shifted and cannot be evaluated.

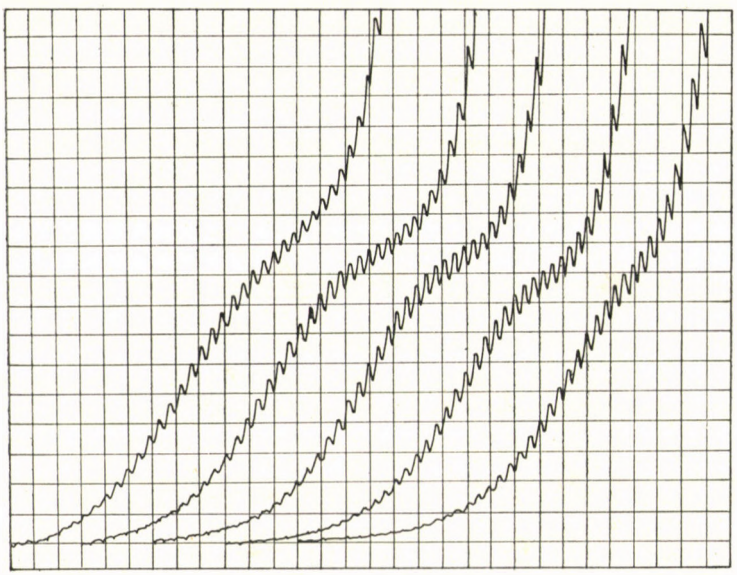

Fig. 7. Effect of the concentration of the depolarisator. Degranol, after standing at pH 8, polarographed in 2.5, 5, 10 and 18 · 10^{-5} *M* concentration in 0.025 *M* phosphate buffer adjusted to pH 6. $S = 4$, 8, 16 and 30 · 10^{-9} A

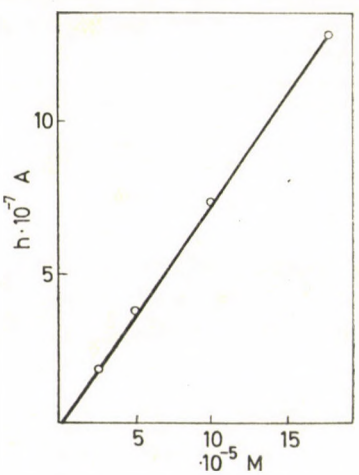

Fig. 8. Graphic representation of the values of Fig. 7, calculated for full galvanometer sensitivity

8. *Effect of the concentration of the depolarisator*

Fig. 7 shows polarograms recorded at concentrations varied within the limits of the measuring range (at sensitivities changed proportionally), while Fig. 8 is a diagram of the relationship between the wave height and concentration. Both figures show that the wave height is proportional to the concentration, again in accord with our results for **II.**

9. *Reaction with thiosulfate*

Similarly, as described in our previous communication, the present substance under examination was reacted with an excess of $Na_2S_2O_3$ and the

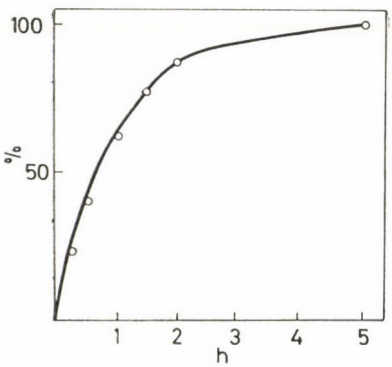

Fig. 9. Reaction with thiosulfate. 10^{-3} *M* Degranol in 0.025 *M* phosphate buffer adjusted to pH 8, 25 °C, allowed to stand for 16 hours; admixed with $3 \cdot 10^{-3}$ *M* $Na_2S_2O_3$, and the time curve of the reaction recorded at pH 4 with a polarograph at a constant potential of —1 V. The values shown in the diagram are expressed as percentages of the highest value of the curve

$h = f(t)$ curve was plotted on the basis of the fact that during the course of the reaction a new compound, giving rise to a polarographic wave, had formed. The time-curve of the reaction is shown in Fig. 9. On this curve, the half-time of the reaction under the given conditions is 36 minutes, which is in good agreement with the 30 minutes found for the cyclic substance in our previous communication.

The examination of the reaction with thiosulfate and the products formed, will be reported in detail in another communication.

10. *Effect of the pH on the polarogram*

On the basis of polarograms not presented here, the dependence of the wave heights has been plotted as a function of the pH of the medium (Fig. 10). Similarly to the ethyleneimino compound [2], it was found that the wave height

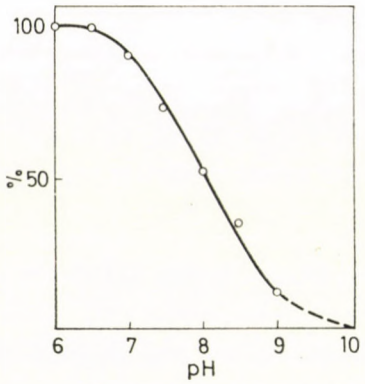

Fig. 10. Effect of the pH on the wave. The wave height of the polarogram of 10^{-4} *M* Degranol after standing in slightly alkaline medium; recorded in 0.025 *M* phosphate buffer adjusted to different pH values, as a function of the pH, expressed as percentages of the highest value

diminishes at alkaline pH values; in fact, the wave may completely disappear. From Fig. 10, the value of *pk'* is 8.2, which is in satisfactory agreement with the value of 8.1, found previously [2] for the ethyleneimino compound.

*

The author's thanks are due to Misses M. DEWATH and É. MAJLÁTH for technical assistance; to the Chemical Works Chinoin for a sample of Degranol and to Dr. P. Irene HORVÁTH for her valuable advice.

REFERENCES

1. JÁMBOR, B., HORVÁTH, I. P., INSTITORISZ, L.: Acta Chim. Acad. Sci. Hung. **53,** 85 (1961); Magyar Kém. Foly. **73,** 332 (1967)
2. JÁMBOR, B.: Acta Chim. Acad. Sci. Hung. (In the press).
3. ANHALT, A., BERG, H.: J. Electronal. Chem. **4,** 218 (1962)

Béla JÁMBOR; Budapest VIII., Múzeum krt. 4/a

Acta Chimica Academiae Scientiarum Hungaricae, Tomus 63 (2), pp. 215—228 (1970)

ANWENDUNG VON AMIDCHLORIDEN IN RINGSCHLUSSREAKTIONEN, I

SYNTHESE VON 4(3H)-CHINAZOLINONDERIVATEN UND ALKYLEN-BIS-3,3'-4(3H)-CHINAZOLINONEN

Z. Csűrös, R. Soós, J. Pálinkás und I. Bitter

(Lehrstuhl für Organisch-Chemische Technologie, Technische Universität, Budapest)

Eingegangen am 13. Februar 1969

Amidchloride aus disubstituierten Säureamiden und Phosgen wurden mit Methylanthranilat in Reaktion gebracht. Aus den entstandenen trisubstituierten Amidin-hydrochloriden wurden 4(3H)-Chinazolinonderivate und Alkylen-bis-3,3'-4-(3H)-chinazolinonderivate hergestellt. Der Ringschluß wurde mit aliphatischen und aromatischen primären Aminen, Hydrazin, Phenylhydrazin, Aminosäuren und Alkylendiaminen bewerkstelligt. Der Mechanismus der Ringschlußreaktion wurde untersucht und ein möglicher Reaktionsweg angegeben.

Die therapeutische Wirkung von Verbindungen, die Pyrimidinringe enthalten, ist längst bekannt. Ein stärkeres Interesse für kondensierte Pyrimidinderivate, besonders für solche mit Chinazolinskelett, besteht jedoch nur neuerdings, seit sich herausgestellt hat, daß sie verschiedenartige chemotherapeutische Wirkungen ausüben. Diesem Interesse entspricht unser Ziel, die Synthese solcher und ähnlicher Verbindungen mit einem neuen Verfahren, unter Anwendung von mit Phosgen hergestellten Amidchloriden durchzuführen.

Amidchloride sind äußerst reaktionsfähige Verbindungen. Ihre Anwendung für präparative organisch-chemische Zwecke erfolgte jedoch nur im letzten Jahrzehnt.

Ein Amidchlorid wurde erstmalig durch Wallach [1] aus Diäthylformamid mit Phosphorpentachlorid hergestellt.

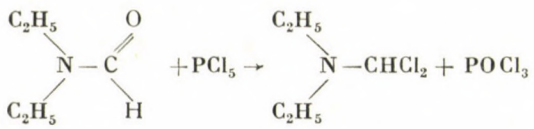

Außer Phosphorpentachlorid werden am häufigsten Thionylchlorid und Phosphoroxychlorid verwendet. Neuerdings wurde festgestellt, daß im ersten Reaktionsschritt ein Additionsprodukt entsteht, welches nur bei höheren Temperaturen in Amidchlorid übergeführt wird. Für praktische Zwecke kann dieses Addukt ebenfalls gut anstelle des reinen Amidchlorids angewendet werden, jedoch erschweren die Nebenprodukte die Verarbeitung.

Hallmann [2] stellte Amidchlorid mit Phosgen her. Dieses Verfahren ist sehr vorteilhaft, da die Reaktion nicht bei dem primären Additionsprodukt

stehen bleibt, sondern bereits bei niedrigen Temperaturen Amidchlorid gebildet wird:

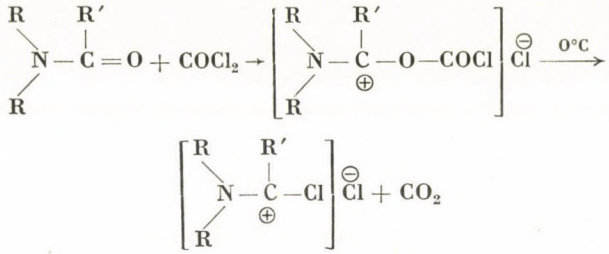

Der weitere Vorteil der Herstellung mit Phosgen besteht darin, daß ein reines Produkt erhalten wird. Aufgrund der hohen Reaktionsfähigkeit wird die Strukturformel des Amidchlorids in Ionenform geschrieben [3, 4].

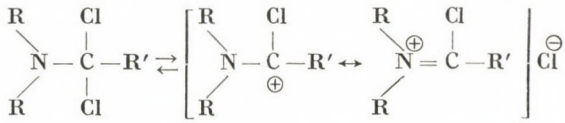

Diese Struktur wird durch Leitfähigkeitsmessungen [5], durch das im IR-Spektrum bei 6μ auftretende, für die Bindung $>C=\overset{\oplus}{N}=$ charakteristische Absorptionsmaximum sowie durch die Tatsache bestätigt, daß die Amidchloride nur in polaren Lösungsmitteln gut löslich sind.

Eine charakteristische Reaktion der Amidchloride ist die Bildung von N,N,N'-trisubstituierten Amidinen mit primären Aminen [6].

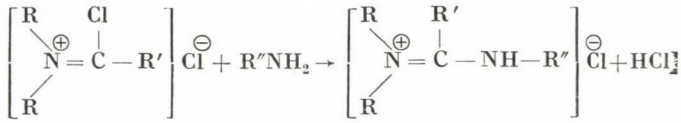

Die frei werdende Salzsäure wird durch das primäre Amin gebunden. Dies stört bei aromatischen Aminen nicht, da das Amidchlorid auch bei Raumtemperatur leicht mit dem Hydrochlorid des aromatischen Amins reagiert. Bei aliphatischen Aminen läuft die Reaktion jedoch nur bei Temperaturen oberhalb von 100 °C vollständig ab. Die Amingruppen im Amidin können mit Ammoniak oder mit einem primären Amin ausgetauscht werden. Ähnlich wie bei der Hydrolyse wird immer zuerst die Aminogruppe mit zwei Substituenten ausgetauscht.

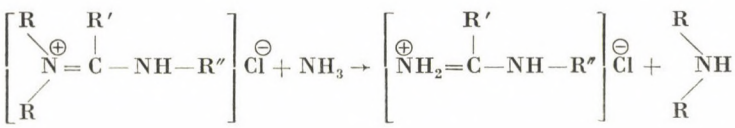

Diese Reaktion wurde durch EILINGSFELD und Mitarb. [7, 8, 9] zum Ringschluß angewendet. Aus β-Ketaminen hergestellte trisubstituierte Amidinhydrochloride wurden mit den Ammoniumsalzen von schwachen Säuren in Reaktion gebracht und auf diese Weise kondensierte Pyrimidinringverbindungen (z. B. Chinazoline) hergestellt.

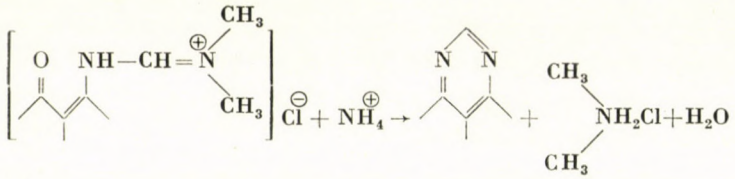

Zur Herstellung des Amidinsalzes wurde nicht das reine Amidchlorid, sondern das Addukt aus Dimethylformamid und Thionylchlorid verwendet. Der Ringschluß wurde in Alkohol durchgeführt. Auf diesem Weg ist es den genannten Verfassern gelungen, u. a. 4-Methylchinazolin, 4-Phenylchinazolin und verschiedene Anthrapyrimidinderivate zu synthetisieren.

Diese aminolytische Spaltung haben wir als Ringschluß der aus *o*-Aminobenzoesäurederivaten hergestellten trisubstituierten Amidinen zu Verbindungen vom Pyrimidinon-Typ verwendet. In diesem Fall besteht außer der Ammonolyse auch die Möglichkeit der Aminolyse, wodurch sich ein Weg zur Herstellung von N-substituierten Derivaten eröffnet.

Methylanthranilat und mit Phosgen hergestelltes Dimethylformamidchlorid wurde in Reaktion gebracht:

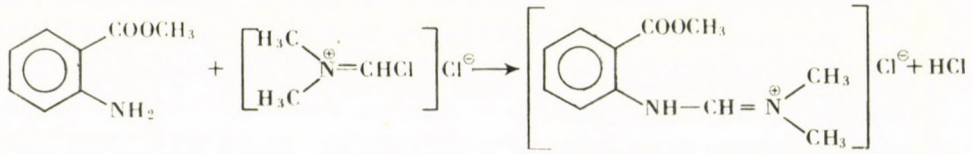

Das erhaltene N,N-Dimethyl-N'-(2-carbomethoxyphenyl)-formamidinhydrochlorid konnte mit Ammoniak bzw. Ammoniumacetat mit recht guter Ausbeute in 4(3H)-Chinazolinon überführt werden:

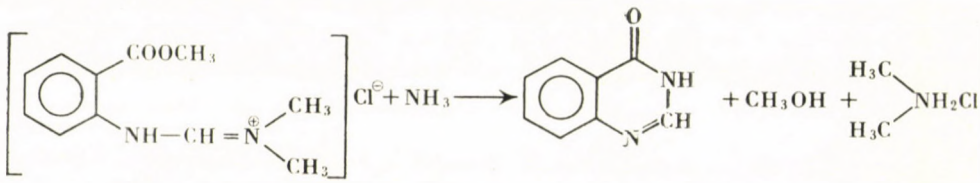

Das 4(3H)-Chinazolinon und seine Derivate sind längst bekannte, für die Industrie wichtige Verbindungen. Eines der ältesten und sehr allgemeinen

Verfahren hat NIEMENTOWSKI [10] ausgearbeitet. Er stellte 4(3H)-Chinazolinon durch Erhitzen von Anthranilsäure mit überschüssigem Formamid her.

Durch Erhitzen von Anthranilsäureamid und N-Acylanthranilsäureamid mit wasserentziehenden Mitteln können ebenfalls 4(3H)-Chinazolinone gewonnen werden [11, 12].

Unter den neueren Verfahren scheint das von GRIMMEL und GUENTHER [13] das einfachste zu sein. Er erhitzte N-Acetylanthranilsäure mit einem primären Amin und Phosphortrichlorid in Toluol:

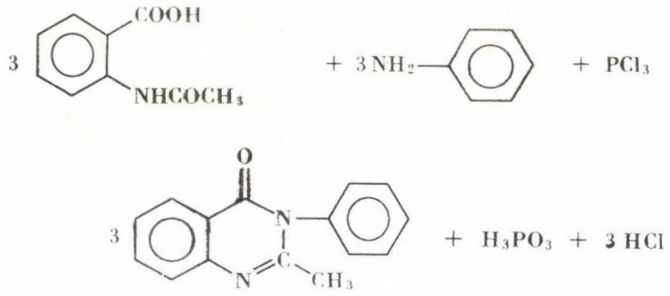

Es sind auch Verfahren bekannt, welche — ähnlich der durch uns ausgearbeiteten Synthese — über N-(2-Carboxy- bzw. Carbalkoxyphenyl)-amidine verlaufen.

So erhält STEPHEN [14] das 4(3H)-Chinazolinon aus Methylanthranilat und N-Arylbenzimidchlorid.

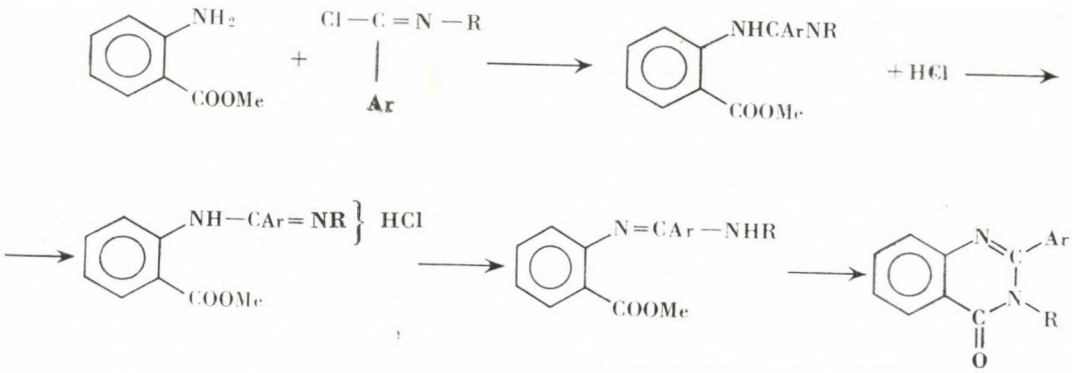

Für den obigen angenommenen Reaktionsweg gibt der Verfasser keinen Beweis. Zur Bindung der Salzsäure benutzt er 100% Aminüberschuß. Das Produkt kann nur mühsam herauspräpariert werden.

PETERSEN und TIETZE [15] stellen durch Reaktion von cyclischen Lactimäthern und Anthranilsäure o-Amidinobenzoesäurederivate her, aus welchen unter energischeren Bedingungen 4(3H)-Chinazolinonderivate gebildet werden.

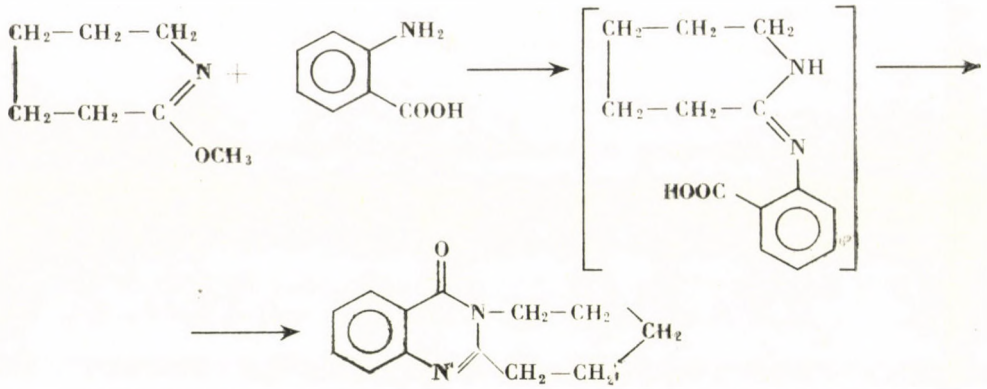

Gegenüber den erwähnten Verfahren besitzt die durch uns ausgearbeitete Synthese mehrere Vorteile. Die überwiegende Mehrzahl der 4(3H)-Chinazolinonderivate wird bei niedrigen Temperaturen, mit guter Ausbeute und auf sehr einfachem Wege erhalten.

Der erste Schritt der Synthese besteht in der Herstellung des Amidchlorids.

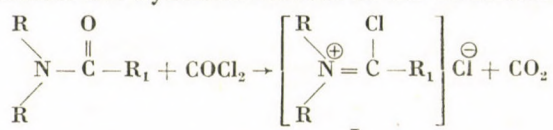

I

(R_1 = H, Alkyl, Aryl, Aralkyl; R = Alkyl)

Das Amidchlorid wird in Toluol aus N,N-disubstituiertem Säureamid und Phosgen hergestellt. Die Dauer und Temperatur der Reaktion hängt vom Säureamid ab. Danach wird aus dem Amidchlorid und der Aminoverbindung das Amidinhydrochlorid hergestellt.

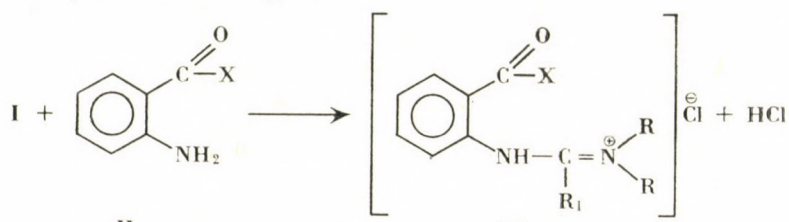

II III

X = OH, NH_2, OCH_3

Die Reaktion wird bei 20—40 °C in absolutem Chloroform durchgeführt. Unter den Anthranilsäurederivaten erwies sich das Methylanhtranilat als bestens geeignet, deshalb befaßten wir uns nur mit dem Ringschluß der daraus hergestellten Amidinsalze.

Als Beweis für die Struktur der Amidinsalze ist in Abb. 1 das IR-Spektrum des N,N-Dimethyl-N'-(2-carbomethoxyphenyl)-formamidin-hydrochlorids wiedergegeben.

Die Bande $\rangle C{=}O$ befindet sich bei 1708 cm^{-1}, die Bande $\rangle C{=}\overset{\oplus}{N}\langle$ bei 1677 cm^{-1}. Die letztere zeigt, daß die Doppelbindung in der Gruppe $\rangle C{=}\overset{\oplus}{N}\langle$ nicht konjugiert ist, daß also die Lage dieser Gruppe in Formel III richtig

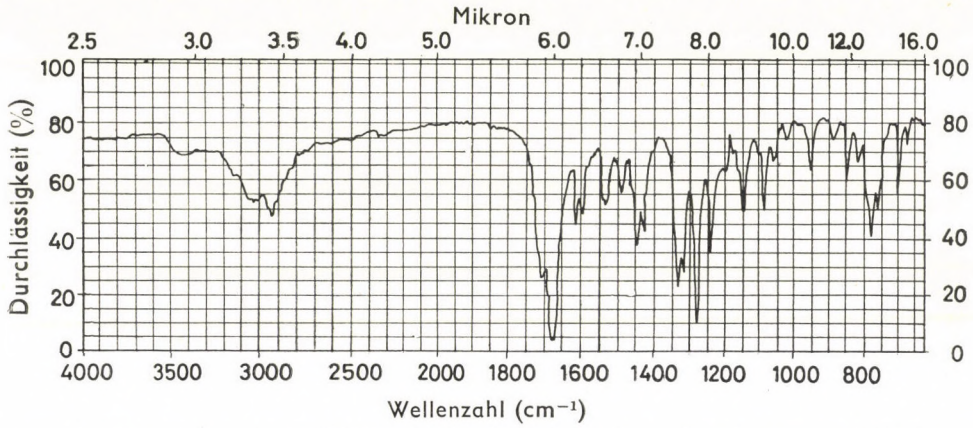

Abb. 1. IR-Spektrum des N,N-Dimethyl-N'-(2-carbomethoxyphenyl)-formamidin-hydrochlorids

wiedergegeben ist. Im IR-Spektrum des N,N-Dimethyl-N'-(2-carbomethoxyphenyl)-benzamidin-hydrochlorids ist nämlich die $\rangle C{=}\overset{\oplus}{N}\langle$ Bande infolge der Konjugation mit der Phenylgruppe nach 1625 cm^{-1} verschoben.

In Tabelle I sind die Zersetzungstemperaturen und der HCl-Gehalt einiger Amidinsalze zusammengestellt.

Der dritte Schritt der Synthese ist der Ringschluß des Amidinsalzes.

Tabelle I

Schmelzpunkt und HCl-Gehalt einiger Amidinsalze

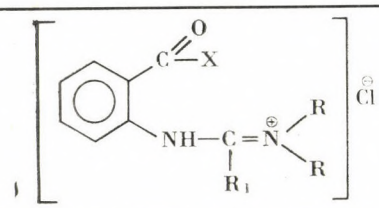	Ausbeute, %	Schmelzpunkt, °C	HCl-Gehalt, %	
			ber.	gef.
$R = CH_3$, $R_1 = H$, $X = OCH_3$	98,2	165—167 Zersetzung	15,03	15,11
$R = C_2H_5$, $R_1 = C_6H_5$, $X = OCH_3$	91,8	168—170 Zersetzung	10,52	10,55
$R = CH_3$, $R_1 = H$, $X = OH$	95,6	168—172 Zersetzung	15,95	15,88
$R = CH_3$, $R_1 = H$, $X = NH_2$	96,4	132—134 Zersetzung	16,02	16,19

1. *Ringschluß zu 4(3H)-Chinazolinonen*

Der Ringschluß des trisubstituierten Amidinhydrochlorids erfolgt auf Einwirkung von primären Aminen bzw. ihrer mit schwachen Säuren gebildeten Salze.

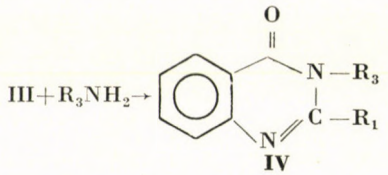

IV

(R_3 = H, Alkyl, Aryl, Aralkyl, NH_2, NHR_1 oder R_3NH_2 = Aminosäure)

Der Ringschluß wird mit der äquimolaren Menge oder einem geringen Überschuß des Reagens durchgeführt. Im allgemeinen verläuft die Reaktion bei Raumtemperatur. Einige Stunden dauerndes Kochen ist nur dann erforderlich, wenn das angewendete Amin eine ziemlich schwache Base ist.

In Abb. 2—5 sind die IR-Spektren einiger charakteristischer 4(3H)-Chinazolinone wiedergegeben.

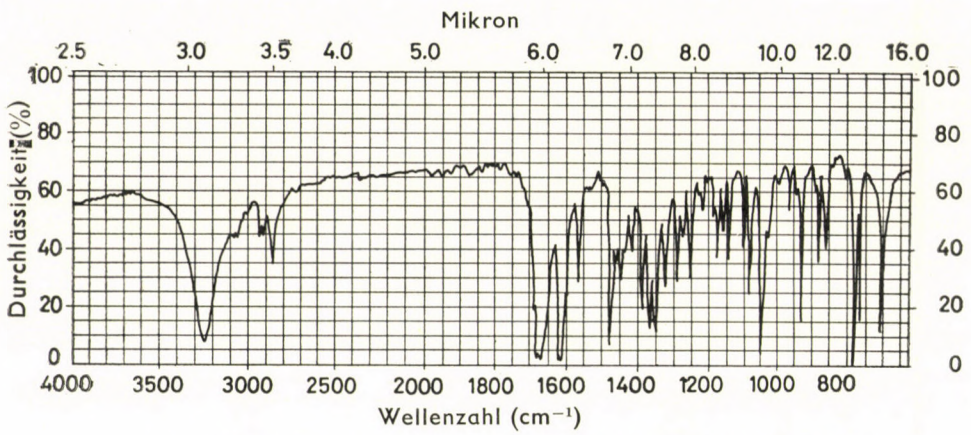

Abb. 2. IR-Spektrum des 3-(2-Hydroxyäthyl)-4(3H)-chinazolinons

In den Spektren zeigen sich zwischen 1500 und 1700 cm^{-1} zwei starke Banden, in Übereinstimmung mit den Ergebnissen von RANDALL [16] und CULBERTSON [17]. Die stärkere N-Acylcarbonyl-Bande kann in sämtlichen Fällen zwischen 1637 und 1704 cm^{-1} identifiziert werden. Die andere, um 1600 cm^{-1} auftretende Bande ist wahrscheinlich für die Bindung $\rangle C{=}N-$ charakteristisch. In den Spektren der durch uns hergestellten 3-substituierten 4(3H)-Chinazolinone wurden außerdem drei charakteristische Banden gefun-

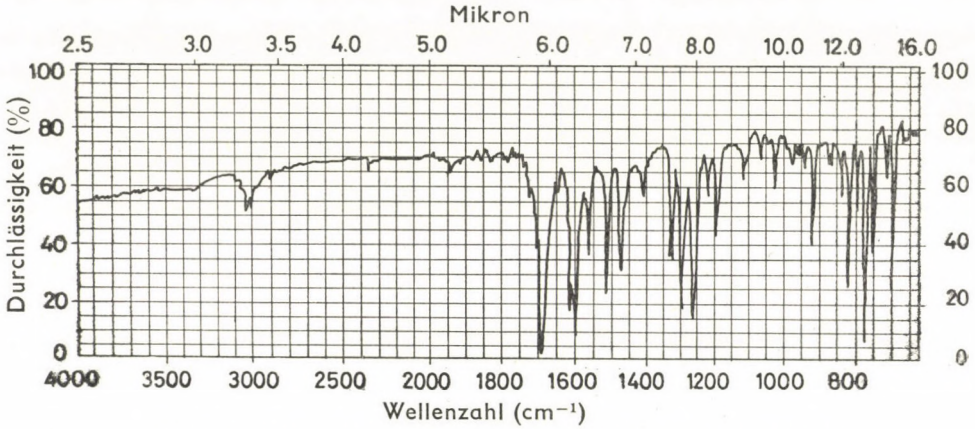

Abb. 3. IR-Spektrum des 3-(4-Methylphenyl)-4((3H)-chinazolinons

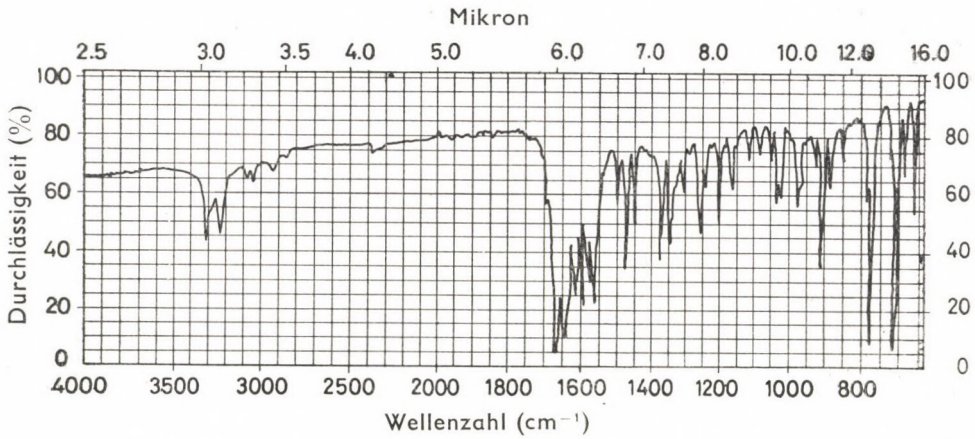

Abb. 4. IR-Spektrum des 2-Phenyl-3-amino-4(3H)-chinazolinons

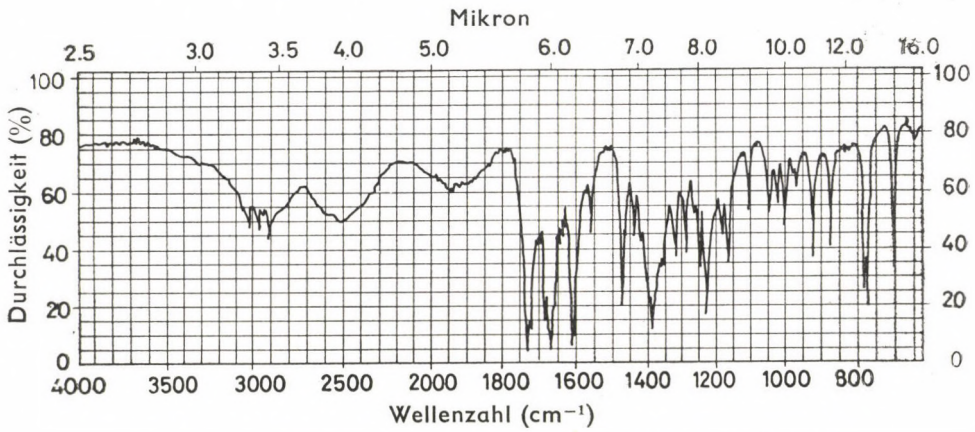

Abb. 5. IR-Spektrum des 3-(2-Carboxyäthyl)-4(3H)-chinazolinons

den. Zwei mittelstarke oder schwache Banden zeigen sich zwischen 1563 und 1580 cm^{-1}, bzw. 1473 und 1484 cm^{-1}; diese sind wahrscheinlich die Valenzschwingungen des aromatischen Gerüstes. Zwischen 769 und 780 cm^{-1} meldet sich die für die aromatische ortho-Disubstitution charakteristische, zur Ebene senkrechte CH-Schwingung. Die letztere Bande ist oft gespalten.

2. *Ringschluß zu Alkylen-bis-3,3'-4(3H)-chinazolinonen*

Diese, unseres Wissens nach bisher noch nicht beschriebenen Verbindungen werden analog zu den Verbindungen (IV) hergestellt, wobei als Ausgangsstoffe trisubstituierte Amidinsalze und Diaminoalkane verwendet werden.

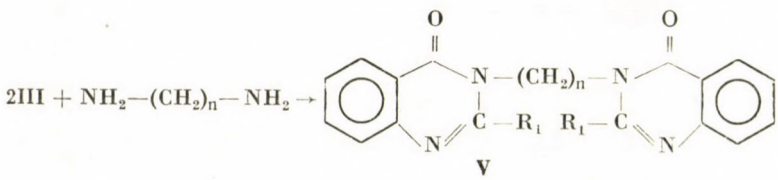

V

$(n = 2,3,\ldots)$

Die Reaktion wird bei äquimolarem Verhältnis der Komponenten und Raumtemperatur in Methanol durchgeführt. Das ausgeschiedene Produkt wird filtriert. Merkwürdigerweise wurde gefunden, daß auch dann (V) entsteht, wenn das Diaminoalkan in dreifachem Überschuß verwendet und das Amidin zum Amin gegeben wird.

In Abb. 6 ist das IR-Spektrum des Äthylen-bis-3,3'-4(3 H)-chinazolinons wiedergegeben.

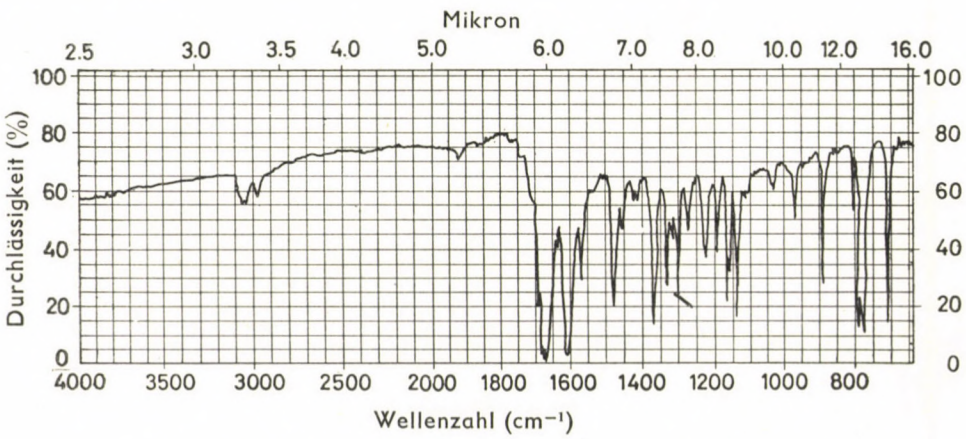

Abb. 6. IR-Spektrum des Äthylen-bis-3,3'-4(3H)-chinazolinons

Die N-Acylcarbonyl-Bande befindet sich bei 1675 cm^{-1}, die Bande >C=N— bei 1611 cm^{-1}, die Valenzschwingungsbanden des aromatischen Gerüstes bei 1568 und 1468 cm^{-1}, die für die aromatische ortho-Disubstitution charakteristische, zur Ebene senkrechte CH-Schwingungsbande in gespaltener Form bei 770 und 778 cm^{-1}.

Die Schmelzpunkte und die Ergebnisse der Elementaranalyse der erhaltenen Chinazolinonderivate sind in Tabelle II zusammengefaßt.

Tabelle II

Schmelzpunkte und Analysenergebnisse der synthetisierten Chinazolinonderivate

Verbindung	Variante	Schmelzpunkt, °C	Ausbeute %	Analyse					
				ber. %			gef. %		
				C	H	N	C	H	N
4(3H)-Chinazolinon = K	a	208—12	96,2	65,76	4,12	19,15	65,70	4,06	19,14
3-CH_3-K	b	104—5	95,0	67,50	5,00	17,50	67,58	5,01	17,42
3-(2-OH-äthyl)-K	b	151—4	90,2	63,15	5,26	14,74	63,10	5,31	14,85
3-Butyl-K	b	69—72	96,9	71,29	6,93	13,86	71,29	6,79	13,90
3-(4-CH_3-phenyl)-K	c	139—43	94,1	76,27	5,08	11,86	76,29	5,09	11,85
3-Benzyl-K	c	117—8	92,7	76,27	5,08	11,86	76,23	5,21	11,90
3-(4-OH-phenyl)-K	c	215—25	91,5	70,58	4,20	11,76	70,67	4,11	11,59
3-(4-NH_2-phenyl)-K	c	Zersetzung 174—7	91,5	70,89	4,64	17,72	70,85	4,66	17,81
3-Phenyl-K	d	135—8	68,2	75,67	4,50	12,61	75,81	4,52	12,60
2-Phenyl-K	d	235—40	82,6	75,67	4,50	12,61	75,72	4,43	12,80
2-Phenyl-3-NH_2-K	d	177—8	78,2	70,89	4,64	17,72	70,90	4,63	17,73
3-(2-Carboxyäthyl)-K	e	155—70	81,9	60,55	4,59	12,84	60,52	4,58	12,80
3-(3-Carboxypropyl)-K	e	Zersetzung 131—3	85,8	62,07	5,17	12,06	62,20	5,21	12,01
3-Phenylamino-K	c	168—70	93,1	70,89	4,64	17,72	70,92	4,61	17,75
3-NH_2-K	f	208—9	91,2	59,62	4,35	26,08	59,54	4,38	26,13
Äthylen-bis-3,3'-K	f	232—6	94,9	67,92	4,40	17,61	68,01	4,34	17,62
Hexylen-bis-3,3'-K	f	178—80	96,3	70,58	5,88	14,97	70,59	5,86	14,90

Die Identifizierung der synthetisierten Verbindungen wurde durch Elementaranalyse, Schmelzpunktbestimmung, gegebenenfalls durch Titration mit Perchlorsäure in nichtwäßriger Lösung und durch IR-Spektroskopie durchgeführt. Die IR-Spektren wurden mit KBr-Pastillen mit dem Perkin-Elmer-Spektrophotometer 237 aufgenommen.

Diskussion des Synthesemechanismus

Die ersten beiden Schritte der Synthese, d. h. die Bildung des Amidchlorids bzw. des Amidins sind geklärt [7].

Der Mechanismus des Ringschlusses ist jedoch noch ungeklärt.

RIED und Mitarb. [18, 19] synthetisierten das 4(3H)-Chinazolinon aus Anthranilsäure und Iminoester und nahmen folgenden Reaktionsmechanismus an:

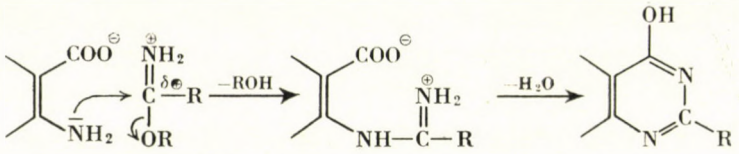

Ihrer Meinung nach benötigt diese Reaktion Säurekatalyse. Dies wird auch durch die Untersuchung von FINGER [20] bestätigt, dem es — aus Methylanthranilat ausgehend — nur bei hohen Temperaturen und mit sehr geringen Ausbeuten gelang, den Ringschluß durchzuführen.

In dem durch uns ausgearbeiteten Verfahren verläuft die Ringschlußreaktion der aus Methylanthranilat hergestellten Amidinsalze leicht und mit recht guter Ausbeute. Zur Interpretierung dieser Reaktion geben wir folgenden Reaktionsmechanismus an:

Der erste Schritt ist eine aminolytische Spaltung des Amidinsalzes, deren primäres Produkt die mono- oder disubstituierte Amidinbase ist:

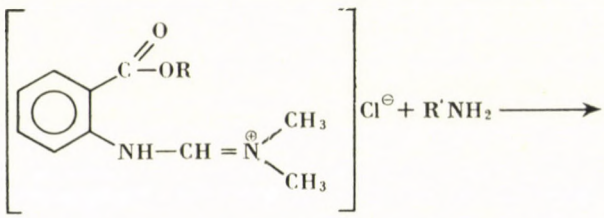

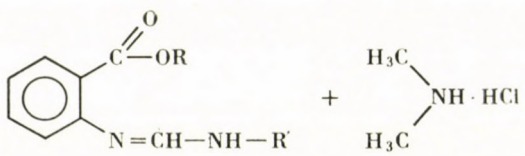

Diese Vorstellung beruht auf der Annahme, daß die Basizität des Amidins — infolge der elektronenanziehenden Wirkung der Estergruppe — dermaßen geschwächt wird, daß die Salzsäure durch das abgespaltene Dimethylamin gebunden wird.

Der Ringschluß der Amidinbase erfolgt dann auf Einwirkung des Protonkatalysators Dimethylaminhydrochlorid in einer Acylierungsreaktion, wobei Alkohol austritt:

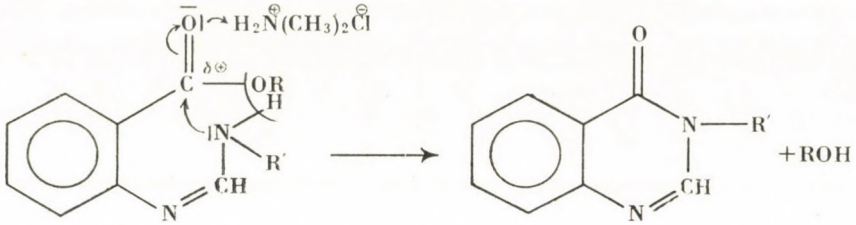

Die als Intermediärprodukt enstehende Amidinbase konnte nicht isoliert werden. Jedoch ist es uns gelungen, das Intermediärprodukt des mit Phenylhydrazin durchgeführten Ringschlusses, d.h. entsprechende Hydrazidinbase in Form einer kristallinen, stabilen Verbindung zu isolieren.

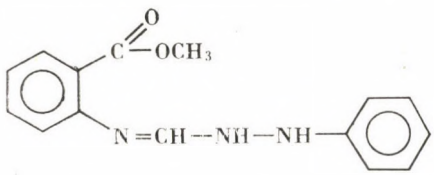

Die Hydrazidinbase ist nämlich in kaltem Alkohol so wenig löslich, daß sie ausgeschieden wird und demgemäß bei Zimmertemperatur keine Cyclisierung erfolgen kann. Wird nun dieses isolierte Intermediärprodukt in Alkohol zum Sieden erhitzt, so setzt es sich nicht zum entsprechenden 4(3H)Chinazolinon um. Wird jedoch Dimethylamin-hydrochlorid zugegeben, so erfolgt der Ringschluß zum Chinazolinonderivat schnell.

Dies ist ein Beweis für unsere obige Annahme, wonach im ersten Schritt der Reaktion die entsprechende Base gebildet wird und ihr Ringschluß infolge der katalytischen Wirkung des als Nebenprodukt entstehenden Dimethylaminhydrochlorids erfolgt.

Über unsere Untersuchungen mit Hydrazidinen und über die Anwendung unseres Verfahrens zur Herstellung mehrerer verschiedenartiger heterocyclischer Verbindungen soll in einer nächsten Mitteilung berichtet werden.

Experimenteller Teil

1. Synthese von Amidchloriden

1.1 *Dimethylformamidchlorid.* 73,09 g (1 Mol) Dimethylformamid werden in 500 ml Toluol gelöst. 118,7 g (1,2 Mol) Phosgengas werden mit einer Geschwindigkeit, bei der die Temperatur des Reaktiongemisches zwischen 10—20 °C bleibt, in die Lösung eingeleitet.

Der ausgeschiedene weiße Niederschlag wird rasch abfiltriert, mit abs. Äther oder Petroläther gewaschen und im Vakuumexsikkator getrocknet.

Die Ausbeute ist praktisch quantitativ.

Schmelzpunkt: 140—145 °C.

1.2 *Diäthylbenzamidchlorid.* 88,5 g (0,5 Mol) Diäthylbenzamid werden in 500 ml Toluol gelöst. 59,35 g (0,6 Mol) Phosgengas werden bei 25—30 °C in die Lösung geleitet. Das abgeschiedene Öl kristallisiert im Laufe von 24 Stunden aus.

Der erhaltene weiße Niederschlag wird rasch filtriert, mit abs. Äther oder Petroläther gewaschen und im Vakuumexsikkator getrocknet.

Ausbeute: 97,5%

Schmelzpunkt: 78—85 °C, unter Zersetzung.

2. Synthese von Amidinen

2.1 *N,N-Dimethyl-N′-(2-carbomethoxyphenyl)-formamidin-hydrochlorid.* 13 g (0,1015 Mol) Dimethylformamidchlorid werden in 150 ml abs. Chloroform gelöst. Eine Lösung von 15,1 g (0,1 Mol) Methylanthranilat in Chloroform wird langsam zugegeben, wobei die Temperatur nicht über 40 °C steigen darf. Die Lösung wird auf dem Wasserbad eingedampft und das Produkt getrocknet.

Ausbeute: 23,8 g (98,2%)

Schmelzpunkt: 165—167 °C, unter Zersetzung.

2.2 *N,N-Diäthyl-N′-(-2-carbomethoxyphenyl)-benzamidin-hydrochlorid.*

2.3 *N,N-Dimethyl-N′-(2-carboxyphenyl)-formamidin-hydrochlorid.*

2.4 *N,N-Dimethyl-N′-(2-carboxamidophenyl)-formamidin-hydrochlorid.*

Die Verbindungen 2.2, 2.3 und 2.4 werden unter den gleichen Bedingungen hergestellt wie 2.1. Bei 2.3 und 2.4 kann ein Teil des Amidinsalzes durch Filtrieren isoliert werden. Der in der Lösung bleibende Teil wird durch Eindampfen gewonnen.

3. Herstellung von 4(3H)-Chinazolinonen und Alkylen-bis 3,3'-4(3H)-chinazolinonen

Die Verbindungen werden aus den entsprechenden Amidin-hydrochloriden und Aminen bei Raumtemperatur oder durch einige Stunden dauerndes Kochen in Methanol hergestellt. Die Produkte werden durch Eindampfen oder Filtrieren isoliert.

Die Varianten des Verfahrens werden an Hand einiger Beispiele vorgeführt. Die übrigen synthetisierten Verbindungen sind in Tab. II zusammengestellt, wobei jeweils die verwendete Variante des Verfahrens angegeben ist.

3.1 *4(3H)-Chinazolinon (a).* 24,25 g (0,1 Mol) N,N-Dimethyl-N′-(2-carbomethoxyphenyl)-formamidin-hydrochlorid werden in 100 ml Methanol gelöst. Die Lösung wird mit Ammoniakgas gesättigt. Nach zweistündigem Stehen wird auf dem Wasserbad eingedampft, das Produkt mit wenig Wasser gewaschen und getrocknet.

Ausbeute: 14,2 g (96,2%)

Schmelzpunkt: 208—212 °C

3.2 *3-Butyl-4(3H)-chinazolinon (b).* 24,25 g (0,1 Mol) N,N-Dimethyl-N′-(2-carbomethoxyphenyl)-formamidin-hydrochlorid werden in 100 ml Methanol gelöst. 7,31 g (0,1 Mol) Butylamin werden zugegeben. Die Lösung wird 1 Stunde lang bei Raumtemperatur gerührt und danach auf dem Wasserbad eingedampft. Das erhaltene hellgelbe Öl kristallisiert sofort. Es wird mit wenig Wasser gewaschen und getrocknet.

Ausbeute: 19,5 g (96,9%)

Schmelzpunkt: 69—72 °C

3.3 *3(4-Aminophenyl)-4(3H)-chinazolinon (c)* 24,25 g (0,1 Mol) N,N-Dimethyl-N′-(2-carbomethoxyphenyl)-formamidin-hydrochlorid werden in 100 ml Methanol gelöst. 10,81 g (0,1 Mol) *p*-Phenylendiamin werden zugefügt. Die Lösung wird 1 Stunde lang im Sieden gehalten und dann abgekühlt. Nach 24stündigem Stehen wird der ausgeschiedene Niederschlag abfiltriert, mit Wasser und wenig Alkohol gewaschen und getrocknet.

Ausbeute: 21,7 g (91,5%)

Schmelzpunkt: 174—177 °C.

3.4 *3-Phenyl-4(3H)-chinazolinon (d).* 24,25 g (0,1 Mol) N,N-Dimethyl-N′-(2-carbomethoxyphenyl)-formamidin-hydrochlorid werden in 100 ml Methanol gelöst. 9,31 g (0,1 Mol) Anilin werden zugegeben. Nach 2 Stunden bei Siedetemperatur wird die Lösung eingedampft. Das erhaltene hellgelbe Öl bildet nach kurzem Stehen einen öligen Kristallbrei. Dieser wird mit wenig Petroläther verrührt, dann wird filtriert, mit wenig Wasser und Alkohol gewaschen und getrocknet.

Ausbeute: 15,14 g (68,2%).

Schmelzpunkt: 135—138 °C.

3.5 3-(2-*Carboxyäthyl*)-4-(3*H*)-*chinazolinon (e)*. 24,25 g (0,1 Mol) N,N-Dimethyl-N'-(2-carbomethoxyphenyl)-formamidin-hydrochlorid werden in 250 ml Methanol gelöst. 8,91 g (0,1 Mol) β-Alanin werden zugegeben. Nach 3 Stunden bei Siedetemperatur wird die Lösung eingedampft. Das erhaltene dunkelgelbe Öl wird stehen gelassen, wobei ein Kristallbrei mit öliger Verunreinigung entsteht. Der Brei wird mit wenig Alkohol verdünnt, die Kristalle werden abfiltriert, mit wenig Wasser und Alkohol gewaschen und getrocknet.

Ausbeute: 17,85 g (81,9%)

Schmelzpunkt: 155—170 °C, unter Zersetzung.

Das salzsaure Salz schmilzt — in Übereinstimmung mit dem Literaturwert — bei 212—214 °C unter Zersetzung.

3.6 *Hexylen-bis*-3,3'-4(3*H*)-*chinazolinon (f)*. 24,25 g (0,1 Mol) N,N-Dimethyl-N'-(2-carbomethoxyphenyl)-formamidin-hydrochlorid werden in 100 ml Methanol gelöst. 5,53 g (0,05 Mol) Hexamethylendiamin werden zugegeben. Die ausgeschiedenen Kristalle werden abfiltriert, mit wenig Wasser gewaschen und getrocknet.

Ausbeute: 18,0 g (96,3%).

Schmelzpunkt: 178—180 °C.

LITERATUR

1. WALLACH, O., KAMENSKY, D.: Liebigs Ann. **214**, 234 (1882)
2. HALLMANN, F.: Ber. **9**, 846 (1876)
3. BOSSHARD, H. H., ZOLLINGER, H. H.: Helv. Chim. Acta **42**, 1659 (1959)
4. ARNOLD, Z.: Chem. Listy **52**, 2013 (1958)
5. KLAGES, F., GRILL, W.: Liebigs Ann. **594**, 21 (1955)
6. BRAUN, J.: Ber. **37**, 2678 (1904)
7. EILINGSFELD, H., SEEFELDER, M., WEIDINGER, H.: Angew. Chem. **72**, 836 (1960)
8. WEIDINGER, H., EILINGSFELD, H., HAESE, G.: DP 1159456 (1963)
9. WEIDINGER, H., EILINGSFELD, H., HAESE, G.: DP 1194867 (1965)
10. NIEMENTOWSKY, S.: J. Prakt. Chem. 2 **51**, 564 (1895)
11. KAUPMANN, W., FUNKE, S.: DP 1168435 (1964)
12. WEDDIGE, A.: J. Prakt. Chem. 2 **31**, 124 (1885)
13. GRIMMEL, H. W., GUENTHER, A.: J. Am. Chem. Soc. **68**, 539 (1946)
14. STEPHEN, L.: J. Chem. Soc. **1956**, 985
15. PETERSEN, S., TIETZE, E.: Liebigs Ann. **623**, 166 (1959)
16. RANDALL, H. N.: Infrared Determination of Organic Structures. D. Van Nostrand Co. Inc., New York. 1949
17. CULBERTSON, H., DECIUS, J. C., CHRISTENSEN, B. E.: J. Am. Chem. Soc. **74**, 4834 (1952)
18. RIED, W., STEPHAN, W.: Ber. **95**, 3042 (1962)
19. RIED, W., STEPHAN, W.: Ber. **96**, 1218 (1963)
20. FINGER, H., SCHUPP, L.: J. Prakt. Chem. **74**, 154 (1906)

Zoltán CSŰRÖS
Rudolf SOÓS
János PÁLINKÁS
István BITTER

Budapest XI., Műegyetem rkp. 3.

Acta Chimica Academiae Scientiarum Hungaricae, Tomus 63 (2), pp. 229—232 (1970)

VIOLEOXANTHIN AND TAREOXANTHIN

(PRELIMINARY COMMUNICATION)

J. SZABOLCS and GY. TÓTH

(Chemical Institute of the Medical University, Pécs)

Received July 21, 1969

Tareoxanthin in dandelion flowers and violeoxanthin in pansy flowers were reported by STRAIN *et al.* [1] and STRAIN [2]. As can be seen from their names, tareoxanthin is similar in many respects to taraxanthin, and violeoxanthin to violaxanthin.

The present paper presents evidence to show that violeoxanthin is a *cis*-violaxanthin [3, 4], and tareoxanthin is a mixture of neolutein epoxide *A*, neolutein epoxide *B*, and a small amount of *cis*-violaxanthin.

Isomerization of violeoxanthin with iodine [5] yielded violaxanthin, and inversely, natural violaxanthin when isomerized with iodine converted into violeoxanthin. Violaxanthin from violeoxanthin has the same physical and chemical properties as natural violaxanthin. Both violaxanthins gave auroxanthins with acid, and zeaxanthin with $LiAlH_4$ [6].

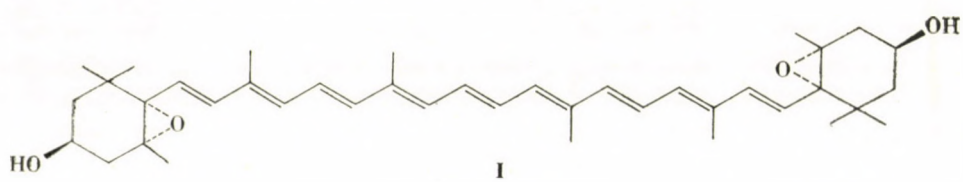

I

The low melting point (m.p. 112 °C), the iodine-catalyzed stereomutation and the light-absorption properties (Fig. 1) show that violeoxanthin is a *cis*-isomer [7] (the IR spectrum of violeoxanthin, Fig. 2, is identical with that of violaxanthin). The λ_{max} shift (4 — 5mμ) and the low *cis*-peak ($10^{-3} \cdot E = 11.6$; 335mμ) indicate that violeoxanthin has a peripheral *cis* double bond. Thus, on the analogy of neoxanthin [8], it seems reasonable to assume that violeoxanthin is 9-mono-*cis*-violaxanthin.

The absolute configuration of the hydroxyl groups and the epoxide ring in violeoxanthin are the same as those of natural violaxanthin because, apart from the same origin, violaxanthin gained from violeoxanthin by iodine-catalyzed stereomutation has the same o.r.d. curve [9] as natural violaxanthin, I.

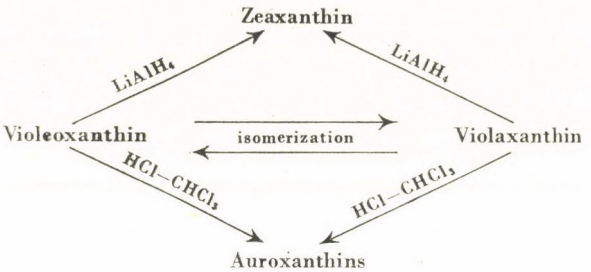

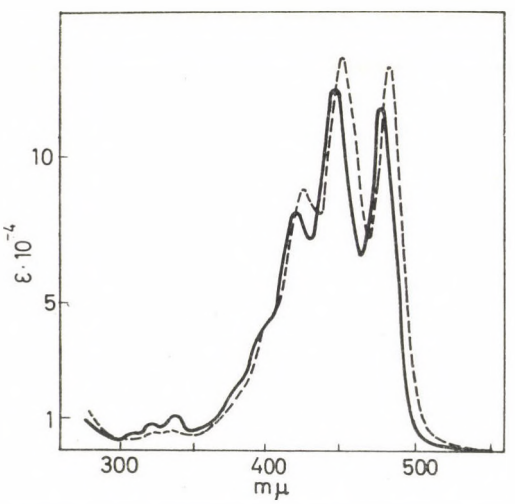

Fig. 1. Extinction curves in benzene, – – – –, violaxanthin; ————, violeoxanthin (λ_{max} 478, 448 and 422 mμ; $10^{-3} \cdot$ E 118.1, 124.7 and 82.5)

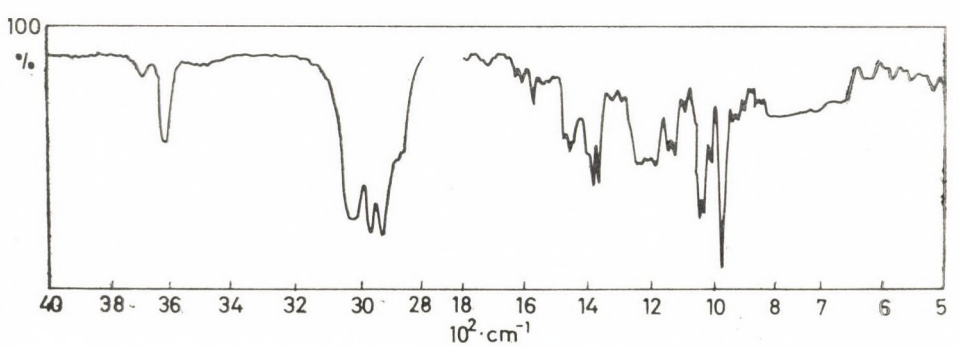

Fig. 2. IR Spectrum of violeoxanthin (in $CHCl_3$)

As it is known, the existence of taraxanthin has often been questioned in the past years, and many authors have concluded that taraxanthin is identical with lutein epoxide [10, 11, 12]. This is in agreement with our experiments reported here, according to which tareoxanthin is a mixture of neolutein epoxide *A*, neolutein epoxide *B* and a small amount of *cis*-violaxanthin.

The chromatogram of the dandelion flower extract* is as follows:

Zones (mm)	Pigments**	λ_{max} (mμ) in benzene		λ_{max} (mμ) in HCl-benzene	
5 yellow	furanoid-derivatives ((494))	457	428	457	428
1 red		460	431	((494))	459
3 yellow		460	432	459	431
12 ochre	neolutein *B*	486	456	486	453
15 ochre	lutein	489	456	488	455
6 yellow	tareoxanthin	479	449	458	430
20 yellow	lutein epoxide	483	453	460	431

* All procedures were carried out under the same conditions as those used by STRAIN *et al.*

** Pigments are listed in the order of decreasing adsorption affinities.

The pigment adsorbed between lutein and lutein epoxide showed the same properties as those described for tareoxanthin in the literature.

Rechromatography of tareoxanthin on a $CaCO_3$ column developed with a mixture of benzene and petroleum ether furnished 2 bands, one of which consisted of neolutein epoxide *A* and the other of neolutein epoxide *B*. The presence of neolutein epoxide *A* and neolutein epoxide *B* in tareoxanthin was also proved by the fact that neolutein epoxide *A* and neolutein epoxide *B* did not separate from each other in the chromatographic system originally used by STRAIN [2].

On isomerization with iodine, tareoxanthin gave the following pigments: neolutein epoxide *A*, neolutein epoxide *B*, a small amount of violaxanthin and all-*trans* lutein epoxide.

These findings make it clear that tareoxanthin is not an individual carotenoid, but a mixture of *cis*-lutein epoxides and *cis*-violaxanthin.

*

We wish to express our gratitude to Professor B. C. L. WEEDON for his useful comment on the optical rotatory dispersion curve of violaxanthin prepared from violeoxanthin.

REFERENCES

1. STRAIN, H. H., MANNING, W. M., HARDIN, G.: Biol. Bull. **86,** 169 (1944)
2. STRAIN, H. H.: Arch. Biochem. and Biophys. **48,** 458 (1954)
3. CURL, A. L., BAILEY, G. F.: Food Res. **22,** 323 (1957)
4. SUBBARAYAN, C., CAMA, H. R.: Indian J. Chem. **3,** 463 (1965)
5. TSUKIDA, K., ZECHMEISTER, L.: Arch. Biochem. and Biophys. **74,** 408 (1958)
6. CHOLNOKY, L., SZABOLCS, J., TÓTH, GY.: Ann. **708,** 218 (1967)
7. ZECHMEISTER, L.: Cis-trans Isomeric Carotenoids, Vitamins A and Arylpolyenes. Springer Verlag, Wien, 1962
8. (the late) CHOLNOKY, L., GYÖRGYFY, K., RÓNAI, Á., SZABOLCS, J., TÓTH, GY., GALASKO, G., MALLAMS, A. K., WAIGHT, E. S., WEEDON, B. C. L.: J. Chem. Soc. (C), **1969,** 1256
9. BARTLETT, L., KLYNE, W., MOSE, W. P., SCOPES, P. M., GALASKO, G., MALLAMS, A. K., WEEDON, B. C. L., SZABOLCS, J., TÓTH, GY.: J. Chem. Soc. (In the press)
10. CROZIER, G. F.: Comp. Biochem. Physiol. **23,** 179 (1967)
11. EGGER, K.: Planta **80,** 65 (1968)
12. TÓTH, GY., SZABOLCS, J.: Acta Chim. Acad. Sci. Hung. (In the press)

József SZABOLCS
Gyula TÓTH
} Pécs, Rákóczi út 80. Hungary

Acta Chimica Academiae Scientiarum Hungaricae, Tomus 63 (2), pp. 233—236 (1970)

BOOK REVIEWS — BUCHBESPRECHUNGEN — РЕЦЕНЗИИ КНИГ

J.C. JUNGERS, et L. SAJUS (avec la collaboration de J. de AGUIRRE et D. DECROOCQ): *L'analyse cinétique de la transformation chimique.* Éditions techniques Paris, 1968, tome II. 1253 Seiten (französisch)

Dieses Buch erschien in einer Serie »Science et technique du pétrole«, dem Inhalt nach geht es aber weit über das spezielle Interesse der in der Erdölwissenschaft Interessierten hinaus. Es ist eine ganz eigenartige Bearbeitung des Problems des chemischen Vorganges, die sich nicht in den klassischen Rahmen der chemischen Stoffaufteilung, wie etwa physikalische Chemie, analytische Chemie usw. einordnen läßt. Es ist ein erstklassiges Werk moderner chemischer Kentnisse, wo die einzelnen traditionellen Wissenschaftszweige integriert zusammenfließen, wie es unser Zeitalter fordert. Die Einteilung des Buches in großen Zügen ist folgende: Das Lösungsmittel (Elektrische Eigenschaften, Kinetische Effekte); Reaktionsschema und Mechanismus (Stöchiometrie und Thermodynamik der Erscheinungen, Kinetik der Umwandlung, Physikalische Methoden der Analyse, Chemische Tests, Kinetische Erwägungen); Zusammenhang zwischen Struktur und molekularen Eigenschaften (Empirische Beziehungen, Über die Effekte der Substituenten, Analytische Beziehungen, Einwirkungen des Lösungsmittels, Zusammenhänge zwischen den Effekten der Substituenten, des Lösungsmittels und der Temperatur). Man findet im Buch Reaktionskinetik, Thermodynamik, Analyse, Strukturchemie, Elektrochemie, organische Chemie usw. in einer sehr interessanten, jedoch sehr konzentrierten Synthese. Der Stoff ist mit Tabellen und graphischen Darstellungen aus der modernsten Literatur (hauptsächlich Zeitschriften) erläutert. Das Buch muß man lesen, um es zu schätzen. Zum Nachschlagen ist es weniger geeignet, da man aufgrund der neuartigen Darlegung nicht nach herkömmlicher Weise suchen kann; das Sachregister wurde jedoch ganz traditionell in erster Linie nach chemischen Verbindungen zusammengestellt, die jedoch im Text zumeist nur als Beweisführung für das eben Vorgeführte dienen. Man könnte hier und da mir der Auffassung der Verfasser wohl disputieren, daß es aber zu den interessantesten Büchern gehört, die ich in letzter Zeit gesehen habe, wage ich zu behaupten.

F. SZABADVÁRY

Arzneimittel, Entwicklung, Wirkung, Darstellung. Herausgegeben von G. Erhart und H. Ruschig. Verlag Chemie, Weinheim, 1968. 1921 Seiten

Dem Neuling auf dem Gebiet der Arzneimittelforschung — sei er Chemiker oder Pharmakologe — stehen nur wenige Handbücher zu Verfügung, die ihm den Überblick über dieses stets ausgedehnter und mannigfaltiger werdende Gebiet erleichtern würden. Es erscheinen zwar von Jahr zu Jahr neue Bände von vielen, hervorragend redigierten Buchreihen, welche einzelne Spezialthemen monographieartig bearbeiten, jedoch sind diese — gerade wegen ihrem Monographiecharakter — für Anfänger, bzw. für ein umfassendes Studium des gesamten Fachgebietes weniger geeignet.

Im letzten Jahrzehnt sind insgesamt nur zwei Werke von allgemeinem Interesse erschienen: Medicinal Chemistry von A. BURGER (USA, 1960) und Grundlagen der Arzneimittelforschung und der synthetischen Arzneimittel von J. BÜCHI (Schweiz, 1963.). Diese, auch heute noch zeitgemäßen Standardwerke können im Bücherschrank eines jeden Arzneimittelforschers aufgefunden werden. Seit der Zeit ihrer Erscheinung wurden jedoch viele neue, hochwirksame Arzneimittel entwickelt und viele neue Angaben über Zusammenhänge

zwischen Struktur und biologischer Wirkung veröffentlicht. Die Herausgabe eines Werkes, welches die Ergebnisse auch der letzten zehn Jahre umfaßt und auswertet, war also höchst aktuell.

Im zweibändigen Werk, welches — redigiert von Herren Professor ERHART und RUSCHIG — unter der Mitwirkung der Forscher der Farbwerke Hoechst AG erschienen ist, wird der Stoff in pharmakologischer Gruppierung behandelt. In den einzelnen Kapiteln werden — nach der Definierung der betreffenden Arzneimittelwirkung — die wichtigsten pharmakologischen Untersuchungsmethoden und anschließend die zur betreffenden Gruppe gehörenden Pharmaka dargestellt. Dabei wird der Entwicklungsweg einiger wichtigen, auch in praktischer Hinsicht bedeutenden Verbindungsgruppen geschildert und auf die eventuellen Nebenwirkungen der Pharmaka und gegebenenfalls auf die Möglichkeiten ihrer Beseitigung eingegangen. Danach folgt die Synthese der behandelten Verbindungen, wobei die bezüglichen Literaturzitate angegeben werden.

Band I befasst sich mit der Pharmakodynamik und enthält folgende Kapitel: Aufbau und Funktionsweise des Nervensystems; Parasympathomimetica; Spasmolytica; Antiparkinsonmittel; Sympathomimetica und Sympatholytica; Muskelrelaxantien; Antihistaminica, Lokalanaesthetica; Narcotica; Hypnotica; Analgetica; Psychopharmaka; Antiepileptica; Analeptica; Kreislaufmittel; herzwirksame Glykoside und Aglykone; Blut; Diuretica; Therapeutica mit Wirkung auf den Magen-Darm-Trakt; Röntgenkontrastmittel; Vitamine; Roborantia und Tonica.

In Band II werden chemoterapeutische Mittel in folgender Gruppierung behandelt: Anthelminthica; Präparate gegen Protozoen; Antimykotica; antibakteriell wirkende Substanzen; Virusmittel; Krebsmittel; Substanzen zur Steigerung der unspezifischen Abwehr; Antisera und Impfstoffe.

In einem kurzen Anhang wird der Weg und das Verhalten der Wirkstoffe im Organismus behandelt.

Anerkennung gebührt den Verfassern der einzelnen Kapitel für die sorgfältige Auswahl des Materials und für die klare, einen guten Überblick gebende Art der Behandlung. Die schöne Ausstattung des Werkes ist das Verdienst des Verlages Chemie.

Das Buch ist ein Wegweiser für die medizinische Grundlagenforschung und ein Helfer auf dem Weg zur gezielten Arzneimittelsynthese.

GY. DEÁK

Ferdinand von STURM: *Elektrochemische Stromerzeugung*. Chemische Taschenbücher-Serie, Verlag Chemie, 1969, herausgegeben von Wilhelm Foerst und Helmut Grünwald, Weinheim, Bergstr. 189 Seiten, 87 Abbildungen, 13 Tabellen

Das Ziel der Serie »Chemische Taschenbücher« ist, einen kurzen Überblick über die heutigen Kenntnisse auf einzelnen Fachgebieten zu geben.

Das vorliegende Buch, gegliedert in Hauptabschnitte über primäre und sekundäre Elemente bzw. Brennstoffzellen, entspricht diesem Ziel in vollem Maße. Der Verfasser geht immer von den thermodynamischen Grundlagen aus und behandelt dann die prinzipiell möglichen und die in der Praxis wirtschaftlich ausführbaren Zellen. Die ökonomische Orientierung ist übrigens — neben der streng chemisch-wissenschaftlichen Behandlung des Themas — für das ganze Buch charakteristisch. Die noch offenen, bzw. zur Zeit in wirtschaftlicher Hinsicht noch ungelösten Probleme werden besonders hervorgehoben, wodurch auf die weiteren Entwicklungsrichtungen hingewiesen wird. Diese Feststellung gilt besonders für das Kapitel über Brennstoffzellen, welches den größeren Teil des Buches ausmacht.

Das klar und verständlich geschriebene Buch ist eine genußreiche Lektüre. Für den Leser, der sich nach dem erhaltenen Überblick in Einzelheiten zu vertiefen wünscht, wird dies durch reichliche Literaturangaben erleichtert.

Das Erscheinen dieses hervorragend gelungenen Buches kann nur wärmstens begrüßt werden. Nur eine einzige kritische Bemerkung wäre vielleicht zu erwähnen: die Kinetik der Elektrodenvorgänge, bzw. die Polarisation wird im Zusammenhang mit den Brennstoffzellen behandelt, obwohl diese Erscheinungen auch bei den primären und sekundären Elementen auftreten.

J. DÉVAY

W. KIRMSE: *Carbene, Carbenoide und Carbenanaloga.* Verlag Chemie, 1969. XII+260 Seiten

Das vorliegende, 260 Seiten starke Büchlein von Professor KIRMSE ist der siebte Band der hier in Ungarn noch nicht allgemein bekannten Serie »Chemische Taschenbücher« des Verlags Chemie. Das Ziel, das sich die Herausgeber (W. Foerst und H. Grünewald) und der Verlag mit der Herausgabe der Reihe gesetzt haben, besteht darin, den Chemie-Studenten, denen es — infolge der stürmischen Entwicklung der modernen Chemie — im Rahmen des normalen Studiums (einschließlich Spezialvorlesungen) heute einfach nicht mehr möglich ist, sich wenigstens einen Überblick über alle wichtigsten Teilgebiete zu verschaffen, billige Büchlein in die Hand zu geben, anhand welcher sie ihr aus den Lehrbüchern gesammeltes Wissen erweitern und vertiefen und bis zu dem neuesten Stand eines Spezialgebietes vordringen können. Diese Zielsetzung entspricht dem Trend, der heute in den wissenschaftlich und industriell höchstentwickelten Ländern zu beobachten ist (man denke an die vielen ausgezeichneten Paperbacks des englischen Sprachgebietes aus allen Zweigen der Wissenschaft), und es ist auch klar, daß ein Buch über Carbene in diese Reihe gehört.

Das vorliegende Werk behandelt alle Aspekte der Carbenchemie, angefangen mit der Bildung der Carbene und ihrem Nachweis sowie den Nomenklaturfragen, über theoretische Probleme der Carbenstruktur und ihre Untersuchungsmethoden, die verschiedenen Reaktionsmöglichkeiten in Abhängigkeit von den Reaktionsbedingungen (Gasphase oder in Lösung, inter- oder intramolekular), die sog. Carbenoide (das sind reaktive Zwischenstufen, man könnte auch sagen, »gebundene« Carbene, die sich in einigen, jedoch nicht allen ihren Reaktionen wie die »freien« Carbene verhalten), die präparativen Anwendungsmöglichkeiten der Carbene und Carbenoide, ganz bis zur Chemie der Carbenanalogen (wie Nitrene, atomarer Sauerstoff, atomarer Kohlenstoff — ein Dicarben — usw.). Zu jedem Kapitel gehört eine Literaturzusammenstellung mit insgesamt über 1000 Literaturzitaten, unter welchen der überwiegende Teil aus den Jahren 1964—1968 stammt. Schon hieraus folgt, daß man es hier mit einem in der Tat auch die neuesten Ergebnisse in Betracht ziehenden Werk zu tun hat, und es ist sehr erfreulich, daß der Verlag durch die rasche Veröffentlichung dazu beigetragen hat, daß das Werk seine Aktualität nicht verlor.

Abgesehen vom letzten Kapitel (»Carben-Analoge«), welches der Verfasser absichtlich recht kurz gehalten hat (da es sich um ein bereits fast selbständiges Arbeitsgebiet handelt), kann man das Werk als eine sehr ausführliche und ausgezeichnete Monographie bezeichnen, an Hand welcher sich der Leser nicht nur eine erste Einführung in das Material, sondern auch ein recht tiefes Wissen auf dem Gebiet der Carbenchemie verschaffen kann. Dies ist ohne Zweifel ein bedeutendes Positivum, andererseits jedoch ist der Rezensent nicht ganz überzeugt davon, daß die Fülle des gebotenen Materials (insbesondere des Tatsachenmaterials) für einen durchschnittlichen Studenten nicht doch zuviel sein wird und das Buch daher nicht etwas abschreckend wirken könnte. Sollten sich diese Befürchtungen des Rezensenten bestätigen, so wird dieses sonst ausgezeichnete Büchlein das w. o. zitierte Ziel, welches der ganzen Serie gesetzt worden ist, nicht leicht erfüllen können.

Der Druck des Buches und seine Ausstattung sind recht gut, das Buch läßt sich sehr gut lesen, die Formeln sind klar. Leider finden sich dagegen im Text verhältnismäßig viele Druckfehler. (Vom Verlag Chemie ist man daran nicht gewöhnt.) Vielleicht hängt dies mit der kurzen Durchlaufszeit zwischen Abgabe des Manuskriptes und der Veröffentlichung des Buches zusammen. Die meisten Druckfehler erschweren das Verstehen des Textes kaum, aber in einer nächsten Ausgabe sollten sie dennoch unbedingt korrigiert werden. Ganz besonders bezieht sich diese Bemerkung auf die anschließend aufgezählten Stellen.

S. 34, zweites Formelschema: in der Formel des Dideuteromethylens sowie des Dideuterotrimethylen-Diradikals fehlt je ein Elektron und dasselbe gilt für die erste Grenzformel des Dideuteroallyl-Radikals;

S. 47, zweites Formelschema: auch hier fehlt wieder ein Elektron, nämlich aus der zweiten Grenzformel des Methallyl-Radikals-^{14}C;

S. 61, erstes Formelschema: in der letzten Formel sollte der Phenylrest durch einen Alkoxycarbonyl-Rest ersetzt werden;

S. 65, Zeile 10 von unten: statt $BrCl_2$, CCH_2Cl müßte es $BrCl_2CCH_2Cl$ heißen;

S. 181, zweites Formelschema: im Ausgangsmaterial müßte es an Stelle von $\ldots = CR'' \ldots = CR''_2$ heißen und im Produkt sollten am C–4 Atom des 3-Oxa-bicyclo-[3,1,0] hexan-Gerüstes zwei R′, am C–6 Atom dagegen zwei R″ Reste haften, nicht je ein R′ und R″ Rest an beiden Stellen;

S. 238, Zeile 10 und 16: statt Äthoxycarbonyl*carben* müßte es Äthoxycarbonyl*nitren* heißen;

S. 242, unterstes Formelschema: die Hälfte der Formel des Reagens R_3P ist »abgeschnitten«.

Zusammenfassend kann der Rezensent die «Carbene, Carbenoide und Carbenanaloga« von Professor KIRMSE allen denjenigen Kollegen empfehlen, die sich für dieses spezielle Teilgebiet interessieren und sich darin vertiefen möchten.

K. LEMPERT

A. D. CROSS and R. A. JONES: *An Introduction to Practical Infrared Spectroscopy*. Third Edition, Butterworths, London, 1969

Doubtlessly not only the review-writer, but all infrared spectroscopists will welcome the third, revised and significantly enlarged edition of CROSS' book which appears with the co-authorship of Dr. R. A. JONES. The main merit of the book is its exceptionally succinct style — even the enlarged edition runs only to 100 pages — and the ease with which the reader can survey the most important group frequencies. These features distinguish this work among the countless uninteresting treatises on the subject of infrared spectroscopy and render the book absolutely necessary.

The book is divided into two parts. The first part containing 60 pages treats with utmost brevity the application possibilities of infrared spectroscopy (rather listing these possibilities than giving details), the most widespread types of instruments (providing in tabular form almost all of their characteristics; the manufacturer's name and country, price, dimensions, main parts; light source, dispersion device, detector, etc., the characteristics of the spectral record: size, linearity, abscissa and ordinate scale, etc., measuring ranges, resolving power, reproducibility, accuracy, etc.), and the different techniques applied in practical spectroscopy.

It devotes a few pages to the theory of infrared spectroscopy, quantitative analytical applications and the possibilities of using infrared spectroscopy for studying association structures.

The chapter ending the first part runs to about 20 pages and illustrates the way in which spectra are interpreted, paying special attention to the structure elucidation role of information obtained by other spectroscopic techniques (NMR, UV, etc.). This is a special contribution to the present edition. There is a literature survey containing about 70 references attached to this chapter which covers all important books on infrared up to 1967.

The second part commences with a set of "maps" illustrating the analytical infrared range (3700—600 cm^{-1}), as divided into five sub-ranges. These contain the characteristic absorption domains of the most frequent functional groups, arranged according to the wavenumber values. These maps render feasible the quick survey of alternative assignment possibilities for a given absorption band of significance.

This part is concluded by a reciprocal scale for the quick interconversion of wavenumbers and wavelengths (although this is nowadays slightly obsolete), a literature list of 12 references and a subject index of 2 pages.

The middle 25 pages of the second part represent the most interesting section of the book. They present the appearance ranges of the characteristic bond- and group frequencies of different types of compounds as classified according to functional groups, together with the wavenumber and wavelength limits, and indications of relative intensities and occasional peculiarities of the spectral bands. These carefully compiled correlation tables, keeping dependability in view, are of great help, indeed, in the interpretation of the spectra. This part has also been significantly enlarged in the new edition, partly by corrections of obsolete data and by including new tables containing mainly the characteristic frequencies of heteroaromatic compounds. The brief explanations appended to the tables, which appear first in this edition, are also contributing to the practical value of this work.

In conclusion, the book should prove a useful reading material both for students and beginners (mainly the first part), and for infrared experts as well (due to the correlation tables in the second part).

P. SOHÁR

INDEX

PHYSICAL CHEMISTRY — PHYSIKALISCHE CHEMIE — ФИЗИЧЕСКАЯ ХИМИЯ

ORGANIC CHEMISTRY — ORGANISCHE CHEMIE — ОРГАНИЧЕСКАЯ ХИМИЯ

Printed in Hungary

A kiadásért felel az Akadémiai Kiadó igazgatója — Műszaki szerkesztő: Farkas Sándor

A kézirat nyomdába érkezett: 1969. X. 7. — Terjedelem: 10,75 (A/5) ív, 78 ábra

70.68408 Akadémiai Nyomda, Budapest — Felelős vezető: Bernát György

The AALC collection, including approx. 5500 punched cards gives the individual the advantages of modern data processing, without the need for expensive machines.

The advantages of cards!

The AALC collection of cards offers many advantages to its user. First, because only a card-file can be kept complete and up-to-date at any time. Book-form bibliographies are difficult to handle and are not apt for cross-indexing. Secondly with a card-file you do not have to make personal notes. If you wish to retain items of information from a book-bound bibliography, you cannot avoid noting them down (if you don't want to tear out the relevant pages!); with the AALC-file, however, you can indulge in the luxury of picking out the cards you are looking for.

The advantages of p u n c h e d cards!

By having the AALC collection on *punched* cards, you never have to replace cards in any particular order. Through the selection operation the cards you are looking for fall unerringly from the whole pack, irrespective of the place they occupy in the card-file. Using simple methods, you can collect all the cards that are particularly important for the topical field you are engaged in at a given time. A punched card file allows any questions to be combined according to the nature of your problem: it allows cross-indexing as well.

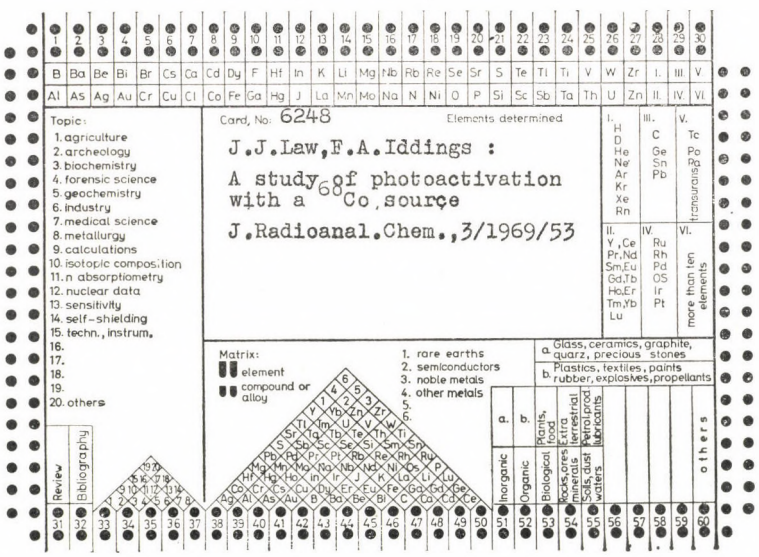

AALC—File
ACTIVATION
ANALYSIS
LITERATURE
CARDS
1935—1968

Unslotted:
US$ 0.05/card

Slotted:
US$ 0.06/card

IN PREPARATION

Ask for leaflets at the following address

AKADÉMIAI KIADÓ

Publicity Department, Budapest 502. P.O.B. 24

ACTIVATION ANALYSIS DOCUMENTATION CENTER

AKADÉMIAI KIADÓ

PUBLISHING HOUSE OF THE HUNGARIAN ACADEMY OF SCIENCES

ACTA CHIMICA

ТОМ 63 — ВЫП. 2

РЕЗЮМЕ

Изучение сольватации хлорида железа (II) с помощью эффекта Мёссбауэра

К. БУРГЕР, А. ВЕРТЕШ и И. Н. ЦАКО

Измерялись параметры Мёссбауэра для $FeCl_2$, $FeSO_2$ и $FeCl_3 \cdot 4H_2O$ в различных органических растворителях. На основе измерений, проведенных при температуре жидкого воздуха, было установлено, что параметры Мёссбауэра позволяют получить информацию относительно строения и состава сольватной оболочки.

Изучение сольватации хлорида железа (II) в смесях метанол-формамид с помощью метода Мёссбауэра

А. ВЕРТЕШ, К. БУРГЕР и Л. ШУБА

Снимались спектры Мёссбауэра $FeCl_2$, растворенного в смесях метанол-формамид, ри температуре жидкого азота.

Было показано, что два различных типа сольватированных частиц железа находятся равновесии в замороженных растворах.

Полуэмпирический метод приблизительного расчета паро-жидкостных равновесий бинарных смесей спирт-углеводород

Ф. РАТКОВИЧ и Л. МЕСАРОШ

Описывается полуэмпирический метод расчета параметров паро-жидкостных равновесий смесей спирт-углеводород. В методе используется в качестве сравнительной системы смесь спиртового компонента рассчитываемой смеси с каким-либо другим углеводородом. При знании свойств смеси, взятой за основу сравнения, могут быть рассчитаны данные паро-жидкостных равновесий бинарных смесей данного спирта с любым другим углеводородом, если известен параметр растворения углеводорода по Гильдебранду. Погрешность расчетных данных не превышала в изученных случаях $\pm$ 3 мол.% или $\pm$ 7 торр. Авторы предлагают данный метод для определения исходных данных, необходимых для расчета многокомпонентных смесей спирт-углеводород (постоянные Вильсона для бинарных смесей).

Электронографическое исследование строения молекулы $(CH_3)_2NSON(CH_3)_2$

И. ХАРГИТТАИ и Л. В. ВИЛКОВ

Электронографическим сектор-микрофотометрическим методом было исследовано строение молекулы $(CH_3)_2NSON(CH_3)_2$. С помощью метода наименьших квадратов были получены следующие длины связей и валентные углы:

r(C—H)	1.103 ± 0.008	Å
r(C—N)	1.460 ± 0.008	Å
r(S—O)	1.480 ± 0.009	Å
r(S—N)	1.693 ± 0.004	Å
∢ HCN	110.7 ± 1.6°	
∢ SNC	116.1 ± 0.5°	
∢ CNC	113.9 ± 1.5°	
∢ NSN	96.9 ± 1.2°	
∢ OSN	105.5 ± 0.8°	

Три формы внутреннего вращения оказались наиболее вероятными. Некоторые проблемы стереохимии атомов серы и азота были обсуждены. В частности, сопоставление данных о конфигурации атома азота в кремний-, фосфор-, серо- и хлор-производных сделало возможным предсказать геометрическую конфигурацию атома азота в некоторых неизученных серо- и хлор-производных.

Изучение тетраэдрически координированных ионов Cu^{+2} в Cu(1-бензазо--N-фенил-2-нафтиламин)$_2$, с помощью электронного парамагнитного резонанса

А. РОКЕНБАУЭР

Измерялись спектры электронного резонанса Cu(1-бензазо-N-фенил-2-нафтиламин)$_2$ в диамагнитно разбавленных поликристаллических образцах. На основе анализа спектров были получены следующие параметры:

$$g_{II} = 2{,}168 \pm 0{,}005, g_{\perp} = 2{,}040 \pm 0{,}005;$$

$$/A_{II}/ = (123 \pm 5) \cdot 10^{-4}\ см^{-1},\ /A_{\perp}/ \leq 20 \cdot 10^{-4}\ см^{-1}.$$

Эти значения, по-видимому, указывают на то, что четыре атома азота в указанном комплексе образуют четырехугольную плоскость, а не тетраэдр, как полагалось ранее по химическим соображениям. Это противоречие однако объяснялось тем, что значения спектральных параметров, в случае значительного тетрагонального искажения, нельзя отличать от значений параметров, характерных для случая расположения атомов азота в одной плоскости. Сильное искажение, соответствующее значениям измеренных параметров, обосновывалось гибкостью молекулы лиганда.

Крайние значения силовых постоянных и средних амплитуд колебаний молекул этилена и его тетрагалогензамещенных, I

C_2H_4 и C_2D_4

Г. ФОГАРАШИ и П. МЕЗЕИ

Изучая в качестве моделей независимо друг от друга молекулы C_2H_4 и C_2D_4, с помощью параметрического метода, предложенного Пулаи и Тёрёкем, был рассчитан многочисленный ряд силовых постоянных, репродуцирующих экспериментальные частоты нормальных колебаний, и средних амплитуд колебаний. Согласно нашему опыту, в случае, если в качестве экспериментальных данных в распоряжении имеются лишь нормальные частоты, силовые постоянные могут принимать совершенно нереальные значения, но несмотря на это, и в данном случае можно получить полезные сведения о силовом поле, изучая его крайние значения. Изучая амплитуды колебаний в очень широком интервале силовых постоянных, результаты в каждом случае отличаются от данных, полученных электрондиффракционным методом, что указывает на неопределенность последних.

Многослойная адсорбция смеси жидкостей, II

Й. ТОТ

Было подробно доказано, что термодинамические проблемы, возникающие вследствие исключительного использования модели однослойной адсорбции, могут быть разрешены с помощью термодинамической интерпретации многослойной адсорбции, равнозначной однослойной (м.р.о.-адсорбция). Было сделано заключение о том, что распределение концентрации в поверхностной фазе, устанавливающейся в результате м.р.о.-адсорбции, по характеру может быть подразделено на две группы, что находится в согласии с положением о конкретных свойствах конкретных адсорбционных систем. К первой группе относится такое распределение, которое обеспечивает непрерывный перепад концентрации между поверхностной и внутренней фазой. В этом случае концентрация в каждом слое поверхностной фазы больше, чем во внутренней фазе, но с уменьшающейся тенденцией (положительная-положительная адсорбция). Согласно другой возможности, в слоях поверхностной фазы устанавливается адсорбция с противоположными знаками (положительная-отрицательная адсорбция). Объясняя выше указанными причинами экспериментальные данные, сообщаемые в литературе, была дана общая интерпретация касательно того, почему в данном случае происходит многослойная адсорбция, которая в конечном итоге однозначна мономолекулярной адсорбции.

Полярографическое исследование цитостатических производных маннитола, II

Дальнейшие исследования с этилениминовыми производными «Дегранола»

Б. ЯМБОР

Производились дальнейшие полярографические исследования для выяснения того, что полярограммы 1,6-этиленимино-маннитола (II) и его изопропилиден-производного (I), изученного в предыдущем сообщении, одинаковы ли по характеру. Ответ на этот вопрос, с большой степенью вероятности, положителен и основывается на следующих заключениях:

1. Высота волны прямо пропорциональна концентрации деполяризатора, корню квадратному от высоты ртутного столбца и не зависит от емкости буфера.

2. Температурный коэффициент высоты волны при 15° С равен приблизительно 3%/° С, а выше 35° С колеблется в пределах теоретического значения, справедливого для диффузионной ступени, однако, он трудно определим.

3. При 50° С и в нейтральной среде в то время как высота волны первого вещества быстро уменьшается, высота волны второго вещества уменьшается лишь медленно.

4. С добавлением желатина высота волны не изменяется, а величина π 1/2 сдвигается в отрицательном направлении.

5. Оба соединения реагируют с одинаковой скоростью с тиосульфатом, образуя при этом соединение, дающее полярограмму. Для полного завершения реакции необходимо 3 часа, в противоположность этиленимониевым соединениям, которые реагируют моментально.

6. Высота волны для обоих соединений при комнатной температуре в слегка кислых средах уменьшается быстро, а в щелочных средах со скоростью в 3 раза ниже.

7. Высота волны в случае обоих соединений с увеличением pH и в слегка щелочных средах уменьшается или исчезается. Точка перегиба, как в случае I, так и в случае II, лежит около pH = 8.

Полярографическое исследование цитостатических производных маннитола, III

Дегранол

Б. ЯМБОР

С точки зрения параметров, рассматриваемых при всех исследованиях, наблюдалась полная идентичность (в пределах экспериментальной погрешности) — полярографического поведения соединения, образующегося в щелочных средах из «Дегранола» и соответствующего этилениминового соединения.

Сравнение и идентификация производились на основе влияния температуры, высоты ртутного столбца, влияний желатина, концентрации буфера и деполяризатора, а также на основе реакции с тиосульфатом. На основе исследований было заключено, что полярограмма, в первую очередь, носит диффузионный характер, смешанный с некоторым кинетическим характером и каталитическим влиянием, но последнее наблюдается лишь на участке после скачка.

Вопрос о том, что образуется ли бис-этилениминовое соединение и в физиологических условиях из «Дегранола», остается открытым.

Использование амидхлоридов в реакциях циклизации, I

З. ЧЮРЁШ, Р. ШООШ, Й. ПАЛИНКАШ и И. БИТТЕР

Амидхлориды, образующиеся под действием фосгена на дизамещенные амиды кислот, подвергались взаимодействию с метилантранилатом. Таким образом, из образующихся в данной реакции гидрохлоридов тризамещенных амидинов были получены производные 4/3*H*/-хиназолинона и алкилен-*бис*-3,3'-4/3*H*/-хиназолинона. В качестве агентов циклизации использовались ароматические и алифатические первичные амины, гидразин, фенилгидразин, аминокислоты и алкилендиамины. Изучался механизм циклизации и предлагается возможный путь реакции.

The Acta Chimica publish papers on chemistry in English, German, French and Russian.

The Acta Chimica appear in volumes consisting of four parts of varying size, 4 volumes being published a year.

Manuscripts should be addressed to

Acta Chimica
Budapest 112/91 Műegyetem

Correspondence with the editors should be sent to the same address.

Orders may be placed with "*Kultura*" Foreign Trade Company for Books and Newspapers (Budapest I., Fő utca 32. Account No. 43-790-057-181) or with representatives abroad.

Les Acta Chimica paraissent en français, allemand, anglais et russe et publient des mémoires du domaine des sciences chimiques.

Les Acta Chimica sont publiés sous forme de fascicules. Quatre fascicules seront réunis en un volume (4 volumes par an).

On est prié d'envoyer les manuscrits destinés à la rédaction à l'adresse suivante:

Acta Chimica
Budapest 112/91 Műegyetem

Toute correspondance doit être envoyée à cette même adresse.

On peut s'abonner à l'Entreprise pour le Commerce Extérieur de Livres et Journaux «*Kultura*» (Budapest I., Fő utca 32. Compte-courant No. 43-790-057-181) ou à l'étranger chez tous les représentants ou dépositaires.

«*Acta Chimica*» издают трактаты из области химической науки на русском, французском, английском и немецком языках.

«*Acta Chimica*» выходят отдельными выпусками разного объема. 4 выпуска составляют один том. 4 тома публикуются в год.

Предназначенные для публикации рукописи следует направлять по адресу:

Acta Chimica
Budapest 112/91 Műegyetem

По этому же адресу направлять всякую корреспонденцию для редакции.

Заказы принимает предприятие по внешней торговле книг и газет «*Kultura*» (Budapest I., Fő utca 32. Текущий счет № 43-790-057-181) или его заграничные представительства и уполномоченные.

Reviews of the Hungarian Academy of Sciences are obtainable at the following addresses:

ALBANIA

Ndermarja Shtetnore e Botimeve
Tirana

AUSTRALIA

A. Keesing
Box 4886, GPO
Sydney

AUSTRIA

Globus Buchvertrieb
Salzgries 16
Wien I

BELGIUM

Office International de Librairie
30, Avenue Marnix
Bruxelles 5
Du Monde Entier
5, Place St. Jean
Bruxelles

BULGARIA

Raznoiznos
1, Tzar Assen
Sofia

CANADA

Pannonia Books
2, Spadina Road
Toronto 4, Ont.

CHINA

Waiwen Shudian
Peking
P. O. B. 88

CZECHOSLOVAKIA

Artia
Ve Smečkách 30
Praha 2
Poštová Novinová Služba
Dovoz tisku
Vinohradská 46
Praha 2
Mad'arská Kultura
Václavské nám. 2
Praha I
Poštová Novinová Služba
Dovoz tlače
Leningradská 14
Bratislava

DENMARK

Ejnar Munksgaard
Nörregade 6
Copenhagen

FINLAND

Akateeminen Kirjakauppa
Keskuskatu 2
Helsinki

FRANCE

Office International de Documentation et Librairie
48, rue Gay Lussac
Paris 5

GERMAN DEMOCRATIC REPUBLIC

Deutscher Buch-Export und Import
Leninstraße 16
Leipzig 701
Zeitungsvertriebsamt
Fruchtstrasse 3—4
1004 Berlin

GERMAN FEDERAL REPUBLIC

Kunst und Wissen
Erich Bieber
Postfach 46
7 Stuttgart S.

GREAT BRITAIN

Collet's Subscription Import Department
Dennington Estate
Wellingborough. Northants.
Robert Maxwell and Co. Ltd.
Waynflete Bldg. The Plain
Oxford

HOLLAND

Swetz and Zeitlinger
Keizersgracht 471—487
Amsterdam C.
Martinus Nijhof
Lange Voorhout 9
The Hague

INDIA

Current Technical Literature Co. Private Ltd.
India House OPP
GPO Post Box 1374
Bombay I

ITALY

Santo Vanasia
Via M. Macchi 71
Milano
Libreria Commissionaria Sansoni
Via La Marmora 45
Firenze

JAPAN

Nauka Ltd.
92, Ikebukur O-Higashi 1-chome
Toshima-ku
Tokyo
Maruzen and Co. Ltd.
P. O. Box 605
Tokyo-Central
Far Eastern Booksellers
Kanda P. O. Box 72
Tokyo

KOREA

Chulpanmul
Phenjan

NORWAY

Johan Grundt Tanum
Karl Johansgatan 43
Oslo

POLAND

Ruch
ul. Wronia 23
Warszawa

ROUMANIA

Cartimex
Str. Aristide Briand 14—18
Bucureşti

SOVIET UNION

Mezhdunarodnaya Kniga
Moscow G—200

SWEDEN

Almquist and Wiksell
Gamla Brogatan 26
Stockholm

USA

Stechert Hafner Inc.
31, East 10th Street
New York, N. Y. 10003
Walter J. Johnson
111, Fifth Avenue
New York, N. Y. 10003

VIETNAM

Xunhasaba
19, Tran Quoc Toan
Hanoi

YUGOSLAVIA

Forum
Vojvode Mišića broj 1
Novi Sad
Jugoslovenska Knjiga
Terazije 27
Beograd

31. I. 1970

Index: 26.007

ACTA CHIMICA

ACADEMIAE SCIENTIARUM HUNGARICAE

TOMUS 63 FASCICULUS 3

AKADÉMIAI KIADÓ, BUDAPEST

1970

ACTA CHIM. ACAD. SCI. HUNG.

ACTA CHIMICA

A MAGYAR TUDOMÁNYOS AKADÉMIA KÉMIAI TUDOMÁNYOK OSZTÁLYÁNAK IDEGEN NYELVŰ KÖZLEMÉNYEI

Az Acta Chimica német, angol, francia és orosz nyelven közöl értekezéseket a kémiai tudományok köréből.

Az Acta Chimica változó terjedelmű füzetekben jelenik meg, egy-egy kötet négy füzetből áll. Évente átlag négy kötet jelenik meg.

A közlésre szánt kéziratok a szerkesztőség címére (Budapest 112/91 Műegyetem) küldendők.

Ugyanerre a címre küldendő minden szerkesztőségi levelezés. A szerkesztőség kéziratokat nem ad vissza.

Megrendelhető a belföld számára az „Akadémiai Kiadó"-nál (Budapest V., Alkotmány utca 21. Bankszámla 05-915-111-46), a külföld számára pedig a „Kultura" Könyv- és Hírlap Külkereskedelmi Vállalatnál (Budapest I., Fő utca 32. Bankszámla: 43-790-057-181) vagy annak külföldi képviseleteinél és bizományosainál.

Die Acta Chimica veröffentlichen Abhandlungen aus dem Bereiche der chemischen Wissenschaften in deutscher, englischer, französischer und russischer Sprache.

Die Acta Chimica erscheinen in Heften wechselnden Umfanges. Vier Hefte bilden einen Band. Jährlich erscheinen 4 Bände.

Die zur Veröffentlichung bestimmten Manuskripte sind an folgende Adresse zu senden:

Acta Chimica
Budapest 112/91 Műegyetem

An die gleiche Anschrift ist auch jede für die Redaktion bestimmte Korrespondenz zu richten.

Bestellbar bei dem Buch- und Zeitungs-Außenhandels-Unternehmen »*Kultura*« (Budapest I., Fő utca 32. Bankkonto No. 43-790-057-181) oder bei seinen Auslandsvertretungen und Kommissionären.

Acta Chimica Academiae Scientiarum Hungaricae, Tomus 63 (3), pp. 237—241 (1970)

THE INTERACTION OF THE $[PtCl_4]^{2-}$ and K^+ IONS IN THE K_2PtCl_4 CRYSTAL ON THE BASIS OF ITS INFRARED SPECTRUM

F. TÖRÖK

(Institute of General and Inorganic Chemistry, L. Eötvös University, Research Group for Inorganic Chemistry of the Hungarian Academy of Sciences, Budapest)

Received May 27, 1968

The force constants compatible with normal frequencies of the K_2PtCl_4 crystal have been calculated without and with taking into consideration the coupling with the lattice vibrations. Our calculations, made with the method of the parameter representation of force constants, show that the coupling can essentially alter the force field of the complex ion. Applying the parameter method useful informations can be obtained on the possible changes in force constants owing to the coupling.

The atoms of the $[PtCl_4]^{2-}$ are placed at vertices of a quadrate, accordingly the ion belongs to the point group D_{4h}. The normal frequencies are divided among the following species:

$$A_{1g} + B_{1g} + B_{2g} + A_{2u} + 2E_u$$

The normal frequencies of the first 3 species are only Raman active, those belonging to the species A_{2u} and E_u appear only in the infrared spectrum, while the B_{1u} frequency is inactive, it cannot be observed in either spectrum.

The vibrations of the K_2PtCl_4 crystal are to be discussed on the basis of the corresponding space group: D^1_{4h}(P4/mm) [1, 2]. The symmetry elements of the space group are made up partly of the operators of the translation group, partly of those of the symmetry group of the unit cell [2]. In the unit cell one $[PtCl_4]^{2-}$ and two K^+ ions can be found. The unit cell, the numbering of atoms and the axes of the Descartes coordinates are shown in Fig. 1. In the harmonic approximation the selection rules for the vibrations of the complex ion are unchanged also in the K_2PtCl_4 crystal, but besides the vibrations of the complex ion also the lattice vibrations must be taken into consideration. The lattice vibrations belong to the following species:

$$A_{2g} + E_g + A_{2u} + B_{2u} + 2E_u.$$

The vibrations of B_{2u} and A_{2u} are inactive, that of E_g is Raman active, the vibrations of E_{2u} and A_{2u} are infrared active.

As far as we know the Raman spectrum of the crystal has not yet been published. The Raman spectrum of $[PtCl_4]^{2-}$ ion was determined by STAMMREICH and FORNERIS [3], their results are summarized in Table I.

Table I

Vibration	Species	Frequency (cm^{-1})
Pt—Cl sym. stretch	A_{1g}	335
Cl Pt Cl sym. def.	B_{1g}	164
Pt—Cl asym. stretch	B_{2g}	304

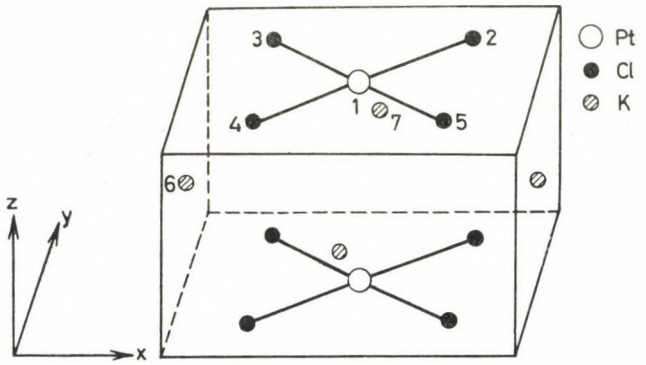

Fig. 1

The infrared spectrum of K_2PtCl_4 crystal has been studied by several authors [4, 5, 6]. In Table II the frequencies and assignment accepted by HIRAISHI and SHIMANOUCHI [6] are shown.

Table II

Vibration	Species	Frequency (cm^{-1})
Pt—Cl asym. stretch.	E_u	325
Cl Pt Cl asym. def	E_u	190
Translational lattice	E_u	116
Translational lattice	E_u	90
$PtCl_4$ out of plane	A_{2u}	170
Translational lattice	A_{2u}	103

The force constants of $[PtCl_4]^{2-}$ ion have been calculated by STAMMREICH and FORNERIS on basis of its Raman spectrum [3]. From the infrared frequencies HIRAISHI and SHIMANOUCHI have determined the UREY-BRADLEY force constants [6]. Besides the Raman frequencies of the solution also the infrared frequencies have been taken into consideration by SABATINI, SACCONI and SCHETTINO [5], but in their calculations the lattice vibrations have been

neglected, and they considered the vibrations of the complex ion as independent from the lattice vibrations. According to the opinion of HIRAISHI and SHIMANOUCHI, it was because of this neglection that the measured frequencies were reproduced by applying the UREY-BRADLEY force constants in a rather poor approximation.

In this paper the possible values of force constants of species A_{2u} and E_u are investigated and compared with each other in two cases:

1. The vibrations of the complex ion are considered independently from the lattice vibrations,

2. The vibrations of the complex ion and those of the lattice are discussed together.

The symmetry coordinates are the following:

$$
\begin{aligned}
A_{2u}: \quad & S_1 = 1/2\,(\varphi_2 + \varphi_3 + \varphi_4 + \varphi_5) \\
& S_2 = 1/\sqrt{2}\,(z_6 + z_7) \\
E_u: \quad & S_3 = 1/1\,(r_2 - r_3 - r_4 - r_5) \\
& S_4 = 1/\sqrt{2}\,(\Phi_{34} - \Phi_{25}) \\
& S_5 = x_6 \\
& S_6 = x_7
\end{aligned}
$$

Here $\varphi_2, \varphi_3, \varphi_4, \varphi_5$ designate the out of plane vibrations, r_i means the stretching of the ith bond, and Φ_{ik} characterizes the deformation of $Cl_i \diagdown Pt \diagup Cl_k$ angle. The matrices G and F are constructed according to SHIMANOUCHI's method for crystals. The matrix G is partitioned into two blocks, one corresponding to the K^+ ions and the other to the complex ion in both A_{2u} and E_u species. The meaning of the elements of matrix F is somewhat more complicated because several of them correspond not only to interactions within a cell but also between cells. In our work these interactions have not been separated, because our aim is to demonstrate how the force constants of the complex ion can be modified by the coupling with the lattice vibrations.

In our previous paper [8] we have dealt with the forming matrices F belonging to a given assignment.

According to this method the matrices F of A_{2u} belonging to the given assignment have been calculated and the force constants as a function of the angle parameter (defined in our paper [8]) are shown in Table III. At the parameter value $\alpha = 0$ there is no coupling between the out of plane vibrations of $[PtCl_4]^{2-}$ ion, and the lattice vibrations. In this case $F_{11} = 0.458$, $F_{22} = 0.253$. But if interactions are allowed, *i.e.* $F_{12} = 0$, F_{11} decreases, F_{22} increases. The amount of decrease or increase depends only on the absolute value of F_{12}. At the border of the assignment: $F_{11} = 0.313$, $F_{22} = 0.453$, $F_{12} = \pm 0.253$.

If the vibrations of the complex ion and those of the lattice are independent, the vibrations of the complex ion can be treated separately. In this case

Table III

Parameter	F_{11}	F_{12}	F_{22}
—0.25	0.313	—0.174	0.453
—0.20	0.357	—0.165	0.388
—0.15	0.398	—0.141	0.329
—0.10	0.430	—0.102	0.283
—0.05	0.450	—0.053	0.253
0.00	0.458	0.000	0.243
0.05	0.450	0.053	0.253
0.10	0.430	0.102	0.283
0.15	0.398	0.141	0.329
0.20	0.357	0.165	0.388
0.25	0.313	0.174	0.453

an F matrix of 2 dimensions is obtained, the possible elements of which belonging to the given assignment are shown in Table IV. When $\alpha = 0$ (*i.e.* at the point of the most expressed assignment [10]), the diagonal force constants are almost the same. When the coupling with the lattice vibrations is not neglected, the G and F matrices of E_u are of 4 dimensions. In this case all the matrices F compatible with the normal frequencies can be formed as function of 6 parameters. Therefore there is no practical possibility for constructing a table similar to Tables I and II. For this reason, to estimate the effect of the coupling with the lattice vibrations, in Table V a matrix F is shown in case of which the coupling is negligible. Starting from this position the maximum and

Table IV

Parameter	F_{33}	F_{34}	F_{44}
—0.25	0.980	—0.421	2.757
—0.20	1.156	—0.394	2.317
—0.15	1.344	—0.279	1.951
—0.10	1.495	—0.087	1.693
—0.05	1.625	0.162	1.570
0.00	1.709	0.445	1.593
0.05	1.741	0.734	1.760
0.10	1.716	1.001	2.005
0.15	1.638	1.219	2.448
0.20	1.514	1.367	2.902
0.25	1.356	1.431	3.372

minimum values (*i.e.* extreme values) of force constants were calculated by applying the parameter method described in our earlier paper [11]. From our results the following conclusions can be drawn:

Table V

1.614	0.135	0.010	0.010
	1.576	0.001	0.001
sym-		0.309	0.001
metric			0.186

The maximum values of F_{33} and F_{44} are not changing when the coupling with the lattice vibrations is taken into consideration. Thus F_{33} cannot be greater than 1.74. But the interaction with the lattice vibrations can essentially decrease these elements, *e.g.* F_{44} can be smaller than 1. The role and the values of F_{34} do not change to a great extent. The method, of course, gives also the change of force constants concerning the lattice vibrations as function of their coupling with the inner vibrations of the complex ion. As it is expected the elements F_{55} and F_{66} have their minimum values at the points in the neighbourhood of the situation given in Table V, when the off diagonal elements of F between lattice and complex ion vibrations are zeros. The diagonal elements of the lattice vibrations F_{55} and F_{66} have their maximum values at the border of the assignment when the coupling with the complex ion is essential and the interaction between the lattice vibrations themselves is small. The maximum values of both F_{55} and F_{66} are almost equal to 1. The extreme values of the element F_{56} coupling the lattice vibrations with themselves are ± 0.4. The maximum and minimum values of elements corresponding to the interaction between lattice and complex ion vibrations are 0.9 and —0.9, respectively.

The presented data clearly demonstrate that the force constants of the complex ion can be essentially altered by the coupling with the lattice vibrations.

REFERENCES

1. Theilacker, W.: Z. anorg. Chem. **234,** 161 (1937)
2. Bhagavantam, S., Venkatarayudu, T.: "Theory of groups and its application to physical problems" 2nd ed. Andkra University Waltair
3. Stammreich, H., Forneris, R.: Spectrochim. Acta **16,** 363 (1960)
4. Adams, D. M.: Spectrochim. Acta **19,** 925 (1963)
5. Sabatini, A., Sacconi, L., Schettino, V.: Inorg. Chem. **3,** 1775 (1964)
6. Hiraishi, J., Shimanouchi, T.: Spectrochim. Acta **22,** 1483 (1966)
7. Shimanouchi, T., Tsuboi, M.: J. Chem. Phys. **35,** 1597 (1964)
8. Török, F.: To be published in Acta Chim. Acad. Sci. Hung
9. Pulay, P., Török, F.: Acta Chim. Acad. Sci. Hung. **44,** 287 (1965)
10. Pulay, P.: Acta Chim. Acad. Sci. Hung. **57,** 373 (1968)
11. Török, F., Pulay, P.: Acta Chim. Acad. Sci. Hung. **56,** 285 (1968)

Ferenc Török; Budapest VIII., Múzeum krt. 6—8.

Acta Chimica Academiae Scientiarum Hungaricae, Tomus 63 (3), pp. 243—256 (1970)

THERMOGRAVIMETRIC AND IR SPECTROPHOTOMETRIC EVALUATION OF TG STEPS OF THERMAL DECOMPOSITIONS PRODUCING TWO GASES

A. B. Kiss

(Tungsram Research Laboratories, Budapest)

Received August 27, 1968

In the course of studies of thermal decomposition reactions with gaseous products, IR spectrophotometry was used in conjunction with thermogravimetry, for recording changes in the concentration of gaseous products. The thermal decomposition of ammonium paramolybdate and ammonium paratungstate has been studied and the concentration changes in the gas cell for evolved ammonia and water have been determined.

The possibilities of a combined quantitative evaluation of IR peaks and TG steps have been explored. When the initial ammonia and water content of the compounds tested is known the proportion in which gaseous products are released at individual TG steps can be determined from measured areas under the corresponding IR maxima.

A method is proposed for determining the contribution of gaseous products to the observed TG steps when the initial ammonia and water contents are not known.

The simultaneous evolution of gaseous products is associated with a weight loss $\Delta m = m_{(NH_3)} + m_{(H_2O)}$ at a given step. We have determined the quotient $\frac{m_{(NH_3)}}{m_{(H_2O)}}$ by means of IR peaks, from which the values for $m_{(NH_3)}$ and $m_{(H_2O)}$ can be found.

Earlier we have discussed how infrared spectrophotometry can be used in studying thermal decomposition reactions. If decomposition produces one or more gases, the continuous observation of the quantitative changes occurring in the gas above the solid phase can be carried out by means of infrared spectrophotometry [1, 2].

On the basis of infrared data on the gas phase combined with TG-curves, it is comparatively easy to assign the TG-steps to gases evolved, or to select reactions which may be responsible for the evolution of the observed gaseous products. Such measurements have been carried out on the thermal decomposition of ammonium paramolybdate and ammonium paratungstate where the amount of ammonia and water released or the equivalent quantity of acetylene, have been recorded continuously by infrared spectrophotometry [2]. We have determined the experimental conditions ensuring that the area of infrared peaks should be proportional to the amount of gas produced [2].

In this work, the possibilities of simultaneous quantitative evaluation of TG-curves and IR-maxima are described. It is necessary to recall that, as known, thermogravimetric data alone are insufficient for the determination of proportions in which two simultaneously evolved gaseous products contribute to the mass change at a given TG-step.

The present experiments indicate that continuous infrared spectrophotometry of gaseous products provides valuable data for solving the problem.

Experimental

The experiments have been performed with a thermobalance of the Chevenard system and an UR-10 type infrared spectrophotometer. Gas spectra were recorded using 10 cm gas cells with a capacity of 125 ml. The rate of the carrier gas (air) was kept on the desired level with a calibrated capillary manometer.

For concrete calculations, in this work too, ammonium paramolybdate (reagent grade Analar product, $3(NH_4)_2O \cdot 7MoO_3 \cdot 4H_2O$ m.w. 1235.96) and ammonium paratungstate ($5(NH_4)_2O \cdot 12WO_3 \cdot 5H_2O$, reagent grade Fluka product m.w. 3133.52) have been selected. According to X-ray diffraction tests, molybdate and tungstate showed the known heptamolybdate [3] and paratungstate [4] structures, their analyses were consistent with the above formulas. These two substances decomposed, via various intermediate phases, to the respective metal oxides, releasing ammonia and water vapour in the course of thermal decomposition.

In Figs 1 and 2, we present the thermogravimetric and infrared spectrophotometric results obtained with the above two test substances. Sample weights were 400 and 800 mg, the flow-rate of air was kept at 16.65 l/hr, and the rate of heating was 300 °C per hour. The reaction with calcium carbide was used for the determination of water [2], and changes in the concentration of acetylene and ammonia were recorded at 728.0 cm^{-1} and 965.0 cm^{-1}, respectively, *i.e.* at the most sensitive maxima.

The curves in Fig. 1 represent data recorded as a function of temperature and show that at all three steps of the TG-curves for molybdate, ammonia and water leave the system simultaneously. At the same time, Fig. 2 shows that, unlike in the case of molybdate, after the removal of water of crystallization at steps I and II, dry ammonia is also evolved at step III of the paratungstate. At steps IV and V, ammonia and water are again set free simultaneously.

We can obtain data suitable for quantitative determinations when, at given wave numbers, transmission *vs.* concentration (milligram substance per cell volume) calibration curves are recorded and the IR-maxima of Figs 1 and 2 are drawn, on the basis of the calibration curve, as functions of the linear millimetre-scale corresponding to the chart-speed (Figs 3 and 4).

It has been shown that the total area of the IR-peaks thus drawn is proportional to the sample weight for both components and that the areas of peaks corresponding to the individual steps are proportional to the amount

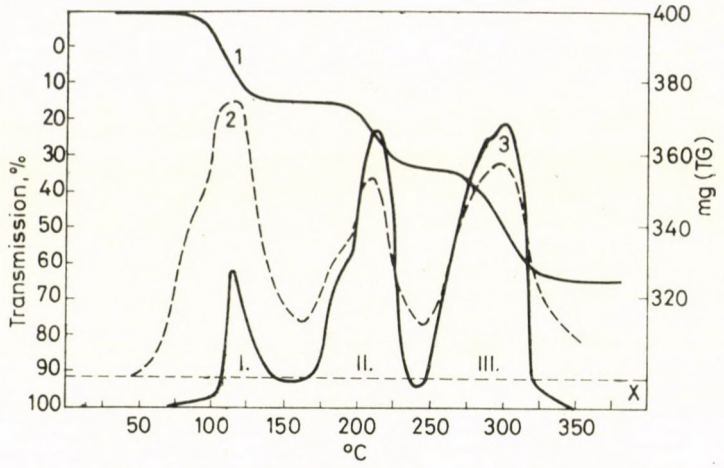

Fig. 1. Ammonium paramolybdate. Sample weight 400 mg. Flow rate 16.65 l/hr. Heating rate 300°/hr. 1. TG curve; 2. IR curve for H_2O (C_2H_2); 3. IR curve for NH_3; x = equilibrium moisture content of the carrier gas

of gas evolved on the sections under consideration [2]. For further studies, these plots will be used. In Fig. 5, the calibration curves for ammonia and acetylene are shown.

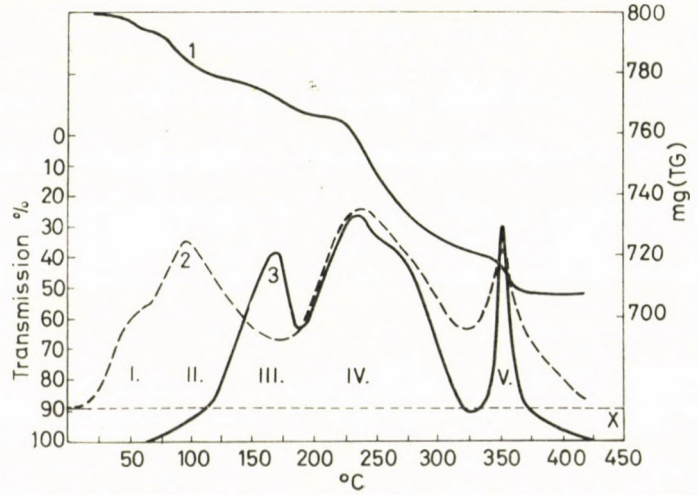

Fig. 2. Ammonium paratungstate. Sample weight 800 mg. Flow rate 16.65 l/hr. Heating rate 300°/hr. 1. TG curve; 2. IR curve for H_2O (C_2H_2); 3. IR curve for NH_3; x = equilibrium moisture content of the carrier gas

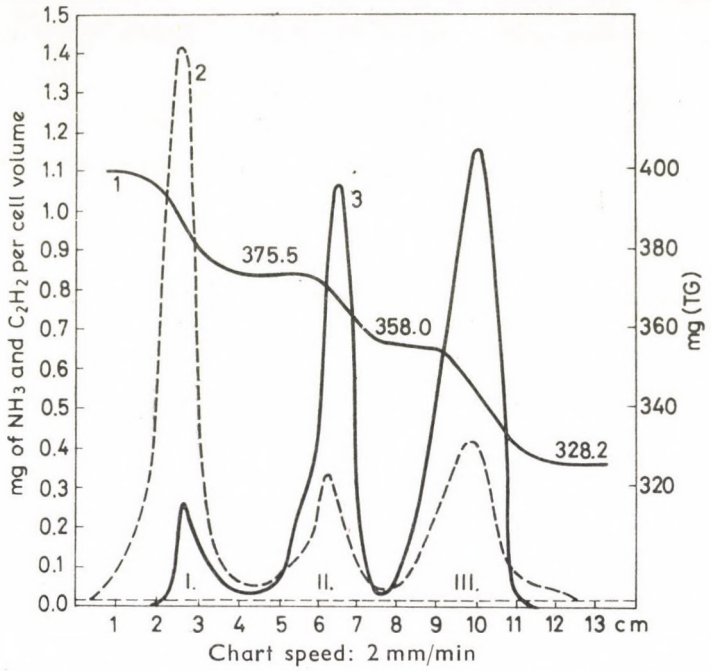

Fig. 3. Ammonium paramolybdate. T(I) = 12.4, T(II) = 67.0, T(III) = 107.0 NH_3; T(I) = = 94.0, T(II) = 23.8, T(III) = 41.0 H_2O; T(NH_3) total = 190.0, T(H_2O, *i.e.* C_2H_2) total = = 158.5; 1 $cm^2 \approx 6.15$ mg of paper ≈ 1.068 mg NH_3 and 1.582 mg H_2O

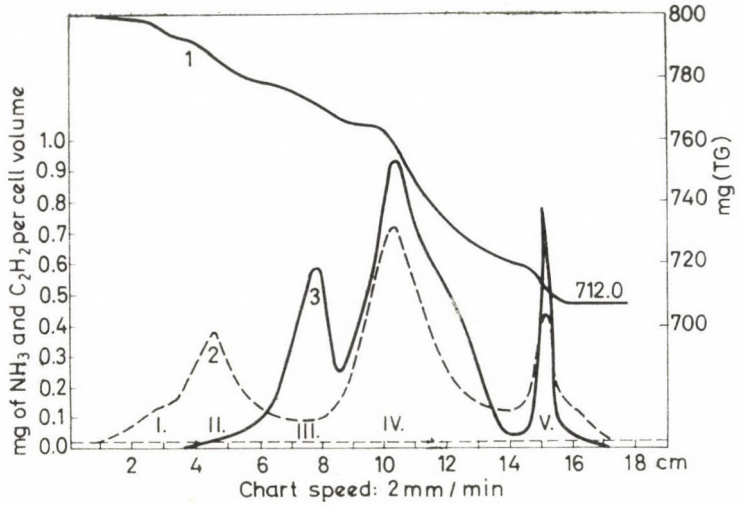

Fig. 4. Ammonium paratungstate. T(NH_3) total = 245.0, T(H_2O, *i.e.* C_2H_2) total = 178.0

Methods for the simultaneous quantitative evaluation of TG-curves and IR-maxima

On the basis of the known thermal decomposition pathway for ammonium paramolybdate [5—9], we intend to examine how the areas of the maxima in Fig. 3 are related to the calculated number of ammonia and water moles set free at individual TG-steps. The principal processes involved in the decomposition reaction are:

$$3\,(NH_4)_2O \cdot 7MoO_3 \cdot 4\,H_2O \xrightarrow{115-130^\circ C} 2\,(NH_4)_2O \cdot 5\,MoO_3 \longrightarrow$$

$$\xrightarrow{225-245^\circ C} 2\,(NH_4)_2O \cdot 8\,MoO_3 \xrightarrow{320-350^\circ C} Mo\,O_3$$

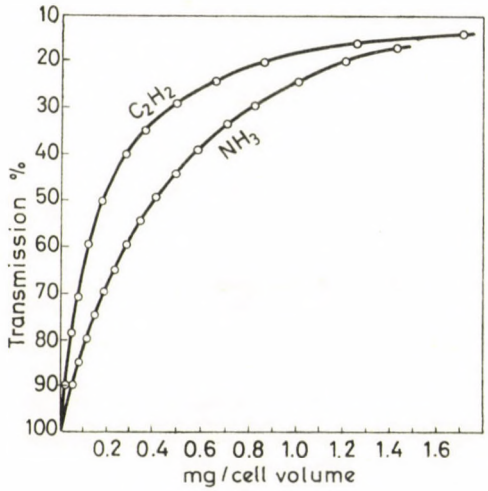

Fig. 5. Calibration curves

The number of moles of ammonia and water evolved at different TG-steps, calculated from the above equation yield the following proportions

$$0.4 : 2.1 : 3.5 = 1.0 : 5.25 : 8.75\ NH_3 \quad (1)$$

$$4.2 : 1.05 : 1.75 = 4.0 : 1.0 : 1.66\ H_2O \quad (2)$$

At the same time, gravimetric determinaton of areas under the corresponding maxima gives the following proportions

$$T(I)\ T(II)\ T(III)$$

$$12.4 : 67.0 : 107.0 = 1.0 : 5.4 : 8.62\ NH_3 \quad (3)$$

$$94.0 : 23.8 : 41.0 = 3.9 : 1.0 : 1.72\ H_2O \quad (4)$$

These data show that, within certain limits of experimental error, the areas under the IR peaks are in the same proportion as the quantities of gaseous products evolved at the individual TG-steps. From the proportion figures referring to IR peak areas, the absolute quantity of ammonia and water, evolved at each thermogravimetric step, can be determined if the initial sample weight and composition are known.

For example, let A mg be the total ammonia content in the initial compound of known composition, and let a_1, a_2 and a_3 stand for the quantities of ammonia evolved at the individual steps. Then

$$A = a_1 + a_2 + a_3 .$$

Since it is known that

$$a_1 : a_2 : a_3 = T(\mathrm{I}) : T(\mathrm{II}) : T(\mathrm{III}) ,$$

it follows that

$$a_1 = K \cdot T(\mathrm{I}),\ a_2 = K \cdot T(\mathrm{II}),\ a_3 = K \cdot T(\mathrm{III})$$

where

$$K = \frac{A}{T(\mathrm{I}) + T(\mathrm{II}) + T(\mathrm{III})} .$$

A is given by

$$A = \frac{n \cdot M(\mathrm{NH_3}) \cdot B}{M} .$$

In this equation, n is the number of moles of ammonia in the initial compound, $M(\mathrm{NH_3})$ is the millimolecular weight of ammonia, M is the millimolecular weight of the initial compound, and B is the sample weight in mg. These data are obtained for the other component in a similar way (water in the present case).

Using the experimental data in Fig. 3, one can compare the results obtained by the present method with those calculated theoretically from sample weight and reaction pathway (*cf.* Table I).

Table I

TG steps	$3(NH_4)_2O \cdot 7\,MoO_3 \cdot 4\,H_2O$					
	mg NH_3 evolved		% error	mg H_2O evolved		% error
	calcd.	found		calcd.	found	
I	2.20	2.20	—	24.2	24.4	+0.83
II	11.50	11.87	+2.77	6.12	6.14	+0.32
III	19.38	18.98	+2.22	10.20	10.20	—

According to the table, the agreement between experimental and theoretical values is satisfactory. This seems to indicate that this method may be suitable for the determination of the ratios in which various gaseous products contribute to a given TG-step.

From now on, let us suppose that the initial composition of the sample is not known. Of course, if the numerical value for A is not known, the data according to Table I cannot be calculated directly from IR peak area ratios on the basis of Eqs (3) and (4). The proportionality in these equations can be satisfied by any set of absolute values, so there is no way of performing actual calculations. However, should a TG-step be found for which infrared spectrophotometry furnishes unambiguous proof that the two gaseous products, *e.g.* ammonia and water, are released simultaneously, then for this step, the absolute quantities of the gaseous components can also be found. Such a step is observed in Figs 3 and 4. If the data for one TG step are known, from the proportionality expressed by Eq. (3) or (4) the corresponding data for the other steps can also be determined. Another possible method is that IR peak areas recorded for the unknown sample are calibrated with compounds of known ammonia and water contents, but there is a simpler method based on the following considerations.

In connection with the fundamental principle of the method, let us first examine various common and different properties of the gases from the point of view of how the nature of the gases affects the areas of IR peaks under otherwise identical conditions. The principle of the measurement is schematically illustrated in Fig. 6.

During the measurement, the carrier gas flows through the system at a constant pressure difference adjusted with the capillary manometer, and at sample holder *e* it is admixed with the gas to be measured; the mixture will then flow into the IR cell. The transmissions of various gases are recorded at the corresponding wave numbers $\lambda_1, \lambda_2, \lambda_3 \ldots \lambda_n$, where the molar absorptivities can be entirely different. As a further limitation, let us assume that there is no mutual interference by various gases at the wave numbers given. If transmission *vs.* concentration (*i.e.* mg per cell volume) data are recorded at each wave number, and the IR maxima recorded under the same experimental conditions are redrawn on this basis, and if we suppose that internal friction and flow characteristics do not change significantly from gas to gas, then at complete passage through the cell of the same molar quantity of each gas we can write

$$\frac{T_1}{M_1} = \frac{T_2}{M_2} = \frac{T_3}{M_3} \ldots \ldots \frac{T_n}{M_n} = K \text{ (constant)} \qquad (5)$$

where $T_1, T_2, T_3, \ldots T_n$ stand for the areas found from the calibration curves of various gases, and $M_1, M_2, M_3, \ldots M_n$ are the corresponding millimole-

cular weights. Thus, when the same molar quantities of gases are measured, the $\frac{T}{M}$ areas are equal.

If the flow characteristics of the gases are different (internal friction coefficients, etc.), the rates of concentration changes in the cell for the gases to be recorded will also be different even at a constant pressure drop for the carrier gas. There will be no laminar flow in the cell, there will be one gas that leaves the cell sooner than the other, though other conditions and the volume

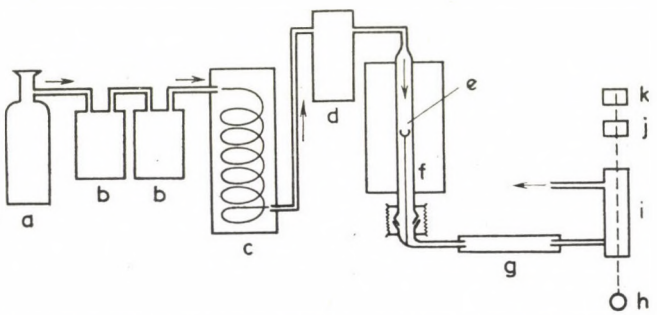

Fig. 6. Schematic diagram of the experimental apparatus. a) pressure cylinder (air); b) cold traps (acetone and dry ice); c) temperature control (ambient temperature); d) capillary manometer; e) sample holder; f) oven; g) calcium carbide reactor; h) IR source; i) IR gas cell; j) monochromator; k) detector

rate remain the same. Obviously, the peak area characteristic for the complete passage through the cell of one mole of the gas that is exchanged slower, will be greater than that for the gas with a lower internal friction.

In this case, equation (5) is valid only when the specific flow characteristics of the gases are taken into account, *i.e.* when the terms are made equal by multiplying them by a factor η.

$$\frac{T_1}{M_1}\eta_1 = \frac{T_2}{M_2}\eta_2 = \ \ldots\ \frac{T_n}{M_n}\eta_k = K \text{ (constant)}. \tag{6}$$

Nothing has been said about the value this factor can assume. This is a matter of convention, *i.e.* for one of the gases η may be set equal to unity and then for the other gases $\eta_k \gtrless 1$.

Now, we may return to the system which is the object of our study and where, during decomposition, gaseous ammonia and water are evolved. In the case of simultaneous evolution of the two reaction products, the loss of weight (Δm, mg) at a given TG step is the sum of the weights of the two components, *i.e.*

$$\Delta m = m_1 + m_2 .$$

Δm can be read directly from the TG curve, but the absolute values for m_1 and m_2 are unknown. However, the $\frac{m_1}{m_2}$ ratio can be calculated, if the IR peak areas of the gaseous components are known. Since the respective IR peak areas are proportional to the quantity of ammonia and water evolved, on the basis of considerations mentioned in connection with Eq. (6), one can write that

$$\frac{\frac{m_1}{M_1}}{\frac{m_2}{M_2}} = \frac{\frac{T_1}{M_1}\eta_1}{\frac{T_2}{M_2}\eta_2}, \quad i.e. \quad \frac{m_1}{m_2} = \frac{T_1 \cdot \eta_1}{T_2 \cdot \eta_2} \tag{7}$$

where subscripts 1 and 2 refer to ammonia and water, respectively.

However, it is not water but acetylene that is determined [2]. Considering that

$$CaC_2 + 2H_2O = Ca(OH)_2 + C_2H_2,$$

i.e. that 2 moles of water are equivalent to 1 mole of acetylene in this context, it is evident that recording of acetylene will produce only about half the area with respect to the denominator in Eq. (7). This area will not be exactly one half because the ratio is a function of η_2 and η_3, too. Consequently,

$$\frac{T_2}{M_2}\eta_2 = \frac{n_e \cdot T_3}{M_3}\eta_3 \tag{8}$$

where T_3, M_3, and η_3 have the same meaning as before but now refer to acetylene, and n_e is the theoretical ratio of the number of moles involved in the transformation reaction ($n_e = 2$).

With this substitution, we obtain

$$\frac{m_1}{m_2} = \frac{T_1 \cdot M_3 \cdot \eta_1}{n_e \cdot T_3 \cdot M_2 \cdot \eta_3}. \tag{9}$$

In a former communication we have shown that in the calcium carbide reactor used under the prevailing conditions, less than the theoretical amount of acetylene is generated by 2 moles of water, *viz.* 0.854 mole only [2]. Accordingly, Eq. (9) must be multiplied by β, a factor defined by the ratio of apparent and theoretical mole numbers,

$$\beta = \frac{n_e}{n_L}.$$

Hence

$$\frac{m_1}{m_2} = \frac{T_1 \cdot M_3 \cdot \eta_1}{n_c \cdot T_3 \cdot M_2 \cdot \eta_3} \beta = \frac{T_1 \cdot M_3}{n_L \cdot T_3 \cdot M_2} B = K \tag{10}$$

where

$$B = \frac{\eta_1}{\eta_3}, \quad \text{and} \quad n_L = \frac{2.0}{0.854} = 2.34 .$$

Hence

$$m_1 = \Delta m \frac{K}{K+1}, \quad \text{or} \quad m_2 = \Delta m \left(1 - \frac{K}{K+1}\right).$$

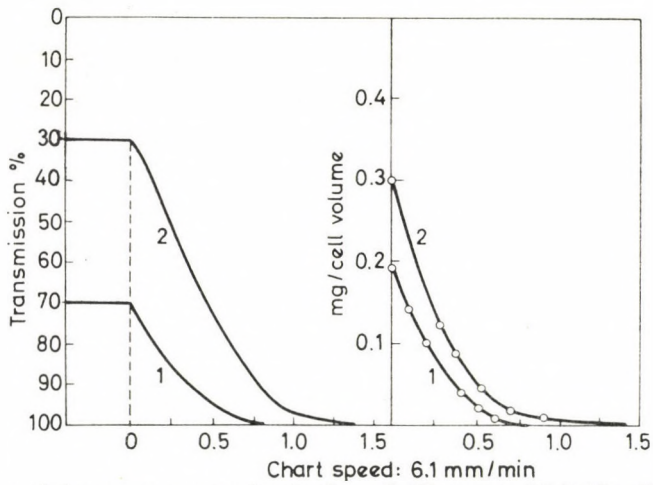

Fig. 7. Variation of the gas concentration in the cell. Flow rate 16.65 l/hr. 1) 0.0112 mmole of NH_3; 2) 0.0115 mmole of C_2H_2

The theoretical calculation of factor B is rather complicated, therefore we deduced an approximate value from certain experimental data.

In a series of tests with gradually increasing concentrations of ammonia and acetylene, in the IR cell the decrease of concentrations in time was followed at constant flow rate of the carrier gas (16.65 l/hr) and constant chart-speed (6.1 mm/min). The recorded curves for nearly identical initial concentrations are shown in Fig. 7.

This figure shows that the concentration of acetylene changes at a slower rate than that of ammonia. For the complete removal of ammonia from the cell 1.3 min, for that of acetylene 2.24 min were noted. Consequently, in case of the same experimental conditions and the same initial gas concentrations, the T/M area for the slower gas determined on the basis of the corresponding calibration curve will be somewhat greater. To demonstrate this, in Table II we have listed the figures pertaining to the concentration-series tested, together with the proportionality factors indicative of the corresponding areas.

Table II

NH_3			C_2H_2		
10^{-3} mole	T	$\frac{T}{M}$	10^{-3} mole	T	$\frac{T}{M}$
0.0112	10.38	0.610	0.00458	7.4	0.284
0.0182	16.50	0.970	0.0115	18.6	0.718
0.0306	27.20	1.600	0.0196	30.4	1.170
0.0777	73.00	4.300	0.0377	61.0	2.340

T = area drawn on the basis of calibration curves
M = millimolecular weight

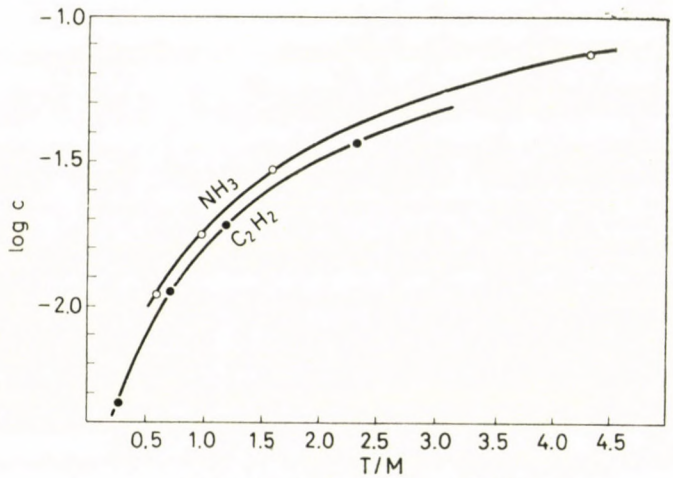

Fig. 8. $\lg c(NH_3, C_2H_2) = f(T/M)$

If the function $\lg c = f(T/M)$ is plotted graphically, the correlations shown in Fig. 8 are obtained.

By selecting from Fig. 8 the T/M quotients referring to the same concentrations, and taking Eq. (6) into consideration, the approximate value for B can be estimated since

$$\frac{\frac{T_1}{M_1}}{\frac{T_3}{M_3}} = \frac{\eta_3}{\eta_1} = \frac{1}{B} .$$

From the data, one obtains $1/B = 0.866 \pm 1.27\%$, or $B = 1.155$. From Fig. 8 it can be seen that B is independent of the absolute values of concentrations.

Since the composition of the model compound is known, the numerical value for B can be determined experimentally, too.

For this purpose we take the third step in Fig. 3 for paramolybdate, for which $T_1 = 107.0$ and $T_3 = 41.0$ (*cf.* Eqs (3) and (4)). The corresponding figures for m_1 and m_2 are also known from Table I: $m_1 = 19.38$, $m_2 = 10.20$. Solving Eq. (10) for these quantities, we obtain $B = 1.178$; there is no great deviation between the values obtained by the two methods.

In connection with this deviation we must note, however, that in the experimental determination of B the flow characteristics of pure gases were studied, whereas it is actually gas mixtures that enter the cells in the course of a decomposition reaction, thus ammonia plus water, when ammonia is measured, and ammonia and acetylene, when water is determined. It can be supposed that the difference between the two values for B is due to disregarding this circumstance. The fact that the discrepancy is not significant suggests that the differences between the flow characteristics of ammonia and acetylene exist also in the gaseous mixture.

If the Δm values corresponding to the individual steps of TG curve in Fig. 3 are known, and it is taken into account that at all three steps the evolution of the two gases occurs simultaneously, the m_1 and m_2 values for the given steps can be calculated according to the latter method, too. Using the numerical values of the measured areas corresponding to proportions (3) and (4), the data collected in Table III were obtained.

Table III

TG steps	$3(NH_4)_2O \cdot 7\,MoO_3 \cdot 4\,H_2O$						
	Δm (mg)	NH_3 (mg)		% error	H_2O (mg)		% error
		calcd.	found		calcd.	found	
I	24.5	2.20	o 2.14 * 2.10	—2.72 —4.55	24.2	o 22.40 * 22.40	—7.45
II	17.5	11.5	o 11.75 * 11.70	+2.18 +1.74	6.12	o 5.75 * 5.81	—7.70 —5.07
III	29.8	19.38	o 19.50 * 19.38	+0.62 —	10.20	o 10.35 * 10.40	+1.54 +1.96

for o, $B = 1.178$, for *, $B = 1.115$

According to Table III, the results obtained with the second method are of satisfactory accuracy, thus the use of different B values does not cause significant deviations.

In practice, a third possibility must also be considered, *viz.* that the composition of the substance is unknown and no step is found where the gases

are evolved simultaneously. Then the numerical value of A required for the application of the first method is not available, but the second method cannot be used, either. However, relationship (10) offers a solution. It has been found that if this correlation is applied for the entire process and, instead of T_1 and T_3, the numerical values of the total areas under the IR curves of Figs 3 and 4 are used and the total change of weight read from the TG curve is regarded as the value for Δm, then Eq. (10) will give the amount of ammonia and water in the initial compound. Thus by IR measurements the respective A values become available for the two components and then one can proceed according to the first method.

In order to verify this, the theoretical amounts of ammonia and water corresponding to given sample weights have been calculated from the empirical formulas and these figures we compared with those obtained from experimental data treated according to Eq. (10). The results are summarized in Table IV.

Table IV

Subst.	Δm (mg)	NH_3 (mg)		% error	H_2O (mg)		% error
		calcd.	found		calcd.	found	
Mo	71.8	33.07	33.20	+0.39	40.80	38.80	—4.90
W	88.0	43.28	43.60	+0.74	46.95	44.50	—5.22

As seen from Table IV, ammonium and water contents of the compounds studied by infrared spectrophotometry can be determined with a fair degree of accuracy.

Discussion

Generally, in the case of special types of compounds, IR spectrophotometry may be useful in the study of thermal decomposition reactions, especially when several gaseous products are formed. Under such conditions, the reaction path can be qualitatively elucidated since gaseous components and the changes in their concentrations in the gas phase are recorded separately by IR spectrophotometry. Thus, individual steps of the overall process can be recognized more easily than by thermogravimetry alone.

The methods of quantitative analysis described in this paper give results that provide sufficient information although with limited accuracy, about the composition of intermediate phases without chemical analysis. Since these methods were applied in the study of only a few systems, accurate chemical analyses of initial and intermediate phases are still required when the decomposition of unknown compounds of a similar type is investigated.

However, if the thermal studies are completed with infrared data as mentioned above, reliable preliminary information on the quantitative aspects of the process are obtained by means of the proposed methods of calculation. On the basis of this information, it will be comparatively easy to decide whether or not accurate chemical analysis is required for the elucidation of some unclearness. In order to draw further conclusions, it is necessary to study numerous unknown compounds by this method.

In the meantime we wish to point out two experimental factors strongly affecting the accuracy of results. The calibration curve must be determined with great care which is not easy at the low concentrations encountered in this study. The correctness of calibration curves must be checked; the most simple way for this is to measure the area under the IR peaks of the gas in question at gradually increasing concentration levels. The calibration curve is acceptable when the corresponding areas are proportional to the sample weight [2].

Contrary to general thermogravimetric practice, here the flow rate of the carrier gas must be kept strictly constant since any fluctuation will considerably affect the areas obtained. Of course, significant errors may occur when the Δm values are read from the TG curves.

Ammonium paramolybdate was used for the experimental verification of calculation method, because the steps of its decomposition can be easily and accurately distinguished. The TG steps and IR maxima are clearly separated, and the areas under maxima corresponding to individual processes can be accurately measured.

As seen from Figs 2 and 4, the decomposition process of paratungstate seems to consist of overlapping steps and this makes the determination of areas rather ambiguous. In similar cases, an adequate graphical method of evaluation of the curve should be found in order to separate the overlapping areas correctly, *i.e.* in conformity with quantitative proportions. In a subsequent paper, the decomposition of paratungstate will be discussed in detail.

REFERENCES

1. HEGEDÜS, J. A., KISS, B. A.: Acta Chim. Acad. Sci. Hung. **51,** 251 (1967). Magyar Kém. Folyóirat, **73,** 41 (1967)
2. KISS, B. A.: Acta Chim. Acad. Sci. Hung. **61,** 207 (1969).
3. LINDQVIST, I.: Nova Acta Soc. Sci. Upsaliensis, IV. 15. Nr. 1 (1950). Arkiv för Kemi, **2,** Nr. 18 (1950)
4. LINDQVIST, I.: Acta Crystallogr. Copenhagen **5,** 667 (1952)
5. DUVAL, C.: Inorganic Thermogravimetric Analysis. p. 332. Elsevier, Amsterdam, 1953
6. FUNAKI, K., SEGEWA, T.: J. Electrochem. Soc. Japan, **18,** 152 (1950)
7. RODE, E. YA., TVERDOKHLEDOV, V. N.: Zhur. Neorg. Khim. **3,** 2343 (1958)
8. HEGEDÜS, J. A., SASVÁRI, K., NEUGEBAUER, J.: Z. anorg. allg. Chem., **56,** 293 (1957)
9. EIKOH, MA.: Bull. Chem. Soc. Japan, **37,** 171 (1964); **37,** 648 (1964)

András B. KISS; Budapest IV., Váci út 77.

Acta Chimica Academiae Scientiarum Hungaricae, Tomus 63 (3), pp. 257—265 (1970)

STRIPPING VOLTAMMETRY OF Se(IV) COMPOUNDS WITH THE HANGING MERCURY DROP ELECTRODE

F. VAJDA

(Mining Research Institute, Budapest)

Received September 27, 1968

In the presence of halide ions, selenous acid forms a complex compound which is adsorbed on the surface of the hanging mercury drop electrode. This adsorption phenomenon can be utilized in the cathodic stripping technique; the current peak permits a sensitive and selective quantitative determination of selenium. Se(IV) gives rise to a current peak also at another potential and it is also suitable for stripping analysis. In this case, the dissolution curve for the solid product of the preceding reduction step is obtained.

After earlier studies by SCHWAER and SUCHY [4], LINGANE and NIEDRACH [2] have carried out fundamental work on elucidating the polarographic behaviour of Se(IV). Many authors dealt with the polarographic determination of selenium. They examined the selenium steps in various base solutions and succeeded in measuring selenium concentrations as ion as a few μg/ml. Their results are presented in a comprehensive work by BOCK and KAU [1].

According to these authors, in acidic solutions (pH < 3) selenous acid undergoes 6-electron reduction to hydrogen selenide at the beginning of the polarogram, but at the same time mercury is oxidized to HgSe:

$$\mathrm{Se(VI)} + \mathrm{Hg} + 4e \rightarrow \mathrm{HgSe}$$

At a more negative potential the oxidation of Hg ceases and the diffusion current reaches the 6-electron value. Thus, the polarogram consists of a 4-electron and a 2-electron step.

The present studies with the hanging mercury drop electrode began on this basis and resulted in the elucidation of voltammetric characteristics and the development of a new sensitive stripping method for the determination of selenium.

Experimental

The measurements were performed with a Radelkis OH 102 type polarograph using the dropping mercury and the hanging mercury drop electrodes. All potential values are given *vs.* the saturated calomel electrode and, to compensate the IR potential drop, the curves were recorded by applying the 3-electrode system. All reagents were of analytical grade and water was deionized on an ion exchange column. Further purification, which is usual in the stripping technique, was found to be unnecessary. Atmospheric oxygen was carefully removed by bubbling an inert gas through the solutions.

Results and discussion

The behaviour of Se(IV) was first studied in a 0.1 *M* solution of perchloric acid which has no tendency for complex formation. When using the dropping mercury electrode two steps were obtained (Fig. 1): a drawn-out irreversible 4-electron step with a half-wave potential of approximately +0.1 V, and a 2-electron step having a half-wave potential of −0.55 V.

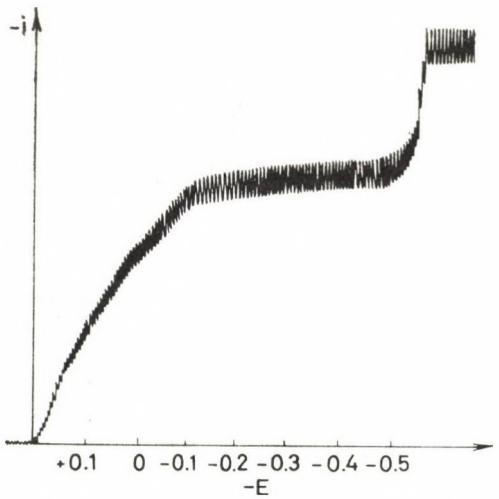

Fig. 1. Selenium(IV) step. 5.10^{-4} *M* Na_2SeO_3 in 0.1 *M* $HClO_4$

The first half of the cyclic voltammogram recorded with the hanging mercury drop electrode consists of an elongated wave and a well-developed peak (Fig. 2). When increasingly negative potentials are applied to the electrode, starting from 0.0 V, a solid HgSe film develops on the drop surface. At −0.58 V, the film dissolves in accordance with the equation: $HgSe + 2e + 2\,H^+ = Hg + H_2Se$, giving rise to a sharp current peak.

In the other half of the cycle only a small anodic peak appears, resulting from incomplete diffusion of hydrogen selenide from the vicinity of the mercury drop.

In the presence of halide ions, the cyclic curve is modified: the wave is shifted to a more negative value and a superimposed sharp peak appears on the wave. In 0.1 *N* HCl, the potential of the new peak is −0.02 V, while in 0.1 *N* HBr it is −0.16 V (Fig. 3). The potential of the second peak remains unchanged in every case. (Instead of half-peak potentials, peak potentials can be measured more accurately for sharply rising peaks.)

1. The new peak is useful for cathodic stripping *i.e.* on polarizing the electrode at +0.05 V in a stirred solution for a given period of time, then

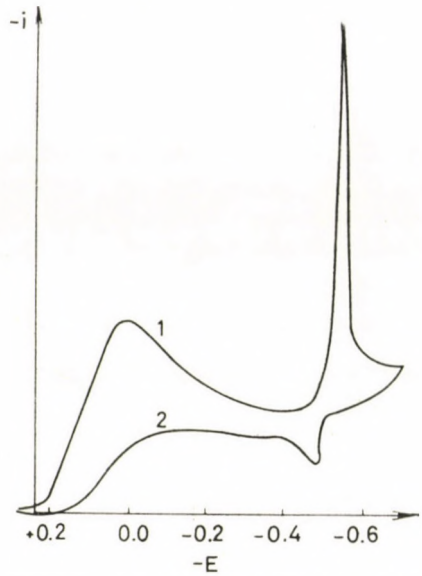

Fig. 2. Cyclic voltammogram for selenium(IV) recorded with the hanging mercury drop electrode. 1.10^{-4} *M* Na_2SeO_3 in 0.1 *M* $HClO_4$

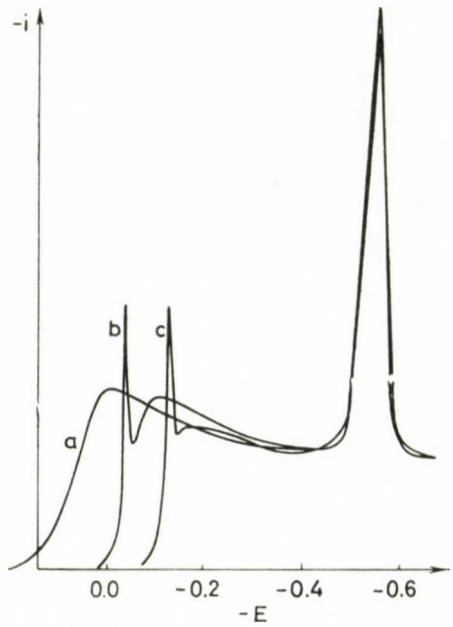

Fig. 3. Voltammogram of 1.10^{-4} *M* Na_2SeO_3 in the following base solutions: (a) 0.1 *M* $HClO_4$. (b) 0.1 *M* HCl, (c) 0.1 *M* HBr

changing the potential to negative values, a reduction current peak is obtained whose height depends on the time of stirring and the amount of Se(IV) present in the solution.

2. The height of the stripping peak recorded at −0.58 V is also dependent on the time of deposition at +0.05 V.

3. Apart from the small residual current at the deposition potential, the cell is free of current even at high concentrations of selenous acid.

4. The stripping peak can also be observed when, after the deposition process, the electrode is placed into a selenium-free basic solution.

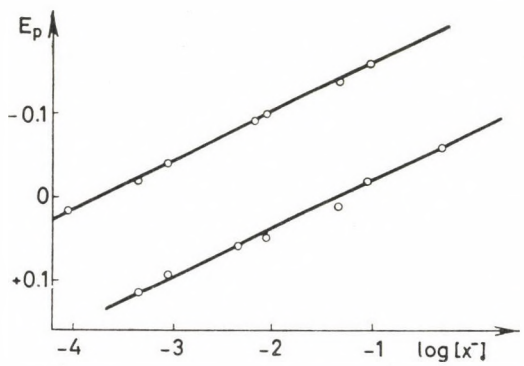

Fig. 4. Variation of the potential of the first Se(IV) peak with the halide concentration of the base solution

5. After recording the curve, the experiment can only be repeated with a new drop while the stripping peak at −0.58 V can be recorded times, using the same drop.

6. The stripping peak can be recorded if the cell is short-circuited or disconnected during the deposition process.

7. The peak potential is directly proportional to the logarithm of the halide concentration (Fig. 4). The data obtained are shown in Table I. The lines corresponding to the HCl and HBr base solutions are parallel, having a slope of 59 mV.

8. On adding gelatin to the solution the height of the peak gradually decreases (Fig. 5).

9. The peak decreases with increasing temperature. These measurements were carried out in a 0.2 *M* HCl solution containing $5 \cdot 10^{-4}$ *M* Se(IV). 30 seconds were allowed to elapse between pressing out the mercury drop and starting the motor so that the solution came to rest. The temperature dependence of the transferred electricity calculated from the area under the peak, is shown in Table II. The decrease is 5% per degree on the average.

Table I

Dependence of the peak potential of Se(IV) on halide concentration (Acid concentration adjusted to 0.2 M by $HClO_4$)

$[X^-]$	E_p Cl^- complex	E_p Br^- complex
1×10^{-4}	—	+0.025
5×10^{-4}	+0.115	—0.02
1×10^{-3}	+0.095	—0.04
5×10^{-3}	+0.060	—
7×10^{-3}	—	—0.09
1×10^{-2}	+0.050	—0.10
5×10^{-2}	+0.010	—0.14
1×10^{-1}	—0.020	—0.16
5×10^{-1}	—0.060	—

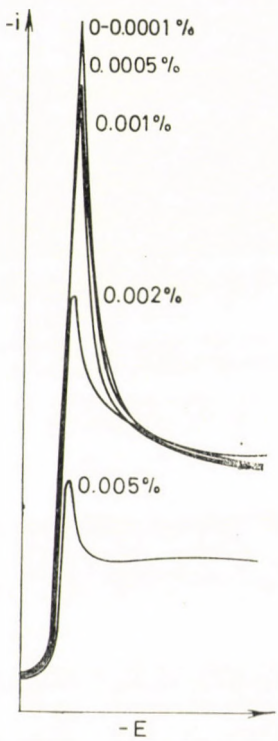

Fig. 5. Peaks for Se(IV) from solutions containing different amounts of gelatin. The percentage of gelatin is given with each peak

Table II

Dependence of Se(IV) current peaks on temperature

t (°C)	e (μ Cb)
13	58
20	51
41	32
50	16
64	4.5

On the basis of the above experiments, it is obvious that from selenous solutions containing halide ions, a selenium compound is deposited on the surface of the mercury drop while no transfer of electricity occurs, but the product is cathodically reducible (*cf.* 1, 3, 4 and 6). The reduction product which forms a solid adherent coating on the drop, is further reducible at −0.58 V, thus it consists of HgSe (*cf.* 2 and 5).

The shift in the peak potential indicates that in halide containing solutions selenous acid is present as a complex compound. This means that in a HCl or HBr base solution hexahaloselenous acid and/or the corresponding singly and double ionized forms exist (*cf.* 7). A simple relation (3) holds for the half-wave potential measured in the presence of complexing agents which, when applied to the present case, becomes:

$$E_p = \text{const} - \frac{0.059}{z} p \log [X^-]$$

where z is the number of electrons involved in the electrode reaction, p is the coordination number in the complex and $[X^-]$ is the concentration of halide ions. The constant includes the reduction potential of selenous acid, and the change in overvoltage due to complex formation, the difference between half-wave and peak potentials, and a term depending on the complex stability constant. Since the coefficient of log $[X^-]$ was found to be 59 mV, z is equal to p and, consequently,

$$H_2SeX_6 + 6e = H_2Se + 6\,X^-.$$

The observation and results so far considered give no explanation for the appearance of the cathodic peak and the possibility for stripping analysis. It can be assumed, however, that the molecules increased in size and weight as a result of complex formation are adsorbed on the surface of the drop due to considerable adhesive forces. Consequently, they can be accumulated at

the mercury drop without any electrode reaction, the phenomenon being useful for stripping technique. The spontaneous adsorption of the depolarizer is convincingly proved by the experiments with a capillary-active substance (*cf.* 8) and by temperature-dependence measurements (*cf.* 9) since a rise in temperature hinders adsorption whereas it increases other (diffusion, kinetic) polarographic currents.

The experimental results do not preclude the theoretical possibility that in a current free cell the adsorbed film is produced by chemical reaction. If this is the case, the interaction of selenious acid as a strong oxidant, with mercury as well as the halides would result in the formation of an insoluble mercury or selenium compound, the reduction of which would give rise to the adsorption current peak. This assumption, however, is not confirmed because of the considerably different reduction potentials, the relatively high solubility and hydrolysis of the possible compounds (*e.g.* Hg_2Cl_2, HgSe, Hg_2SeO_3, Se_2Cl_2).

Determination of Se(IV) by stripping voltammetry

On the basis of the foregoing, there are to possible ways of determining Se(IV) by cathodic stripping voltammetry using either one of two different electrode reactions. In both cases a 0.2 *M* HCl solution can be best used as supporting electrolyte.

For the anodic stripping peak, the deposition of the substance is accomplished at +0.05 V while the solution is kept stirred. After stopping the stirring, 20 seconds are allowed to pass and then the reduction curve for the adsorption layer is recorded (Fig. 6). It can be more accurately evaluated by measuring the area under the curve. Table III shows the relationship between the quantity of electricity calculated from the peak-area, the concentration and the deposition time.

As can be seen from the data given in the Table, the adsorption peak is suitable for analytical purposes. Because of its relatively positive potential, only a few ions interfere. It is unaffected by large excess of Pb, Cd, As, Te, Ti, Mn, Tl and Zn but interference is encountered from Fe(III) and Cu when present in two-fold excess. Sb(III) and Bi are also troublesome when their concentrations are ten times greater than that of selenium.

The stripping technique is not performed according to the usual mechanism also in the case of the other selenium peak, *i.e.* it is not a reversible process allowed to proceed in the forward and reverse directions but a two-stage reduction, the subsequent steps of which are used as working-process: one step is the film-formation and the other is the electro-dissolution process. The dissolution curve for HgSe formed at the deposition potential (−0.4 V) is also a sharp cathodic peak, which is well-suited for analytical purposes.

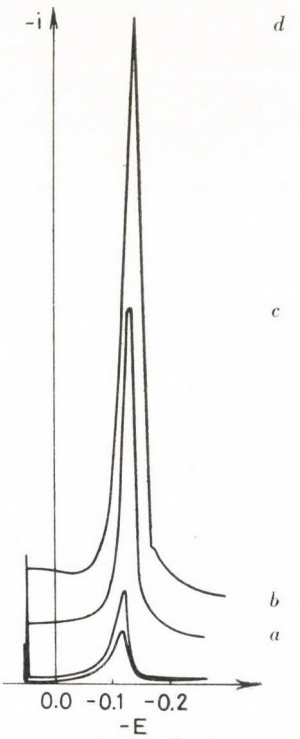

Fig. 6. Stripping curves of Se(IV). 5.10^{-6} *M* Na_2SeO_3 in 0.2 *M* HCl. Time of deposition: (a) 30 sec, (b) 1 min (c) 4 min (d) 8 min.

Table III

Variation with concentration of the adsorption peak of Se(IV)

C (M)	t (sec)	e (μ Cb)	$\frac{e}{ct}\ 10^4$
1×10^{-5}	60	16	2.67
5×10^{-6}	60	7.7	2.57
5×10^{-6}	120	16	2.67
1×10^{-6}	300	7.8	2.60
5×10^{-7}	120	1.47	2.45
2×10^{-7}	120	0.60	2.50
2×10^{-7}	300	1.54	2.57
1×10^{-7}	300	0.70	2.34

Fe(III), Cu, Pb, Cd, As and Tl cause interference even when they are present in concentrations equal to that of selenium.

By the application of the stripping technique, the sensitivity of the determination of Se has been markedly increased as compared to the polarographic technique. In addition, the well-separated adsorption peak provides a higher selectivity. The smallest Se(IV) concentration detectable by this method was 7×10^{-8} M at the adsorption peak and 5×10^{-9} M at the second peak. In practice, selenium concentrations of a few hundredth of a μg/ml can be detected, but under favourable circumstances, concentrations as low as a few thousandths of a μg/ml are accessible by the cathodic stripping method. For the determination of 10^{-5} M or higher concentrations of selenium, voltammetry without electro-deposition or classical polarography methods can be employed more successfully.

REFERENCES

1. Bock, R., Kau, H.: Z. anal. Chem. **188,** 28 (1962)
2. Lingane, J. J., Niedrach, L. W.: J. Am. Chem. Soc. **70,** 4115 (1948)
3. Proszt, J., Cieleszky, V., Győrbiró, K.: Polarography. p. 104—106. Akadémiai Kiadó, Budapest, 1964
4. Schwaer, L., Suchy, K.: Collection Czechoslov. Chem. Communs. **7,** 25 (1935)

Ferenc Vajda; Budapest III., Mikoviny u. 2.

Acta Chimica Academiae Scientiarum Hungaricae, Tomus 63 (3), pp. 267—277 (1970)

POSSIBILITIES OF THE JOINT APPLICATION OF X-RAY DIFFRACTOMETER AND DERIVATOGRAPH TO THE QUANTITATIVE PHASE ANALYSIS OF BAUXITES AND SIMILAR ROCKS

G. BÁRDOSSY

(Research Laboratory for Geochemistry of the Hungarian Academy of Sciences)

Received October 8, 1968

102 Hungarian and foreign bauxite samples were examined by the author using X-ray diffractometer, derivatograph, and analyzed by chemical methods. The purpose of the work has been to compare the efficiency of X-ray diffractometric and derivatographic measurements and to study the possibilities of their joint application.

The possibilities of detecting various minerals are treated. Data on the detection limits are given in Table I. The derivatograms of some minerals detected in bauxite are presented which have not yet been published in the literature.

In the third part of the paper the problems of the quantitative determination of minerals are treated. According to the author, in the case of well homogenized samples the results obtained by the two methods agree within 0.5%. Both methods yielded 0.2 to 2.2% water excess compared to the results of chemical analysis. It has been cleared up by the author that this water excess is due to adsorbed (chemisorbed) water molecules which leave above 100 °C. In loose, porous bauxite types the amount of adsorbed water is greater than in compact ones. Besides, greatest water amounts are adsorbed by bauxites rich in iron and manganese minerals.

The joint application of the two methods has special importance in the mineralogic elaboration of new, so far unexamined deposits, owing to the so called mineralogical error, which may change the results by 5—20%. By means of derivatograms and chemical analyses the constants can be appropriately modified and the results made accurate. By combining the two methods the mineral composition of other sedimentary and pyroclastic rocks can be determined with adequate accuracy.

Introduction

The accurate quantitative determination of the mineral composition of bauxite is of great importance both from the scientific point of view and in the practice of bauxite processing. NÁRAY-SZABÓ and NEUGEBAUER were first to use X-ray diffraction method to the investigation of Hungarian bauxite (1944). The possibilities of the quantitative phase analysis of bauxite by X-ray diffractometry have been studied all over the world since 1953 (TERTIAN 1953, TERTIAN–HOUSSEMAINE 1954, BLACK 1953, BRINDLEY–SUTTON 1957, GINSBERG–WEFERS 1957, ROHNER 1957, MENCZEL 1958, BEZJAK 1962, GUTKIN–SKRIPKO 1963). The method elaborated earlier by NÁRAY-SZABÓ and PÉTER (1964) for clays and soils was used by the author of the present paper with some modifications for studying bauxite; he also proved that the so called mineralogical error is the greatest uncertainty factor in the determinations (1966).

ERDEY, PAULIK and PAULIK were first to use derivatograph for examining bauxite (1955), later they also dealt with the thermal decomposition of gibbsite (ERDEY, PAULIK 1959), with the determination of calcite (PAULIK, LIPTAY, GÁL 1963) and pyrite (PAULIK, GÁL, ERDEY 1963) in bauxite. The thermal decomposition of various bauxite minerals was investigated by ÜVEGES and MÁRIÁSSY (1959) by means of the derivatograph. KOTSIS (1962, 1964) developed a method for the quantitative determination of some bauxite minerals.

The purpose of the present work has been to compare the two methods of investigation, and to find the possibilities of their joint application. Bauxite samples have been chosen, thoroughly homogenized and examined by derivatograph, X-ray diffractometer and chemical methods. The samples were the 40 samples of the bauxite collection of the Research Laboratory for Geochemistry of the Hungarian Academy of Sciences and the 62 samples of the collection of the Research Institute for Metal Industry. The author wishes to thank for supplying the data of the latter samples also here.

X-ray diffraction measurements were made with a Müller Mikro 111 generator and a Philips counter-recorder, with Cu, Co and Mo K α radiation. The data for the conditions of the measurements are the same as given in an earlier paper (BÁRDOSSY 1966).

2. Problems of the detection and qualitative determination of minerals

By X-ray diffractometer all crystalline minerals and by supplementary measurements (by so-called addition methods) also the amount of the amorphous phase can be determined. Those minerals can be detected by means of a derivatograph which undergo thermal changes (weight change, structural change) on heating. So from among the usual bauxite minerals hematite, magnetite, ilmenite, anatase, rutile and corundum cannot be detected by this method. Quartz is very difficult to detect in bauxite by means of a derivatograph, it is only possible by repeated heating, while it is readily and accurately determined by an X-ray diffractometer.

The detection limits of some minerals in the main types of bauxite by X-ray diffractometer have been calculated and the result checked by means of synthetic mixtures (BÁRDOSSY 1966). The detection limits in the case of the derivatograph were determined by KOTSIS (1962, 1964) for goethite, pyrite, kaolinite, dolomite and calcite, by means of synthetic mixtures. In the present studies the author has determined the limits of detection of the minerals by the derivatograph in all the 102 samples available, which can be detected by an X-ray diffractometer. Also those minerals have been determined which interfere with the determination of the mineral in question. All these data are given in Table I.

Table I

Detection limit of minerals in bauxite

Mineral	Diffracto-metrically %	Derivatographically			
		According to T. Kotsis 1964 %	Measurements by the author		
			Undis-turbed %	Dis-turbed %	Interfering mineral in the presence of
gibbsite	0.5		2.6	7	great amount of goethite
				4	goethite in about the same amount
boehmite	0.5		4	9	diaspore, chamosite, kaolinite
diaspore	0.5		4	9	boehmite, chamosite, kaolinite
goethite	0.3	5—6	2	8	great amount of gibbsite
				3	gibbsite in about the same amount
pyrite	0.3	0.4	0.3	1	organic materials
chamosite	1.2		5	15	boehmite, diaspore, kaolinite
kaolinite	2.2	2	2.5	—	(its exothermic peak is not disturbed by peaks from other minerals)
halloysite	2.5		2.5	10	great amounts of boehmite, diaspore, kaolinite
chlorite	2.7		6	25	kaolinite, halloysite, chamosite
illite	3.0		8	30	kaolinite, halloysite, chamosite
siderite	0.2		1	—	(its exothermic peak is not disturbed by peaks from other minerals)
calcite	0.2	0.4	1	5	dolomite, alunite, pyrite
dolomite	0.2	4	4	10	calcite, alunite, pyrite
lithiophorite	3.0		8	15	pyrite, organic materials

The data reflect that the X-ray diffractometer is more advantageous from the point of view of detectability of minerals than the derivatograph and also, that the clay minerals in bauxite are most difficult to detect by both methods.

Any organic substance present can also be detected by the derivatograph on the basis of the exothermic peak between 400—500 °C on the DTA curve. Its identification is more difficult in the presence of pyrite, although still possible according to Paulik, Gál and Erdey (1963). The detection limit of organic matter in bauxite is 0.3—0.5%, while it cannot at all be detected by an X-ray diffractometer.

Different minerals can be recognized by means of an X-ray diffractometer on the basis of the position and intensity of reflections. Connected problems have been dealt with in detail earlier (Bárdossy 1966). The bases for the recognition of minerals by means of derivatograms are the temperatures

of endothermic and exothermic peaks. The fact that the temperatures belonging to the peaks in some cases depend on the amount of mineral makes the detection more difficult. This effect is greatest for calcite. According to PAULIK, LIPTAY and GÁL (1963) the temperature of the endothermic peak is 900 °C for 100% calcite, while 730 °C for 1% calcite. Similar behaviour can be observed with dolomite.

There are no such data available for other minerals occurring in bauxite. Therefore the data of the derivatograms were evaluated by statistical method: the distribution, arithmetic mean and most frequent value (modus) of the peak temperatures were determined. The peak temperatures change only by 10—40 °C in the case of various amounts of minerals. Isomorphous substitution, however, may cause much greater shifts. Small differences in peak temperatures are brought about by lattice defects, differences in the crystalline order and the grain size of crystallites.

The temperature of the exothermic peak of goethite varies between 290 and 390 °C according to its amount. The arithmetic mean is 349 °C, the modus 340 °C. The reason for this great deviation is probably that the Fe^{3+} ions in goethite can be substituted by Al^{3+} ions isomorphously. According to the experience of the author the degree of substitution varies from 1—2 to 30 mole per cent in bauxites. The temperature of the endothermic peak rises with increasing degree of substitution by Al. This increase in thermal stability is due to the fact that the introduction of Al changes the lattice to a small extent into the direction of that of diaspore which gives the goethite crystal greater stability.

For gibbsite the temperature of the main endothermic peak of the DTG curve varies between 280 and 350 °C, the arithmetic mean being 313 and the modus 320 °C. As no isomorphous substitution is possible in this case, the deviations are caused by differences in the degree of order of the lattice and in the size of crystallites. The appearance of small endothermic peaks before and after the main endothermic peak in the case of some gibbsite samples can also be ascribed to the above factors. Connected problems were elucidated by ERDEY and PAULIK on the basis of thorough investigations (1959).

The temperature of the endothermic DTG peak of boehmite was found to vary between 520 and 565 °C, the arithmetic mean being 540 °C and the modus 550 °C. The deviation of data is even smaller than with gibbsite, the reason of which may be 1—2% Fe^{3+} substitution, lattice defects and differences in grain size.

Only 13 diaspore samples were available since this mineral is present in Hungarian bauxites in very small amount only. We had to rely on data obtained with bauxite samples from Greece, Yugoslavia and the Soviet Union. The temperatures of the endothermic peak were between 530 and 555 °C, the arithmetic mean being 535 °C.

The difference between the peak temperatures of diaspore and boehmite is so small that in boehmite-diaspore bauxites the two minerals cannot be distinguished, the endothermic peaks merge into one single peak (Fig. 1).

The most frequent clay mineral in bauxite is kaolinite. It is known that there may be great differences in the degree of order of kaolinite crystals, and this can be demonstrated by X-ray measurements. According to data measured by FIEDLER and STEINIKE (1967) the thermal properties of kaolinites of different degrees of order are different. The main endothermic DTA peak of highly

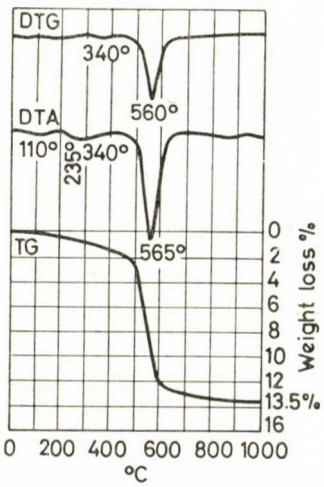

Fig. 1. Diaspore-boehmite bauxite from Distomon (Greece) with some chamosite and goethite

crystalline kaolinites appears at 583 ± 3 °C, while that of kaolinites disordered along the axis *b* at 550—562 °C, and of samples loosened also along the axis *c* at 527—564 °C. The last named type has been identified by the authors.

The DTA peaks of kaolinites appear at 520—600 °C, which indicates the different degrees of order of the samples. The arithmetic mean is 576 °C, modus 580 °C which indicates that mostly crystalline modifications of kaolinite are present in bauxite. The data of X-ray experiments also support this statement.

The accurate measurement of the temperature of the endothermic peak of kaolinite is rather difficult in the presence of great amounts of boehmite and diaspore, therefore it is advisable to take also the exothermic peaks into consideration. According to FIEDLER and STEINIKE (1967) this temperature is 980 ± 3 °C for highly crystalline kaolinite, 940—950 °C for samples disordered along the axis *b*, and 914—940 °C for those disordered along the axis *c*. On the derivatograms taken by the author the exothermic peaks appeared between

910 and 1000 °C, the arithmetic mean being 958 °C, the modus 960 °C. These data are in good agreement with earlier statements of the author.

It can be established that the evaluation of the derivatograms helps in determining the degree of order of kaolinite present in bauxite.

Recently the author has succeeded in detecting in some Hungarian and foreign bauxites by X-ray diffractometric measurements a dioctahedral chlorite mineral — sudoite — similar in composition to kaolinite. According to the present knowledge and experience of the author the thermal properties of sudoite in bauxite do not differ from those of kaolinite in noticeable extent. Therefore the presence of sudoite in bauxite can only be detected by an X-ray diffractometer.

Some laterite-bauxites are rich in halloysite. Its presence can be noticed easily on the basis of the high endothermic peak at 130—150 °C. Its exothermic peak appears between 930 and 970 °C, according to the eight derivatograms given in the book by LANGIER-KUZNIAROWA (1967). This peak of a bauxite sample rich in halloysite from Greece has been found to be at 990 °C. If also kaolinite is present, the exothermic peaks of the two minerals cannot be distinguished.

In some bauxite types kaolinite is partly or completely substituted by chamosite. It is characterized by a high endothermic peak at 480 °C, according to the derivatogram given in the book by LANGIER-KUZNIAROWA (1967). With chamosite-bauxites from Greece this peak appeared at 560 °C. It is probable that the temperature of the endothermic peak depends on the composition of chamosite. The exothermic peak at 960 °C lacks, what makes its distinguishing from kaolinite easier. In other bauxites trioctahedral chlorite occurs in varying amounts, and rarely also illite and montmorillonite. Owing to the overlapping of thermal reactions in this case certain clay minerals cannot be detected reliably, so both diffractograms and derivatograms have to be evaluated. In this work a valuable aid can be the book by LANGIER-KUZNIAROWA (1967) in which the derivatograms of clay minerals are given.

To illustrate the above said, the derivatograms of a bauxite sample containing chlorite and of one containing illite are shown in Fig. 2.

In the course of the present work some minerals have also been studied the derivatograms of which have not yet been given in the literature.

Lithiophorite — $Li_2Al_8Mn_2^{2+}Mn_{10}^{4+}O_{35} \cdot 14H_2O$ — has been detected in bauxite samples from Eplény, Halimba (Hungary) and Greece. The degree of crystallinity is widely varying, therefore the derivatograms are somewhat different (see Fig. 3). From the point of view of detection the intensive endothermic peak at 476—496 °C on the DTA curve and 470—492 °C on the DTG curve, accompanied by a remarkable water release is of importance. On the DTA curves of highly crystalline samples also a small exothermic peak can be observed at 268 °C. On the derivatograms of less crystalline samples this peak

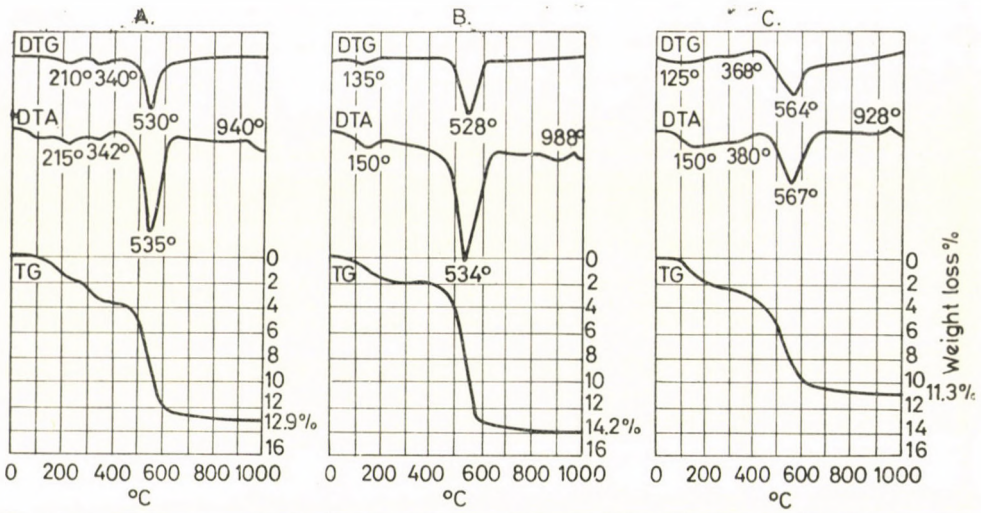

Fig. 2. A. Light green chlorite rich bauxite from Kamnik (Slovenia, Jugoslavia). B. The same sample after boiling with 10% HCl. Chlorite and goethite were dissolved; C. Red illite-clayey bauxite from the Parnassus mountains (Greece)

does not appear, but there is a flat endothermic peak on the DTA curve at 130 °C, indicating gradual water release. This is probably not structural, but strongly adsorbed or chemisorbed water.

The derivatogram of aluminite — $Al_2SO_4(OH)_4 \cdot 7H_2O$ — which occurs in the bauxite from Szőc in form of white nests, is characterized by a high initial endothermic peak, on which four partial minima appear at 130, 175,

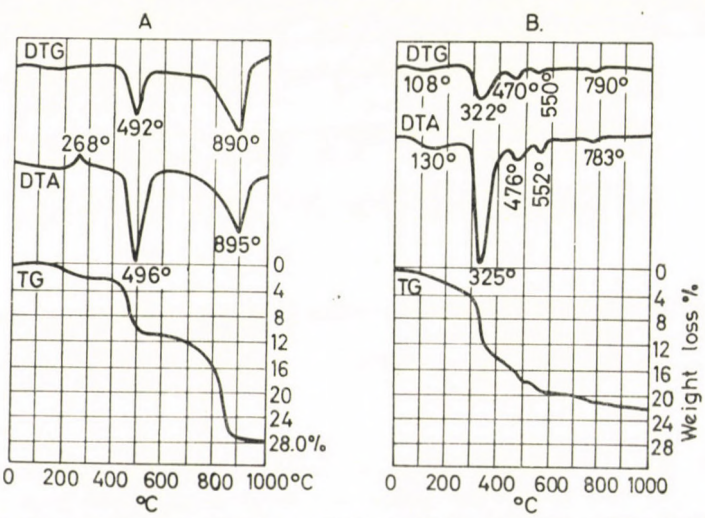

Fig. 3. A. Black crust between bauxite and footwall limestone from Eleusis (Greece). 62% lithiophorite +38% calcite; B. Black nests in red bauxite from Halimba, Malomvölgy X. Minerals: lithiophorite, gibbsite, boehmite and calcite, all of low degree of crystallization

198 and 222 °C (Fig. 4). This corresponds to the stepwise removal of water. SO_3 begins to leave above 700 °C, which proceeds in two steps at 910 and 945 °C according to the DTG curve. The small exothermic peak at 850 °C is

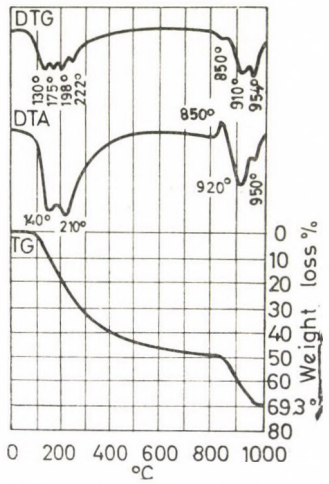

Fig. 4. White pure aluminite nest in red bauxite from Szőc, Nyíreskút (Hungary)

indicative of the formation of γ and α Al_2O_3. The correctness of this interpretation of the process has been checked by X-ray diffractograms of gradually heated aluminite samples.

Takovite — $(2Al_2O_3 \cdot 5NiO \cdot 9H_2O) \cdot 6H_2O$ — has been detected in bauxites from the South of France and from Greece in form of nests and crusts. On the DTG curve endothermic peaks appear at 288 and 292 °C (Fig. 5). The intensive endothermic peak at 550 °C is caused by accompanying boehmite.

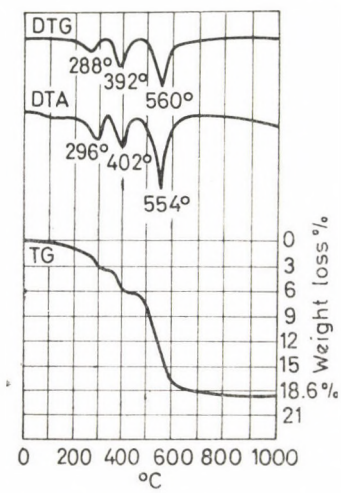

Fig. 5. Yellowish takovite nests in red bauxite, accompanied by boehmite (France)

3. Problems of quantitative determination of minerals

The way of the quantitative evaluation of diffractograms and derivatograms will not be given here, since it can be found in papers cited in the introduction. The comparison of the performance of the two methods will be given in detail.

The mineral composition of the bauxite samples of the Research Institute for Metal Industry was determined independently by an X-ray diffractometer and a derivatograph. The results differed by 0—3%. Based on this experience the results obtained by the author with 40 samples by the two methods differed by 0.5%. By converting the mineral composition obtained by the two methods to chemical composition, good agreement was found with the results of chemical analysis. The only systematic error was that the water content was found by 0.2—2.2% higher by the given two methods than by chemical analysis.

According to measurements this excess water is strongly adsorbed (chemiadsorbed) water which leaves the sample between 100 and 400 °C. This initial gradual water release is indicated on the TG curves in the derivatograms of even those samples which do not contain minerals from which water leaves at this temperature. This statement is supported by the fact that greater water excess was found in the case of loose, porous bauxites than of hard, solid ones. Furthermore, the — H_2O content of samples with higher water excess is higher in the air-dry form, than that of samples with small water excess. This phenomenon was most striking with the samples of laterite from Guinea, where an average of 2% adsorption water excess was found in the loose, lateritic-iron ore, while in the hard, solid iron ore ("cuirasse") above the former only 0.7%. Their mineral composition was practically the same.

According to the measurements of the author the amount of adsorbed water which leaves above 100 °C depends also on the mineral composition. Adsorbed water is mostly bound by iron minerals: goethite, hematite and magnetite. Thus *e.g.* the adsorbed water which leaves above 100 °C amounts to 0.9% in the red bauxite mined in the Ghiona mountains in Greece, which contains 20—30% hematite and goethite, while it is only 0.2% in the light grey spots in this red bauxite, which contains little iron ($Fe_2O_3 \approx 1\%$).

By removing iron minerals *e.g.* by dissolving in hydrochloric acid the amount of adsorbed water leaving above 100 °C may be remarkably reduced. *E.g.* in the red bauxite mined at Distomon which contained 28% hematite 1% adsorbed water was present. Most of the hematite was extracted by warm 10% hydrochloric acid. The derivatogram taken after the treatment showed only 0.4% adsorbed water (Fig. 6).

Manganese hydroxides adsorb even more water owing to their higher degree of dispersion: for instance in lithiophorite rich nests 1.5—2.2%.

The amount of water remaining adsorbed above 100 °C cannot be determined by an X-ray diffractometer alone, since, owing to the nature of the method, the sum of the crystalline phases is calculated as 100%. If, in a second step the non-crystalline fraction is also determined by addition method, then the non-crystalline fraction appears to be greater by the amount of this water.

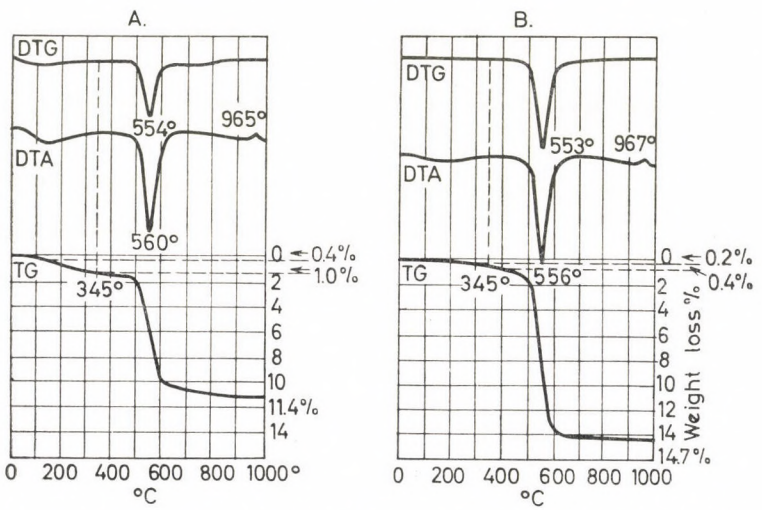

Fig. 6. Effect of acid treatment on the amount of water remaining adsorbed above 100 °C. A. Rusty brown boehmite-hematite bauxite from Distomon (Greece); B. The same sample after boiling with 10% HCl. Hematite was dissolved

When both diffractometer and derivatograph are used, the following sequence of operations can be suggested: First the quantitative crystalline composition of the sample is determined by a diffractometer. Then the chemical composition corresponding to the minerals is calculated. The amounts of H_2O, SO_3 and CO_2 are compared to those shown by the TG curve in the derivatogram. The water given by the initial section (100—400 °C) of the TG curve is the adsorbed water. If the calculations were made on the basis of the derivatogram only, then this water would increase the amount of minerals which have a weight loss in the initial section (*e.g.* gibbsite, goethite etc.).

The organic material in bauxite, as already mentioned, can only be determined by the derivatograph. The results obtained diffractometrically have to be corrected by this value. The organic material is generally below 0.1% in red, yellow and brown bauxite types, while it can reach 1—2% in some green and grey bauxites.

The joint application of the two methods has special importance when the samples from a new deposit have to be analyzed. The mineralogical error, which influences the X-ray diffractometric constants, may change the results

by 5—20%. The elimination of this error is rather difficult, since pure standard samples from the given deposit are necessary, or if these are not available, the constants have to be modified on the basis of a great number (20—50) of analyses.

In such cases derivatograms are of great help since according to experience the chemical composition and the structural water content of the minerals is less variable than the X-ray constants. The TG curves can be used — together with the results of chemical analysis — for correcting X-ray constants.

4. Further possibilities of application

The complex method of quantitative phase analysis described in the paper can be applied to other sedimentary and pyroclastic rocks. A similar complex method applicable to the investigation of clay rocks was published by BÁLINT (1964). It has to be pointed out that just in the case of clay rocks in the presence of various clay minerals there may be so many overlappings on the derivatograms and on the diffractograms that reliable results can only be obtained by thoroughly comparing them and also using the data of chemical analysis.

*

Derivatograms were taken by PAULIK–PAULIK–ERDEY MOM derivatographs with 0.1—1.0 g samples, at heating rates of 10°C/min and 11°C/min. The derivatograms of the 62 samples from the Research Institute of Metal Industry were recorded by the derivatograph working in this institute, while those of the further 40 samples by the equipment of the Institute for Mineralogy and Geochemistry of the L. Eötvös University, Budapest. The author wishes to express his thanks to Mr. FEHÉR for preparing the derivatograms.

REFERENCES

1. BÁLINT, P.: Építőanyag. (In Hungarian.) 449, 1964
2. BÁRDOSSY, GY.: Kohászati Lapok **99,** 355 (1966)
3. BEZJAK, A., FRIS-GACESA, F., UZELAC, V., ARAPOVIC, I.: Groatica Chimica Acta **34,** 51 (1962)
4. BLACK, R. H.: Analytical Chemistry **25,** 743 (1953)
5. BRINDLEY, G. W., SUTTON, W. H.: Economic Geology **52,** 391 (1957)
6. ERDEY, L., PAULIK, F.: Acta Chim. Acad. Sci. Hung. **21,** 205 (1955)
7. ERDEY, L., PAULIK, F., PAULIK, J.: MTA Kém. Tud. Oszt. Közl. **7,** 55 (1955)
8. FIEDLER, G., STEINIKE, K.: Ber. d. Ges. geol. Wiss. **B12,** 187 (1967)
9. GINSBERG, H., WEFERS, K.: Erzmetalle **10,** 499 (1957)
10. GUTKIN, E. SZ., SZKRIPKO, M. L.: Sovetskaa Geologya 133 (1957)
11. KOTSIS, T.: FÉMKUT Közleményei 7 (1962)
12. KOTSIS, T.: Géologie 159 (1964)
13. LANGIER-KUZNIAROWA, A.: Termogramy mineralow ilastych. Warszawa, 1967
14. MENCZEL, GY.: Magy. Kém. Folyóirat **64,** 143 (1958)
15. NÁRAY-SZABÓ, I., PÉTER, T.: Földtani Közlöny **94,** 444 (1964)
16. PAULIK, F., GÁL, S., ERDEY, L.: Anal. Chim. Acta **29,** 381 (1963)
17. PAULIK, F., LIPTAY, G., GÁL, S.: Talanta **10,** 551 (1963)
18. ROHNER, F.: Chimia **12,** 287 (1958)
19. TERTIAN, R., HOUSSEMAINE, R., LEGRAND, CH., TERTIAN, R.: Bull. Soc. chim. France 423 (1953)
20. TERTIAN, R., HOUSSEMAINE, R.: Chimie Analytique 182 (1954)
21. ÜVEGES, J., MÁRIÁSSYI M.: Acta Techn. Acad. Sci. Hung. **16,** 381 (1959)

György BÁRDOSSY; Budapest VIII., Múzeum krt. 4/a

Acta Chimica Academiae Scientiarum Hungaricae, Tomus 63 (3), pp. 279—291 (1970)

ELECTRON-MICROSCOPICAL INVESTIGATION OF THE OXIDE LAYER FORMED ON THE SURFACE OF CHEMICALLY TREATED GERMANIUM SINGLE CRYSTALS

EFFECT OF SOME CORROSIVE AGENTS ON THE MORPHOLOGY OF THE SURFACE OXIDE LAYER

J. GIBER,* L. E. CZÁRÁN,** and M. WÉGNER*

*(*United Incandescent Lamp and Electrical (TUNGSRAM) Co. Ltd. Semiconductor Development Department and **Central Research Institute for Chemistry of the Hungarian Academy of Sciences, Budapest)*

Received July 24, 1968

In revised form September 24, 1969

The effect of various etchants (that contain nitric acid, or hydrogen peroxide as an oxidant) has been investigated by electron microscopy in a study of morphological and structural features of oxide layers formed on the surface of germanium single crystals.

With etching agents CPI, CP4A, and H_2O_2 containing KOH, a continuous, homogeneous, smooth oxide layer can be produced by prolonged treatment.

In the temperature range from 25° to 50°C, nitric acid, and corrosive mixtures which contain nitric acid, produce oxide grains of hexagonal structure.

When hydrogen peroxide does not contain any alkali compound, at room temperature and at 110°C the hexagonal oxide is produced by it.

After treatment with hydrogen peroxide at 110°C containing potassium hydroxide or lithium carbonate, in the form of grains not joined together, respectively in the form of structures grown on to the foundation oxide layer, the presence of the tetragonal oxide can be observed.

The formation of the tetragonal modification has been found to be due to the presence of a basic alkali compound and to high temperature.

It is generally known that in the technological practice of semiconductor instruments based on germanium, the chemical corrosive agents produce an oxide layer on the surface of germanium single crystals, besides etching this surface in a characteristic way.

Studies of such germanium surfaces reveal [9] that surfaces resulting from treatment with various etchants exhibit various physical, and physicochemical peculiarities. Of this one presumable cause is the formation of various types or modifications of the germanium oxides according to the treatment applied, the various modifications having diverse properties. Thus an attempt at the elucidation of the structure, of crystallographical and morphological features within this structure, is sufficiently well motivated.

Practical significance is added by the fact that chemical treatment of semiconductors is unavoidable since the removal of the layer shattered during

mechanical shaping, as well as the formation of surfaces covered with oxides less sensitive to external influence, cannot be carried out otherwise.

Comparatively little attention has been paid to the morphology of oxide layers formed on the surfaces of germanium single crystals: authors seem to have been interested rather more in the investigation of so-called etch figures and in the production of smooth surfaces. Still fewer in number are those who tackled this question with direct methods like electronmicroscopy, electron-diffraction, or X-ray diffraction [1, 2, 3, 4, 5].

BERLAGA *et al.* [2] were the first to study by means of electronmicroscopy the crystal structure of oxide layers produced on the surface of germanium single crystals by chemical treatment (etching, and thermal oxidation, respectively). These authors found that hexagonal forms of crystals appear on the surface treated with concentrated nitric acid and supposed these to be due to the formation of $GeO_{2(hex)}$ particles. These authors were the first to have prepared by thermal oxidation the crystalline hexagonal oxide, and to have identified it by means of electronmicroscopy [5].

Even recent communications in the literature [3, 4] adhere to a morphological study of oxide layers prepared by treatment with pure nitric acid, and describe the reproduction by various routes of the results communicated by BERLAGA, and the finding which support his deductions.

Starting with the idea that, apart from concentrated nitric acid, various other corrosive agents, or mixtures of these, may be important and seeing that no data are available in the literature concerning oxide surface layers prepared with their use, we decided to study, by means of electronmicroscopy, the morphology of germanium oxide surface layers prepared with various etchants or with mixtures of these. Our aim was to obtain data concerning grain sizes and crystal forms in these layers.

Experimental

An ELMI-D2 type Zeiss electronmicroscope was used. Acceleration potential was 50 kV at 5.10^{-5} torr.

Since our interest was centered upon the morphology of surface layers, only the replica methods generally used in studies of surfaces were applied for the preparation of specimen. Generally the so-called single-stage replica was used since the resolution thus obtainable (25 to 50 Å) is better by one order of magnitude than the two-stage replica which reproduces surfaces by the interposition of a plastic film. This was resorted to only when the single-stage replica could not be separated from the original surface.

The carbon single-stage replica with palladium shadowing was prepared in the usual way: a palladium layer was applied (evaporated at an angle of 40°) to give sharply contrasting shadows and this was covered vertically with a suitably thick layer of spectroscopically pure carbon made in a HBA-2 type Zeiss evaporator. A hydrogen fluoride solution of 20 per cent concentration was used for flotation. When specimen plates were immersed obliquely into this solution, the replica became easily detached and drifted on to the liquid surface. After several washings in distilled water this film was transferred upon the object grid to be viewed in transmitted light.

The two-stage replica was prepared according to the standard technique [10], with a drop of a 5 per cent solution of collodion in amyl acetate. The dry and detached plastic film — shadowed and covered with carbon as before — was removed by dissolving in amylacetate and the residual carbon film was used for viewing.

Comparison, according to surface types, of the results collected by the application of these two techniques showed that, except in resolving power, no deviation exists between the two sets.

For the preparation of hexagonal, respectively of tetragonal* powders, these methods were unsuitable.

To establish the morphology of the hexagonal powder, this was suspended in carbon tetrachloride and the suspension was allowed to sediment upon the surface of a sodium chloride crystal. After evaporation of the solvent, shadowing with palladium followed, this surface was covered with carbon and the resulting film was collected on the surface of disstilled water. The so-called packing replica, formed after GeO_2 dissolved (the hexagonal modification is soluble in water) was placed into the electronmicroscope for examination. This technique was not applicable in the case of the tetragonal modification since its solubility in water is rather poor. Thus this substance was made to settle from its suspension in carbon tetrachloride directly upon the object grid previously provided with a zapon-lacquer supporting film. Thus in the electron microscope, and on the photographic pictures, the shadow image of the particles is seen, respectively recorded.

For the studies germanium single crystal plates ($D = 5000 \pm 3000/cm^2$ dislocation density, N-type (1.1.1.) orientation, 1.5 to 2 ohm.cm) were used which were ground, after cutting, on both sides with an aqueous suspension of a 10-μm silicium carbide powder and then, with the exception to be mentioned later on, were polished with an aqueous suspension of a 0.3 to 0.6 μm alumina powder removing a thickness of 30 μm on both sides. After cleaning (removal of fatty substances) with carbon tetrachloride the chemical treatment chosen followed, the duration of which varied according to the character of the experiment, and was always long enough to remove the mechanically shattered layer. This was carefully checked by X-ray diffraction. (With this technique of grinding and polishing, our experiments suggest that it is enough to remove 50 μm per side from surfaces only ground, and 20 μm from surfaces polished as well.)

Etching with concentrated (67 per cent) nitric acid

This treatment was carried out at 25 °C, or 50 °C.

Etching with a CPI-type etchant

This treatment, while vigorous stirring was maintained, consisted in submersion at 25 °C in a mixture of 67 per cent nitric acid (125 ml), 40 per cent hydrogen fluoride (75 ml), glacial acetic acid (75 ml) and iodine (330 mg).

Etching with an alkaline hydrogen peroxide solution

The mixture contained 30 per cent hydrogen peroxide (250 ml), and 25 per cent potassium hydroxide (2 ml). The etching was maintained at 110 °C, with vigorous stirring. It should be noted that this fluid etches slower by a factor of about ten than the former one.

Etching with CP4A-type etchant

The mixture contained 67 per cent nitric acid (100 ml), 40 per cent hydrogen fluoride (60 ml), and glacial acetic acid (80 ml). Temperature 25 °C; vigorous stirring.

After chemical treatment the etching liquid was removed from the samples. As a rule, care was taken to preserve the oxide structure produced by etching therefore the surfaces were rinsed with some water (since $GeO_{2(hex)}$ or $GeO_{2(amorph)}$ among the oxides are soluble in water, and since water in contact with a germanium surface can produce oxides on the

* The hexagonal powder was spectrometrically pure GeO_2 produced by Hoboken. The tetragonal variant was prepared in the Research Institute for Technical Physics, by hydrothermal conversion.

semiconductor which were not characterized by the etchant used) or with carbon tetrachloride. The samples were dried at room temperature in vacuum and stored in dust-free dry air. The fact that some ionic contamination may have persisted on the surface did interfere the electron microscopic study of morphology less than a thorough washing would have done by changing the prepared surfaces.

Of course, the so-called standard surfaces needed in other tests (adsorption of ions, gas, or vapour) were washed carefully in a stream of de-ionized water. In such cases the characteristics of the state of surface after washing were studied.

The results presented in this paper were found to be reproducible for surfaces prepared in 10 to 15 separate parallel experiments, and, as witnessed by the photographs of the several types of surfaces always recorded from various areas of one surface, are characteristic of that particular surface.

Results and discussion

First, only the surfaces mechanically worked were studied. A ground surface (Fig. 1) is shown to be rough, broken up; according to its electron microscopic picture of the same magnification, a polished surface (Fig. 2) is smooth. On the polished surface tracks of the polishing grains can be seen.

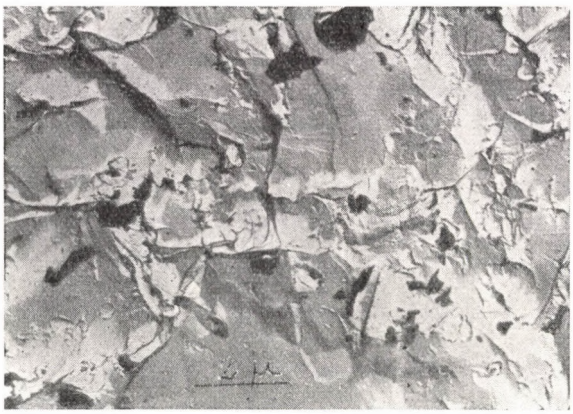

Fig. 1. Ground surface. Direct magnification, ×6000

In the study of the effect of concentrated nitric acid, the surface oxide structure produced by BERLAGA [2], and by VALYOCSIK [4], at room temperature by etching with concentrated nitric acid could be reproduced here by etching with the same acid at 50 °C for 5 minutes: on the surface of germanium, well developed crystal nuclei with clearly developed hexagonal symmetry are to be seen (Fig. 3). As the result of etching at 25 °C for 71 hours, a thick, laminated oxide layer is formed. This can be studied by means of X-ray diffraction, which reveals that the layer consists of $GeO_{2(hex)}$. The electron microscope photographs containing only angles of 60° and 120°, respectively, indicate a possible hexagonal symmetry (Fig. 4).

In the course of etching with a CPI mixture, the oxide layer is the result of two processes since nitric acid acts as an oxidant and hydrogen fluoride as a solvent for the oxide. In view of the fact that also in this mixture nitric acid is the oxidizing agent it seems reasonable to expect that here too hexa-

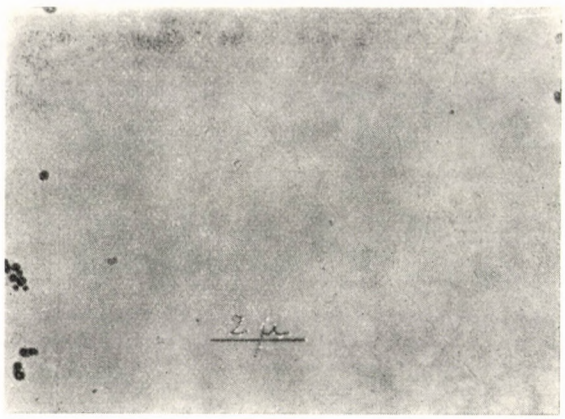

Fig. 2. Polished surface. Direct magnification, ×6000

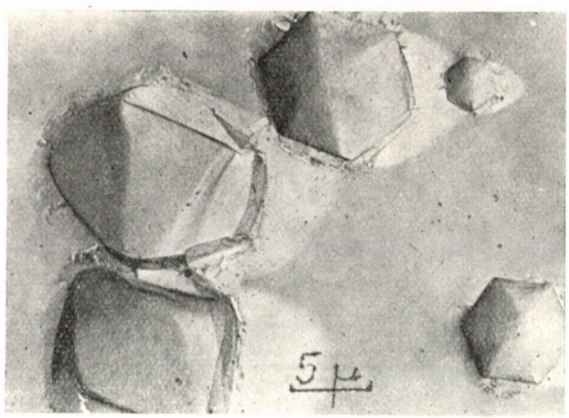

Fig. 3. Surface treated with concentrated nitric acid, at 50 °C, for 5 minutes. Direct magnification, ×2000

gonal structure will be characteristic of the oxide produced. This view is supported by the electron microscope photographs. Exposed to the etching agent for one minute, the sample contained surface areas where distinctly separated crystal grains were formed with (Fig. 5) hexagonal symmetry. That in an otherwise continuous oxide layer the formation of such nuclei is a consequence of the inhomogeneous temperature distribution due to exo-

thermal reactions because temperature coefficients of the oxidation reactions on the one hand, and that of the dissolution of the oxide on the other, differ, seems to be a tenable hypothesis.

When etching with CPI is allowed to proceed for a longer time, a continuous and homogeneous smooth oxide layer is formed (*cf.* Fig. 6). Since the

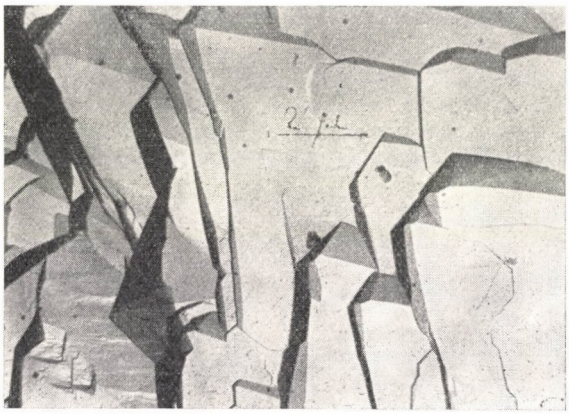

Fig. 4. Surface treated with concentrated nitric acid, at 25 °C, for 71 hours. Direct magnification, ×6000

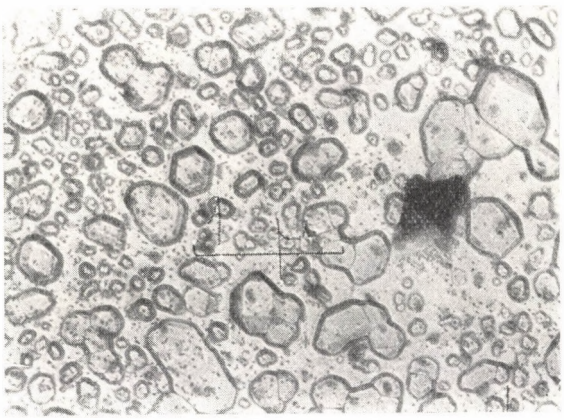

Fig. 5. Surface treated with the etching mixture CPI, for 1 minute. Direct magnification, ×12 000

CPI mixture contains hydrogen fluoride, which latter is a solvent for the oxides, no grains with dimensions comparable to those shown in Fig. 3 could be expected.

The morphology of the hexagonal oxide prepared on the surface was compared with that of powdered germanium oxide. Using the packing method

described before, electron microscopic photographs of the powder were made (Fig. 7). Germanium oxide obtained by etching and precipitated, in the course of alcoholic washing, upon the surface shows an electron microscopic picture (Fig. 8) that closely resembles Fig. 7. No hexagonal symmetry is recognizable in these photographs — though by X-ray diffraction the hexagonal structure of the powdered substance was established.

Fig. 6. Surface treated with the etching mixture CPI, continuous oxide layer. Direct magnification, ×32 000

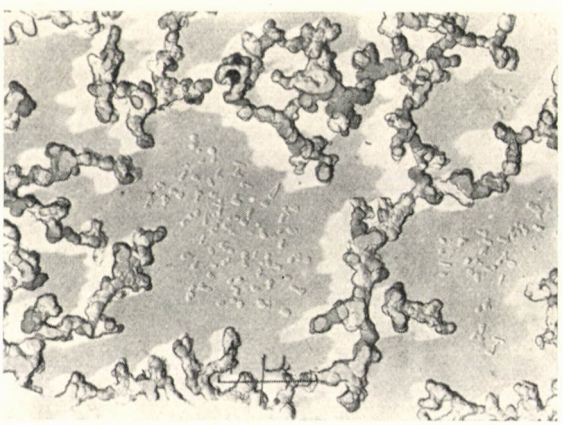

Fig. 7. Packing replica of commercial hexagonal germanium dioxide powder. Direct magnification, ×12 000

The shattered layer having been removed with CPI, a 5-minute etching at 110 °C with concentrated hydrogen peroxide produced separate grains visible by electron microscopy (Figs 9 and 10). The photographs show structures with tetragonal crystal symmetry, *i.e.* tetragonal germanium dioxide grains, according to our supposition. On polished surfaces without preliminary

etching with CPI, grains with tetragonal symmetry were produced by alkaline hydrogen peroxide when applied for a longer time, grown on to the basic oxide layer. Fig. 11 is particularly convincing: the photograph shows that the crystal grains became detached from the surface and stuck in the replica. When rinsing with carbon tetrachloride, which instead of water was applied,

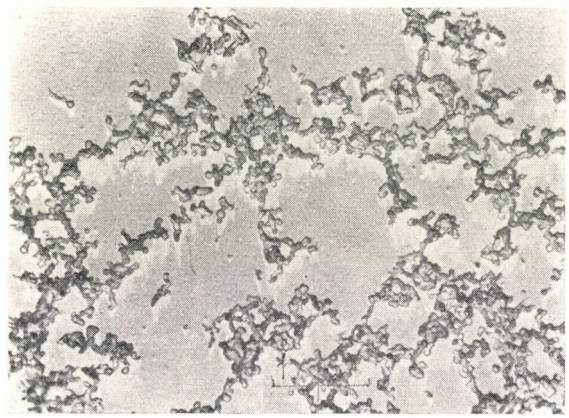

Fig. 8. Germanium dioxide precipitated on to the surface. Direct magnification, ×12 000

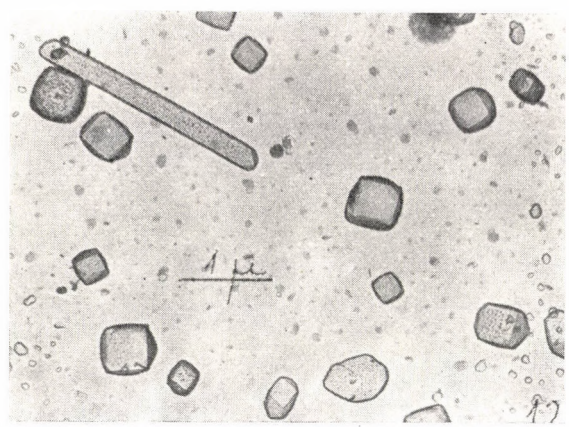

Fig. 9. Surface treated with hydrogen peroxide containing potassium hydroxide, at 110°C; pre-etching with CPI for 5 minutes. Direct magnification, ×12 000

developed tetragonal structures could be found (Fig. 12). An inhomogeneous surface covered with coalesced grains is shown in Fig. 13.

For the identification of tetragonal structures, photographs also of powdered germanium (tetragonal) oxide were taken (Fig. 14). The morphological similarity to structures on Fig. 9 are well discernible.

We wish to note that structures identified by means of electron microscopy do not justify any conclusion concerning crystal structures within

the entire surface oxide layer. Neither can the simultaneous presence of various crystalline and amorphous phases be excluded. Especially probable is this beside tetragonal structures: here too the oxide layer may contain hexagonal forms in substantial amounts. In these details the question may be studied by means of slow electron diffraction.

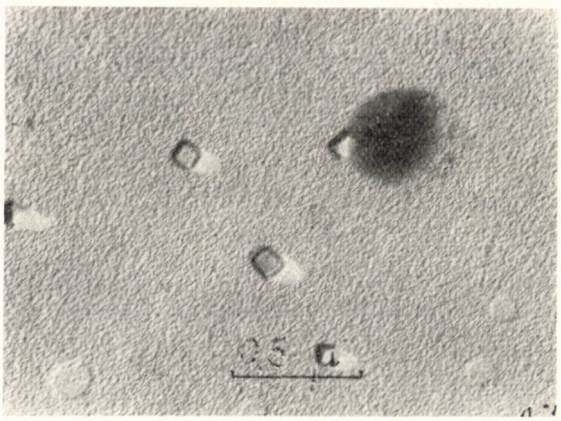

Fig. 10. Polished surface, treated with hydrogen peroxide containing potassium hydroxide, at 110 °C for 15 minutes. Direct magnification, ×32 000

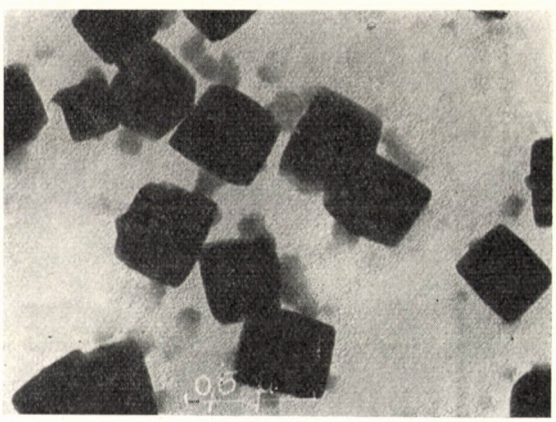

Fig. 11. Polished surface, treated with hydrogen peroxide containing potassium hydroxide at 110 °C for 15 minutes. Direct magnification, ×32 000

Since the literature data suggest that the conversion of $GeO_{2(hex)}$ into the tetragonal modification is facilitated* by traces of alkali compounds in

* In case of [6] the hexagonal dioxide is converted into the tetragonal form when an aqueous solution of $GeO_{2(hex)}$ is evaporated in the presence of traces of sodium hydroxide; in the case of [7] this conversion occurs when the surface layer of $GeO_{2(hex)}$ is embedded into germanium oxide powder containing lithium carbonate, and heated.

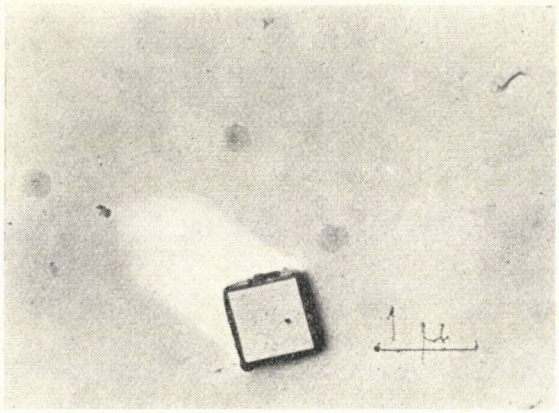

Fig. 12. Polished surface, treated with hydrogen peroxide containing potassium hydroxide, rinsed with carbon tetrachloride. Direct magnification, ×12 000

warm aqueous solutions [6] as well as in the solid surface phase at 860 °C [7], we suppose that also in our experiments potassium hydroxide contents are responsible for the appearance of tetragonal structures on the surface. In some experiments we replaced potassium hydroxide with lithium carbonate, *i.e.* treated the surface with a mixture of 250 ml concentrated hydrogen peroxide and 2 ml of a 1 per cent solution of lithium carbonate. As shown by the photograph (Fig. 15), the crystal grains with tetragonal symmetry appear again. In order to check whether for the production of tetragonal structures traces of alkali compounds and high temperature are needed, surfaces treated with concentrated hydrogen peroxide (free from alkali compounds) were studied. Within a few hours at 110 °C a thick oxide layer formed (Fig. 16) which could

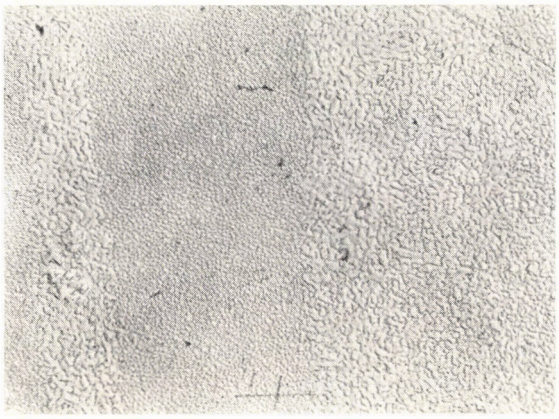

Fig. 13. Grains joined together by growth, after treatment with hydrogen peroxide. Direct magnification, ×3000

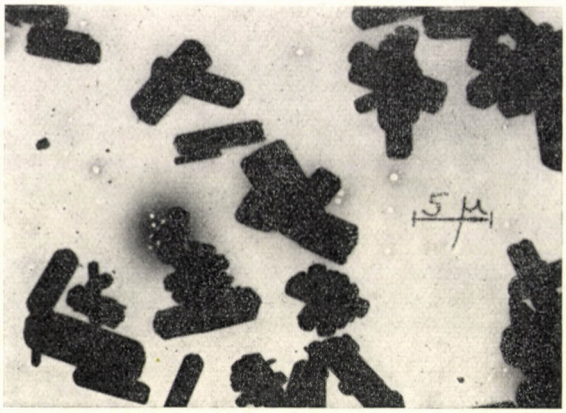

Fig. 14. Electron microscopic picture of tetragonal germanium dioxide powder. Direct magnification, ×2000

be tested by X-ray diffraction. According to these tests the layer was composed of hexagonal structures. At room temperature, neither a solution contained potassium hydroxide nor one contained lithium carbonate produced a tetragonal phase; under these conditions and in a few days a thick oxide layer grew (Fig. 17) that was proven by X-ray diffraction to be of hexagonal character.

The so-called standard surfaces used for other tests were prepared by directly etching the polished surface with CPI, CP4A, or alkaline hydrogen peroxide at temperatures and compositions mentioned (for 3 to 5 minutes in the former case, and for 30 minutes in the latter case). Since here the perfect cleanness of the surface was important, rinsing for 15 minutes in a stream of

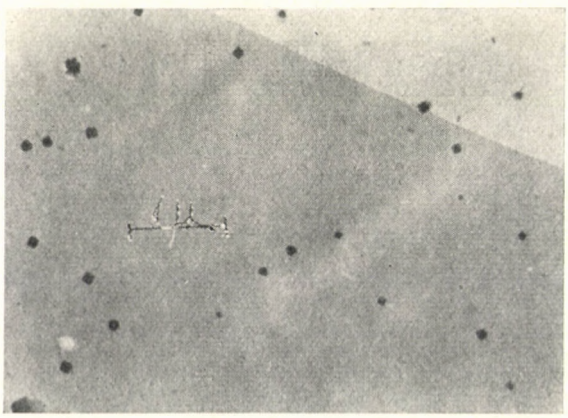

Fig. 15. Surface treated with hydrogen peroxide containing lithium carbonate, at 110 °C, for 15 minutes. Direct magnification, ×6000

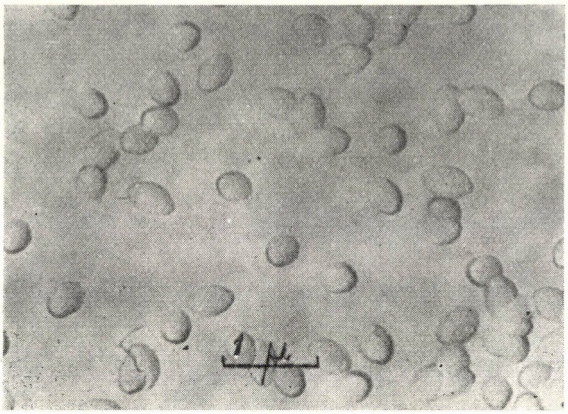

Fig. 16. Surface treated with pure concentrated hydrogen peroxide, at 110 °C, for 3 hours Direct magnification, ×12 000

de-ionized water (conductivity water) was applied. Surfaces thus prepared with CPI and CP4A were morphologically the same as that shown in Fig. 6. The "standard hydrogen peroxide surface" (Fig. 18) is less even; with medium magnification etch figures due to the differences of the etching rate on different plates are clearly discernible, and, according to other tests, are covered with a uniform oxide layer. Standard surfaces do not change their character when duration of etching and of rinsing is increased.

From our experimental data, together with those in the literature, we may state that etchants applied by us at low temperature produce hexagonal oxide layers. At higher temperatures, in the presence of basic alkali compounds a conversion $GeO_{2(hex)} \rightarrow GeO_{2(tetr)}$ or formation of $GeO_{2(tetr)}$, is observable.

Fig. 17. Surface treated with hydrogen peroxide containing lithium carbonate, at 25 °C for 71 hours. Direct magnification, ×2000

From the literature [8] we also know that below 1033 °C $GeO_{2(hex)}$ is less stable thermodynamically than the tetragonal modification. We suppose that certain compounds (perhaps only certain ions in them) *and* higher temperature facilitate that the unstable modification should not be "frozen in" and thus thermodynamically stable tetragonal germanium dioxide should be allowed to form. Supposedly, the basic alkali compounds facilitate octahedral arrangement and thus lead to the formation of tetragonal grains.

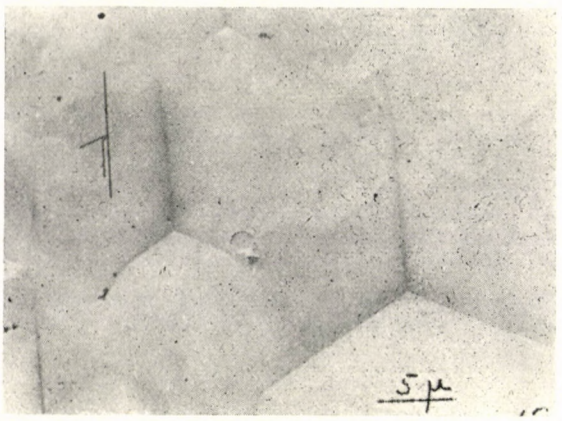

Fig. 18. Etching with hydrogen peroxide containing potassium hydroxide, for 30 minutes rinsing for 15 minutes. Direct magnification, ×2000

REFERENCES

1. Ellis, S. G.: J. Appl. Phys. **28,** 1262 (1957)
2. Berlaga, R. Ja., Konorov, P. P., Rudenok, M. I.: Radiotechn. i Elektron. **6,** 1370 (1961)
3. Konorov, P. P., Romanov, O. V.: Sov. Phys. Solid State **5,** 2225 (1964)
4. Valyocsik, E. W.: J. Electrochem. Soc. **114,** 176 (1967)
5. Berlaga, R. Ja., Bolsakov, L. P., Konorov, P. P., Rudenok, M. I.: Fiz. Tvjord. T. **5,** 2991 (1963)
6. Pflugmacher, A., Kellermann, J.: Angew. Chem. **68,** 374 (1956)
7. Albers, W. A., Valyocsik, E. W., Mohan, P. V.: J. Electrochem. Soc. **113,** 196 (1966)
8. Laubengayer, A. W., Morton, D. S.: J. Am. Chem. Soc. **54,** 2303 (1932)
9. Many, A., Goldstein, Y., Grover, N. B.: Semiconductor Surfaces. p. 377. North Holland Publ. Co., Amsterdam, 1965.
10. Kay, D.: Techniques for Electron Microscopy. p. 86. Blackwell Scientific Publ., Oxford, 1961

János Giber
Erzsébet L. Czárán
Mária Wégner
Budapest IV. Váci út 77.

Acta Chimica Academiae Scientiarum Hungaricae, Tomus 63 (3), pp. 293—299 (1970)

DETERMINATION OF THE REAL COMPOSITION OF ACETIC ACID–CARBON TETRACHLORIDE MIXTURE FROM ITS DIELECTRIC BEHAVIOUR ACCORDING TO THE A—A_2—B TERNARY MIXTURE MODEL, II

J. Liszi

(Department of Physical Chemistry, University of Chemical Engineering Sciences at Veszprém; Research Group for Electrochemistry of the Hungarian Academy of Sciences)

Received October 1, 1968

The interpretation of the data given in the first part is extended. The error in the calculated composition of the mixtures is traced back to the uncertainty in the data used.

In the first part [1] of this communication the composition of mixture, modelled as an $A—A_2—B$ ternary mixture, of acetic acid and carbon tetrachloride has been determined from dielectric properties (A symbolizes monomeric acid, A_2 dimeric acetic acid, and B stands for carbon tetrachloride). In this part the author continues the interpretation of the results reported in the first part, and examines how far the uncertainty in the data used have led to errors in the calculated compositions of the mixtures.

1. Permanent dipole moment of dimeric acetic acid

In the literature two opinions, contradicting each other, are to be found about the association structures formed in liquid acetic acid. According to the one, chain-like structures are formed [2, 3]. In the vapour phase, and in solution in non-polar solvents, dimeric ring structures are judged to occur [4]. In the present work the latter model is accepted to study mixture of acetic acid with a non-polar substance. Accordingly, the nominal binary mixture of acetic acid and carbon tetrachloride was treated as a ternary mixture of $A—A_2—B$ type, and the real composition was considered to be the composition of the ternary mixture so defined.

For the determination of the true composition of the mixture, the following molecular model was used. Carbon tetrachloride was held to be a substance composed of spherical molecules with average polarizability α_3 and zero permanent dipole. Molecules of monomeric, and of dimeric, acetic acid we held — from the point of view of dielectric behaviour — to be point dipoles within an ellipsoidal cavity. To monomeric acetic acid μ_1 permanent dipole

and α_1 average polarizability, to dimeric acetic acid μ_2 permanent dipole and α_2 average polarizability was attributed. The calculations followed the fundamental work of SCHOLTE [5].

Several acceptable explanations offer themselves for the view that dimeric acetic acid molecules at all possess a permanent dipole moment. If these dimeric molecules are not of a cyclic structure but possess only one hydrogen bond then the emergence of a permanent dipole moment is evident. However, this arrangement does not find favour in the literature though in liquid formic acid the presence of chain-like association structures have been detected [6]. According to HARRIS and ALDER [7], self-ionization in carboxylic acids plays an important part in the shaping of their dielectric character: self-ionization described by the scheme

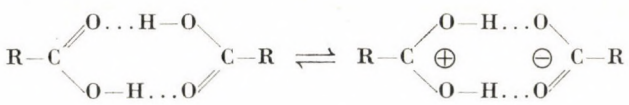

may be responsible for the generation of a permanent dipole in dimeric carboxylic acids. According to PIMENTEL and MCCLELLAN [4] there is no evidence whatever forthcoming in favour of the view that cyclic dimers in the liquid phase are planar. It may be supposed that due to strong molecular interactions the planar structure becomes distorted and that the distortion produces a permanent dipole moment. Among the possible explanations here briefly sketched, the first is discarded, *i.e.* the presence of chain-like association structures because also the literature seems reluctant to adopt it. The evolution of a self-ionization equilibrium is denied in the literature on grounds of infrared studies because existence of such ion-pairs cannot be detected by the spectra [4]. Thus the most probable explanation seems to remain the one that ascribes the permanent dipole moment of dimeric acetic acid molecules to the deformation perpendicular to the plane of the ring. This explanation is supported by the fact that hydrogen bonding which holds these associated parts together is significantly weaker than the classic chemical bond and consequently much more mobile.

The present studies lead to the following results. If in the calculations $\mu_2 = 0.00$ D was used then a lower degree of dimerization offered for liquid acetic acid than that determined for the vapour phase [8] and this is, on thermodynamic grounds, not likely to be the case. If the value determined by POHL, HOBBS and GROSS [9], was used *viz.* $\mu_2 = 0.92$ D, then real values for pure liquid acetic acid are obtainable, but for the more diluted solutions in carbon tetrachloride negative mole fractions would result, thus figures are obtained which lack physical meaning. Therefore it was concluded that the permanent dipole moment of dimeric acetic acid is a function of dilution.

It is supposed that the explanation of this is to be found therein that in concentrated solutions monomeric, and dimeric, acetic acid molecules interact so that the force of interactions suffices to deform dimeric acetic acid in a direction normal to the plane of the ring and thus to produce a permanent dipole in it. With a decrease of the concentration of acetic acid this interaction grows weaker, and at infinite dilution — like in the vapour phase — dimeric acetic acid molecules have no dipole moment at all.

2. Errors in calculated compositions

In the following a brief discussion is given about the consequences of the uncertainty of the quantities used for the calculating of true compositions for the mixtures.

True compositions, corresponding to the ternary model $A-A_2-B$, of the mixtures were calculated using Eq. [1].

$$\frac{\varepsilon-1}{4\pi N_A}\,\frac{1}{\varrho}\,(M_1 x_1+M_2 x_2+M_3 x_3)=\frac{36\,\varepsilon n_\infty^2}{17\varepsilon n_\infty^2+7n_\infty^4+7\varepsilon+5n_\infty^2}$$

$$\left\{x_1\frac{\alpha_1}{1-f_1\alpha_1}+x_2\frac{\alpha_2}{1-f_2\alpha_2}+x_3\frac{\alpha_3}{1-f_3\alpha_3}\right\}+x_1\frac{\varepsilon}{\varepsilon+(1-\varepsilon)A_1} \tag{1}$$

$$\frac{\mu_1^2}{3kT}\,\frac{p\cdot q_1^2}{(1-f_{\mu_1}\cdot\alpha_{\mu_1})^2}+x_2\frac{\varepsilon}{\varepsilon+(1-\varepsilon)A_2}\,\frac{\mu_2^2}{3\,kT}\,\frac{p\cdot q_2^2}{(1-f_{\mu_2}\cdot\alpha_{\mu_2})^2}$$

where ε = dielectric constant
N_A = Avogadro's number
x_1, x_2, x_3 = mole fractions
M_1, M_2, M_3 = molecular weights
$\alpha_1, \alpha_2, \alpha_3$ = average polarizabilities
μ_1, μ_2 = permanent dipole moments
k = Boltzmann's constant
T = absolute temperature
ϱ = density
n_∞ = refractive index extrapolated to infinite wavelength

$$A=\frac{abc}{2}\int_0^\infty\frac{ds}{(s+a^2)^{\frac{3}{2}}\,(s+b^2)^{\frac{1}{2}}\,(s+c^2)^{\frac{1}{2}}} \tag{2}$$

where a, b and c stand for the half-axes of the ellipsoid that geometrically represents the space of the molecules, a is the half-axis in the direction of the

permanent dipole moment. A_1 and A_2, in Eq. (2) are the factors referring to monomeric, and dimeric molecules.

$$f = \frac{1}{abc} \frac{2n_\infty^2 - 2 + \frac{3(\varepsilon - n_\infty^2)}{17\varepsilon + 7n_\infty^2}}{2n_\infty^2 + 1 - \frac{3(\varepsilon - n_\infty^2)}{17\varepsilon + 7n_\infty^2}} \tag{3}$$

f must be calculated separately for the three components (f_1, f_2 and f_3, in Eq. (1)).

$$f_\mu = \frac{3}{abc} \frac{A(1-A)(n_\infty^2 - 1)}{\varepsilon + (1-\varepsilon)A} \tag{4}$$

f_μ must be calculated separately for monomeric, and for dimeric, acetic acid (f_{μ_1} and f_{μ_2} in Eq. (1))

$$p = \frac{36\varepsilon n_\infty^2}{17\varepsilon n_\infty^2 + 7n_\infty^4 + 7\varepsilon + 5n_\infty^2} \frac{2\varepsilon + 1}{3\varepsilon} \tag{5}$$

$$q = \frac{1}{1 - f\alpha_\mu} \left\{ 1 - \frac{\alpha_\mu}{abc} \frac{2n_\infty^2 - 2}{2n_\infty^2 + 1} \right\} \tag{6}$$

where α_μ is the polarizability of the molecule in the direction of its dipole (α_{μ_1} for monomeric, α_{μ_2} for dimeric, acetic acid); q must be calculated separately for monomeric, and for dimeric acetic acid (q_1 and q_2 in Eq. (1)).

In what follows, the examination of the effect is given upon the calculated figures of composition of the uncertainty of the quantities in Eq. (1).

a) Effect of the uncertainty of the dielectric constant ε

The dielectric constant of mixtures was measured with a TR-9701 type bridge allowing ± 2 per cent accuracy. If we regard all the quantities, with the exception of the dielectric constant, to be accurate, then the error $\Delta\varepsilon$ in measured figures, on the basis of the function

$$x_i = f[x_B(\varepsilon), \varepsilon] \tag{7}$$

may cause the error

$$\Delta x_i = \left(\frac{\partial x_i}{\partial \varepsilon} \right)_{x_B} \Delta\varepsilon = \left\{ \frac{dx_i}{d\varepsilon} - \left(\frac{\partial x_i}{\partial x_B} \right)_\varepsilon \frac{dx_B}{d\varepsilon} \right\} \tag{8}$$

in the true mole fraction values pertaining to the given x_B composition. This value is $\Delta x_i = \pm 0.003$ in the entire range of concentrations, according to Eq. (1).

b) Effect of the uncertainty in the refractive index extrapolated to infinite wavelength, n_∞

For carbon tetrachloride, since its molecules do not possess permanent dipole moments, the square of the refractive index extrapolated to light of infinite wavelength corresponds to the dielectric constant. Thus the uncertainty in $n^2_{\infty B}$ is ± 2 per cent. The refractive index extrapolated to light of infinite wavelength we have calculated from dispersion data [1]. It is extremely difficult to estimate the uncertainty in data for resonance frequencies and force constants taken from the literature, especially if we consider that the latter show great deviations [10, 11, 12]. Therefore the uncertainty of figures for refractive indices extrapolated to light of infinite wavelength in pure liquid acetic acid is estimated as follows. It is supposed that a refractive index which appertains to a frequency just higher than relaxation frequency does differ but slightly from a refractive index referred to light of infinite wavelength. If Eq. (1) is written for a frequency above relaxation frequency then, for pure acetic acid, we arrive at the correlation

$$\frac{n^2-1}{4\pi N_A}\frac{1}{\varrho}(M_1 x_1+M_2 x_2)=\frac{3n^2}{2n^2+1}\left\{x_1\frac{\alpha_1}{1-f_1\alpha_1}+x_2\frac{\alpha_2}{1-f_2\alpha_2}\right\} \tag{9}$$

where

$$f=\frac{1}{abc}\,\frac{2n^2-2}{2n^2+1} \tag{10}$$

(f must be calculated separately for monomeric and dimeric acetic acid). In the first part of this communication, the value arrived at from dispersion data is $n^2_{\infty\mathrm{ac}}=2.6991$; Eq. (9) leads to the figure $n^2_{\mathrm{ac}}=2.6500$. The deviation between the two figures is 2 per cent. If we accept, based upon this, that the error in the second power of the refractive index referred to light of infinite wavelength is ± 2 per cent in the whole range of concentrations, then this uncertainty causes an error of $\Delta x_i=\pm 0.0002$ in the real mole fractions. Similarly to the calculation of the error caused by the uncertainty of dielectric constants, the error calculated according to the equation

$$\Delta x_i=\left\{\frac{dx_i}{dn^2_\infty}-\left(\frac{\partial x_i}{\partial x_B}\right)_{n^2_\infty}\frac{dx_B}{dn^2_\infty}\right\} \tag{11}$$

However, we ought to mention that due to the approximation made in the course of the estimation, the uncertainty of the refractive index referred to light of infinite wavelength should be regarded only as an informative figure.

c) Effect of the uncertainty of other terms in Eq. (1)

Compared with that of the measured dielectric constants, the errors in density figures are negligibly small, therefore their effect upon the uncertainty of mole fraction figures can be left out of account. Average polarizability figures and permanent dipoles were taken from the literature [9, 13]. If significant figures given in the literature are regarded as accurate, then the uncertainty in these is in the order of tenths of per cents, and has no effect. The case is similar concerning molecular dimensions deduced from X-ray studies [3]; in the literature inaccuracies amounting to ± 0.01 Å or ± 0.02 Å are mentioned.

On the basis of the foregoing we may state that, in essence, inaccuracy in figures calculated for true mole fractions is due to errors committed in the measurement of dielectric constants. Calculated figures, and the measure of their inaccuracy, are shown in Table I.

Table I

x_B	x_1	x_2	x_3
0.0	0.115 ± 0.003	0.885 ± 0.003	0.000
0.2	0.055	0.621	0.324 ± 0.003
0.4	0.027	0.409	0.564
0.6	0.012	0.243	0.746
0.8	0.004	0.109	0.887
1.0	0.000	0.000	1.000

It should be noted that the errors indicated in the table refer to the worst instances. Per cent proportion of errors increases, of course, with the decrease of mole fraction figures. Deviations cause the greatest uncertainty in the mole fraction figures of monomeric acetic acid since, nearly over the entire range of concentrations, monomeric acetic acid has the lowest mole fractions.

Symbols

A = monomeric acetic acid
A = the constant defined by Eq. (2)
A_2 = dimeric acetic acid
B = carbon tetrachloride
a, b, c = half-axes of the ellipsoid which represents the geometry of monomeric, and dimeric, acetic acid
f = factor defined by Eqs (3) and (10)
f_μ = factor defined by Eq. (4)
k = Boltzmann's constant
M = molecular weight

n = refractive index
n_∞ = refractive index extrapolated to light of infinite wavelength
p = factor defined by Eq. (5)
q = factor defined by Eq. (6)
s = space co-ordinate
T = absolute temperature
x = mole fraction
α = average polarizability
α_μ = polarizability in the direction of the permanent dipole
ε = dielectric constant
μ = permanent dipole moment
ϱ = density

Indices for the designation of components

1 = monomeric acetic acid in a real mixture
2 = dimeric acetic acid in a real mixture
3 = carbon tetrachloride in a real mixture
ac = acetic acid in a nominal mixture
B = carbon tetrachloride in a nominal mixture

REFERENCES

1. Liszi, J.: Acta Chim. Acad. Sci. Hung. **62,** 263 (1969)
2. Allen, G., Caldin, E. F.: Quart. Rev. **7,** 255 (1953)
3. Jones, R. E., Templeton, D. H.: Acta Cryst. **11,** 484 (1958)
4. Pimentel, C. C., McClellan, A. L.: The Hydrogen Bond. Freeman, San Francisco and London 1960
5. Scholte, T. G.: Physica **XV,** No. 5—6, p. 347 (1949)
6. Chapman, D.: J. Chem. Soc. **1965,** 225
7. Harris, F. E., Alder, B. J.: J. Chem. Phys. **21,** 1306 (1953)
8. Ritter, H. L., Simons, J. H.: J. Am. Soc. **67,** 757 (1945)
9. Pohl, H. A., Hobbs, M. E., Gross, P. M.: J. Chem. Phys. **9,** 408 (1941)
10. Moelwyn-Hughes, E. A.: Physical Chemistry. Pergamon, London, NewYork, Paris 1964
11. Herzberg, G.: Infrared and Raman Spectra of Polyatomic Molecules. New York, 1945
12. Brooks, W. V. F., Haas, C. M.: J. Phys. Chem. **71,** No. 3. p. 650 (1967)
13. Affsprung, H. E., Findenegg, G. H., Kohler, F.: J. Chem. Soc. A. **1968,** p. 1364

János Liszi; Veszprém, Schönherz Z. u. 12. Hungary

Acta Chimica Academiae Scientiarum Hungaricae, Tomus 63 (3), pp. 301—317 (1970)

ADSORPTION ON SOLIDS FROM SOLUTIONS CONTAINING A POLAR COMPONENT

S. K. SURI and V. RAMAKRISHNA*

(Chemistry Department, Indian Institute of Technology, New Delhi-29)

Received December 19, 1968

Adsorption from binary solutions of nitromethane and nitrobenzene respectively in benzene, cyclohexane and dioxane on chromatographic silica gel at 20 °C and alumina at 30 °C has been determined. On silica, the adsorption from the solutions extends close to a monolayer while on alumina, mostly multilayer adsorption occurs. Adsorption from dioxane–nitromethane solutions has been found to occupy about half a monolayer or less on these two solids.

The thermodynamic treatment outlined by SCHAY and NAGY [3, 4] and by EVERETT [5, 6] has been extended to the adsorbed phase from these solutions. In most cases, results obtained by the alternate methods show a fair agreement. Adsorption at the free liquid surface has also been compared with the adsorbed layer on the solids. The extent of adsorption per unit area on the solid surfaces has been found to be some 2 –4 times higher than on the free liquid surface.

Theoretical treatment

It has been recognised for some time [1] that there is a similarity between the free liquid surface of a binary solution and the adsorbed phase between the solution and an inert solid. This similarity extends not only to the nature of adsorptions that occur at these interfaces, but also to the thermodynamic treatment of the data and the models used for the adsorbed phase. Experimentally, however, while the surface tensions of binary liquid mixtures can be measured directly, the interfacial tension between the liquid and a solid surface cannot be so measured. It has to be computed by indirect methods. A simple treatment of the adsorbed phase in solid–liquid systems analogous to that of the free liquid surface, can be given — using both the ideal solution and the regular solution models [1, 2]. If γ_i is the interfacial tension of pure components in contact with the solid, and γ that of the solution, the following equations can be written for the chemical potentials (μ_i) in the liquid (l) and the adsorbed (σ) phase respectively:

$$\mu_i^l = \mu_i^{l0} + RT \ln a_i^l \tag{1}$$

$$\mu_i^\sigma = \mu_i^{l0} + (\gamma_i A_i - \gamma \bar{A}_i) + RT \ln a_i^\sigma . \tag{2}$$

* To whom all correspondence may be addressed.

In the above equation A_i stands for the surface occupancy of the molecules (cm^2/mol) and $a_i = x_i f_i$ the thermodynamic activity. It can be shown that

$$x_1^\sigma = \frac{x_1^l}{x_1^l + \frac{f_2^l}{f_1^l} \cdot \frac{f_1^*}{f_2^*} x_2^l} \tag{3}$$

where

$$\frac{f_1^*}{f_2^*} = \frac{f_1^\sigma}{f_2^\sigma} \cdot \frac{\exp \cdot (\gamma_1 - \gamma) A_1/RT}{\exp \cdot (\gamma_2 - \gamma) A_2/RT}$$

$$= \frac{f_1^\sigma}{f_2^\sigma} \cdot \exp \cdot \frac{(\gamma_1 A_1 - \gamma_2 A_2)}{RT} \exp \cdot \frac{(A_2 - A_1)\gamma}{RT} . \tag{4}$$

$$= \frac{f_1^\sigma}{f_2^\sigma} \cdot \frac{1}{K_a} . \tag{5}$$

Here, K_a is a constant for the system at constant temperature. Eq. (3) can be considered to be the most general form of the adsorption isotherm. The shape of the isotherm then depends on the following four factors [3, 4]:

(i) the nature of the bulk phase, as given by the term f_1^l/f_2^l; the ratio of activity coefficients in liquid phase;

(ii) the nature of the adsorbed phase, as given by the term f_1^σ/f_2^σ;

(iii) the magnitude of the term exp. $(\gamma_1 A_1 - \gamma_2 A_2)/RT$ which may be considered to represent the difference in the adsorption potentials of the two components;

(iv) the magnitude of the term exp. $(A_2 - A_1)\gamma/RT$ which may be considered to represent the variation of surface energy with the composition of the bulk solution.

It has generally been observed [1, 3] that the influence of the first factor, (f_1^l/f_2^l) on the nature of the adsorbed phase is profound, as in the case of the free liquid surface.

When the approximation $A_1 \approx A_2 = A$ can be made, and the behaviour at the surface can be expected to near the ideal, it will be observed from Eq. (5) that

$$K_a = \exp.(\gamma_2 - \gamma_1) A/RT . \tag{6}$$

Under similar circumstances, for the liquid–vapour interface [2],

$$c = \exp.(\gamma_1' - \gamma_2') A/RT . \tag{7}$$

The close similarity between Eqs (6) and (7) may be noted. In such cases, the free liquid surface and the adsorbed phase on a solid can be directly com-

pared using YOUNG's equation:

$$\gamma_{LS} = \gamma_{SV} - \gamma_{LV} \cos \Theta \tag{8}$$

where subscripts L, S and V refer to liquid, solid and vapour, respectively. If the liquids are completely wetting, $\cos \Theta = 1$, and it can be shown that

$$(\gamma_{LV})_2 - (\gamma_{LV})_1 = (\gamma_{LS})_1 - (\gamma_{LS})_2 . \tag{9}$$

Hence from Eqs (6) and (7),

$$C = 1/K_a . \tag{10}$$

It follows therefore that if the adsorption at these interfaces are both expressed in terms of unit surface area, the curve for one must be rotated by an angle 2π with respect to the x_i^l axis to obtain that of the other. The convention we will use for comparing adsorptions at the free liquid surface and the liquid-solid interface will be in terms of $\Gamma_1^{(N)}$ which gives the excess of component 1 in the surface per unit area, compared to the same total number of moles in the bulk. Thus,

$$\Gamma_1^{N)} = \Gamma_1 - x_1^l(\Gamma_1 + \Gamma_2) \tag{11}$$

where Γ_1 is the actual surface concentration of the component. Such comparisons have been found to hold good in a few cases (1).

In case of non-ideal behaviour in the adsorbed layer, the analysis of the other factors of Eqs (3) and (5) needs to be carried out. Two approaches are used in practice. The first is due to SCHAY and NAGY [3, 4]. If m grams of a solid having a specific surface area Σ, is equilibrated with n_0 moles of a binary liquid mixture, which undergoes a change of composition Δx_1^l due to adsorption, it can be shown that

$$\frac{n_0 \Delta x_1^l}{\Sigma m} = \Gamma_1^{(N)} = - \frac{(1 - x_1^l)}{RT} \frac{d\gamma}{d \ln a_1^l} . \tag{12}$$

This equation is a form of GIBB's adsorption isotherm. Hence, from Eq. (12),

$$(\gamma_1 - \gamma) A_1 = \frac{RTA_1}{\Sigma} \int_{a_1=1}^{a_1} \frac{n_0 \Delta x_1^l}{(1 - x_1^l) m} d \ln a_1^l . \tag{13}$$

SCHAY carries out the integration graphically, using experimental data, to obtain $(\gamma_1 - \gamma)$. Further, the surface composition can be written in terms

of the amount of adsorption ($n_0 \Delta x_1^l/m$); thus,

$$x_1^\sigma = \frac{\Sigma x_1^l + A_2(n_0 \Delta x_1^l/m)}{\Sigma + (A_2 - A_1)(x_0 \Delta x_1^l/m)} \tag{14}$$

It is, therefore, possible to calculate $\ln f_1^\sigma$, using Eqs (13) and (14). Thus

$$\ln f_1^\sigma = \ln a_1^l - \ln x_1^\sigma - (\gamma_1 - \gamma) A_1/RT. \tag{15}$$

The other approach is due to EVERETT [5, 6]. If the ratio of activity coefficients, $f_1^l f_2^\sigma / f_2^l f_1^\sigma$, in Eqs (3)—(5) can be approximated to unity, then

$$x_1^\sigma = \frac{x_1^l}{x_1^l + x_2^l/K_a} = \frac{K_a x_1^l}{K_a x_1^l + x_2^l}. \tag{16}$$

Also,

$$\frac{n_0 \Delta x_1^l}{m} = \frac{n^\sigma}{m}(x_1^\sigma - x_1^l). \tag{17}$$

Combining Eqs (16) and (17), it follows that

$$\frac{n_0 \Delta x_1^l}{x_2^l m} = \frac{n^\sigma}{m}\left(\frac{K_a - 1}{K_a}\right) - \frac{n_0 \Delta x_1^l}{m} \cdot \frac{1}{K_a x_1^l}. \tag{18}$$

or

$$-\frac{x_1^l x_2^l}{n_0 \Delta x_1^l/m} = \frac{m}{n^\sigma}\left[x_1^l - \frac{1}{1 - K_a}\right]. \tag{19}$$

Eqs (18) and (19) can be applied directly to the experimental data of adsorption. The former, due to ERDŐS [7], is more suitable for the calculation of K_a, while the latter, due to EVERETT [5], is more suitable for the calculation of n^σ. Once n^σ has been obtained, Eq. (17) will yield the value of x_1^σ. Further, the activity coefficients can then be calculated [6] from

$$\ln f_2^\sigma = x_1^\sigma \ln\left(\frac{x_1^\sigma}{x_2^\sigma} \cdot \frac{a_2^l}{a_1^l}\right) - \int_0^{x_1^\sigma} \ln\left(\frac{x_1^\sigma}{x_2^\sigma} \cdot \frac{a_2^l}{a_1^l}\right) dx_1^\sigma. \tag{20}$$

A similar expression can be written for $\ln f_1^\sigma$. EVERETT [6] has discussed in detail the difference between his derivation and the earlier treatments of ERDŐS [7] and KISELEV [8]. If the two components occupy vastly different

areas, *i.e.* if A_2/A_1, is far different from unity, an extra term $r = A_2/A_1$ has to be introduced into the equation expressing the distribution coefficient of the components between the adsorbed phase and the bulk solution; thus

$$(a_1^\sigma/a_1^l)\,(a_2^l/a_2^\sigma)^{1/r} = K_a. \tag{21}$$

This equation cannot be solved analytically, excepting by introducing various simplifications [9]. Also, if r is very large, as in the case of polymer solutions, it is difficult to define an exact boundary between the adsorbed phase and the bulk solution [1, 10].

Scope of the present work

In the present investigation we have studied binary systems where the size ratio A_2/A_1 is not far different from unity (see Table I); hence the method of SCHAY and NAGY as well as that of EVERETT can be applied for the calculation of x_i^σ and f_i^σ for the adsorbed phase. It will be noted, however, that in both the methods, the experimental data have to be put through a graphical integration, which renders the process tedious and somewhat less accurate.

Table I

Some physical properties of the liquids used

Liquid (i)	F.P. (°C)	ϱ_i (20 °C) (g/ml)	ϱ_i (30 °C) (g/ml)	γ_i (20 °C) (dyne/cm)	γ_i' (30 °C) (dyne/cm)	A_i^* (30 °C) (cm²/mole) × 10^{-10}
Benzene	5.50	0.8790	0.8685	28.85	27.55	0.169
	(5.53)	(0.8790)	(0.8685)	(28.88)	(27.57)	
Cyclohexane	6.60	0.7786	0.7694	25.00	23.85	0.193
	(6.68)	(0.7785)	(0.7690)	(25.20)	(23.82)	
1,4-Dioxane	11.75	1.0338	1.0220	33.75	32.20	0.165
	(11.80)	(1.0337)	(1.0223)	(33.74)	(32.20)	
Nitrobenzene	5.70	1.2035	1.1933	43.40	42.20	0.185
	(5.70)	(1.2032)	(1.1936)	(43.35)	(42.17)	
Nitro-	—	1.1386	1.1239	37.19	35.50	0.121
methane		(1.1311)**	(1.1245)	(36.98)	(35.51)	

* Calculated from $A_i = (V_i)^{2/3}\,(N)^{1/3}$.
** Density at 25 °C as compared to our average value 1.1312 g/ml.
All values in parantheses indicate the literature values [14].

EVERETT's method has the advantage of yielding x_i^σ values without recourse to a knowledge of A_i, provided the adsorption data obey the linear relationship, Eq. (19). Also, the constant K_a can be evaluated without a discussion of the surface activity coefficients. SCHAY's approach, on the other hand, requires a prior estimate of the surface occupancy of the molecules in order to calculate x_i^σ (see Eq. (14)) and thence f_i^σ. To the best of the authors' knowledge, the results obtained from these two approaches have been compared only for a few systems [11, 12]. SURI and RAMAKRISHNA [11, 12] made the following observations: (i) the values obtained from the two approaches for the adsorption on silica and alumina, n^σ/m, from the binary solutions of benzene, cyclohexane and dioxane agree extremely satisfactorily; (ii) a judicious combination of these two methods may enable the calculation of A_i, the actual surface occupancy of the molecules and hence throw light on surface orientation. However, some questions remained unanswered; namely, (*a*) what would happen to such comparisons if one of the components was strongly polar? (*b*) what would happen if the adsorption isotherm was *S*-shaped instead of the *U*-shaped curves obtained in the previous systems? To find some answers to these questions, we have extended our investigations to the study of adsorption from binary solutions of benzene, cyclohexane or dioxane respectively, with nitrobenzene and nitromethane. The solids used for the investigations were the same as before [12], namely chromatographic silica (412 m^2/g) and alumina (65.2 m^2/g).

Experimental procedure and results

The liquids have been purified according to standard procedures [13]. Some physical properties of these liquids measured in the laboratory have been recorded in Table I and compared with the literature values [14]. It will be observed that there is an excellent agreement between these values, excepting in a few cases. The surface tension for nitromethane at 30 °C agrees very well with a recent report of SNEAD and CLEVER [15]; but the $d\gamma/dT$ reported by them varies from our data by 0.032 dyne/cm degree, while agreeing with other literature values [14]. The density of our sample agreed very closely with the most carefully purified sample described in literature [16]. According to COETZEE *et al.* [16], the density of nitromethane can be used as the best criterion for its purity. We have, therefore, proceeded with the rest of the determinations.

The surface tensions of the binary liquid mixtures were measured according to the procedure already described [17, 18] with an expected accuracy of ± 0.1 dyne/cm. The results are shown in terms of $\gamma^E (= \gamma - \gamma_1' x_1^l - \gamma_2' x_2^l)$ *vs.* mole fraction in Fig. 1.

A weighed quantity (1.5 gms) of the solid (dried at 140 °C) was taken in glass ampoules and degassed for about 24 hours. The ampoules were then filled with about 7—8 ml of a previously prepared binary liquid solution of known composition (prepared by weighing). The sealed ampoules were then placed in a constant temperature bath (±0.02 °C) and allowed to equilibrtat for 48 hours or more with frequent stirring. The liquid was subsequenlye separated from the solid by centrifuging. The change in concentration of the

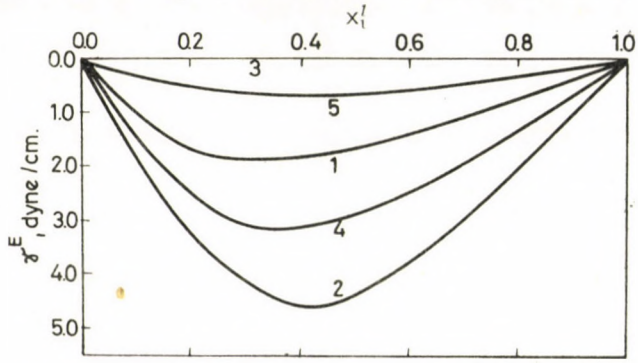

Fig. 1. Excess surface tension (γ^E) of binary solutions at 20 °C. 1. Benzene(1) + nitrobenzene(2); 2. Cyclohexane(1) + nitrobenzene(2); 3. Dioxane (1) + nitrobenzene(2); 4. Benzene(1) + nitromethane(2; 5. Dioxane(1) + nitromethane(2)

solution was calculated from the change in refractive index measured using a Rayleigh interference refractometer, mercury arc radiation, $\lambda = 5461$ Å, being used for the calibration of the instrument. Several checks for the determinations were made by duplicating some of the points, running blanks, and also by equilibrating pure solvents with alumina to see if the instrument indicated any change of refractive index.

The adsorption data are recorded in Tables II and III for the alumina and silica surfaces respectively. The last two columns in Tables II and III record x_1^σ calculated from the equations of EVERETT (Eq. 17) and of SCHAY and NAGY (Eq. 14), respectively. The constants used for the application of these equations have been recorded in Tables IV and V. These constants have been obtained from the experimental data in the following manner: The results of adsorption are plotted in Figs 2 and 3 in terms of $n_0 \Delta x_1^l/m$ *vs.* x_1^l which gives the "composite" isotherms for each binary mixture and solid. The straight line portion of the adsorption isotherm is extrapolated to obtain intercepts on the $x_i^l = 0$ and $x_i^l = 1$ axis (see 3, 4). Assuming that the composition of adsorbate remains constant (3) these intercepts give the values of n^σ/m (Tables IV and V). It is to be emphasized that in the above calculation for n^σ/m, the assumption of a monolayer adsorption is not involved. On the other hand, if this value of n_i^σ/m is divided by the number of moles required for monolayer capacity based on BET (N_2) areas of the solid, we can obtain the thickness

Table II

Adsorption from binary liquid mixtures on alumina (surface area 65.2 m^2/g) at 30 °C

System	x_1^l	$\Delta x_1^l \times 10^2$	n_0	m	$\frac{n_0 \Delta x_1^l}{m} \times 10^4$	x_1^σ Eq. (17)	x_1^σ Eq. (14)
Benzene(1) +	0.1252	0.517	0.04110	1.0828	1.963	0.4334	0.4033
nitrobenzene(2)	0.1880	0.376	0.07463	1.2684	2.210	0.5350	0.4985
	0.2376	0.427	0.04942	1.1148	1.892	0.5346	0.5032
	0.3388	0.287	0.04685	1.1927	1.128	0.5159	0.4973
	0.3664	0.230	0.05850	1.1305	1.190	0.5532	0.5330
	0.4365	0.246	0.05016	1.1151	1.108	0.6105	0.5907
	0.5379	0.263	0.06120	1.3071	1.230	0.7310	0.7074
	0.6313	—0.057	0.05211	1.0323	— 0.290	0.5858	0.5909
	0.7014	—0.181	0.05721	1.2847	— 0.800	0.5758	0.5899
	0.8607	—0.205	0.05964	1.1315	— 1.085	0.6904	0.7112
	0.9088	—0.181	0.05544	1.1252	— 0.890	0.7691	0.7871
Cyclohexane(1) +	0.1667	1.187	0.05813	1.2186	5.663	0.3309	0.3137
nitrobenzene(2)	0.3212	0.438	0.08749	1.3682	2.802	0.4024	0.3941
	0.4890	—0.573	0.07261	0.9590	— 4.341	0.3631	0.3793
	0.5304	—0.685	0.09307	1.0887	— 5.860	0.3605	0.3825
	0.6616	—1.793	0.07931	1.3456	—10.570	0.3561	0.3949
	0.8485	—2.290	0.05821	1.2423	—10.730	0.5373	0.5798
Dioxane(1) +	0.1966	0.359	0.06661	1.2767	1.873	0.5712	0.6837
nitrobenzene(2)	0.3790	0.339	0.08228	1.2789	2.184	0.8158	0.9299
	0.5756	0.258	0.07983	1.2751	1.615	0.8986	0.9802
	0.7069	0.217	0.06918	1.2734	1.180	0.9449	0.9985
	0.8602	0.065	0.08914	1.0723	0.540	0.9682	0.9952
Benzene(1) +	0.1084	—0.140	0.13463	1.1211	— 1.684	0.0175	0.0082
nitromethane(2)	0.2343	—0.354	0.09653	0.9751	— 3.505	0.0450	0.0129
	0.3915	—0.761	0.09317	1.2722	— 5.575	0.0905	0.0438
	0.4053	—0.668	0.09859	1.2193	— 5.780	0.0932	0.0449
	0.5303	—0.936	0.08553	1.1183	— 7.161	0.1516	0.1023
	0.7358	—1.273	0.06354	0.9908	— 8.167	0.2948	0.2743
Dioxane(1) +	0.1140	—0.031	0.08950	1.1753	— 0.237	0.0465	0.0034
nitromethane(2)	0.2097	—0.083	0.10228	2.1288	— 0.399	0.0960	0.0161
	0.3886	—0.062	0.11124	1.0211	— 0.678	0.1954	0.0656
	0.5639	—0.206	0.06664	1.9604	— 0.697	0.3653	0.2552
	0.7537	—0.073	0.08031	1.0760	— 0.542	0.5992	0.5410

Table III

Adsorption from binary liquid mixtures on silica gel (surface area 412 m^2/g) at 20 °C

System	x_1^l	$\Delta x_1 \times 10^2$	n_0	m	$\frac{n_0 \Delta x_1^l}{m} \times 10^4$	x_1^σ Eq. (17)	x_1^σ Eq. (14)
Benzene(1) +	0.1213	0.345	0.07474	0.9001	2.864	0.2645	0.2722
nitrobenzene(2)	0.2288	0.197	0.07274	1.2362	1.160	0.2847	0.2898
	0.3389	—0.316	0.06867	1.1597	— 1.187	0.2745	0.2732
	0.4441	—0.551	0.05990	1.0703	— 3.079	0.2942	0.2737
	0.5478	—0.901	0.05680	1.0525	— 4.798	0.2973	0.2820
	0.6452	—0.747	0.07017	0.8962	— 5.850	0.3527	0.3202
	0.7431	—1.141	0.05946	0.9898	— 6.856	0.3998	0.3608
	0.8237	—1.026	0.06918	0.9602	— 7.395	0.4539	0.4096
	0.9165	—0.764	0.07184	1.0314	— 5.321	0.6504	0.6133
Cyclohexane(1) +	0.1133	—0.557	0.06777	0.9746	— 3.874	0.0281	0.0086
nitrobenzene(2)	0.1880	—0.817	0.06614	0.9890	— 5.464	0.0678	0.0405
	0.2887	—1.541	0.06674	1.0468	— 9.824	0.0726	0.0234
	0.3863	—1.918	0.06290	1.0686	—11.290	0.1379	0.0026
	0.5113	—3.243	0.06946	1.0640	—18.431	0.1058	0.0134
	0.6097	—3.076	0.07016	0.8652	—24.950	0.0608	0.0086
	0.7310	—5.171	0.05824	1.1210	—26.860	0.1401	0.0052
	0.8353	—5.281	0.05208	0.9560	—28.770	0.2024	0.0595
	0.9224	—3.852	0.05771	0.9895	—22.460	0.4283	0.3227
Dioxane(1) +	0.1126	1.315	0.06680	0.8879	9.893	0.6320	0.6820
nitrobenzene(2)	0.2181	1.202	0.07557	0.8958	10.139	0.7504	0.7937
	0.3316	1.170	0.06591	0.8145	9.464	0.8285	0.8641
	0.4313	1.338	0.07107	1.1183	8.501	0.8775	0.9070
	0.5322	1.425	0.05808	1.0907	7.588	0.9306	0.9544
	0.6378	0.769	0.07454	0.9389	6.105	0.9583	0.9764
	0.7419	0.575	0.07461	0.9750	4.398	0.9729	0.9854
	0.8210	0.435	0.07547	1.0188	3.235	0.9908	0.9996
	0.9098	0.230	0.07771	1.0494	1.707	0.9994	0.9917
Benzene(1) +	0.0668	—0.141	0.11336	0.8258	— 1.936	0.0155	0.0154
nitromethane(2)	0.1405	—0.405	0.10409	0.8947	— 4.712	0.0156	0.0153
	0.2126	—0.848	0.09325	1.0430	— 7.577	0.0118	0.0109
	0.2982	—1.139	0.10126	1.1195	—10.285	0.0257	0.0261
	0.3883	—1.216	0.10270	0.9558	—13.066	0.0421	0.0453
	0.4987	—2.186	0.08321	1.1206	—16.240	0.0683	0.0781
	0.6171	—2.274	0.06707	1.1289	—17.113	0.1636	0.1953
	0.7159	—2.269	0.07906	1.1080	—16.184	0.2870	0.3426

Table III (cont.)

System	x_1	$\Delta x_1 \times 10^2$	n_0	m	$\frac{n_0 \Delta x_1^l}{m} \times 10^4$	x^σ Eq. (17)	x Eq. (14)
Dioxane(1) +	0.0668	0.446	0.11215	0.7875	6.356	0.4577	0.4589
nitromethane(2)	0.1333	0.685	0.08989	0.7276	8.464	0.6538	0.6935
	0.2104	0.716	0.11320	1.0460	7.622	0.6792	0.7184
	0.2834	0.773	0.09242	1.0802	6.605	0.6897	0.7244
	0.3743	0.527	0.10409	1.0592	5.302	0.7076	0.7284
	0.5942	0.291	0.08365	1.0025	2.425	0.7434	0.7575
	0.7007	0.093	0.07469	0.9737	0.716	0.7447	0.7488
	0.8435	—0.083	0.09256	1.4018	— 0.548	0.8098	0.8232

of the adsorbed film, as shown in the last column of Tables IV and V. Further in the use of Eq. (14) for calculating x_i^σ, we have considered it reasonable to use the value of $\Sigma_\tau [= (n_1^\sigma A_1 + n_2^\sigma A_2)/m]$ rather than impose the restriction of monolayer adsorption. This we consider an improvement over that of the previous calculations of SCHAY and NAGY [4], especially when the adsorption is multilayer in nature, as in some of our systems A_i is of course obtained in the usual way: $A_i = (V_i)^{2/3}(N)^{1/3}$.

Table IV

Adsorption from binary solutions on alumina at 30 °C
Characteristics of adsorbed layer

System	Slope $\times 10^{-3}$ Eq. (19)	$n^\sigma/m \times 10^4$ (moles/g)	K_a Eq. (19)	n^σ/m, Fig. 2 intercepts $\times 10^4$ (moles/g)	p.a.c.*	$\frac{n^\sigma_{\text{ads.}}}{n^\sigma_{\text{mono.}}}$**
Benzene(1) + nitrobenzene(2)	1.57	6.4	4.97	7.2	Benzene + nitrobenzene (4.3 : 2.9)	1.95
Cyclohexane(1) + nitrobenzene(2)	0.29	34.5	0.21	38.4	Cyclohexane + nitrobenzene (14.8 : 23.6)	11.13
Dioxane(1) + nitrobenzene(2)	2.00	5.0	5.30	4.0	Dioxane	1.01
Benzene(1) + nitromethane(2)	0.58	18.5	0.15	15.75	Nitromethane	2.92
Dioxane(1) + nitromethane(2)	2.85	3.5	0.40	2.05	Nitromethane	0.38

* Preferentially adsorbed component.
** n^σ (monolayer) $= \Sigma$ BET$(N_2)/A_i$.

Table V

Adsorption from binary solutions on silica gel at 20 °C
Characteristics of the adsorbed layer

System	Slope $\times 10^{-2}$ Eq. (19)	$n^{\sigma}/m \times 10^4$ (moles/g)	K_a Eq. (19)	n^{σ}/m, Fig. 3 intercepts $\times 10^4$ (moles/g)	p.a.c.*	$\frac{n^{\sigma}_{\text{ads.}}}{n^{\sigma}_{\text{mono.}}}$ **
Benzene(1) + nitrobenzene(2)	5.00	20.0	6.0	19.0	Benzene + nitrobenzene (5.4 : 13.6)	0.83
Cyclohexane(1) + nitrobenzene(2)	2.20	45.45	0.05	37.0	Nitrobenzene	1.66
Dioxane(1) + nitrobenzene(2)	5.25	19.0	10.21	18.1	Dioxane	0.70
Benzene(1) + nitromethane(2)	2.66	37.7	0.13	37.4	Nitromethane	1.09
Dioxane(1) + nitromethane(2)	6.15	16.3	11.98	14.85	Dioxane + nitromethane (11.2 : 3.65)	0.53

* Preferentially adsorbed component.
** n^{σ} (monolayer) $= \Sigma$ BET$(N_2)/A_l$.

The slope m/n^{σ} and K_a for the application of EVERETT's equation, Eq. (17), have been obtained by plotting $x_1^l x_2^l/(n_0 \Delta x_1^l/m)$ *vs.* x_1^l. In those cases where the composite isotherm is of the *S*-shape, only the points on the rising part of the curve, at either end of the isotherm have been used. The calculated values of n^{σ}/m according to this procedure are also recorded in Tables IV and V. In Figs 4 to 8, the adsorption at the liquid/vapour interface of the binary solutions is compared with the adsorption at the liquid/solid interface normalised to unit surface area. It will be observed that for the convenience of plotting and also showing the curvature of the lines, the scale used for liquid/vapour adsorption is larger than that for the corresponding liquid/solid adsorption.

Discussion

Comparison of different methods of calculation

It is of interest to compare the values of n^{σ}/m obtained by the methods of SCHAY and NAGY (intercept method) and of EVERETT (Eq. (19)). From Tables IV and V, it will be observed that the values recorded agree fairly well; for the adsorption on silica the values agree much more closely than for that on alumina. However, considering the assumptions involved in the intercept method of SCHAY and NAGY [3, 4], and that EVERETT's Eq. (17) was derived

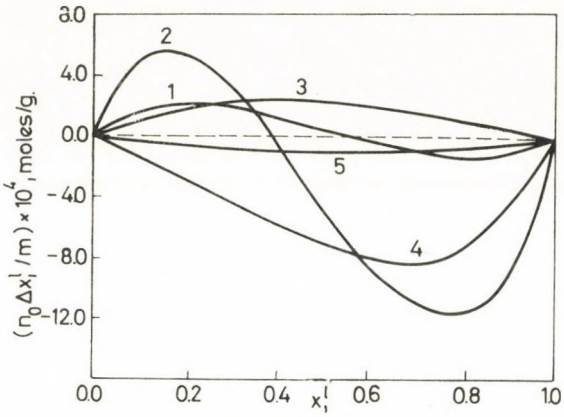

Fig. 2. Composite adsorption isotherms: Binary liquid mixtures + alumina, at 30 °C. 1. Benzene(1) + nitrobenzene(2); 2. Cyclohexane(1) + nitrobenzene(2); 3. Dioxane(1) + nitrobenzene(2); 4. Benzene(1) + nitromethane(2); 5. Dioxane(1) + nitromethane(2)

for a perfect monolayer of adsorption, the agreement between the two sets of n^σ/m is surprisingly good.

Attention is also drawn to the x_i^σ values recorded in Tables II and III calculated from Eqs (14) and (17). Here again the two sets of values are

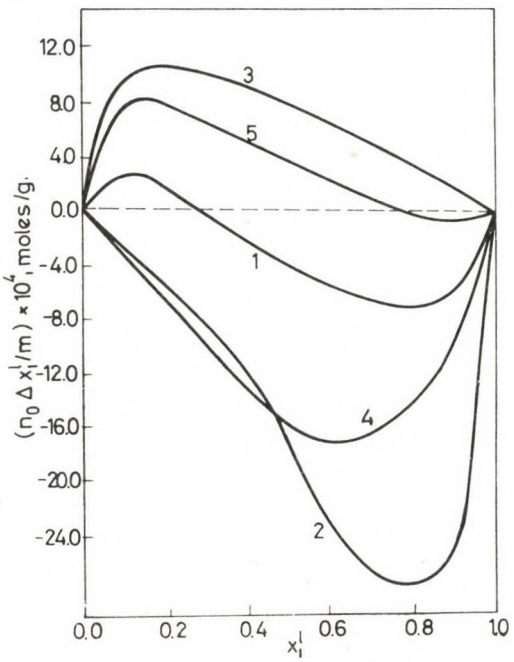

Fig. 3. Composite adsorption isotherms: Binary liquid mixtures + silica gel, at 20 °C. 1. Benzene(1) + nitrobenzene(2); 2. Cyclohexane(1) + nitrobenzene(2); 3. Dioxane(1) + nitrobenzene(2); 4. Benzene(1) + nitromethane(2); 5. Dioxane(1) + nitromethane(2)

in good agreement, although the x_i^σ values for the preferentially adsorbed components obtained by SCHAY's equation are slightly higher than those calculated from EVERETT's expression. For systems cyclohexane + nitrobenzene and benzene + nitrobenzene on alumina, and benzene + nitrobenzene and dioxane + nitromethane on silica, where the composite adsorption isotherm crosses the composition axis (Figs 2 and 3), the values of m/n^σ from Eq. (19) have been obtained from the rising branch of the curves at either end. Interestingly enough when these values obtained towards the end of the less preferentially adsorbed component are used for the calculation of x_i^σ, the results obtained follow closely the corresponding values calculated from the equation of SCHAY and NAGY (Tables II and III). We conclude, therefore, that within the limits of applicability of these equations, the values obtained for n^σ/m and x_i^σ for the adsorbed layer are in satisfactory agreement; when the isotherms are *S*-shaped, the constants for EVERETT's equation are best obtained from the rising part of the isotherms towards the side of the less preferentially adsorbed component.

The nature of the adsorbed layer

In the last columns of Tables IV and V, we compare the number of moles in the adsorbed layer with the number of moles of the components that are required to form a monolayer on the surface, $n^\sigma_{\text{mono.}}$, assuming BET(N_2) areas for the solids. In the case of alumina, excepting for the systems containing dioxane, multilayer adsorption is observed which is rather surprising in view of the observation of SCHAY [3, 4] that, for a number of systems including polar components on alumina, the adsorbate is confined to a single molecular layer within 5%. It has also been suggested that for regular solutions adsorption is essentially confined to a single layer [19], provided the system is well above the temperature at which phase separation occurs. The binary solutions under study approximate to a regular solution behaviour. The temperature of our measurements, particularly with alumina is fairly high, the solutions showing no tendency towards phase separation in its vicinity. In view of these points, the multilayer adsorption observed on alumina cannot be accounted for with the data at our disposal.

In the case of silica, near monolayer adsorption is prevalent, except again for the dioxane systems. The adsorption from dioxane–nitromethane systems is exceptional in that only a small fraction of the surface is covered (40—50%). The near monolayer adsorptions in the case of silica are more closely in accordance with the data available in literature for the adsorption from several binary solutions on silica gel [1]. In such cases, when the adsorbate can be considered to be confined to a single layer on the surface, a suitable shape factor for the packing of the adsorbate molecules or a specific surface

disposition of these molecules (*e.g.* flat lying rings on the solid surface) can be adopted to bring closer agreement between the areas calculated from liquid adsorption and BET(N_2) values. In those cases where multilayer adsorption prevails, both A_i and the thickness of the adsorbate layer become uncertain; and hence it becomes extremely difficult to estimate the monolayer capacity and the corresponding surface areas.

The adsorption from the dioxane systems merits additional comments. The binary solutions of dioxane + nitrobenzane show $\gamma^E = 0$ at 20 °C (Fig. 1)

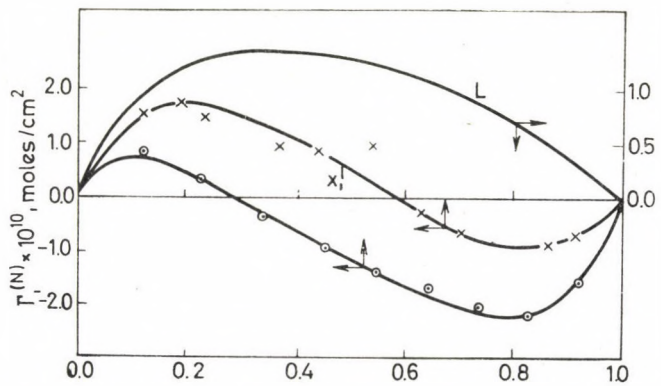

Fig. 4. Isotherms of surface excess for the system benzene(1) + nitrobenzene(2). L Free liquid surface; × Alumina surface; ⊙ Silica gel surface

and slight positive values at 30 °C [17], indicating that the component of the lower surface tension, dioxane, does not rise to the free liquid surface as anticipated. This behaviour, on the basis of Eq. (10), would lead us to expect a preferential adsorption of dioxane on a solid surface, provided it resulted in a perfectly adsorbed phase. The results recorded in Tables IV and V, and shown in Fig. 5 bear out this expectation. In the case of dioxane + nitromethane systems, although the difference in surface tensions of the two components is smaller than in the previous system, the γ^E values are significantly negative, indicating that dioxane does enrich the surface as anticipated. One would, therefore, expect nitromethane to be preferentially adsorbed on a solid surface on the basis of Eq. (10). However, although nitromethane is preferentially adsorbed on alumina, only 40% of the surface is covered; and on silica the adsorption is exceptional, dioxane being adsorbed in greater excess than nitromethane, while the total adsorption is confined to only ~50% of the surface. There is not enough information available in literature for this binary system to explain this behaviour conclusively.

The differences in the behaviour of solutions discussed above are more sharply brought out by comparing the corresponding liquid/vapour and

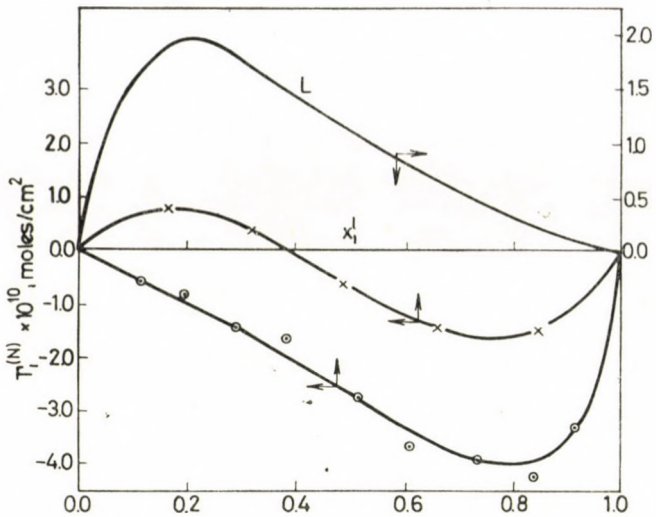

Fig. 5. Isotherms of surface excess for the system cyclohexane(1) + nitrobenzene(2). L Free liquid surface; × Alumina surface; ⊙ Silica gel surface

liquid/solid interfaces. In all the cases where the same component is adsorbed preferentially (Figs 5, 6, 7), excellent agreement is obtained for the adsorption on the two solids over most of the composition range. This is to be expected because of the method of calculation used. When the composition of the mixture $x_i^l \to 1$, i, being the preferentially adsorbed component, some differences are observed for the two solids. In the case of adsorption from cyclohexane + nitrobenzene on alumina, the curve actually crosses the composition axis at mole fraction of nitrobenzene greater than 0.85, indicating a reversal of adsorption in solution containing very small quantities of cyclohexane. Comparing the adsorption on the corresponding free liquid surfaces, the general nature

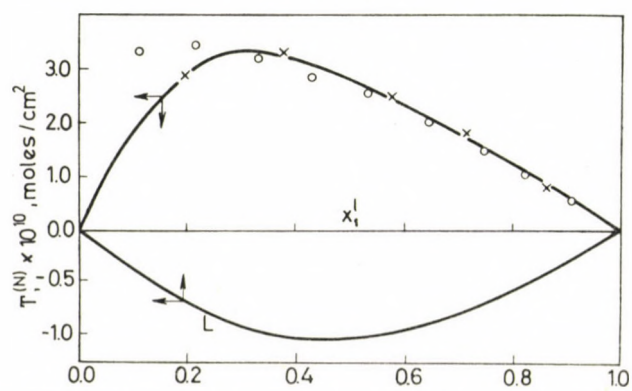

Fig. 6. Isotherms of surface excess for the system dioxane(1) + nitrobenzene(2). L Free liquid surface; × Alumina surface; ○ Silica gel surface

of the curves agrees fairly well with the prediction of Eq. (10). Figure 6 reflects the peculiarity of the free liquid surface of the dioxane + nitrobenzene system, which has $\gamma^E = 0$ (Fig. 1). The actual values of the adsorption per unit area on the solid surface shown in Figs 5—7 are about 2—4 times as high as the corresponding adsorption at the free liquid surface. We have used the values

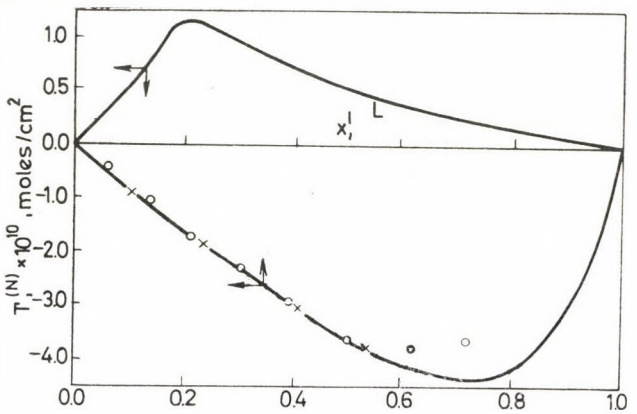

Fig. 7. Isotherms of surface excess for the system benzene(1) + nitromethane(2). L Free liquid surface; × Alumina surface; ○ Silica gel surface

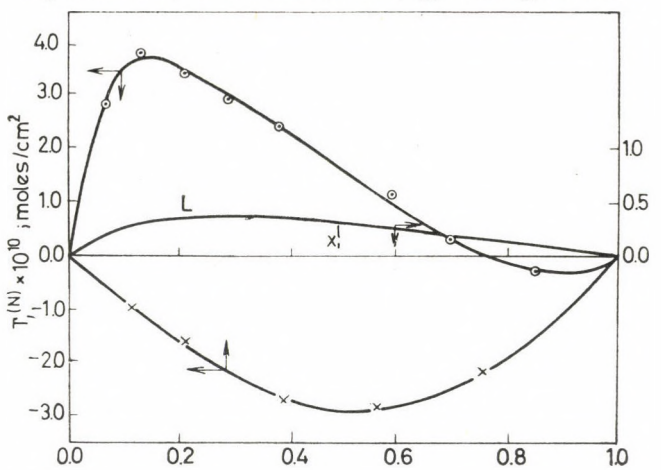

Fig. 8. Isotherms of surface excess for the system dioxane(1) + nitromethane(2). L Free liquid surface; × Alumina surface; ⊙ Silica gel surface

Σ_τ for the surface rather than Σ BET(N_2) as explained earlier. It may, therefore, be concluded that although the systems studied do not conform to the requirements of Eq. (10), in the sense that the components in the free liquid surface and the adsorbed layer on the solids do not follow ideal behaviour, nevertheless, the general nature of the adsorption curves follows the trend predicted by this equation.

The composite adsorption isotherms for benzene + nitrobenzene on both solids and dioxane + nitromethane on silica gel (Figs 4 and 8), cross the composition axis and do not conform to the above analysis. In these systems, it appears that specific molecular interactions with the respective solid surfaces occur vitiating comparisons with the free liquid surface.

REFERENCES

1. KIPLING, J. J.: Adsorption From Solutions of Non-electrolytes. Academic Press, London and New York 1965
2. HILDEBRAND, J. H., SCOTT, R. L.: The Solubility of Non-electrolytes, 3rd Edition. Dover, New-York, 1964
3. SCHAY, G., NAGY, L. GY., SZEKRÉNYESY, T.: Periodica Polytechnica **6**, 91 (1962); NAGY, L. GY.: *ibid.* **7**, 75 (1963)
4. NAGY, L. GY., SCHAY, G., SZEKRÉNYESY, T.: Acta Chem. Acad. Sci. Hung. **53**, 145 (1967). NAGY, L. GY., SCHAY, G.: *ibid* **39**, 365 (1963). SCHAY, G., NAGY, L. GY.: *ibid* **50**, 207 (1966)
5. EVERETT, D. H.: Trans. Farad. Soc. **60**, 1803 (1964)
6. EVERETT, D. H.: Trans. Farad. Soc. **61**, 2487 (1965)
7. SISKOVA, M., ERDŐS, E.: Coll. Czech. Chem. Comm. **25**, 1729 (1960), *ibid* **25**, 2599 (1960), *ibid* **25**, 3086 (1960)
8. KISELEV, A. V. *et al.*: Izvestia Acad. Nauk. S.S.R. Ser. Khim. **NI**, 18 (1965) and erlier References
9. ERIKSSON, J. C.: Advances in Chemical Physics, Vol. VI. Interscience, New York, 1964. Arkiv For Kemi., **26**, 49 (1966)
10. SCHMIDT, R. L., CLEVER, H. L.: J. Colloid and Interface Sci. **26**, 19 (1968)
11. SURI, S. K., RAMAKRISHNA, V.: J. Phys. Chem. **72**, 1555 (1968)
12. SURI, S. K., RAMAKRISHNA, V.: Trans. Farad. Soc. (In Print)
13. WEISSBERGER, A.: Technique of Organic Chemistry, Vol. VII., 3rd Edition. Interscience, New York, 1950
14. TIMMERMANS, J.: Physicochemical Constants of Pure Organic Compounds. Elsevier, Amsterdam, 1950
15. SNEAD, C. C., CLEVER, H. L.: J. Chem. Engg. Data. **7**, 393 (1962)
16. COETZEE, J. F., CUNNINGHAM, G. P.: J. Am. Chem. Soc. **87**, 2529 (1965)
17. SURI, S. K., RAMAKRISHNA, V.: J. Phys. Chem. **72**, 3073 (1968)
18. SURI, S. K., RAMAKRISHNA, V.: Ind. J. Chem. (In Print)
19. DELMAS, G., PATTERSON, D.: Off. Dig. Fed. Paint Varn. Prod. Cl. **31**, 1129 (1959)

S. K. SURI
V. RAMAKRISHNA
Chemistry Dept., Indian Institute of Technology, New Delhi-29 India

Acta Chimica Academiae Scientiarum Hungaricae, Tomus 63 (3), pp. 319—327 (1970)

INVESTIGATION OF THE DIFFUSION POTENTIAL IN SOLUTIONS OF CONSTANT IONIC STRENGTH

L. BARCZA, L. STRÓBL and B. LEHOCZKY

(Institute for Inorganic and Analytical Chemistry of the L. Eötvös University, Budapest)

Received December 19, 1968

In the course of our measurements of the electrode potential in solutions of constant ionic strength, the development and the possible calculation of the diffusion potential has been studied for the case, when the monovalent cation is replaced up to about 50 per cent by hydrogen ion.

Assuming that up to a certain limit the single activity and conductivity coefficients are constant, a relationship, formally similar to the equation of HENDERSON, has been deduced:

$$E_d = -59.15 \log \left(1 + h \cdot \frac{\lambda_{m,HB} - \lambda_{m,AB}}{m \cdot \lambda_{m,AB}}\right)$$

where h is the total concentration of the acid, and m the original concentration of the supporting electrolyte. It follows from our starting concept that $\lambda_{m,HB}$ is the equivalent conductivity of the acid in the m molar supporting electrolyte (which, though hypothetical, can be suitably measured and calculated), and $\lambda_{m,AB}$ is the conductivity of the m molar supporting electrolyte.

When these values are determined by independent conductivity measurements, a constant value (K) is obtained for the fractional term of the above equation within the same system. The value of this constant (in units of M^{-1}) was found to be 1.819 in 1.00 M (K)Cl; 10.86 in 0.20 M (K)Cl and 2.929 in 1.00 M (Na)ClO_4.

The relationship was checked by potential measurements, and was found to be valid up to the limit mentioned, which, in the given case, represented an acid concentration of 0.5 M.

One of the most important methods for the investigation of chemical equilibria is based on the determination of electrode potentials with the aid of various cells. Within this scope, the measurement of the hydrogen ion concentration with systems of various type is perhaps the most essential.

During the investigation of electrode potentials, and particularly in that of the latter mentioned case, the problem of the diffusion potential often arises, since this value must be taken into consideration in the calculation of the value of the potential:

$$E = E_{id} + E_d \tag{1}$$

where E is the measured and E_{id} the theoretical electrode potential difference, while E_d is the diffusion potential. Both values depend on the activity of the given substance in the solution. Generally, the objective of the measurements

is the determination of the well defined E_{id} value, however, this necessitates the knowledge of the value of E_d.

In general, it can be shown on the basis of thermodynamical or kinetical considerations [1, 2, 3] that during the contact of two solutions the potential

$$dE_d = -\frac{RT}{F} \sum_i \frac{n_i}{z_i} d \ln a_i \tag{2}$$

is established, where R, T and F are the usual symbols of the constants, and n_i, z_i and a_i are the transport number, charge and activity, respectively, of the i-th ion passing through the interface.

Theoretically, the value of the diffusion potential can be obtained by the integration of Eq. (2) where the limits of integration are given by the initial activity of the two solutions in contact (since in practice the objective is the calculation of a diffusion potential corresponding to finite differences in concentration).

However, the situation is rendered very complicated by the fact that both transport number and activity are dependent on the concentration, and assumptions should be made on the structure of the interface layer and its reversibility (or irreversibility).

When in first approximation the transport number and the activity (equal to the concentration) are taken as constants, there should be made assumptions only in respect of the structure of the interface layer.

This structure was examined optically by SITTE [4], who showed, as was to be expected, that no simple assumptions (a continuous transition or a sharp boundary) are strictly true.

It follows that a measurable and reproducible diffusion potential can be ensured only by a very careful development of the interface(s) and only in the case of cylindrical symmetry, *i.e.* the shape of the electrode vessels is of great importance from the viewpoint of the measurements [5].

The next problem arises from the simplifications involved in our assumption that our solutions are ideal ones. However, discussions concerning this problem must be restricted to the system which is of primary interest to the cell

$$\text{reference electrode} \;\Big\|\; m\ M\ AB \;\Big|\; \begin{matrix}(m-x)\ M\ AB \\ x\ M\ HB\end{matrix} \;\Big|\; \text{measuring electrode}$$

where A is a monovalent (alkali metal) cation, and B a monovalent anion. (It should be mentioned here that theoretically a diffusion potential forms also at the interface: reference electrode — salt bridge, however, this potential may be taken as constant and has a very low value, so that it can be neglected

in comparison to the diffusion potential at the interface: salt bridge — solution.)

Our system corresponds to one of the limit cases of the HENDERSON theory: two electrolytes of the same concentration, containing monovalent ions come into contact, and one of the ions (B) is common. In this case, HENDERSON's equation for the diffusion potential reads:

$$E_d = -\frac{RT}{F} \ln \frac{u_{k2} + u_{a2}}{u_{k1} + u_{a1}} \tag{3}$$

where $u_{i,c}$ is the mobility of the i-th ion in the 1st or 2nd solution. According to the assumptions made in the deduction of the equation, $u_{i,c}$ is the mobility of the ion in ideal solutions, *i.e.* in such of infinite dilution. Thus Eq. (3) will give only for near ideal, *i.e.* strongly dilute solutions results approaching those found experimentally [5].

Taking into consideration the fact that in our solutions of finite dilution the value of $u_{i,c}$ is other than $u_{i,0}$, and the equivalent conductance of the given solution is

$$\lambda_c = u_{k,c} + u_{a,c} \tag{4}$$

the LEWIS–SARGENT [6] relationship is obtained:

$$E_d = -\frac{RT}{F} \ln \frac{\lambda_2}{\lambda_1} . \tag{5}$$

This relationship takes into consideration the interaction between the ions, because λ_c is dependent also on the ionic strength of the solution, and on the other hand, introduces values, determined separately by other method, into the calculation of the diffusion potential.

BIEDERMAN and SILLÉN [7] examined on the basis of Eq. (3) one case of the system mentioned, in which m M AB was 3 M $NaClO_4$, from the practical point of view. They obtained a relationship similar to Eq. (5) (at 25 °C)

$$E_d = -59.16 \log \left(1 + \frac{d \cdot h}{3000}\right) \tag{6}$$

where h is the concentration of perchloric acid, while the value of d is given by the following relation:

$$d = \frac{\lambda_{HClO_4} - \lambda_{NaClO_4}}{\lambda_{NaClO_5}} \tag{7}$$

Potentiometric measurements resulted for the value of d 1.95 $\pm$ 0.08. while on the basis of HENDERSON's equation the value of d, according to their calculations, is 3.3.

These authors next introduce simplifications on the basis that

$$\frac{d \cdot h}{3000} \ll 1 ,$$

so that

$$\ln \left(1 + \frac{d \cdot h}{3000}\right) \cong \frac{d \cdot h}{3000} . \tag{8}$$

Accordingly, Eq. (6) will take the following form:

$$E_d = - \frac{59.16}{\ln 10} \frac{d \cdot h}{3000} = K \cdot h = 0.0167\, h \tag{9}$$

This relationship (provided that the condition in Eq. (8) is satisfied) can be used readily for the potentiometric determination of the K value, characteristic of the diffusion potential, since in this case Eq. (1) attains the simplified form:

$$E' = A \cdot \log h + K'h \tag{10}$$

When K' is known, the equation is suitable for the calculation of unknown h values. Indeed, this equation is very often used for equilibrium measurements in solutions of constant ionic strength.

The fact that Eqs (3) and (6)—(7) do not describe the real situation in concentrated solutions, is evidently due to the circumstance that assumptions made in connection with Eq. (2) are not correct.

SPIRO [8] and COVINGTON [9] studied systems similar to our system mentioned. Both authors started from the consideration that in Eq. (2) the activity can not be simply replaced by the concentration, but the activity coefficients must also be taken into account. Thus, the diffusion potential can be divided into two parts, one of which is dependent on the concentration, and the other on the activity coefficient:

$$E_d = (E_d)_m + (E_d)_f \tag{11}$$

The first term gives as solution the Henderson equation, as the starting point is identical. The calculation of the second term

$$dE'_{d,f} = - k \sum_i \frac{n_i}{z_i} d \log f_i \tag{12}$$

necessitates several considerations, on the basis of which the authors obtained a rather complicated final result, which however, can be handled.

As concerns details, we refer here to the original publications, and would like to mention only that SPIRO [8] dealt also from theoretical viewpoints with the system of BIEDERMAN and SILLÉN [7]. Introducing some neglections and approximations, he obtained instead of the measured value of -0.0167 and the calculated value of -0.0283 a value of -0.023_3.

The equation of LEWIS–SARGENT is not valid either in all the cases: with solutions of higher concentration the change in activity occurring in the boundary layer, which can be ascribed to ion association, must also be considered. Theoretical and practical aspects of this problem were examined by BIANCHI *et al.* [10] in detail.

Considering our cell I, where the ionic strength is the same throughout the system, and disregarding within certain limits the special ion association mentioned above, it may be assumed that

$$f_A = \text{constant} \quad f_B = \text{constant} \quad f_H = \text{constant} \tag{13}$$

Substituting this into the equation derived for our case, we obtain:

$$\frac{dE_d}{k'} = -\left(n_H \frac{dc_H}{c_H} + n_A \frac{dc_A}{c_A}\right) \tag{14}$$

where c_i is the concentration.

(Since the anion concentration is constant throughout the system, it does not participate in the development of the diffusion potential.)

According to definition, the transport number n_i is

$$n_i = \frac{u_i c_i}{\sum_i u_i c_i} \tag{15}$$

where u_i is the ionic mobility of the ith ion in the solution of given concentration.

On introducing the notation

$$u_i = f_{\lambda,i} u_{i,0} \tag{16}$$

where $f_{\lambda,i}$ is the conductivity coefficient, it may be also assumed at constant ionic strength, that

$$f_{\lambda,i} = \text{constant}. \tag{17}$$

Resubstituting these values into Eq. (14), the following relation is obtained after integration for the diffusion potential:

$$E_d = -59.15 \log \frac{h(u_H - u_A) + m(u_A + u_B)}{m(u_A + u_B)} . \tag{18}$$

Since

$$u_A + u_B = \lambda_{m,AB}$$

and

$$u_H - u_A = (u_H + u_B) - (u_A + u_B) = \lambda_{m,HB} - \lambda_{m,AB} \tag{19}$$

finally, a relation, formally completely similar to the HENDERSON's equation (and used also by BIEDERMAN and SILLÉN) is obtained:

$$E_d = -59.15 \lg\left(1 + \frac{h}{m} \frac{\lambda_{m,HB} - \lambda_{m,AB}}{\lambda_{m,AB}}\right) \tag{20}$$

where only the definition of $\lambda_{m,HB}$ differs from the usual: $\lambda_{m,HB}$ *being the equivalent conductance of the given acid in the solution* $m\,M\,AB$ (and it is not equal to the equivalent conductance of m M acid).(It goes without saying that $\lambda_{m,AB}$ is the equivalent conductance measured in the $m\,M\,AB$ solution.) Since these (and m) are constant within one system, our Eq. (20) is further simplified to

$$E_d = -59.15 \log (1 + Kh) . \tag{21}$$

Substituting this expression into Eq. (1) we obtain

$$E' = 59.15 \log h - 59.15 \log (1 + Kh) = 59.15 \log \frac{h}{1 + Kh} . \tag{22}$$

This relation can be very easily handled (when K is known) for h (the hydrogen ion concentration to be determined). Moreover, it will be seen that (except for the interpretation of the designations) Eq. (9) actually is a limit case of Eq. (22).

Theoretically, Eq. (21) is also suitable for the calculation of K on the basis of potentiometric measurements. However, this approach is not recommended, as the problem can be solved much easier and more accurately by conductivity measurements.

The procedure is as follows: the specific conductance of the $m\,M\,AB$ solution is measured, and, titration-like, portions of $m\,M\,HB$ solution are added to it. As long as our assumptions (Eqs (13) and (17)) are valid, the plotting of the conductance values measured against the $[HB]$ values will give a straight line.

Since the specific conductivity of m M AB ($\varkappa_{AB}$) is known, for each (m — $[HA]$) M point the part due to it can be calculated, and thus, the conductivity corresponding to the acid ($\varkappa_{HB}$) can be obtained from the specific conductivity measured ($\varkappa_{\text{meas.}}$):

$$\varkappa_{HB} = \varkappa_{\text{meas.}} - \varkappa_{AB} \cdot C_{AB}. \tag{23}$$

From the specific conductivities the equivalent conductivities are obtained without any further difficulties.

Our measurements were made on 1.0 M and 0.2 M KCl and 1.0 M $NaClO_4$ systems. In our investigations the metal ions were replaced up to about 50 per cent by hydrogen ions.

For our measurements, reagents purified and checked very carefully were used. The conductivity was determined with a Radiometer Model CDM 2d instrument. On the basis of the values obtained with this instrument, the validity of Eq. (21) was checked with a Radelkis Model OP 205 instrument. A glass electrode Radelkis OP/711—1/A was used as measuring electrode, and the reference electrode was an Ag/AgCl electrode prepared suitably [11], which dipped into a potassium chloride solution of suitable concentration saturated with silver chloride, or into a 0.99 M $NaClO_4$ solution, 0.01 molar with respect to NaCl. The design of the whole reference electrode (comprising also the salt bridge) was of the W—J type [7, 12]. According to our experiences, this type ensures the symmetry requirements concerning the boundary layer.

From the conductivities measured the values $\lambda_{m,AB}$, $\lambda_{m,HB}$,

$$K \cdot m = \frac{\lambda_{m,HB} - \lambda_{m,AB}}{\lambda_{m,AB}} \tag{24}$$

and K have been calculated.

These K values were used in Eq. (22), after some transformation:

$$E_0 = E_{\text{meas.}} - 59.15 \log \frac{h}{1 + Kh} \tag{25}$$

in the investigation of the dependence of the electrode potentials on $[H^+]$. The E_0 values were calculated also without taking into account of the diffusion potentials:

$$E_0' = E_{\text{meas.}} - 59.15 \log h. \tag{26}$$

To illustrate our results, the two series of E_0 and E_0' values in dependence on h, measured in 1 M $NaClO_4$ solution, are shown also graphically (Fig. 1), while our results are compiled in the following table:

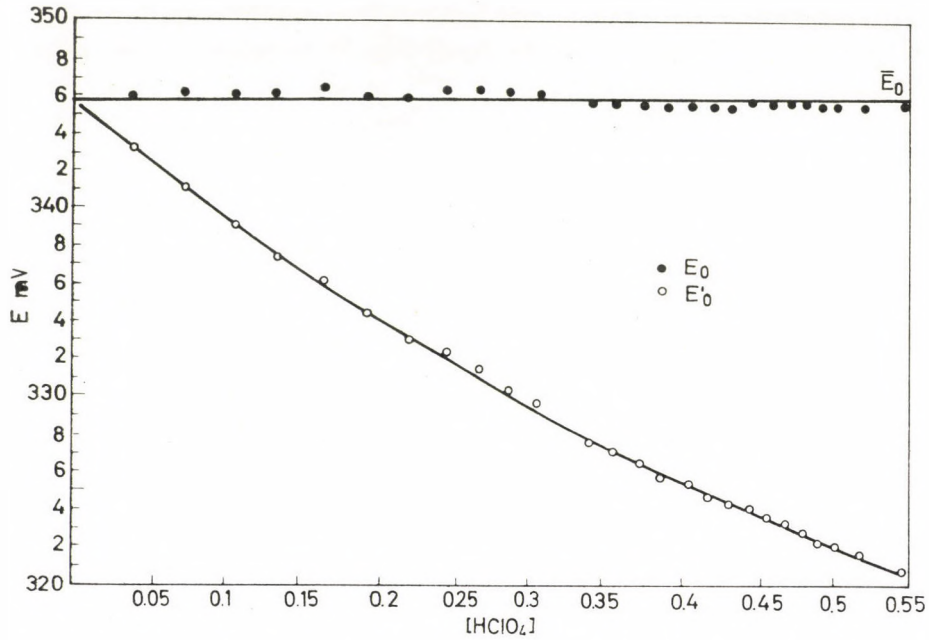

Fig. 1

Table I

System investigated	1.00 *M* (K)Cl	0.20 *M* (K)Cl	1.00 *M* (Na)ClO_4
Conductivity measurements:			
Number of points	26	22	27
h_{max}	0.51 *M*	0.10 *M*	0.38 *M*
h_{max}/m	0.51	0.50	0.38
$\lambda_{m,HB}$	315.2 $ohm^{-1}\,cm^2$	391.4 $ohm^{-1}\,cm^2$	315.9 $ohm^{-1}\,cm^2$
$\lambda_{m,AB}$	111.8 $ohm^{-1}\,cm^2$	123.4 $ohm^{-1}\,cm^2$	80.4 $ohm^{-1}\,cm^2$
$K \cdot m$	1.819	2.172	2.929
K	1.819 M^{-1}	10.86 M^{-1}	2.929 M^{-1}
Electrode potential measurements:			
Number of points	35	32	28
h_{max}	0.52 *M*	0.104 *M*	0.55 *M*
h_{max}/m	0.52	0.52	0.55
$E_{d,max}$	17.06_6 mV	19.3_9 mV	24.5_2 mV
E_0	474.0_1 mV	424.5_7 mV	345.7_1 mV
σE_0	0.04 mV	0.09 mV	0.07 mV

The table and the diagram (the other two cases show a similar course), clearly demonstrate that relations (19), (20), (21), deduced on the basis of the assumptions made in Eqs from (13) to (17), are valid within wide limits, up to a substitution of 50 per cent of the metal ions. Thus, for the case of our cell I, the validity of the assumptions (13) and (17) could be proved. This however, means both theoretically and practically a considerable broadening of the sphere of systems which can be investigated.

It should be mentioned finally that we tried to extrapolate our results to the result obtained by BIEDERMAN and SILLÉN [7] in 3 M $(Na)ClO_4$ solution. According to our calculations, this value is -0.0179, and is still closer to -0.0167, the value measured, than the value calculated by SPIRO (-0.0233) [8].

REFERENCES

1. NERNST, W.: Z. phys. Chem. **2,** 613 (1888); **4,** 129 (1889)
2. PLANCK, M.: Ann. Physik **39,** 161 (1890); **40,** 561 (1890)
3. HENDERSON, P.: Z. phys. Chem. **59,** 118 (1907); **63,** 325 (1908)
4. SITTE, K.: Z. Phys. **91,** 622; 642; 651 (1934)
5. SZABÓ, Z. G.: Z. phys. Chem. **174A,** 33 (1935); Magy. Kém. Folyóirat **39,** 145 (1933); **41,** 130 (1935); **42,** 1 (1936)
6. LEWIS, G. N., SARGENT, L. W.: J. Am. Chem. Soc. **31,** 363 (1909)
7. BIEDERMAN, G., SILLÉN, L. G.: Arkiv Kemi **5,** 425 (1953)
8. SPIRO, M.: Electrochim. A. **11,** 569 (1966)
9. COVINGTON, A. K.: Electrochim. A. **11,** 959 (1966)
10. BIANCHI, G., FAITA, G., GALLI, R., MUSSINI, T.: Electrochim. A. **12,** 439 (1967)
11. BROWN, A. S.: J. Am. Chem. Soc. **56,** 646 (1934)
12. FORSLING, W., HIETANEN, S., SILLÉN, L. G.: Acta Chem. Scand. **6,** 905 (1952)

Lajos BARCZA
László STRÓBL
Béla LEHOCZKY
Budapest VIII., Múzeum krt 4/b

Acta Chimica Academiae Scientiarum Hungaricae, Tomus 63 (3), pp. 329—342 (1970)

POLAROGRAPHIC INVESTIGATION OF CYTOSTATIC MANNITOL DERIVATIVES, IV

A KINETIC INVESTIGATION OF THE REACTIONS OF DEGRANOL

B. JÁMBOR

(Institute for Plant Physiology, L. Eötvös University, Budapest)

Received June 26, 1968

The mechanism of the conversion of Degranol into ethyleneimino compounds, and the influence of the experimental conditions on this conversion have been investigated, and the following results obtained:

1. At pH < 6, predominantly the monoethyleneimino derivative is formed at 25 °C. This compound does not give the wave produced by the bis derivative. In a few hours, it reacts with thiosulfate, to yield a compound giving rise to a readily evaluable wave. The compound formed in the reaction of the bis-ethyleneimino derivative with thiosulfate gives a wave which is twice as high as the former.

2. At pH < 6, the cyclization of the second ethylamino group proceeds very slowly. At higher pH values, complete cyclization of the monoethyleneimino compound takes place readily. In a solution having a pH adjusted initially to a higher value (*e.g.*, pH 8), these two steps do not separate.

3. In an ionic environment similar to that of blood, Degranol reacts at 37 °C with hydrocarbonate to yield predominantly an inactive oxazolidone compound. Only about 10 to 15% is cyclized.

4. Cyclization is hindered by buffers present in high concentrations, but the cleavage of chlorine is decreased only very slightly, or not at all. Sodium sulfate has no effect.

5. In the presence of trivalent buffers, the cyclization of freshly dissolved Degranol begins only after a certain "induction period". The length of this period depends on the nature, concentration, etc., of the buffer.

6. The concentration of Degranol has practically no influence on the percentage reaction rate, as shown by measurements either of the cyclization or the cleavage of halogen.

In our earlier communications [1—3] the polarographic behaviour of the ethyleneimino derivatives of Degranol (**I** and **II**) and of the compound formed from Degranol (**III**) in slightly alkaline medium has been studied. It has been found that in all three cases a reduction wave corresponding to the uptake of four electrons is produced, which exhibits a slight kinetic character. As the principal object of the above investigations, it could also be established that, under the given conditions, Degranol gave the corresponding ethyleneimino compound (**II**).

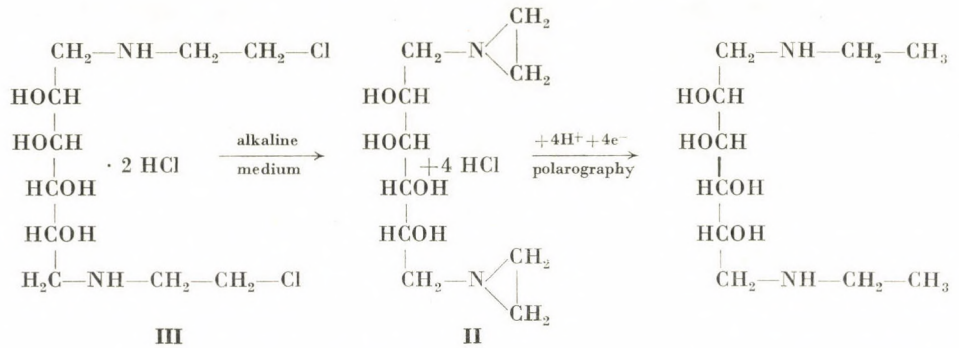

The object of our present investigation was the study of the conversion of Degranol as a function of time, and to establish the effect of the pH, the nature and the concentration of the buffer, and of other experimental conditions on the reaction. Our main purpose was to clarify the course of the reaction under conditions similar to physiological circumstances.

Experimental part and discussion of the results

1. *Materials and methods.* In general, the methods and materials described in our earlier communications have been used [1—3]. Moreover, the quantity of halogen split off in the reaction **III** → **II** was also measured by the well known method of VOLHARD. Besides the phosphate buffer used in the earlier experiments, hydrocarbonate, borate, citrate and acetate buffers were used, further non-buffered sodium sulfate solution (adjusted with NaOH), and finally, the reaction was also studied in a solution which had a composition similar to the ionic composition of blood:

$NaHCO_3$	0.2%
NaCl	0.25%
KCl	0.15%
$CaCl_2$	0.02%
$MgCl_2 \cdot 6H_2O$	0.03%
Phosphate buffer	10^{-2} *M*

The temperature of the reaction solution was maintained at 25 and 37 °C, respectively. In plotting the wave heights, percentage values were given instead of the corresponding values of the current, taking the wave height of the synthetic ethyleneimino compound (**II**) of identical concentration as 100%.

2. *The progress in time of the cyclization reaction.* First, the conversion of Degranol (**III**) into **II** was examined in phosphate buffer (0.025 *M*) at 25 °C

and various pH values. We wished to clarify in this way the basic characteristics of the reaction in a simple system, and to study the effect of physiological conditions subsequently. The Degranol concentration was 10^{-3} *M* during the reactions in which the splitting off of the halogen was studied, to ensure hereby accurate results in the Volhard titration. The samples for polarography were withdrawn at given intervals from this solution, in order to study the development of the ethyleneimino wave.

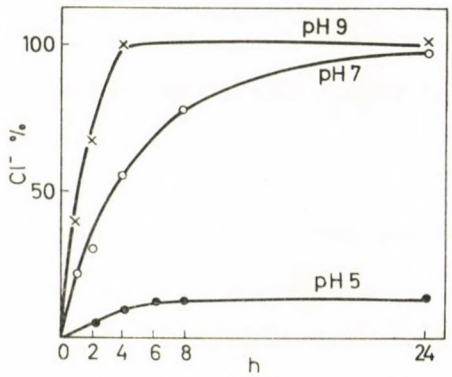

Fig. 1. Time curves of cleavage of chlorine at 25 °C; 10^{-3} *M* **III** in 0.025 *M* phosphate buffer of various pH's. Ordinate: covalent chlorine split off, in percentage of the final value

Figs 1 and 2 give the quantity of the halogen in covalent bond split off as a function of time, in solutions adjusted to pH's between 5 and 9. For pH 6 and 8, Fig. 2 shows the progress of cyclization both on the basis of the ethyleneimino wave, and the polarogram of the compound formed with thiosulfate. From these figures, the following can be established:

(*a*) at pH > 7, the total halogen is split off during a reaction time of 24 hours,

(*b*) at pH < 6, the reaction proceeds only partially: at pH 6, the curve seems to have a limit value at about 50%, and at pH 5 at about 15%, similarly to the time curves of equilibrium reactions.

It is evident on the basis of theoretical considerations that the cyclization of the first halogenethylamino group of Degranol probably requires a smaller activation energy than the reaction of the second such group. Moreover, it is reasonable to presume that the derivative containing one ethyleneimino ring (further on: **IV**) is more stable than **II**. Probably, this may be of importance also from the aspect of toxicity.

(*c*) At higher pH values, the development of both kinds of waves remains only slightly behind the curve representing the elimination of the halogen, while at pH 6 the ethyleneimino wave heights amount only to half of the height of the halogen curve. On the other hand, the wave height of the com-

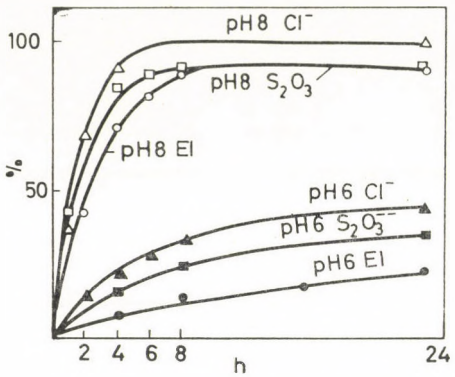

Fig. 2. Time curves of the cyclization reaction at 25 °C. The splitting off of covalent chlorine (Cl^-), the height of the ethyleneimino wave (EI), and the wave of the samples withdrawn during cyclization, after their reaction with thiosulfate ($S_2O_3^{2-}$). For the experimental conditions, see Fig. 1. Ordinate: Cl^-, EI and $S_2O_3^{2-}$, in percentage of the theoretical final value

pound formed with thiosulfate is fairly close to the halogen curve. This fact also indicates a different reaction mechanism: at pH 6, a considerable part of the halogen is split off under conditions where scarcely any compound giving an ethyleneimino wave is formed, and presumably, a part even of this small quantity is split by hydrolysis. This latter fact seems to be supported by findings reported in our earlier communications [2], [3], according to which the wave height of **II** diminished on standing in solution, particularly at low pH values. The problem, which of these alternatives is valid for our case, is answered by the reaction curve measured by means of the wave of the thiosulfate compound in Fig. 2. In slightly acid medium, mostly a compound containing only one ethyleneimino group is formed, which, however, does not give rise to an ethyleneimino wave; on the other hand, its reaction product

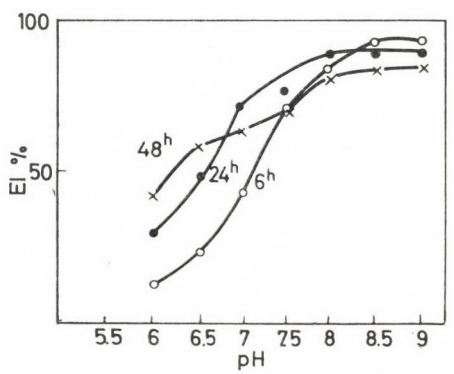

Fig. 3. Effect of the pH and reaction time on the height of the ethyleneimino wave. 5.10^{-4} *M* **III**, after standing in 0.025 *M* phosphate buffers of various pH for 6, 24 and 48 hours, respectively, at 25 °C. After standing, the polarograms were recorded with 10^{-4} *M* **III** in 0.025 *M* phosphate buffer (pH 6)

with thiosulfate gives the same wave as the thiosulfate compound of **II**, only the wave is lower. This indicates that the compound under investigation is different from **II**, still it contains one ethyleneimino ring. Herewith, the formation of the monoethyleneimino derivative, **IV**, in slightly acid medium can be regarded as proved.

Fig. 3 shows the height of the ethyleneimino wave as a function of the pH, on the basis of polarograms recorded after a cyclization reaction

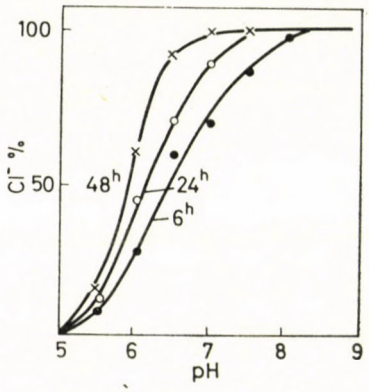

Fig. 4. The splitting off of covalent chlorine as a function of the pH and the reaction time. (For conditions, see Figs 1 and 3, data of which were obtained in identical experiments)

of 6, 24 and 48 hours, respectively. It can be established on the basis of this figure that:

(*a*) In a solution whose pH is adjusted to 8—9, the wave height attains its maximum value within 6 hours while at pH 6, even after 48 hours, only about 50% of the theoretical wave height is attained.

(*b*) The curve corresponding to a reaction time of 48 hours seems to be anomal, as compared with the curves for 6 or 24 hours: at a pH higher than 7, it lies lower than the 24-hour curve, obviously owing to hydrolytic ring splitting as mentioned above. On the other hand, below pH 7 it lies above the 24-hour curve. This effect has not been investigated in detail.

(*c*) The influence of the pH on the reaction can be expressed with the inflexion point of the curves. With a reaction of 6 hours, this value occurs at about pH 7.2, and with a reaction of 24 hours at about pH 6.6. In the case of the 48-hour curve, due to its anomalous character mentioned, the establishing of the inflexion point is meaningless.

The halogen values corresponding to Fig. 3 are shown in Fig. 4. The following main conclusions may be drawn:

(*a*) The maximum value of the curves is 100%, since the quantity of halogen split off is not limited by the hydrolytic splitting of the ring.

(*b*) For the same reason, the 48-hour curve does not exhibit an anomalous character.

(*c*) The inflexion points of the curves are shifted towards acid regions, as compared with Fig. 3. The inflexion point occurs after 6 hours at pH 6.5, and after a reaction of 24 hours at pH 6.1. This shift is in good accordance with time curves shown in Fig. 2, where in slightly acid medium the degree of halogen splitting considerably exceeds the formation of the ethyleneimino wave.

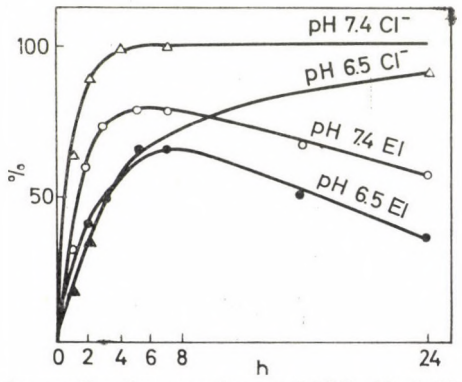

Fig. 5. Time curves of the cyclization reaction at 37 °C. 10^{-3} *M* **III** standing in 0.025 *M* phosphate buffer (pH 7.4 and 6.5, respectively). Wave heights of the EI polarograms of samples, withdrawn after various periods of standing, and the amount of covalent chlorine split off in percentage of the theoretical value (10^{-4} *M*; 0.025 *M* phosphate buffer; pH 6; 25 °C)

The conversion of Degranol was also studied under conditions more similar to physiological conditions. Fig. 5 shows the halogen splitting and the development of the ethyleneimino wave as a function of time, when the reaction proceeds at 37 °C in 0.025 *M* phosphate buffer whose pH-value has been adjusted to 7.4 and 6.5, respectively. The following conclusions can be made:

(*a*) The maximum wave height is attained in about 6 hours (80 and 65%, respectively); after this, the wave height diminishes rapidly.

(*b*) At a pH value of 7.4, characteristic of blood, the splitting off of the halogen occurs to 100% as soon as after 4 hours, while at pH 6.5 100% cleavage is not attained even after 24 hours.

(*c*) The "half-time" of halogen cleavage is about 30 minutes and 3 hours, respectively. It can be established, therefore, that in the physiological pH range the reaction rate is strongly affected by the pH of the medium. Probably, the selective effect of Degranol on cancerous tissues is to be ascribed to this fact.

3. *Effect of hydrocarbonate.* The investigations on the reaction mechanism discussed so far were carried out in phosphate buffer solutions, to avoid complex

side effects. However, Degranol is administered by the intravenous route and as it is known blood contains, besides other ions, hydrocarbonate in 23 m*M* concentration. It was shown on true nitrogen mustards [4—6] that the halogenethylamino group reacted with hydrocarbonate to give an oxazolidone which had no cytoactivity. Hydrocarbonate does not react with the cyclic compound. Thus, a great part of the nitrogen mustard introduced into the blood becomes ineffective. This effect becomes still more pronounced owing

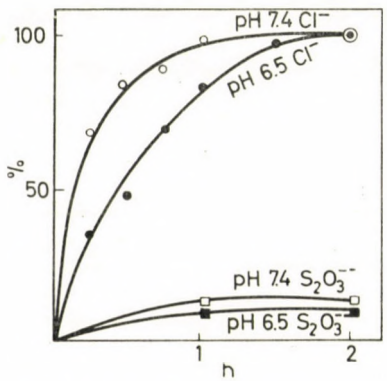

Fig. 6. The course of the reaction in the ionic environment of blood. 10^{-3} *M* **III**, after standing at 37 °C for various times in a solution of an ionic composition similar to that of blood at pH 7.4 and 6.5, respectively. Ordinate: halogen split off, and the wave heights of the samples after reaction with thiosulfate, in percentage of the theoretical value

to the fact that blood contains an enzyme catalyzing this reaction [7], increasing its rate to several times of the normal value.

For this reason, the effect of hydrocarbonate on Degranol has been investigated in detail. These investigations involved also the study of the reaction in the presence of the other inorganic ions contained in blood. Fig. 6 shows the degree of halogen splitting at 37 °C, at pH values characteristic of blood and of cancerous tissues (7.4 and 6.5, respectively) in a solution having an ion composition corresponding to that of blood. The time required for the cleavage of 50% of the halogen is about 12 minutes in the first case, and about 30 minutes in the second. In phosphate buffer containing no hydrocarbonate, these two values were found to be 30 minutes and 3 hours (Fig. 5). In the presence of hydrocarbonate, the splitting off of the whole quantity of halogen required one and two hours, respectively.

This shows that the reaction with hydrocarbonate proceeds also with Degranol, and moreover, at such a high rate that the cyclization reaction may take place only to a very small extent. The assumed scheme of the reaction between Degranol and hydrocarbonate is the following:

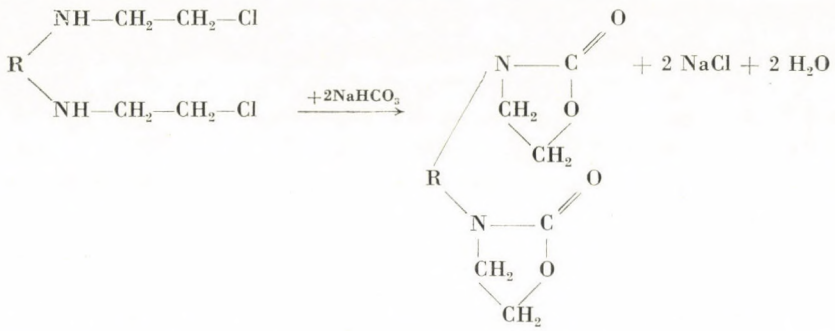

The next problem was to establish to what degree the reaction, used as the basis of the time curves of halogen splitting shown in Fig. 6, proceeds in the direction leading to the formation of oxazolidone, or in that yielding ethyleneimino groups. Simultaneously with the measuring of the halogen polarograms were obtained for both solutions. However, the appearance of the wave, characteristic of the ethyleneimino group, could not be observed. Therefore, the latter experiment was repeated with the difference that the samples taken at intervals were first reacted with thiosulfate, and subsequently polarographed. As it can be seen from the two lower curves in Fig. 6, a wave corresponding to 10 and 14%, respectively, of the theoretically possible maximum value could be measured.

4. *Formation of the monoethyleneimino derivative.* After these experiments it was still an open question, whether this wave of about 10% was indicative of the mono- or bis-ethyleneimino derivative. The lack of the wave characteristic of the ethyleneimino group appears to indicate the mono derivative. However, the possibility must be taken into consideration that the bis derivative might be present, but its very low ethyleneimino wave is protracted and cannot be observed on the polarogram. On the other hand, the waves of the thiosulfate compounds, as mentioned already, are steep, and therefore, can be readily observed even at small wave heights.

Fig. 7 shows the reaction of compound **IV** (which has stood at pH 6 and lost about half of its halogen content), at 37 °C in a solution at pH 7.4. The splitting off of halogen, the ethyleneimino wave and the wave of the product of the reaction with thiosulfate have been examined over 6 hours. The solution adjusted to pH 7.4 contained in one of the cases 0.025 *M* phosphate buffer, and in the other case also 23 m*M* sodium hydrocarbonate. Samples were withdrawn periodically for determination of the halogen content; on the other hand, the samples were reacted with an excess of sodium thiosulfate, and polarographed next day; finally, also the heights of the ethyleneimino waves were plotted. The following conclusions can be drawn from Fig. 7:

(*a*) Further cleavage of the halogen proceeds in the presence of sodium hydrocarbonate somewhat quicker than when standing in phosphate buffer

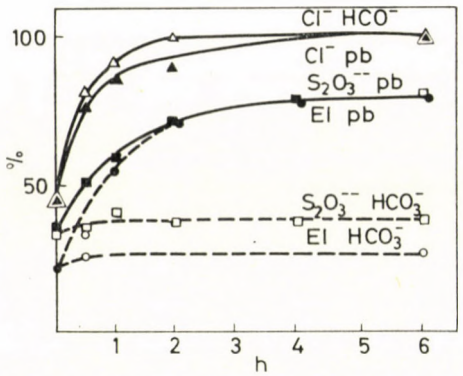

Fig. 7. Complete cyclization of semi-cyclized Degranol and its oxazolidone reaction. Pretreatment: 10^{-3} *M* **III** standing for 48 hours at 25 °C in a solution adjusted with NaOH to pH 6. One half of this solution was then adjusted with 0.025 *M* phosphate buffer (pb), the other half with 0.023 *M* $NaHCO_3$ to pH 7.4, and allowed to stand at 37 °C. Samples were withdrawn at intervals for determination of the amount of halogen split off (Cl^-), the height of the ethyleneimino wave of the solution diluted to 10^{-4} *M* (EI), and the wave height of the reaction product with thiosulfate ($S_2O_3^{2-}$)

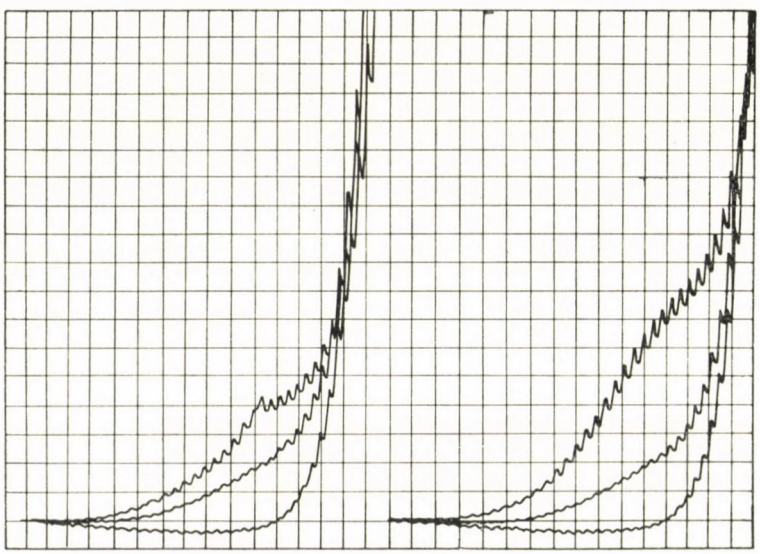

Fig. 8. 10^{-3} *M* **III** was allowed to stand for 16 hours in 0.025 *M* phosphate buffer (pH 6), then half of the solution was adjusted with 0.23 m*M* $NaHCO_3$ (curves on the left) and the other half with NaOH (curves on the right) to pH 8.5. Curves from the bottom to the top: untreated solution of **III**; **III** allowed to stand at pH 6; **III** allowed to stand for further 3 hours at pH 8.5. The polarograms were recorded on 10^{-4} *M* **III**, at pH 6. S = 16.10^{-9} A; Hg level 30 cm; 25 °C; from −0.8 V on; ΔE = 0.05 V

only. Thus, here too, the reaction yielding oxazolidone proceeds at a higher rate than cyclization.

(*b*) In the presence of hydrocarbonate, the ethyleneimino wave hardly rises above the initial value of 22%, while in phosphate buffer it reaches 80% of the theoretical value.

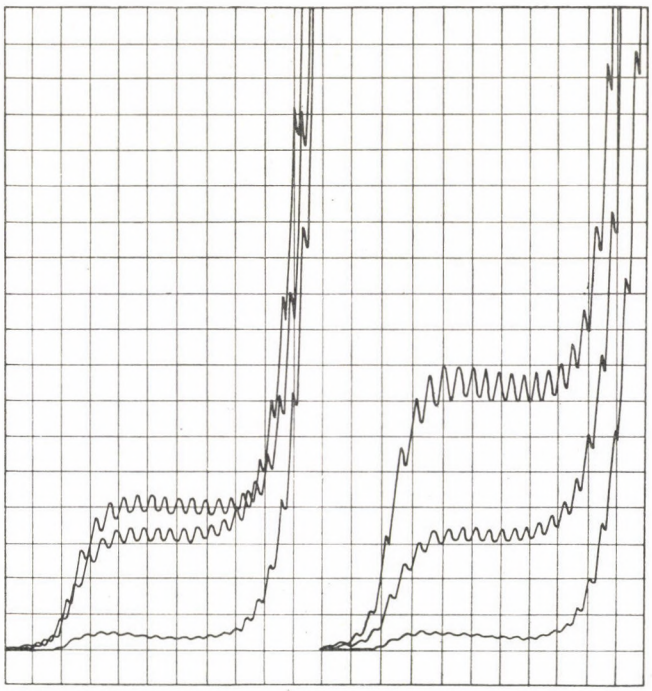

Fig. 9. Continuation of the experiment in Fig. 8: the solutions described there were reacted before recording the polarograms at 25 °C and pH 4, with a tenfold quantity of $Na_2S_2O_3$; $S = 3.10^{-8}$ A; recording from —0.5 V on; $\Delta E = 0.1$ V

(*c*) The wave of the thiosulfate compound also remains at its original level in the presence of hydrocarbonate, while in phosphate buffer after 2 hours, it has the same value as the ethyleneimino wave.

(*d*) In the presence of hydrocarbonate, the heights of the two kinds of waves differ considerably: that of the thiosulfate compound is 40% (its height can be exactly measured), and that of the ethyleneimino wave is about 26%.

These results support the assumption that on standing at pH 6, the greater part of Degranol is converted into compound IV containing one ring; this product does not give an ethyleneimino wave, but its thiosulfate compound products a wave, the height of which is about half of that of the wave of the thiosulfate compound of the bis-ethyleneimino derivative. The existence of the ethyleneimino wave even after standing at pH 6, and the slight increase of this wave in the buffer solution containing hydrocarbonate indicate that

the pH ranges of the various reactions overlap, and each principal reaction is accompanied by side reactions.

The polarograms serving as the basis for the relationships shown in Fig. 7, recorded for a reaction of 3 hours, proceeding however at 25 °C instead of 37 °C, are shown in Figs 8 and 9. It will be seen how difficult it is to evaluate the height of the low ethyleneimino wave, while the height of the wave of the thiosulfate compound can be easily measured. Moreover, it can be seen that the ratio of the waves of two kinds is similar to that at 37 °C.

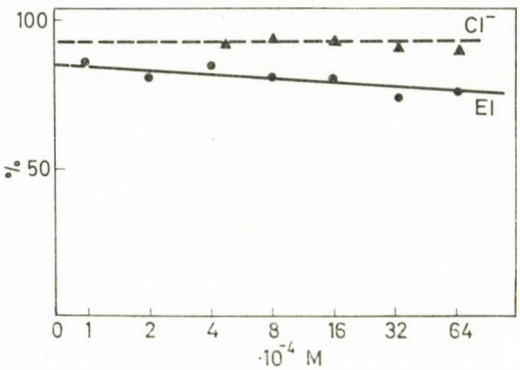

Fig. 10. 1, 2, 4, 8, 16, 32 and $64 \cdot 10^{-4}$ *M* **III** allowed to stand at 25 °C in 0.025 *M* phosphate buffer (pH 8) for 6 hours: the polarograms were recorded on a solution of 10^{-4} *M* concentration. Wave height, in percentage of the theoretical (●———●); percentage halogen split off (▲———▲)

The fact that the reaction proceeds at pH 6 according to a different mechanism than at pH 8, is also shown by considering again Fig. 2: in the first case the wave height does not attain even half the value of halogen splitting, while in the second case it reaches the expected value almost completely.

5. *Effect of the concentration of Degranol on the rate of the reaction.* Assuming that the cleavage of the halogen and cyclization proceed as reactions of first order, the conversion yields must be proportional to the initial concentration of Degranol. This means that, *e.g.*, in 6 hours identical percentages of dissolved Degranol should be converted, independently of the initial concentration. Fig. 10 shows that this relationship is actually valid, both with respect to the quantity of halogen splitt off and the height of the ethyleneimino wave. At Degranol concentrations below $8 \cdot 10^{-4}$ *M*, the splitting off of the halogen has not been investigated, owing to the limited accuracy of the Volhard titration.

A comparison of the values in Figs 10 and 2 shows that in the latter case the splitting off of the halogen is 100% and the wave 82%, while in the

former instance 93 and 80%, respectively, could be observed, under the same experimental conditions. Owing to the versatile reaction possibilities of Degranol and to its high sensitivity to experimental conditions, such deviations were often encountered in the course of our work. However, these deviations do not affect the validity of the tendencies shown by the results, or the conclusions drawn from them, as an uncertainty of 10% has always been taken into account, or the error was minimalized by many repetitions of the experiments in those cases, where greater accuracy was required.

The slight diminution of the wave height with increasing Degranol concentrations falls similarly within the limits of experimental error, therefore it was not further investigated.

It should be mentioned that the polarographic wave of Degranol becomes distorted or melts almost completely with the final catalytic section of the polarogram, if the concentration of Degranol, standing in solution, is increased. This also contributes to the inaccuracy in the determination of the wave height. The limiting current part of the wave is represented, even if solutions of rather low concentrations are allowed to stand, by an inflexion, instead of a horizontal section. At higher concentrations, even this inflexion straightens out completely, and in this case, the height of the polarogram measured at the potential of −1.4 V was taken as the probable value of the wave height.

The polarogram of the pure synthetic ethyleneimino derivative (**II**) shows this factor of inaccuracy to a lesser extent. This indicates that side reactions occur, besides the formation of **II**, when **III** is allowed to stand under the experimental conditions used, and the products of these side reactions are responsible for the indistinct character of the polarogram. The circumstance that in none of the many hundred experiments made in the course of this work did the wave height of Degranol increase during standing to a value corresponding to the wave height of pure synthetic **II**, but amounted only to 80—90% of this value, is also indicative of side reactions.

6. *Effect of the buffer concentration and ionic strength.* The effects of the buffer concentration and ionic strength of the reaction mixture on the splitting off of halogen, accompanying cyclization, and on the ethyleneimino wave height have also been investigated. It can be seen from Fig. 11 that on raising the phosphate buffer concentration to a value higher than 10^{-1} *M*, the splitting off of the halogen decreases slightly, and the wave height considerably. When the reaction is carried out in the presence of 0.64 *M* phosphate, splitting diminishes to about 80% and the wave height to about 30% of their initial values. On the other hand, sodium sulfate, which has no buffer effect, did not influence at all, within the concentration limits examined, either the splitting off of the halogen, or the development of the ethyleneimino wave.

The problem arose whether the effect of the phosphate buffer is specific, and whether this result is actually due to a buffer effect or to the effect of

the multivalent ion. Therefore, also other buffers were included in our investigations. To attain maximum effect, these compounds were used in high (0.64 *M*) concentrations. The results are summarized in Table I.

Our experiments showed inexplicable anomalies from time to time, when fresh stock solutions were used. Therefore, the experiments reported

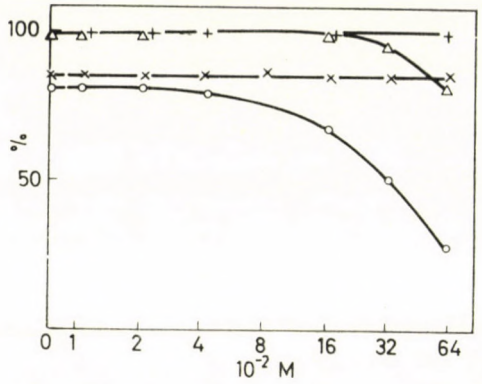

Fig. 11. Effect of the concentration of Na_2SO_4 on the splitting off of halogen (+ ——— +) and the wave height (× ——— ×) of 10^{-3} *M* **III**. Effect of the concentration of the phosphate buffer on the splitting off of halogen (△ ——— △) and on the wave height (○ ——— ○) of 10^{-3} *M* **III**. Standing for 6 hours at 25 °C, at pH 8. Recorded on a solution of 10^{-4} M III.

n Table I, were carried out both on fresh and on 2-week old stock solutions. The results were the following:

(*a*) In a solution which had been allowed to stand, the splitting off of chlorine was slightly influenced only by phosphate. Within the limit of experimental error, borate, citrate, acetate and sulfate had no effect.

(*b*) On the other hand, the wave height was markedly reduced by phosphate, moderately by borate and citrate, slightly by acetate, while sulfate had no effect on the wave height.

Table I

The reaction of 10^{-3} M **II** *in the presence of various buffers or Na_2SO_4 at 25 °C after a reaction time of 6 hours*

	Stock solution, 2-week-old		Fresh stock solution	
0.64 *M*, pH 8	Wave, %	Halogen, %	Wave, %	Halogen, %
Sulfate	82	95	80	90
Borate	53	95	41	85
Citrate	54	93	48	81
Acetate	67	97	63	88
Phosphate	29	83	29	62

(*c*) In the case of freshly dissolved Degranol the wave height was identical in the presence of sulfate and acetate with that of Degranol which had been allowed to stand, while in the presence of borate and citrate, the height of the wave in the fresh solution is lower.

It follows from this that the cyclization reaction is hindered by buffers, but not by the anion (SO_4^{-2}). Moreover, it becomes evident that fresh Degranol and such which was let to stand behave differently. On standing, Degranol undergoes structural changes, which favour cyclization. According to our experiments in progress, in the presence of phosphate, borate and citrate, freshly dissolved Degranol is converted into **II** only after an "induction period". The length of this period depends on the experimental conditions, and the cleavage of halogen starts only after this period.

This problem will be dealt with in another publication, because its elucidation has no direct bearing on the use of Degranol as a cytostatic agent; under the conditions prevailing in blood, this induction period is negligible.

*

The author is indebted to Misses M. DEWATH and É. MAJLÁTH for their assistance in the experimental work.

REFERENCES

1. JÁMBOR, B., HORVÁTH, I. P., INSTITORIS, L.: Acta Chim. Acad. Sci. Hung. **53,** 85 (1967)
2. JÁMBOR, B.: Acta Chim. Acad. Sci. Hung. **63,** 193 (1970)
3. JÁMBOR, B.: Acta Chim. Acad. Sci. Hung. **63,** 205 (1970)
4. ARNOLD, H., BEKEL, H.: Arzneim. F. **14,** 750 (1964)
5. RAUEN, H. M.: Ibid. **14,** 855 (1964)
6. RAUEN, H. M., NORPOTH, K., KRÁMER, K. P.: Ibid. **15,** 1048 (1965)
7. WILLIAMSON, CH. E. *et al.:* Cancer Res. **26,** 323 (1966)

Béla JÁMBOR; Budapest VIII. Múzeum krt 4/a

Acta Chimica Academiae Scientiarum Hungaricae, Tomus 63 (3), pp. 343—352 (1970)

SOLANUM GLYCOSIDES, IV*

SOLARADIXINE

P. BITE, M. M. SHABANA,** L. JÓKAY and L. PONGRÁCZ-STERK

(Research Institute for Pharmaceutical Chemistry, Budapest)

Received December 8, 1968

It has been established that the structure of solaradixine isolated from the bark of the root of *Solanum laciniatum*, is 0-L-rhamnopyranosyl(1α → 2)-0-[0-D-glucopyranosyl(1β → 2)-D-glucopyranosyl] (1β → 3)-0-D-galactopyranosyl(1β → 3)-solasodine.

The root of *Solanum laciniatum* and *S. aviculare*, which grow readily also in Hungary [1], and the fruit of *Solanum mammosum*, indigenous to Venezuela [2], contains a solasodine glycoside, whose sugar moiety consists of galactose, glucose and rhamnose in the molar ratio of 1 : 2 : 1. In a preliminary communication [1], we called this solasodine glycoside, found in the radix of *Solanum laciniatum*, solaradixine.

Solaradixine is present in the bark of the root, while the internal part of the root contains no steroid glycosides. The melting point of the compound is 275—278 °C (decomposition), $[\alpha]_D^{20}$ — 69.7° (c = 1, pyridine), $[\alpha]_D^{20}$ — 51.9° (c = 0.23, methanol). It gives negative Fehling reaction, and positive ALBERTI and BIAL reactions [3]. The equivalent weight, titrated in the presence of TASCHIRO's indicator [4] is 1020, and on the basis of potentiometric titration with perchloric acid it is 1069. The aglycone obtained in its hydrolysis with a mineral acid has been found identical with solasodine on the basis of its physical properties, infrared spectrum, and the N-nitroso derivative. Our investigations by qualitative paper chromatography and thin-layer chromatography, using various solvent mixtures, have shown that the sugars obtained on total hydrolysis are D-galactose, D-glucose and L-rhamnose. The molar ratio of the sugars was found to be 1 : 2 : 1 by the formazan method of FISCHER and DÖRFEL [5], and the anthrone method of SCOTT and MELVIN [6], as well as by gas chromatography.

From the determination of the equivalent weight and the C, H, N, O elemental analysis, the empirical formula of solaradixine, after drying at 105 °C over phosphorus pentoxide in a vacuum of 0.5 mm Hg, is $C_{51}H_{83}O_{21}N \cdot H_2O$ (M = 1064).

* Part III: Acta Chim. Acad. Sci. Hung. **62**, 283 (1969)

** United Arab Republic Scholar from Cairo University, Faculty of Pharmacy.

After oxidation with sodium metaperiodate and subsequent hydrolysis, the reaction mixture contained only galactose, and no other sugars can be detected.

On subjecting solaradixine to partial hydrolysis with 0.01 *N* sulfuric acid, solasonine can be isolated from the reaction mixture. The identity of this solasonine has been established by its physical properties, the preparation and the physical data of its N-nitroso derivative, and by an examination of the aglycone and the sugars obtained in its total hydrolysis.

To clarify the site of linkage of the second glucose unit, solaradixine has been permethylated [7]. After hydrolysis, 2,3,4-tri-O-methyl-L-rhamnose, 2,3,4,6-tetra-O-methyl-D-glucose, 4,6-di-O-methyl-D-galactose and 3,4,6-tri-O-methyl-D-glucose were identified in the reaction mixture.

When solaradixine is dissolved in 0.01 *N* hydrochloric acid, no sugar is split off even on standing for 24 days, therefore the second glucose molecule must also have pyranose structure [8]. This was verified by the structures of the isolated methylated monosaccharides. Though solaradixine is not affected when exposed for 14 days to the action of β-glucosidase enzyme, due to its D-structure, the second glucose molecule can be considered to be present in β-linkage.

Therefore, the complete structure of solaradixine, assuming for all sugars pyranose structure, is the following:

L-rhamnose($1\alpha \rightarrow 2$)
D-glucose($1\beta \rightarrow 2$)-D-glucose($1\beta \rightarrow 3$) — D-galactose($1\beta \rightarrow 3$)-solasodine.

Solaradixine is the first tetroside in which a sugar moiety consisting of four monosaccharides is linked to position three of an unsaturated steroid alkaloid aglycone having a Δ^5 double bond [9], and it contains in the sugar residue the structural unit D-glucopyranosyl($1\beta \rightarrow 2$)-D-glucopyranose, which occurs only seldom in nature.

Experimental

All m.p.'s were determined with a Boetius apparatus, and are uncorrected. The following solvent mixtures were used for chromatography:

1. For the glycosides on paper: (*a*) *n*-butanol–acetic acid–water (10 : 2 : 5) [10]; (*b*) ethyl acetate–acetic acid–water (11 : 2 : 1.85) [11]; (*c*) *n*-butanol–acetic acid–water (4 : 1 : 2).

2. For the glycosides in TLC: (*a*) *n*-butanol saturated with water [1]; (*b*) ethyl acetate–pyridine–water (3 : 1 : 3), upper phase [11]; (*c*) chloroform–ethanol–1% NH_4OH-solution (4 : 5 : 1) [12], (*d*) chloroform–methanol–water (65 : 35 : 10) [13].

3. For the aglycones on paper: (*a*) cyclohexane–methylcellosolve–pyridine–water (8 : 4 : 4 : 1) [14].

4. For the aglycones in TLC: (*a*) chloroform–ethanol (99 : 1) [1]; (*b*) chloroform–methanol (19 : 1) [15]; (*c*) benzene–methanol (9 : 1) [16].

5. For the sugars on paper: (*a*) *n*-butanol–pyridine–water (6 : 4 : 3) [17]; (*b*) *n*-butanol–ethanol–water (8 : 1 : 2) [16]; (*c*) *n*-butanol–ethanol–water (4 : 1 : 5) [18].

6. For the sugars in TLC: (*a*) *n*-butanol–acetic acid–diethyl ether–water (9 : 6 : 3 : 1) [19]; (*b*) ethyl acetate–isopropanol–water (65 : 23 : 12) [22].

Both in paper chromatography and TLC, the glycosides as well as the aglycones were visualized with saturated antimony trichloride solution in chloroform, or with Dragendorff's reagent, while the sugars were detected with analine phthalate, triphenyltetrazolium hydroxide or anisaldehyde–sulfuric acid.

Isolation of the glycoside mixtures

1 kg of ground *Solanum laciniatum* root, dried at 60 °C, was stirred at room temperature for each 5 hrs. subsequently with 1×10 l. and 1×5 l. of 0.5% nitric acid solution. The combined extracts were adjusted with conc. aqueous ammonia to pH 6, heated to 60 °C, and made alkaline with conc. aqueous ammonia, to obtain pH 9. After standing for a day, the precipitate was separated by decantation and subsequent centrifuging. The dry precipitate (19.8 g) was extracted by boiling for 1 hr. with 2×300 ml and then 1×200 ml portions of methanol. The evaporation residue of the combined extracts, a very slightly yellowish solid substance, was 7.9 g.

Both paper and thin-layer chromatograms were run with this product, simultaneously with solasonine, solamargine and solaradixine for comparison. The spots of the glycoside mixture, in the decreasing order of the R_f values were marked by *A*, *B*, *C*, *D*, and *E*. The results, obtained are summarized in Table I.

Table I

Examination of the glycoside mixture by paper chromatography and by thin-layer chromatography

Substance	R_f values						
	SS 2043b	MN 214		Silicagel-G			
	Solvent mixture 1*a*	1*b*	1*c*	2*a*	2*b*	2*c*	2*d*
Solamargine	0.64	0.75	0.65	0.27	0.46	0.63	0.46
A	0.63	0.75	0.65	0.27	0.45	0.63	0.46
Solasonine	0.55	0.51	0.55	0.22	0.25	0.58	0.38
B	0.55	0.50	0.54	0.22	0.25	0.58	0.38
Solaradixine	0.45	0.33	0.45	0.15	0.15	0.44	0.30
C	0.44	0.33	0.44	0.15	0.15	0.45	0.30
D				0.09		0.39	0.24
E	0.29	0.08		0.05		0.33	0.20

A, which seems to be identical with solamargine, could not be detected in each root material, and even when present, it gave only a weak spot.

Isolation of B

A column of 5 cm diameter was prepared from 250 g of neutral alumina of Brockmann II activity with *n*-butanol saturated with water. 5.9 g of the glycoside mixture was introduced into the column, and eluted with *n*-butanol saturated with water. Fractions of 15 ml were collected. The chromatographic results are summarized in Table II.

Recrystallization from methanol of the evaporation residue of fractions 10—38, giving only the spot of *B*, yielded colourless needles, m.p. 285—287 °C (d.), $[\alpha]_D^{25} = -90°$ ($c = 1$, pyridine), $[\alpha]_D^{25} = -70.5°$ ($c = 0.5$, methanol).

Table II

Separation of the glucoside mixture by chromatography on an alumina column

Fractions, No.	Weight of the evaporation residue (g)	Components as shown by TLC
1— 9	0.05	$A + B$
10— 38	0.87	B
39— 45	0.51	$B + C$
46— 87	3.24	C
88—125	0.72	$C + D + E$

On the basis of the melting point, mixed melting point, rotation, C, H, N, O analysis [20, 21], *B* is identical with solasonine, prepared from the leaves of *Solanum aviculare* and *S. laciniatum;* its behaviour in paper chromatography and TLC was also consistent with the properties of solasonine.

N-nitroso-B

100 mg of *B* was dissolved in 1 ml of acetic acid, and admixed with a conc. aqueous solution of 50 mg of sodium nitrite. After a few minutes, a white precipitate was obtained. The mixture was allowed to stand in a refrigerator, then filtered off, washed with water, and dried (90 mg). Attempted crystallization from 96% ethanol gave a gelatinous substance. This was dissolved again by boiling, and hot water was added until beginning turbidity. On cooling, a crystalline substance separated. Filtration yielded a product (40 mg), m.p. 250 °C. The m.p. was the same as that of the N-nitroso derivative prepared from an authentic sample of solasonine (m.p. 251 °C, see [22]); no depression of the mixed m.p. was observed.

Isolation of C

The evaporation residues of the mixed fractions containing *C* (which was called in our earlier communication [1] solaradixine) were combined, and chromatographed again as described above. The evaporation residue of the combined fractions giving only the spot of solaradixine (3.92 g) was then repeatedly dissolved in hot ethanol and precipitated with ether. Recrystallization from 50% aqueous acetone of the colourless product yielded needle crystals. Solaradixine, after drying in vacuum at 105 °C for 5 hrs. over phosphorus pentoxide, had m.p. 275—278 °C (d.) $[\alpha]_D^{20} = -69.7°$ ($c = 1$, pyridine), $[\alpha]_D^{20} = -51.9$ ($c = 0.23$, methanol).

$C_{51}H_{83}O_{21}N \cdot H_2O$ (1064.2). Calcd. C 57.57; H 8.05; O 33.08; N 1.31. Found C 57.92; H 8.06; O 33.11; N 1.33%.

Dissolution in an excess of 0.01 *N* HCl and titration in the presence of Taschiro's indicator [4] with 0.01 *N* NaOH gave the equivalent weight as 1020 (values measured: 1030, 1010); potentiometric titration with 0.025 *N* perchloric acid in glacial acetic acid yielded the equivalent weight 1069 (values measured: 1100, 1038).

A solution of 10 mg of solaradixine in 5 ml of ethanol mixed with 5 ml of a 1% digitonine solution in 90% ethanol did not give any turbidity even after 24 hrs.

The product gave negative Fehling reaction, and positive Alberti, Molisch. α-naphthol and Bial reactions.

Total hydrolysis of solaradixine (C)

1 g of solaradixine was dissolved in 10 ml of ethanol, 10 ml 3 *N* HCl was added, and the mixture was boiled for 4 hrs.

Examination of the aglycone

The mixture was let to stand in a refrigerator, the precipitate filtered off, washed with a small amount of ice-water, dissolved in 80% hot methanol, and the free base precipitated with conc. ammonia (dry weight 376 mg).

The free base gave two spots in TLC (solvent mixture 4*c*) after visualization with antimony trichloride. The R_f of the principal spot (0.34) was the same as that of solasodine, and the R_f value of the weaker spot (0.70) agreed with that of solasodiene.

The mixture was dissolved in benzene, and chromatographed on a column 1.2 cm in diameter, prepared from neutral Woelm's alumina of activity II, using solvent mixture 4*c* for elution. The evaporation residue of the combined fractions giving one spot with R_f 0.34 was recrystallized from methanol. The product had m.p. 200—202 °C, $[\alpha]_D^{22} = -101^\circ$ ($c = 1$, ethanol). The analysis (C 78.40; H 10.48 and N 3.4%) was also in good agreement with the data published for solasodine [20]. The infrared spectrum of the product was identical with that of solasodine, obtained from the leaves of *Solanum laciniatum*.

On the basis of the 376 mg of free base, obtained as described above, and shown to be a mixture of solasodine and solasodiene, the molecular weight of solaradixine is 1100.

Examination of the sugar moiety

After the removal of the hydrochloride precipitate, methanol was evaporated from the solution, then the residual aqueous acid solution was neutralized with Amberlite IR-4B resin, and a stock solution was prepared.

From this stock solution a portion containing about 100 μg of total sugar was applied onto Whatman 1 chromatographic paper, and an ascending chromatogram was made with solvent mixtures 5*a* and 5*b*, respectively, to a front distance of 30 cm. The sugar mixture was also studied by TLC on a Silicagel-G layer with solvent mixture 6*a*, and on Kieselguhr-gypsum layer with solvent mixture 6*b*. To achieve a better separation of glucose and galactose, double runs were made with the same solvent both in paper chromatography and TLC. The final results of the comparative runs made with analytically pure hexoses and pentoses, are summarized in Tables III and IV.

Table III

Chromatography of sugars obtained in the total hydrolysis of solaradixine, on Whatman 1 paper

Substance	R_f values in ascending chromatography run with					
	5*a*			5*b*		
	solvent mixtures					
Hydrolyzate	0.55	0.61	0.81	0.21	0.27	0.60
D-Galactose	0.54			0.21		
D-Glucose		0.61			0.27	
L-Rhamnose			0.81			0.60

Table IV

Thin-layer chromatography of the sugars obtained in the total hydrolysis of solaradixine

Substance	R_f values					
	Silicagel-G 6*a*			Kieselguhr-gypsum 6*b*		
	solvent mixtures					
Hydrolyzate	0.57	0.62	0.77	0.10	0.14	0.44
D-Galactose	0.57			0.10		
D-Glucose		0.62			0.14	
L-Rhamnose			0.77			0.44

Quantitative determination of the molar ratio of galactose, glucose and rhamnose

The quantitative determination of the sugars was made on total sugar stock solutions, prepared on the one hand from the stock solution mentioned above and kept at 0 °C, and, on the other hand, from case to case from 5 mg of solaradixine (heated with 0.5 ml of 1 *N* HCl at 100 °C for 3 hrs. in a sealed tube, centrifuged and the acid evaporated in vacuum). The determinations were carried out by the formazan method of FISCHER and DÖRFEL [5], by the anthrone method of SCOTT and MELVIN [6], and by gas chromatography using an instrument Model Gasofract 400 C (Dr. Virus K.G.). In the formazan and anthrone methods, the chromatograms were run twice on Whatman 1 paper with solvent mixture 5*a* to a front distance of 30 cm. The experimental results are summarized in Tables V and VI.

Table V

Quantative molar ratio of the sugars in solaradixine determined by the formazan method

	μg	$\times 10^{-8}$ mole	Molar ratio
D-Galactose	12.0	6.66	1.0
D-Glucose	23.5	13.05	1.96
L-Rhamnose	13.1	7.96	1.20

Table VI

Quantitative molar ratio of the sugars in solaradixine determined by the anthrone method

	μg	$\times 10^{-8}$ mole	Molar ratio
D-Galactose	14.5	8.05	1.0
D-Glucose	31.1	17.20	2.1
L-Rhamnose	15.7	9.55	1.2

Gas chromatographic determinations gave for D-galactose 24.5, for D-glucose 51.3 and for L-rhamnose 24.8% *i.e.* a molar ratio of 1 : 2.1 : 1.1.

Oxidation of solaradixine with periodate

45 mg of solaradixine was dissolved in 4 ml of 0.1 *N* acetic acid, 9 ml of 0.1 *N* sodium periodate was added, and the mixture was allowed to stand for 3 days at room temperature. After this period, 2 ml of ethyleneglycol was added, and the mixture was processed according to KUHN and LÖW [21]. The evaporation residue was dissolved in 50% methanol. Paper chromatography detected only D-galactose in this solution.

Partial hydro ysis of solaradixine

10 g of solaradixine was refluxed for 24 hrs. with 500 ml of 0.01 *N* sulfuric acid. The hot solution was made alkaline with conc. ammonium hydroxide solution and placed in a refrigerator. The precipitate was separated on a centrifuge, washed with water, and dried.

The glycoside mixture (5.27 g) obtained in this partial hydrolysis had five marked chromatographic spots. The mixture was separated on a chromatographic column of 1500 g Brockman II alumina, using for elution a 1 : 1 *n*-butanol–ethylacetate mixture saturated with water. Only fractions containing two or more glycosides were obtained.

The fractions shown by TLC and paper chromatography to contain a component with the same R_f as solasonine were combined and evaporated, and the residue (1.1 g) was chromatographed again with butanol saturated with water on a column packed with 240 g of wide-pore silicagel and having a grain size between 0.5 and 0.15 mm [23]. A good separation was obtained. The evaporation residue of the combined fractions containing only the substance of an R_f value identical with that of solasonine, was 0.5 g. Repeated recrystallizations (dissolution in hot 60% ethanol and adding hot acetone) gave the substance with m.p. 287—290 °C. This product showed no depression of the m.p. with pure solasonine. The results of C, H, N, O analysis were also consistent with those of solasonine, and qualitative chromatography of the hydrolysis products showed the presence of the same aglycone and sugar components as obtainable from solasonine.

The N-nitroso derivative was prepared in the same way as described for substance *B*. This gave no depression of the m.p. with the N-nitroso derivative of authentic solasonine, and showed in TLC an identical behaviour ($R_f = 0.37$, on silicagel G, with solvent 2*d*).

Permethylation of solaradixine

4.2 g of solaradixine (dried in a vacuum of 0.5 mm-Hg over magnesium perchlorate for 48 hrs. at 110 °C) was dissolved in 90 ml of freshly purified dimethylformamide, and 30 g of freshly prepared silver oxide was added [7]. The internal temperature was maintained below 5 °C and 30 ml of methyl iodide was added in small portions, under shaking. The mixture was then shaken for 70 hrs. The precipitate was filtered off, and 25 g of freshly prepared silver oxide and 25 ml of methyl iodide were added to the solution, and the mixture was shaken for 30 hrs. After this period, the new precipitate was filtered off, washed with a small amount of dimethylformamide, and 100 ml of chloroform was added to the filtrate.

The precipitate was dissolved in a solution of 20 g of potassium cyanide in 300 ml of water, and the chloroform phase was separated from the aqueous layer. The aqueous phase was extracted with further 6×100 ml portions of chloroform, and the combined chloroform phases were washed with 2×50 ml of water. After drying over sodium sulfate, the chloroform solution was evaporated to dryness. The evaporation residue was a yellowish-white solid (5.53 g), m.p. 126—138 °C. Drying in vacuum over phosphorus pentoxide for 3 hrs. at 100 °C did not alter the m.p.

5 g of the product was dissolved in 150 ml of methanol. 30 ml of water and 10 g of freshly precipitated silver oxide were added, and the mixture was shaken for 12 hrs. at room temperature. After the removal of the precipitate, the solution was evaporated to dryness. The residue was a pale yellow solid, m.p. 146—151 °C, $[\alpha]_D^{22} = 43.1°$ ($c = 1$, methanol). According to the infrared spectrum, the substance did not contain free hydroxyl group.

$C_{64}H_{109}O_{21}N$ (1228.5). Calcd. C 62.2; H 8.9; OCH_3 (12) 30.3. Found C 61.5; H 9.02; OCH_3 28.43%.

Total hydrolysis of permethyl-solaradixine

5.3 g of permethyl-solaradixine was refluxed for 6 hrs. with 120 ml of a 5% solution of HCl in abs. methanol. After cooling, 100 ml of water was added, and the mixture was concentrated in vacuum to about 90 ml. 7 ml of conc. HCl was added, and the mixture was boiled for 4 hrs. After cooling, the precipitate was filtered off (1.7 g after drying).

The acid solution was treated with clarifying carbon, and extracted with 10×150 ml of chloroform.

(*a*) *Examination of the chloroform phase*

The combined pale yellow chloroform solutions were washed with $NaHCO_3$ solution, then with water until neutral, dried with sodium sulfate, and evaporated. A sticky brown residue (1.52 g) was obtained. Gas-liquid chromatography showed this substance to be a mixture of 2,3,4,6-tetra-O-methyl-D-glucose and 2,3,4-tri-O-methyl-L-rhamnose.

A mixture of 25 g of Darco-G 60 and 25 g of Celite 535 was treated with conc. HCl, washed neutral with distilled water, then washed with abs. ethanol. From this adsorbent mixture a column of 3 cm diameter was prepared using 5% aqueous methyl ketone. 1.4 g of the evaporation residue was dissolved in the same solvent, and eluted on the column. Fractions of 15 ml were taken. The chromatographic results are shown in Table VII.

Table VII

Chromatography of the evaporation residue of the chloroform phase on a Darco-Celite column

Fraction, No.	Weight of the evaporation residue (g)	Whatman 1 paper, solvent mixture 5*c*, detection with aniline phthalate
1—15	0.61	2,3,4-trimethyl-L-rhamnose
16—24	0.13	no spot
25—38	0.52	2,3,4,6-tetramethyl-D-glucose

Run in a mixture, 2,3,4-tri-O-methyl-L-rhamnose and 2,3,4,6-tetra-O-methyl-D-glucose did not give separate spots. In pure state, and detected with aniline phthalate, the spot of 2,3,4-tri-O-methyl-L-rhamnose was brown, that of 2,3,4,6-tetra-O-methyl-D-glucose red, while visualization with triphenyltetrazolium hydroxide gave pink colour with 2,3,4-tri-O-methyl-L-rhamnose, and no colour with 2,3,4,6-tetra-O-methyl-D-glucose.

The evaporation residue of fractions 1—15 was dissolved in choroform, filtered, and the clear solution evaporated again in vacuum. The residue was a pale yellow syrup, which gave on Whatman 1 paper with solvent mixture 5*c* an R_f value of 0.81, $[\alpha]_D^{23} = +25.3$ ($c = 1$, water) (lit [7] $[\alpha]_D^{24} = +27.5°$, $c = 1$, water). The infrared spectrum of the substance was identical with that of authentic 2,3,4-tri-O-methyl-L-rhamnose; the C, H and OCH_3 analyses were in good agreement with the calculated values.

The anilide of the substance, prepared according to KUHN *et al.* [7], gave after sublimation and recrystallization from petroleum ether, fine needle crystals, m.p. 120—122 °C, $[\alpha]_D^{23} = +138°$ ($c = 0.66$, ethanol); lit. [7] m.p. 124—125 °C. The C, H and N analyses were in good agreement with the calculated values.

The brown resinous evaporation residue of fractions 25—38 was dissolved in water, centrifuged, and the clear solution evaporated. Repeated recrystallizations from ether-petroleum ether yielded colourless needles, m.p. 90—93 °C; the substance did not give m.p. depression with authentic 2,3,4,6-tetra-O-methyl-α-D-glucose, $[\alpha]_D^{23} = +92°$ ($c = 1$, water) → 84.5° (24 hrs.) (lit. [24] m.p. 90—96 °C; $[\alpha]_D^{20} = +91.5° \rightarrow +84°$). Using solvent mixture 5*c*, the R_f value, 0.80, was the same as that of an authentic sample. The infrared spectrum and the C and H analyses were also consistent with the given structure.

(*b*) *Examination of the aqueous phase*

After the extraction with chloroform, the residual aqueous phase was neutralized with Amberlite IR-4B, and evaporated in vacuum. The residue (2.38 g) was a dark brown syrup, which gave three chromatographic spots (Whatman 1 paper, solvent mixture 5*c*). Of these, the topmost was due to an impurity (contamination of the methylated sugar mixture, recovered from the chloroform phase as described above). Under this spot two new spots were exhibited (R_f 0.70 and 0.42; R_G 0.85 and 0.51). An authentic sample of 4,6-di-O-methyl-α-D-galactose gave the same R_f as the lower spot. Authentic 2,3,6-, 2,4,6- and 3,4,6-tri-O-methyl-D-glucose samples had all nearly identical R_f values with that of our substance migrating to a greater distance.

Preparative separation by paper chromatography

2.2 g of the above evaporation residue was dissolved in 5 ml of 90% methanol, and 0.5 ml of the solution was applied with a micropipette on each of ten Whatman 3 papers (40×36 cm) in a strip of 5 mm width, parallel to the lower edge of the paper, and at a height of 5 cm from the same. The chromatograms were run with the upper phase of solvent mixture 5*c*, with ascending technique, to a front distance of 28 cm. After the drying of the chromatograms, 3 indicator strips (3 mm wide) were cut out from each sheet (from the two ends and the middle). The spots on the indicator strips were visualized with aniline phthalate, and using this indication as a guide, the required bands were cut out from the untreated paper parts. The papers with identical bands were collected and cut to small pieces, then placed into a centrifuging

tube, strirred for 1 hr. with 300 ml of 90% methanol, and centrifuged. Extraction with methanol was twice repeated, and the combined extracts were evaporated in vacuum.

Evaporation of the extract of the slower running substance gave a brown syrup (400 mg), which became crystalline. It was dissolved in 2 ml of boiling abs. ethanol, 6 ml of ethyl acetate was added, and the mixture was allowed to stand in a refrigerator. Colourless crystal needles separated, m.p. 141—142 °C, $[\alpha]_D^{22} = +138°$ ($c = 0.5$, water) → 75.7° (18 hrs.); lit [24] m.p. 140.5 °C. $[\alpha]_D^{20} = +135° \rightarrow +76°$ (16 hrs.). The product did not give m.p. depression with authentic 4,6-di-O-methyl-α-D-galactose, and had an identical infrared spectrum. The C, H and OCH_3 analyses were in good agreement with the calculated values.

The osazone prepared according to BACON *et al.* [25] was yellow needles, m.p. 159—161 °C, $[\alpha]_D^{22} = +50.3°$ ($c = 0.5$, chloroform) → $+121°$ (24 hrs.) → $-21°$ (150 hrs.); lit. [25] m.p. 160—162 °C, $[\alpha]_D^{20} = +50° \rightarrow -21°$ (143 hrs.).

Evaporation of the extract of the substance migrating to a greater distance gave 470 mg of a brown syrup. Using small Darco-Celite (1 : 1) column (2 cm×15 cm), the substance was clarified in 0.5% aqueous methyl ethyl ketone solution, then evaporated to yield a pale yellow syrup, which could not be crystallized; $[\alpha]_D^{20} = +71°$ ($c = 0.5$, water); this value did not change on standing. Authentic 2,3,6-, 2,4,6- and 3,4,6-tri-O-methyl-D-glucoses and this substance gave (Whatman 1 paper, solvent mixture 5*c*) the R_f and R_G values shown in Table VIII.

Table VIII

Paper chromatography of trimethyl-D-glucoses

Substance	Whatman 1, ascending, solvent mixture 5*c*	
	R_f	R_G
2,3,6-Tri-O-methyl-D-glucose	0.69	0.88
2,4,6-Tri-O-methyl-D-glucose	0.67	0.84
3,4,6-Tri-O-methyl-D-glucose	0.71	0.86
Isolated substance to be identified	0.70	0.85

The authentic trimethylglucose samples and our own substance were investigated on Whatman 1 paper with four different sugar reagents. The results of these tests, supplemented with the literature data of 2,3,4-tri-O-methyl-D-glucose, which was not available to us, are summarized in Table IX.

On the basis of its colour reactions, the sugar derivative to be identified is 3,4,6-tri-O-methyl-D-glucose.

Table IX

Colour reactions of trimethyl-D-glucoses

Reagent	Tri-O-methyl-D-glucose				Substance investigated	Colour
	2,3,4-	2,3,6-	2,4,6-	3,4,6-		
Triphenyltetrazolium hydroxide	— [26]	—	—	+	+	pink
Periodate–permanganate	— [27]	—	—	+	+	yellowish brown
Periodate–benzidine	— [28]	—	—	+	+	colourless in blue background
Dimethylaniline	— [29]	+	—	—	—	purple

We wish to thank Mr. B. KOCH, assistant director (Tápiószele, National Agrobotanical Institute), and the Research Institute for Medicinal Plants (director: Dr. P. TÉTÉNYI) for making available the plant material.

Best thanks are due to the Analytical Department of our Institute, headed by A. MIZSEI for the various analytical tests; to Prof. Sir Edmund HIRST, University of Edinburgh, and to Dr. Irmentraut LÖW, Heidelberg, Max Planck Institute, for samples of authentic methylated sugars.

We thank Miss É. SZEBENYI for her valuable help in the experimental work.

REFERENCES

1. BITE, P., JÓKAY, L., PONGRÁCZ-STERK, L.: Acta Chim. Acad. Sci. Hung. **34,** 363 (1962)
2. SEELKOPF, C.: Arch. Pharmaz. **301,** 111 (1968)
3. SCHREIBER, K.: Die Pharmazie **10,** 379 (1955)
4. FRESENIUS, R.: Z. analyt. Chem. **114,** 278 (1938)
5. FISCHER, F. G., DÖRFEL, H.: Hoppe-Seylers Z. f. physiol. Chem. **297,** 164 (1954)
6. SCOTT, T. A., MELVIN, E. H.: Anal. Chem. **25,** 1656 (1953)
7. KUHN, R., LÖW, I., TRISCHMANN, H.: Chem. Ber. **88,** 1492, 1690 (1955)
8. HAWORTH, W. N.: Chem. Ber. **65,** 50 (1932)
9. TSCHESCHE, R., WULFF, G.: Planta Med. **12,** 283 (1964)
10. SZENDEY, G. L.: Arch. Pharmaz. **290,** 563 (1957)
11. BRIGGS, L. H., CAMBIE, R. C., HOARE, J. L.: J. Chem. Soc. **1961,** 4645
12. BOGNÁR, R., MAKLEIT, S.: Acta Chim. Acad. Sci. Hung. **46,** 205 (1965)
13. KAWASAKI, T., MIYAHARA, K.: Chem. Pharm. Bull. (Japan) **11,** 1546 (1963)
14. TSCHESCHE, R., FREYTAG, W., SNATZKE, G.: Chem. Ber. **92,** 3053 (1959)
15. BOLL, P. M.: Acta Chem. Scand. **16,** 1819 (1962)
16. RASMUSSAN, H. P., BOLL, P. M.: Acta Chem. Scand. **12,** 802 (1958)
17. DJATLOVICKAJA, E. V., VORONKOVA, V. V., BERGELSON, L. D.: Dokl. Akad. Nauk, S.S.S.R. **145,** 325 (1962)
18. HIRST, E. L., HOUGH, L., JONES, J. K. N.: J. Chem. Soc. **1949,** 928
19. HAY, G. W., LEWIS, B. A., SMITH, F.: J. Chromatog. **11,** 479 (1963)
20. BELL, R. C., BRIGGS, L. H.: J. Chem. Soc. **1942,** 1
21. KUHN, R., LÖW, I.: Chem. Ber. **88,** 289 (1955)
22. SCHREIBER, K., AURICH, O.: Z. f. Naturforschung **18b,** 471 (1963)
23. BITE, P., RETTEGI, T.: Acta Chim. Acad. Sci. Hung. **52,** 79 (1967)
24. BRIGGS, L. H., CAMBIE, R. C., HOARE, J. L.: J. Chem. Soc. **1963,** 2848
25. BACON J. S. D., BELL, D. H., LORBER, J.: J. Chem. Soc. **1940,** 1147
26. TREVELYAN, W. E., PROCTOR, D. P., HARRISON, J. S.: Nature **166,** 444 (1950)
27. LEMIEUX, R. U., BAUER, H. F.: Anal. Chem. **26,** 920 (1954)
28. CIFONELLI, J. A., SMITH, F.: Anal. Chem. **26,** 1132 (1954)
29. HOUGH, L., JONES, J. K. N., WADMAN, W. H.: J. Chem. Soc. **1950,** 1702

Pál BITE
M. Marruan SHABANA
László JÓKAY
Lili PONGRÁCZ-STERK

Budapest IV.,
Szabadságharcosok útja 47—49

INDEX

Printed in Hungary

A kiadásért felel az Akadémiai Kiadó igazgatója — Műszaki szerkesztő: Farkas Sándor

A kézirat nyomdába érkezett: 1969. X. 22. — Terjedelem: 10,50 (A/5) ív, 59 ábra

70.68504 Akadémiai Nyomda, Budapest — Felelős vezető: Bernát György

ACTA CHIMICA

ТОМ. 63 — ВЫП. 3

РЕЗЮМЕ

Взаимодействие между $[PtCl_4]^{-2}$ и K^+ на основе ИК-спектров кристалла $K_2P(Cl_4$

Ф. ТЁРЁК

Изучались силовые постоянные, совместимые с ИК активными частотами спектра кристалла K_2PtCl_4 с одной стороны, с учетом, связи между внутренними колебаниями в комплексном ионе и колебаниями решетки, а, с другой стороны, пренебрегая этим. Производилось параметрическое определение силовых постоянных и было установлено, что взаимодействие с колебаниями решетки оказывает значительное влияние на силовое поле комплексных ионов. С помощью параметрического метода можно было судить о характере и степени взаимодействия.

Исследования в области количественной оценки ступеней ТГ в реакциях термического разложения, связанных с образованием двух газообразных продуктов, на основе термогравиметрических и ик-спектрофотометрических измерений

А. Б. КИШШ

При изучении термического разложения, связанного с образованием газообразных продуктов, измерение концентрации последних проводилось как термогравиметрическим, так и ИК-спектрофотометрическим методами. Таким образом, исследовалось термическое разложение парамолибдата аммония и паравольфрамата аммония, где измерялось изменение концентрации образующихся NH_3 и H_2O в газовом пространстве.

Изучались возможности одновременной количественной оценки ИК-максимумов и ступеней ТГ-кривых. При знании исходных содержаний NH_3 и H_2O в изучаемых соединениях, после определения площади ИК-максимумов с помощью простых зависимостей определялись отношения количеств газообразных продуктов, образующихся на отдельных ТГ-ступенях. Для случая, когда начальные содержания NH_3 и H_2O не известны, был разработан метод определения того, в каком количественном отношении образующиеся газообразные продукты принимают роль в образовании соответствующей ТГ ступени.

При условии одновременного выделения газообразных продуктов, из зависимости потери в весе на соответствующей ступени $\Delta м = м_{(NH_3)} + м_{(H_2O)}$ и отношения $м_{(NH_3)}$: $м_{(H_2O)}$, определяемого с помощью ИК-кривых с максимумами, могут быть определены уже сами величины $м_{(NH_3)}$ и $м_{(H_2O)}$.

Растворяющая вольтамперометрия соединений Se IV на электроде висячей ртутной капли

Ф. ВАЙДА

Селенистая кислота в присутствии галогенидов дает комплекс, который адсорбируется на поверхности электрода висячей ртутной капли. Явление адсорбции может быть использовано в технике удаления покрытия катодным растворением. Токовый пик позволяет чувствительное и селективное количественное измерение. Se(IV) дает токовый пик растворения и при другом потенциале, а именно, где появляется кривая растворения твердого продукта, образовавшегося в предыдущей ступени восстановления.

Возможности совместного применения рентгено-диффрактометрических и дериватографических измерений для количественного фазового анализа бокситов и подобных им пород

ДЬ. БАРДОШШИ

Во введении автор приводит обзор работ в области рентгено-диффрактометрических и дериватографических исследований бокситов. Было исследовано 102 образца венгерских и иностранных бокситов, для которых вместе с рентгено-диффрактограммами снимались также дериватограммы и проводился химический анализ. Целью исследований являлись их сравнение и определение возможностей их совместного использования.

Помимо возможностей определения отдельных минералов, автор рассматривает также пределы их обнаружения. В табл. 1 приводятся результаты обнаружения минералов.

Дериватограммы оценивались статистическими методами. Подробно описываются наблюдения, полученные с отдельными бокситными минералами. Помимо этого, приводится несколько дериватограмм таких минералов, найденных в бокситах, о которых до сих пор в литературе не приводились такого рода данные. Это — литиофорит, алюминит и таковит.

В 3-ей части сообщения автор занимается вопросами количественного определения минералов. В случае хорошо гомогенизированных образцов результаты двух методов совпадают в пределах 0,5%. По сравнению с результатами химического анализа оба метода показывают избыток воды на 0,2—2,2%. Автором экспериментально было доказано, что этот избыток воды обусловлен адсорбированной (хемосорбированной) водой, которая выделяется при температуре выше 100° С. В рыхлых пористых бокситах количество адсорбированной воды выше, чем в твердых уплотненных образцах. Помимо этого, в богатых железными и манганoвыми минералами бокситах, связывается наибольшее количество воды.

В разработке новых, до сих пор неисследованных месторождений совместное применение этих двух методов приобретает особенно важное значение, вследствие, так наз., минералогических источников ошибок, влияющих на рентгеновские константы на 5—20%. С помощью дериватограмм и химического анализа эти константы могут быть соответственно модифицированы, и тем самым может быть обеспечена точность измерений. При совместном использовании рентгенодиффрактометра и дериватографа минеральный состав других осадочных и пирокластических пород может быть определен с достаточной точностью.

Электронно-микроскопическое исследование окисного слоя образовавшегося на поверхности химически обработанного монокристалла германия

Й. ГИБЕР, Э. Л. ЦАРАН и М. ВЭГНЕР

Исследовалось методом электронной микроскопии влияние разных травителей содержащих в качестве окисляющих компонентов азотную кислоту или перекись водорода на морфологические и структурные свойства окисных слоев, полученных на поверхности монокристалла германия.

Установлено, что в случаях травления в «CP1, CP4A» и в перекиси водорода, содержащем гидроокись калия достаточно длительное время травления приводит к образованию непрерывных, однородных, гладких окислых слоев.

В случаях использования азотной кислоты и травителей, содержащих азотную кислоту обнаружены окисные зерна гексагональной структуры в температурном диапазоне травления 25—50° С.

В случаях более толстых слоев (GeO_2) гекс был идентифицирован и методом рентгеновского структурного анализа.

При травлении в перекиси водорода не содержащем соединения щелочных металлов как при комнатной температуре, так и при 110° С получается окись гексагональной структуры.

В случаях травления при 110° С в перекиси водорода, содержащем карбонат лития или гидроокись калия наблюдалось присутствие тетрагональной окиси в форме несращенных зерен или образований вырастающих на основной окиси.

Наши результаты находятся в согласии с часто наблюдавшимся экспериментальным фактом, высказанным в правиле Гей—Люсака—Освальда: при более низких температурах образуется термодинамически менее стабильный (GeO_2) гекс.

Предполагается, что основные соединения щелочных металлов, а также повышенная температура совместно предупреждают «замерзание» нестабильной модификации и ускоряют образование тетрагональной окиси германия, стабильной термодинамически при температурах ниже 1033° С.

Определение истинного состава смеси уксусной кислоты с четыреххлористым углеродом из диэлектрических свойств и на основе модели трехкомпонентной смеси типа $A—A_2—B$, II

Я. ЛИСИ

В данном сообщении проводится интерпретация данных, изложенных в первой части. Изучалась погрешность, вводимая в расчет истинного состава смеси в связи с неточностью данных для расчета. Было установлено, что среди этих данных наибольшую неопределенность расчетного состава вызывает погрешность в экспериментальной диэлектрической постоянной.

Адсорбция на твердой фазе из растворов, содержащих полярный компонент

С. К. СУРИ и В. РАМАКРИШНА

Определялась адсорбция из бинарных растворов нитрометана, а также нитробензола в бензоле, циклогексане и диоксане, соответственно, на хроматографическом силикагеле при 20° С и на окиси алюминия при 30° С. В то время, как на силикагеле происходит почти однослойная, на окиси алюминия — многослойная адсорбция. Адсорбция же из диоксан-нитрометановых растворов, как было найдено, является почти полуоднослойной или даже меньше.

Термодинамическая обработка, описанная в общих чертах Шай и Надь (3,4) и Эверетт (5,6), распространялась на адсорбированную фазу для данных случаев. В большинстве случаев результаты, полученные различными методами, имеют хорошее согласие. Адсорбция на свободной поверхности жидкости также сравнивалась с адсорбированным слоем на поверхности твердой фазы. Степень адсорбции на единицу поверхности твердой фазы оказалась в 2—4 раза выше степени адсорбции на свободной поверхности жидкости.

Изучение диффузионного потенциала в растворах с постоянной ионной силой

Л. БАРЦА, Л. ШТРОБЛ и Б. ЛЕХОЦКИ

В растворах с постоянной ионной силой изучалось путем измерений электродного потенциала появление диффузионного потенциала и возможность его расчета для случая, когда вплоть до 50%-ов одновалентного катиона (щелочной металл) замещалось ионами водорода.

Полагая, что до некоторых пределов отдельные коэффициенты активности и проводимости постоянны, для потенциала диффузии было выведено следующее уравнение (формально подобное уравнению Хендерсона):

$$E_d = -59.15 \lg \left(1 + h \frac{\lambda_{m,HB} - \lambda_{m,AB}}{m \cdot \lambda_{m,AB}}\right),$$

где 59,15 представляет собой постоянную, выраженную в *мв* и характерную для 25° С; h — общая концентрация кислоты и m — исходная концентрация электролита. Согласно нашему исходному положению, $\lambda_{m,HB}$ — эквивалентная проводимость (которая может быть измерена и рассчитана соответствующим методом) кислоты в m молярном растворе основного электролита и $\lambda_{m,AB}$ — эквивалентная проводимость m молярного раствора основного электролита.

Определяя эти величины с помощью независимых измерений проводимости, могут быть рассчитаны отношение, фигурирующее в вышеприведенном уравнении, которое в пределах одной системы является постоянным (K). Для них были получены следующие значения: в 1,00 М растворе (K)Cl — 1,819, в 0,20 М растворе (K)Cl — 10,86 и в 1,00 М растворе (Na)ClO_4 — 2,929 (в единицах M^{-1}).

С помощью величины K и принимая во внимание диффузионный потенциал, величина измеряемой электродвижущей силы может быть описана весьма простым и удобным для использования уравнением:

$$E_m = E_0 + 59{,}15 \lg \frac{h}{1+Kh} .$$

Справедливость данной зависимости проверялась и была доказана потенциометрическими измерениями в вышеупомянутых пределах, что означает в данном случае концентрацию кислоты 0,5 М. Это, в свою очередь, позволяет потенциометрическое изучение таких систем, которые до сих пор не удалось изучить потенциометрически или лишь с большой погрешностью.

Полярографическое исследование цитостатических производных маннитола, IV

Кинетическое изучение реакций «Дегранола»

Б. ЯМБОР

Изучался механизм превращения «Дегранола» в этилениминовые соединения, а также исследовалось влияние экспериментальных условий, на основе чего были сделаны следующие заключения:

1. При pH < 6 и при 25° С образуется, в основном, моноэтилениминовое производное. Это соединение не дает полярограммы, соответствующей бис-производным. Реагирует с тиосульфатом в течение нескольких часов, образуя при этом соединение, дающее хорошо определенную полярограмму. Такую же полярограмму, но с волной вдвое выше дает соединение, образующееся при взаимодействии бис-этилениминового производного с тиосульфатом.

2. При pH $\cong$ 6 циклизация второй этиламиновой группы происходит весьма медленно. При более высоких pH полная циклизация моноэтилениминового производного протекает весьма легко. В растворе с исходно установленным более высоким значением pH (напр. pH $= 8$), эти две ступени не отделяются.

3. При 37° С в ионной среде, приближающейся к ионной среде крови большая часть «Дегранола» реагирует с гидрокарбонатом воды, давая неэффективное оксазолидоновое соединение, при этом циклизуется лишь около 10—15%.

4. Присутствие буферов (при высоких концентрациях) понижает циклизацию, а не, или лишь незначительно влияет на отщепление хлора. Сульфат натрия не оказывает никакого влияния.

5. Циклизация свеже растворенного «Дегранола» в присутствии трехвалентного буфера начинается лишь по истечении некоторого индукционного периода. Продолжительность последнего зависит от природы буфера, его концентрации и т. д.

6. Концентрация «Дегранола» практически не оказывает влияния на скорость реакции, выраженной в %-ах, как при циклизации, так и при отщеплении галогена.

Глизкозиды видов Solanum, IV

Соларадиксин

П. БИТЕ, М. М. ШАБАНА, Л. ЙОКАИ и Л. ПОНГРАЦ-ШТЕРК

Было установлено, что строение соларадиксина, изолированного из коры корня Solanum laciniatum соответствует строению O—L-рамнопиранозил (1$\alpha \rightarrow$ 2)-0-[O—D-глюкопиранозил (1$\beta \rightarrow$ 2)-D-глюкопиранозил] (1$\beta \rightarrow$ 3)-O — D-галактопиранозил(1$\beta \rightarrow$ 3)-соласодина.

The Acta Chimica publish papers on chemistry in English, German, French and Russian.

The Acta Chimica appear in volumes consisting of four parts of varying size, 4 volumes being published a year.

Manuscripts should be addressed to

Acta Chimica
Budapest 112/91 Műegyetem

Correspondence with the editors should be sent to the same address.

Orders may be placed with "*Kultura*" Foreign Trade Company for Books and Newspapers (Budapest I., Fő utca 32. Account No. 43-790-057-181) or with representatives abroad.

Les Acta Chimica paraissent en français, allemand, anglais et russe et publient des mémoires du domaine des sciences chimiques.

Les Acta Chimica sont publiés sous forme de fascicules. Quatre fascicules seront réunis en un volume (4 volumes par an).

On est prié d'envoyer les manuscrits destinés à la rédaction à l'adresse suivante:

Acta Chimica
Budapest 112/91 Műegyetem

Toute correspondance doit être envoyée à cette même adresse.

On peut s'abonner à l'Entreprise pour le Commerce Extérieur de Livres et Journaux «*Kultura*» (Budapest I., Fő utca 32. Compte-courant No. 43-790-057-181) ou à l'étranger chez tous les représentants ou dépositaires.

«*Acta Chimica*» издают трактаты из области химической науки на русском, французском, английском и немецком языках.

«*Acta Chimica*» выходят отдельными выпусками разного объема. 4 выпуска составляют один том. 4 тома публикуются в год.

Предназначенные для публикации рукописи следует направлять по адресу:

Acta Chimica
Budapest 112/91 Műegyetem

По этому же адресу направлять всякую корреспонденцию для редакции.

Заказы принимает предприятие по внешней торговле книг и газет «*Kultura*» (Budapest I., Fő utca 32. Текущий счет № 43-790-057-181) или его заграничные представительства и уполномоченные.

Reviews of the Hungarian Academy of Sciences are obtainable at the following addresses:

ALBANIA

Ndermarja Shtetnore e Botimeve
Tirana

AUSTRALIA

A. Keesing
Box 4886, GPO
Sydney

AUSTRIA

Globus Buchvertrieb
Salzgries 16
Wien I

BELGIUM

Office International de Librairie
30, Avenue Marnix
Bruxelles 5
Du Monde Entier
5, Place St. Jean
Bruxelles

BULGARIA

Raznoiznos
1, Tzar Assen
Sofia

CANADA

Pannonia Books
2, Spadina Road
Toronto 4, Ont.

CHINA

Waiwen Shudian
Peking
P. O. B. 88

CZECHOSLOVAKIA

Artia
Ve Smečkách 30
Praha 2
Poštová Novinová Služba
Dovoz tisku
Vinohradská 46
Praha 2
Mad'arská Kultura
Václavské nám. 2
Praha I
Poštová Novinová Služba
Dovoz tlače
Leningradská 14
Bratislava

DENMARK

Ejnar Munksgaard
Nörregade 6
Copenhagen

FINLAND

Akateeminen Kirjakauppa
Keskuskatu 2
Helsinki

FRANCE

Office International de Documentation et Librairie
48, rue Gay Lussac
Paris 5

GERMAN DEMOCRATIC REPUBLIC

Deutscher Buch-Export und Import
Leninstraße 16
Leipzig 701
Zeitungsvertriebsamt
Fruchtstrasse 3—4
1004 Berlin

GERMAN FEDERAL REPUBLIC

Kunst und Wissen
Erich Bieber
Postfach 46
7 Stuttgart S.

GREAT BRITAIN

Collet's Subscription Import Department
Dennington Estate
Wellingborough. Northants.
Robert Maxwell and Co. Ltd.
Waynflete Bldg. The Plain
Oxford

HOLLAND

Swetz and Zeitlinger
Keizersgracht 471—487
Amsterdam C.
Martinus Nijhof
Lange Voorhout 9
The Hague

INDIA

Current Technical Literature
Co. Private Ltd.
India House OPP
GPO Post Box 1374
Bombay I

ITALY

Santo Vanasia
Via M. Macchi 71
Milano
Libreria Commissionaria Sansoni
Via La Marmora 45
Firenze

JAPAN

Nauka Ltd.
92, Ikebukur O-Higashi 1-chome
Toshima-ku
Tokyo
Maruzen and Co. Ltd.
P. O. Box 605
Tokyo-Central
Far Eastern Booksellers
Kanda P. O. Box 72
Tokyo

KOREA

Chulpanmul
Phenjan

NORWAY

Johan Grundt Tanum
Karl Johansgatan 43
Oslo

POLAND

Ruch
ul. Wronia 23
Warszawa

ROUMANIA

Cartimex
Str. Aristide Briand 14—18
Bucureşti

SOVIET UNION

Mezhdunarodnaya Kniga
Moscow G—200

SWEDEN

Almquist and Wiksell
Gamla Brogatan 26
Stockholm

USA

Stechert Hafner Inc.
31, East 10th Street
New York, N. Y. 10003
Walter J. Johnson
111, Fifth Avenue
New York, N. Y. 10003

VIETNAM

Xunhasaba
19, Tran Quoc Toan
Hanoi

YUGOSLAVIA

Forum
Vojvode Mišića broj 1
Novi Sad
Jugoslovenska Knjiga
Terazije 27
Beograd

ACTA CHIMICA

ACADEMIAE SCIENTIARUM HUNGARICAE

TOMUS 63 FASCICULUS 4

AKADÉMIAI KIADÓ, BUDAPEST

1970

ACTA CHIM. ACAD. SCI. HUNG.

ACTA CHIMICA

A MAGYAR TUDOMÁNYOS AKADÉMIA KÉMIAI TUDOMÁNYOK OSZTÁLYÁNAK IDEGEN NYELVŰ KÖZLEMÉNYEI

Az Acta Chimica német, angol, francia és orosz nyelven közöl értekezéseket a kémiai tudományok köréből.

Az Acta Chimica változó terjedelmű füzetekben jelenik meg, egy-egy kötet négy füzetből áll. Évente átlag négy kötet jelenik meg.

A közlésre szánt kéziratok a szerkesztőség címére (Budapest 112/91 Műegyetem) küldendők.

Ugyanerre a címre küldendő minden szerkesztőségi levelezés. A szerkesztőség kéziratokat nem ad vissza.

Megrendelhető a belföld számára az „Akadémiai Kiadó"-nál (Budapest V., Alkotmány utca 21. Bankszámla 05-915-111-46), a külföld számára pedig a „Kultúra" Könyv- és Hírlap Külkereskedelmi Vállalatnál (Budapest I., Fő utca 32. Bankszámla: 43-790-057-181) vagy annak külföldi képviseleteinél és bizományosainál.

Die Acta Chimica veröffentlichen Abhandlungen aus dem Bereiche der chemischen Wissenschaften in deutscher, englischer, französischer und russischer Sprache.

Die Acta Chimica erscheinen in Heften wechselnden Umfanges. Vier Hefte bilden einen Band. Jährlich erscheinen 4 Bände.

Die zur Veröffentlichung bestimmten Manuskripte sind an folgende Adresse zu senden:

Acta Chimica
Budapest 112/91 Műegyetem

An die gleiche Anschrift ist auch jede für die Redaktion bestimmte Korrespondenz zu richten.

Bestellbar bei dem Buch- und Zeitungs-Außenhandels-Unternehmen »*Kultúra*« (Budapest I., Fő utca 32. Bankkonto No. 43-790-057-181) oder bei seinen Auslandsvertretungen und Kommissionären.

Acta Chimica Academiae Scientiarum Hungaricae, Tomus 63 (4), pp. 353—361 (1970)

POLAROGRAPHIC AND VOLTAMMETRIC CHARACTERISTICS OF Te(IV) AND Te(VI) COMPOUNDS

F. VAJDA

(Mining Research Institute, Budapest)

Received September 27, 1968

The behaviour of Te(IV) and Te(VI) ions at the dropping mercury and hanging mercury drop electrodes has been studied. Both ionic species have been found to produce an anodic step or an anodic-cathodic voltammetric peak-couple in the positive potential range. In addition to the reduction peaks, maxima also occur on the cyclic voltammograms recorded in the potential range of the reduction processes. The processes accompanied by the formation of solid films are well-suited for the determination of tellurium by stripping voltammetry and thereby an increased sensitivity of the polarographic method is obtained.

Various tellurium compounds have been studied by many authors. SCHWAER and SUCHY [7] carried out the first studies, then LINGANE and NIEDRACH [4], HANS and STACKELBERG [2] and recently SCHMIDT and STACKELBERG [6] investigated the polarographic behaviour of Te(IV). The polarogram from weakly alkaline solutions (pH = 8—9) consists of a single step and a maximum occurring at the limiting current plateau. The diffusion current has the same value before and after the maximum. The 4-electron step corresponds to reduction to elementary tellurium.

$$TeO_3^{2-} + 4\,e + 3\,H_2O = Te + 6\,OH^- \qquad (1)$$

The occurrence of the maximum is interpreted as follows. At the potential at which the maximum develops and which coincides with the half-wave potential of Te^{2-}, the tellurium deposited on the drop surface dissolves while in the vicinity of the drop a vigorous streaming action ensues. The phenomenon can be observed under a microscope. After the maximum, the process is

$$TeO_3^{2-} + 6\,e + 3\,H_2O = Te^{2-} + 6\,OH^- \qquad (2)$$

The limiting current, however, does not rise to the 6-electron value, since the resulting Te^{2-} ions react with TeO_3^{2-} diffusing to the electrode:

$$2\,Te^{2-} + TeO_3^{2-} + 3\,H_2O = 3\,Te + 6\,OH^- \qquad (3)$$

Hence, only 2/3 of the tellurite ions reach the electrode unchanged and the limiting current remains at the 4-electron value.

In contradiction to the negative findings of LINGANE and NIEDRACH [4], NORTON, STOENNER and MEDALIA [5] obtained well-defined tellurate steps with half-wave potentials varying with the pH. The half-wave potentials were determined in a variety of base electrolytes and were found to be between 1.2 V and 1.7 V. By microcoulometric measurements, the reduction was found to involve 8 electrons, consequently the reduction proceeds to the telluride state. As an intermediate product, elementary tellurium is also assumed by these authors to appear in the reduction. This is indicated by the fact that in KCN base solutions more concentrated than 0.1 *M* the anodic Te^{2-} step is replaced by a maximum.

GOKHSTEIN [1] examined the reduction of Te(IV) at the hanging mercury drop electrode. The measurements were performed with an oscillopolarograph using a mercury anode. After a pre-electrolysis procedure, at —0.32 V, which is much more positive than the reduction potential of Te(IV), a cathodic-anodic peak-couple was obtained whose origin remained unexplained. On the voltammogram recorded with increasingly negative potentials, a wave and a current peak occurred in accordance with the two-step reduction. The stirring action ensuing in the neighbourhood of the electrode with the appearance of the peak was observed under a microscope.

In the present work, the characteristics of tellurium(IV) and tellurium(VI) were examined by polarographic and voltammetric methods in the complete useful potential range. Consideration of the voltammetric curves suggested the possibility of applying the stripping technique which permitted the determination of small amounts of tellurium.

Experimental

The measurements were made with a Radelkis OH 102 type polarograph using the dropping mercury and the hanging mercury drop electrodes. The potential values are reported *vs.* the saturated calomel electrode. To compensate the IR potential drop, the curves were recorded by employing the three-electrode system. All reagents were of analytical grade and water has been deionized on an ion exchange column. Further purification, which is usual in the stripping technique, was found to be unnecessary. Oxygen was carefully removed by bubbling an inert gas through the solutions. A 0.5 *M* $NaClO_4$ solution was used as supporting electrolyte whose pH was adjusted to 8.3 $\pm$ 0.2 by the addition of Na_2CO_3.

Tellurium(IV) ion

LINGANE and NIEDRACH [4] found that the maximum occurring on the polarogram of TeO_3^{2-} ions was unaffected by usual maximum-suppressors. According to our observations, it can be greatly decreased by the addition of gelatin to the solution, though it is not completely eliminated even at a gelatin concentration of 0.01%. That is, the incorporation of gelatin into the solution

stops the turbulence, but it does not stop the adherence and dissolution of the deposited tellurium film, and this process is appreciable even on the continuously renewed mercury surface (Fig. 1).

In view of the foregoing, the cyclic voltammogram recorded with the hanging mercury drop electrode from a carbonate buffer containing 0.01% of gelatin is interpreted as follows.

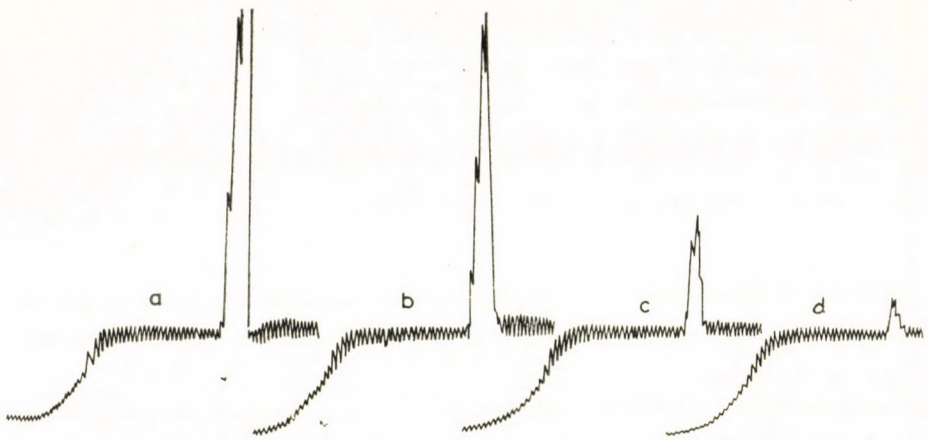

Fig. 1. Polarograms for $5 \cdot 10^{-4}$ *M* TeO_3^{2-} in a carbonate buffer of pH 8.3 containing *a:* 0%, *b:* 0.001%, *c:* 0.005%, *d:* 0.010% of gelatin

The wave corresponds to process (1) and the peak represents the dissolution of the tellurium deposit:

$$Te + 2\ e = Te^{2-} \tag{4}$$

No current peak was observed in the second half of the cycle (Fig. 2).

In the absence of capillary-active substances, the cyclic voltammogram is modified. The peak in the first half of the cycle is higher, but a more prominent feature is the large cathodic current peak produced in the second half of the cycle (Fig. 3). The latter cannot be explained by any electrode process since the potential of the cathodic current peak is attained from the direction of negative potentials. The explanation is given by microscopic examinations. In view of Eqs (2) and (3), at potentials more negative than that of the peak, elementary tellurium is accumulated in the solution layer covering the mercury drop, the process being easily observed under microscope or a high-powered magnifier. When the peak in the second half-cycle begins to rise, a vigorous motion of the tellurium 'cloud' ensues and the solution layer adherent to the mercury drop is disrupted and scattered into the bulk of the solution. Thus the observed peak is not a stripping phenomenon but a pure maximum occurring at the hanging mercury drop and, on adding gelatin to the solution, it can be

suppressed in the same way as ordinary polarographic maxima. If the solution is kept stirred until the moment that the maximum begins to rise, that is the tellurium formed in the process is driven away from the neighbourhood of the drop, a considerably lower maximum appears. This means that the moment the production of telluride ions ceases at the electrode, the tellurium "cloud" plays an important part in bringing about the turbulence.

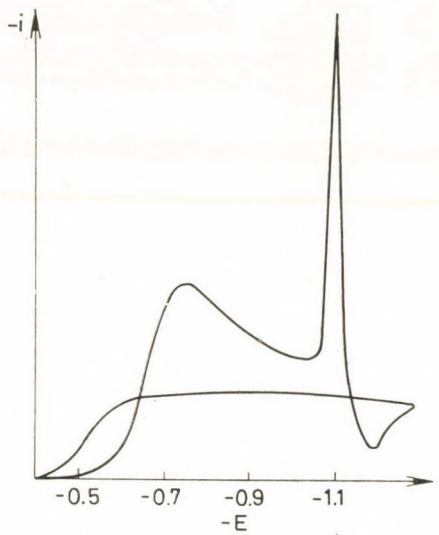

Fig. 2. Cyclic voltammogram of $5 \cdot 10^{-4}$ *M* Te(IV) in a carbonate buffer + gelatin base solution; pH = 8.3

The peak in the first half-cycle is considerably higher than it is from solutions containing gelatin. In this case, the peak is composed of the stripping current and the maximum produced by turbulence.

The anodic-cathodic peak-couple which is reported by GOKHSTEIN [1] to appear at —0.4 V *vs.* SCE was obtained in the positive potential range, in the region of +0.1 V from a halide free carbonate buffer solution (Fig. 4). The height of the cathodic peak proved to be a function of the time elapsed between recording the two peaks. Consequently, with the appearance of the anodic wave, an oxidation process takes place in the presence of TeO_3^{2-} ions and the solid product deposited on the mercury surface can be reversibly dissolved. The peak potentials are: +0.12 V and +0.07 V for anodic and cathodic peaks, respectively.

A well-defined polarographic step with a half-wave potential of +0.11 V was obtained with the dropping mercury electrode. As compared with the known 4-electron Te(IV) step (Fig. 5), a reversible 2-electron anodic process is

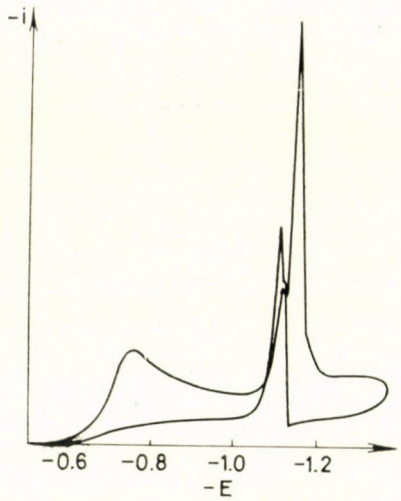

Fig. 3. Te(IV) cycle in a gelatin-free carbonate buffer base solution; pH = 8.3

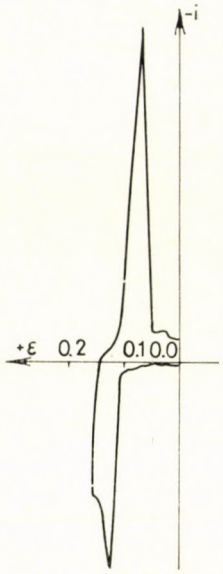

Fig. 4. Te(IV) cycle in the positive potential range. $1 \cdot 10^{-4}$ *M* Te(IV) in a carbonate buffer base solution of pH 8.3

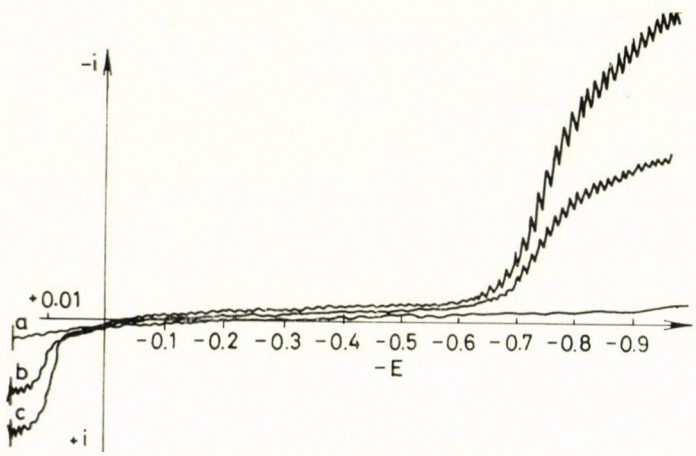

Fig. 5. Anodic and cathodic Te(IV) steps. *a:* 0, *b:* $4 \cdot 10^{-4}$ *M*, *c:* $8 \cdot 10^{-4}$ *M* TeO_3^{2-} in a carbonate buffer base solution of pH 8.3

to be assumed, resulting in the formation of an off-white Hg_2TeO_3 film which is insoluble in this medium

$$TeO_3^{2-} + 2\ Hg = Hg_2TeO_3 + 2\ e \qquad (5)$$

Tellurium(VI) ion

In our experiments first the polarographic step (Fig. 6) reported by NORTON et al. [5], then the cyclic voltammogram (Fig. 7) have been recorded for tellurate ions. In the anodic half-cycle the maximum observed also with Te(IV) occurs accompanied by turbulence around the mercury drop. This

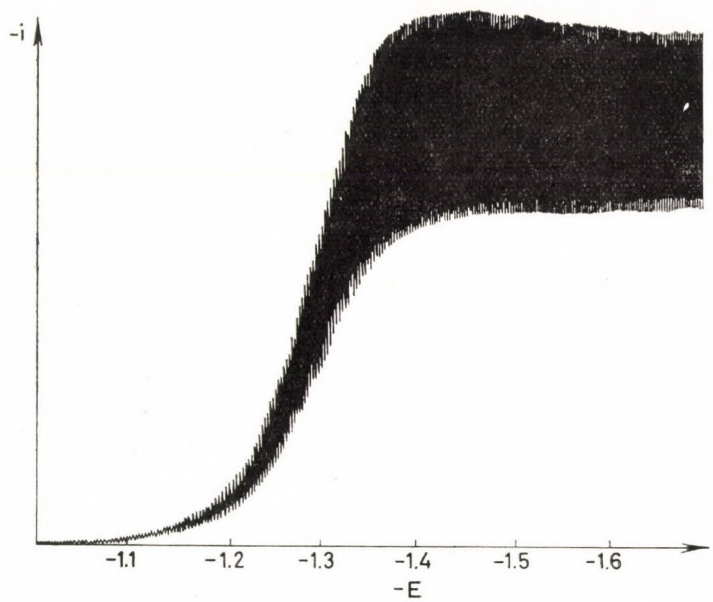

Fig. 6. Polarogram of Te(IV). $2 \cdot 10^{-4}$ *M* Te(VI) in a carbonate buffer of pH 8.3

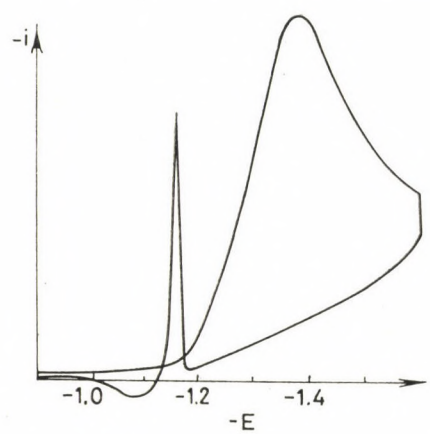

Fig. 7. Cyclic voltammogram of Te(VI). $2 \cdot 10^{-4}$ *M* Te(VI) in a carbonate buffer of pH 8.3

maximum is, however, readily removed by adding gelatin to the solution. This behaviour confirms the assumption of NORTON *et al.* concerning the appearance of elementary tellurium as an intermediate.

Similarly to tellurite ions, tellurate ions also gave rise to an anodic step at the dropping mercury electrode with a half-wave potential of +0.06 V

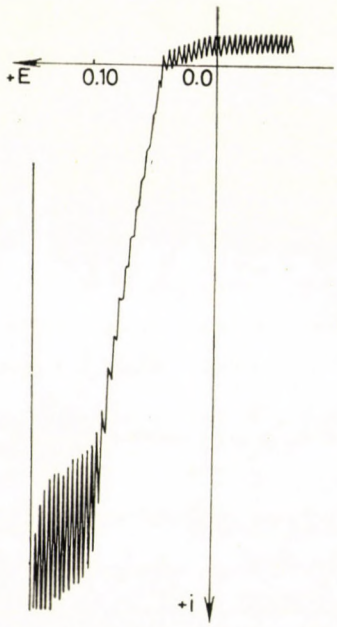

Fig. 8. Anodic step for Te(VI). $2 \cdot 10^{-4}$ *M* Te(VI) in a carbonate buffer of pH 8.3

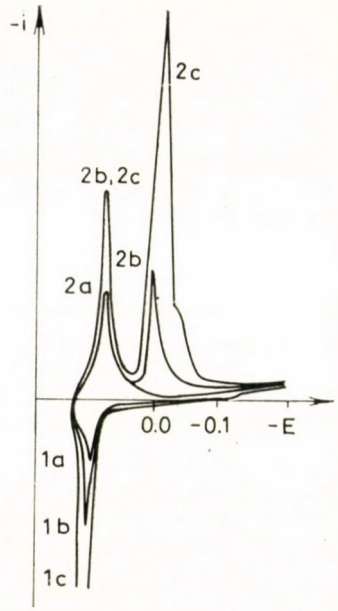

Fig. 9. Te(VI) cycle in the positive potential range. *a:* $4 \cdot 10^{-5}$ *M*, *b:* $1 \cdot 10^{-4}$ *M*, *c:* $3 \cdot 10^{-4}$ *M* Te(VI) in a carbonate buffer base solution of pH 8.3

which may be attributed to the oxidation of mercury and the formation of Hg(I) tellurate. (Hg_2TeO_4 forms a yellow precipitate in neutral or slightly alkaline media.) *(cf.* Fig. 8).

The cyclic voltammogram, recorded with the hanging mercury drop electrode in the potential range corresponding to the polarographic step comprises an anodic and a cathodic peak. With an increase in the concentration, a gradually increasing second cathodic peak appears. The peak potentials are: +0.070 V for the anodic and +0.035 V and 0.0 V for the cathodic peaks. The difference between the anodic and cathodic peak potentials is 35 mV, which corresponds to a rapid 2-electron charge transfer in accordance with the expression (3)

$$\Delta Ep = \frac{0.068}{z} \qquad (6)$$

(cf. Fig. 9).

The stripping method

The new voltammetric results permit the application of the stripping technique to the determination of small amounts of tellurium in both oxidation states.

In the case of tellurite ions, there are two cathodic peaks which are suitable for stripping analysis. For one peak the electro-deposition is accomplished at the potential of the anodic process, *i.e.* at +0.16 V, while the solution is being stirred, the resulting Hg_2TeO_3 is then removed by cathodic stripping. For the other peak, the potential is adjusted to a value between the two steps of the stepwise reduction, *e.g.* to —0.9 V, and after the electrodeposition is completed, the elementary tellurium on the mercury drop is reduced further by applying increasingly negative potentials to the electrode. The peak-height is proportional to the concentration and the time of electrolysis, but as it appears from Table I, better results are obtained by measuring the area (the coulombs transferred) under the peak. The smallest Te(IV) concentration detected in this way was $3 \cdot 10^{-7}$ *M*. In practice, Te(IV) can be determined down to a concentration of 0.05 μg/ml.

For the determination of tellurate ions by the stripping techniqe, only the anodic process taking place in the positive potential range is suitable the electrodeposition potential being +0.10 V. If two peaks are obtained in the subsequent stripping procedure, the sum of the two peak-areas is to be taken into account. Since the peak potential is somewhat more negative than that for

Table I

Variation of the height and area of the cathodic peak of tellurium with concentration and pre-electrolysis time

C (*M*)	t (sec)	e (μ Cb)	I_p (μA)	$\frac{e}{ct} \cdot 10^3$	$\frac{Ip}{ct} \cdot 10^3$
5×10^{-5}	60	23	10.2	7.65	3.4
5×10^{-5}	15	5.5	2.7	7.35	3.6
5×10^{-5}	90	34	15.2	7.57	3.4
3×10^{-5}	60	14	6.4	7.78	3.6
1×10^{-5}	45	3.15	1.6	7.00	3.6
1×10^{-5}	120	9.2	3.7	7.68	3.1
7×10^{-6}	90	5.0	2.1	7.94	3.3
5×10^{-6}	360	14.2	2.8	7.32	1.5
2×10^{-6}	60	0.83	0.35	6.93	2.5
1×10^{-6}	60	0.44	0.20	7.33	3.3

tellurite ions, small amounts of chloride impurities in the base electrolyte do not interfere with the determination. The smallest concentration detected for Te(VI) was $2 \cdot 10^{-6} M$.

REFERENCES

1. GOKHSTEIN, A. Y.: Polarography. p. 661. Proc. of the Third Intern. Conf., Southampton, 1964.
2. HANS, W., STACKELBERG, M.: Z. Electrochem. **54,** 62 (1950).
3. KEMULA, W., KUBLIK, Z., AXT, A.: Roczniki Chem. **35,** 1009 (1961).
4. LINGANE, J. J., NIEDRACH, L. W.: J. Am. Chem. Soc. **71,** 196 (1949).
5. NORTON, E., STOENNER, R. W., MEDALIA, A. I.: J. Am. Chem. Soc. **75,** 1827 (1953).
6. SCHMIDT, H., STACKELBERG, M.: J. Polarogr. Soc. **8,** 49 (1963).
7. SCHWAER, L., SUCHY, K.: Collection Czechoslov. Chem. Communs. **7,** 25 (1935).

Ferenc VAJDA; Budapest III., Mikoviny u. 2.

Acta Chimica Academiae Scientiarum Hungaricae, Tomus 63 (4), pp. 363—370 (1970)

ENTHALPY OF MIXING FOR ACETIC ACID–CARBON TETRACHLORIDE, I

J. Liszi

(Department of Physical Chemistry, University of Veszprém)

Received November 1, 1968

The volumetric properties of the acetic acid–carbon tetrachloride mixture have been investigated. It was found that the molar volume of acetic acid, as a mixture of monomeric and dimeric acetic acid, is formed by contraction at 20°C. A quasi-crystalline structure was assumed for the liquid phase. It was found that at 20°C the acetic acid–carbon tetrachloride mixture can be represented by a cubic lattice of face centered symmetry. These results will be used in the second part of this communication, in the investigation of the enthalpy of mixing for the acetic acid–carbon tetrachloride mixture.

Introduction

In a previous communication [1], the composition of acetic acid–carbon tetrachloride mixtures corresponding to the $A—A_2—B$ ternary mixture model has been determined from dielectric behaviour together with some molecular properties of the components. A, A_2 and B stand for monomeric and dimeric acetic acid, and carbon tetrachloride, respectively. In this paper, the enthalpy changes associated with isothermal mixing of acetic acid and carbon tetrachloride will be presented.

The data used in the determination of the enthalpy of mixing are taken from a previous communication [1], and collected in Table I. Permanent dipole moments μ_2 listed in the last column have been calculated, as shown in a former communication [1], according to the approximation that $\mu_2 = 0.92\ (1 - x_3)$.

Table I

x_B	x_1	x_2	x_3	μ_2 (D)
0.0	0.115±0.003	0.885±0.003	0.000	0.92
0.2	0.055±0.003	0.621±0.003	0.324±0.003	0.62
0.4	0.027±0.003	0.409±0.003	0.564±0.003	0.40
0.6	0.012±0.003	0.242±0.003	0.746±0.003	0.23
0.8	0.004±0.003	0.109±0.003	0.887±0.003	0.10
1.0	0.000	0.000	1.000	0.00

Molecular data [1] for the components of the $A—A_2—B$ type ternary mixture are shown in Table II.

Table II

Property	Monomeric acetic acid	Dimeric acetic acid	Carbon tetrachloride
$M\left(\frac{\text{g}}{\text{mole}}\right)$	60.1	120.2	153.8
μ (D)	1.68	variable	0
α (cm^3)	$4.85 \cdot 10^{-24}$	$15.65 \cdot 10^{-24}$	$10.5 \cdot 10^{-24}$

The data shown in Tables I and II, combined with the known molecular dimensions permit the determination of the enthalpy changes on isothermal mixing of acetic acid with carbon tetrachloride. In Part I of the present paper, the determination of average molecular radii and the coordination number will be described. These data will then be utilized as shown in Part II.

Average molecular radii and the coordination number

Interchange energies play a very important role in the present calculations. If i and j denote the different molecular species, u is the average interaction energy effective between molecules, and z is the number of the nearest neighbours of a molecule in the mixture, *i.e.* the coordination number, then the interchange energy is defined by the following equation [2]:

$$w_{ij} = w_{ji} = z\left(u_{ij} - \frac{1}{2}\,u_{ii} - \frac{1}{2}\,u_{jj}\right) \tag{1}$$

Thus, interchange energy is defined as half the energy associated with replacing a single molecule of pure substance i by a single molecule of pure substance j. Eq. (1) takes into account only molecular interactions between nearest neighbours; however, this approximation is the one generally accepted in the literature [3].

This definition of interchange energy requires the knowledge of molecular dimensions. In this respect, molecular dimensions play a twofold role.

a) The concept of interchange energy involves the a priori assumption that the molecules possess dimensions and shapes which allow their interchange within a set that is similar to a crystal lattice.

b) The dimensions and shape of molecules unequivocally determine the number of possible nearest neighbours, *i.e.* the maximum coordination number.

There is no calculation method in the literature which would give the coordination number for arbitrary molecular dimensions and shapes. In the determination of the coordination number, the analogy to a regular crystal lattice may be utilized. For this purpose, however, a *simplifying assumption* will be introduced, *viz.* it will be disregarded that monomeric and dimeric acetic acid molecules have ellipsoidal shapes. We assume that all the components consist of spherical molecules with a perfectly random distribution within the bulk liquid. It is possible that local "islands" with compositions different from the average are formed (due to non-spherical geometry and strong molecular interaction) but, according to GUGGENHEIM [3], this does not practically affect the calculated macroscopic thermodynamic properties. Thus, in the calculation of the thermodynamic properties of acetic acid–carbon tetrachloride mixtures, the use of two different microphysical models could not be avoided. From the point of view of dielectric behaviour, monomeric and dimeric acetic acid molecules are modelled by point-dipoles located inside an ellipsoidal cavity. In the calculation of macroscopic thermodynamic properties, because of the difficulties encountered in the determination of the coordination number, we had to disregard that monomeric and dimeric acetic acid molecules have ellipsoidal shapes and to consider the liquid mixture as a phase with a quasi-crystalline structure composed of spherical molecules.

The condition of interchangeability described in Par. *a)* is fulfilled for spherical molecules if the ratio of molecular volumes is 1 and 2, *i.e.* if the ratio of molecular diameters is between 1 and 1.26. From the pressure dependence of the relaxation frequency of ultrasonic absorption LITOVITZ and CARNEVALE [4] have deduced that the molar volume of dimeric acetic acid is twice as great as that of the monomeric species. The above assumption, *i.e.* that monomeric and dimeric acetic acid molecules which in fact have ellipsoidal shapes are treated as spheres, together with the findings of LITOVITZ and CARNEVALE indicate that the condition of interchangeability is fulfilled for the acetic acid–carbon tetrachloride model mixture used by the present author. As will be shown later, the volume of the carbon tetrachloride molecule is between the volumes of monomeric and dimeric acetic acid. It is necessary to note that by molecular volume and molecular dimensions, we mean the space or "cavity" and its dimensions available, for a molecule within the quasi-crystalline liquid.

In Table III we list the coordination number and the third power of molecular radii (r) (which for spherical molecules, can be calculated directly from the molecular volume [2]) for the lattice types common in the literature. In this Table, v is the molecular volume and N_A is the Avogadro number.

The comparison of Eq. (1) and Table III shows that the interchange energies are the same in simple cubic and face-centered cubic lattices. Thus no decision on the basis of interchange energies can be arrived at in the question of the lattice type attributed to acetic acid–carbon tetrachloride mix-

Table III

Type of lattice	z	r^3
Simple cubic	6	$\frac{1}{8 N_A} v$
Body-centered cubic	8	$\frac{3\sqrt{3}}{32 N_A} v$
Face-centered cubic	12	$\frac{\sqrt{2}}{8 N_A} v$

tures. However, a comparison of molecular dimensions calculated from Table III, with those determined by diffraction in solid acetic acid affords a possibility to find the right type of lattice.

According to Table III, the calculation of average molecular radii requires the knowledge of the respective molecular volumes. The molecular weight of carbon tetrachloride is 153.84, its density is 1.5940 $g \cdot cm^{-3}$ at 20°C, thus its molecular volume, $v_B = 96.487$ cm^3 $mole^{-1}$.

Monomeric and dimeric acetic acids form a non-ideal mixture with each other; this is evident from the dipole-dipole character of interactions to be verified later numerically by the interchange energy values. Therefore, the molar volume of acetic acid as a mixture (v_{ac}) will be represented in the following form

$$v_{ac} = x_1 v_1 + x_2 v_2 + \beta v_1 x_1 x_2 \tag{2}$$

proportionality factor β will be regarded, in a first approximation as independent on the temperature. Accepting that the molar volume of the dimer is twice that of the monomer [4], *i.e.*

$$v_2 = 2v_1 \tag{3}$$

Eq. (2) can be written as

$$v_{ac} = (x_1 + 2x_1)v_1 + \beta v_1 x_1 x_2 \tag{4}$$

The molar volume of monomeric and dimeric acetic acids will be determined from the temperature dependence of the molar volume of acetic acid. Therefore Eq. (4) is written for two different temperatures T_1 and T_2. After elimination of β, one obtains

$$\frac{v_{acT_1} - v_{1T_1}(x_1 + 2x_2)_{T_1}}{V_{1T_1}(x_1 x_2)_{T_1}} = \frac{v_{acT_2} - v_{1T_2}(x_1 + 2x_2)_{T_2}}{v_{2T_2}(x_1 x_2)_{T_2}} \tag{5}$$

According to definition, the molar volume of acetic acid is

$$v_{ac} = \frac{\overline{M}}{\varrho_{ac}} \tag{6}$$

where $\overline{M}$ is the average molecular weight

$$\overline{M} = 60.1\, x_1 + 102.2\, x_2 \tag{7}$$

and ϱ_{ac} is the density of acetic acid. The temperature dependence of the composition is expressed by the following equations

$$K = \frac{x_2}{x_1^2} \tag{8}$$

$$x_1 + x_2 = 1 \tag{9}$$

$$\frac{d \ln K}{dT} = \frac{\Delta h_r}{RT^2} \tag{10}$$

In Eq. (10), Δh_r is the enthalpy of dimerization. For the enthalpy of hydrogen bond formation values from 2 to 9 (kcal per mole hydrogen bond) are given in the literature [5]. The values determined depend on the experimental conditions (vapour phase, liquid phase, solvent etc.). For pure carboxylic acids in the liquid phase the best values are obtained from ultrasonic absorption data [5, 6, 7]. Therefore, for pure liquid acetic acid the value of —6200 cal per 2 moles of hydrogen bond is used as determined by FREEDMAN from ultrasonic absorption [8]. When the composition is known, the average molecular weight $\overline{M}$ as a function of temperature is also available the density of acetic acid being easily measured. The molar volume of monomeric acetic acid changes with temperature according to the equation

$$v_{1T_2} = v_{1T_1}(1 + \bar{a}\,\Delta T) \tag{11}$$

where a is the coefficient of cubical thermal expansion. From Eqs (5) and (11)

$$\frac{v_{acT_1} - v_{1T_1}(x_1 + 2x_2)_{T_1}}{v_{1T_1}(x_1 x_2)_{T_1}} = \frac{v_{acT_2} - v_{1T_1}[1 + \bar{a}(T_2 - T_1)](x_1 + 2x_2)_{T_2}}{v_{1T_1}[1 + \bar{a}(T_2 - T_1)](x_1 + 2x_2)_{T_2}} \tag{12}$$

In Eq. (12), the mole fractions and the molar volume of acetic acid are known as a function of temperature, thus only unknowns are the molar volume v_{1T} of acetic acid at temperature T_1, and the coefficient of cubical thermal expansion a of monomeric acetic acid. The latter may be regarded as temperature independent within a narrow range of about 30°C. With this assumption Eq. (12) is written for another pair of temperatures T_1 and T_3 and, in this manner, $\bar{a}$ can be eliminated so that a direct way is opened for the determination of the molar volume of monomeric acetic acid at temperature T_1. The required data for this are listed in Table IV.

Table IV

	$T_1 = 293.2°K$	$T_2 = 308.2°K$	$T_3 = 323.2°K$
x_1	0.115	0.146	0.181
x_2	0.885	0.854	0.819
ϱ_{ac}	1.0493 g · cm^{-3}	1.0326 g · cm^{-3}	1.0165 g · cm^{-3}
v_{ac}	108.8 cm^3 · mole^{-1}	107.7 cm^3 · mole^{-1}	107.4 cm^3 · mole^{-1}

From density values and molar volumes in the table, the role of shifts in the association equilibrium is conspicuously evident. A greater mole volume would be expected in case of lower densities at higher temperatures. However, the opposite is observed due to the shift of the association equilibrium, *i.e.* due to the change of the average molecular weight.

The molar volumes calculated for 293.2°K on the basis of Table IV, are

$$v_1 = 58 \pm 1 \text{ cm}^3 \text{ mole}^{-1}, \; v_2 = 116 \pm 2 \text{ cm}^3 \text{ mole}^{-1},$$

taking into account the uncertainties associated with the determination of mole fractions.

AFFSPRUNG, FINDENEGG and KOHLER [7] have found, on the basis of model calculations, that at 20°C the molar volume of acetic acid as a mixture is the result of a contraction by about 3 per cent. Owing to the uncertainty involved in the determination of mole fractions, the present method is not suitable for the determination of the magnitude of this contraction, only a qualitative demonstration of its occurrence being possible. According to our calculations, the molar volume of acetic acid as a mixture at 20°C is obtained as a result of a contraction of 2 ± 1 cm^3. For the calculation of contraction we accepted the results of LITOVITZ and CARNEVALE [4] who state that, from a volumetric point of view, association is an ideal process, *i.e.* it is not accompanied either by contraction or by dilatation. In this case, contraction is due only to interactions between molecules. If the above statement that v_2 is equal to $2v_1$ is true only within certain limits of error, then the calculated contraction represents the total volume change due to association processes and intermolecular interactions. Unfortunately, our method of study does not allow the separation of these two kinds of volume change. However, the fact that monomeric and dimeric acetic acids form a mixture with a negative deviation, as shown numerically by interchange energies discussed in Part II, indicates that, owing to intermolecular interactions, contraction should occur. Qualitatively, this contraction is confirmed in the present calculations, thus the utilization of the correlation $2v_1 = v_2$ as a first approximation seems to be justified.

JONES and TEMPLETON [9] have shown by X-ray diffraction that the dimensions of the elementary cell of crystalline acetic acid consisting of 4 monomers are $l_1 = 13.32 \pm 0.02$ Å, $l_2 = 4.08 \pm 0.01$ Å, $l_3 = 5.77 \pm 0.01$ Å. As deduced from these data, the volume available for one monomeric molecule is about 77 Å^3, and the third power of the radius of the molecule considered to be spherical, $r_1^3 = 18.3$ Å. Accordingly, for various lattice types the third powers of molecular radii calculated from the molar volume of monomeric acetic acid are:

$r_1^3 = 12.1$ Å for a simple cubic lattice,
$r_1^3 = 15.7$ Å for a body-centered cubic lattice,
$r_1^3 = 17.1$ Å for a face-centered cubic lattice.

These show that modelling the acetic acid at 20°C as a face-centered cubic lattice gives the best approximation. In the present study, this lattice type is used for modelling liquid mixtures of acetic acid–carbon tetrachloride at 20°C. This is based on the assumption that if the conditions of interchangeability are fulfilled for the components of the real mixture then the quasi-crystalline structure of acetic acid should not be altered by the admixture of carbon tetrachloride.

From known molar volumes, the average molecular radii for a face-centered cubic lattice are:

$$r_1 = 2.58 \pm 0.02 \text{ Å}; \quad r_2 = 3.15 \pm 0.02 \text{ Å}; \quad r_3 = 3.05 \pm 0.02 \text{ Å}.$$

In the calculation of interaction energies between non-identical pairs of molecules, mean molecular radii have been used. The results are

$$r_{12} = \frac{r_1 + r_2}{2} = 2.91 \pm 0.02 \text{ Å}$$

$$r_{13} = \frac{r_1 + r_3}{2} = 2.81 \pm 0.02 \text{ Å}$$

$$r_{23} = \frac{r_2 + r_3}{2} = 3.15 \pm 0.02 \text{ Å}$$

The above radii, and the coordination number $z = 12$, corresponding to the face-centered cubic lattice, will be used in Part II for the calculation of the enthalpy of mixing.

Symbols

A = monomeric acetic acid
A_2 = dimeric acetic acid
B = carbon tetrachloride
$\bar{a}$ = coefficient of cubical thermal expansion of monomeric acetic acid
Δh_r = enthalpy of the association reaction
K = chemical equilibrium constant of the association reaction expressed with mole fractions
M = molecular weight
$\overline{M}$ = average molecular weight
N_A = Avogadro number
R = gas constant
r = molecular radius
u = average molecular interaction energy
v = molar volume
z = coordination number
w = interchange energy
x = mole fraction
α = average polarizability
β = constant
μ = permanent dipole moment
ϱ = density
l_1, l_2, l_3 = distances
T_1, T_2, T_3 = absolute temperatures

Subscripts

1 = monomeric acetic acid in the real mixture
2 = dimeric acetic acid in the real mixture
3 = carbon tetrachloride in the real mixture
ac = acetic acid in the real mixture
B = carbon tetrachloride in the nominal mixture
i, j = components in general

REFERENCES

1. Liszi, J.: Acta Chim. Acad. Sci. Hung. **63,** 293 (1970)
2. Moelwyn-Hughes, E. A.: Physical Chemistry. Pergamon Press, 1964.
3. Guggenheim, E. A.: Mixtures. Clarendon Press, 1952.
4. Litovitz, T. A., Carnevale, E. H.: J. Acoust. Soc. Amer. **30,** No. 2, 434 (1958).
5. Pimentel, G. C., McClellan, A. L.: The Hydrogen Bond. Freeman, 1960.
6. Posch, H., Kohler, F.: Monatschr. 98, 1451 (1967).
7. Affsprung, H. E., Findenegg, C. H., Kohler, F.: J. Chem. Soc. Ser. A., 1968, 1346.
8. Freedman, E.: J. Chem. Phys. **21,** 1784 (1963).
9. Jones, R. E., Templeton, D. H.: Acta Cryst. **11,** 484 (1958).

János Liszi; Veszprém, Schönherz Z. u. 12. Hungary.

Acta Chimica Academiae Scientiarum Hungaricae, Tomus 63 (4), pp. 371—383 (1970)

ENTHALPY OF MIXING FOR ACETIC ACID–CARBON TETRACHLORIDE, II

J. Liszi

(Department of Physical Chemistry, University of Veszprém)

Received November 1, 1968

Regarding the nominally binary mixture acetic acid–carbon tetrachloride as a ternary mixture of the type $A—A_2—B$, the average interaction energies between the true components and the interchange energies have been determined. The components of the ternary system $A—A_2—B$, *i.e.* monomeric acetic acid, dimeric acetic acid, and carbon tetrachloride are regarded as the true components. In the calculations it has been taken into account that the enthalpy of mixing is due to both the shift of the association equilibrium and the interaction energies between the molecules. Accordingly, the following processes have been considered:

1. separation of monomeric from dimeric acetic acid,
2. dissociation of dimeric acetic acid present in an amount corresponding to the association constant K° (expressed in mole fractions) referred to pure acetic acid,
3. formation of dimeric acetic acid in an amount corresponding to the association constant K (expressed in mole fractions) referred to the prevailing conditions,
4. mixing of monomeric acetic acid, dimeric acetic acid and carbon tetrachloride.

In order to check the calculations, the enthalpy of isothermal mixing of acetic acid with carbon tetrachloride have been experimentally determined at 20°C.

In Part I, the volumetric characteristics of acetic acid–carbon tetrachloride mixtures have been described. From the temperature dependence of the molar volume of acetic acid, the molar volumes of monomeric and dimeric acetic acid have been determined. From the known molar volumes, the molecular volumes have been calculated for various lattice types attributing a quasi-crystalline structure to the liquid. The comparison of the molecular volumes with X-ray diffraction data for solid acetic acid indicates that a face-centered cubic lattice is the model that furnishes the best approximation for the liquid phase at 20°C. A simplifying assumption was that we considered the ellipsoidal molecules of monomeric and dimeric acetic acid to be spherical, and supposed that in the mixture the distribution of molecules is random. From molar volumes of monomeric and dimeric acetic acid and carbon tetrachloride, the molecular radii corresponding to the face-centered cubic lattice have been determined. Using the results reported in the former Part I, in this paper we describe the calculation of the enthalpy of isothermal mixing of acetic acid with carbon tetrachloride. The calculated results are then compared with the experimental data.

1. Average interaction and interchange energies

Before describing the calculation of average interaction energies it is necessary to return to the dielectric model of SCHOLTE [1]. This model had been used as the basis for the calculation of the composition of $A-A_2-B$ ternary mixtures. According to this model, the point dipole is located in the centre of a sphere of radius r. Within the molecule, the dipole is surrounded by vacuum, thus r is the distance between the dipole and the nearest polarizable environment and $2r$ is the distance from the nearest neighbouring dipole. Accordingly, the average molecular interaction energies (u) are given [2] by the following equations

$$u_{11} = -\frac{2\alpha_1 \mu_1^2}{r_{11}^6} \tag{1}$$

$$u_{22} = -\frac{2\alpha_2 \mu_2^2}{r_{22}^6} \tag{2}$$

$$u_{33} = 0 \tag{3}$$

$$u_{12} = -\frac{\alpha_1 \mu_2^2 + \alpha_2 \mu_1^2}{r_{12}^6} \tag{4}$$

$$u_{13} = -\frac{\alpha_3 \mu_1^2}{r_{13}^6} \tag{5}$$

$$u_{23} = -\frac{\alpha_3 \mu_2^2}{r_{23}^6} \tag{6}$$

The data used in the calculations are listed in Tables I and II. Table I contains data which vary with the composition, as a function of the nominal mole fraction x_B of carbon tetrachloride. Table II contains data which do not change with concentration.

Table I

x_B	x_1	x_2	x_3	μ_2 (D)
0.0	0.115±0.003	0.885±0.003	0.000	0.92
0.2	0.055±0.003	0.621±0.003	0.324±0.003	0.62
0.4	0.027±0.003	0.409±0.003	0.564±0.003	0.40
0.6	0.012±0.003	0.242±0.003	0.746±0.003	0.23
0.8	0.004±0.003	0.109±0.003	0.887±0.003	0.10
1.0	0.000	0.000	1.000	0.00

The average interaction energies calculated from the data of Tables I and II according to Eqs (1) to (6) are shown in Table III and Fig. 1. The average interaction energies refer to one mole of an isolated pair of molecules $\left[\frac{\text{cal}}{2 \text{ moles}}\right]$.

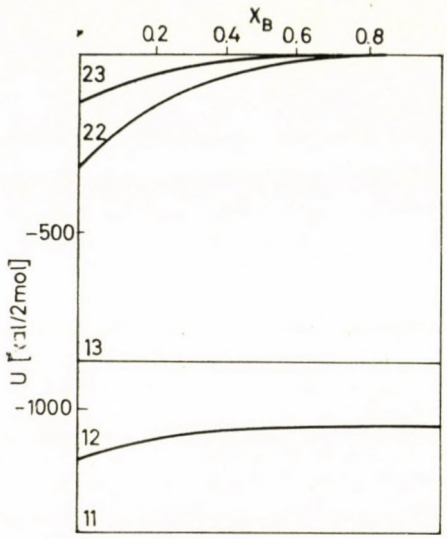

Fig. 1. Average molecular interaction energies as a function of nominal composition

Table II

$r_{11} = 2.58 \pm 0.02$ Å	$r_{22} = 3.49 \pm 0.02$ Å	$r_{33} = 3.05 \pm 0.02$ Å
$r_{12} = 2.91 \pm 0.02$ Å	$r_{13} = 2.81 \pm 0.02$ Å	$r_{23} = 3.15 \pm 0.02$ Å
$\alpha_1 = 4.85 \times 10^{-24}$ cm^3	$\alpha_2 = 15.65 \times 10^{-24}$ cm^3	$\alpha_3 = 10.5 \times 10^{-24}$ cm^3
$\mu_1 = 1.68$ *D*	variable	$\mu_3 = 0.0$ *D*

Table III

x_B	u_{11}	u_{22}	u_{12}	u_{13}	u_{23}
0.0	—1342	—325	—1138	—862	—132
0.2	—1342	—148	—1085	—862	—60
0.4	—1342	—62	—1060	—862	—25
0.6	—1342	—21	—1048	—862	—9
0.8	—1342	—4	—1042	—862	—2
1.0	—1342	0	—1041	—862	0

For the calculation of the interchange energies the following equation has been used

$$w_{ij} = w_{ji} = z\left(u_{ij} - \frac{1}{2}u_{jj} - \frac{1}{2}u_{ii}\right) \tag{7}$$

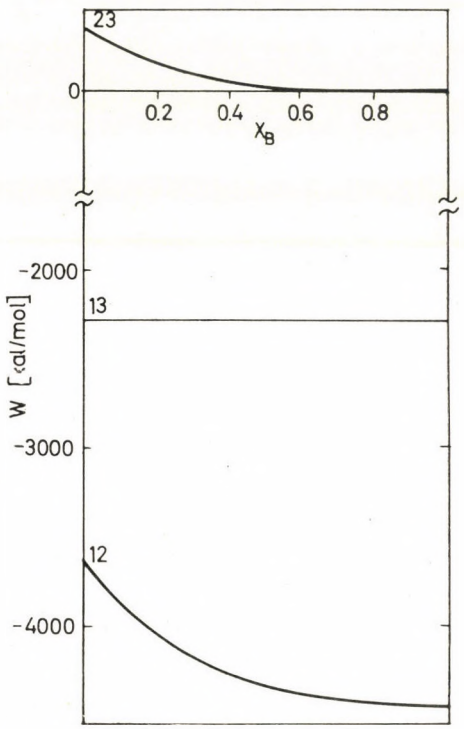

Fig. 2. Interchange energies as a function of nominal composition

Table IV

X_B	$w_{12}\left(\frac{\text{cal}}{\text{mole}}\right)$	$w_{13}\left(\frac{\text{cal}}{\text{mole}}\right)$	$w_{23}\left(\frac{\text{cal}}{\text{mole}}\right)$
0.0	−3655	−2291	+369
0.2	−4082	−2291	+168
0.4	−4292	−2291	+70
0.6	−4391	−2291	+24
0.8	−4432	−2291	+5
1.0	−4458	−2291	0

together with the data in Table III. $z = 12$ was taken as the coordination number in accordance with the face-centered cubic lattice structure. The results are shown in Table IV and Fig. 2. The interchange energies indicate that the mixtures monomeric–dimeric acetic acid, monomeric acetic acid–carbon tetrachloride, and dimeric acetic acid–carbon tetrachloride are characterized by extremely strong and strong negative, and a slight positive deviation, respectively.

The error due to the uncertainties in the determination of the mole fractions is not more than 4% of the interchange energy values.

2. Calculation of the enthalpy of mixing

For the calculation of the heat of mixing of ordinary (non-reactive) mixtures, the knowledge of the composition and interchange energy is sufficient. In the case of acetic acid–carbon tetrachloride mixtures the situation is more complex because it is a reactive mixture. This is due to the facts that:

a) no pure components are available; in fact, when preparing a mixture, monomeric and dimeric acetic acids are diluted with carbon tetrachloride,

b) the association equilibrium is disturbed by dilution and the heat of association is measured together with the heat of mixing.

Accordingly, in the calculation of the true (total) heat of mixing the following processes must be taken into account:

1. separation of the monomeric acid from the dimeric one;

2. dissociation of dimeric acetic acid present in an amount corresponding to equilibrium constant K° (expressed in mole fractions) for pure acetic acid;

3. formation of dimeric acetic acid in an amount corresponding to equilibrium constant K (expressed in always actual mole fractions);

4. mixing of monomeric acetic acid, dimeric acetic acid and carbon tetrachloride.

Furthermore, the fact that the experimentally measured heat of mixing refers to one mole of the nominal mixture requires that the calculations should also yield the heat of mixing for one of the nominal mixture.

For processes 2 and 3, the equilibrium constant of association

$$K = \frac{x_2}{x_1^2} \tag{8}$$

(expressed in mole fractions) is used. We have found that K, as defined by Eq. (8), increases strongly with dilution [3], which shows that with increasing concentration of carbon tetrachloride the association equilibrium is shifted toward dimerization. However, we must point out that in non-ideal mixtures

the value of the equilibrium constant is affected also by the activity coefficients. Therefore, in a subsequent study, we shall return to the problem of the concentration dependence of the equilibrium constant when the activity coefficients of the components will be available.

Let us examine first the *enthalpy change for the association step.* The calculations refer to one mole of the nominal mixture:

$$N_{ac} + N_B = 1 \tag{9}$$

where N_{ac} and N_B are the number of moles of acetic acid N_B and carbon tetrachloride, respectively, in the nominal mixture. Since two monomeric molecules form one dimeric acetic acid molecule

$$N_1 + 2N_2 + N_3 = 1 \tag{10}$$

At the same time, the actual total number of moles N_T is less than unity, *i.e.*

$$N_T = N_1 + N_2 + N_3 = 1 - N_2 \tag{11}$$

The number of moles of carbon tetrachloride is equal to its mole fraction referred to the nominal mixture

$$N_3 = N_B - x_B \tag{12}$$

and

$$1 - x_B = x_{ac} \tag{13}$$

The number of moles of monomeric acetic acid in one mole of the binary mixture is

$$N_1 = 1 - 2N_2 - x_B = x_{ac} - 2N_2 \tag{14}$$

The true mole fractions are

$$x_1 = \frac{N_1}{N_T} = \frac{N_1}{1 - N_2} \tag{15}$$

$$x_2 = \frac{N_2}{N_T} = \frac{N_2}{1 - N_2} \tag{16}$$

Substitution of these expressions into Eq. (8) gives

$$K = \frac{N_2(1 - N_2)}{N_1^2} \tag{17}$$

Using Eq. (14) one obtains

$$K = \frac{N_2 (1 - N_2)}{(x_{ac} - 2N_2)^2} \tag{18}$$

from which the number of moles of dimeric acetic acid in one mole of the nominal mixtures is

$$N_2 = \frac{4 K x_{ac} + 1 - \sqrt{8 K x_{ac} + 1 - 4 K x_{ac}^2}}{2 (4 K + 1)} \tag{19}$$

The positive sign of the square root is left out of consideration since the criterion that if $x_{ac} = 0$ then $N_2 = 0$, is not fulfilled when the sign is positive. From Eq. (19) the enthalpy of the association process can be determined:

$$N_{2a} \Delta h_r = \Delta h_{ra} \tag{20}$$

The enthalpy change corresponding to the process of dissociation is given by the equation

$$\Delta h_{rd} = - N_{2d}^0 x_{ac} \Delta h_r \tag{21}$$

where N_2^0 is the number of moles of dimeric acetic acid in case when $x_{ac} = 1$. The validity of Eq. (21) is evident since the starting substance is always pure acetic acid of the amount of x_{ac} (referred to monomeric acetic acid) with equilibrium constant K°.

From Eqs (20) and (21) the enthalpy change due to chemical reactions during mixing is

$$\Delta H_r = (N_{2a} - N_{2d}) \Delta h_r \tag{22}$$

The results of calculations are collected in Table V.

Table V

x_B	N_{2a}	N_{2d}	$\Delta H_r \left(\frac{\text{cal}}{\text{mole}}\right)$
0.0	0.4695	0.4695	0.0
0.2	0.3831	0.3756	−46.5
0.4	0.2903	0.2817	−53.3
0.6	0.1952	0.1878	−45.9
0.8	0.0974	0.0939	−21.7
1.0	0.0000	0.0000	0.0

On the basis of considerations applied in the case of dissociation, the enthalpy change of the separation process is

$$\Delta h_{\text{sep}} = -x_1^0 x_2^0 w_{12}^0 x_{ac} \tag{23}$$

The enthalpy of formation of one mole of the ternary mixture is

$$\Delta h_f = x_1 x_2 w_{12} + x_1 x_3 w_{13} + x_2 x_3 w_{23} \tag{24}$$

With reference to Eq. (11), the total enthalpy change associated with processe of mixing and separation is

$$\Delta H_e = (\Delta h_f + \Delta h_{\text{sep}})\ (1 - N_2) \tag{25}$$

The results of the calculations are summarized in Table VI. ΔH_e is expressed in $\left(\frac{\text{cal}}{\text{mole nominal mixture}}\right)$ units; the enthalpies of mixing and separation refer to one mole of the actual mixture.

Table VI

x_B	$\Delta h_f \frac{\text{cal}}{\text{mole}}$	$\Delta H_{\text{sep}} \frac{\text{cal}}{\text{mole}}$	$\Delta H_e \frac{\text{cal}}{\text{mole}}$
0.0	−372.0	+372.0	0.0
0.2	−144.7	+297.6	+94.3
0.4	−67.2	+223.2	+110.5
0.6	−28.8	+148.8	+96.5
0.8	−9.0	+74.4	+59.0
1.0	0.0	0.0	0.0

The heat of mixing actually measured is the sum of values in the last columns of Tables V and VI, *i.e.*

$$H^E = \Delta H_r + \Delta H_e \tag{26}$$

Before describing the experimental determination of the heat of mixing we shall discuss briefly the effect of errors in the determination of composition on calculated enthalpies of mixing. The calculation of errors has been carried out for the whole interval of concentrations, but only those for two greatly different compositions, *viz.* $x_B = 0.2$ and $x_B = 0.8$, will be presented here. The error limits always refer to the worst result.

The uncertainty of interchange energies has been shown to be $\pm 4\%$. The uncertainties of the mole fractions and interchange energies lead to an error of about $\pm 6\%$ in the enthalpy of mixing calculated from Eq. (24) for a nominal composition $x_B = 0.2$, whereas there is an error of about $\pm 33\%$ for the nominal composition $x_B = 0.8$. In the entire range of concentrations, the error in the enthalpy of mixing calculated according to Eq. (23) is $\pm 6\%$. Since errors committed in the determination of mole fractions appear with

Table VII

x_B	$H^E \frac{\text{cal}}{\text{mole}}$
0.0	0.0
0.2	+47.8
0.4	+57.2
0.6	+50.6
0.8	+37.3
1.0	0.0

the same sign both in the separation and mixing processes, at nominal composition $x_B = 0.2$ the errors due to the two processes are cancelled. At nominal composition $x_B = 0.8$ the enthalpy change $+74.4 \left(\frac{\text{cal}}{\text{mole}}\right)$ due to the process of separation is significantly higher than $-9.0 \left(\frac{\text{cal}}{\text{mole}}\right)$ associated with the process of mixing. Thus, though an error of $\pm 33\%$ is possible in the enthalpy of mixing, the combined error of the two processes is not more than 9%. In the calculation of enthalpy changes due to the shift of the association equilibrium, the errors caused by the inaccuracy of composition data have the same sign, thus the errors due to the two processes practically cancel. The error in the term $(1 - N_2)$ necessary for the calculation of the enthalpy of mixing for one of the nominal mixture (*cf.* Eq. (25), is $\pm 1\%$ if $x_B = 0.2$, and $\pm 0.5\%$ if $x_B = 0.8$. In view of this, the error of the measured (total) enthalpy of mixing is $\pm 1\%$ at a nominal composition $x_B = 0.2$ and $\pm 9.5\%$ at $x_B = 0.8$. These are the worst expectations and are surprisingly low considering the rather crude simplifications used in the calculation of the overall enthalpy of mixing. As seen, this is due to the convenient structure of the formulas used in the calculation of the enthalpy of mixing, *viz.* that the errors caused by the uncertainty of composition date tend to cancel. Perhaps this is the reason for the usefulness of the quasi-crystalline model of liquid mixtures, though the application of this model often implies gross simplifications. Of course, great care must be taken whenever conclusions concerning the quasi-crystalline structure of liquid mixtures are drawn from enthalpies of mixing.

In order to perform an experimental check on the values obtained by calculation, the enthalpy of mixing acetic acid with carbon tetrachloride was measured.

3. Determination of heats of mixing

The apparatus used for the determination of heats of mixing is shown sketchily in Fig. 3. One of the liquids to be mixed is put in a thermos bottle while the other vessel is surrounded with a jacket permitting to adjust the

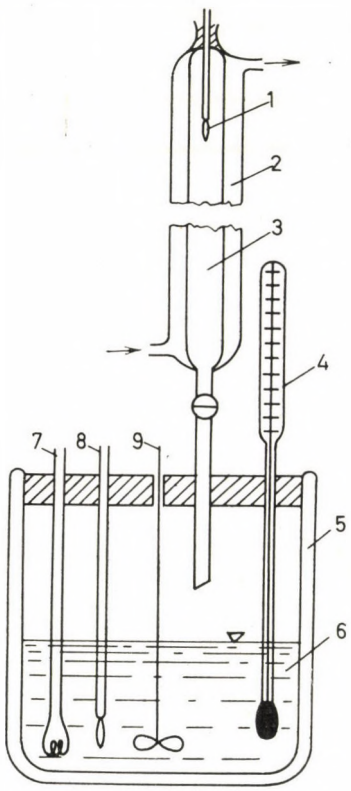

Fig. 3. Schematic drawing of the apparatus used for measuring enthalpies of mixing

temperature as desired. The latter vessel has a volume scale with 0.1 ml divisions on its inner wall. The thermos bottle (placed under the other) is provided with variable electric heating, a stirrer a Beckmann thermometer, and a thermistor which is part of a thermometer system described below. The measurement is performed at constant temperature. An important part of the apparatus is the thermometer system consisting of two thermistors, by which the temperatures of the two liquids to be mixed can be adjusted to the same value. The two thermistors are linked to a Wheatstone bridge, a galvanometer

serving as a zero indicator. The liquid in the thermos bottle attains a certain temperature close to ambient (between 19.5 and 20.4°C). The two thermistors are then immersed in this liquid and the bridge current is adjusted to zero. After this, one of the thermistors is placed into the liquid in the upper vessel and, by means of a thermostat, the temperature of the upper liquid is varied until the galvanometer indicates zero current again. In this case the temperature of the upper liquid is the same as that of the lower liquid. Then under slow stirring, the heating is started and the liquid from the upper vessel is added to the lower one at such a rate that the Beckmann thermometer should not show

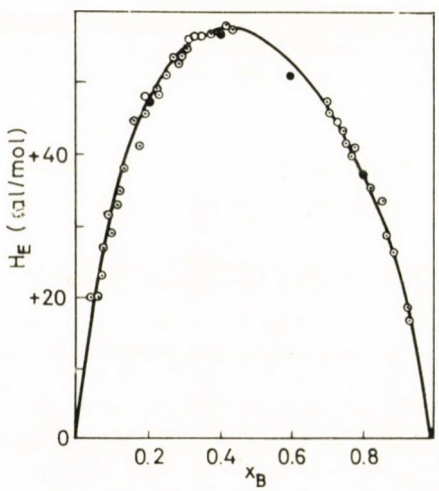

Fig. 4. The enthalpy of mixing as a function of nominal composition. ○ measured; ● calculated

any change of temperature. Time is measured with a stop-watch, time *vs.* volume data being obtained. From time and the output of the electric heater, the amount of heat, while from volume and density data, the mole fractions can be calculated. A drawback of this method is that only endothermic heats of mixing can be measured and the temperature of the measurement cannot be chosen at will. A source of error is that the temperature cannot be adjusted to the same value in various series of experiments. The other sources of error, including the heat generated by the stirrer, have been found to be negligible. The results are collected in Table VIII and Fig. 4.

The uncertainty of volume and temperature measurement causes an overall error of $\pm 2.5\%$. The variation of the temperature during the measurement caused, through the shift of the association equilibrium, a maximum error of 1% in this series. As shown by Fig. 4, the agreement between calculated and experimental values is good.

Table VIII

x_B	$H^E \frac{\text{cal}}{\text{mole}}$	x_B	$H^E \frac{\text{cal}}{\text{mole}}$	x_B	$H^E \frac{\text{cal}}{\text{mole}}$
0.0471	19.8	0.2560	51.1	0.7005	45.6
0.0587	20.0	0.2790	53.5	0.7180	44.6
0.0736	23.0	0.2818	53.4	0.7213	44.3
0.0810	27.1	0.2920	54.1	0.7356	43.4
0.0911	31.5	0.2961	54.0	0.7518	41.2
0.0938	28.9	0.3061	54.8	0.7690	39.6
0.1112	32.8	0.3157	55.8	0.7708	41.0
0.1215	34.4	0.3320	56.5	0.8002	37.4
0.1323	38.0	0.3480	56.6	0.8161	35.2
0.1624	44.8	0.3700	57.0	0.8429	33.7
0.1755	41.2	0.3895	57.6	0.8605	28.1
0.1950	45.6	0.3915	57.5	0.8832	26.3
0.1980	48.0	0.4070	57.8	0.9191	18.5
0.2230	48.5	0.4283	57.5	0.9226	16.6
0.2280	49.0	0.6998	46.8		

Symbols

A = monomeric acetic acid,
A_2 = dimeric acetic acid,
B = carbon tetrachloride,
Δh = enthalpy change in the actual mixture,
ΔH = enthalpy change in the nominal mixture,
H^E = measured enthalpy of mixing,
K = chemical equilibrium constant of the association reaction expressed with mole-fractions,
N = number of moles,
r = molecular radius,
u = average molecular interaction energy,
w = interchange energy,
z = coordination number,
x = mole fraction,
α = average polarizability,
μ = permanent dipole moment.

Subscripts

1 = monomeric acetic acid in the actual mixture,
2 = dimeric acetic acid in the actual mixture,
3 = carbon tetrachloride in the actual mixture,
ac = acetic acid in the nominal mixture,
B = carbon tetrachloride in the nominal mixture,
T = total,
r = reaction,
a = association,

d = dissociation,
f = mixing,
sep = separation (de-mixing),
0 = refers to pure acetic acid (upper index).

REFERENCES

1. SCHOLTE, T. G.: Physica, XV, No. 5—6, 347 (1949).
2. MOELVYN-HUGHES, E. A.: Physical Chemistry. Pergamon, 1964.
3. LISZI, J.: Acta Chim. Acad. Sci. Hung. **63,** 293 (1970)

János LISZI; Veszprém, Schönherz Z. u. 12. Hungary

Acta Chimica Academiae Scientiarum Hungaricae, Tomus 63 (4), pp. 385—402 (1970)

INVESTIGATION OF ADSORPTION PHENOMENA ON PLATINIZED Pt ELECTRODES BY TRACER METHODS, I

THE EXPERIMENTAL PROCEDURE AND H_2SO_4 ADSORPTION

J. SOLT, G. HORÁNYI and F. NAGY

(Central Research Institute for Chemistry, Hungarian Academy of Sciences, Budapest)

Received November 29, 1968

A method has been developed for the investigation of adsorption phenomena on platinum electrodes by tracer techniques, using isotopes emitting soft β-radiation.

The relation between apparatus parameters and the systematic error of measurements was analyzed.

The adsorption of HSO_4^- ions was investigated on platinized Pt electrodes in 1 *N* $HClO_4$ supporting electrolyte solution as a function of the electrode potential. The following has been established:

1. the adsorption of HSO_4^- ions is specific and is a function of both the electrode potential and HSO_4^- concentration;

2. HSO_4^- adsorption is reversible at potentials below 750 mV as referred to the RHE and irreversible at higher potentials;

3. in the concentration range between 10^{-7} and 10^{-4} mole/l the concentration dependence of adsorption can be described by the superposition of three Langmuir-type isotherms corresponding to three different kinds of adsorption sites. The adsorbed amounts required for the saturation of different sites (Γ_I^0) are potential dependent.

In earlier communications [1], studies on the individual steps of liquid (aqueous) phase heterogeneous catalytic hydrogenation have been described. One of the steps is the adsorption of the substrate which has not yet been treated in detail though an attempt was made [2] to estimate the extent of substrate adsorption indirectly, from results obtained for hydrogen adsorption. In the above paper, the difficulties encountered in the course of the indirect measurement have been pointed out. It seemed desirable, therefore, to turn to a direct method, and accordingly, a method had to be chosen or devised that was suited to the determination of the adsorption of dissolved species including the substrate on the most commonly used metal catalysts.

The conclusion was arrived at that the radioactive tracer method, more than any other method, was suited to this purpose and that a combination with other techniques might be very fruitful.

Accordingly, the radioactive tracer method to be employed has to fulfill the following requirements.

1. Application must be possible under the conditions prevailing in hydrogenation and electrohydrogenation.

2. As the rate of hydrogenation in aqueous solutions on metal catalysts is a function of the electrode potential, adsorption, too, has to be measured as a function of the potential.

3. A continuous measurement is required, *i.e.* the relationship between adsorption and potential must be determined without disturbing the system.

4. As labelling of the components (*e.g.* H_2SO_4, organic compounds, water) is generally possible by isotopes emitting soft β radiation (^{35}S, ^{14}C, ^{3}H) the equipment must be suitable for the measurement of such radiation.

The method of measurements

A number of tracer methods for the measurement of adsorption from aqueous solutions have been described in the literature [3—14]. Most suited to the present study are techniques similar to those described in papers [6], [8] and [11].

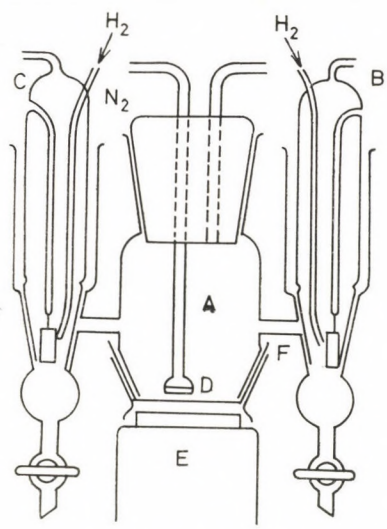

Fig. 1. The measuring cell

The above tracer techniques are essentially modifications of the JOLIOT method [15], originally developed for the investigation of electrolytic metal deposition. The apparatus essentially consists of an electrolytic cell with a platinum or gold foil cathode which at the same time, serves as detector "window". The apparatus developed here, too, is essentially a modification of this method, adapted to the aims and requirements of the present study.

A. *The measuring cell*

The measuring cell is of the three-compartment type commonly used in electrochemical work. Such a cell was also used in the investigation of electrohydrogenation. The bottom of the central compartment (*A*) is a gold-plated

plastic foil (D) on which the metal to be investigated is deposited subsequently. This is the main electrode on which adsorption is investigated. The gold-plating also serves as electric contact (F). Electrodes B and C are immersed in the same electrolyte as the main electrode. The cell compartments of the side electrodes are connected to the central compartment by greaseless glass stopcocks. Both are hydrogen electrodes and serve as auxiliary and reference electrodes to polarize the main electrode and to measure its potential.

Under the plastic foil and at a constant distance is placed the scintillation counter (E) used to measure radiation. The central compartment is provided with gas in- and outlets for the removal of O_2 from the solution and the space above it.

B. *The main electrode*

The main electrode, serving at the same time as the "window" of the scintillation counter, has to fulfill the following requirements.

1. It should have sufficient mechanical strength because it serves as the bottom of the cell.

2. It should be thin enough to transmit soft β radiation without apreciable absorption.

3. It should resist the electrolytes employed.

The first two requirements evidently are in conflict, therefore, a compromise was necessary in the practical realization.

In the experiments, a PVC foil with a thickness of 1.0—2.5 mg/cm^2 was used which satisfies requirement 1.

In order to form a conducting layer, a thin (0.5—1.0 μm; 1—2 mg/cm^2) layer of gold was deposited on the PVC foil by vacuum plating. Direct deposition of platinum is not possible because evaporated platinum does not form a uniform layer, and the temperature required for vacuum plating with platinum destroys the PVC foil in the given evaporation chamber.

After adequate pretreatment, the gold deposit of the above thickness shows excellent adhesion and a suitable conductivity. (The resistance of a 1 cm wide gold-plated strip of PVC is 0.8—1 Ω cm^{-1}).

The foil thus prepared was fastened to the open bottom of the cell by a tapered ground glass rim. Electric contact was ensured by attaching a copper clamp to the gold-plated side of the foil outside the cell. The electrode was platinized in the cell using a solution of H_2PtCl_6 and an apparent current density of about 1.5 mA/cm^2. After rinsing and alternate cathodic and anodic polarization in 1 N $HClO_4$, the preparation of the electrode was regarded as complete.

C. *Electric apparatus*

The described cell was used with conventional electric apparatus.

a) Potentiostat. Maximum current: 10 mA, range: —400 and +1,600 mV, accuracy ±1 mV.

b) Galvanostat. Continuous control in ranges of 0.1, 0.3, 1, 3, 10 and 30 mA.

c) VT voltmeter. Total range ±1.5 V in steps of 100 mV. Accuracy ±1 mV.

Radiation detector was a GAMMA F029 type 4—5—1—14 scintillation detector with a plastic β phosphor, shielded against light by an Al foil of 1 mg/cm^2 overall thickness. The detector was attached to a GAMMA type NK 108 automatic scaler with an energy discriminator.

D. *Fundamental principle of the method*

Dependence of systematic error on parameters

The described method is based on the principle that an accumulation of the labelled compound on, or in the vicinity of the electrode is reflected by an increase of the number of counts.

If accumulation is due to adsorption, *i.e.* to binding of molecules or ions to the surface, the concentration of the solution in the immediate vicinity of the electrode, neglecting the very thin adsorption layer, can be regarded as equal to that in the bulk of the solution.

In this case, the adsorbed amount can be determined from the radiation intensity using relations described in the literature [7]. The intensity I_A originating from the adsorption layer is

$$I_A = \lambda \Gamma$$

Assuming a uniform distribution of the labelled compound in the solution surrounding the main electrode, the background intensity I_B from the solution is

$$I_B = \lambda \bar{c} \int_0^\infty e^{-\mu x} \, dx = \lambda \frac{\bar{c}}{\mu} \tag{1}$$

(The upper limit of integration can be extended to infinity with regard to the small penetration of soft β radiation.) Thus the total intensity (I_T) from adsorption layer and solution is

$$I_T = \lambda \left(\frac{\bar{c}}{\mu} + \Gamma \right) \tag{2}$$

where $\lambda = AI^\circ \beta$ (A is the geometric surface of the electrode, I° is the specific activity of the labelled component in the solution in Ci/mole), $\bar{c}$ is the concentration of the dissolved substance (mole/mg), β is the efficiency of counting, μ is the mass absorption coefficient ($cm^2 \cdot mg^{-1}$), and Γ is the adsorbed amount ($mol \cdot cm^{-2}$). β includes geometric efficiency, absorption by electrode, detector, etc., and the responding probability of the counter. (Intensities I_T, I_A and I_B are count rates.) Since in expression (2), the mass absorption coefficient, independent of the nature and density of the medium, is for convenience given in cm^2/mg units, x (in mg/cm^2) is equivalent to the distance from the electrode (thickness of the absorbing layer). Subsequently, this quantity will be referred to as distance.

Eq. (2) is valid only if geometric and true surface areas are identical, *i.e.* the roughness factor is equal to 1. Eq. (2), therefore, can generally be written as

$$I_T = \lambda \left(\frac{\bar{c}}{\mu} + \gamma \Gamma \right) \tag{3}$$

where γ is the roughness factor. Thus, $\frac{\lambda \bar{c}}{\mu}$ is the activity originating from the solution (I_B) while $\lambda \gamma \Gamma$ is the activity due to adsorbed substances (I_A).

$$I_T = I_B + I_A \tag{4}$$

The last equation illustrates limitations of the method, too. The systematic error is determined predominantly by the ratio of the magnitudes of $\frac{\bar{c}}{\mu}$ and $\gamma \Gamma$.

The latter can be influenced by increasing the value of γ. In case of a given platinizing procedure, when the specific surface area of the deposited particles is fixed, γ can only be increased by increasing the amount of platinum deposited. In the present method, however, the increasing amounts of deposited Pt black reduce the counting efficiency, as the counter is placed outside the cell. Obviously this dual influence of the amount of the deposit involves the existence of an optimum amount for which the systematic error is minimal. This condition was strictly observed in the preparation of electrodes.

Ion adsorption from electrolyte solutions on metal surfaces

In case of ions, two main types of adsorption are distinguished [16]:

a) electrostatic adsorption,

b) specific adsorption.

Electrostatic adsorption is a phenomenon to be expected on the basis of the nature of the electrical double layer. In this case, the enrichment corresponding to adsorption in the layer(s) in direct contact with the surface is due to electrostatic forces. On the solution side plate of the double layer condenser an excess of positive or negative ions must appear, as determined by the electrode capacity. According to the Gouy—Chapman theory, the concentration of the individual ionic species in the double layer is given by the following equation

$$\varepsilon = C(E_a - \Psi_1) = \sqrt{\frac{\delta RT}{2}} \sqrt{\sum_i \left[\exp\left(\frac{Z_i F \Psi_1}{RT}\right) - 1\right] c_i} \qquad (5)$$

where ε is the charge density, C the double layer capacity, E_a is the electrode potential, ψ_1 is the potential at a distance of one ion radius from the surface, δ is the dielectric constant of the medium, z_i and c_i are the number of charges (with the appropriate sign) and the concentration in the bulk of the solution, respectively, of the i-th ionic species.

It is evident from Eq. (5) that the concentration of the individual ionic species in the double layer is different from that in the bulk of the solution. In addition to the electrode potential, the dielectric constant of the solution and the double layer capacity, this difference also depends on the concentration and charge of the ions in question as well as on the concentration and charge of the other ions present. Accordingly, if measurement of the quantity adsorbed specifically is desired, *i.e.* electrostatic adsorption is to be rendered negligible, supporting electrolyte has to be employed in large concentration beside the labelled ionic species. The supporting electrolyte, in principle, disturbs the specific adsorption of ionic species under investigation. The adsorption of solutes differs from gas adsorption, since the wetting solution produces complete coverage of the adsorbent surface and adsorption is possible only by displacement of the solvent. This means that all measurable characteristics of adsorption, such as adsorption coefficients and heats of adsorption, are values relative to the solvent. In the presence of large amounts of supporting electrolyte, therefore, specific adsorption of the investigated ions takes place as the result of competition not only with the solvent but also with the supporting electrolyte. Consequently, the supporting electrolyte must be selected in such a manner that its adsorption would not be strong enough to completely suppress adsorption of the ions under investigation. 1 N perchloric acid has been found suitable for this purpose if an acidic solution is required.

The use of 1 N $HClO_4$ solution has other advantages, too, beside the one mentioned. If it is desired to examine the concentration dependence of adsorption of a weak acid or an acid capable of stepwise dissociation, in a solution without a supporting electrolyte, the varying ratio of ions produced by

dissociation has to be taken into account, a complicating factor in the evaluation of adsorption measurements. For example, in a H_2SO_4 solution, dissociation produces H^+, HSO_4^- and SO_4^{--} ions, *i.e.* the adsorption of two kinds of anions, HSO_4^- and SO_4^{--} has to be reckoned with. The amount of these ions, however, is not proportional to the total sulfuric acid concentration, since the second dissociation constant (K_2) of sulfuric acid in water at room temperature is 1.2×10^{-2} mole/l, and the dissociation of the first proton is practically complete. Thus neither the concentration of HSO_4^-, nor that of the SO_4^{--} ions is proportional to the total sulfuric acid concentration. The charge, and consequently the electrostatic adsorption, *i.e.* accumulation in the double layer, is different for the two ions. Probably there is also a difference in the strength of specific adsorption. Consequently, under such conditions, the results obtained with the tracer method cannot be assigned unambiguously to a single ionic species.

If measurement of sulfuric acid adsorption is carried out in 1 *N* $HClO_4$, the degree of dissociation of HSO_4^- ions is $\alpha \leq 1.2 \cdot 10^{-2}$ regardless of the total sulfuric acid concentration, *i.e.* the concentration of SO_4^{--} ions is less than 1.2% of the total sulfuric acid concentration and practically only HSO_4^- ions have to be considered.

Experimental

A. Solutions

Since the surface of Pt is very sensitive towards impurities, the solutions have been prepared with extreme care. Doubly distilled and freshly reboiled water and analytical grade chemicals were used. Oxidizable trace impurities were destroyed by H_2O_2, excess H_2O_2 being removed by boiling over Pt powder. A stock solution of 0.5 *N* H_2SO_4 was prepared and the necessary solutions were prepared by dilution.

Labelling was performed immediately before use, with H_2SO_4 prepared from unsupported ^{35}S (activity: 5 Ci/ml). As H_2SO_4 prepared from unsupported ^{35}S contains considerable amounts of Cl^- ions which, due to competitive adsorption, lead to false results on H_2SO_4 adsorption, chloride ions had to be eliminated. This was done by diluting H_2SO_4 prepared from ^{35}S with inactive H_2SO_4 to obtain a $5 \cdot 10^{-5}$ molar solution and titrating Cl^- ions with an $AgClO_4$ solution. The AgCl precipitate was removed by filtering. Thus the concentration of Cl^- ions introduced in the labelling procedure is reduced to less than 10^{-8} mole/l.

B. The main Pt electrode

Preparation and platinizing of the main electrode was carried out as described previously. The amount of Pt deposited varied between 2 and 4 mg/cm^2 (as referred to the geometric surface of the main electrode). The roughness factor (γ) was calculated from the double layer section of the charging curve determined in 1 *N* $HClO_4$ solution. The double layer capacity was taken as 30 μF/cm^2. (This value is, to a certain extent, arbitrary.) As, however, the charging curve was always determined in the same electrolyte solution, the relative roughness factors are correct even if the absolute values are not. The value of γ in the present investigation varied between 200 and 300.

Immediately before the adsorption measurements, the main electrode was submitted to repeated (3 to 4 times) anodic and cathodic treatment (2 minutes each). The last 5 min treatment was cathodic. The current density used in regeneration was 0.7 mA/cm^2, as referred to the geometric surface. By this kind of regeneration adsorbed sulfuric acid, too, could be completely removed from the electrode surface.

C. Determination of the adsorbed amounts

The quantity of substance adsorbed was computed from the measured I_T and I_B values, using Eqs (3) and (1). The adsorption of H_2SO_4 (SO_4^{--}, HSO_4^- ions) at E = 0 mV with respect to the RHE is pratically naught. Thus counts received during cathodic polarization may be identified with I_B. From (1), λ can be calculated for given I_B and known $\bar{c}$ and μ. $\bar{c}$ is known from the preparation of the solution, μ is the mass absorption coefficient of the β radiation of ^{35}S (0.314 cm^2/mg). From λ, the measured I_T and the roughness factor γ, the specific adsorption can be calculated by (3).

$$I_A = I_T - I_B = \lambda \gamma \Gamma \tag{6}$$

As the individual counts are not listed among the results, some illustrative data are given here. The values of I_T for HSO_4^- ions varied between $4—6 \times 10^4$ and $2—3 \times 10^5$ cpm, depending on the concentration, while the value of I_B was 500—1500 cpm in the region of maximal adsorption, the true background being 2—300 cmp. It can be seen that the value of I_T/I_B varies between 30 and 600, giving a sufficient accuracy in determining the difference I_A. Under the above conditions, the radiation coming from adsorbed species was measured with an efficiency of a few %, depending on the roughness factor. (Efficiency β appearing in the proportionality factor λ of Eq. (2).)

The concentration and potential dependence of Γ, was determined by measuring I_T at various concentrations and potentials. In the determination of equilibrium concentrations, changes in concentration due to adsorption have been taken into account.

However carefully solutions were made up, poisoning of the electrode was observed during the process of adsorption, as shown by the decrease of the activities with time.

Therefore, the electrode had to be regenerated after the measurement of adsorption at each potential, especially in case of low concentrations.

At higher (10^{-2}, 10^{-1} N) concentrations, omission of regeneration did not noticeably alter the adsorption measured, so that a continuous passage from one potential to another was possible. This, obviously, simplified the measurements.

Adsorption of H_2SO_4

Using the above procedure the adsorption of sulfuric acid (HSO_4^-, SO_4^{--}) was measured at room temperature on a platinized Pt electrode as a function of potential, in solutions of various H_2SO_4 concentration with and without 1 N $HClO_4$ as supporting electrolyte. The results are shown in Fig. 2. As may be seen, adsorption becomes manifest at 100—200 mV and rises monotonously up to 700—800 mV.

At potentials more positive than those belonging to maximal adsorption, the measured values of adsorption cannot be regarded as equilibrium values since the measured activities decrease monotonously with time. On proceeding from such potentials to more negative ones, an adsorption hysteresis is observed. The hysteresis lag increases with increasing positive starting potentials. This trend of the adsorption curves agrees with those described in the literature [9].

As seen from Fig. 2, the adsorption maxima appear at 700—800 mV for solutions both with and without perchloric acid support. The values of adsorption, however, are rather different for the two kinds of measurement. As a rule, adsorption is greater for solutions with perchloric acid. This may be due to differences in the ψ_1 potential, and to the fact, that the concentra-

tion ratio $[HSO_4^-]/[SO_4^{--}]$ varies with sulfuric acid concentration and is different for the two cases. The adsorption potentials of the two ions are presumably different.

The adsorption of HSO_4^- ions in 1 N $HClO_4$ solution must be regarded as specific adsorption. Since both ClO_4^- and HSO_4^- ions are univalent, their participation in the formation of the double layer should depend only on their relative concentration, if only electrostatic forces were operative. On the ba-

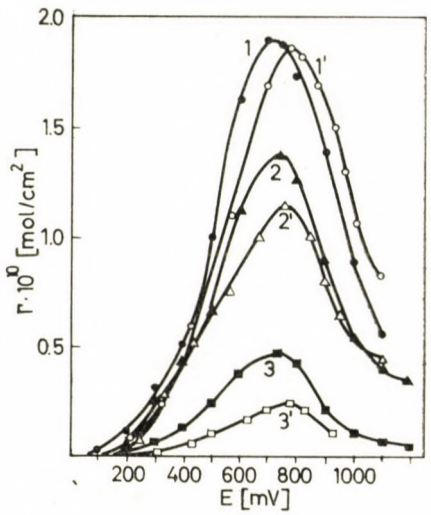

Fig. 2. Potential dependence of sulfuric acid adsorption. 1.: 5×10^{-3} mole/l $H_2SO_4 + 1$ N $HClO_4$; ●; 1'.: 5×10^{-3} mole/l H_2SO_4; ○; 2.: 5×10^{-4} mole/l $H_2SO_4 + 1$ N $HClO_4$; ▲, 2'.: 5×10^{-4} mole/l H_2SO_4; △, 3.: 5×10^{-5} mole/l $H_2SO_4 + 1$ N $HClO_4$; ■, 3'.: 5×10^{-5} mole/l H_2SO_4; □

sis of this, the quantity of ions participating in the formation of the double layer can be estimated. Let us consider the simplified model in which the solution side plate of the double layer capacitor consists of anions only. In this case, a potential change of ΔE causes a change of the quantity of ions in the double layer equivalent to the change of charge $\Delta Q = C\Delta E$ depending on the capacity. If the concentration of the two ions of equal charge in the solution is c_1 and c_2, the charges ΔQ_1 and ΔQ_2 represented by them in the double layer obey the following relations:

$$\Delta Q = \Delta Q_1 + \Delta Q_2 \tag{7}$$

$$\Delta Q_1 : \Delta Q_2 = c_1 : c_2 \tag{8}$$

giving

$$\Delta Q_2 = \frac{\Delta Q}{1 + \frac{c_1}{c_2}} \tag{9}$$

Taking the double layer capacity as constant, one obtains

$$\Delta Q = C\Delta E \tag{10}$$

Since the charge represented by 1 mole of a univalent ion is approximately 10^5 Coul, $\Delta\Gamma_{\text{el.stat}} = 10^{-5}\ \Delta Q = 10^{-5}\, C\Delta E$

$$\Delta\Gamma^{(2)}_{\text{el.stat}} = \Delta\Gamma_{\text{el.stat}} \frac{1}{1 + \frac{c_1}{c_2}} \tag{11}$$

Using an average double layer capacity of 30 $\mu F/\text{cm}^2$ for the potential interval $\Delta E = 500$ mV in the region of reversible adsorption, one obtains

$$\Delta Q = 1.5 \times 10^{-5}\ \text{coul/cm}^2, \textit{ i.e. } \Delta\Gamma_{\text{el.stat}} = 1.5 \times 10^{-10}\ \text{mole/cm}^2$$

Values of $\Delta\Gamma^{(2)}_{\text{el.stat}}$ calculated from (11) and the experimental values of $\Delta\Gamma$ are given in Table I (index$^{(2)}$ refers to HSO_4^- ions).

Table I

Values of electrostatic adsorption ($\Delta\Gamma_{\text{el.stat}}$ and $\Delta\Gamma^{(2)}_{\text{el.stat}}$) calculated from Eq. (11) compared with measured values $\Delta\Gamma$ of HSO_4^- ion adsorption

$\Delta E = 700—200 = 500$ mV; $c_1\,[ClO_4^-] = 1$ mole/l

c_2 (mole/l)	5×10^{-5}	5×10^{-4}	5×10^{-3}
$\Delta\Gamma_{\text{el.stat}} \cdot 10^{10}$ (mole/cm^2)	1.5	1.5	1.5
$\Delta\Gamma^{(2)}_{\text{el.stat}} \cdot 10^{10}$ (mole/cm^2)	0.75×10^{-4}	0.75×10^{-3}	0.75×10^{-2}
$\Delta\Gamma \cdot 10^{10}$ (mole/cm^2)	0.43	1.30	1.80

It can be seen from Table I that the accumulation of HSO_4^- ions expected from electrostatic causes is less than 1% of the adsorption values actually measured even at a H_2SO_4 concentration of 5×10^{-3} mole/l.

It cannot be expected, of course, that values of HSO_4^- adsorption and charges calculated from the double layer capacity should coincide. The latter quantity is an excess charge resulting from the charges of all the anions and cations in the double layer, whereas labelling accounts only for the HSO_4^- ions (or, generally speaking, for the labelled compound) in the immediate vicinity of the electrode surface.

In conclusion, it can be stated that the adsorption of HSO_4^- ions on Pt is, beyond doubt, specific. In establishing this, the use of the $HClO_4$ support

played an important part. The use of perchloric acid is of advantage for reasons, in part already mentioned: it stabilizes the pH, the concentration ratio $[HSO_4^-]/[SO_4^{2-}]$, the ionic strength and, therefore, the dimensions of the double layer.

The significant adsorption of HSO_4^- ions calls attention to the fact that a H_2SO_4 support is not, of necessity, an inert electrolyte in investigations of hydrogenation or the adsorption of other solutes.

Concentration dependence of adsorption

Experimental values (Γ_i^m) of HSO_4^- ion adsorption as a function of potential (E) and H_2SO_4 equilibrium concentration (c_i) are given in Table II.

The measurements were carried out at room temperature in 1 N $HClO_4$ solution. The concentrations pertaining to equilibrium were calculated from the equation

$$c_0 = \frac{\gamma F \Gamma_i^m}{V} = c_i$$

where c_0 is the initial concentration, F is the geometric surface area of the electrode, γ is the roughness factor and V is the volume of solution. Consequently, the equilibrium concentration varies with the potential even for a given initial concentration. (The change of background radiation due to this change in concentration was corrected for, too.)

Table II

$E = 300$ mV		$E = 400$ mV		$E = 500$ mV		$E = 600$ mV		$E = 700$ mV	
$c_i \times 10^6$ mole/l	$\Gamma_i^m \times 10^{12}$ mole/cm²	$c_i \times 10^6$ mole/l	$\Gamma_i^m \times 10^{12}$ mole/cm²	$c_i \times 10^6$ mole/l	$\Gamma_i^m \times 10^{12}$ mole/cm²	$c_i \times 10^6$ mole/l	$\Gamma_i^m \times 10^{12}$ mole/cm²	$c_i \times 10^6$ mole/l	$\Gamma_i^m \times 10^{12}$ mole/cm²
0.834	0.49	0.203	0.405	0.171	0.75	0.100	1.15	1.53	11.10
1.41	0.75	0.735	1.10	0.590	1.95	0.392	3.15	3.15	16.90
1.99	0.95	1.25	1.70	1.02	3.10	0.732	4.90	6.47	31.9
5.35	1.75	1.80	2.10	1.53	3.75	1.13	6.10	14.2	57.6
11.0	2.65	2.88	2.80	2.47	5.30	1.94	8.60	31.0	94.5
22.3	4.55	4.94	4.35	4.15	8.15	3.53	13.30	45.8	116.5
44.3	7.35	10.4	7.25	9.25	14.50	7.65	24.00	77.9	151
62.4	7.80	21.0	12.90	19.1	25.95	16.3	43.5	128	183
98.5	9.90	42.1	21.65	39.1	41.5	34.6	71.5	231	221
153	13.25	59.7	24.25	56.1	48.2	50.6	85.5	386	290
263	15.55	95.8	30.0	91.1	62.0	83.8	110.5		
447	21.55	149	35.0	143	78.5	135	138		
810	22.00	256	51.5	250	91.0	241	168		
1350	28.10	436	76.5	426	139	414	219		

The results do not fit either Temkin's or Langmuir's isotherm equation. Certain authors [9] are in favour of the validity of the Temkin isotherm, but the underlying experiments have — in our opinion — not been carried out under comparable conditions for the different concentrations. At different sulfuric acid concentrations, the pH, ionic strength and thus the structure of the double layer are subject to changes. The ratio $[HSO_4^-] / [SO^{2}_4^-]$, too, changes continuously with sulfuric acid concentration. All this tends to complicate the interpretation of the results.

If, however, adsorption measurements are carried out in 1 N $HClO_4$ solution, changes in the sulfuric acid concentration only moderately influence the other parameters of the system. The $[HSO_4^-] / [SO^{2}_4^-]$ ratio remains unchanged with increasing sulfuric acid concentrations as far as those are not excessive, and though it cannot be decided which form of sulfuric acid is adsorbed, we can be assured that there prevails proportionality between the concentrations of the ionic species adsorbed and sulfuric acid in the solution. It is very likely, of course, that the adsorption of HSO_4^- ions, present in greater concentration, is predominant, but it cannot be excluded in principle that $SO^{2}_4^-$ ions, too, are present in the adsorption phase.

As already demonstrated, in 1 N $HClO_4$ medium specific adsorption is observed unambiguously because of the excess supporting electrolyte, and because accumulation due to electrostatic reasons can be disregarded. In 1 N $HClO_4$ solution, the ionic strength, and consequently, the activity coefficients are unchanged by the relatively insignificant quantities of sulfuric acid added. These circumstances also contribute to the fact that the experimental conditions may be regarded as well defined even when the sulfuric acid concentration is varied.

The experimental task was to study adsorption phenomena in 1 N $HClO_4$ solution at very low (10^{-7}—10^{-4} mole/l) concentrations of sulfuric acid. In the concentration interval so far treated in the literature (10^{-4}—10^{-1} N), adsorption changes only weakly. In view of experimental errors, therefore, it is very difficult to obtain an isotherm from these results, and it is unjustified to draw general conclusions concerning the entire course of the isotherm — even in case of extremely accurate measurements — as these data are related to a relatively uncharacteristic part of the isotherm.

The measurements were carried out at activities in the range of 10^3 Ci/mole—0.1 Ci/mole, depending on the sulfuric acid concentration. Generally, the sulfuric acid concentration was increased by the addition of inactive sulfuric acid without disassembling the apparatus. Thus the highest specific activities occurred at the lowest concentrations.

As already mentioned, the concentration dependence of the HSO_4^- ion adsorption cannot be described by either Langmuir's or the logarithmic isotherms. As known from literature, the adsorption of hydrogen at the platinum-

electrolyte interface can be represented by the superposition of several (3—4) Langmuir isotherms. It seems justified, therefore, to look for a similar interpretation in the present case. As a first approximation the following relation was examined:

$$\Gamma_i^c = \Gamma_{\mathrm{I}}^0 \frac{b_{\mathrm{I}} c_i}{1 + b_{\mathrm{I}} c_i} + \Gamma_{\mathrm{II}}^0 \frac{b_{\mathrm{II}} c_i}{1 + b_{\mathrm{II}} c_i} + \Gamma_{\mathrm{III}}^0 \frac{b_{\mathrm{III}} c_i}{1 + b_{\mathrm{III}} c_i} \tag{12}$$

where the Γ^0-s and b-s are the adsorption constants and Γ_c^i is the calculated amount adsorbed.

The validity of Eq. (12) means that on the Pt surface there exist three kinds of active centers with different energies of adsorption, and the concentration dependence of adsorption on each kind of active sites can be described by a Langmuir isotherm.

The constants of Eq. (12) have been determined from experimental values (Table II) on a computer. The program is based on an iteration procedure. The values of Γ^0 and b are determined by minimizing the standard deviation of the relative errors. The results are compiled in Table III, together with the standard deviations (Δ) computed from the relative errors (δ_i)

$$\delta_i = \frac{\Gamma_i^m - \Gamma_i^c}{\Gamma_i^m} 100\ [\%] \tag{13}$$

using the definition equation:

$$\Delta \equiv \left(\frac{1}{n} \sum_{i=1}^{n} \delta_i^2 \right)^{1/2} \tag{14}$$

As may be seen from Table III, Eq. (12) adequately describes the adsorption of HSO_4^- ions on Pt surface within the usual experimental error

Table III

Constant of Eq. (12) and the standard deviation of computed adsorption values

E; mV		300	400	500	600	700
l/mole;	$b_{\mathrm{I}} \cdot 10^{-6}$	0.65±0.35	1.50±0.47	2.07±0.53	3.31±0.33	10±21
	$b_{\mathrm{II}} \cdot 10^{-4}$	1.59±1.10	2.24±0.52	2.31±0.36	2.21±0.18	2.32±0.42
	$b_{\mathrm{III}} \cdot 10^{-2}$	13.6±13.0	1.98±0.31	1.76±0.26	4.60±0.60	2.02±0.67
	$\Gamma_{\mathrm{I}}^0 \cdot 10^{12}$	0.95±0.40	1.08±0.27	1.78±0.54	3.39±0.23	3.66±2.43
mole/cm²;	$\Gamma_{\mathrm{II}}^0 \cdot 10^{12}$	10.7±6.8	28.5±4.7	65.8±7.2	131.5±8.9	195.6±21.1
	$\Gamma_{\mathrm{III}}^0 \cdot 10^{12}$	24.8±4.1	560±5	997±42	590±17	1376±129
Δ,	%	5.0	5.1	4.0	2.2	2.9

(+5%) in a wide range of concentrations (10^{-7}—10^{-3} mole/l) and at different potentials.

As a further proof of the applicability of Eq. (12), the values Γ_i^m (measured and Γ_i^c (computed) are given for $E = 500$ and 600 mV, together with the relative errors in column A of Table IV.

To establish the potential dependence of constants b of Eq. (12), these constants are represented as functions of E in Fig. 3.

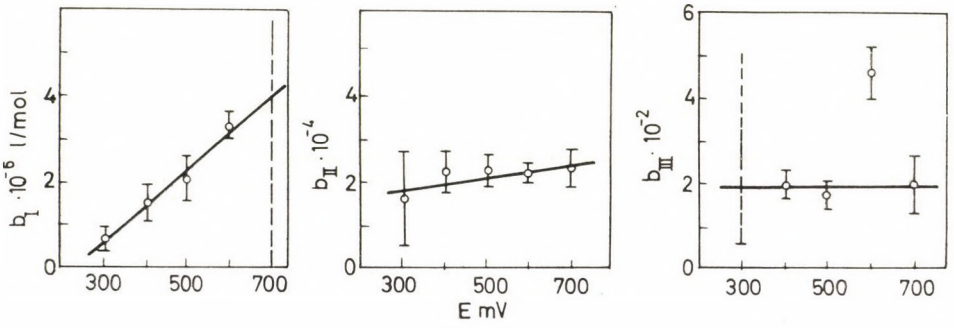

Fig. 3

It appears justified to represent the potential dependence of the b constants by the straight lines drawn in Fig. 3. Using these values of $\tilde{b}_{\mathrm{I}}$, $\tilde{b}_{\mathrm{II}}$, and $\tilde{b}_{\mathrm{III}}$, constants $\tilde{\Gamma}_{\mathrm{I}}^0$, $\tilde{\Gamma}_{\mathrm{II}}^0$, $\tilde{\Gamma}_{\mathrm{III}}^0$ of Eq. (12) can also be calculated by means of a least squares procedure. By comparing the $\tilde{\Gamma}_i^c$ values calculated using these constants in Eq. (12) with the measured values (Table II), the standard deviations as defined by relations (13) and (14) can also be obtained. The results of this calculation are shown in Table V.

The standard deviations indicate that the assumption made about the potential dependence of constants b is justified as the standard deviations exceed the experimental error of $\pm 5\%$ only in some cases and only insignificantly. As a further verification of the procedure, the adsorption values (Γ_i^c) calculated from Eq. (12) using the adsorption constants determined in the above manner are presented in column B of Table IV together with the relative errors.

From Table V, graph of the potential dependence of $\tilde{\Gamma}^0$ can be obtained. The result is shown in Fig. 4 indicating that the $\tilde{\Gamma}^0$ values for all three kinds of active sites depend on the potential.

The concentration dependence of adsorption is thus adequately described by Eq. (12). However, the analysis of the corresponding physical concept points to some —apparently contradictory — consequences that require further clarification.

Table IV

Comparison of values (Γ_i^c and Γ_i^c) calculated from Eq. (12) using data of Tables III and V with the measured values (Γ_i^m) of adsorption

$E = 500$ mV						$E = 600$ mV					
		A		*B*				*A*		*B*	
$c_i \times 10^6$ mole/l	$\Gamma_i^m \times 10^{12}$ mole/cm²	$\Gamma_i^c \times 10^{12}$ mole/cm²	δ_i %	$\tilde{\Gamma}_i^c \times 10^{12}$ mole/cm²	δ_i %	$c_i \times 10^6$ mole/l	$\Gamma_i^m \times 10^{12}$ mole/cm²	$\Gamma_i^c \times 10^{12}$ mole/cm²	δ_i %	$\tilde{\Gamma}_i^c \times 10^{12}$ mole/cm²	δ_i %
0.171	0.75	0.754	−0.6	0.769	−2.5	0.100	1.15	1.161	−0.9	1.143	+0.6
0.590	1.95	1.967	−0.9	1.962	−0.6	0.392	3.15	3.150	0.0	3.153	−0.1
1.02	3.10	2.903	+6.4	2.874	+7.3	0.723	4.90	4.654	+5.0	4.666	+4.8
1.53	3.75	3.870	−3.2	3.820	−1.9	1.13	6.10	6.182	−1.3	6.213	−1.9
2.47	5.30	5.479	−3.4	5.401	−1.9	1.94	8.60	8.859	−3.0	9.916	−3.7
4.15	8.15	8.090	+0.8	7.980	+2.1	3.53	13.30	13.58	−2.1	13.68	−2.9
9.25	14.50	14.92	−2.9	14.80	−2.1	7.65	24.00	24.32	−1.3	24.43	−1.8
19.1	25.95	25.25	+2.7	25.26	+2.7	16.3	43.5	42.50	+2.5	42.53	+2.2
39.1	41.5	39.85	+4.0	40.17	+3.2	34.6	71.5	69.54	+2.7	69.21	+1.6
56.1	48.2	48.77	−1.0	49.25	−2.2	50.6	85.5	86.17	−0.8	85.53	0.0
91.1	62.0	62.17	−0.3	62.85	−1.4	83.8	110.5	110.65	−0.1	109.49	+0.9
143.0	78.5	76.84	+2.1	77.35	+1.5	135.0	138	136.4	+1.2	134.9	+2.2
250	91.5	99.98	−9.9	99.51	−9.4	241	168	173.0	−3.0	172.2	−2.5
426	139	131.2	+5.6	128.3	+7.7	414	219	216.4	+1.2	219.3	−0.2

As demonstrated above, the potential dependence of adsorption can be attributed primarily to the potential dependence of the Γ^0 values. On ground of the physical model underlying the Langmuir isotherm, the maximum coverage (Γ^0) attainable on the different kinds of active sites should — according to the present concept — be essentially potential independent. Thus, if such a dependence is found, the reason must be sought in some other phenomenon occurring in the adsorption phase and depending on potential. As other studies (*e.g.* the adsorption of Cl^- ions) lead to similar conclusions, this question will be discussed in a subsequent paper.

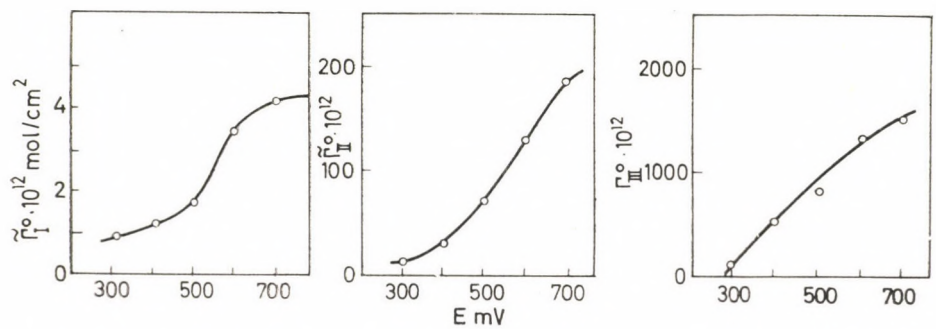

Fig. 4

The existence of centers of different energies of adsorption is also supported by other experimental evidence, as *e.g.* the phenomena observed in the displacement of adsorbed labelled sulfuric acid by the unlabelled species. The time course of this displacement is shown in Fig. 5.

Table V

Constants of Eq. (12) from Fig. 3 and the standard deviations of adsorption values calculated therefrom

E,	mV	300	400	500	600	700
	$\tilde{b}_I \times 10^{-6}$	0.59	1.44	2.31	3.16	4.02
1 mole;	$\tilde{b}_{II} \times 10^{-4}$	1.85	1.99	2.13	2.28	2.42
	$\tilde{b}_{III} \times 10^{-2}$	2.00	2.00	2.00	2.00	2.00
	$\tilde{\Gamma}^0_I \times 10^{12}$	0.856	1.16	1.71	3.43	4.17
mole/cm^2;	$\tilde{\Gamma}^0_{II} \times 10^{12}$	11.97	30.8	71.6	129.0	187.5
	$\tilde{\Gamma}^0_{III} \times 10^{12}$	81.14	517.7	797.3	1298	1501
$\tilde{\Delta}$,	%	6.8	5.2	4.2	2.3	2.9

After the equilibrium in a 10^{-4} mole/l H_2SO_4 solution had been attained at 600 mV (section 1), a large excess of inactive sulfuric acid was added and the change in activity coming from the adsorption layer was measured (section 2). As may be seen, the activity rapidly drops to about one half of its initial value. Subsequently, the process slows down and the change in activity almost ceases at a considerable level. Under the prevailing conditions the specific activity is lowered by dilution to such an extent that even in the case of increased adsorption due to the increased concentration, the number of counts per minute should not have exceeded a few hundred, if rapid equilibration between solution and adsorption phase had taken place. This means that exchange is very slow on some sites of the surface.

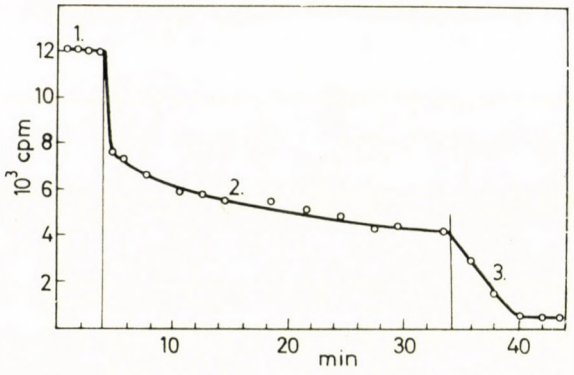

Fig. 5

As a result of shifting the potential to more negative values, *i.e.* regeneration, adsorbed labelled substance can be displaced very rapidly, as shown by section 3 of Fig. 5. If the electrode is subsequently polarized to the initial potential, the activity from the adsorption layer is extremely small, in accordance with the expectation.

All this supports the view that adsorbed particles are differently bound on various sites of the electrode, which is reflected in their rate of desorption.

A dependence of desorption rate on potential (section 3), however, also seems to contradict the fact that constants b_{II} and b_{III} of Eq. (12) are practically independent of the potential with the exception of b_I, whereas the quantity of HSO_4^- on sites I is only an insignificant fraction of the total quantity adsorbed at a concentration of 10^{-4} mole/l.

This phenomenon is necessarily connected with the potential dependence of I^0 as, on shifting to more negative potentials, the quantity of HSO_4^- adsorbed on the surface by far exceeds the possible, maximal HSO_4^- coverage at the given (negative) potential.

A clarification of the above questions and a resolution of the contradictions may be expected from the investigation of systems in which the differences of the individual kinds of adsorption sites — here only assumed — are more pronounced. Preliminary experiments show that the study of Cl^- ion adsorption might be suited to this end.

*

The authors are indebted to Mr. A. NESZMÉLYI for preparing the computer program and carrying out computations.

REFERENCES

1. NAGY, F., TELCS, I., HORÁNYI, GY.: Acta Chim. Acad. Sci. Hung. **37,** 295 (1963).
NAGY, F., HORÁNYI, GY.: Magy. Kém. Folyóirat **68,** 479 (1962).
2. HORÁNYI, GY., NAGY, F.: Magy. Kém. Folyóirat **72,** 370 (1966).
3. RICHERT, J., LORENZ, W.: Z. physik. Chem. **217** 136 (1961).
4. KAFALAS, J. A., GATOS, H. C.: Rev. Sci. Instr. **29,** 47 (1958).
5. COOK, H. D.: Rev. Sci. Instr. **27,** 1081 (1956).
6. DAHMS, H., GREEN, M., WEBER, J.: Nature **196,** 1310 (1962).
DAHMS, H., GREEN, M.: J. Electrochem. Soc. **110,** 1075 (1963).
7. BLOMGREEN, E. A., BROCKRIS, J. O'M.: Nature **186,** 305 (1960).
8. GILEADI, E., RUBIN, B. T., BOCKRIS, J. O'M.: J. Phys. Chem. **69,** 3335 (1965).
9. BALASHOVA, N. A., MERKULOVA, N. S.: Transactions of the Fourth Conference on Electrochemistry (in Russian) 1956. p. 48.
BALASHOVA, N. A.: Dokl. A. N. SSSR **103,** 639 (1955).
BALASHOVA, N. A., IVANOV, V. A., KAZARINOV, V. E.: Dokl. A. N. SSSR **134,** 864 (1960).
BALASHOVA, N. A.: Dokl. A. N. SSSR **143,** 358 (1962).
KAZARINOV, V. E.: Z. Phys. Chem. **226,** 167 (1964).
BALASHOVA, N. A.: Zh. Fiz. Khim. **32,** 2266 (1958).
KAZARINOV, V. E., BALASHOVA, N. A.: Dokl. A. N. SSSR **134,** 864 (1960).
BALASHOVA, N. A.: Electrochim. Acta **7,** 559 (1962).
KAZARINOV V. E., BALASHOVA, N. A.: Dokl. A. N. SSSR **157,** 1174 (1964).
KAZARINOV, V. E., BALASHOVA, N. A.: Dokl. A. N. SSSR **139,** 641 (1961).
KAZARINOV, V. E., BALASHOVA, N. A.: Collect. Czech. Chem. Commun. **30,** 4184 (1965).
FRUMKIN, A. N., MANSUROV, G. N., KAZARINOV, V. E., BALASHOVA, N. A.: Dokl. A. N. SSSR **31,** 806 (1966).
BALASHOVA, N. A.: Wiss. Z. d. Techn. Univ. Dresden, **12,** (5) 1177.
10. BALASHOVA, N. A., KAZARINOV, V. E.: Usp. Khim. **34,** 1721 (1956).
11. POWER, W. H., HEYD, J. W.: Anal. Chem. **28,** 523 (1956).
12. SCHWABE, K.: Electrochim. Acta **6,** 1003 (1964).
13. SCHWABE, K.: Electrochim. Acta **6,** 223 (1962).
14. IMRE, L., NAGY, J.: Kolloid-Z. **183,** 134 (1962).
15. JOLIOT, F.: J. Chim. Phys. **27,** 119 (1930).
16. DELAHAY, P.: Double Layer and Electrode Kinetics. Interscience Publishers, 1965.

János SOLT
György HORÁNYI
Ferenc NAGY
Budapest II., Pusztaszeri út 57—69.

Acta Chimica Academiae Scientiarum Hungaricae, Tomus 63 (4), pp. 403—415 (1970)

THE BOND STRUCTURE OF COMPOUNDS CONTAINING ALLYLSILICON GROUPS

J. NAGY, J. RÉFFY and P. ÉLIÁS

(Department of Inorganic Chemistry, Technical University, Budapest)

Received December 2, 1968

Approximate quantum chemical calculations were made concerning the σ- and π-bond systems of trimethylallylsilane and 1-trimethylsilylcyclopentene-2 in order to elucidate the structure of the allyl-silicon (and allyl-germanium) group. The calculations indicated in trimethylallylsilane the combined action of the hyperconjugation of the CH_2 group and of the long bond between the silicon atom and the carbon atom in β-position. The bond order of the bond between the silicon atom and the neighbouring carbon atom is about 8%, while the π-bond character of the long bond is about 3.5%. The π-bond character of these bonds in the cyclic allylic compound is higher. The calculated resultant dipole moment of trimethylallylsilane is 0.448 D, in good agreement with the experimental value of 0.58 D.

Several authors have studied the bond structure of vinylsilanes [1, 2, 3] with the conclusion that conjugation occurs, that is a $d\pi$—$p\pi$ bond is formed, between one of the empty d orbitals of silicon and the π-electron system of the double bond. (A similar $d\pi$—$p\pi$ interaction has been observed in case of a silicon atom bound to a phenyl group.) In the course of the present work we have investigated whether a $d\pi$—$p\pi$ bond will also be formed in case of allylsilanes and, whether the hyperconjugation effect of the methylene group situated between the double bond and the silicon atom gives rise to a more extensive conjugated system.

It is known that the ultraviolet spectrum of trimethylvinylsilane has an absorption maximum at 178 nm, and that of trimethylallylsilane (I) at 192 nm [4]. There is a remarkable resemblence between germanium compounds and the analogous silicon derivatives. This similarity is also indicated by the ultraviolet absorption spectra of trimethylvinylgermanium (with a maximum at 182.5 nm) and of trimethylallylgermanium (with a maximum at 197 nm). The considerable bathochromic shifts in the spectra of allyl derivatives compared with the vinyl compounds is the result of the extension of the conjugated system. In case of vinyl derivatives the delocalized π-electron system is tricentric. When the allyl group is bound to silicon (or to germanium), there are three possible conjugated systems as shown in Fig. 1. (In the figure the numbers pertaining to the atoms mark at the same time the numbers applied to π-systems in quantum chemical calculations.) The π-electron system with five centres shown in Fig. 1/a may be explained by the hyperconjugation of the hydrogen atoms bound to the C-2 atom. This hyperconju-

gation may be discussed as two hydrogen atoms forming a pseudo p orbital, which produces overlapping with the p orbital of the C-2 atom (and through this with the π-electron system of the double bond and with one of the empty d orbitals of the silicon atom). Fig. 1/b reflects the case when the hyperconjugation effect due to the CH_2 group is neglected (hence the CH_2 group does not participate in the conjugated system and is shown therefore by a dashed line), while one of the d orbitals of the silicon atom overlaps with the $p\pi$ orbital of the C-2 atom in β position, producing a so-called 'long bond' [5]. This case corresponds to a tricentric π-system in the same way as in the conjugated system of trimethylvinylsilane. In Fig. 1/c the simultaneous presence of hyper-

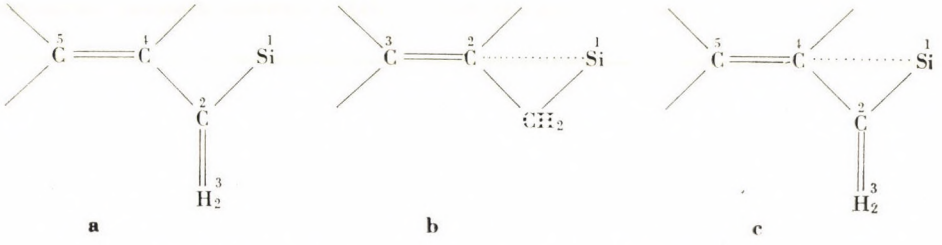

Fig. 1. Assumed conjugated π-systems in trimethylallylsilane

conjugation and long bond results again in a delocalized π-system with five centres. In this system the $d\pi$—$p\pi$ interaction between the silicon atom, rotating around the axis connecting the C-2 and C-4 atoms, and the C-4 atom changes depending on the angle of rotation and is statistically only half as great as the value for a fixed C^2—C^4 axis. Such a fixed axis and, with respect to the silicon atom, an allylic double bond occurs in the 1-trimethylsilylcyclopentene-2 molecule (**II**). The ultraviolet spectra of trimethylallylsilane and of cyclic allylic type derivatives may furnish useful experimental data to the elucidation of structural problems. The spectral data of the required cyclic silicon compounds were not available, but it is known that the spectrum of the analogous germanium derivative ($\lambda_{max} = 204$ nm) shows a bathochromic shift compared with trimethylallylgermanium ($\lambda_{max} = 197$ nm) [4, 6]. PETUHOV *et al.* [4] obtained the spectrum of a compound of allyl-germanium character (**III**) in which the germanium is situated in a five-membered ring, and its d orbitals have no possibility to form long bonds.

The ultraviolet absorption maximum of compound **III** appears below 180 nm, that is at a shorter wavelength, than the maxima of the other two allylic compounds. This experimental fact allows the conclusion that the long bond may indeed contribute to the formation of a delocalized π-system in the molecules, and the lack of a long bond will reduce the conjugated character of the mole-

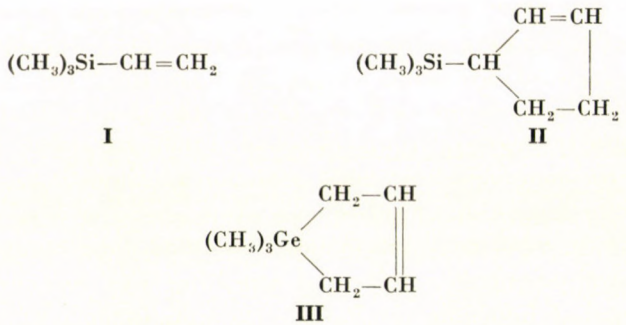

cule. In order to be able to study the role of the hyperconjugation effect and of the long bond, we carried out quantum chemical calculations with respect to the σ and π systems of compounds **I** and **II.** Calculations with respect to the σ-bond system were performed by means of the modified method of DEL RE [7], and with respect to the π-bond system by means of the single-electron Hückel LCAO-MO method. The similarity between silicon and germanium compounds offers a possibility of applying the conclusions derived from the spectral data of germanium compounds to the silicon analogues (*e.g.*, in case of compound **II**), and to compare the results with those obtained by quantum chemical calculations for the silicon derivatives. (Calculation of the germanium compounds involves considerable difficulties.)

The DEL RE parameters used in the calculation of the σ-bond systems are listed in Table I, where δ^0 stands for the Coulomb parameters, γ is the so-called induction parameter, and ε the resonance integral. Numbering of the compounds is shown in Fig. 2.

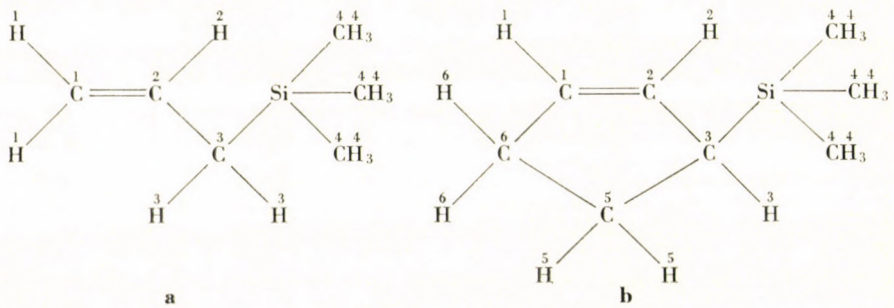

Fig. 2. Numbering of the atoms in the calculation of the σ-bond systems: *a)* trimethylallylsilane; *b)* 1-trimethylsilylcyclopentene-2

For compound **I** the following linear inhomogeneous system of equations, consisting of nine equations, may be written:

1. $\delta_C^1 = \delta_C^0 (sp^2) + \gamma_{C(C)}\,\delta_C^2 + 2\gamma_{C(H)}\,\delta_H^1$
2. $\delta_H^1 = \delta_H^0 + \gamma_{H(C)}\,\delta_C^1$
3. $\delta_C^2 = \delta_C^0 (sp^2) + \gamma_{C(C)}\,\delta_C^1 + \gamma_{C(C)}\,\delta_C^3 + \gamma_{C(H)}\,\delta_H^2$
4. $\delta_H^2 = \delta_H^0 + \gamma_{H(C)}\,\delta_C^2$
5. $\delta_C^3 = \delta_C^0 (sp^3) + \gamma_{C(C)}\,\delta_C^2 + \gamma_{C(Si)}\,\delta_{Si} + \gamma_{C(H)}\,\delta_H^3$
6. $\delta_H^3 = \delta_H^0 + \gamma_{H(C)}\,\delta_C^3$
7. $\delta_{Si} = \delta_{Si}^0 + \gamma_{Si(C)}\,\delta_C^3 + 3\gamma_{Si(C)}\,\delta_C^4$
8. $\delta_C^4 = \delta_C^0 (sp^3) + \gamma_{C(Si)}\,\delta_{Si} + 3\gamma_{C(H)}\,\delta_H^4$
9. $\delta_H^4 = \delta_H^0 + \gamma_{H(C)}\,\delta_C^4$

Table I

DEL RE *parameters*

Parameters	A—B bond		
	C—C	C—H	Si—C
δ_A^0	sp^2 : 0.12; sp^3 : 0.07	sp^2 : 0.12; sp^3 : 0.07	—0.1
δ_B^0	sp^2 : 0.12; sp^3 : 0.07	0	sp^2 : 0.12; sp^3 : 0.07
$\gamma_{A(B)}$	0.1	—0.2	0.2
$\gamma_{B(A)}$	0.1	0.4	0.4
ε_{AB}	1	1	1

In a similar manner, compound **II** may be characterized by a linear inhomogeneous system consisting of 13 equations. The solution of the system of equations furnishes the Coulomb parameters, and when these are known, the bond polarity degrees Q_{A-B} may be calculated with the help of the equation

$$Q_{A-B} = \frac{\delta_A - \delta_B}{2\varepsilon_{AB}},$$

and the bond dipole moments m_{A-B} from the equation

$$m_{A-B} = Q_{A-B} \cdot e \cdot R$$

(where e is the elementary charge, R the bond distance); the q_A partial charges are obtained from the equation:

$$q_A = \sum_B Q_{A-B},$$

The values of the bond polarity degrees and bond dipole moments are listed in Table II.(When writing the bonds, the atom shown on the left-hand side has the negative polarity.) The negative signs of the $Q_{C_2-C_1}$ and $m_{C_2-C_1}$ values pertaining to compound **II** indicate that the polarity of the bond between the C-1 and C-2 atoms in compound **II** is opposite to that in compound **I.** For the calculation of the bond dipole moments the following bond distance values were used:

C—H	1.09 Å
C—C (alkyl)	1.54 Å
C—C (double bond)	1.353 Å
Si—C	1.87 Å

The σ-charge distribution in compound **I** is shown in Fig. 3/a, that in compound **II** in Fig. 3/b.

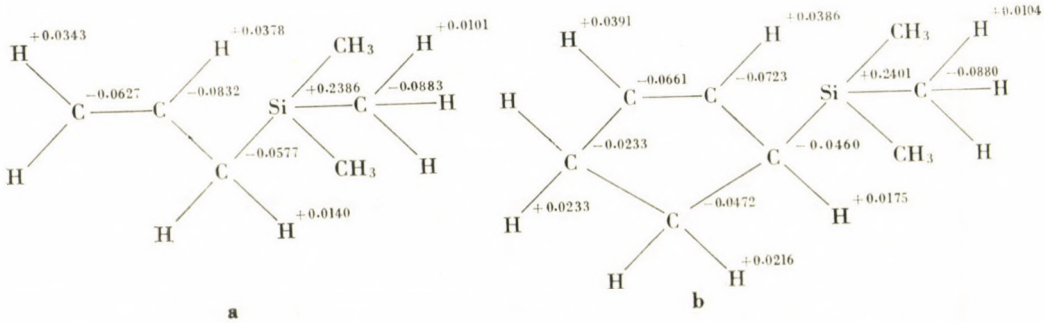

Fig. 3. σ-charge distributions: *a)* trimethylallylsilane; *b)* 1-trimethylsilylcyclopentene-2

In Fig. 1 the three possible forms of the π-system in trimethylallylsilane are shown. The energy of the molecular orbitals and the energy of lowest electron transition (Δm) have been calculated for all three cases. In the first case, due to the hyperconjugation of the CH_2 group, a five-centre delocalized system is formed and the solution of the matrix equation of fifth order will furnish the energy of the molecular orbitals. The values of the Coulomb and resonance integrals for the calculation were chosen partly from literature data [8], partly from our earlier calculations [9, 10], and may be summed up as follows. (For integrals written in the parametric form it is usual to take as basis the Coulomb integral marked α of the carbon in the benzene ring and at the same time the resonance integral β of the carbon–carbon bond in the benzene ring, hence the following integral values should be interpreted in this way. For example, the carbon–carbon resonance integral of the double bond in the allyl group has been converted into the resonance integral units of the carbon–carbon bond of benzene.)

$$H_{11} = \alpha - 1.8152\,\beta, \quad H_{12} = H_{21} = 0.3374\,\beta, \quad H_{22} = H_{44} = H_{55} = \alpha,$$
$$H_{23} = H_{32} = 3.06\,\beta, \quad H_{33} = \alpha - 0.5\,\beta, \quad H_{24} = H_{42} = 0.8\,\beta,$$
$$H_{45} = H_{54} = 1.0324\,\beta$$

After these values are known, and supposing hyperconjugation, a matrix of fifth order may be written:

$$\begin{bmatrix} \alpha - 1.8152\,\beta - \varepsilon & 0.3374\,\beta & 0 & 0 & 0 \\ 0.3374\,\beta & \alpha - \varepsilon & 3.06\,\beta & 0.8\,\beta & 0 \\ 0 & 3.06\,\beta & \alpha - 0.5\,\beta - \varepsilon & 0 & 0 \\ 0 & 0.8\,\beta & 0 & \alpha - \varepsilon & 1.0324\,\beta \\ 0 & 0 & 0 & 1.0324\,\beta & \alpha - \varepsilon \end{bmatrix} = 0$$

Table II

Calculated bond polarity degree and bond dipole moment values of trimethylallysilane **(I)** *and 1-trimethylsilyl-cyclopentene-2* **(II)**

	Q_{A-B}		m_{A-B} (DEBYE)	
	I	II	I	II
C_2-C_1	0.0059	−0.0008	0.038	−0.005
C_2-C_3	0.0400	0.0346	0.029	0.255
C_3-Si	0.0651	0.0699	0.588	0.623
C_4-Si	0.0578	0.0568	0.522	0.510
C_5-C_3		0.0069		0.051
C_6-C_5		0.0029		0.021
C_1-C_6		0.0262		0.195
C_1-H_1	0.0343	0.0391	0.179	0.204
C_2-H_2	0.0378	0.0386	0.198	0.202
C_3-H_3	0.0141	0.0175	0.074	0.092
C_4-H_4	0.0102	0.0104	0.053	0.054
C_5-H_5		0.0216		0.113
C_6-H_6		0.0233		0.122

If a long bond without hyperconjugation is assumed for compound **I** (Fig. 1/b), in the tricentric system the long bond between the silicon atom and the C-2 carbon atom (marked in the figure by a dotted line) will have a smaller resonance integral because of the lengthened bond distance (2.78 Å, instead of 1.54 Å of the normal bond) and also because the $3d$ orbital of silicon and the $2p\pi$ orbital of carbon make an angle, and the rotation of the silicon atom around the axis reduces the possibility of favourable overlappings (to 0.1283 β) compared with the case of a simple carbon–silicon bond (0.3374 β). The tricentric matrix is as follows:

$$\begin{bmatrix} \alpha - 1.8152\,\beta - \varepsilon & 0.1283\,\beta & 0 \\ 0.1283\,\beta & \alpha - \varepsilon & 1.0324\,\beta \\ 0 & 1.0324\,\beta & \alpha - \varepsilon \end{bmatrix} = 0$$

If the conjugated system is brought about by hyperconjugation and long bond (Fig. 1/c), a five-centre system is obtained as in the first case. The only difference appears in the value of the resonance integral between the silicon atom and the C-4 atom, which, instead of zero, has now the value corresponding to the long bond, *i.e.* $H_{14} = H_{41} = 0.1283\,\beta$.

Solution of the secular equations gives in all three cases the energies of the molecular orbitals.

Hyperconjugation	Long bond	Hyperconjugation + long bond
$\varepsilon_1 = \alpha + 2.9686\,\beta$	$\varepsilon_1 = \alpha + 1.0353\,\beta$	$\varepsilon_1 = \alpha + 2.9717\,\beta$
$\varepsilon_2 = \alpha + 0.9750\,\beta$	$\varepsilon_2 = \alpha - 1.0221\,\beta$	$\varepsilon_2 = \alpha + 0.9755\,\beta$
$\varepsilon_3 = \alpha - 1.0138\,\beta$	$\varepsilon_3 = \alpha - 1.8284\,\beta$	$\varepsilon_3 = \alpha - 1.0019\,\beta$
$\varepsilon_4 = \alpha - 1.7961\,\beta$		$\varepsilon_4 = \alpha - 1.8174\,\beta$
$\varepsilon_5 = \alpha - 3.4489\,\beta$		$\varepsilon_5 = \alpha - 3.4432\,\beta$
$\Delta m = 1.9888\,\beta$	$\Delta m = 2.0574\,\beta$	$\Delta m = 1.9774\,\beta$

The Δm values stand for the transition energies in β units, between the highest occupied and the lowest unoccupied molecular orbital.

Similar calculations may also be carried out for compound **II**. In this case, too, assuming a hyperconjugational effect a five-centre, in the case of long bond tricentric, and in the simultaneous presence of hyperconjugation and long bond again a five-centre π-system is formed. In Fig. 4/a, 4/b and 4/c the atoms which do not take part in the π-system are marked with dotted lines. There are two main differences between the assumed π-systems of molecule **I** and molecule **II**: in **I** hyperconjugation is caused by the CH_2 group, whereas in **II** by the CH group; secondly, in **II** overlapping giving rise to the long bond (between the *d* orbital of silicon and the $p\pi$ orbital of the carbon atom in β position) has twice as great probability than in the case of **I** because of the fixed C^2—C^4 axis. These discrepancies are manifest in the changes of two resonance integrals: in the first and third system accounting for hyperconjugation $H_{23} = H_{32} = 2.16\,\beta$, whle the resonance integral of the long bond is $0.2566\,\beta$ (from the numberingn Fig. 4/b $H_{12} = H_{21}$, in Fig. 4/c $H_{14} = H_{41}$).

Solution of the corresponding secular equations leads also in this case to the energy levels of the molecular orbitals and to the transitions:

Hyperconjugation	Long bond	Hyperconjugation + long bond
$\varepsilon_1 = \alpha + 2.1634\,\beta$	$\varepsilon_1 = \alpha + 1.0440\,\beta$	$\varepsilon_1 = \alpha + 2.1762\,\beta$
$\varepsilon_2 = \alpha + 0.9096\,\beta$	$\varepsilon_2 = \alpha - 0.9933\,\beta$	$\varepsilon_2 = \alpha + 0.9107\,\beta$
$\varepsilon_3 = \alpha - 0.9946\,\beta$	$\varepsilon_3 = \alpha - 1.8659\,\beta$	$\varepsilon_3 = \alpha - 0.9530\,\beta$
$\varepsilon_4 = \alpha - 1.7690\,\beta$		$\varepsilon_4 = \alpha - 1.8520\,\beta$
$\varepsilon_5 = \alpha - 2.6248\,\beta$		$\varepsilon_5 = \alpha - 2.5967\,\beta$
$\Delta m = 1.9042\,\beta$	$\Delta m = 2.0373\,\beta$	$\Delta m = 1.8677\,\beta$

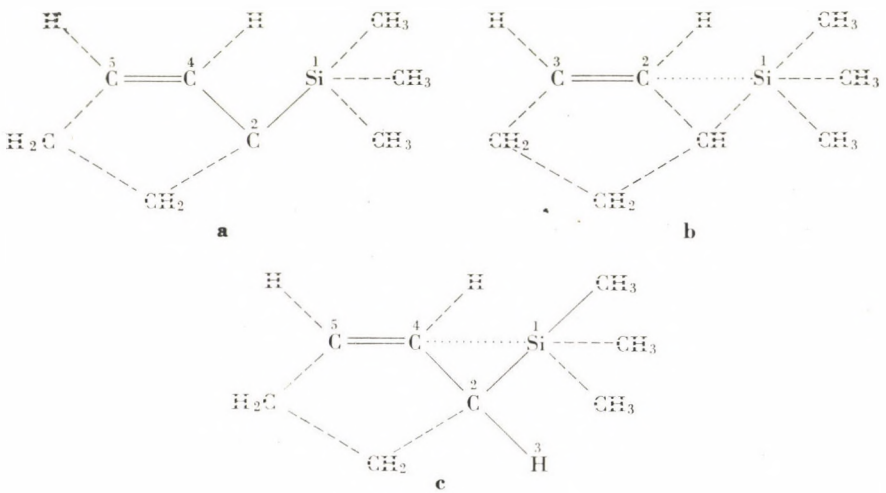

Fig. 4. Assumed conjugated π-systems in 1-trimethylsilylcyclopentene-2

Starting with similar parameters, we obtain the following simple matrix for the π—π^* transition in ethylene:

$$\begin{bmatrix} \alpha - \varepsilon & 1.0324\,\beta \\ 1.0324\,\beta & \alpha - \varepsilon \end{bmatrix} = 0$$

from which $\Delta m = 2.0648\,\beta$. The position of the corresponding ultraviolet maximum is at 165 nm. The calculated Δm transitions of compounds **I** and **II** are smaller for all three assumed conjugated systems than the Δm value of ethylene. The tricentric system with long bond but without hyperconjugation shows only a slight decrease in transition energy (considerably smaller than might be expected from the ultraviolet spectrum). For both the first and third assumed structures a considerable drop in the value of Δm was found, and in accordance with spectral data the Δm transition for compound **I** is higher than for compound **II**. To decide which of these is the actual structure, the Δm tran-

sition value for the tricentric conjugated system of trimethylvinylsilane was calculated. The system has the following eigenenergy matrix:

$$\begin{bmatrix} \alpha - 1.8152\,\beta - \varepsilon & 0.3374\,\beta & 0 \\ 0.3374\,\beta & \alpha - \varepsilon & 1.0324\,\beta \\ 0 & 1.0324\,\beta & \alpha - \varepsilon \end{bmatrix} = 0$$

The eigenenergies of the three molecular orbitals are:

$$\varepsilon_1 = \alpha + 1.0524\,\beta;\ \varepsilon_2 = \alpha - 0.9675\,\beta;\ \varepsilon_3 = \alpha - 1.9001\,\beta.$$

The value of the Δm transition is: $2.0199\,\beta$.

According to Karapetyanc's comparative theorem, a linear correlation should be obtained when the wavelengths of the ultraviolet maxima of similar compounds are plotted *vs.* the Δm transition. Table III shows the frequencies of the absorption maxima of ethylene, trimethylvinylsilane and trimethylallylsilane, and the calculated Δm values. (For the last compound the Δm values of all three variations are given.) In Fig. 5 the related points are plotted. If we assume hyperconjugation and long bond for trimethylallylsilane, the three points will lie on a perfectly straight line, *i.e.* the linear correlation really exists, whereas if the exclusive presence of the hyperconjugation effect (point surrounded by a circle) or long bond (point surrounded by a square) is assumed, the point corresponding to trimethylallylsilane lies far from the straight line. The point corresponding to compound **II** cannot be included in the diagram, since the experimental data on its ultraviolet absorption maximum is lacking.

Table III

Absorption maxima and transition energies of ethylene, trimethylvinylsilane and trimethylallylsilane

	λ (nm)	γ^* (cm^{-1})	Δm
CH_2CH_2	165	60610	$2.0648\,\beta$
$(CH_3)_3SiCHCH_2$	178	56180	$2.0199\,\beta$
$(CH_3)_3SiCH_2CHCH_2$	192	52080	$1.9888\,\beta$ (Hyperconjugation)
			$2.0574\,\beta$ (long bond)
			$1.9774\,\beta$ (hyperconjugation and long bond)

Starting with the assumption that the conjugated system of trimethylallylsilane may be described with the greatest probability by the simultaneous presence of a hyperconjugation effect and a long bond, the system of linear

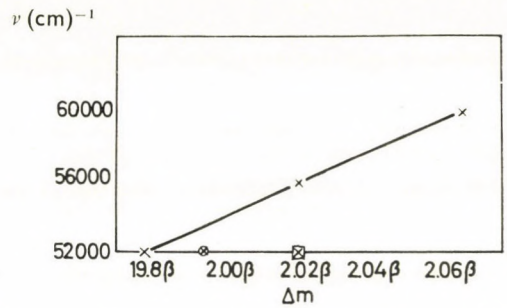

Fig. 5. Correlation between the wave numbers of the absorption maxima and the transition energies

coefficients was calculated from the appropriate eigenenergy matrix and the eigenvalues. For the cyclic compound containing a double bond in allylic position to the silicon atom (denoted by **II** in our calculations), a structure

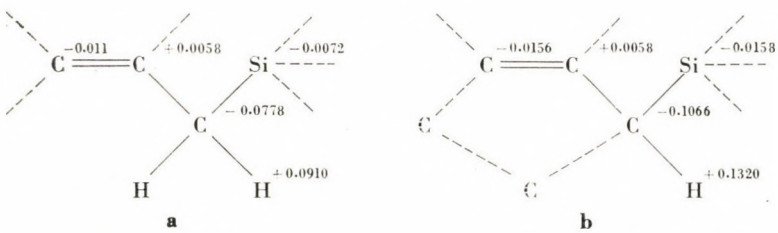

Fig. 6. π-charge distribution in *a)* trimethylallylsilane; *b)* 1-trimethylsilylcyclopentene-2

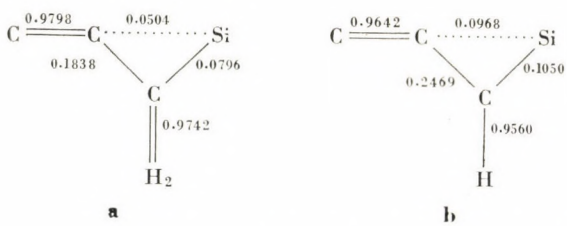

Fig. 7. π-bond systems i. *a)* trimethylallylsilane; *b)* 1-trimethylsilylcyclopentene-2

corresponding to the third variation may similarly be assumed, and the linear coefficient system characteristic of the molecule may be calculated. By means of the linear coefficients the π-charge distribution in the molecules can also be determined. It appears from Fig. 6 that the silicon atom has a small partial negative charge, the carbon atom in β-position to it is partially positive, while

the γ-carbon atom is partially negative. This result is in good agreement with the theory of the decomposition mechanism of allylsilanes [11], according to which during acid decomposition the γ-carbon atom first takes up a proton and the acid anion is then added to the β-carbon atom of the cation thus formed.

If the linear coefficients are known, the π-bond orders of the bonds in the π-systems may be calculated. According to Fig. 7, in molecule **I** the π-character of the bond between the carbon atom of the methylene group and the silicon atom is about 8%, while the π-bond order of the long bond is significantly lower (5%). The double bond character of the bond connecting C-4 and

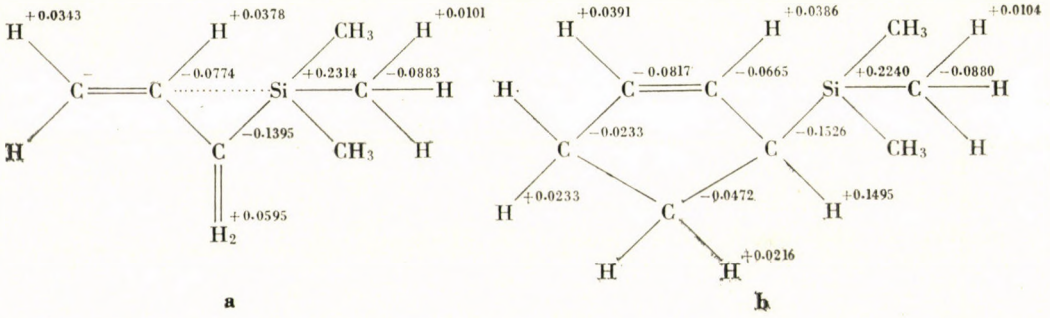

Fig. 8. Total charge distribution in *a)* trimethylallylsilane; *b)* 1-trimethylsilylcyclopentene-2

C-5 decreases only slightly when the silicon atom is introduced into the conjugated system. In molecule **II**, the order of the bond between the silicon and the C-2 atom (in α-position), as well as the π-bond order of the long bond is greater than in compound **I**, while the π-bond order of the double bond in the ring has a somewhat lower value.

The total charge of the various atoms can be determined from the σ-charge distribution shown in Fig. 3 and the π-charge distribution given in Fig. 6. The combined σ, π-molecular diagrams are shown in Fig. 8. From the results of the calculations referring to the σ and π-electron systems the approximate δ-, π- and resultant (σ, π) dipole moments of trimethylallylsilane were calculated and the last was compared with the experimental data reported in the literature. Calculation of the σ dipole moment started from the bond dipole moments m_{A-B} given in Table II (the numbering of the atoms is illustrated in Fig. 2). The three methyl groups bound to the silicon atom and making tetrahedral bond angles with one another may vectorially be replaced by a single methyl group lying on the same straight line as the Si—C^3 bond, and similarly, the bond vectors pointing from the three hydrogen atoms of the methyl group in the direction of the carbon atom may also be replaced by a single m_{C^4-H} bond moment vector lying on the straight line of the Si—C^3 bond. The

rotation of the silicon atom around the Si—C^3 axis may be neglected, since the three methyl groups are symmetrically arranged. The vectorial resultant of the $m_{C^4-H^4}$, m_{C^4-Si} and m_{C^3-Si} bond moments lying on a straight line was denoted by the symbol M. The vectorial resultant (group moment vector) of the two bond moments $m_{C^1-H^1}$ and of the bond moments $m_{C^2-C^1}$ and $m_{C^2-H^2}$ can also be calculated; this is denoted by the symbol m_e. Fig. 9 shows the simplified vector model obtained after these summing up operations (m_0 is the symbol of the bond moment vector $m_{C^2-C^3}$ and the symbol of $m_{C^3-H^3}$). The m_e vector rotates freely around the C^2—C^3 rotation axis. The average moment given by

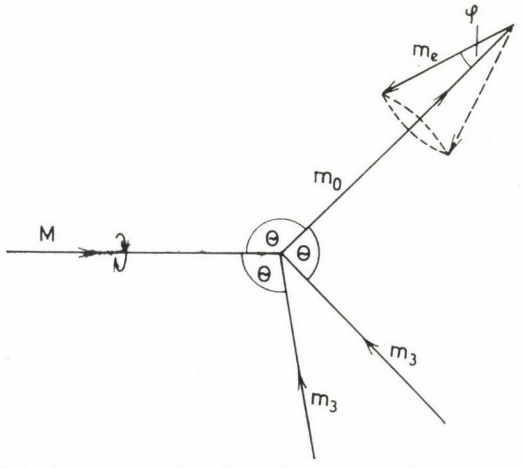

Fig. 9. Vectorial model of trimethylallylsilane for the calculation of the dipole moment

m_e and m_0, as well as the moments m_3 rotate freely around the C^3—Si rotation axis (lying in the direction of the vector), assuming the absence of any rotation hindrance. The resultant average σ-dipole moment was calculated by the method known from the literature, using the following expression [12, 13]:

$$\mu_\sigma^2 = M^2 + 2m_3^2 + m_0^2 + m_e^2 + 2\,(Mm_0\,\cos\Theta + Mm_e\,\cos\Theta\cos\varphi + 2\,Mm_3\,\cos\Theta + m_3^2\,\cos\Theta - 2\,m_3m_0\,\cos\Theta - 2\,m_3m_e\,\cos\Theta\,\cos\varphi + m_0m_e\,\cos\varphi).$$

In this formula Θ is the tetrahedral bond angle and φ the angle between the precessing group moments and the C^2—C^3 rotation axis.

For the calculation of the π-dipole moments the value and direction of the bond moments had to be determined from the π-charge distribution shown in Fig. 6. The adding up of the bond moments involved a similar problem as already discussed in connection with the σ-dipole moment, with the simplification that the group moments M and m_e are formed only by the bond moments between the atoms which figure in the calculation of the π-system.

Calculation of the resultant (σ, π) dipole moment from the total charge distribution of the molecule (Fig. 8) was made in the same way as the calculation of the σ-moment. The following dipole moments were obtained:

$$\mu\delta = 0.253 \text{ D}$$
$$\mu\pi = 0.293 \text{ D}$$
$$\mu\delta,\pi = 0.448 \text{ D}$$

If the resultant (σ, π) dipole moment is known, the angle between the σ and π dipole moment vectors may be calculated by means of the cosine theorem, and it is 70°.

The experimentally determined resultant dipole moment of trimethylallylsilane is 0.58 D [14] in good agreement with the calculated value, proving (together with other experimental results) that the calculations present a true picture of the structure of the molecules investigated.

REFERENCES

1. Nagy, J., Ferenczi-Gresz, S., Mironov, V. F.: Acta Chim. Acad. Sci. Hung. **45,** 190 (1966).
2. Armstrong, D. R., Perkins, P. G.: Theoret. Chim. Acta **5,** 69 (1966).
3. Nagy, J., Réffy, J., Kuszmann-Borbély, A., Pálossy-Becker, K.: Periodica Polytechnica **13,** 215 (1969).
4. Petuhov, V. A., Mironov, V. F., Sorigin, P. P.: Izv. A. N. SSSR, OHN **1964,** 2203.
5. Nagy, J., Becker-Pálossy, J., Réffy, J.: Periodica Polytechnica **11,** 43 (1967).
6. Éliás, P.: Thesis (Department of Inorganic Chemistry, Technical University, Budapest, 1968).
7. Del Re, G.: J. Chem. Soc. **1958,** 4034.
8. Streitwieser, A.: Molecular Orbital Theory for Organic Chemists. J. Wiley and Sons Inc., New York—London, 1962.
9. Nagy, J., Réffy, J., Kuszmann-Borbély, A., Pálossy-Becker, K.: J. Organomet. Chem. **7,** 393 (1967).
10. Nagy, J., Réffy, J.: Paper presented at the Bordeaux Congress, 1968.
11. Pálossy-Becker, K.: Physical-chemical Investigations with Allyl-ethoxysilanes. (In Hungarian) Thesis (1966).
12. Svirbely, W. T., London, J. J.: J. Am. Chem. Soc. **70,** 4121 (1948).
13. Eyring, J.: Phys. Rev. **39,** 746 (1932).
14. Nagy, J., Ferenczi-Gresz,S., Mironov, V. F.: Acta Chim. Acad. Sci. Hung. **47,** 191 (1966)

József Nagy
József Réffy
Pál Éliás
Budapest XI., Gellért tér 4.

Acta Chimica Academiae Scientiarum Hungaricae, Tomus 63 (4), pp. 417—423 (1970)

ON THE IR AND NMR SPECTRA OF THE $[(CH_3)_2N]_2S$, $[(CH_3)_2N]_2SO$, $[(CH_3)_2N]_2SO_2$ AND $(CH_3)_2NSO_2Cl$ MOLECULES

F. Török, E. Páldi, S. Dobos and G. Fogarasi

(Research Group for Inorganic Chemistry of the Hungarian Academy of Sciences, Institute for General and Inorganic Chemistry of the L. Eötvös University, Budapest)

Received January 30, 1969

Infrared and NMR spectra of $[(CH_3)_2N]_2S$, $[(CH_3)_2N]_2SO$, $[(CH_3)_2N]_2SO_2$ and $(CH_3)_2NSO_2Cl$ have been recorded. In the infrared spectra, the S—N bond frequency was found to be higher and the C—N symmetric stretching frequency lower than expected. On the basis of the spectra, for the p—d bond strength the following order can be given:

$$[(CH_3)_2N]_2SO < [(CH_3)_2N]_2SO_2 < (CH_3)_2NSO_2Cl$$

Neither the IR nor the NMR spectra of $[(CH_3)_2N]_2S$ fit into the order expected for the spectral data of the compounds investigated.

Introduction

The stretching frequency of S—N bond may vary within very wide limits: from 620 to 1690 cm^{-1} [1]. This can be explained partly by the possible formation of a $d\pi - p\pi$ bond between the lone electron pair of N and the empty d orbitals of the S atom [2].

The primary object of our investigations was to study the S—N bonds of the compounds listed above.

Out of the compounds investigated, the infrared spectrum of $(CH_3)_2NSO_2Cl$ is reported in the literature [3, 4]. In our investigations, the spectrum of this compound has been recorded for a broader region of wave number, than published in literature, and the spectrum is discussed in the knowledge of the spectra of the other analogue compounds.

Preparation of the compounds

Sulfinyldimethylamide and thiodimethyldiamide were prepared as described in the publications [5] and [6, 7], respectively, involving the following reactions:

$$4(CH_3)_2NH + SOCl_2 \xrightarrow[\text{ether}]{-78°C} [(CH_3)_2N]_2SO + 2(CH_3)_2NH.HCl$$

$$4(CH_3)_2NH + SCl_2 \xrightarrow[\text{ether}]{-78°C} [(CH_3)_2N]_2S + 2(CH_3)_2NH.HCl.$$

The boiling points of the compounds were the same as reported in the literature. Melting points of the products were 31°C and 20°C, respectively. To obtain a better yield and to eliminate side reactions resulting in the formation of di- and trithiodimethyldiamide derivatives, the compounds were prepared at —78°C instead of 0°C, recommended in literature, and on the other hand, the system was allowed slowly to attain, in 18—24 hours, room temperature after the termination of the reaction. To meet the requirements for purity necessary in our investigations, the products were subjected to vacuum sublimation.

Dimethylamidosulfonyl chloride has been prepared by different ways [8, 9]:

$$(CH_3)_2NH.HCl + SO_2Cl_2 \xrightarrow{60°C} (CH_3)_2NSO_2Cl + 2\ HCl$$

$$2(CH_3)_2NH + SO_2Cl_2 \xrightarrow[ether]{-78°C} (CH_3)_2NSO_2Cl + (CH_3)_2NH.HCl$$

Physical constants were the same as those given in the literature, and vacuum distillation yielded a product of satisfactory purity.

Sulfonyldimethyldiamide was prepared according to the following reactions [8]:

$$2(CH_3)_2NSO_2Cl + Zn \xrightarrow[25°C]{HCl} [(CH_3)_2N]_2SO_2 + ZnCl_2 + SO_2$$

$$(CH_3)_2NSO_2Cl + 2(CH_3)_2NH \xrightarrow[ether]{-78°C} [(CH_3)_2N]_2SO_2 + (CH_3)_2NH.HCl$$

The latter reaction proceeds at a considerably higher rate, and higher yields were obtained. After recrystallization from ethyl alcohol, the end product was purified by vacuum sublimation.

The purity of the compounds was checked by gas chromatography.

Infrared spectrum of the compounds

Infrared spectra were recorded with a Perkin—Elmer Model 225 instrument, in case of $[(CH_3)_2N]_2SO_2$ on a solution of the compound in carbon tetrachloride and dioxane, respectively, while in those of the other compounds on a liquid film.

Spectra of the compounds examined are shown in Fig. 1, in the wave number region from 200 to 1500 cm^{-1}. Owing to several identical bonds and groups involved, the spectra show many similar characteristics. Thus, a strong absorption can be observed near the wave numbers 650 cm^{-1} and 950 cm^{-1}. These bands correspond to the C—N and S—N stretching frequencies, respectively. An assignment is made difficult by the fact that the wave number of

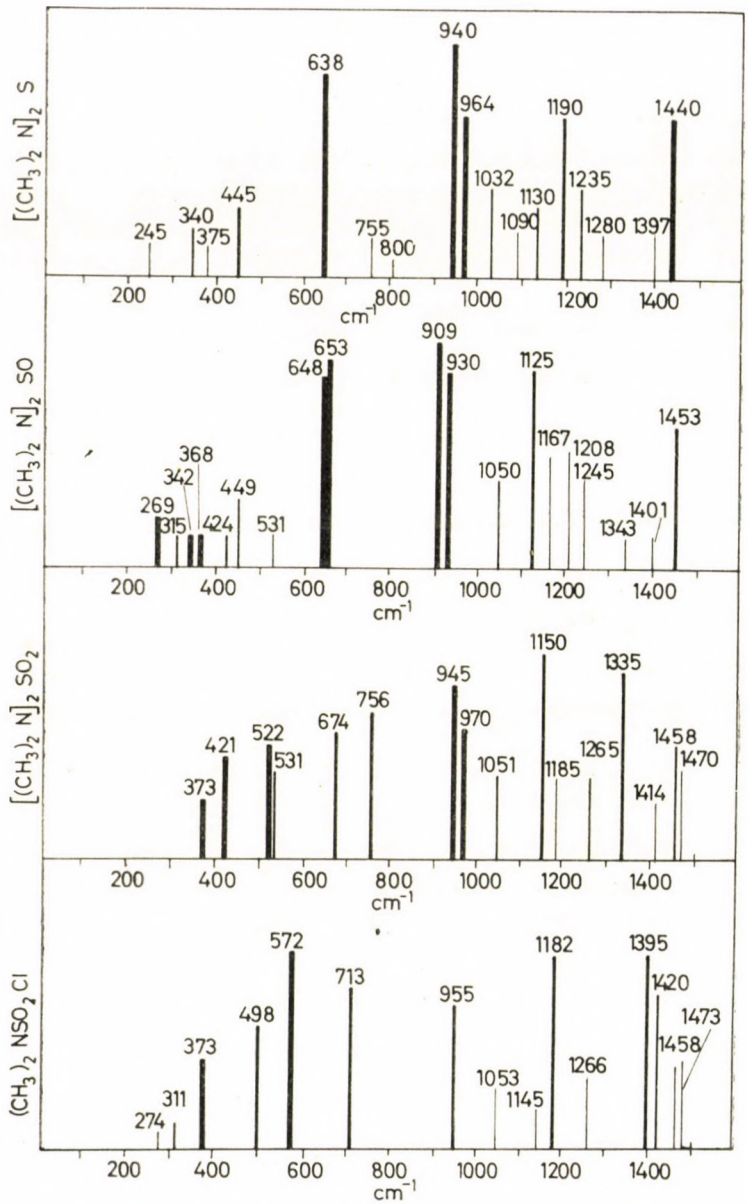

Fig. 1

the vibration observed at 650 cm^{-1} is too low to be considered as the symmetric stretching frequency of either the S—N or the C—N bonds. The symmetric stretching frequency of C—N bonds may also vary within wide limits. With dimethylamine, this vibration appears at 928 cm^{-1} [10]. It can be observed that ν_sCN diminishes, when electron attracting groups are linked to the tri-

methylamine group. Thus, for $(CH_3)_3NSO_3$ a value of 799 cm^{-1} was found [11], while for $(CH_3)_3NO$ a value of 757 cm^{-1} [12]. When the lone electron pair of N participates to a considerable degree in the formation of the bond, as for example in the case of $(CH_3)_3NBH_3$, the frequency may diminish to a wave number of 667 cm^{-1} [11]. However, it seems improbable that the lone electron pair of N has a role of this importance in the formation of the bonds in the compounds investigated by us.

As has been pointed out already in the introductory part, also the stretching frequency of S—N may vary within wide limits. The higher the electron attracting effect of the groups attached to S is, the more pronounced will be the double bond character, and the higher the frequency of the S—N bond [13]. Naturally, the double bond character is reflected also by the length of the S—N bond. Based on known S—N stretching frequencies and equilibrium distances of several compounds, BANISTER, MOORE and PADLEY give an empirical relationship between the two values [1]. Out of the compounds investigated, the electron configuration, determined by X-ray diffraction, has been published for $(CH_3)_2NSO_2Cl$ and for $[(CH_3)_2N]_2SO$ [14, 15]. The length of the S—N bond was found to be in these compounds 1.69 Å. Similarly, a length of 1.69 Å was found for the distance of the S—N bond in $[(CH_3)_2N]_2S$ [17]. In case of solid $[(CH_3)_2N]_2SO_2$, X-ray diffraction yielded for this distance 1.623 Å [16]. The distance of the S—N bond, determined by electron diffraction on the same compound in the gaseous state is greater, having a value of 1.65 Å [17]. An application of the empirical relationship between the bond length and the stretching frequency of the bond, mentioned above [1], 1.70 Å correspond to 803 cm^{-1}, and 1.62 Å to 926 cm^{-1}. In view of this, the stretching frequency of wave number 950 cm^{-1}, determined in solution or in liquid phase, appears to be too high. According to our approximate calculations, a deviation of this magnitude of the two frequencies from the usual values cannot be explained by a mechanical coupling of the vibrations.

Notwithstanding this, in Table I the vibration of higher wave number has been assigned to the S—N symmetric vibration, and that of lower wave number to the C—N bond. MØLLENDAL, GRUNDNES and KLABOE proceeded in the same way in case of $(CH_3)_2NSO(CH_3)$ and $(CH_3)_2NSO_2(CH_3)$: these having structures similar to our molecules [18]. It should be mentioned in connection with the C—N bond frequencies that, on the one hand, the frequency near the wave number 1050 cm^{-1} has been assigned to the asymmetric stretching frequency and, on the other hand, that the spectrum of the $[(CH_3)_2N]_2SO_2$ molecule is different from those of the other molecules, as it exhibits besides the 674 cm^{-1} band also an absorption band at 758 cm^{-1}.

The frequencies of the SO_2 and SO groups are also shifted towards higher wave numbers, when electron attracting groups are attached to S [20, 25]. S—O stretching frequencies measured by us are lower than those measured

for the SO_2F_2 molecule (1502, 1269) or for the SO_2Cl_2 molecule (1414, 1182), but are higher than the corresponding frequencies of $(CH_3)_2NSO_2CH_3$ (1328, 1150) [18]. The S—O stretching frequencies show a similar change in case of the SOF_2, $SOCl_2$, $[(CH_3)_2N]_2SO$ and $(CH_3)_2NSOCH_3$ molecules, with values of 1308 cm^{-1}, 1229 cm^{-1}, 1125 cm^{-1} and 1070 cm^{-1}, respectively.

Table I

Assignment of some stretching vibrations

	$[(CH_3)_2N]_2S$	$[(CH_3)_2N]_2SO$	$[(CH_3)_2N]_2SO_2$	$(CH_3)_2SO_2Cl$
ν_sS—N	940	909	945	955
ν_{as}S—N	964	930	970	—
ν_sC—N	683	646, 653	674, 758	713
ν_{as}C—N	1032	1050	1051	1053
ν_sS—O	—	1125	1150	1182
ν_{as}S—O	—	—	1335	1395

Neither is the assignment of deformation vibrations free of problems. The spectrum of each compound containing an N—S—N group exhibited an absorption band near 440 cm^{-1}. In view of the relatively great mass of the atomic nuclei, this frequency seems to be too high. The deformation vibration of the C—N—C angle appears at 340 cm^{-1}, similarly as in the case of compounds containing other dimethylamine groups. Absorption bands observed in the spectrum of $[(CH_3)_2N]_2SO_2$ at 522 cm^{-1} and 530 cm^{-1}, and in the spectrum of $(CH_3)_2NSO_2Cl$ at 572 cm^{-1} can be ascribed to the deformation vibration of the SO_2 group. In the case of the latter compound, the band exhibited at 498 cm^{-1} is assigned to the stretching frequency of the S—Cl bond.

The symmetric stretching frequencies of the C—H bond are also indicative of the participation of the lone electron pair of the dimethylamine group in the formation of the bond [21]. If the lone electron pair of N participates in the bond, the frequency of the C—H bond shifts towards higher values. For the compounds investigated by us, 4—5 overlapping bands were found in the wave number region corresponding to the stretching of the C—H bond. All these bands are shifted in the investigated compounds in the following order:

$$[(CH_3)_2N]_2SO < [(CH_3)_2N]_2S < [(CH_3)_2N]_2SO_2 < (CH_3)_2NSO_2Cl.$$

Concerning the development of $p_\pi - d_\pi$ bond, a study of the infrared spectra yielded in general the expected pattern: the $p_\pi - d_\pi$ bond is most pronounced in the case of $(CH_3)_2SO_2Cl$ and $[(CH_3)_2N]_2SO_2$ molecules, and less distinct in the case of $[(CH_3)_2N]_2SO$, while it is somewhat remarkable that we found the $[(CH_3)_2N]_2S$ molecule to fall between these two extreme po-

sitions. This is the more remarkable, as the order of stability of the complexes of the compounds investigated formed with BF_3, where BF_3 is attached through the lone electron pair of N, is as follows [19]:

$$[(CH_3)_2N]_2S > [(CH_3)_2N]_2SO > [(CH_3)_2N]_2SO_2.$$

The NMR spectra of the compounds

NMR spectra were recorded with a Zeiss Model ZKR-60 apparatus at a frequency of 60 Mc, in CCl_4 solutions, with TMS as internal standard. The spectrum of all the four compounds consisted of a single sharp band. There was no possibility to undertake measurements at low temperatures. Also in case of compounds of a certain similarity, such as N-methylsulfineamides [22] and S-yields [23], the two methyl groups linked to N (or to S) were represented even at as low temperature as —60°C by a single signal. This phenomenon can be attributed to the fact that, owing to the shape of the *d* orbitals, even when the $p_\pi - d_\pi$ bond has formed, no hindered rotation is to be expected about the S—N bond.

In Table II, the values of the chemical shifts for the compounds investigated by us are given. For comparison, data available in literature for sulfides, sulfoxides and sulfons have been summarized in Table III [24]. It will be noticed that in case of these latter compounds the change in chemical shift proceeds parallel to the electron attracting effect of the groups attached to S. In our compounds this tendency is shown only at the SO, SO_2 and

Table II

Chemical shifts in τ units of the compounds investigated, measured in CCl_4 *at 60 Mc*

$[(CH_3)_2N]_2S$	$[(CH_3)_2N]_2SO$	$[(CH_3)_2N]_2SO_2$	$(CH_3)_2NSO_2Cl$
7.05	7.46	7.26	7.00

Table III

Chemical shifts in τ units of R—X—R' molecules measured in CCl_4 *at 56.4 Mc* [24]

	X = S	X = SO	X = SO_2
R = CH_3, R' = CH_3	7.94	7.49	7.15
R = CH_3, R' = C_2H_5 (CH_3 signal)	8.76	8.71	8.62

SO_2Cl derivatives, while the S derivative exhibits a remarkably large shift. Thus, neither the IR nor the NMR spectrum of $[(CH_3)_2N]_2S$ fits into the expected order of the spectral data of the compounds investigated.

REFERENCES

1. BANISTER, A. J., MOORE, L. F., PADLEY, L. S.: Spectrochim. Acta **23A**, 2705 (1967).
2. GLEMSER, O., MÜLLER, A., BÖHLER, D., KREBS, B.: Z. anorg. allg. Chem. **357**, 184 (1968).
3. MERIAN, E.: Helv. Chim. Acta **43**, 1122 (1960).
4. SCHNEIDER, W., KESSLER, G., LEHMANN, H. A.: Z. anorg. allg. Chem. **356**, 239 (1968).
5. MICHALEIS, A., LUXEMBURG, K.: Ber. **28**, 165 (1895).
6. BLAKE, E. S.: J. Am. Chem. Soc. **65**, 1267 (1943).
7. LEVCHENKO, E. S., SHEINKMAN, I. E., KIRSANOV, A. V.: Zh. Obsh. Khim. **33**, 3068 (1953).
8. BEHREND, R.: Annales **222**, 133 (1884).
9. BINKLEY, W. N., DEGERING, E. F.: J. Am. Chem. Soc. **61**, 3250 (1939).
10. PERCHARD, J., FOREL, M., JOSIEN, M.: J. Chim. Phys. **61**, 652 (1964).
11. WATARI, F.: Z. anorg. allg. Chem. **332**, 322 (1964).
12. GIGUERE, P. A., CHIN, D.: Can. J. Chem. **39**, 1214 (1961).
13. KHARASCH, N.: Organic Sulfur Compounds. Pergamon Press, 1961.
14. VILKOV, L. V., HARGITTAI, I.: Acta Chim. Acad. Sci. Hung. **52**, 423 (1967).
15. HARGITTAI, I., VILKOV, L. V.: Acta Chim. Acad. Sci. Hung. (in press).
16. JORDAN, T., SMITH, H. W., LOHR, L. L., LIPSCOMB, W. N.: J. Am. Chem. Soc. **85**, 846 (1963).
17. HARGITTAI, I.: Acta Chim. Acad. Sci. Hung. (under publication).
18. MØLLENDAL, H., GRUNDNES, J., KLABOE, P.: Spectrochim. Acta **24A**, 1669 (1968).
19. BURG, A. B., WOODROW, H. W.: J. Am. Chem. Soc. **76**, 219 (1954).
20. LINDBERG, J. B.: Acta Chem. Scand. **21**, 841 (1967).
21. DABROWSKY, J., KAMIENSKA-TRELA, K.: Bull. Acad. Polon. Sci. Ser. Chim. **15**, 587 (1967).
22. MORIARTY, R. M.: Tetrahedron Letters **509** (1964).
23. RATTS, K. W.: Tetrahedron Letters **4707** (1964).
24. TADDEI, F., ZAULI, C.: Nuclear Magnetic Resonance in Chemistry, Proc. Symp. Cagliari, Italy, 1964. Publ. 1965, Academic Press, New York, London, pp. 179—184.
25. BUTCHER, F. K. CHARALAMBOUS, J., FRAZER, M. J., GERARADR, W.: Spectrochim. Acta **23A**, 2399 (1967).

Ferenc TÖRÖK
Emil PÁLDI
Sándor DOBOS
Géza FOGARASI

Budapest VIII., Múzeum krt. 6—8.

Acta Chimica Academiae Scientiarum Hungaricae, Tomus 63 (4), pp. 425—435 (1970)

INCLUSION COMPOUNDS OF DEOXYCHOLIC ACID WITH AROMATIC SOLVENTS

Z. Csűrös, Gy. Deák and M. Novák-Kiss

(Department of Organic Chemical Technology, Technical University, Budapest)

Received September 27, 1968

Inclusion compounds have been prepared from deoxycholic acid, examined by thin-layer chromatographically and found to be free of fatty acids (m.p. 174°C), using various aromatic solvents (benzene and nine other liquid substituted benzene derivatives) as the guest components. The compositions of the inclusion complexes were determined by UV spectrophotometry. It has been found that with an increase in the amount of the guest component during preparation, the host to guest molar ratio approaches 2 : 1 but it never reaches that value, even if a large excess of the aromatic compound is used.

If two guest components are employed simultaneously, mixed inclusion compounds are obtained. The host to guest molar ratio depends on the ratio of the solvents applied, and on the relative stabilities of the particular inclusion compounds. The term "relative stability" has been defined to characterize the affinity, under identical conditions, of deoxycholic acid towards the two competing guest components. The stability of the inclusion compounds depends, *inter alia*, on the molecular size and dipole moment of the guest component.

There are contradictory data in the literature concerning the melting point of the long-known deoxycholic acid (3α, 12α-dihydroxycholanic acid, Fig. 1). For example, the melting point of deoxycholic acid samples, obtained

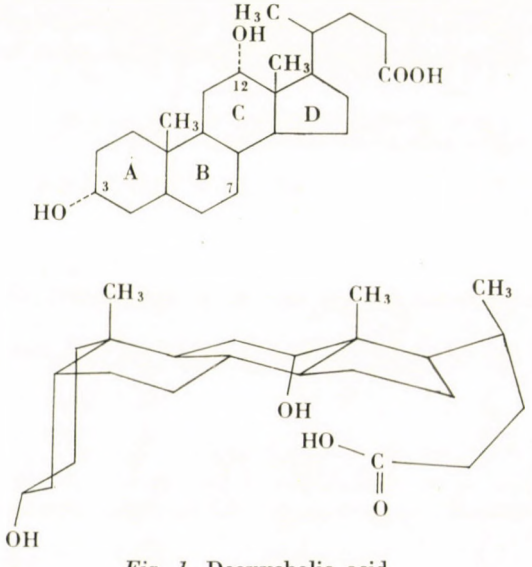

Fig. 1. Deoxycholic acid

in different ways, was reported to be 173—175°C by SIFFERD [1], 176—177°C by WIELAND [2] and REICHSTEIN [3], 190°C by CHARONNAT and GAUTHIER [4], and 189°C by PATTERSON [5]. Examination of comercially available A.R. and pss. grade deoxycholic acid samples in the authors' laboratory led to similar results.

In order to clarify this problem, the various procedures used for the preparation of deoxycholic acid [1, 5, 6, 7] were reproduced and the obtained samples, as well as a number of commercially available substances subjected to thin-layer chromatography. It was found that homogeneous, chromatographically pure deoxycholic acid melts at 174°C, while all samples of higher melting point contained fatty acid.

As known [7], deoxycholic acid is obtained from bile by means of a complex purification procedure. The greatest difficulties are encountered in the removal of fatty acids, with which deoxycholic acid gives well-known, stable inclusion compounds [8]. Simple recrystallization fails to be effective in separating the two components. All procedures which have successfully been applied for the removal of fatty acids are based on the selective extraction of the fatty acid content with some aromatic solvent (*e.g.*, benzene, xylene), when the aromatic component enters the inclusion compound to replace the fatty acid molecule. This new, transformed deoxycholic acid inclusion compound can be decomposed more easily.

Reproducing the described procedures, it was found in the authors' laboratory that xylene is significantly superior to benzene in the selective extraction of fatty acids, presumably because of the preference with which deoxycholic acid forms an inclusion compound with the former solvent.

A survey of the literature of deoxycholic acid inclusion compounds gave, however, no reference to any difference in the formation of various inclusion compounds, or to the factors on which such differences would depend.

In order to find the most suitable solvent for the removal of fatty acid content, it is necessary to learn the tendency of deoxycholic acid for the formation of inclusion compounds with different solvents.

Therefore, we decided to study the factors which influence, and the way how, the formation of inclusion compounds of deoxycholic acid with aromatic solvents. Inclusion compounds of deoxycholic acid were prepared with a number of liquid benzene derivatives available in our laboratory. Deoxycholic acid free of any inclusion impurity was refluxed in a ten-fold excess of the component investigated with the simultaneous addition of small portions of methanol until the complete dissolution of the former. The solution was refluxed for a further hour and the silky needles deposited on cooling from the filtered solution were collected and washed with some methanol. The melting points and compositions of the inclusion compounds were determined. Several methods have been employed for the determination of the molar ratio

of deoxycholic acid to the guest component aromatic compound. Alkaline titration made possible the determination of the deoxycholic acid content of the inclusion compound. Whenever it was possible, the functional group of the aromatic partner was determined. Spectrophotometric determination of the absorption of the aromatic component in the ultraviolet region proved to be the most suitable method. This technique was also effective in the structure determination of mixed inclusion compounds to be described later.

The characteristic data of the inclusion compounds are summarized in Table I.

On the basis of the data of Table I the following conclusions may be drawn:

1. In many cases the melting point of the inclusion compound is higher than that of deoxycholic acid. These derivatives melt at their elevated melting point without decomposition.

2. In each inclusion compound 2 moles of deoxycholic acid is accompanied by approximately 1 mole of the guest component, but this value is somewhat less than 1 mole in all cases. On repetition of the preparation of the inclusion compound under identical conditions, the molar ratio remains unchanged.

As it is known from the literature [9], the deoxycholic acid molecule, owing to the *cis* fusion of its A/B rings, possesses an arched architecture and the connection of two molecules by hydrogen bonds gives hollow space inside the crystal.

Table I

Inclusion compounds containing a single guest component

Guest component	Host to guest molar ratio on the basis of		
	determination of deoxycholic acid	UV determination of the guest component	M.p., °C*
Benzene	2 : 0.564	2 : 0.566	162—170
Toluene	2 : 0.890	2 : 0.892	171—175
Ethylbenzene	2 : 0.868	2 : 0.866	170—172
m-Xylene	2 : 0.896	2 : 0.926	176—179
Bromobenzene	2 : 0.982	2 : 0.974	174—176
Chlorobenzene	2 : 0.808	2 : 0.818	169—171
Anisole	2 : 1.001	2 : 0.998	169—173
Benzaldehyde	2 : 0.906	2 : 0.906	164—167
Nitrobenzene	2 : 0.896	2 : 0.918	169—172
Phenylacetonitrile	2 : 0.850	2 : 0.854	162—165

* The inclusion-free pure deoxycholic acid melted at 173—174°C.

Deoxycholic acid crystallizes from solutions with this structure, and apart from a few exceptions (*e.g.* methanol) the adduct encloses one molecule of the solvent, as far as the solvent molecule finds room in the cavity.

In such cases the inclusion compound has the stoichiometric ratio of the components 2 : 1. All inclusion compounds prepared in the present work fall in this class, therefore the case when the solvent molecule finds no room in the cavity formed by the two connected deoxycholic acid molecules will not be considered.

The types of inclusion complexes in which one of the components contains the other enclosed in the inside of itself, are called clathrates [10]. The inclusion compound is schematically shown in Fig. 2.

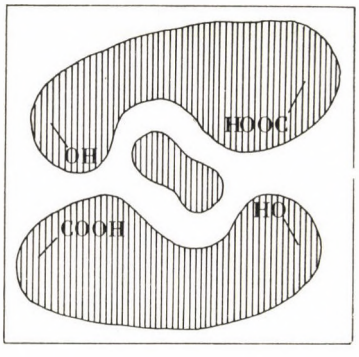

Fig. 2. Schematic structure of deoxycholic acid inclusion compounds

However, connection of two molecules of deoxycholic acid may also occur without the formation of an inclusion complex. The IR spectrum of deoxycholic acid crystallized from methanol shows no band characteristic of a free OH group, indicating that the molecules are linked to each other with hydrogen bonds in the pure deoxycholic acid crystal, too.

Hence, if the formation of the inclusion complexes is accompanied by the connection of deoxycholic acid molecules containing no guest component, the crystalline product will contain both inclusion-containing and inclusion-free deoxycholic acid dimers. Any kind of determination of the composition will give the total amount of deoxycholic acid present in both types of units, therefore the guest to host molar ratio will be somewhat lower than stoichiometric. The more complete the formation of the inclusion compound, the more close is the proportion of the two components to the stoichiometric ratio.

Since the two processes occur simultaneously, an excess of the guest component in the reaction mixture, used also as the solvent, has a decisive role. The higher the ratio of guest to host is in the solution, the more complete is the formation of the inclusion compound, as in this case the connection of two

molecules of deoxycholic acid without enclosing a solvent molecule is less probable.

Table II shows the results of experiments in which the effect of excess toluene upon extent of formation of the inclusion compound was studied.

When deoxycholic acid is crystallized from a two-component (binary)

Table II

Effect of the relative amount of the guest component upon the composition of the inclusion compound

Toluene (moles)	deoxycholic acid (moles)
During preparation	In the crystal
11 : 1	0.900 : 2
19 : 1	0.915 : 2
30 : 1	0.936 : 2
43 : 1	0.963 : 2
59 : 1	0.969 : 2

solvent mixture, the two types of solvent molecules will compete for inclusion compound formation, and two kinds of inclusion complexes will be obtained. The process can be represented analogously to the case of an equilibrium reaction:

$$[DC - S_I] + [S_{II}] \rightleftharpoons [DC - S_{II}] + [S_I]$$

where [DC — S] denotes the concentration of the inclusion compound and [S] that of the solvent. The ratio of the two types of inclusion compounds depends, on the one hand, upon the relative amounts of the solvents present and, on the other, upon the relative stabilities of the inclusion adducts. The term "relative stability" has been defined to characterize the affinity of deoxycholic acid under identical conditions to the two guest components.

The above equilibrium means, at the same time, that a given inclusion compound can be converted into another one by refluxing it in a suitable solvent. The new component, being present in higher excess, replaces the original solvent molecule in a degree determined by the molar ratio of the competing solvent to the original one and the relative stabilities of the two inclusion compounds. Such conversions of inclusion compounds were carried out in the present work, using benzene, toluene and xylene. The entering solvent was applied in 10 : 1 molar proportion to the original solvent. The results are summarized in Table III.

While toluene and xylene extrude benzene practically completely from the inclusion compound, in the reverse reactions, despite the large excess of benzene, about 50% of the original inclusion compound remains unchanged.

Table III

Conversion of deoxycholic acid inclusion compounds by replacement of the guest component

In the starting inclusion compound		In the transformed inclusion compound			
Starting guest component	Molar ratio to deoxycholic acid	New guest component	Molar ratio	Starting guest component	Molar ratio
Benzene	2 : 0.74	Toluene	2 : 0.99	Benzene	2 : 0.005
		m-Xylene	2 : 0.985		2 : 0.010
Toluene	2 : 0.970	Benzene	2 : 0.412	Toluene	2 : 0.336
		m-Xylene	2 : 0.013		2 : 0.945
m-Xylene	2 : 0.985	Benzene	2 : 0.415	Xylene	2 : 0.560
		Toluene	2 : 0.80		2 : 0.196

Table IV

Composition of inclusion compounds containing two guest components

Components	Molar ratio of host to guest
DC–benzene–*toluene*	2 : 0.166 : 0.810
DC–benzene–*m–xylene*	2 : 0.128 : 0.850
DC–toluene–*m–xylene*	2 : 0.371 : 0.570
DC–benzene–*benzyl cyanide*	2 : 0.109 : 0.536*
DC–phenylacetonitrile–*nitrobenzene*	2 : 0.102 : 0.768
DC–phenylacetonitrile–*xylene*	2 : 0.270 : 0.730*
DC–phenylacetonitrile–*anisole*	2 : 0.000 : 0.960*
DC–phenylacetonitrile–*benzaldehyde*	2 : 0.220 : 0.736*
DC–phenylacetonitrile–*chlorobenzene*	2 : 0.220 : 0.536*
DC–chlorobenzene–*toluene*	2 : 0.448 : 0.552
DC–nitrobenzene–*chlorobenzene*	2 : 0.318 : 0.408*
DC–nitrobenzene–*m–xylene*	2 : 0.204 : 0.638*
DC–nitrobenzene–*bromobenzene*	2 : 0.280 : 0.520*
DC–benzaldehyde–*nitrobenzene*	2 : 0.470 : 0.504
DC–benzaldehyde–*bromobenzene*	2 : 0.171 : 0.782
DC–benzaldehyde–*m–xylene*	2 : 0.120 : 0.632
DC–benzaldehyde–*anisole*	2 : 0.080 : 0.876
DC–*m*–xylene–*anisole*	2 : 0.444 : 0.592
DC–bromobenzene–*m–xylene*	2 : 0.214 : 0.624*
DC–bromobenzene–*anisole*	2 : 0.230 : 0.642
DC–toluene–*bromobenzene*	2 : 0.432 : 0.496*

If the two guest components are applied in the same molar proportion, the inclusion compound having higher stability will be formed predominantly. Hence, determination of the proportion of the two inclusion compounds formed in solvent pairs of equal molar ratio makes possible to determine the relative stabilities of the respective inclusion compounds.

The composition of the prepared mixed inclusion adducts is shown in Table IV. These mixed inclusion compounds were prepared under analogous conditions to those of the compounds, the common proportion of the solvent mixture to deoxycholic acid being 30 : 1, *i.e.* 15 : 1 and 15:1 for either solvent. In Table IV the more stable component is shown in italics and the method of determination is also indicated.

As it has been mentioned, the UV photometric technique is suitable for the simultaneous determination of two aromatic components in a mixture, but exact results can only be obtained if the molar extinction coefficients of the two components are of comparable order of magnitude.

In the cases where inaccuracy of the measurements rendered the result unreliable, functional group determinations were also carried out, but this method, too, furnished approximative data only. These determinations are marked with an asterisk in the Table and are unsuitable for numerical evaluation.

The numerical evaluation was done by dividing the amounts of the two aromatic components present in the mixed inclusion compound by each other. The result has been termed relative stability constant, and the component appearing in the denominator is the basis of reference. For inclusion compounds in which one of the aromatic component is common, the stability constant may be calculated based on this common component, and thus an order of the stabilities can be established. Table V shows these stability coefficients and the order of the stabilities.

The inclusion compounds containing one aromatic component were subjected to derivatographic analysis. The composition of the inclusion compound was calculated from the TG weight loss curve of the derivatogram, while the melting point was determined from the DTA curve. These results are summarized in Table VI. The composition of the inclusion compounds determined by the UV spectrophotometric technique and the melting point values determined earlier are also included.

From Table VI it can be seen that according to the composition values calculated from the derivatogram in the usual way, the relative amount of the aromatic component is somewhat smaller than the values obtained by UV spectrophotometry. The melting point values shown by the derivatogram differ from each other from one guest component to the other, and the decrease of the melting points reveals an identical tendency with the stability order established in the foregoing.

Table V

Stability constants calculated from the compositions of inclusion compounds containing two guest components

Basis of reference	Component referred to	Stability constant	Order of stability
Benzaldehyde	Phenylacetonitrile	0.33	PhA < BA < NO_2 < Br < X < An
	Nitrobenzene	1.07	
	Bromobenzene	4.57	
	m-Xylene	5.23	
	Anisole	22.0	
Toluene	Benzene	0.206	B < K < T < X
	Chlorobenzene	0.81	
	m–Xylene	1.53	
Anisole	Phenylacetonitrile	0	PhA < BA < Br < X < An
	Benzaldehyde	0.091	
	Bromobenzene	0.36	
	m–Xylene	0.75	
Nitrobenzene	Phenylacetonitrile	0.133	PhA < BA < NO_2
	Benzaldehyde	0.93	
Phenylacetonitrile	Anisole	∞	PhA < BA < NO_2 < An
	Nitrobenzene	7.5	
	Benzaldehyde	3.3	

Table VI

Derivatographically determined compositions and melting points of deoxycholic acid inclusion compounds

Guest component	Composition of the inclusion compound as determined by		M.p., °C	
	UV	deriv.	Measured*	Deriv.
Anisole	1 : 0.499	1 : 0.48	169–173	175
m–Xylene	1 : 0.463	1 : 0.39	176–179	174
Bromobenzene	1 : 0.49	1 : 0.46	174–176	172
Benzene	1 : 0.28	1 : 0.19	168–170	171.5
Toluene	1 : 0.396	1 : 0.33	171–175	170.5
Nitrobenzene	1 : 0.48	1 : 0.40	168–171	169
Ethylbenzene	1 : 0.43	1 : 0.37	170–172	166
Chlorobenzene	1 : 0.40	1 : 0.38	169–171	166
Benzaldehyde	1 : 0.45	1 : 0.35	164–167	160
Phenylacetonitrile	1 : 0.42	1 : 0.43	162–165	159

* The melting points were determined with a Büchi—Tottoli apparatus.

Further, it was attempted to find some explanation for the different stabilities of the inclusion compounds. The characteristic features of the enclosed aromatic guest component were considered, and the change of stability with a change in these features was analyzed.

The examined characteristic properties of the compounds are listed in Table VII.

On the basis of the data in Table VII it can be assumed that the stability of the inclusion compounds is influenced by the size of the enclosed aromatic molecule.

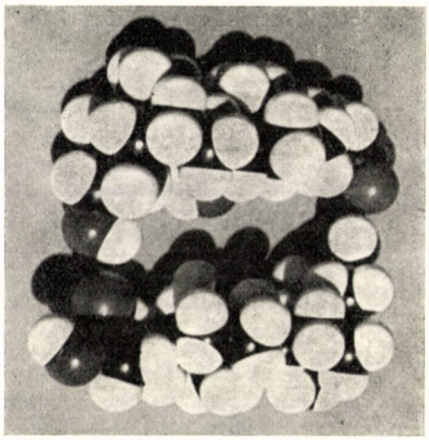

Fig. 3. Model of the inclusion-forming deoxycholic acid molecule pair

The molecular dimensions were measured with the aid of molecular models. The molecular model of the deoxycholic acid molecule pair, the host component of inclusion compound formation, is shown in Fig. 3.

The two molecules of deoxycholic acid, like two cockle shells, fold and enclose the aromatic component which is like a flat disc. The height of the channel or cavity in the "shell" is about 4.5 Å. Whenever a disc-molecule of a height somewhat greater than 4.5 Å is enclosed in the cavity formed by the two deoxycholic acid molecules bound together by hydrogen bonds, the latter will be strained, and will open up easily. In our opinion, this is the factor responsible for the low stability of the inclusion compounds formed with benzaldehyde, phenylacetonitrile and nitrobenzene.

It is also clear from Table VII that the strength of inclusion bonding depends on the dipole moment of the enclosed molecule, too.

The decrease in the dipole moment of anisole $>$ *m*-xylene $>$ toluene $>$ benzene is accompanied by a decrease in the stability of the inclusion compounds made with these guests. This can be explained by the assumption that the dipole-induced dipole interaction part of the secondary van der Waals

Table VII

Some characteristic properties of the guest components

Guest component	Dipole moment	Height of the molecule, Å
Anisole	1.46	4.09
m–Xylene	0.36	3.73
Toluene	0.31	3.73
Benzene	0	2.60
Chlorobenzene	1.23	2.93
Bromobenzene	1.52	3.24
Nitrobenzene	4.69	4.73
Benzaldehyde	2.79	4.24
Phenylacetonitrile		4.68

forces holding together the inclusion complexes play an important role in the formation of the inclusion compound.

However, there are a few interesting facts, which cannot be accounted for by the above considerations. Thus, for instance, the inclusion adduct formed with bromobenzene of higher dipole moment is less stable than those formed with anisole or *m*-xylene of about the same size. Obviously, there are several other factors in addition to those examined by us which play a part in the formation of inclusion compounds.

Experimental

Materials

Deoxycholic acid, Fluka, pss. grade, was used.
The guest components were commercial products purified by distillation.

Preparation of the inclusion compounds

5 g (0.0127 mole) of deoxycholic acid was refluxed in 50 ml of the guest component, and methanol was added in small portions until the mixture became homogeneous. After refluxing for 1 hr., the solution was filtered and slowly cooled. The deposited silky white needles were collected, washed with some ice-cold methanol and dried in air.

Thin-layer chromatographic analyses

The deoxycholic acid samples were chromatographed on thin-layer using a solvent system of petroleum ether–ether–glacial acetic acid (70 : 30 : 2), and the spots were visualized with chromic acid–sulphuric acid.

REFERENCES

1. U. S. Pat. 2.606.912 (Aug. 12, 1952); C. A. **46,** 11593 (1952).
2. WIELAND, H., WEYLAND, P.: Z. physiol. Chem. **110,** 123 (1920).
3. REICHSTEIN, T., SORKIN, M.: Helv. Chim. Acta **25,** 797 (1942).
4. CHARONNAT, R., GAUTHIER, B.: Compt. rend. **223,** 1009 (1946).
5. Brit. Pat. 695,504 (Aug. 12, 1953); C. A. **48,** 1938 (1954).
6. U. S. Pat. 2,661,356 (Dec. 1, 1953); C. A. **48,** 1281 (1954).
7. BIOS Report 142.
8. WIELAND, H., SORGE, H.: Z. physiol. Chem. **97,** 1 (1916).
9. FIESER, L., FIESER, M.: Steroids. Reinhold Publ. Corp., New York, 1959.
10. POWELL, H.: J. Chem. Soc., **1948,** 61.

Zoltán CSŰRÖS
Gyula DEÁK
Magda NOVÁK-KISS

Budapest XI., Műegyetem rkp. 3.

Acta Chimica Academiae Scientiarum Hungaricae, Tomus 63 (4), pp. 437—442 (1970)

UNTERSUCHUNGEN AUF DEM GEBIET DER AROMATISCHEN SULFENYLCHLORIDE, I

DIE REAKTION VON SULFENYLCHLORIDEN MIT ALKYLTHIOSULFATEN UND XANTHOGENATEN

F. KLIVÉNYI, E. VINKLER und A. E. SZABÓ

(Institut für Pharmazeutische Chemie der Medizinischen Universität, Szeged)

Eingegangen am 17. Oktober 1968

Es wurde festgestellt, daß die bei der Reaktion zwischen aromatischen Sulfenylchloriden und Alkylthiosulfaten erwarteten O-Arylsulfenyl-S-alkylthiosulfate in nur kleinen Mengen anfallende, labile Produkte sind, da sie sich unter Schwefeltrioxydverlust in Disulfide umwandeln.

In der Reaktion von Arylsulfenylchloriden mit Xanthogenaten bilden sich mit guter Ausbeute (Alkoxythioformyl)-aryldisulfide. Diese Verbindungen sind gelbe Öle, die chromatographisch gereinigt werden können. Auf Einwirkung von Wärme werden sie zu den entsprechenden Thiophenol- und Olefinderivaten zersetzt, wobei gleichzeitig Carbonylsulfid und Schwefel freigesetzt werden. Die (Alkoxy-thioformyl)-aryldisulfide zeigen eine starke, selektive antimikrobielle Aktivität gegenüber grampositiven Mikroorganismen.

Theoretischer Teil

Zahlreiche Publikationen (z.B. [1] und [2]) befassen sich mit der Untersuchung der Reaktionen von Sulfenylchloriden. Diese Verbindungsgruppe ist durch ihre besondere Reaktionsfähigkeit gekennzeichnet. Wir beschäftigen uns nun schon seit längerer Zeit mit den Reaktionen der Sulfenylchloride und haben unter anderem den Verlauf der Hydrolyse dieser Verbindungen geklärt sowie ihre Reaktionen mit Sulfinsäuren [3, 4].

Als Forsetzung unserer Studien erschien es von Interesse, die Reaktionen der Arylsulfenylchloride **(I)** mit Alkylthiosulfat-**(II)**- und mit aliphatischen Xanthogenat-**(VI)**-Anionen als nukleophile Substrate zu untersuchen. Auf Grund der bekannten Reaktionsbereitschaft der Sulfenylhaloide [2] ist die folgende ionische Primärreaktion zu erwarten:

$$\underset{\textbf{I.}}{Ar-\overset{\overset{\oplus}{\delta}}{S}-\overset{\overset{\ominus}{\delta}}{Hal}} + \overset{\ominus}{Y} \rightarrow Ar-S-Y + \overset{\ominus}{Hal} \qquad (1)$$

$$\overset{\ominus}{Y} = RSSO_2O^-,\ ROC(S)S^-$$

Die zu erwartenden Produkte der Primärreaktion, die O-Arylsulfenyl-S-alkylthiosulfate bzw. die (Alkoxythioformyl)-aryldisulfide sind bisher unbekannte Verbindungen.

I. *Reaktion mit Alkylthiosulfat*

Wenn S-Alkylthiosulfate (»Bunte-Salze«) [5] in einem wasserfreien Lösungsmittel (zweckmäßigerweise in Dioxan) bei Zimmertemperatur mit Arylsulfenylchlorid (**I**) umgesetzt werden, verschwindet alsbald unter schwacher Erwärmung die rote Farbe des Reaktionsgemisches. Aus dem Reaktionsgemisch können zwei einfache Disulfide (**III** und **IV**) sowie Schwefeltrioxid (als Sulfation) isoliert verden:

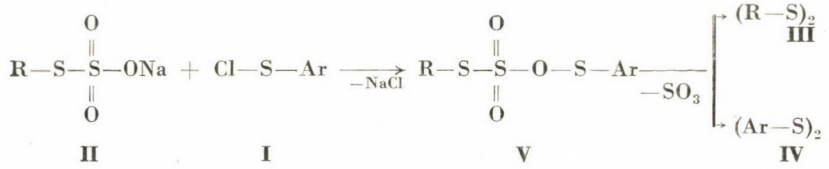

(2)

II **I** **V** **III** **IV**

R = z. B. *n*-Butyl

Ar = *p*-Tolyl

Vermutlich kann die durch die Reaktionsgleichung beschriebene Brutto-Änderung derart gedeutet werden, daß das unter Bildung von Natriumchlorid entstehende Zwischenprodukt (**V**) instabil ist, und schließlich unter Verlust von Schwefeltrioxyd in Form von Disulfiden stabilisiert wird. Im Laufe der Zersetzung der Verbindung **V** kann auch sog. »gemischtes« Disulfid entstehen, welches dann mittels der bekannten Radikal-Spaltung in zwei »einfache« Disulfide umgewandelt werden kann. Dioxan bildet mit dem aus Verbindung **V** sich abspaltenden Schwefeltrioxyd eine Additionsverbindung von bekannter Zusammensetzung [6]. Aus der im Laufe der Aufarbeitung des Reaktionsgemisches gewonnenen wäßrigen Lösung kann das Sulfation fast quantitativ gefällt werden.

Um eine eventuelle Zersetzung während der Destillation zu vermeiden, versuchten wir, das Reaktionsgemisch auch mittels Chromatographie bei Zimmertemperatur aufzuarbeiten. Bei der Elution isolierten wir neben den Disulfiden **III** und **IV** eine kleine Menge von instabilem gelbem Öl, dessen Analyse, auf Grund des Schwefelgehaltes, auf Verbindung **V** gut stimmte. Selbst in kaltem Zustand setzte sich die Verbindung in kurzer Zeit zu den entsprechenden zwei Disulfiden um.

Auf Grund unserer Versuchsergebnisse kann festgestellt werden, daß die O-Arylsulfenyl-S-alkylthiosulfate (**V**) unter solchen Umständen nur kurzlebige Verbindungen sind.

II. *Reaktion mit Xanthogenaten*

Im weiteren studierten wir die Reaktion der Sulfenylchloride mit den Alkalisalzen des O-Esters der Thiokohlensäure (»Xanthogenate«) (**VI**). Der zu erwartende Verbindungstyp, das [Alkoxy-thioformyl]-aryldisulfid (**VII**) ist

nach den uns bisher zugänglich gewordenen Literaturdaten noch unbekannt. Analoge Derivate vom S-Trichlormethylsulfenyl-Typ wurden jedoch von HAWLEY und KITTLESON bereits hergestellt [7]. Diese Verbindungen sind wirksame Insekticide und Fungicide.

Zu unseren Experimenten wurde als eine Komponente das ziemlich stabile *p*-Methylphenyl- bzw. *p*-Chlorophenylsulfenylchlorid gewählt. Die Lösung dieser Verbindungen in wasserfreiem Dioxan wurde mit der Suspension der Xanthogenate (**VIa**, b, c) in Dioxan bei Zimmertemperatur umgesetzt (Gl. 3).

$$\underset{\mathbf{VI}}{RO{-}C(=S){-}SNa} + \underset{\mathbf{I}}{Cl{-}SAr} \xrightarrow[-NaCl]{} \underset{\mathbf{VII}}{RO{-}C(=S){-}S{-}S{-}Ar} \qquad (3)$$

a) R = Cyclohexyl Ar = *p*-Methylphenyl bzw. *p*-Chlorophenyl
b) R = Äthyl Ar = *p*-Methylphenyl bzw. *p*-Chlorophenyl
c) R = Isopropyl Ar = *p*-Methylphenyl

Die Reaktion verläuft in allen fünf Fällen glatt. Die erhaltenen Verbindungen vom Typ **VII** sind Öle von lebhaft gelber Farbe und können selbst in hohem Vakuum nur unter Zersetzung destilliert werden. Im Destillat erscheinen dabei verschiedene schwefelhaltige Zersetzungsprodukte. Für die Reinigung der rohen Produkte erwies sich die chromatographische Methode als geeignet. Auf Einwirkung von Wärme spielt sich im Falle dieser Verbindungen höchstwahrscheinlich die von TSCHUGAEV [8] und dann von SISOEVA [9] beobachtete thermische Zersetzung der Xanthogensäureester ab. Nach diesen Forschern bildet sich durch homolytische *cis*-Elimination unter Ausscheidung von Schwefel das entsprechende Thiophenol- und Olefinderivat sowie Carbonylsulfid (Gl. 4). Jedes dieser Zersetzungsprodukte ist im Destillat der Verbindungen von Typ **VII** nachweisbar.

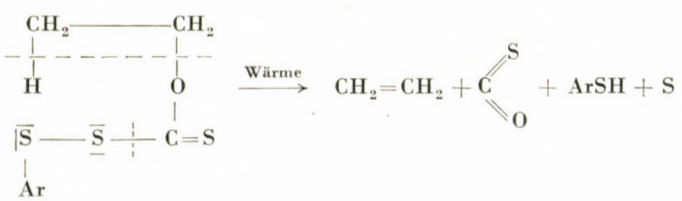

(4)

Nach Untersuchungen von FERENCZY zeigen die hergestellten Xanthogenatsäure-arylthioester (**VII**) gegenüber einigen Mikroorganismen eine starke antimikrobielle Aktivität. Diese Aktivität ist gegenüber grampositiven Erregern, Kokken und Streptomyces-Arten selektiv wirksam. Gramnegativen Arten sowie Hefen- und Fadenpilzen gegenüber erwiesen sich diese Verbindungen als praktisch umwirksam [10].

Experimenteller Teil

(Die Schmelzpunkte sind unkorrigiert)

1. Die Reaktion von n-Butanthiosulfonsäure-Natrium mit p-Methylphenylsulfenylchlorid

Zu einer Suspension von 6,15 g (0,032 m) *n*-butanthiosulfonsaurem Natrium (siehe [11]) in 60 ml absolutem Dioxan wurde unter Rühren bei Zimmertemperatur tropfenweise die Lösung von 4,5 g (0,03 *M*) *p*-Methylphenylsulfenylchlorid in 40 ml absolutem Dioxan zugegeben. Das Reaktionsgemisch erwärmte sich. Nach halbstündigem Rühren wurde das feste Produkt durch Filtrieren getrennt. Das Lösungsmittel wurde bei vermindertem Druck abdestilliert. Das zurückbleibende gelbe, viskose Öl wurde in Äther gelöst und mit Wasser gewaschen, bis die Lösung neutral reagierte (Entfernung der Schwefelsäure). Der Rückstand der über Natriumsulfat getrockneten Ätherlösung wurde im Vakuum fraktioniert. Das übergehende Destillat betrug 0,6 g (18,5%).*

Kp_2: 82—83° n_D^{22}: 1,495

Mit authentischem *n*-Dibutyldisulfid [12] identisch. Der Destillationsrückstand beträgt 3,3 g (74,1%). Aus Methanol umkristallisiert farblose Nadeln.
Fp. 44—45°C Mit authentischem *p,p'*-Ditolyldisulfid [13] identisch.

2. Versuch Nr. **1** wurde unter Kühlung mit Eiswasser wiederholt. Das erhaltene trockene Dioxan-Filtrat wurde in einer mit Silikagel gefüllten Kolonne (90 g Adsorbens, 25 mm Durchmesser) empirisch chromatographiert. Die einzelnen Eluate wurden mittels Dünnschicht-Chromatographie untersucht (Lösungsmittel: *n*-Hexan, Entwickler: alkalische Kaliumpermanganatlösung). Die identische Flecke liefernden Eluate wurden kombiniert. Das Lösungsmittel wurde bei Zimmertemperatur entfernt. Die drei Hautpfraktionen wurden mit Petroläther auf die gleiche Weise noch zweimal chromatographiert, sodann wurde das Lösungsmittel entfernt.

Fraktion Nr. 1**: 0,80 g; n_D^{22}: 1,574; $C_{11}H_{16}O_3S_3$ (276,44)
S ber.: 32,8%
S gef.: 32,2%
Fraktion Nr. 2: 1,30 g; *p,p'*-Ditolyldisulfid (mit dem authentischen Präparat identisch)

Fraktion Nr. 3: 1,90 g; Dibutyldisulfid, $C_8H_{18}S_2$ (178,36)
S ber.: 35,9%
S gef.: 35,9%

3. Die Herstellung der Xanthogensäure-arylthioester

Verfahren: Zu einer Suspension der in der Tabelle angegebenen Menge von Xanthogenat **(VI)** in 50—70 ml wasserfreiem Dioxan wurde tropfenweise unter Rühren die 5%ige Lösung der angegebenen Menge von Arylsulfenylchlorid **(I)** in Dioxan zugegeben. Nach Verschwinden der roten Farbe der Lösung wurde das Reaktionsgemisch noch eine Stunde in einem Wasserbad von 50°C erwärmt. Das ausgeschiedene Salz wurde herausfiltriert und das Lösungsmittel bei vermindertem Druck abdestilliert. Das zurückbleibende viskose, gelbe, ölige Produkt wurde in Äther gelöst, mit Wasser gewaschen und getrocknet. Der lösungsmittelfreie Rückstand wurde in einer kleinen Menge Petroläther gelöst und in einer mit aktivem Silikagel gefüllten Kolonne (90 g Adsorbens) zweimal chromatographiert, wobei durchwegs Petroläther als Eluent verwendet wurde. Die Eluate mit dem gleichen Brechungsindex wurden vereinigt.

* Unter Mitwirkung von Elza Kis.
** Die erste Fraktion ist im Kühlschrank etwa eine Woche beständig. Nach einer Zeit sind nur die **III** und **IV** Disulfide mit Chromatographie nachgewiesen worden.

Tabelle I

Xanthogenat VI g (*M*)	Arylsulfenylchlorid I g (*M*)	Isolierte Substanz VII g (%)	Charakterisierung: Brechungsindex	Analyse: berechnet %	Analyse: gefunden %
R = Cyclohexyl	Ar = *p*-Tolyl			C: 56,3	C: 55,9
9,9	7,9	9,7	n_D^{20} : 1,6282	H: 6,0	H: 5,7
(0.05)	(0,05)	(65,20)		S: 32,2	S: 32,5
				M. Gew. : 298,5	
R = Cyclohexyl	Ar = *p*-Chlor-			C: 48,9	C:48,8
	phenyl	11,8	n_D^{20} : 1,6420	H: 4,7	H: 4,5
9,9	9,05				
(0.05)	(0,05)	(74,2)		M. Gew. : 318,9	
R = Äthyl	Ar = *p*-Tolyl			C: 49,1	C: 49,3
9,46	10,31	14,0	n_D^{20} : 1,6311	H: 4,9	H: 5,2
(0,065)	(0,065)	(88,1)		M. Gew. : 244,3	
R = Äthyl	Ar = *p*-Chlor-			C: 40,8	C: 40,5
	phenyl				
18,7	23,5	23,9	n_D^{20} : 1,6550	H: 3,4	H: 3,5
(0,13)	(0,13)	(75)		M. Gew. : 264,8	
R = Isopropyl*	Ar = *p*-Tolyl			C: 51,1	C: 50,9
8,4	10,6	9,0	n_D^{20} : 1,6438	H: 5,5	H: 4,7
(0,035)	(0,07)	(52,1)		S: 37,2	S: 36,7
				M. Gew. : 258,4	

* Das Ausgangsmaterial war Zinkdiisopropylxanthogenat

4. Thermische Zersetzung von (Äthoxy-thioformyl)-p-tolyldisulfid

Das nach Versuch 3 hergestellte rohe Reaktionsprodukt (5 g) von Äthylxanthogenat (**VIb**) und *p*-Tolylsulfenylchlorid wurde eine Stunde lang in einem Ölbad von 150—160°C gehalten. Die entweichenden Dämpfe wurden durch eine mit Eiswasser gekühlte, verdünnte wäßrige Alkalilauge enthaltende Waschflasche und durch eine Tetrachlorokohlenstoff enthaltende Waschflasche geleitet. Im wäßrigen Teil konnte etwas Schwefelwasserstoff und Kohlendioxyd, im alkalischen Teil viel Alkalisulfid und -carbonat nachgewiesen werden.

Die Tetrachlorkohlenstoff-Lösung wurde mit verdünnter Bromlösung in geringem Überschuß versetzt. Der lösungsmittelfreie Rückstand (0,2 g) ist ein blaßgelbes Öl, welches auf starkes Kühlen kristallisiert.

Brechungsindex n_D^{20}: 1,538 (theoretisch 1,5378) Dibromäthan. Wenn der Rückstand der thermischen Zersetzung einer Wasserdampfdestillation unterworfen wird, destilliert *p*-Thiocresol über (0,5 g). Oxydiert wurde es als Disulfid charakterisiert: Fp.: 44—45°C, *p*-Ditolyldisulfid. Mit dem authentischen Präparat identisch. Der thiocresolfreie Rückstand wurde mit kaltem Petroläther mehrmals verrieben, sodann dekantiert und filtriert (0,30 g).

Aus Benzol umkristallisiert gelbe Plättchen, Fp.: 111—112°C. Mit authentischem elementarem Schwefel identisch.

LITERATUR

1. Organic Sulfur Compounds, Vol. I. S. 375, 377, 394, 396. Ed. N. Kharasch. Pergamon Press 1961, California.
2. Quarterly Reports on Sulfur Chemistry, Vol. I. No. 2. Z. S. ARIYON, A. J. HAVLIK, Ed. N. Kharasch, California, Santa Monica. Intra-Science Research Foundation, California, 1966.
3. VINKLER, E., KLIVÉNYI, F.: Acta Chim. Acad. Sci. Hung. **22,** 345 (1960).
4. KLIVÉNYI, F.: Magy. Kém. Folyóirat, **64,** 121 (1958).
5. BUNTE, H.: Ber. **7,** 646 (1874).
6. SUTER, C. M.: J. Am. Chem. Soc. **68,** 139 (1946).
7. HAWLEY, R. S., KITTLESON, A. R.: Amer. Pat. 2 553 777 (1949) (C. A. **45,** 7742 (1951).
8. TSCHUGAEV, L.: Ber. **32,** 3332 (1899).
9. SISOEVA, N. D.: Uspehi Himii **20,** 498 (1951).
10. FERENCZY, L.: Acta Biol. Acad. Sci. Hung. (in the press)
11. VESTLAKE, DOUGHTERY: J. Am. Chem. Soc. **63,** 658 (1941).
12. GILMAN, H., SMITH, L., PARKER, H.: J. Am. Chem. Soc. **47,** 859 (1925).
13. VOGT: Liebigs Ann. **119,** 149 (1861).

Ferenc KLIVÉNYI
Elemér VINKLER
Angela Enikő SZABÓ
Szeged, P. O. B. 121, Ungarn

Acta Chimica Academiae Scientiarum Hungaricae, Tomus 63 (4), pp. 443—446 (1970)

THE CHEMISTRY OF HETEROCYCLIC PSEUDOBASIC AMINOCARBINOLS, XXXVII

REACTION OF 6,7-DIMETHOXY-3,4-DIHYDROISOQUINOLINE WITH FORMALDEHYDE*

GY. KALAUS, L. TŐKE and CS. SZÁNTAY

(Department of Organic Chemistry, Technical University, Budapest)

Received January 18, 1969

The reaction of 6,7-dimethoxy-3,4-dihydroisoquinoline with formaldehyde was studied and the structure of the product was proved.

In the course of earlier investigations in this laboratory, the reaction of 3,4-dihydroisoquinolines with α, ω-dihalogen compounds was studied. The purpose of the work was the synthesis of bis-quaternary salts with curare-like effect. On alkaline treatment of the salts formed, a particular redox process was observed, which gave rise to molecules containing both isocarbostyryl and tetrahydroisoquinoline units.

In the bis-quaternization reaction with α, ω-bis-halogen compounds, the yield markedly depended upon the number of CH_2 groups between the two halogen atoms. Thus, in the case of 1,2-dibromoethane the reaction could not be accomplished at all.

We found, however, that when 6,7-dimethoxy-3,4-dihydroisoquinoline (**I**) was treated with formaldehyde compound **II** was obtained.

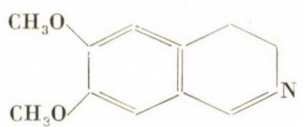

I

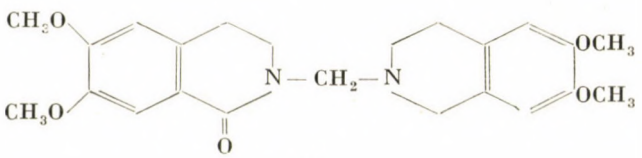

II

The structure of the compound was supported by its empirical formula, and its ultraviolet and infrared spectroscopic data were consistent with those of compounds described earlier [1].

* Part XXXVI: L. SZABÓ and CS. SZÁNTAY: Chem. Ber. 102, 529 (1969).

Compound **II** gives a monohydrochloride salt and a monomethiodide derivative, hence it contains one basical group. Reduction with lithium-aluminium-hydride, on the other hand, gives rise to a dibasical derivative, **III**.

The same product, compound **III**, is formed in the condensation reaction of 6,7-dimethoxy-1,2,3,4-tetrahydroisoquinoline (**IV**) with formaldehyde.

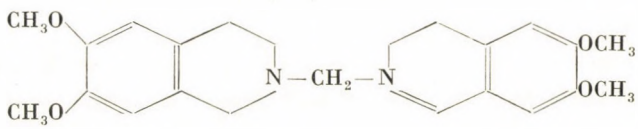

III

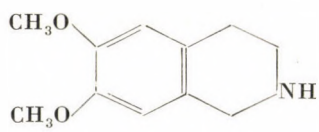

IV

All these reactions unequivocally support structure **II**.

Formation of **II** may presumably be characterized by the following elementary processes. Reaction of **I** and aqueous formaldehyde gives rise to the pseudobase **V**, which then transforms to **II** *via* a mechanism studied in detail and described earlier [1].

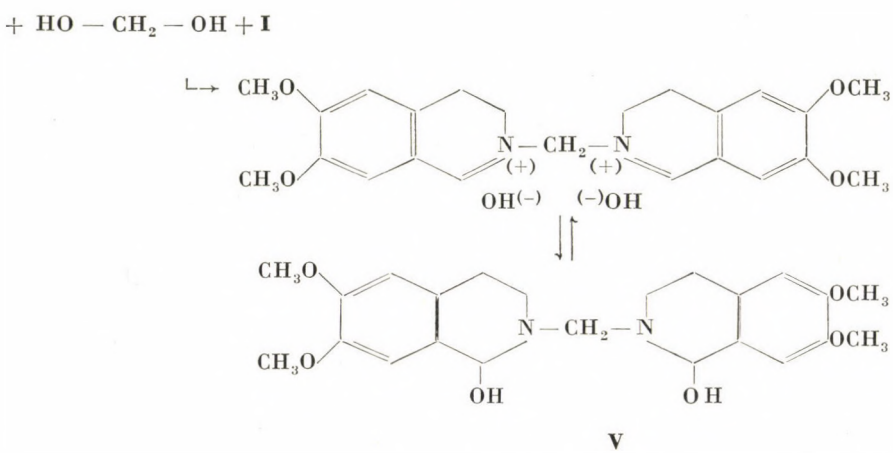

V

The hydrochloride salt of compound **II** possesses a significant spasmolytic effect, however, it is markedly toxic (KNOLL).

Experimental

1. (1-Oxo-6,7-dimethoxy-1,2,3,4-tetrahydroisoquinolinyl-2) - (6,7-dimethoxy-1,2,3,4-tetrahydroisoquinolinyl-2)-methane (II)

6,7-Dimethoxy-3,4-dihydroisoquinoline (**I**; 5.00 g; 26.2 mmole) was dissolved in ethanol (20 ml) and a 26% aqueous formaldehyde solution (6.10 ml; 56.3 mmole) was added. The solution was let to stand at room temperature for six days, when on scratching a white crystalline material deposited. It was filtered off and washed with 3 × 10 ml ethanol to yield 4.00 g of compound **II**, m.p. 158—161°C. Recrystallizations from four times ethanol raised the m.p. to 163—164°C. Yield 3.85 g (71.6%).

$C_{23}H_{28}N_2O_5$ (412.47) Calcd. C 66.97; H 6.84; N 6.79. Found C 66.92; H 6.86; N 6.78%.

UV spectrum: λ_{max} Methanol 269 nm (log ε = 3.953); 289 nm (log ε = 3.918)

λ_{max} *N* HCl 271 nm (log ε = 4.037); 286 nm (log ε = 3.889); 302 nm (log ε = 3.883)

IR spectrum: ν_{max} KBr 1649 cm^{-1} (carboxamide CO).

Hydrochloride (from ethanol): m.p. 175—176°C.

$C_{23}H_{29}N_2O_5Cl$ (448.92). Calcd. C 61.53; H 6.51; N 6.24. Found C 61.27; H 6.44; N 5.96%.

Methiodide: Compound **II** was allowed to stand in nitrobenzene with 1 equivalent methyl iodide at room temperature for 5 days to deposit 77.8% of the methiodide, m.p. 221—222°C (d.).

$C_{24}H_{31}N_2O_5I$ (554.42). Calcd. C 51.98; H 5.63; N 5.05%. Found C 51.72; H 5.58; N 4.94%.

2. Bis-(6,7-dimethoxy-1,2,3,4-tetrahydroisoquinolinyl-2)-methane (III)

(a) Lithium-aluminium-hydride (0.80 g; 21.2 mmole) was refluxed in abs. ether (100 ml) for 30 min. in a flask equipped with a mechanical stirrer, dropping funnel and reflux condenser, and then compound **II** (1.85 g; 4.50 mmole) was added, with stirring and cooling, in portions. Stirring was continued for a further 30 min. at room temperature and for 4 hrs. at reflux temperature. After cooling, water (1 ml), 20% aqueous NaOH (1 ml), and water (3 ml) again were added to the reaction mixture.

The solvent was evaporated and the residue extracted with hot ethanol (50 + 20 ml). After filtration the ethanol solution was concentrated to one half of its original volume and kept in a refrigerator for several hours to deposit crystals, which were collected and washed with 3 × 3 ml ethanol to yield 1.40 g, product, m.p. 123—126°C. Recrystallization from two parts of ethanol gave 1.25 g (67.8%) of the white crystalline base III, m.p. 126—127°C.

$C_{23}H_{30}N_2O_4$ (398.49). Calcd. C 69.32; H 7.59; N 7.03. Found C 69.47; H 7.59; N 6.87%.

Dihydrochloride (from ethanol); m.p. 241—242°C. (d).

$C_{23}H_{32}N_2O_4Cl_2$ (471.42). Calcd. C 58.59; H 6.84; N 5.94. Found C 58.34; H 6.84; N 5.85%.

Bis-methiodide: Compound **III** was allowed to stand in nitrobenzene with 2 equivalents of methyl iodide overnight at room temperature to deposit 68.2% bis-methiodide, m.p. 234—235°C (d).

$C_{25}H_{36}N_2O_4I_2$ (682.38). Calcd. C 44.00; H 5.32; N 4.10. Found C 44.18; H 5.38; N 3.98%.

(b) Base **IV** (2.35 g; 11.6 mmole) was dissolved in ethanol (8 ml) and paraformaldehyde (0.2 g; 6.65 mmole) was added. The mixture was heated on a water bath for 2 hrs. The white crystals deposited on cooling were collected and washed with 3 × 5 ml of ethanol to yield 2.20 g of the product, m.p. 125—126°C which on recrystallization from two parts of ethanol gave 2.00 g (86.4%) of a substance, which was identical in all respects with the product obtained in procedure (a).

*

The authors express their thanks to the Hungarian Academy of Sciences for support of this work, and to the Microanalytical Laboratory of the Department of Organic Chemistry for the microanalyses.

REFERENCE

1. SZÁNTAY, Cs., NOVÁK, L.: Chem. Ber. **96**, 1779 (1963); Magyar Kém. Foly. **69**, 366 (1963).

György KALAUS
László TŐKE
Csaba SZÁNTAY

Budapest XI., Gellért tér 4.

Acta Chimica Academiae Scientiarum Hungaricae, Tomus 63 (4), pp. 447—452 (1970)

BENZAZOLES, VIII*

6,7-DIHYDRO-5-PHENYL-5H-[1,3]-THIAZINO[2,1-b]-IMIDAZOLES AND 2,3-DIHYDRO-1-PHENYL-1H-[1,3]-THIAZINO-[3,2-a]-BENZIMIDAZOLES

H. O. HANKOVSZKY and K. HIDEG

(Institute of Pharmacology, University Medical School, Pécs)

Received January 31, 1969

Imidazole-2-thiols (benzimidazole-2-thiol, 5,6-dimethyl-benzimidazole-2-thiol, 4,5-diphenylimidazole-2-thiol) have been reacted with 3-chloropropiophenone to yield 3-(imidazolylthio)-propiophenones. The ketones are reduced with sodium borohydride to the secondary alcohols, then the secondary alcohol group is substituted by chlorine by treatment with $SOCl_2$. The 2-[(3-chloro-3-phenylpropyl)thio] imidazol derivatives undergo self-alkylation on heating in the presence of excess alkali, to yield the corresponding thiazinoimidazoles.

In continuation of our series dealing with the preparation and reaction of benzazole derivatives, the present paper describes a new condensed thiazinoimidazole ring system.

When equivalent amounts of an imidazole-2-thiol (**I**) (benzimidazole-2-thiol, 5,6-dimethylbenzimidazole-2-thiol, 4,5-diphenylimidazole-2-thiol) and 3-chloropropiophenone are refluxed in the presence of an alkali, S-alkylation takes place to yield the corresponding substituted or condensed imidazolylthiopropiophenone (**II**).

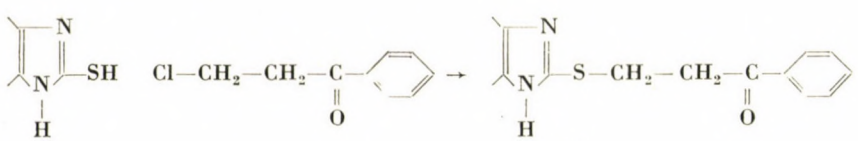

I **II**

The keto group in **II** can be reduced with sodium borohydride in anhydrous ethanol to obtain the secondary alcohol, **III**.

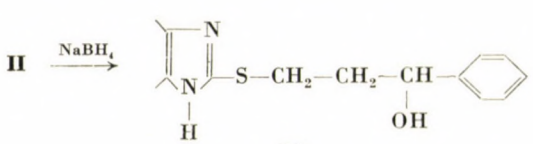

III

* Part VII: HANKOVSZKY, H. O., HIDEG, K.: Acta Chim. Acad. Sci. Hung. **61**, 69 (1969).

Table I

Compd. No.	Structure	Yield, %	M.p., °C	Formula (Molecular weight)	Analysis, %				
					C	H	N	S	Cl
					Calcd. / Found				
1	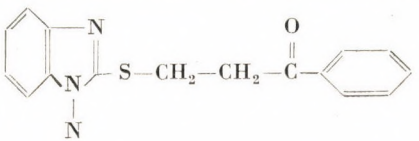	90	136—137	$C_{16}H_{14}N_2OS$ (282.36)	68.06 68.16	5.00 4.92	9.92 9.83	11.35 11.21	—
2	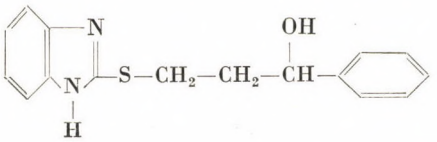	75	54—56	$C_{16}H_{16}N_2OS$ (284.38)	67.58 67.62	5.67 5.83	9.85 9.72	11.28 11.09	—
3	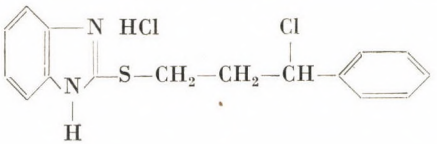	87	172—174	$C_{16}H_{15}ClN_2S.HCl$ (339.29)	56.64 56.56	4.75 4.78	8.26 8.39	9.45 9.38	20.90 20.72
4	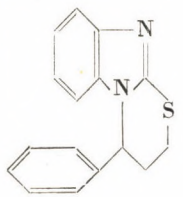	90	126—128	$C_{16}H_{14}N_2S$ (266.37)	72.15 72.08	5.30 5.23	10.51 10.45	12.04 12.00	—

5	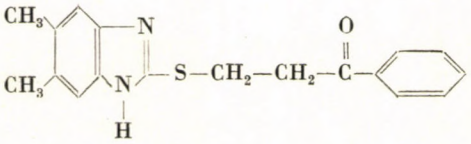	88	190—193	$C_{18}H_{18}N_2OS$ (310.43)	69.67 69.74	5.84 5.90	9.04 9.20	10.32 10.50	—
6	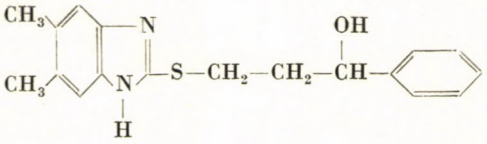	77	134—135	$C_{18}H_{20}N_2OS$ (312.44)	69.20 69.12	6.45 6.50	8.97 8.79	10.26 10.16	—
7	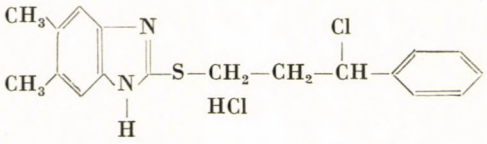	90	246—248	$C_{18}H_{19}ClN_2S.HCl$ (367.36)	58.85 58.74	5.49 5.60	7.62 7.76	8.73 8.80	19.30 19.25
8	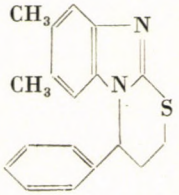	90	248—250	$C_{18}H_{18}N_2S$ (294.43)	73.43 73.45	6.16 6.26	9.52 9.64	10.89 10.92	—
9	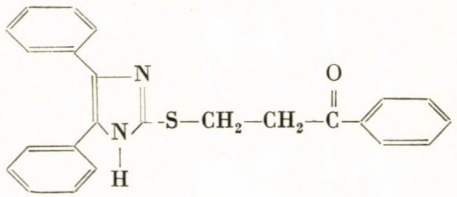	82	218—220	$C_{24}H_{20}N_2OS$ (384.50)	74.97 75.06	5.24 5.25	7.29 7.40	8.34 8.31	—

Table I (cont.)

Compd. No.	Structure	Yield, %	M.p., °C	Formula (Molecular weight)	Analysis, %				
					C	H	N	S	Cl
					Calcd. / Found				
10	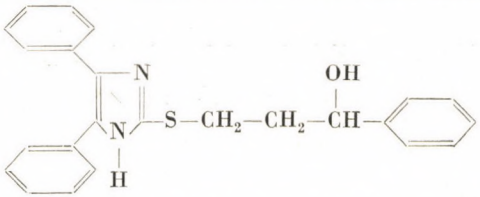	74	184—186	$C_{24}H_{22}N_2OS$ (386.52)	74.58 74.67	5.73 5.85	7.25 7.12	8.30 8.13	—
11	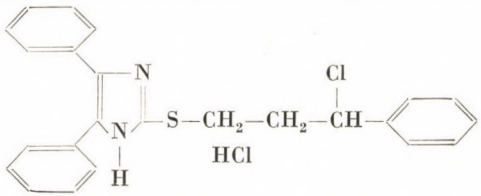	65	137—139	$C_{24}H_{21}ClN_2S.HCl$ (440.42)	65.45 65.32	4.81 4.78	6.36 6.22	7.28 7.34	16.10 16.25
12	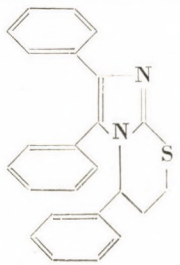	95	211—213	$C_{24}H_{20}N_2S$ (368.50)	78.23 78.40	5.47 5.50	7.60 7.52	8.70 8.81	—

Treatment of **III** with $SOCl_2$ in chloroform results in substitution of the hydroxyl group by chlorine; the product is obtained as the hydrochloride salt, **IV**.

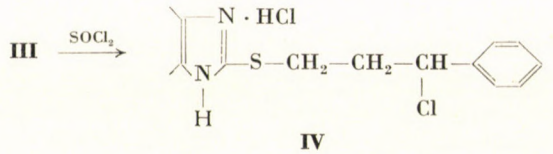

IV

When **IV** is treated with alkali in ethanol, the imino group and the chlorine atom of the molecule interact to give a thiazinoimidazole ring system, (**V**).

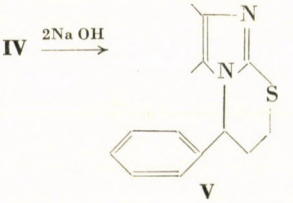

V

The compounds prepared by the method described are listed in Table I.

Experimental

All m.p.'s were obtained on a Boetius melting point apparatus and are uncorrected. IR spectra were determined in KBr disks, with a Beckman IR-4 spectrophotometer.

Several compounds of each type have been prepared by the same method, but only one example is given.

Pertinent data regarding each compound are recorded in Table I.

Type II

3-[(2-Benzimidazolyl)thio]propiophenone (No. 1)

A solution of 15.0 g (0.1 mole) of benzimidazole-2-tiol and 16.8 g (0.1 mole) of 3-chloropropiophenone in 300 ml of ethanol was treated with 4.4 g (0.11 mole) of sodium hydroxide dissolved in 20 ml of water. The mixture was refluxed for 3 hrs.

After cooling, the mixture was diluted with 100 ml of water, when the product precipitated.

The crystals were filtered off and washed with water to remove NaCl, to obtain 25.4 g (90%) of the crude product.

Recrystallization gave a white crystalline substance, m.p. 136—137°C; ν_{max}^{KBr} 3200 cm^{-1} (NH), 1700 cm^{-1} (CO).

Type III

α-{2-[(2-Benzimidazolyl)thio]ethyl}benzyl alcohol (No. 2)

A suspension of 14.1 g (0.05 mole) of the above product (No. 1) in 200 ml of anhydrous ethanol was treated with 3 g of sodium borohydride and the reaction mixture was refluxed for 3 hrs. The complex was decomposed with water, the solvent evaporated, and the aqueous residue extracted with chloroform.

The chloroform solution was evaporated to dryness in vacuum. The product was recrystallized twice from aqueous ethanol to give 10.7 g (75%) of No. 2, as white crystals, m.p. 54—55°C; νKBr 3400 cm^{-1} (OH), 3100 cm^{-1} (NH).

Type IV

2-[(3-Chloro-3-phenylpropyl)thio]benzimidazole hydrochloride (No. 3)

A solution of 14.2 g (0.05 mole) of the above product (No. 2) in 100 ml of chloroform was mixed with 5 ml of $SOCl_2$ in 50 ml of chloroform, and refluxed for 3 hrs. The solvent was evaporated under reduced pressure, and the residue rubbed with acetone to give the product in 87% yield, m.p. 172—174°C. A sample for analysis was recrystallized from ethanol–acetone 1 : 1, m.p. 172—174°C.

Type V

2,3-Dihydro-1-phenyl-1H[1,3]thiazino[3,2-a]benzimidazole (No. 4)

A solution of 8.5 g (0.025 mole) of the previous compound (No. 3) in 100 ml of ethanol was mixed with 2.4 g (0.06 mole) of sodium hydroxide dissolved in 10 ml of water, and the mixture was refluxed for 1 hr.

The precipitated NaCl was filtered off from the hot reaction mixture. The filtrate was cooled and diluted with water. The almost white solid which deposited was filtered off to obtain 6.0 g (90%) of the desired product, m.p. 120—124°C.

Two recrystallizations from ethanol–water gave No. 4 as white crystals, m.p. 126—128°C.

*

The authors' thanks are expressed to Mrs. M. Ott, Mrs. A. Halász and Miss T. Huszár for the microanalyses and technical assistance.

Olga H. Hankovszky
Kálmán Hideg

Pécs, Rákóczi út 2. Hungary

Acta Chimica Academiae Scientiarum Hungaricae, Tomus 63 (4), pp. 453—456 (1970)

APPLICATION OF RADIATION POLYMERIZATION FOR THE PRODUCTION OF WATER-INSOLUBLE ENZYME PREPARATIONS

(SHORT COMMUNICATION)

J. DOBÓ

(Plastics Research Institute, Budapest)

Received July 9, 1969

The preparation of water-insoluble enzymes has attained considerable interest in recent years [1]. Enzymes bound to insoluble carriers act as heterogenous specific catalysts and can be used successfully both in analytical and preparative chemistry. In most of the papers published, covalent binding of the protein to a water-insoluble carrier is brought about, in some others the physical entrapping of the enzyme is utilized.

One of the physical methods consists in entrapping the enzyme into a crosslinked network of a hydrophilic polymer as it forms. This method seems to be universal, simple, and best suited for practical application.

As entrapping matrices more or less crosslinked polyacrylamide gels proved to be especially suitable. For initiation of the polymerization of acrylamide and crosslinking agents, BERNFELD and WAN used a redox-system at 35°C [2]. For labile enzymes [3], photoinitiation was proposed too.

In this work we report some experiments on the entrapping of enzymes nto radiation polymerized polyacrylamide gels.

Experimental

Recrystallized acrylamide and bisacrylamide were used as monomers and liophylized trypsin as the enzyme.

The insoluble enzyme was prepared — unless stated otherwise — by dissolving 200 mg of acrylamide and 120 mg of bisacrylamide in 10 ml of borax buffer solution, to which 0.1—10 mg trypsin had been added. The solutions were deaerated by bubbling purified argon for 15 minutes and, in some control experiments, by sealing off in high vacuum after repeated freezing and thawing. Irradiation was carried out by a 150 kV/10 mA X-ray apparatus at dose rates of 2300 r/hr and 4700 r/hr.

The resulting gel containing the insoluble enzymes was centrifuged and washed repeatedly in the centrifuge until no activity could be detected in the wash water (6—8 washing cycles). The activity was determined by a casein digestion method (30 minutes digestion time at 40°C) through comparison with the activity of 0.02—0.03 mg of pure trypsin. The activity of the enzyme precipitate was determined in a similar manner, good contact between solution and precipitate being ensured by slow bubbling of argon.

Results

1. Polymerization reaction

Pure acrylamide, when thoroughly degassed, polymerizes spontaneously even in the absence of initiators [4]. In the presence of added substances, however, acrylamide is much less inclined to spontaneous polymerization. In fact, in the presence of enzymes, we could not observe any spontaneous polymerization. On the other hand, good deaeration is a prerequisite for low-dose processing. With good deaeration an opaque precipitate begins to form within 2 to 5 minutes of irradiation even in the presence of enzymes.

Enzymes somewhat retard the polymerization reaction (*cf.* Table I). The retarding effect of certain additives on the polymerization of monomers in aqueous solution has been studied already by CHARLESBY [5].

Table I

Polymerization of 200 mg of acrylamide + 120 mg of bisacrylamide in 10 ml of borax buffer (20°C, 4700 r/hr)

Irradiation time	% polymerized	
	without trypsin	with 10 mg of trypsin
15 min	80	63
30 min	81	64
60 min	91	75
3 hrs	100	100

2. Monomer composition

As monomers, 200 mg of acrylamide + 120 mg of bisacrylamide, and 120 mg of bisacrylamide (without acrylamide) have been used. The precipitate obtained from the mixture of monomers was easier to handle and required lower doses. According to preliminary experiments, higher monomer concentrations ensure higher enzyme activities in the precipitate.

3. Radiation damage of enzymes

Solutions of enzymes are known to be sensitive to high energy radiation. After 30 minutes of irradiation with 4700 r/hr, trypsin solutions showed a marked decrease while 1—2 hours of irradiation resulted in a strong decrease in activity. It is assumed that large amounts of monomers provide effective protection against the attack of free radicals.

4. Activity of the insoluble enzymes

The behaviour of the insoluble preparations can be illustrated by the following example:

200 mg of acrylamide and 120 mg of bisacrylamide were polymerized by 3 hours of irradiation at 0°C and at a dose rate of 2300 r/hr, in 10 ml of a borax buffer, in the presence of 1 mg (**I**) and 3 mg (**II**) of trypsin, respectively. The insoluble enzymes were repeatedly used in casein digestion tests; in 3 and 9 subsequent digestions, **I** and **II**, respectively, have shown higher activity than 0.03 mg of pure trypsin. The digestions were continued and after 12 cycles **I** showed only a poor, while **II** a rather good activity.

On the next day, a distinct regeneration of the enzyme activity was observed. The digestion tests have been continued to a total of 50 cycles during 8 days after which **I** has completely, and **II** partly lost its activity. A regeneration of the activity has been observed after each night of standing. During these digestion experiments the insoluble enzymes suffered a thermal treatment of 25 hours at 40°C. The soluble trypsin, on the other hand, lost over 90% of its activity during a thermal treatment of 4 hours at 40°C.

Preparations of good activity have been obtained in the presence of polyurethane foams, too.

Discussion

A general drawback of the entrapping of enzymes into gels formed *in situ* is the sensitivity of enzymes against free radical attack. This question would merit a closer examination since, probably, there are differences between enzyme and monomer reactivities against different kinds of free radicals. Toward hydroxyl radicals, both acrylamide [4] and trypsin [6] seem to be especially reactive. As monomer and enzyme compete for the free radicals, it seems to be advisable to work with excess monomer, not conducting the polymerization to 100 per cent conversion.

Radiation initiation has two distinct advantages over chemical initiation. The first one is the better heat control.

In polymerization reactions, as in any process where considerable heat is evolved and where the reaction is accelerated by higher temperatures, there is a danger of thermal explosion, *i.e.* sudden acceleration and overheating. The temperature rise ΔT, where this acceleration occurs, is after SEMENOV

$$\Delta T = \frac{T_1}{\frac{E}{RT_1} - 2}$$

where T_1 is the initial temperature, E is the overall activation energy of the reaction, and R is the gas constant [7]. From this, the paramount importance of a low activation energy is obvious. The activation energy of polymerization reactions is

$$E = E_i/2 + E_p - E_t/2$$

where i, p and t refer to initiation, propagation and termination, respectively. For the radiation polymerization of acrylamide, where $E_i = 0$, an activation energy of only about 1.5 kcal/mole has been found [4]. Moreover, at high conversion, E_t generally becomes higher. Thus, it can be assumed, that under ordinary conditions the activation energy of radiation polymerization is close to 0 and a sudden selfacceleration of the reaction is impossible.

In case of redox initiation, the activation energy of initiation may be *e.g.* some 14 kcal/mole, and so the polymerization reaction has an overall activation energy of about 7 kcal/mole. This is a low value, too, but when judging the danger of overheating, one should take into account the high heat of polymerization reactions, the poor heat transfer of gels especially at high conversion and in large reaction vessels as well as the extreme thermal sensitivity of enzymes. The danger of overheating with redox initiators has been considered by other authors, too [3].

The second advantage of radiation initiation is that it can be stopped at any moment and no undecomposed initiator remains in the preparation. Chemically initiated polymerization is seldom conducted to dead-end, *i.e.* to complete decomposition of the initiator. Upon decomposition the remaining initiator can cause further damage, its complete elimination being difficult, especially from viscous gels or from foams, membranes, etc.

*

The author is indebted to Mrs. Dr. E. UDVARDY-NAGY of the Gedeon Richter Chemical Works, Budapest, for her continuous advices and help and to Mrs. P. KÁRPÁTHY for her technical assistance.

REFERENCES

1. SILMAN, I. H., KATCHALSKI, E.: Ann. Rev. Biochem. **35,** 873 (1966).
2. BERNFELD, P., WAN, J.: Science **142,** 678 (1963).
3. MOSBACH, K., MOSBACH, R.: Acta Chem. Scand. **20,** 2807 (1966).
4. COLLINSON, E., DAINTON, F. S., MCNAUGHTON, G. S.: Trans. Faraday Soc. **53,** 476, 489 (1957).
5. CHARLESBY, A., KOPP, P. M.: Int. J. Rad. Biol. **5,** 521 (1962).
6. SANNER, T., PIHL, A.: Biochem. Biophys. Acta **146,** 298 (1967).
7. TÜDŐS, F., GÁL, K.: Magyar Kém. Folyóirat **64,** 270 (1958).

János DOBÓ; Budapest XIV., Hungária krt. 114.

Experimental Thermodynamics, Vol. I. Ed. by J. P. McCullough and D. W. Scott, Butterworths, London, 1968. 606 pages

Experimental Thermodynamics, Volume I (Calorimetry of Non-reacting Systems) prepared under the sponsorship of the IUPAC (International Union of Pure and Applied Chemistry) Commission on Thermodynamics and Thermochemistry was edited with the aim to give an authoritative knowledge on experimental thermodynamics to contemporary and future scientists of the world. In accordance with the sub-title of the book, the authors deal with the determination of the specific heat of substances in different states in the range from the absolute zero up to the highest temperatures attainable at present, and discuss the measurement of the change in enthalpy for various phase transformations. The contents of the book differ substantially from that of "Experimental Thermochemistry"* which discusses the determination of heats of reactions. The book is divided into chapters on the basis of the types of calorimeters and the ranges of applicability (temperature, state). Though each chapter has been written by a different author, the book is uniform and there are no unjustified overlaps, while those present, further a better understanding, as they are concerned with different aspects of the same method or apparatus.

The principal fundamental physical quantities measured in calorimetry are temperature, energy and mass. Therefore, the general historical survey is followed by two chapters, of which one is devoted to the measurement of temperature, the other to that of energy. It becomes clear from the discussion that while aiming at higher accuracy, the difficulties of the measurement increase exponentially. Today, the highest attainable accuracy is about 0.01%.

The fourth chapter deals with the general aspects of calorimeter design and with general techniques in this field. This helps researchers to select or to design the most suitable calorimeter for the solution of a given problem. Consideration of heat flow forms the backbone of this chapter, because it is believed that lack of understanding of heat flow is the source of most errors in accurate calorimetry.

The following ten chapters discuss special kinds of calorimeters. The authors of these chapters give a detailed description of a few characteristic, well-functioning instruments from their special field of research, and a short general survey of other instruments. Thus, the book is a fortunate combination of everything that is expected from a good textbook and an exhaustive handbook. For a better understanding, the authors give the necessary thermodynamic relationships, detailed instructions for calculations, and even numerical examples.

GY. RÁCZ

Annual Review of NMR Spectroscopy. Edited by E. F. Mooney. Academic Press, London and New York, 1969. 467 pages

After the favourable reception of the first volume of this series, it was only natural that readers interested in this field of science looked forward to the publishing of further vollumes. The high standard of the second volume and the careful selection of material come up

* Vol. I. Editor F. D. ROSSINI, 1956
Vol. II. Editor H. A. SKINNER, 1962.

to these expectations in every respect. The book offers valuable guidance to chemists to find their way, in the steadily swelling sea of data on NMR spectroscopy.

Obviously, it is more or less a matter of individual opinion, which papers should be reviewed out of the immense number of publications dealing with NMR spectroscopy. The editor has given an example of excellent discrimination in this respect. Compared with the first volume, much greater emphasis is laid here on the magnetic spectroscopy of nuclei other than protons (nitrogen, phosphorus, etc.). This branch of NMR spectroscopy is steadily gaining importance in structural analysis.

The first chapter (P. BLADON: General Review of Proton Magnetic Resonance, pp. 34) gives a review of recent technical developments, and surveys the factors affecting chemical shift and coupling constants. Special attention is paid in this chapter to equilibrium problems, such as keto-enol tautomerism, studied by PMR techniques.

The second chapter (T. D. INCH: NMR Spectroscopy in the Study of Carbohydrates and Related Compounds pp. 47) deals with the conformation, configuration and other structural problems of carbohydrates and their derivatives, *e.g.* nucleosides.

The third chapter (J. RONAYNE and D. H. WILLIAMS: Solvent Effects in PRM Spectroscopy, pp. 41), discussing the role of solvents, is of particular interest and very useful in the everyday practice of NMR spectroscopy.

The fourth chapter (E. F. MOONEY and P. H. WINSON: Nitrogen Magnetic Resonance Spectroscopy, pp. 27) reviews the role of nitrogen; it is followed by the fifth part (E. F. MOONEY and P. H. WINSON: Carbon-13 NMR Spectroscopy; Carbon-13 Chemical Shifts and Coupling Constants, pp. 65), which can be particularly recommended to organic chemists. Many chemists do not pay due attention to the carbon-13 satellite signals appearing in simple PMR spectra, though their study may yield very valuable information, as it is shown in this chapter.

The sixth chapter (W. G. HENDERSON and E. F. MOONEY: Boron-11 NMR Spectroscopy, pp. 72) deals with the spectra of tetracovalent heterocyclic and other boron compounds.

The next part (R. A. DWEK, R. E. RICHARDS and D. TAYLOR: Nuclear Electron Double Resonance in Liquids, pp. 49) helps to a better understanding of the concept of nuclear Overhauser effect, and illustrates the scope of its applications. This method is not yet in general use in chemical laboratories, however, this survey of the possibilities is very useful.

The last chapter (J. F. NIXON and A. PIDCOCK: Phosphorus-31 NMR Spectra of Coordination Compounds, pp. 76) deals with the structural investigation of complex compounds containing phosphorus.

The book, impeccable also from the viewpoint of printing techniques, is completed with an Author and Subject Index.

CS. SZÁNTAY

INDEX

INORGANIC AND ANALYTICAL CHEMISTRY – ANORGANISCHE UND ANALYTISCHE CHEMIE – НЕОРГАНИЧЕСКАЯ И АНАЛИТИЧЕСКАЯ ХИМИЯ

PHYSICAL CHEMISTRY– PHYSIKALISCHE CHEMIE – ФИЗИЧЕСКАЯ ХИМИЯ

ORGANIC CHEMISTRY – ORGANISCHE CHEMIE – ОРГАНИЧЕСКАЯ ХИМИЯ

CHEMICAL TECHNOLOGY– CHEMISCHE TECHNOLOGIE – ХИМИЧЕСКАЯ ТЕХНОЛОГИЯ

Printed in Hungary

A kiadásért felel az Akadémiai Kiadó igazgatója — Műszaki szerkesztő: **Farkas Sándor**

A kézirat nyomdába érkezett: 1969. XI. 24. — Terjedelem: 9,25 (A/5) ív, 31 ábra

70.68663 Akadémiai Nyomda, Budapest — Felelős vezető: Bernát György

ACTA CHIMICA

ТОМ 63—ВЫП. 4

РЕЗЮМЕ

Полярографические и вольтамперометрические свойства соединений Te(IV) и Te(VI)

Ф. ВАЙДА

При изучении ионов (Te(IV) и Te(VI) на ртутном капельном электроде и на электроде висячей ртутной капли, для обоих ионов было найдено появление анодной волны при положительных потенциалах и пары анодно-катодных вольтамперометрических пиков. На циклических вольтаграммах, снятых в области потенциалов, соответствующих процессам восстановления, помимо пиков восстановления наблюдаются также максимумы. Процессы, сопровождаемые образованием твердой пленки, могут быть использованы для определения теллура с помощью растворяющей вольтамперометрии, тем самым повышая чувствительность полярографического определения теллура.

Изменение энтальпии при смешении уксусной кислоты с четыреххлористым углеродом, I

Я. ЛИСИ

Изучались волюметрические свойства смесей уксусной кислоты с четыреххлористым углеродом. Было найдено, что на величину молярного объема уксусной кислоты, как смеси, состоящей из мономера и димера, при 20°C сказывается контракция. Жидкой фазе приписывалось квазикристаллическое строение. Было установлено, что смесь уксусной кислоты с четыреххлористым углеродом можно моделировать как кубическую решетку центрированную на плоскость. Эти результаты используются во второй части сообщения, где рассматривается изменение энтальпии при смешениее уксусной кислоты с четыреххлористым углеродом.

Изменение энтальпии при смешении уксусной кислоты с четыреххлористым углеродом, II

Я. ЛИСИ

Рассматривая номинально бинарную смесь уксусной кислоты с четыреххлористым углеродом как трехкомпонентную типа $A—A_2—B$, определялись средние энергии взаимодействия между действительными компонентами, а также энергии обмена. При расчете изменения энтальпии при смешении учитывались смещение равновесия ассоциации и различные энергии взаимодействия молекул. Для проверки расчетов экспериментально определялись изменения энтальпии для случая изотермического смешения при 20°C.

Изучение адсорбционных явлений на платинированной платине методом радиоактивных индикаторов, I. Экспериментальная методика и адсорбция H_2SO_4

Я. ШОЛТ, Дь. ХОРАНИ и Ф. НАДЬ

Был разработан метод изучения адсорбционных явлений на платиновом электроде с помощью техники изотопов с мягким β-излучением.

Анализировалось влияние параметров оборудования на систематическую погрешность измерений.

Изучалась адсорбция иона HSO^-_4 в 1N-ом растворе $HClO_4$ в зависимости от потенциала электрода. На основе измерений было установлено:

1. Адсорбция ионов HSO^-_4 является специфической. Величина адсорбции зависит от потенциала электрода и от концентрации $[HSO^-]$.

2. Адсорбция HSO^-_4 является обратимой при потенциалах более отрицательных, чем 750 мв и необратимой при потенциалах больших, чем 750 мв.

3. Зависимость величины адсорбции от концентрации в области $10^{-7} + 10^{-4}$ моль/л описывается суммой трех изотерм типа Лангмюра, отвечающих трем типам активных центров с различной адсорбционной силой. Количество адсорбата, необходимого для насыщения центров различной активности, (Γ_i°) является функцией потенциала.

Изучение структуры связей соединений, содержащих аллил-кремниевую группу

Й. НАДЬ Й. РЕФФИ и П. ЭЛИАШ

С целью определения структуры аллил-кремниевой (и аллил-германиевой) группы проводились приблизительные квантово-химические расчеты относительно структуры δ- и π-связей триметил-аллил-силана и 1-триметил-силил-циклопентена-2. Расчеты показали, что в триметил-аллил-силане, гиперконъюгационное влияние CH_2-группы а также длинная связь между атомом кремния и атомом углерода, находящимся в β-положения к нему, оказывают совместное влияние, так что связь между атомом кремния с соседним атомом углерода обладает характером π-связи на 8%, а длинная связь обладает характером π-связи на 3,5%. В циклических же соединаниях аллильного типа характер π-связи еще выше. Расчетное значение результирующего дипольного момента триметил-аллил-силанов равно 0,448 D, что находится в хорошем согласии с экспериментальным значением, равным 0,58 D.

Об ИК и ЯМР спектрах молекул $[(CH_3)_2N]_2S$, $[(CH_3)_2N]_2SO$, $[(CH_3)_2N]_2SO$, и $(CH_3)_2NSO_2Cl$.

Ф. ТЁРЁК, Е. ПАЛДИ, Ш. ДОБОШ и Г. ФОГАРАШИ

Снимались ИК и ЯМР спектры молекул $[(CH_3)_2N]_2S$, $[(CH_3)_2N]_2SO$, $[(CH_3)_2N]_2SO_2$ и $CH_3)_2NSO_2Cl$. Частота связи S—N в ИК спектрах оказалась слишком высокой по сравнению с ожидаемой, а частота симметричного растяжения связи C—N — слишком низкой. На основе спектров, соединения по силе связи $p_\pi—d_\pi$ могут быть расположены в следующем ряду:

$$[(CH_3)_2N]_2SO < [(CH_3)_2N]_2SO_2 < (CH_3)_2NSO_2Cl.$$

Молекула $[(CH_3)_2N]_2S$ ни по ИК, ни по ЯМР спектрам не может быть включена в ожидаемый ряд спектроскопических данных изученных соединений.

Введение ароматических соединений в качестве включений в дезоксихолевую кислоту

З. ЧЮРЁШ, Дь. ДЭАК и М. КИШШ-НОВАК

В дезоксихолевую кислоту с темп. пл. 174°C, свободную от жирных кислот, что подтверждалось тонкослойной хроматографией, вводились включения с помощью различных, включаемых компонентов (бензол и его девять жидких, замещенных производных). Состав определялся с помощью ультрафиолетовой спектроскопии. Было установлено, что с увеличением количества включемого компонента отношение дезоксихолевой кислоты к включенному компоненту в соединении с включениями приближается к значению 2 : 1, но, однако, не достигает этого значения даже и при большом избытке включаемого компонента.

Было обнаружено образование смешанного соединения одновременно с двумя включаемыми компонентами. Отношение компонентов во включении определяется, с одной стороны, отношением компонентов в смеси растворителей, применяемых для включения, а с другой стороны, относительной стабильностью включаемых компонентов. Относительная стабильность определялась для охарактеризования сродства дезоксихолевой кислоты отдельным компонентам смеси при прочих равных условиях. Стабильность соединений с включениями зависит также от величины молекулы компонента включения и от его дипольного момента.

Исследования в области ароматических сульфенилхлоридов, I

Взаимодействие сульфенилхлоридов с алкилтиосульфатами и ксантогенатами

Ф. КЛИВЕНИ, Е. ВИНКЛЕР и А. Е. ШТАЙЕР-САБО

Было установлено, что О-арилсульфенил-S-алкилтиосульфаты образуются лишь в небольших количествах при взаимодействии сульфенилхлоридов с алкилтиосульфатами. Продукты неустойчивы и при потере трехокиси серы переходят в дисульфиды.

При взаимодействии арилсульфенилхлоридов с ксантогенатами образуются с хорошим выходом (алкокси-тиоформил)-арилдисульфиды. Эти соединения представляют собой желтые масла, которые могут быть хорошо очищены хроматографическим путем. Под влиянием тепла они разлагаются на соответствующие тиофенол и олефин с выделением при этом карбонил-сульфида и серы. (Алкокси-тиоформил)-арил-дисульфиды обладают высоким селективным антимикробным действием на Грам — положительные микроорганизмы.

Некоторые данные к химии гетероцикличных псевдоосновных аминокарбинолов, XXXVII

Реакция 6,7-диметокси-3,4-дигидро-изохинолина с формальдегидом

Дь. КАЛАУШ, Л. ТЁКЁ и Ч. САНТАИ

Изучалась реакция 6,7-диметокси-3,4-дигидроизохинолина с формальдегидом и оказалась структура образующегося продукта.

Бензазолы, VIII

6,7-Дигидро-5-фонил-5Н-[1,3] тиазино [2,1-б] имидазолы и 2,3-дигидро-1-фенил-1Н-[1,3] тиазино-[3,2-а] бензимидазолы.

Х. О. ХАНКОВСКИЙ и К. ХИДЕГ

Имидазол-2-тиолы (бензимидазол-2-тиол, 5,6-диметил-бензимидазол-2-тиол, 4,5-дифенил-имидазол-2-тиол) реагируют с 3-хлоропропиофеноном, образуя 3-(имидазолил-тио)-пропиофенон.

С помощью борогидрида натрия кетон восстанавливается до вторичного спирта.

Вторичная спиртовая группа замещалась с помощью $SOCl_2$ на хлор и получаемое 2-[(3-хлоро-3-фенилпропил)-тио] имидазола подвергалось самоалкилированию путем нагрева последнего в присутствии избытка щелочи, образуя при этом соответствующий тиазиноимид-азолы.

The Acta Chimica publish papers on chemistry, in English, German, French and Russian.

The Acta Chimica appear in volumes consisting of four parts of varying size, 4 volumes being published a year.

Manuscripts should be addressed to

Acta Chimica
Budapest 112/91 Műegyetem

Correspondence with the editors should be sent to the same address.

Orders may be placed with "*Kultúra*" Foreign Trade Company for Books and Newspapers (Budapest I., Fő utca 32. Account No. 43-790-057-181) or with representatives abroad.

Les Acta Chimica paraissent en français, allemand, anglais et russe et publient des mémoires du domaine des sciences chimiques.

Les Acta Chimica sont publiés sous forme de fascicules. Quatre fascicules seront réunis en un volume (4 volumes par an).

On est prié d'envoyer les manuscrits destinés à la rédaction à l'adresse suivante:

Acta Chimica
Budapest 112/91 Műegyetem

Toute correspondance doit être envoyée à cette même adresse.

On peut s'abonner à l'Entreprise pour le Commerce Extérieur de Livres et Journaux «*Kultúra*» (Budapest I., Fő utca 32. Compte-courant No. 43-790-057-181) ou à l'étranger chez tous les représentants ou dépositaires.

«*Acta Chimica*» издают трактаты из области химической науки на русском, французском, английском и немецком языках.

«*Acta Chimica*» выходят отдельными выпусками разного объема. 4 выпуска составляют один том. 4 тома публикуются в год.

Предназначенные для публикации рукописи следует направлять по адресу:

Acta Chimica
Budapest 112/91 Műegyetem

По этому же адресу направлять всякую корреспонденцию для редакции.

Заказы принимает предприятие по внешней торговле книг и газет «*Kultúra*» (Budapest I., Fő utca 32. Текущий счет № 43-790-057-181) или его заграничные представительства и уполномоченные.

Reviews of the Hungarian Academy of Sciences are obtainable at the following addresses:

ALBANIA

Ndermarja Shtetnore e Botimeve
Tirana

AUSTRALIA

A. Keesing
Box 4886, GPO
Sydney

AUSTRIA

Globus Buchvertrieb
Salzgries 16
Wien I

BELGIUM

Office International de Librairie
30, Avenue Marnix
Bruxelles 5
Du Monde Entier
5, Place St. Jean
Bruxelles

BULGARIA

Raznoiznos
1, Tzar Assen
Sofia

CANADA

Pannonia Books
2, Spadina Road
Toronto 4, Ont.

CHINA

Waiwen Shudian
Peking
P. O. B. 88

CZECHOSLOVAKIA

Artia
Ve Směčkách 30
Praha 2
Poštová novinová služba
Dovoz tisku
Vinohradská 46
Praha 2
Mad'arská Kultura
Václavské nám. 2
Praha I
Poštová novinová služba
Dovoz tlače
Leningradská 14
Bratislava

DENMARK

Ejnar Munksgaard
Nörregade 6
Copenhagen

FINLAND

Akateeminen Kirjakauppa
Keskuskatu 2
Helsinki

FRANCE

Office International de Documentation et Librairie
48, rue Gay Lussac
Paris 5

GERMAN DEMOCRATIC REPUBLIC

Deutscher Buch-Export und Import
Leninstraße 16
Leipzig 701
Zeitungsvertriebsamt
Fruchtstrasse 3—4
1004 Berlin

GERMAN FEDERAL REPUBLIC

Kunst und Wissen
Erich Bieber
Postfach 46
7 Stuttgart S.

GREAT BRITAIN

Collet's Subscription Import Department
Dennington Estate
Wellingborough. Northants

Robert Maxwell and Co. Ltd.
Waynflete Bldg. The Plain
Oxford

HOLLAND

Swetz & Zeitlinger
Keizersgracht 471—487
Amsterdam C.

Martinus Nijhof
Lange Voorhout 9
The Hague

INDIA

Current Technical Literature
Co. Private Ltd.
India House OPP
GPO Post Box 1374
Bombay I

ITALY

Santo Vanasia
Via M. Macchi 71
Milano
Libreria Commissionaria Sansoni
Via La Marmora 45
Firenze

JAPAN

Nauka Ltd.
92, Ikebukur O-Higashi 1-chome
Toshima-ku
Tokyo
Maruzen and Co. Ltd.
P. O. Box 605
Tokyo-Central
Far Eastern Booksellers
Kanda P. O. Box 72
Tokyo

KOREA

Chulpanmul
Phenjan

NORWAY

Johan Grundt Tanum
Karl Johansgatan 43
Oslo

POLAND

RUCH
ul. Wronia 23
Warszawa

ROUMANIA

Cartimex
Str. Aristide Briand 14—18
Bucureşti

SOVIET UNION

Mezhdunarodnaya Kniga
Moscow G—200

SWEDEN

Almquist & Wiksell
Gamla Brogatan 26
Stockholm

USA

Stechert Hafner Inc.
31, East 10th Street
New York, N. Y. 10003
Walter J. Johnson
111, Fifth Avenue
New York, N. Y. 10003

VIETNAM

Xunhasaba
19, Tran Quoc Toan
Hanoi

YUGOSLAVIA

Forum
Vojvode Mišića broj 1
Novi Sad
Jugoslovenska Knjiga
Terazije 27
Beograd

20. III. 1970 Index: 26.007